UNIVERSITÉ DU QUÉBEC À TROIS-RIVIÈRES

TECHNIQUES INFORMATIQUES AVANCÉES ET PILOTÉES PAR L'INTELLIGENCE ARTIFICIELLE POUR LA MANIPULATION DE BRAS ROBOTIQUES INDUSTRIELS : UN CADRE INTÉGRÉ POUR LA MODÉLISATION, L'APPRENTISSAGE, L'OPTIMISATION ET LA COMMANDE

THÈSE PRÉSENTÉE
COMME EXIGENCE PARTIELLE DU

DOCTORAT EN GÉNIE MÉCANIQUE

PAR
MEHDI FAZILAT

AVRIL 2026

UNIVERSITÉ DU QUÉBEC À TROIS-RIVIÈRES

AI-DRIVEN AND ADVANCED COMPUTATIONAL TECHNIQUES FOR THE INDUSTRIAL ROBOTIC ARM MANIPULATION: AN INTEGRATED FRAMEWORK FOR MODELING, LEARNING, OPTIMIZATION, AND CONTROL

A THESIS PRESENTED
IN PARTIAL FULFILLMENT OF
THE REQUIREMENTS FOR THE DEGREE
DOCTOR OF PHILOSOPHY IN MECHANICAL ENGINEERING

BY
MEHDI FAZILAT

APRIL 2026

UNIVERSITÉ DU QUÉBEC À TROIS-RIVIÈRES

DOCTORAT EN GÉNIE MÉCANIQUE (PH.D.)

Direction de recherche :

Nadjet Zioui Université du Québec à Trois-Rivières	directeur de recherche

Jury d'évaluation :

Nadjet Zioui Université du Québec à Trois-Rivières	directeur de recherche
Sasan Sattarpanah Karganroudi Université du Québec à Trois-Rivières	président du jury
Hamed Sohrabpoor Indiana University Bloomington	évaluateur externe
Toufik Souanef Cranfield University, UK	évaluateur externe

Thèse soutenue le 13 MARS 2026

UNIVERSITÉ DU QUÉBEC À TROIS-RIVIÈRES

DOCTOR OF PHILOSOPHY IN MECHANICAL ENGINEERING (PH.D.)

Research Supervision :

Nadjet Zioui — research director
Université du Québec à Trois-Rivières

Evaluation jury :

Nadjet Zioui — research director
Université du Québec à Trois-Rivières

Sasan Sattarpanah Karganroudi — jury president
Université du Québec à Trois-Rivières

Hamed Sohrabpoor — external evaluator
Indiana University Bloomington

Toufik Souanef — external evaluator
Cranfield University, UK

Thesis defended on 13 MARCH 2026

Abstract

This dissertation proposes an integrated and interdisciplinary framework for enhancing the modeling, learning, optimization, and control of industrial robotic arms by intersecting advanced computational methods in fundamental artificial intelligence and robotics. Motivated by the growing demand for high-precision, energy-efficient, and adaptive robotic systems in industrial automation, this research addresses core challenges in dynamic modeling, inverse kinematics, parameter identification, and robust control under nonlinear and uncertain conditions. The study is structured around six core investigations, each represented by a peer-reviewed publication and synthesized into a unified research trajectory. First, a systematic review assesses the landscape of quantum computing in robotics, highlighting the roles of quantum machine learning, quantum neural networks, quantum-inspired algorithms, and quantum-enhanced control strategies. Second, the impact of dynamic model simplifications on energy consumption and torque prediction is rigorously quantified using multi-fidelity CAD models of a six-jointed industrial robot. Third, a QNN-based inverse kinematics framework is proposed, demonstrating superior accuracy and singularity robustness compared to classical neural network approaches. Fourth, dynamic parameter identification is accomplished through a comparative study between classical Particle Swarm Optimization and Quantum-behaved PSO, with results confirming the quantum approach's improved convergence and resilience to disturbances. Fifth, a quantum-inspired Sliding Mode Control method is developed, integrating quantum principles into control laws to reduce chattering, enhance tracking precision, and improve energy efficiency. Additionally, a sixth investigation introduces a Quantum Sinusoidal

Pulse Width Modulation strategy, implemented as the actuator-level control mechanism to realize the optimized trajectory tracking tasks derived from the proposed quantum-enhanced methods. This technique minimizes Total Harmonic Distortion in motor drives, thereby enhancing power quality, voltage utilization, and overall energy efficiency across the robotic control framework. The proposed framework is not just a theoretical concept, but a practical solution that has been validated using both simulation and empirical data on the ABB IRB 140 industrial robotic manipulator. Across all analyses, quantum-enhanced techniques consistently outperform classical counterparts in terms of accuracy, adaptability, and computational robustness. This dissertation provides novel insights into the scalability and practicality of quantum-AI integration, establishing methodological pathways for the next generation of intelligent robotic systems.

Résumé

Cette thèse propose un cadre intégré et interdisciplinaire visant à améliorer la modélisation, l'apprentissage, l'optimisation et la commande des bras robotiques industriels, en croisant des méthodes computationnelles avancées issues de l'intelligence artificielle fondamentale et de la robotique. Motivée par la demande croissante en systèmes robotiques industriels à haute précision, à faible consommation énergétique et à forte capacité d'adaptation, cette recherche s'attaque aux défis fondamentaux liés à la modélisation dynamique, la cinématique inverse, l'identification des paramètres et la commande robuste dans des conditions non linéaires et incertaines. L'étude s'articule autour de six axes de recherche principaux, chacun ayant donné lieu à une publication évaluée par des pairs et synthétisé dans une trajectoire scientifique cohérente. Premièrement, une revue systématique évalue l'état de l'art du calcul quantique appliqué à la robotique, en mettant en lumière les rôles du Machine Learning quantique, des réseaux de neurones quantiques, des algorithmes inspirés du quantique, et des stratégies de commande améliorées par le quantique. Deuxièmement, l'impact des simplifications du modèle dynamique sur la consommation d'énergie et la prédiction du couple est quantifié rigoureusement à l'aide de modèles CAO multi-fidélité d'un robot industriel à six articulations. Troisièmement, un cadre de cinématique inverse basé sur les réseaux de neurones quantiques est proposé, démontrant une précision supérieure et une meilleure robustesse face aux singularités comparativement aux approches neuronales classiques. Quatrièmement, l'identification dynamique des paramètres est réalisée via une étude comparative entre l'optimisation par essaim particulaire classique et celle à comportement quantique, les résultats confirmant la

meilleure convergence et la résilience accrue de l'approche quantique face aux perturbations. Cinquièmement, une méthode de commande par modes glissants inspirée du quantique est développée, intégrant des principes quantiques dans les lois de commande afin de réduire le chattering, améliorer la précision de suivi et optimiser l'efficacité énergétique. En outre, une sixième investigation présente une stratégie de Modulation de Largeur d'Impulsion Sinusoïdale Quantique, mise en œuvre comme mécanisme de commande au niveau des actionneurs pour réaliser les trajectoires optimisées issues des méthodes quantiques proposées. Cette technique permet de réduire la Distorsion Harmonique Totale dans les entraînements de moteurs, améliorant ainsi la qualité de l'alimentation, l'utilisation de la tension et l'efficacité énergétique globale du cadre de commande robotique. Le cadre proposé ne se limite pas à une conceptualisation théorique, mais se concrétise par des validations empiriques et en simulation, notamment sur le manipulateur robotique industriel ABB IRB 140. Dans l'ensemble des analyses, les techniques augmentées par le quantique surpassent systématiquement leurs équivalents classiques en termes de précision, d'adaptabilité et de robustesse computationnelle. Cette thèse offre ainsi des perspectives inédites sur la scalabilité et la viabilité pratique de l'intégration IA-quantique, ouvrant des voies méthodologiques pour la prochaine génération de systèmes robotiques intelligents.

Acknowledgement

I wish to convey my profound and heartfelt gratitude to **Prof. Dr. Nadjet Zioui** for her outstanding supervision, illuminating intellectual guidance, and unwavering encouragement throughout the course of my doctoral journey. Her remarkable scholarly rigor, far-reaching vision, and steadfast support have been instrumental in shaping both the direction and depth of this research. With exceptional patience, integrity, and a truly generous spirit of mentorship, she guided me through the most challenging stages of this work and continually inspired me to pursue excellence with perseverance, curiosity, and purpose. I remain deeply grateful for the trust she placed in my abilities and for the enduring impact she has had on my academic formation as well as my personal growth.

In memory of my father, A. H. Fazilat.

Table of Contents

List of Tables

List of Figures

List of Abbreviations

Abbreviation	Full Description
AI	Artificial Intelligence
ANN	Artificial Neural Network
CAD	Computer-Aided Design
CAO	Computer-Aided Optimization
CCNOT	Controlled-Controlled NOT gate (Toffoli gate)
CNOT	Controlled NOT gate (Quantum logic gate)
DE	Differential Evolution
DH	Denavit–Hartenberg (Kinematic Convention)
DOF	Degrees of Freedom
EKF	Extended Kalman Filter
GWO	Grey Wolf Optimizer
IK	Inverse Kinematics
MAE	Mean Absolute Error
MAPE	Mean Absolute Percentage Error
ML	Machine Learning
MLP	Multi-Layer Perceptron

MPC	Model Predictive Control
NN	Neural Network
PID	Proportional–Integral–Derivative
PSO	Particle Swarm Optimization
PWM	Pulse Width Modulation
QSPWM	Quantum Sinusoidal Pulse Width Modulation
SPWM	Sinusoidal Pulse Width Modulation
THD	Total Harmonic Distortion
VSI	Voltage Source Inverter

Chapter 1 - Introduction

1.1 Motivation

In recent decades, global industries have faced increasing demands for elevated productivity, operational precision, and energy efficiency, all essential for maintaining competitiveness, economic viability, and environmental sustainability. These imperatives appear not only from intensified demand pressures but also from the critical requirement to adhere to strict energy regulations and meet advancing consumer expectations for quality and performance. Advanced sectors such as precision manufacturing, autonomous logistics, minimally invasive robotic surgery, and cleanroom assembly increasingly depend on robotic systems to carry out intricate, high-accuracy tasks. The effectiveness of these systems directly impacts production throughput, safety, and energy consumption. However, any shortcomings in control fidelity, kinematic accuracy, or dynamic responsiveness can lead to cumulative errors, increased operational costs, and higher energy usage. Consequently, the incorporation of advanced control techniques, intelligent kinematic modeling, and energy-aware algorithms has appeared as an essential research priority for both academia and industry.

A particularly noticeable area where these multifaceted challenges intersect is in industrial robotics. Within this domain, articulated robotic arms are essential components of modern automated manufacturing systems. Their intrinsic intricacy emanates from nonlinear kinematics, tightly coupled dynamic behavior, and vulnerability to both internal uncertainties and external disturbances. Collectively, these factors present considerable

hurdles to achieving high-precision control, robust performance, and energy-efficient operations. Among such systems, the ABB IRB-140, a widely utilized six-degree-of-freedom industrial manipulator, serves as a notable benchmark, highlighting the real-world applicability and practical constraints associated with these platforms. Its application across various sectors, from automotive manufacturing to electronics assembly, underscores the urgent need to refine control strategies and dynamic modeling to meet excellent performance and sustainability standards. Enhancing the control dedication, adaptive responsiveness, and energy efficiency of robotic manipulators like the IRB-140 is not exclusively a technical endeavor; it defines a direct pathway to increased industrial throughput, precision, and accuracy, reduced downtime and maintenance costs, and significant reductions in energy consumption and environmental impact. These modifications align with more all-around societal goals, including resource optimization and intelligent automation in the context of Industry 4.0 and beyond.

Addressing these convoluted challenges, the literature has investigated a variety of innovative solutions, including robust control strategies, comprehensive dynamic modeling techniques, and data-driven approaches like neural networks for inverse kinematics and parameter identification. While Advanced Control provides effective resilience to external disturbances and model uncertainties, it often leads to issues such as chattering and an increased computational burden, which can hinder its effectiveness in precision-focused tasks [1]. Neural network-based methods, on the other hand, enhance flexibility and capabilities for nonlinear mapping in solving inverse kinematics, but may struggle under real-time constraints due to their inherent computational complexity [2, 3]. Dynamic modeling, essential for accurate predictions of system behavior, often demands substantial

labor and computational resources, making it less practical for situations requiring rapid adaptation [4, 5]. An important element of effective dynamic modeling is parameter identification, where swarm optimization has recently shown faster convergence, greater robustness, and enhanced accuracy compared to classical swarm algorithms. In this context, quantum computing has emerged as a promising frontier to overcome existing limitations. Approaches such as Quantum Machine Learning (QML), Quantum Neural Networks (QNNs), and quantum-inspired metaheuristics leverage the unique properties of quantum mechanics, such as superposition, entanglement, and quantum parallelism, to achieve accelerated convergence, improved generalization, and scalable computation. Their application in robotics has already led to significant enhancements in speed, robustness, and efficiency, often surpassing classical benchmarks across various metrics.

Despite these promising advancements, several persistent challenges hinder the full realization of quantum-based robotic Control:

- Limited availability and maturity of the classical method.
- Susceptibility of control systems to decoherence and noise.
- High complexity and abstraction of computational algorithms.
- Lack of standardized evaluation frameworks for standard methods in robotics.
- Fragmentation of interdisciplinary collaboration between robotics, advanced computational methods, and control theory.

Current research launched a systematic and rigid exploration into the modeling, analysis, optimization, and Control of industrial robotic arms by progressively integrating classical and quantum computational techniques. It began by developing a highly accurate

and advanced kinematic and dynamic model of an industrial robotic arm. The impact of common simplifications in kinematic and dynamic modeling was then examined, revealing important trade-offs that are academically and practically significant [5]. Building on this foundation, the study conducted a comprehensive literature review that identified the transformative potential of quantum computing in robotics. Guided by this perspective, the research explored hybrid neural network solutions, both classical and quantum, to address the inverse kinematics problem, indicating notable improvements in robotic accuracy and singularity avoidance [2, 6]. To further enhance dynamic modeling, the study applied both classical and quantum swarm optimization algorithms for precise parameter identification, confirming the robustness of quantum-inspired methods in high-dimensional, nonlinear settings. Finally, the research implemented a robust Sliding Mode Control strategy and extended it through a quantum-enhanced version, comparing their performance in terms of precision, robustness, and energy efficiency [1]. Together, these contributions establish a cohesive and interdisciplinary framework that advances the modeling, optimization, and Control of industrial robotic arms by effectively harnessing quantum computing technologies. The comparative analysis conducted across different methodologies clearly reveals the benefits of quantum-enhanced approaches over classic methods. The current thesis addresses this crucial issue through an interdisciplinary framework that unifies classical and quantum methodologies. It focuses on refining dynamic and kinematic models, advancing hybrid quantum-classical optimization techniques, and designing quantum-enhanced control algorithms. By doing so, the research aims to deliver practical and scalable solutions for the next generation of intelligent, energy-efficient industrial robotic systems.

1.2 Literature Review

The rapid evolution of industrial robotics, particularly in high-precision and high-flexibility applications, has prompted a substantial transformation in the methodologies underpinning robotic modeling, control, and learning. These transformations are promoted by pressing industrial demands for systems that can operate under stringent constraints of accuracy, adaptability, and energy efficiency [5]. Against this backdrop, the convergence of artificial intelligence and quantum computing has materialized as a disruptive lane, one that promises to redefine the computational boundaries of intelligent robotics. The present literature review serves as a foundational platform for the following thesis, aiming to consolidate and critically assess contemporary advances in techniques across robotic modeling, parameter identification, learning architectures, and robust control mechanisms.

Over the last two decades, classical AI algorithms such as artificial neural networks (ANNs), support vector machines (SVMs), and various swarm optimization techniques have played an instrumental role in enhancing robotic capabilities [7, 8]. These techniques have demonstrated their value in solving inverse kinematics, improving dynamic model estimation, and enabling real-time trajectory planning. Nonetheless, as the dimensionality and nonlinearity of robotic systems increase, particularly in the context of articulated manipulators with six or more degrees of freedom (DOF), classical approaches have shown signs of restrictions. Issues such as computational overhead, convergence instability, sensitivity to noise, and difficulty in maintaining robustness under unstructured environments remain formidable challenges [2, 9].

Concurrently, the emergence of quantum computing has opened a new computational frontier. Unlike classical computers that process information in bits, quantum systems utilize quantum bits (qubits), which harness principles such as superposition, entanglement, and quantum tunneling to represent and process information in fundamentally new ways [10]. In robotics, this paradigm has given rise to a relative of quantum-inspired algorithms, ranging from quantum neural networks (QNNs) and quantum machine learning (QML) to quantum-enhanced control strategies and swarm optimization heuristics [11]. These developments offer influential advantages in terms of computational scalability, learning efficiency, and resilience to noise, essential attributes for real-world robotic systems operating in dynamic and uncertain settings.

Despite notable advancements, the body of literature on quantum-enhanced robotics remains quite fragmented. Research efforts primarily focus on isolated components, such as control or learning, often lacking an integrative framework that links modeling, parameter estimation, and decision-making processes. Moreover, many quantum methodologies are introduced in theoretical or simulated contexts, lacking standardized benchmarking against their classical counterparts. This absence of comparative analysis complicates the evaluation of the actual benefits of quantum methods, especially when implemented on real robotic platforms constrained by hardware limitations and operational challenges [1]. In other hand, the literature study addresses existing research gaps by synthesizing findings across five essential dimensions of robotic system development: the integration of quantum-AI principles, modeling simplification strategies, learning architectures for inverse kinematics, parameter identification via optimization, and robust control enhancement. These five domains are central to building intelligent, adaptive, and energy-

efficient robotic systems capable of operating in dynamic and uncertain industrial settings. The subsequent sections of the literature review will explore each of these five dimensions in depth, providing critical insights into their theoretical underpinnings, practical applications, and comparative performance assessments. Cooperatively, they constitute the conceptual and empirical foundation of the thesis, leading the reader through the interdisciplinary landscape of essential investigation in robotics.

1.2.1 Quantum AI Foundations in Robotics

Synergy between quantum computing and artificial intelligence (AI) is revolutionizing computational paradigms with profound implications on the way robotic systems will be developed in the future. Termed Quantum Artificial Intelligence (QAI), the union has shortened the route to intelligent devices where non-classical resources like superposition, entanglement and quantum parallelism are merging with learning protocols and decision-taken protocols. These advances are not purely theoretical, as they represent a paradigm shift towards improving robotic autonomy, robustness of control, and computational efficiency – especially in the high-dimensional and highly non-linear regimes where more classical approaches reach their limitations.

Quantum computing is constructed for the growing computational requirements of AI-powered robotics. While in a classical system, states are calculated in sequence, in a quantum processor, we can compute and store many states at the same time [12, 13]. This native parallelism enables much faster training of machine learning models and efficient resolution of complex optimization problems, both of which are indispensable for robotic perception, control, and decision making. Quantum learning systems have been found to

perform exceptionally well in large-scale pattern recognition, combinatorial problems, and on-the-fly adaptation, all of which are essential traits for autonomous robotic systems working in unpredictable and dynamic settings [14]. There has been enormous interest from multiple domains, including energy optimization, cybersecurity, autonomous vehicles, medical diagnostics, etc., due to the theoretical promise that Quantum Artificial Intelligence (QAI) offers in robotics [15, 16]. More specifically, for robotic systems, QAI has been considered for the improvement of energy efficiency in control systems, better understanding sensor data, real-time decision-making in high-dimensional state spaces, and motion planning. For instance, it has been suggested that entanglement-based classification of high-dimensional vectors can be used for accelerating machine learning processes in robotics, outperforming standard classifiers in terms of speed and robustness. Moreover, nature-inspired perception models that use qubits to represent sensory information are hoped not only to develop robotic vision and environmental perception further, but also in other fields [17, 18]. Despite this progress, direct execution of QAI on robotics is at its early stages. While classical AI frameworks have reached a certain level of maturity concerning deployment, there are mounting limitations in terms of computational overhead, power demand, and expansion as a practical robotic platform. Their capabilities are limited and not only constrained to static environments with structured setups, making them less flexible and precise for applications in need of continuous learning, real-time control, and working in unstructured conditions. Quantum computing, with its ability to compute in potentially hundreds of gigabytes, also provides hope in transcending most of these limitations [19]. Nevertheless, the real-world integration of quantum processors with robots introduces new challenges, including hardware immaturity, the cost of error correction, and

the complexity of many quantum algorithms [20, 21]. To tackle these challenges, new research has recently centred on categorising QAI developments across four key domains as they apply to robotics: Quantum Machine Learning (QML); Quantum Neural Networks (QNNs); Quantum-Inspired Algorithms; and Quantum-Enhanced Control Strategies. Each of these is a new area that span several limitations the classical ones have, and provides quantum or inspiration from quantum solutions for better system-level performance.

Quantum Machine Learning (QML) focuses on leveraging quantum computing to accelerate and generalize classical learning algorithms. QML includes quantum-enhanced support vector machines, reinforcement learning models, and generative techniques, many of which have shown exponential or polynomial speedups in theoretical and empirical settings [22]. In robotics, QML has been applied to learning inverse dynamics, improving path planning under uncertainty, and optimizing control policies. One notable application includes quantum reinforcement learning agents that outperform classical counterparts in exploration efficiency, especially in deterministic environments where classical models tend to overfit or converge prematurely [23].

QNNs, a specific subclass of QML, provide a quantum-native framework for computations. Differing from typical neural networks, QNNs store information in quantum form and employ quantum gates to perform transformation and training procedures [24, 25]. These networks have been found to have properties that can cause the model to be less complex and generalize better, along with other qualities that provide for the extraction of higher-dimensional features with fewer computational resources. In robotics, QNNs have been shown to improve the prediction of Inverse kinematics, learned path, and sensorimotor coordination, especially in systems for which singularities and discontinuities are

challenging issues for the classical models. Moreover, the inclusion of QAFs, the Quantum ReLU and cosine-dependent interferometer model, has expanded the capacity of QNNs to approximate complex, nonlinear functions with greater accuracy.

Quantum-Inspired Algorithms (QIA) adopt principles of quantum mechanics, such as tunneling, interference, and probabilistic superposition, but implement them on classical hardware [26]. These algorithms have gained traction in robotics for solving optimization problems, including path planning, task allocation, swarm coordination, and resource scheduling. Quantum-behaved Particle Swarm Optimization (Q-PSO), for example, improves convergence and robustness in estimating dynamic parameters such as link inertia and center of mass, key components in high-fidelity robotic modeling [27]. Unlike classical PSO, Q-PSO introduces a probabilistic search space governed by quantum potential wells, enabling better avoidance of local minima and faster global convergence. Quantum-Enhanced Control (QEC) refers to the integration of quantum computing principles directly into feedback and control systems [28]. By embedding quantum operators into the control laws such as in quantum-inspired Sliding Mode Control (QSMC) these strategies achieve improved robustness against disturbances and reduced control energy [29]. Although the potential of these quantum technologies is considerable, significant barriers remain. Foremost among them is the current limitation of quantum hardware. Noisy Intermediate-Scale Quantum (NISQ) devices still struggle with qubit decoherence, gate fidelity, and scalability. These technical limitations affect the practical deployment of QAI algorithms in physical robotic systems [30]. Additionally, many quantum algorithms lack standardized evaluation metrics, making it difficult to benchmark performance relative to classical models in real-world tasks. The absence of cross-disciplinary integration between quantum

computing, robotics, and AI further hinders the translation of theoretical advancements into deployable robotic architectures [31].

Quantum-enhanced controllers can also exploit quantum parallelism to evaluate multiple control paths simultaneously, enabling more adaptive and precise trajectory tracking [1, 32]. By embedding quantum operators into the control laws, such as in quantum-inspired Sliding Mode Control (QSMC), these strategies achieve improved robustness against disturbances and reduced control energy [29, 33]. Quantum-enhanced controllers can also exploit quantum parallelism to evaluate multiple control paths simultaneously, enabling more adaptive and precise trajectory tracking [34]. In medical robotics and collaborative manipulators, QEC has shown promise in managing high precision tasks, reducing chattering, and improving transient response time [35].

To address these challenges, the literature emphasizes the need for scalable quantum protocols, hybrid classical-quantum frameworks, and enhanced quantum software engineering. Hybrid systems, in which classical processors handle deterministic low-level control while quantum modules manage probabilistic learning or global optimization, offer a promising compromise [36, 37]. For example, using IBM's quantum cloud infrastructure, researchers have demonstrated hybrid learning architectures capable of executing robot navigation and control tasks in partially structured environments, with notable improvements in training efficiency and decision robustness [36]. The evolution of quantum-inspired perception systems has further motivated researchers in the field to design multi-sensory data fusion models that represent and process complex environmental signals in terms of qubits [38]. These models not only improve the interpretability and robustness of data obtained from sensors but also help make robot behavior more adaptive

and responsive. Including such features in mobile robots, manipulators, and swarm systems is a dynamic frontier in quantum augmented robotics [39].

Overall, the intersection of quantum computing and AI in the context of robotics is full of promises and complexities. Quantum-AI approaches offer computational capabilities that go beyond classical constraints in terms of speed, adaptivity, and scalability. However, the field as such is still in its infancy, and it needs more rigorous theoretical grounding, empirical verifications, and interdisciplinary efforts to realize its values.

1.2.2 Modeling and Simplification in Robotic Dynamics

The dynamic model is the foundation of robot system design, which affects the performance of the control strategy, energy consumption, and trajectory planning [4]. In the field of industrial robotics, as is also the case for articulated robotic arms, the grade of a dynamic model is important. The model's capability to predict joint torques and system energy depends on its ability to precisely represent the mass distribution, inertial properties, and kinematic configurations of each robot link; however, this precision comes at the expense of increased computation cost. As a result, researchers are frequently confronted with a trade-off in model complexity and performance, particularly when applying real-time control or simulation in low-resource scenarios [5].

Robots have their end-effector devices carrying out operations through revolute or prismatic joints, and the dynamic equations of these devices will govern the forces or the torques at these joints. They are equations for which the leaves can be determined through the Newton–Euler or Euler–Lagrange approach. The Newton–Euler formulation gives an efficient way to calculate dynamic forces and moments using a recursive algorithm and is

well suited for numerical realizations [40]. On the other hand, the Euler–Lagrange formulation is based on the theory of analytical mechanics, which provides a more systematic way to describe the system using generalized coordinates and energy functions [41]. Although elegant and intuitive from a physical perspective, the definition of the Euler–Lagrange model requires detailed information about the center of mass and inertia tensor of each link, as well as the structure of the potential and kinetic energy terms in their entirety [42].

In high-fidelity dynamic models, mass properties are typically extracted through engineering-grade methods such as Computer-Aided Design (CAD) tools, Experimental Modal Analysis, or the use of Inertial Measurement Units (IMUs) [43]. CAD software such as SOLIDWORKS enables the extraction of precise geometric and physical characteristics of each link, including the center of mass and principal moments of inertia [44]. This data becomes especially important when modeling systems with coupled dynamics, where the effect of one joint's motion influences others due to inertial cross-terms.

Nevertheless, acquiring such precision through CAD modeling or physical measurement is not always feasible, particularly when dealing with legacy robots, incomplete specifications, or when simulation speed is a primary concern. To address these constraints, several levels of model simplification are commonly employed. These simplifications include treating complex geometries as uniform rods or boxes, using approximated mass distributions, or neglecting cross-coupling terms [45-47]. While such reductions pointedly reduce computational overhead, they may introduce modeling errors that adversely affect control accuracy, energy estimation, and disturbance rejection.

A larger view of this modeling difficulty emerges from the literature. In recent years, some novel developments in dynamic parameter identification have been made to improve further the accuracy of identifying the dynamic parameters and to handle the model's complexity [48-50]. For instance, methods such as virtual mass manipulation have been applied to improve the performance of the controller by tuning parameters during online operation [51]. A learning-based approach has recently been proposed in the literature where compensation for gravity and inertia may be learned over a neural network, thus allowing for high tracking performance without requiring an explicit dynamic model [52]. Other work has used Lie group theory and differentiable physics models to achieve better estimates of the inertial parameters, even when the payload could change.

They also cited an increasing trend towards hybrid physics-and learning based modelling. In hybrid systems, the classical physical interpretability is carried over, supplemented in some manner with data-driven or learning type elements to be able to adjust to unmodelled dynamics and measurement noise [53, 54]. In mobile manipulators, such as, for example, payload estimation techniques have been incorporated into dynamic models to be able to consider changing operational conditions [55]. Online mass and inertia estimation has been used in aerial robotics for control purposes, such as improving trajectory tracking and stabilizing flight despite disturbances [56].

However, the systematic comparison of how the dynamic model accuracy may affect the performance of articulated robotic arm control systems is lacking in the literature. Many of the existing methodologies are fine-tuned to optimize for either high-fidelity off-line modeling or highly abstracted online control, and with sparse attention paid to the regimes in between where relevant simplifications can be gradually exploited to the fullest extent

[57]. In addition, their combination with robust control techniques, like Sliding Mode Control or Model Predictive Control, is yet to be developed, in particular for real-time operation [58, 59].

In conclusion, dynamic model simplification plays a pivotal role in robotic system design, particularly in balancing fidelity and computational efficiency. Through a comparative analysis of CAD-derived models at varying levels of detail, this research highlights the practical implications of model abstraction for torque estimation, energy consumption, and control reliability. As robotic systems become more intelligent and adaptive leveraging AI and quantum-inspired algorithms the foundational understanding of how model simplifications affect system dynamics remains crucial. The following stages of this review will address how such modeling challenges intersect with learning-based inverse kinematics, parameter optimization techniques, and robust control architectures.

1.2.3 Neural Network Approaches to Inverse Kinematics

The issue of Inverse Kinematics (IK) still constitutes a important problem in robotic manipulation, especially when it comes to redundant degrees of freedom solutions and nonlinear joint space to task space mappings. In recent years, artificial neural networks (ANNs) have been relatively popular as an alternative to classic analytical and numerical solutions of the IK. These learning-based controllers, based on supervised and reinforcement learning, have demonstrated strong performances in terms of flexibility, learning ability, overall speed, and adaptability on numerous robotic systems [3].

Artificial neural network-based approaches have been successfully used to enhance the accuracy of motion control or to eliminate singularities and discontinuities that typically

plague classical IK methods. Feed-forward neural network (FNN) structures, such as multilayer perceptron (MLP), have been popularly used in robotic arm model-free control, operating effectively with or without known system dynamics, or with structural redundancy [2, 60]. For example, it was shown that feeding the network input with joint position feedback can lead to an improvement in convergence and control stability. These models also enable offline training and sim-to-real transfer learning, which is particularly useful for soft robotics and other compliant manipulators for which accurate analytical models might be infeasible [61-63].

Another major trend has been the design of hybrid systems, in which ANNs are combined with well-established controllers, such as PID or impedance control, resulting in data-driven adaptable systems that still exhibit model-based robustness [64]. These methods of hybrid control allow fine control whilst also acting to model tracking errors or uncertainties in the mechanical system [65]. Moreover, these architectures could integrate additional novelties like Gaussian Mixture Models, hierarchical structures, and function approximators that enhance the functional capability of NNs to solve IK problems, mainly when applied to redundant or continuum robots [66-68]. As they are trained to estimate the inverse kinematics end-to-end by adapting to various trajectory datasets, the network-based solution is expected to generalize and also reduce computational time during online motion in real time.

Even though classical ANNs work well on robotic kinematics, they are determined by the need for large training data sets, overfitting, and scalability issues in higher-order, high-dimensional input spaces [69, 70]. These disadvantages have also created much interest in Quantum Neural Networks (QNNs), which incorporate ideas from quantum computing into

the processing and learning process of neural systems [71, 72]. QNNs change the way we encode and process data by exploiting quantum mechanical effects such as superposition, entanglement, and interference [73, 74]. Unlike conventional networks that work with scalar or vector inputs, QNNs consider data as quantum states, thereby allowing for parallel analysis of several solution spaces [71, 75]. This parallelism enables QNNs to successfully solve complex high-dimensional problems, such as IK, faster and generalize better, especially in the vicinity of singularities and among ambiguous joint configurations.

In robotics, there have been efforts to apply QNNs to forward and inverse kinematics, trajectory prediction, and adaptive control [3]. Initial research has shown that QNNs can achieve better accuracy and computational cost than classical ANNs [76]. Matterport3D and ScanNet. Some related works describe the use of quaternions and Pauli gates to represent spatial rotations, which capture pose and orientation representations more compactly and accurately [2]. Some authors incorporate QNNs into swarm optimization to address IK problems with more favorable convergence properties and fewer local minima [77]. Given that QNNs are versatile for the representation of spatial data and inherently parallel, they are particularly suitable for real-time robotic scenarios with an uncertain, nonlinear environment [78].

A central novelty in QNN design was the introduction of quantum-inspired activation functions. Traditional neural networks often rely on rectified linear units (ReLU), which, despite being computationally efficient, have several drawbacks, including the dying ReLU problem, where a ReLU unit becomes inactive and halts learning [79, 80]. Quantum activation functions (QAFs) solve those problems by generalizing the transformation as periodic, entanglement-respecting, or interference-sensitive ones [81, 82]. For instance,

cosine-inspired periodic functions or entangled-state-induced QAFs have proven to accelerate the learning dynamics, expedite convergence, and improve (regression and classification) function approximation.

Several hybrid quantum-classical models have been developed to model inductive biases of QAFs for convolutional and/or recurrent neural network architectures [83, 84]. Not only in robotics, such networks have also been deployed in challenging problems such as medical diagnosis and environmental modelling, and the quantum layer can act as a feature enhancer or encoder. In robotics, this promises new frontiers in fast disturbance rejection, on-the-fly motion planning, or improved IK controllers. Nevertheless, QNNs remain impractical in robotics due to the current state of quantum hardware. Most of such calculations depend on simulators or classical models that have a quantum foundation, rather than on genuine quantum computing. Moreover, although the theory of quantum activation function and learning layer suggests speedups, the interfacing of these with sensor feedback, real-time control loops, and actuator interfaces is still an active research area.

One such related line of development is to adopt the quantum swarm intelligence in the form of quantum-inspired (QI) swarm optimization search as an auxiliary for learning in QNN-centric IK systems [11, 85]. By integrating global optimization approaches with quantum-inspired deep learning networks, new solution spaces have been recently investigated for joint trajectory planning, particularly in complex or congested spaces [77, 86]. These methods also have the advantage of being robust to noisy inputs, which is particularly important for deploying robots in the real world [87]. On the whole, the intersection of conventional ANNs and QNNs offers encouraging prospects for IK in

robotics [88]. Employing QNNs enables the development of weightless, scalable solutions that can learn intricate mappings with fewer parameters and improved generalization. Finally, integrating quantum mechanics into activation functions and network topology gives rise to a vast design space in which to explore novel neural architectures designed for robotic applications [71, 89].

In summary, classical and quantum neural networks are powerful and versatile building blocks for inverse kinematics problems in robotics. Although traditional ANNs work well in different setups and control missions, their scalability and accuracy call for even more advanced quantum-based models. QNNs, owing to their unique computational approaches and theoretical benefits, mark out an intriguing paradigm to address the current problems in robotics, covering planning, control for uncertain systems, as well as under uncertainty. In what follows, we shall continue adding further insights into how these architectures relate to trap parameter identification directly, mainly in the context of high-dimensional, nonlinear operations, such as what occurs with articulated industrial robotic manipulators.

1.2.4 Parameter Identification in Robotic Arm Dynamic Model

As industrial robotics advances toward greater autonomy and precision, the accurate identification of dynamic parameters becomes increasingly essential for achieving robust control, smooth motion, and energy-efficient operation. This need is particularly evident in articulated robotic manipulators, where the configuration, mass distribution, and inertia characteristics of individual links significantly affect the system's dynamic response. Parameters such as the center of mass and elements of the inertia matrix directly determine how the robot interacts with its environment and responds to control inputs. Precise

modeling of these properties supports not only high-fidelity simulation and predictive control but also enhances fault detection and adaptive performance under variable load conditions.

Most of the standard parameter estimation techniques for quantifying the optimal values of the robotic system parameters are deterministic and analytic. Most popular methods, such as LS, Recursive LS (RLS), and Newton Raphson, provide low complexity and nice mathematical theory [90, 91]. However, the traditional methods are not ideal for complex, high-dimensional, or nonlinear systems. They shall, however, be seen as limited when it comes to real industrial applications where noise, time-varying dynamics, and unmodelled nonlinearities deteriorate the estimation quality. For example, LS and RLS rely on a linear assumption, which does not hold in the case of many robotic systems [92, 93]. On the other hand, Newton-Raphson type algorithms are sensitive to the initial condition, and challenging to handle non-convex solutions. Additionally, filtering methods such as extended Kalman filters (EKF) and particle filters are robust to noise [94, 95]. However, they heavily rely on accurate models of system dynamics and noise statistics, which are not available in practical implementation.

To overcome these challenges, researchers have increasingly turned to metaheuristic optimization algorithms. Among them, Particle Swarm Optimization (PSO) has emerged as a particularly effective method for parameter estimation in robotics. Inspired by the collective behavior of swarms in nature, PSO navigates the solution space through a population of candidate solutions (particles) that iteratively update their positions based on personal and collective experience [96, 97]. This stochastic approach enables PSO to

escape local minima and explore highly nonlinear landscapes, making it well-suited to identifying inertial parameters in articulated robotic arms [98, 99].

Applications of PSO in robotic parameter identification span a wide range of configurations and systems [100]. In space robotics, PSO has been used to estimate dynamic parameters under microgravity conditions [101, 102]. At the same time, hybrid approaches combining PSO with LS or Differential Evolution (DE) have been successfully applied to terrestrial manipulators [103, 104]. These methods have demonstrated improvements in convergence speed and estimation accuracy, especially in scenarios involving large parameter sets and dynamic coupling between links [105]. For instance, increased variants of PSO that employ time-varying inertia weights or adaptive coefficients have been shown to improve stability and robustness during the estimation process [106]. Additionally, hybrid frameworks that integrate PSO with Grey Wolf Optimization (GWO) or other evolutionary strategies further enhance the algorithm's capacity to handle complex, multidimensional identification tasks [107, 108].

Even though PSO has good flexibility, it may still suffer from early convergence and sensitivity to parameter settings. In order to overcome these drawbacks, Quantum-behaved Particle Swarm Optimization (Q-PSO) is proposed as an advanced PSO [109, 110]. Q-PSO incorporates quantum mechanics ideas, such as the probabilistic location of the particle, the quantum potentials, and the quantum force fields, into an ordinary PSO scenario. This allows for a broader spread in the solution space and a higher global search performance of the algorithm [111]. In Q-PSO, unlike classical PSO (which makes deterministic updates of positions), quantum probability distributions are used to represent particle trajectories, which enhances the convergence characteristics and robustness of the solution [112, 113].

The superiority of Q-PSO is confirmed in different engineering applications such as robotics kinematics, trajectory tracking, and inverse dynamics. In particular, it has been found that the Q-PSO performs well in estimating both kinematic and dynamic parameters of parallel as well as serial manipulators [114, 115]. It has been applied to the optimization of trajectory profiles and inverse kinematics accuracy in some examples, showing better convergence speed and a smaller error bound than traditional methods [116, 117]. These enhancements are especially significant for real-time applications where solution quality and speed are equally important [39, 118].

While the body of literature surrounding PSO and Q-PSO is substantial, most studies have focused on simplified systems with low degrees of freedom or have relied on abstract simulation models. There is not any study, which explored the application of these algorithms to high-degree-of-freedom (DOF) manipulators within realistic modeling frameworks. Additionally, although many studies validate their findings through numerical experiments, only a limited number assess the performance of identified parameters in closed-loop control scenarios under external disturbances. To conclude, optimization-based methods, in particular PSO and its quantum-inspired derivatives, provide a useful design tool for dynamic parameter identification in involved robot settings. The capability of these algorithms to search nonlinear, high-dimensional spaces makes them particularly suitable for articulated manipulators in the presence of uncertainty.

1.2.5 Advanced Control in Robotic Systems

In robotic systems, especially those featuring articulated arms with high degrees of freedom, maintaining consistent performance amid uncertain conditions and external

disturbances poses a significant challenge. Among various control strategies, Sliding Mode Control (SMC) has gained widespread adoption due to its robustness in managing nonlinearities and parameter variations. The fundamental principle of SMC involves driving the system state towards a predefined manifold, known as the sliding surface, where the system's dynamics are constrained and ideally governed by simpler, linear behavior. Once the system arrives on this surface, it exhibits a high resistance to disturbances and unmodeled dynamics, allowing for reliable performance in demanding tasks such as trajectory tracking, impedance regulation, and force control [63, 119-121].

Conventional sliding mode control methods face significant challenges that impede their effectiveness in high-precision applications. A primary concern is the control signal discontinuity near the sliding surface, commonly known as chattering, which can trigger unmodeled dynamics, cause actuator wear, and diminish overall system efficiency. Furthermore, traditional SMC strategies often entail high computational costs, particularly when applied to systems with intricate dynamic structures or in real-time control settings [122-127]. To ease these limitations, recent efforts have turned to advanced modeling and novel control formulations, one of which is the integration of quantum-inspired principles into SMC frameworks.

A significant approach in this evolution involves the development of highly detailed kinematic and dynamic models utilizing CAD tools like SolidWorks. This enables the precise extraction of physical properties such as mass distribution and inertia. These models facilitate the design of refined control algorithms customized for specific robotic configurations. Recently, the incorporation of quantum mechanics-inspired features—such as quantum superposition and qubit operators, into the formulation of control laws has

emerged as a promising strategy to enhance the resilience, adaptability, and energy efficiency of robotic systems [5].

Recent studies have introduced a new class of controllers known as quantum-inspired sliding mode controllers (QSMCs). These controllers aim to maintain the robustness characteristic of classical sliding mode control while addressing its inherent weaknesses. Typically, these approaches replace discontinuous control laws with smoother alternatives or incorporate probabilistic reasoning based on quantum theory to achieve adaptive gains and improve chattering suppression. In the broader field of robotics, numerous contributions have sought to refine traditional SMC through structural enhancements or hybridization with intelligent techniques. Variations such as terminal SMC, integral SMC, and adaptive backstepping SMC have been employed to enhance transient performance and reduce sensitivity to modeling errors. These methods have demonstrated promising results in applications involving low-DOF manipulators, SCARA robots, and mobile systems. However, challenges related to real-time implementation and parameter tuning remain to be addressed [58, 128-140]. Hybrid controllers integrating neural networks or fuzzy inference systems into the SMC framework have also demonstrated improvements in precision and learning capabilities, particularly for highly nonlinear systems.

Quantum-inspired control, while still in its early stages, signifies a substantial advancement in addressing the shortcomings of classical controllers. Techniques derived from quantum mechanics, such as quantum-behaved particle swarm optimization (Q-PSO), quantum fuzzy logic, and entanglement-based computational models, have been effectively utilized in robotic systems to enhance learning, adaptability, and energy efficiency. For instance, hybrid controllers that integrate Q-PSO within the sliding mode control

framework have demonstrated superior performance compared to traditional SMC in terms of convergence speed and accuracy when implemented in complex, high-dimensional environments [6, 141].

Quantum principles have also been applied to kinematic modeling and pose estimation. By utilizing quaternion representations, spinor mathematics, and Pauli matrices, researchers have developed compact and efficient models for rigid body orientation, suitable for both simulation and real-time implementation [142]. These models reduce computational load and improve estimation precision, thereby enhancing controller responsiveness. Alongside mathematical formulations, quantum algorithms like the Harrow-Hassidim-Lloyd (HHL) algorithm have been introduced to resolve state-space equations in control systems with greater efficiency than classical methods. The application of these algorithms in control design has shown significant reductions in computational complexity, making them particularly well-suited for systems that require rapid response times [143]. Furthermore, quantum fuzzy neural networks and reinforcement learning-based strategies have proven to be powerful tools for adapting controllers and optimizing policies in uncertain environments. These models incorporate probabilistic decision-making layers and quantum-informed feedback mechanisms that dynamically adjust control parameters, ultimately enhancing generalization and robustness in unstructured or dynamic operating conditions [144-148]. Other quantum-enhanced strategies focus on integrating quantum information theory with conventional control laws. For instance, integrating Q-PSO with fast terminal SMC or backstepping techniques has enabled smoother transitions, better disturbance rejection, and improved tracking performance in servo systems and helicopter

dynamics [148-150]. Such hybrid designs demonstrate the potential for quantum-inspired mechanisms to address performance bottlenecks in existing SMC formulations.

The literature study in this field can introduce a substantial gap persists in the application of these sophisticated strategies to full-scale industrial manipulators operating under realistic conditions. Current implementations are primarily confined to simulated platforms or simplified models featuring only two or three degrees of freedom. Furthermore, there is a notable absence of systematic validation regarding QSMC performance when subjected to real-world disturbances or high-speed trajectories. To address this gap, future research should concentrate on integrating CAD-based physical modeling with QSMC architectures and deploying these systems within embedded hardware environments. This integration would enable a smoother transition from theoretical concepts to practical control systems capable of adaptive real-time operation. Additionally, assessing energy consumption, transient stability, and response robustness in the context of variable payloads and external forces will lead to a more thorough evaluation of performance.

In conclusion, the incorporation of quantum-inspired strategies into sliding mode control frameworks marks a significant advancement towards the development of more intelligent, adaptable, and efficient robotic systems. By addressing the shortcomings of traditional methods, quantum sliding mode control opens up new possibilities for enhancing robotic precision, autonomy, and reliability in uncertain and dynamic environments.

1.2.6 Literature analyzes and gap investigations

Upon the previous five subsections of this literature review, which examined the intersections of quantum artificial intelligence (QAI), robotic modeling, learning architectures, parameter identification, and control strategies, a characteristic set of gaps within the existing body of research comes to light. These gaps, both thematic and methodological, inform consequential limitations in the current approaches to addressing the challenges of precision, scalability, real-time adaptability, and energy efficiency in high-dimensional robotic systems. To address these challenges, the dissertation adopts an integrated research trajectory structured across five key chapters. Each chapter is thus positioned to target a specific knowledge gap, as detailed below:

Chapter 2 lays the theoretical and methodological foundation by systematically reviewing the state-of-the-art in Quantum-AI applications to robotics. Existing studies on QML, QNNs, and quantum-inspired algorithms often operate in isolation, lacking a unified framework for robotics applications, and this chapter consolidates these areas into a cohesive foundation.

Chapter 3 focuses on evaluating the fidelity-performance trade-off in dynamic modeling by investigating the impact of model simplifications. The chapter addresses a lack of systematic studies comparing how different levels of model fidelity affect control performance and energy consumption by analyzing detailed vs. simplified models.

Chapter 4 explores the challenge of inverse kinematics by presenting a Quantum Neural Network (QNN) framework specifically designed to improve accuracy and robustness in the presence of singularities. Classic neural networks used for inverse kinematics often

struggle with issues related to generalization and stability, particularly when approaching singularities. This chapter highlights the application of QNNs to enhance the precision and reliability of inverse kinematics solutions.

Chapter 5 focuses on developing and comparing methods for parameter identification using both classical and quantum swarm optimization strategies to improve the precision of dynamic modeling. Traditional identification techniques often face challenges when dealing with nonlinear dynamics and high-dimensional spaces. This chapter introduces and contrasts Particle Swarm Optimization (PSO) and Quantum-Particle Swarm Optimization (Q-PSO) for identifying dynamic parameters in computer-aided design (CAD)-based modeling.

Chapter 6 presents and validates a robust control strategy inspired by quantum principles, utilizing Sliding Mode Control (SMC) to enhance energy efficiency, trajectory tracking, and resilience against disturbances. While traditional SMC is effective, it faces challenges such as chattering and energy inefficiency. This chapter introduces a Quantum-Inspired Sliding Mode Control strategy aimed at improving robustness and minimizing energy consumption.

Chapter 7 advances the research framework to the actuator-control level by introducing a Quantum Sinusoidal Pulse Width Modulation (QSPWM) strategy. This chapter highlights the necessity of integrating quantum-enhanced control concepts into motor drive systems, which are essential for executing the optimized trajectories generated by the proposed methods. The QSPWM technique is employed to control the robot's actuators with enhanced precision and energy efficiency. Its objective is to reduce Total Harmonic

Distortion (THD) in the motor drives while ensuring the smooth and accurate execution of the quantum-optimized trajectory tracking tasks.

1.3 Thesis Problem Statement and Conceptual Framework

1.3.1 Thesis Problem Statement

Robotic systems, especially articulated industrial manipulators, require high precision, adaptability, and operational efficiency. However, as these systems become more complex, with higher degrees of freedom, tighter tolerance constraints, and real-time energy efficiency requirements, their modeling, control, and learning architectures face increasingly severe challenges. Classical computational approaches often fall short in addressing these challenges, particularly when subjected to nonlinear dynamics, external disturbances, and uncertain environments. The limitations are further exacerbated by the computational load of accurate dynamic modeling, the instability near singularities in inverse kinematics, the sensitivity of parameter estimation to noise, and the energy-intensive nature of conventional control laws.

The intersection of quantum computing and artificial intelligence offers a transformative way to overcome these limitations. Quantum-inspired algorithms, such as Quantum Neural Networks (QNNs), Quantum-behaved Particle Swarm Optimization (Q-PSO), and Quantum-Inspired Sliding Mode Control (QSMC), provide theoretical advantages in computational speed, convergence behavior, and robustness to uncertainty. However, despite growing interest, the practical integration of these quantum-based methodologies into robotic systems remains fragmented and underexplored. There exists a considerable gap in systematically evaluating how these advanced classical methods and

quantum-inspired practices can be engaged interdisciplinarity to improve all stages of robotic architecture, from modeling and parameter identification to control and decision-making.

This thesis addresses that gap by proposing and experimentally evaluating the advanced classic method with a unified quantum-enhanced architecture, interdisciplinary for an industrial high degree of freedom robotic arm assessments. The focus lies on enhancing the modeling accuracy, learning efficiency, and control robustness of a six-degree-of-freedom industrial robot (ABB IRB-140) through a modular yet interconnected application of classic, standard techniques and quantum-behaved methods. The core research question navigating this study is as follows:

"How can we enhance the kinematic and dynamic modeling, along with the identification and control of a high-degree-of-freedom robotic arm using advanced classical techniques?

Furthermore, what would be the effects of systematically integrating quantum-inspired artificial intelligence algorithms into a robotic manipulator, particularly in terms of improving precision, energy efficiency, and robustness in uncertain conditions?"

1.3.2 Conceptual Framework

The conceptual framework guiding this thesis is built on the hypothesis that intelligent robotic systems can achieve quite improved performance when their core computational modules are restructured using quantum-inspired techniques. These modules span the entire control stack, from the modeling of kinematics and dynamics of the robot to parameter estimation and trajectory control. Every chapter of this thesis addresses a specific

bottleneck or limitation that is known in the field of classical robotic architectures and introduces a quantum-enhanced alternative. The framework supports a side-by-side evaluation of both classical and quantum methods, establishing performance improvements across modeling accuracy, learning efficiency, and control robustness. The Table 1-1 provides a summary and an outline of the thesis framework as follows and A detailed system-layer interpretation of this framework is provided in Appendix1:

Table 1-1 Comparative Framework of the thesis.

Framework Layer	Chapter	Classical Method	Quantum Innovation	Objective
Theoretical Foundation and Taxonomy	Chapter 2	Review of classical AI & control methods	QML QNN, Q-PSO, QSMC (Systematic Review)	To categorize and benchmark classical vs. quantum approaches in robotics
Modeling and Fidelity Trade-off Analysis	Chapter 3	Detailed vs. Simplified Euler Lagrange models (CAD-based)	Providing the Benchmark for research path	To quantify trade-offs between model detail, energy accuracy, and computation
Inverse Kinematics Resolution	Chapter 4	Multi-Layer Perceptron (MLP) ANN	Quantum Neural Network (QNN)	To enhance singularity avoidance and improve inverse mapping accuracy
Dynamic Parameter Identification	Chapter 5	Classical Particle Swarm Optimization (PSO)	Quantum-behaved Particle Swarm Optimization	To increase accuracy, reduce sensitivity to noise, and accelerate convergence
Robust Trajectory Tracking Control	Chapter 6	Classical Sliding Mode Control (SMC)	Quantum-Inspired Sliding Mode Control (QSMC)	To reduce chattering, save energy, and enhance tracking robustness
Harmonic Reduction in Motor Drives	Chapter 7	Classical Sinusoidal PWM (SPWM)	Quantum Sinusoidal PWM (QSPWM)	To minimize Total Harmonic Distortion (THD), improve power quality, and enhance motor efficiency

1.3.3 Theoretical Integration of the Framework

The conceptual foundation of this research is constructed upon a rigid synthesis of established theories in robotics, system assessments, and quantum computing. Each component of the proposed framework is anchored in a particular theoretical domain, ensuring methodological coherence and scientific validity across all investigative layers.

- ✓ Euler–Lagrange Mechanics provides the core analytical framework for the dynamic modeling of the robotic manipulator, enabling the derivation of equations of motion that accurately capture the interplay of inertial, Coriolis, and gravitational forces (Chapters 3, 5, and 6).
- ✓ Denavit–Hartenberg (D-H) Kinematic Formalism serves as the geometric backbone for representing joint transformations and computing forward and inverse kinematics, particularly in high-DOF articulated systems (Chapters 3 and 4).
- ✓ Artificial Neural Network Architectures, specifically Multi-Layer Perceptron (MLPs), are employed as baseline function approximators for learning-based inverse kinematics. These are systematically extended into Quantum Neural Networks (QNNs) to exploit quantum-inspired mechanisms such as parallel encoding, entanglement-influenced activation functions, and improved generalization (Chapter 4).
- ✓ Quantum Computational Principles, including quantum superposition, entanglement, and quantum-behaved search heuristics, are operationalized through the integration of QNNs, Quantum-behaved Particle Swarm Optimization (Q-PSO), and Quantum-Inspired Sliding Mode Control (QSMC). These techniques simulate probabilistic behaviors and non-classical search spaces to achieve superior convergence, stability, and learning adaptability (Chapters 4–6).

- ✓ From a unified mathematical perspective, the quantum-inspired methods proposed in this thesis represent distinct realizations of a common computational logic. In each case, a classical robotic quantity, such as position and orientation data, dynamic parameters, tracking error, torque-related information, or modulation signals, is first converted into an enriched representation via an encoding stage. This representation is subsequently processed by a quantum-inspired transformation stage, which introduces probabilistic structure, parallel state consideration, or modified decision behavior, depending on the application. The result is then converted back to a classical form through measurement and collapse, enabling its use in prediction, optimization, control, or actuation. Within this framework, the quantum-inspired neural network for inverse kinematics, quantum-behaved particle swarm optimization for parameter identification, quantum-inspired sliding mode control for trajectory tracking, and quantum sinusoidal pulse width modulation for motor-drive operation are not isolated developments. Instead, they constitute mathematically coherent variations of a unified computational framework applied at different layers of the robotic system. Appendix 2 provides a detailed description of this unified framework.
- ✓ Sliding Mode Control (SMC) Theory is adopted for robust control under model uncertainty and external perturbations. It is subsequently enhanced via quantum-inspired adaptations to mitigate chattering, reduce control energy consumption, and improve transient response in nonlinear and uncertain dynamic environments (Chapter 6).
- ✓ Quantum Sinusoidal Pulse Width Modulation (QSPWM) Theory extends the framework toward the domain of motor drive control by incorporating quantum computational principles into classical modulation schemes. Building on sinusoidal PWM fundamentals, QSPWM leverages quantum interference and probabilistic

amplitude modulation to minimize Total Harmonic Distortion (THD), enhance voltage utilization, and improve overall energy efficiency in three-phase motor drives (Chapter 7).

Collectively, these theoretical constructs combine into a readable and innovative quantum-AI robotic architecture, whose validity is demonstrated through detailed modeling, algorithmic development, and extensive simulation-based benchmarking using an industrial-grade manipulator, A structured mapping of these quantum-inspired methods across the robotic control stack is provided in Appendix 3.

1.4 Contribution of the Research

1.4.1 Motivation for Quantum-AI Integration in Robotics

Robotic systems, especially those deployed in industrial contexts, are increasingly expected to operate with promoted precision, adaptability, and energy efficiency under problematic dynamic conditions. Classical control and modeling approaches, while mature, encounter substantial limitations when faced with nonlinear dynamics, high-dimensional parameter spaces, real-time constraints, and uncertain environments.

These challenges are particularly critical in articulated robotic manipulators with multiple degrees of freedom, where control dedication and dynamic modeling accuracy critically impact performance. Against this backdrop, quantum computing, through compactional mechanisms such as superposition, entanglement, and probabilistic parallelism, offers a transformative framework for reconsidering the core computational modules of robotic architectures. The thesis is motivated by the potential of quantum-

inspired and hybrid quantum-classical methods to overtake the limitations of conventional robotics in terms of learning accuracy, modeling efficiency, and control robustness.

1.4.2 Research Objectives Summary

The overarching purpose of this dissertation is to enhance the modeling, identification, and control capabilities of high-degree-of-freedom industrial robotic manipulators through the systematic integration of advanced classical techniques and quantum-inspired methodologies, with following detailed objectives include:

- ✓ Establishing a comprehensive taxonomy and literature synthesis of quantum-AI applications in robotics.
- ✓ Quantifying the trade-offs between dynamic model fidelity and computational complexity in articulated manipulators.
- ✓ Designing quantum-inspired neural networks for high-precision inverse kinematics with singularity avoidance.
- ✓ Developing accurate, CAD-informed dynamic models enhanced through quantum-behaved swarm optimization techniques.
- ✓ Proposing and validating a quantum-inspired sliding mode control strategy to improve trajectory tracking and reduce energy consumption.
- ✓ Introducing a quantum-based sinusoidal pulse width modulation (QSPWM) approach to reduce Total Harmonic Distortion (THD) and improve power quality and energy efficiency in three-phase motor drive control systems.

1.4.3 Key Scientific Contributions

This dissertation presents several key scientific contributions, each corresponding to one of the main chapters (Chapters 2 through 6), which are adapted from peer-reviewed publications. Together, these contributions enhance the integration of quantum computing and artificial intelligence into robotic modeling, optimization, and control. Specifically:

1. ***Foundational Synthesis:*** A systematic review and taxonomy of quantum computing-based AI methodologies in robotics, organizing 245 peer-reviewed sources across four domains, Quantum Machine Learning (QML), Quantum Neural Networks (QNNs), Quantum-Inspired Algorithms, and Quantum-Enhanced Control. This contribution establishes the intellectual landscape and identifies critical research gaps in real-world implementation, scalability, and algorithmic standardization.
2. ***Modeling Trade-off Framework:*** A comprehensive analysis of model simplification in robotic dynamics using three SolidWorks-based fidelity levels (detailed, semi-detailed, simplified). This study quantifies the trade-off between modeling precision and computational efficiency, establishing practical thresholds for energy-aware modeling in resource-constrained industrial applications.
3. ***Quantum Neural Networks for Inverse Kinematics:*** The development of a QNN framework incorporating quantum-inspired activation functions within a multi-layer perceptron architecture. The proposed QNN achieves up to 16.67% lower mean absolute error than classical ANNs, with superior performance in singularity avoidance and precision under high-dimensional input conditions.
4. ***CAD-Based Quantum-Enhanced Parameter Identification:*** The introduction of a quantum-behaved particle swarm optimization (Q-PSO) technique for estimating

inertial and mass center parameters from a high-fidelity CAD-derived dynamic model. Compared to PSO, Q-PSO demonstrated significantly lower MAPE values (0.76% for inertia, 0.43% for mass center), improved convergence, and better performance under disturbance conditions when evaluated using a sliding mode control benchmark.

5. ***Quantum-Inspired Sliding Mode Control (QSMC):*** A novel control architecture embedding quantum principles via multiple qubit operators into a robust SMC framework. The QSMC method achieves enhanced tracking performance and reduces energy consumption by approximately 3.79% over its classical counterpart, with effective mitigation of chattering and superior disturbance rejection.
6. ***Quantum Sinusoidal Pulse Width Modulation (QSPWM):*** The formulation of a quantum-enhanced modulation framework that integrates quantum interference and probabilistic amplitude principles into classical sinusoidal PWM. The proposed QSPWM method effectively reduces Total Harmonic Distortion (THD) by 35.6%, enhances voltage utilization, and improves overall motor drive efficiency compared to traditional SPWM, marking a significant advancement in energy-optimized quantum-based control for industrial actuators.

1.4.4 Methodological and Practical Contribution

Introduces a cohesive suite of methodological innovations and practical implementations that advance the current capabilities of industrial robotic systems. Each innovation is directly validated on the ABB IRB-140 six-DOF industrial manipulator to confirm the theoretical development with practical applicability in measurable

enhancements in computational efficiency, learning generalization, and energy performance. These contributions are synthesized in Table 1-2.

Introduces innovative hybrid classical–quantum strategies and demonstrates their feasibility through comprehensive applications in a standardized industrial context. By consistently utilizing a real robot as a case study, we ensure comparability, reproducibility, and a practical perspective for evaluating advancements in algorithms and modeling. Collectively, our findings establish a novel, multi-layered architecture that employs a systematic interdisciplinary approach. This framework is designed to support the development of intelligent, quantum-augmented robotic systems, aligning with the goals of next-generation automation, sustainability, and adaptive intelligence.

The proposed contribution structure of this dissertation supports major objectives such as adaptive decision-making, real-time learning, sustainable energy consumption, and operational resilience in uncertain and dynamically changing environments. More importantly, it provides a coherent and scalable foundation for linking these objectives across different layers of robotic system design, from modeling and learning to optimization, control, and actuation. The dissertation goes beyond reporting isolated methodological improvements. Instead, it establishes a structured precedent for the systematic integration of quantum technologies into industrial robotics, contributing to the advancement of smart manufacturing, intelligent automation, and next-generation quantum-driven robotic systems.

Table 1-2 Summary of Methodological and Practical Contributions of the thesis.

Chapter	Contribution	Methodological Innovation	Practical Implementation	Impact
2	Systematic Review	Developed a four-pillar taxonomy (QML, QNNs, Q-Inspired Algorithms, Q-Enhanced Control) based on analysis of 245 studies	Identified gaps in real-world quantum-Al robotic integration	Established a structured foundation for future research and unified fragmented literature
3	Model Simplification Analysis	Created and compared three CAD-based fidelity levels (detailed, semi-detailed, simplified) for dynamic modeling	Applied to IRB-140 to assess energy vs. computational trade-offs	Demonstrated that simplified models achieve ~93% accuracy with significantly reduced computational load
4	Inverse Kinematics via NNs	Designed a QNN using quantum-inspired activation functions in a multi-layer perceptron	Trained on 167,000 real motion data points; evaluated on ABB IRB-140	Achieved 15.60-16.67% lower MAE than ANN; enhanced singularity avoidance
5	Dynamic Parameter Identification	Applied Quantum-behaved Particle Swarm Optimization (Q-PSO) for inertial/mass parameter estimation	Integrated CAD-derived parameters into optimization loop validated by Simulink SMC	Reduced MAPE to 0.76% (inertia) and 0.43% (mass centers); improved torque smoothness and disturbance resilience
6	Robust Quantum Inspired Control	Developed a Quantum-Inspired Sliding Mode Control (QSMC) using qubit-based operators and exponential reaching law	Implemented in Simulink for trajectory tracking under disturbances	Reduced energy consumption by 3.79%; improved chattering rejection and control accuracy
7	Quantum Sinusoidal PWM (QSPWM)	Developed a quantum-based Sinusoidal Pulse Width Modulation framework integrating quantum interference and probabilistic amplitude modulation into classical SPWM.	Implemented and simulated in MATLAB/Simulink for three-phase motor drive control to evaluate THD reduction and efficiency improvement.	Reduced Total Harmonic Distortion (THD) by 35.6%, enhanced voltage utilization, and improved overall motor-drive energy efficiency compared to classical SPWM.

1.5 Methodology

The methodological architecture of this dissertation adopts a modular and interdisciplinary approach that integrates classical robotic modeling with quantum-inspired computational paradigms. The methodology is structured across five central posts: systematic literature analysis, physical system modeling, algorithmic development, simulation-based validation, and comparative performance evaluation. Each stage is designed to progressively build toward a cooperative framework that enhances the modeling, learning, and control of high-degree-of-freedom industrial robotic manipulators, using both classical and quantum-enhanced methods.

1.5.1 Research Design Overview

This dissertation employs a multi-layered methodology that links analytical modeling, quantum-AI algorithm design, and empirical evaluation, which is rooted in both theoretical rigor and practical applicability. A detailed kinematic and dynamic model of the ABB IRB-140 six-joint robotic manipulator is first developed using established mechanical principles alongside a thorough CAD design of the robot arm in the initial step. Classical techniques are then systematically extended using quantum-inspired computational frameworks, namely, Quantum Neural Networks (QNN), Quantum-behaved Particle Swarm Optimization (Q-PSO), and Quantum-Inspired Sliding Mode Control (QSMC). Each quantum-enhanced technique is evaluated against its classical counterpart, ensuring a controlled, side-by-side comparison across learning, identification, and control tasks.

1.5.2 System Modeling Framework

The physical modeling of the robotic platform begins with a comprehensive kinematic representation based on the Denavit–Hartenberg (D-H) convention. Forward and differential kinematics are established to define the spatial configuration and velocity relationships of the end-effector. The dynamic modeling phase is governed by the Euler–Lagrange formalism, capturing the system's inertial, Coriolis, and gravitational dynamics. Three levels of model fidelity, such as detailed, semi-detailed, and simplified, are developed through SolidWorks CAD representations, enabling a controlled study of trade-offs between computational sophistication and modeling accuracy. Mass properties, including inertia matrices and center-of-mass vectors, are extracted directly from the CAD environment to ensure physical realism.

1.5.3 Literature Review Methodology

The theoretical foundation of this work is established through a systematic literature review, structured using the PICO (Population, Intervention, Comparison, Outcome) framework. The review spans over 10,000 initial records, from which 245 peer-reviewed studies are selected following strict inclusion and exclusion criteria. Searches were conducted across major scientific databases. The literature is organized into four thematic disciplines: Quantum Machine Learning (QML), Quantum Neural Networks (QNNs), Quantum-Inspired Algorithms, and Quantum-Enhanced Control Strategies, forming the abstract taxonomy that conducts the thesis.

This review focuses on quantum-inspired and quantum-enhanced approaches in robotics, as its primary purpose is to establish the conceptual and methodological

foundation for the research presented in subsequent chapters. Traditional robotics, control, and identification methods are included only where necessary to provide context, comparison, and baseline interpretation. The review does not aim to offer a comprehensive survey of conventional robotic methodologies. Instead, it clarifies the positioning of quantum-inspired computational strategies within robotics and explains how these approaches motivate the specific framework proposed in this thesis.

1.5.4 Quantum and Classical Algorithm Design

To examine the computational benefits of quantum-enhanced approaches, classical baseline algorithms are precisely developed and then expanded with quantum principles. For inverse kinematics, a Multi-Layer Perceptron (MLP) architecture is trained and evaluated alongside a QNN with quantum-inspired activation functions. In the domain of dynamic parameter identification, classical Particle Swarm Optimization (PSO) is compared with Q-PSO, which introduces probabilistic position encoding based on quantum mechanics. For trajectory tracking control, classical Sliding Mode Control (SMC) is re-engineered into a Quantum-Inspired Sliding Mode Control (QSMC) architecture employing exponential reaching laws and qubit-based operators. These parallel implementations enable straightforward benchmarking across performance, robustness, reliability, and efficiency comparisons of the techniques.

1.5.5 Simulation and Validation

All models and algorithms are validated through high-fidelity simulations implemented in MATLAB and Simulink, and Simscape Multibody. A wide dataset comprising over 170,000 joint-space and end-effector trajectories is collected using the ABB IRB-140 robot

under various path-planning scenarios, including elliptical, polygonal, and random trajectories. The dataset is used to train, test, and evaluate the learning-based models and control strategies. Performance metrics include Mean Absolute Error (MAE), Mean Absolute Percentage Error (MAPE), tracking error, control smoothness, energy consumption, and resilience to disturbances. Real-world disturbances and perturbation scenarios are explicitly simulated to assess the performance and robustness of the robot's character through various validation methods.

1.5.6 Evaluation and Benchmarking

To facilitate a comprehensive and rigorous evaluation, the proposed methods are assessed using a multi-criterion benchmarking strategy that spans all system layers. The evaluation framework incorporates multiple performance indicators, including predictive accuracy, learning generalization, convergence behavior, disturbance robustness, transient and steady-state performance, control smoothness, computational efficiency, and spectral quality. The specific assessment criteria applied throughout this thesis comprise torque profiles, energy consumption, computational demand, Mean Absolute Error, Mean Absolute Percentage Error, position error, orientation error, singularity-related loss, convergence curves, final fitness across repeated runs, tracking error, rise time, settling time, overshoot, steady-state error, chattering attenuation, Root Mean Square Error, speed ripple, Total Harmonic Distortion, voltage utilization, torque ripple, and frequency-domain spectral distribution. The integration of these complementary indicators establishes a robust and wide-ranging basis for comparing the developed algorithms in terms of accuracy, robustness, convergence, efficiency, and practical control relevance.

Beyond core performance metrics, the evaluation strategy incorporates practical indicators of robustness and sensitivity tailored to each subsystem. These indicators include repeated-run comparisons for optimization performance, analysis of final fitness distributions and variance, assessment of training-versus-validation consistency for learning models, and systematic hyperparameter exploration for neural architectures by varying layers, nodes, learning rates, and batch sizes. In optimization studies, multiple independent runs mitigate sensitivity to random initialization and enable assessment of convergence consistency. In learning studies, comparisons between training and validation losses, as well as activation-function and architecture tuning, facilitate examination of generalization and model stability. Collectively, these elements provide an empirical robustness assessment that complements comparative evaluations of accuracy, convergence, control behavior, and efficiency across the proposed methods.

A structured benchmarking protocol is employed to compare classical and quantumized approaches across modeling, learning, and control tasks. Each quantum-inspired method is evaluated against its classical counterpart using the same kinematic and dynamic models, initial conditions, and performance metrics. Graphical analyses, including convergence curves, error distributions, and control signal profiles, are introduced to visualize relative performance. Statistical measures are computed across multiple trials to ensure reproducibility and robustness. The comparative framework underlines not only absolute gains in accuracy or efficiency but also the computational trade-offs introduced by quantum interpretation methods.

This comparative design is intentionally pairwise, so that the contribution of each quantum-inspired modification can be isolated under matched modeling, training, and

evaluation conditions. Broader benchmarking against other classical algorithmic families is important for future studies, but it lies outside the primary scope of the present dissertation.

1.6 Thesis structure

The dissertation is systematized into nine chapters, each corresponding to a different layer in the modeling, learning, and control architecture of a high-degree-of-freedom industrial robotic manipulator, and also introduction, conclusion, and appendices. The submitted structure reflects a refined integration of classical methods and quantum techniques:

- ✓ **Chapter 1:** Introduction: Presents the research motivation, literature background, problem statement, conceptual framework, contributions, and methodological foundation.
- ✓ **Chapter 2:** Advancements in Quantum Computing-based AI for Robotics: Provides a systematic review of literature across four domains: Quantum Machine Learning (QML), Quantum Neural Networks (QNNs), Quantum-Inspired Algorithms, and Quantum-Enhanced Control Strategies, establishing a foundation for quantum-AI integration in robotics.
- ✓ **Chapter 3:** The Impact of Simplifications: Investigates how varying levels of dynamic model fidelity (detailed, semi-detailed, simplified) influence torque estimation and energy consumption, highlighting the trade-offs between computational efficiency and physical accuracy.
- ✓ **Chapter 4:** Quantum Neural Networks for Inverse Kinematics: Proposes a QNN architecture using quantum-inspired activation functions to solve inverse kinematics

problems with improved accuracy and singularity avoidance, compared to classical MLP-based ANNs.

- ✓ **Chapter 5:** Dynamic Model Parameter Identification: Develops a CAD-derived dynamic model and compares classical PSO with Quantum-behaved PSO (Q-PSO) for accurate identification of mass center and inertia matrix elements, demonstrating improved convergence and robustness.
- ✓ **Chapter 6:** Quantum-Inspired Sliding Mode Control: Introduces a quantum-inspired enhancement of the Sliding Mode Control (SMC) technique. The QSMC design improves tracking performance and energy efficiency while reducing chattering under nominal and disturbed conditions.
- ✓ **Chapter 7:** Quantum Sinusoidal Pulse Width Modulation (QSPWM): Presents a quantum-enhanced modulation strategy that integrates quantum interference and probabilistic amplitude modulation principles into classical SPWM to reduce Total Harmonic Distortion (THD), enhance voltage utilization, and improve overall energy efficiency in three-phase motor drive systems.
- ✓ **Chapter 8:** General Conclusion: Summarizes key findings, discusses limitations, and outlines future research directions focused on expanding quantum-AI methods in robotics.
- ✓ **Chapter 9:** Appendices: Presents the supplementary materials supporting the dissertation, including the integrated system-layer framework, the unified quantum-inspired computational framework, the mapping of quantum-inspired methods across the robotic control stack, and the quantitative summary of the thesis contributions.

Chapter 2 - Advancements in Quantum Computing based AI for Robotics

2.1 Chapter Overview

The intersection of quantum computing and artificial intelligence (AI) marks a considerable shift in computational science, with substantial potential for advancing next-generation robotic systems. This systematic review examines the literature at this intersection, proposing an in-depth analysis of how quantum technologies are transforming AI-driven robotics. As data-intensive operations and increasingly intricate robotic functions proliferate, conventional AI techniques often encounter limitations in scalability, responsiveness, and energy consumption. Quantum computing is an effective alternative, utilizing principles such as superposition, entanglement, and quantum parallelism to enhance algorithmic efficiency, decision throughput, and adaptability in robotic platforms.

The review organizes recent developments into four primary categories: Quantum Machine Learning (QML), Quantum Neural Networks (QNNs), Quantum-Inspired Algorithms, and Quantum-Enhanced Control Mechanisms. Each classification addresses unique challenges in robotics, including perception, localization, motion planning, and autonomous control. Quantum-driven learning models and optimization methods have demonstrated enhanced capabilities in dynamic and uncertain settings, leading to faster convergence, higher precision, and improved resilience. The review further underscores notable progress in secure quantum communication protocols for robotic networks, as well

as the deployment of quantum models in domains such as swarm coordination, prosthetic robotics, and nanorobotic systems.

Nevertheless, critical obstacles remain, particularly those related to the developing state of quantum hardware, susceptibility to decoherence, and the theoretical complexity of many quantum algorithms. Additionally, the lack of collaborative disciplines and standardized evaluation metrics makes it challenging to benchmark quantum AI against classical AI in robotic applications. Overcoming these challenges requires integrated efforts across quantum science, systems engineering, computer science, and cognitive modeling.

The purpose of the review is to make a coherent foundation for future inquiry by integrating foundational theory, real-world applications, and emerging directions in quantum-AI robotics. It offers targeted guidance for scholars and practitioners, presenting quantum-augmented intelligence as a promising route toward more capable, autonomous, and efficient robotic technologies. The flowchart content of this research is explained in Figure 2-1, outlining key areas such as quantum machine learning, neural networks, algorithms, and robust control in robotics, along with the study's methodology, applications, and concluding insights. Each main section is divided into focused subsections that highlight advancements in control, optimization, and decision-making. This structured layout provides a clear overview of how quantum technologies are integrated across various robotic domains.

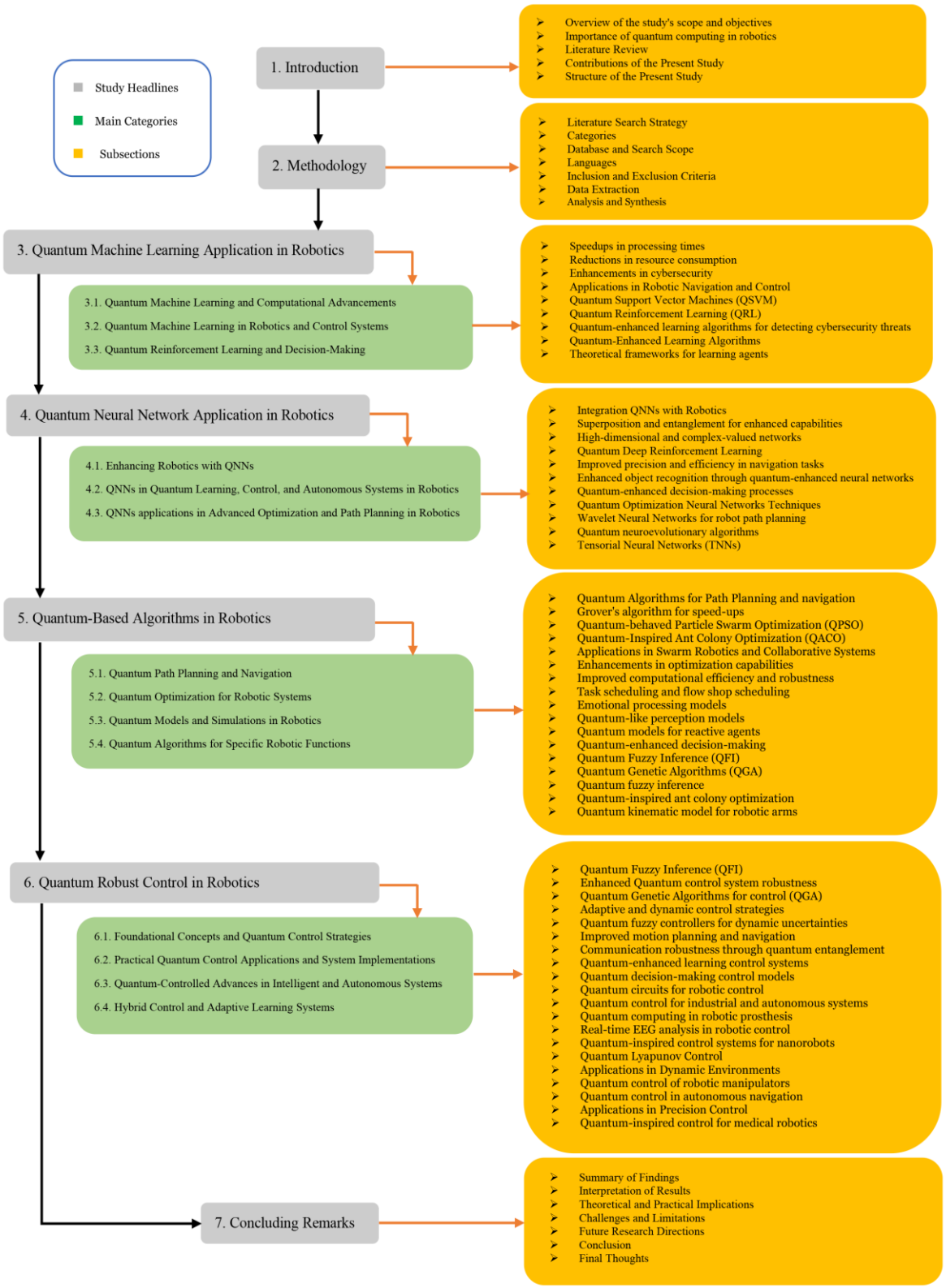

Figure 2-1 The flowchart content of this research.

2.2 Paper 1: Quantum Computing-Based Artificial Intelligence for Robotics: A Systematic Review of Theoretical Foundations, Practical Applications, and Future Trends.

Authors : Mehdi Fazilat, Nadjet Zioui.

Journal: Journal of King Saud University – Engineering Sciences.

Submission date and status: 21/Nov/2025 - Under Review.

2.2.1 Methodology

This systematic review, conducted with the utmost methodological rigor, examines the influence of quantum computing-driven artificial intelligence (AI) algorithms on the development and operational efficiency of robotic systems. The structured methodology, based on the PICO framework, ensures clarity and replicability in the selection and evaluation of relevant studies, providing a solid foundation for our research.

2.2.2 PICO Framework

Population (P): A variety of robotic platforms, including autonomous systems, mobile robots, humanoid robots, articulated robotic arms, and unmanned vehicles.

Intervention (I): AI algorithms enhanced by quantum computing, featuring quantum machine learning, quantum-enhanced control schemes, quantum-inspired optimization, and decision-support mechanisms.

Comparison (C): Traditional AI or robotics approaches that rely on classical computational paradigms, such as rule-based systems, neural networks, or classical optimization algorithms.

Outcome (O): The practical implications of this research are significant. We assess the performance improvement, adaptability, computational efficiency, and potential applications of quantum computing-driven AI algorithms in robotic systems, providing valuable insights for future developments in these fields.

2.2.3 Literature Search Strategy

The search encompassed both open-access and subscription-based scholarly sources. Primary databases consulted included IEEE Xplore, Scopus, SpringerLink, Web of Science, ScienceDirect, PubMed, and the ACM Digital Library. The institutional search engine, Sofia, supplemented the search for broader access to restricted content.

2.2.4 Search Terms and Boolean Logic

Keywords were categorized into three thematic areas: Robotics, Quantum Computing, and Artificial Intelligence, and optimized using Boolean logic (AND, OR, NOT). Key terms comprised “Quantum computing,” “Quantum algorithms,” “Quantum machine learning,” “Quantum-enhanced,” “Robotic control,” “Autonomous robots,” “AI,” and “Neural networks,” among others.

2.2.5 Inclusion and Exclusion Criteria

Studies were considered eligible if they explicitly examined the convergence of quantum computing and AI within robotic domains, were published in English between 2008 and 2025, and were available in full text. Eligible sources included peer-reviewed journal articles, conference proceedings, and comprehensive reviews. Excluded were

publications lacking direct relevance to robotics, non-peer-reviewed documents, abstracts without accompanying full texts, and redundant entries.

2.2.6 Selection Process and Results

From an initial pool of 10,361 records, 193 duplicates were removed. After a thorough review of titles, abstracts, and full texts, 245 studies met the inclusion criteria, comprising 239 from the primary selection and six identified in a subsequent review cycle. Figure 2-2 depicts the selection workflow.

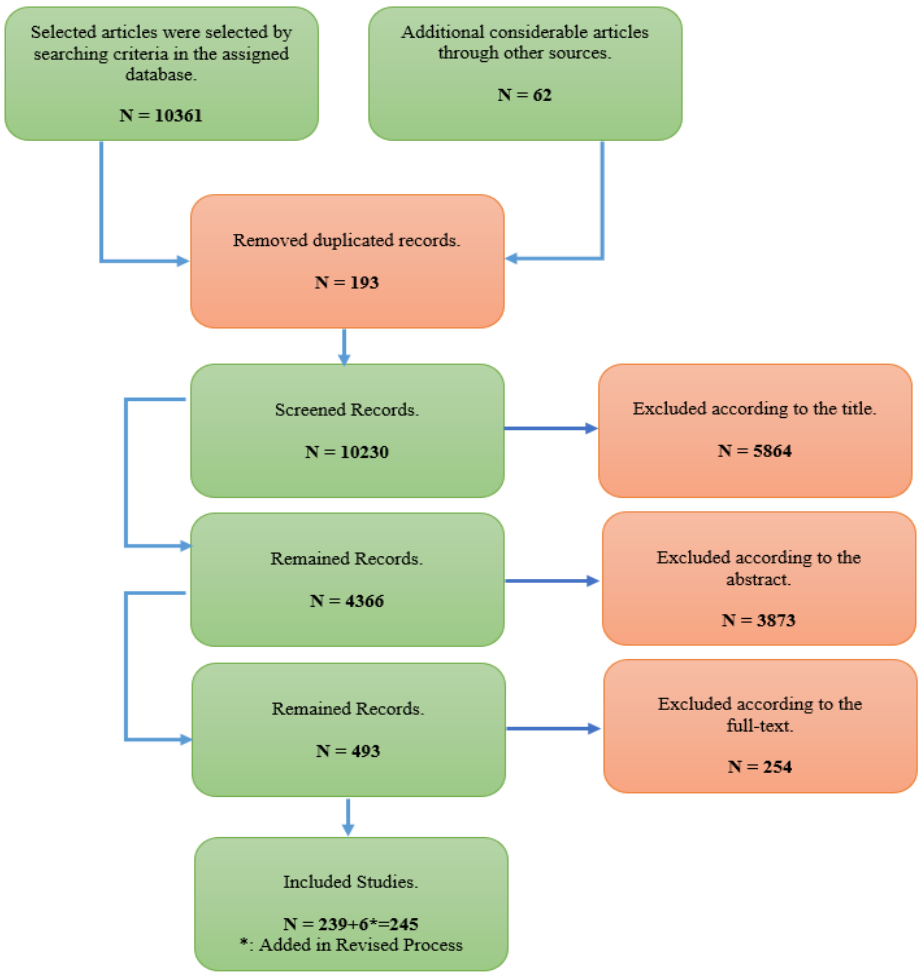

Figure 2-2 Flowchart of the selection process.

Figure 2-3 and Figure 2-4 provide insights into the distribution of the studies, presenting a graphical representation of various types of selected documents, and illustrating the reference distributions across the four main categories analyzed in this study.

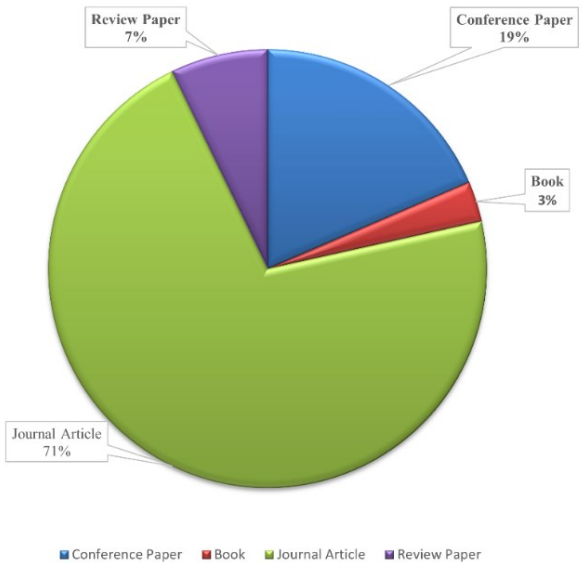

Figure 2-3 Graphical representation of various types of the selected documents.

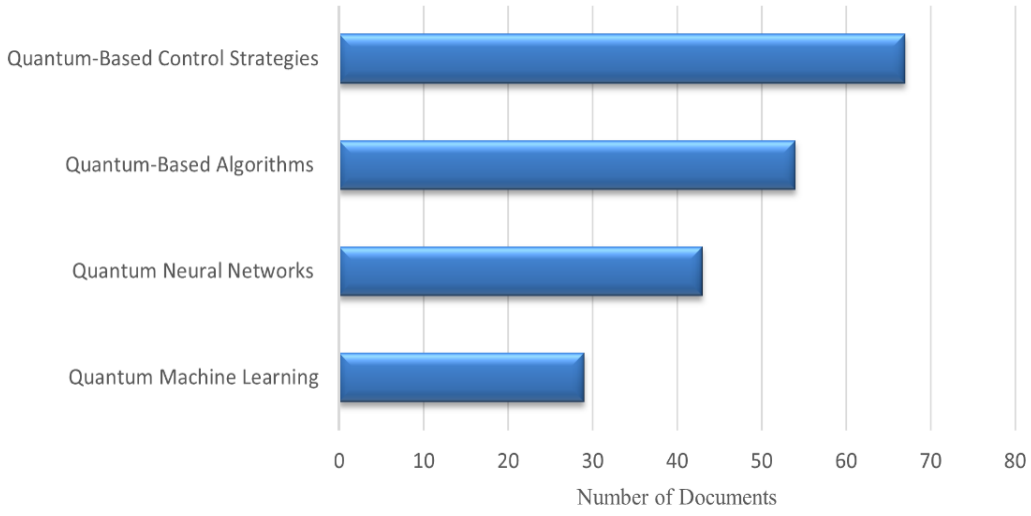

Figure 2-4 Selected reference distributions of the four main categories in the present study.

2.2.7 Data Extraction and Analysis

A standardized extraction template captured key elements, including citation details, research objectives, methodologies, contributions, limitations, and quantitative metrics. Both thematic qualitative analysis and quantitative synthesis were conducted to identify prevailing patterns, key challenges, and comparative outcomes. Findings were grouped into four principal domains: Quantum Machine Learning, Quantum Neural Networks, Quantum Algorithms, and Quantum-Based Control Strategies.

Quantum Computing-Based Artificial Intelligence for Robotics: A Systematic Review of Theoretical Foundations, Practical Applications, and Future Trends

Mehdi Fazilat, Nadjet Zioui *

Université du Québec à Trois-Rivières, 3351 Bd des Forges, Trois-Rivières, QC G8Z 4M3, Canada

* Email of corresponding Author: nadjet.zioui@uqtr.ca

ABSTRACT

This systematic review explores the intersection of quantum computing and artificial intelligence (AI) in robotics, evaluating their theoretical underpinnings, practical applications, limitations, and emerging trends. Employing the PICO framework and adhering to PRISMA guidelines, peer-reviewed studies published from 2008 to 2025 were systematically identified across major scientific databases, including Scopus, Web of Science, IEEE Xplore, and ScienceDirect. Explicit inclusion and exclusion criteria were applied to ensure the quality and relevance of the selected studies, which were then categorized into four primary domains: Quantum Machine Learning (QML), Quantum Neural Networks (QNNs), Quantum-Inspired Algorithms, and Quantum-Enhanced Control Strategies. The findings reveal that QML and QNNs significantly enhance robotic intelligence by accelerating computations, improving perception accuracy, and optimizing decision-making and control processes. Quantum-inspired optimization techniques demonstrate superior convergence rates and robustness compared to their classical counterparts, while quantum control strategies provide higher precision and adaptability in dynamic environments. However, challenges such as quantum decoherence, limited qubit scalability, hardware noise, and the absence of standardized hybrid frameworks continue to hinder real-world applications. This review emphasizes that integrating quantum and classical paradigms can yield hybrid intelligent systems with transformative capabilities across areas such as autonomous navigation, industrial manipulation, and medical robotics. It provides a thorough overview of current advances in quantum-driven robotics and highlights future research priorities, including developing scalable quantum processors, improving error-correction models, and implementing real-time hybrid quantum-classical control architectures. As the first study to unify the literature on QML, QNNs, quantum-inspired optimization, and quantum control in robotics, it provides a roadmap for the next generation of quantum-enabled autonomous systems.

Key words: *Quantum Computing, Quantum Machine Learning, Quantum Neural Networks, Quantum-enhanced Control, Artificial Intelligence, Robotics*

1. INTRODUCTION

The convergence of quantum computing and artificial intelligence marks a paradigm shift in advancing fields such as cybersecurity, medical diagnostics, energy management, engineering, autonomous vehicles, and robotics. The capacity of quantum computing to process large datasets rapidly enables progress in machine learning (ML) algorithms and robotic systems, opening new horizons in technology. While classical artificial intelligence (AI) and machine learning support renewable energy forecasting and management, Quantum AI refines efficiency and predictive accuracy. This integration can yield sustainable energy systems in which robotic platforms can manage resources with precision [1]. The acceleration of machine learning through quantum computing is a major research direction. The entanglement-based classification of high-dimensional vectors promises faster learning with applications in robotics [2]. Quantum computing enhances AI by increasing the computational speed and power of the training algorithms, thereby improving AI-driven robotic systems [3]. Barral demonstrated how Quantum AI can transform sustainable energy management by embedding quantum machine learning (QML) models into autonomous robots [4].

Learning and control in dynamic environments rely on computational principles such as qubits, quantum algorithms, and quantum-enhanced machine learning, to improve efficiency, decision-making, and adaptability [5]. Quantum-based methods, including Qubits, Markov Chains, and Grover's algorithm, provide a foundation for applying quantum concepts to AI and robotics [6, 7]. Integrating quantum computation into traditional systems enhances the computational speed and performance, thereby improving AI and robotics [8]. Intelligent robots using quantum cloud services or co-processors have demonstrated the practical benefits of quantum computing for robotic intelligence [9]. Advances in AI have influenced robotics, enabling human robot collaboration, cognitive augmentation, and autonomous intelligence, reflecting the expanding potential of AI-driven robotics [10]. Reviews of quantum computing outline applications in quantum machine learning relevant to robotics, highlighting decoherence, error correction, and the role of quantum computing in its implementation [11]. The potential of quantum computers to create AI machines necessitates the redesign of the qubit algorithms. These developments link mechatronics and quantum technologies, advancing robotics through the application of quantum effects [12]. A quantum-like perception model for robot multi-sensory inputs utilizes qubits to manage data and decision-making, demonstrating how quantum computing enhances efficiency and precision in perception [13]. Quantum principles enhance AI efficiency in terms of speed and energy use, highlighting the benefits of integrating quantum computing with AI for improved performance and reduced energy demands [14]. A new paradigm for quantum robots utilizes learning algorithms, including quantum searching and reinforcement learning, to accelerate learning speed [15]. Quantum computing applications in AI and robotics have demonstrated progress in interpretation and optimization [16]. Reviews of quantum optimization for engineering highlight challenges such as fault tolerance and noise sensitivity, but emphasize the potential for solving complex optimization problems [17, 18]. Quantum algorithmic gates in robotic control enhance computational speed and accuracy, which are essential for refined systems [19]. Exploring quantum applications in robotics, such as quantum-enhanced machine learning and

optimization, provides a roadmap for integrating methods to address the challenges in robotic science and realize the reciprocal benefits of AI and quantum computing [9, 20]. Scalable protocols and efficient quantum algorithms are crucial for robotic tasks [21]. Android and humanoid robots provide nursing-care companionship and, raise ethical, psychological, and spiritual concerns. The literature notes the limitations of robot companions and proposes AI models that use quantum computation to simulate human cognition more effectively [22]. Quantum computing also supports the analysis of complex datasets in spine care, enhancing predictive modeling and AI-driven decision-making, thereby confirming its broad applicability in medical diagnostics [23]. Advances in artificial perception for precision forestry highlight the ongoing challenges in sensing technologies and the need for continued research in robotics and intelligent systems [24]. Recent studies on quantum computing and AI in robotics have revealed innovative opportunities. Research on quantum computing in cybersecurity focuses on improving threat detection [25].

Integrating QML with robotics is a milestone in autonomous systems [26]. Studies on Quantum Deep Reinforcement Learning (QDRL) show that it can match classical navigation in hybrid quantum-classical settings [27]. Meta-learning analyses suggest that quantum approaches may improve efficiency despite the complexity of the reinforcement dataset [28]. Implementing Quantum AI (QAI) in machine learning presents both opportunities and challenges [29] that are addressed by quantum-enhanced reinforcement learning, particularly in deterministic environments [30]. Theoretical work on QML, including quantum-enhanced reinforcement learning and gradient estimation, highlights rapid growth and curiosity-driven exploration [31]. Other studies document the convergence of quantum computing and machine learning, outlining advances and applications in QAI, QML, robotics, and healthcare [32-35].

Quantum Neural Networks (QNNs) combine quantum computing and neural networks to enhance AI and enable autonomous systems to perform complex tasks with high accuracy [36-40]. Quantum neurons use quantum states for inputs and outputs and operate through circuits that model next-generation AI in robotics [41, 42]. Research has highlighted the importance of parallelism and entanglement in addressing challenges in classical networks, such as the von Neumann bottleneck and the curse of dimensionality [43].

Quantum-inspired algorithms support robotics by solving optimization problems more efficiently than classical methods [44-51]. Swarm robotics, which coordinate multiple robots for collective tasks, benefits from advanced computation [52].

Quantum-enhanced control improves precision, efficiency, and capabilities, boosting overall performance [53, 54]. It also enables new solutions in multi-robot systems for better coordination and behavior. Integrating quantum principles expands capabilities and fosters research in healthcare, manufacturing, and secure communication [55, 56]. Medical robotic surgery research highlights the potential of quantum computing for faster and less invasive procedures with secure direct communication [57, 58].

Studies on multi-robot systems demonstrate that quantum-inspired approaches enhance the understanding of collective behavior and social organization [59]. Integrating quantum and soft computing enables robots to manage quantum information and improve control quality [60].

This integration supports more effective operations, underscoring the benefits of combining cognitive intelligence with advanced computing.

Quantum-controlled mobile robots combine quantum controls with classical sensors and effectors for navigation and decision-making [61]. Quantum algorithms for optimizing control strategies and stochastic quantum dynamics with homodyne measurement have shown promise in engineering [62]. Research on intelligent machining for robotic end -effectors emphasize the importance of intelligent control in enhancing performance [63-70]. Work on entanglement and cryptography in robotics involves photon-based experiments for mobile systems, underscoring the importance of secure quantum communication in multi-agent networks [71].

Current research remains fragmented across domains, with limited interdisciplinary collaboration hindering cohesive insights. This review addresses the gap by categorizing advances in quantum machine learning, quantum neural networks, quantum-inspired algorithms, and quantum-enhanced control, establishing a structured foundation for future research and applications.

It synthesizes the literature on quantum computing-based AI in autonomous systems and robotics, examining the effects of quantum machine learning and neural networks on robotic systems, algorithms for control and decision-making, and implementations of quantum control. The scope covers studies that apply quantum computing-based AI to autonomous robots, mobile robots, humanoids, manipulators, and unmanned vehicles. The sources include empirical studies, theoretical papers, and implementations published between January 2008 and October 2025. Figure 1 shows the yearly publication trends in quantum computing in robotics. Data were retrieved from Scopus and the Web of Science on October 17, 2025, using the query string "quantum computing" AND "robotics" in titles/abstracts/keywords. Only journal articles and conference papers were included, and duplicates were removed by DOI or title. Publications explicitly mentioning both "quantum computing" and "robotics" were included, while those mentioning "quantum-inspired" or generic algorithms without a robotics focus were excluded. The 2025 decline reflects partial coverage and indexing delays rather than reduced activity; the counts are preliminary. Differences in coverage between Scopus and the Web of Science, especially for conference and non-English sources, affect totals, but overall growth remains evident. The counts were absolute and not normalized against the robotics publication volume.

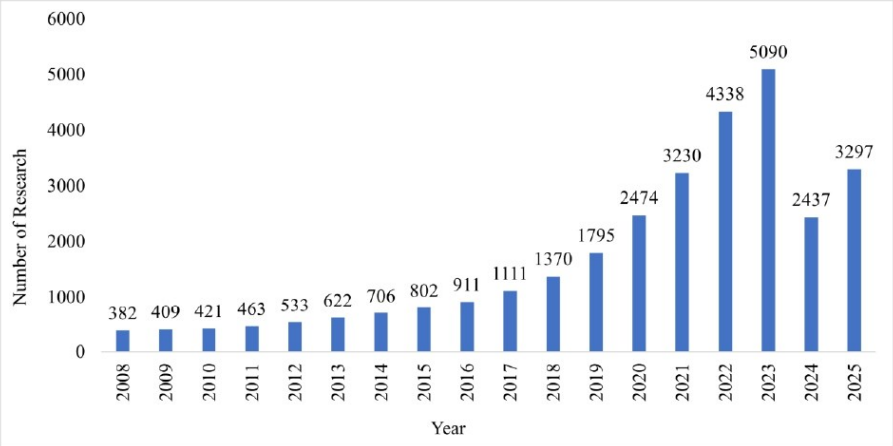

Fig. 1. Annual publications on quantum computing–based methods in robotics (2008–2025): Data from Scopus and Web of Science.

The literature reveals a gap in cross-disciplinary studies linking quantum computing, AI, and robotics. Declining collaboration limits the exploration of new paradigms and refinements that could emerge from synergy. Rapid advances in Quantum Computing and AI often outpace research output, leaving gaps in the academic literature where trends and innovations must be quickly assessed. Although the intersection of these fields presents unique challenges, these issues point to areas where further research could yield substantial benefits.

This review contributes to the synthesis of the existing research on integrating quantum computing and robotics. It examines methodologies and frameworks for applying quantum AI algorithms to autonomous and robotic systems, clarifies future research directions, and outlines the potential applications of quantum-based algorithms, particularly quantum-inspired control strategies. Figure 2 illustrates the country-level distribution of publications on quantum computing in robotics, based on data from Scopus and the Web of Science. The query "quantum computing" AND "robotics" was applied to selected fields from January 2008 to October 2025. The chart indicates that China (n = 8,349) and the United States (n = 5,488) were the leading contributors, followed by India, the United Kingdom, and Germany. These values represent raw publication counts and do not account for the total robotics and AI output, which should be considered when comparing countries.

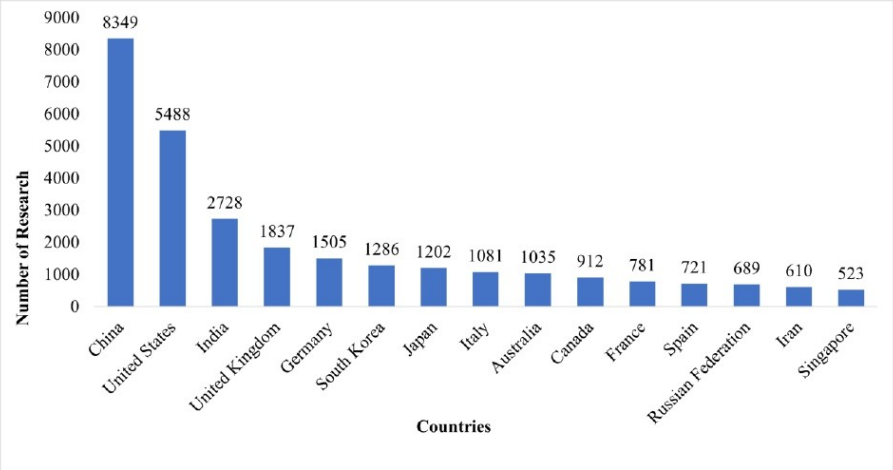

Fig. 2. Country-level contributions to quantum-computing-in-robotics publications; data: Scopus and Web of Science (retrieved October 17, 2025).

This review provides a structured analysis of the intersection of quantum computing, artificial intelligence, and robotics, synthesizing the advancements, challenges, and future research directions in this rapidly evolving field. Unlike fragmented studies on the isolated aspects of quantum-enhanced AI or robotics, it integrates diverse findings into a cohesive framework, identifying gaps and emerging trends. Ultimately, the study consolidates existing knowledge, proposes frameworks for overcoming barriers, and envisions the future of quantum-enhanced robotics across various domains, including automation, medical robotics, cybersecurity, and industry.

This paper is organized as follows: Section 1 introduces the topic and context; Section 2 outlines the methodology for selecting and analyzing the literature; Section 3 explores Quantum Machine Learning in autonomous systems and robotics; Section 4 examines Quantum Neural Networks and their potential to enhance robotic capabilities; Section 5 reviews approaches to Quantum-Based Algorithms; Section 6 discusses advanced Quantum-Based Control Strategies; and Section 7 summarizes the findings and proposes future research directions. The flowchart of the study design is shown in Figure 3.

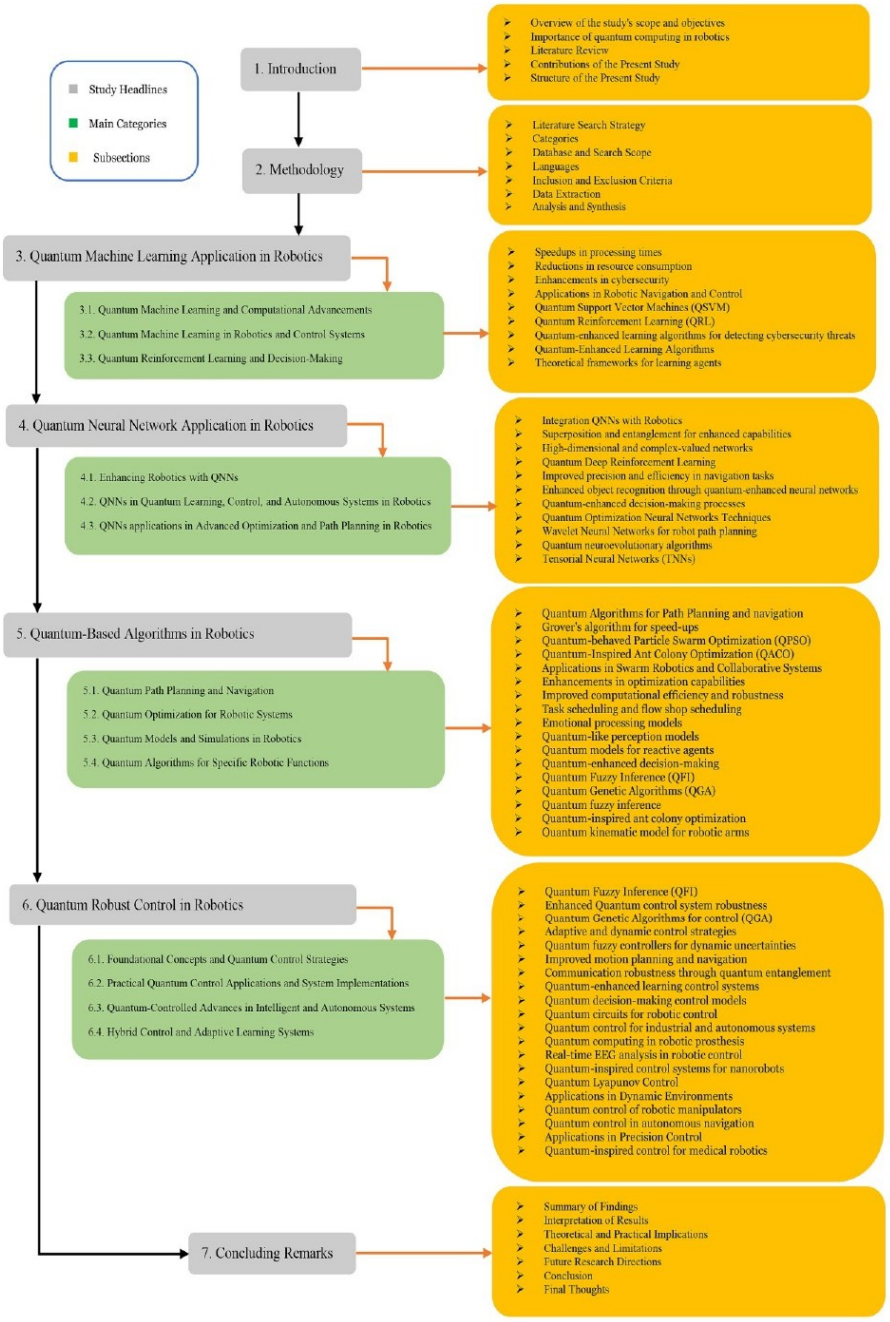

Fig. 3. Flowchart of the contents of the present research.

2. METHODOLOGY

The PICO framework [72-76] in this review addresses the impact of quantum computing-based AI on robotics. The Population includes robotic systems, such as autonomous, mobile, humanoid, manipulator arms, and unmanned vehicles. The Intervention involves implementing quantum AI algorithms such as quantum-enhanced machine learning, quantum algorithms, and quantum-based control strategies to enhance intelligence and efficiency. The Comparison is made against traditional AI or classical computing approaches used in robotics, enabling the evaluation of the distinct contributions of quantum methods. The Outcome emphasizes performance gains and future applications, particularly in terms of processing speed, efficiency, adaptability, and complex task management, highlighting its advantages over conventional techniques.

The search strategy encompasses a broad range of studies, including key studies on integrating quantum computing and AI in robotics. The databases searched were IEEE Xplore, Scopus, ScienceDirect, SpringerLink, Web of Science, PubMed, and ACM Digital Library, all of which host extensive research on robotics, computer science, and engineering. For non-open-access documents, additional searches were conducted using the Sofia platform at the University of Quebec in Trois-Rivières, which provides access to proprietary databases and special collections necessary to capture the latest research.

The search terms were organized into three categories: Robotics, Quantum Computing, and Artificial Intelligence. The Robotics category included “Robotic systems,” “Autonomous robots,” “Mobile robots,” “Humanoid robots,” “Robotic control strategies,” and “Manipulator robotic arms.” Quantum Computing terms include quantum computing, “Quantum computing,” “Quantum algorithms,” “Quantum-inspired,” “Quantum machine learning,” “Quantum Neural Networks” “Quantum-enhanced,” and “Quantum sensors.” The Artificial Intelligence category included terms such as “AI,” “Artificial intelligence,” “Machine learning,” “Deep learning,” and “Neural networks.” Boolean operators (AND, OR, NOT) were applied to refine and track the search queries effectively.

The search spanned publications from January 2008 to October 2025, with a focus on recent and relevant advancements. Only English-language texts with full access to institutional subscriptions or open access platforms were included.

The exclusion criteria eliminated studies outside the intersection of quantum computing, AI, and robotics, such as those addressing only broader aspects of quantum computing or AI without robotic relevance. Non-peer-reviewed sources (gray literature, opinion pieces, editorials), works available only as abstracts, posters, or presentations, and duplicate reports of the same data were also excluded to ensure quality and originality. Figure 4 details the study selection flow, whereas Figure 5 illustrates the distribution of document types after applying the selection protocol.

Figure 6 illustrates the four main concentrations of related studies. This visualization provides an insight into how the selected literature is allocated to these categories. By depicting the balance of studies across these categories, Figure 6 enhances the systematic synthesis and provides valuable context for subsequent analysis sections.

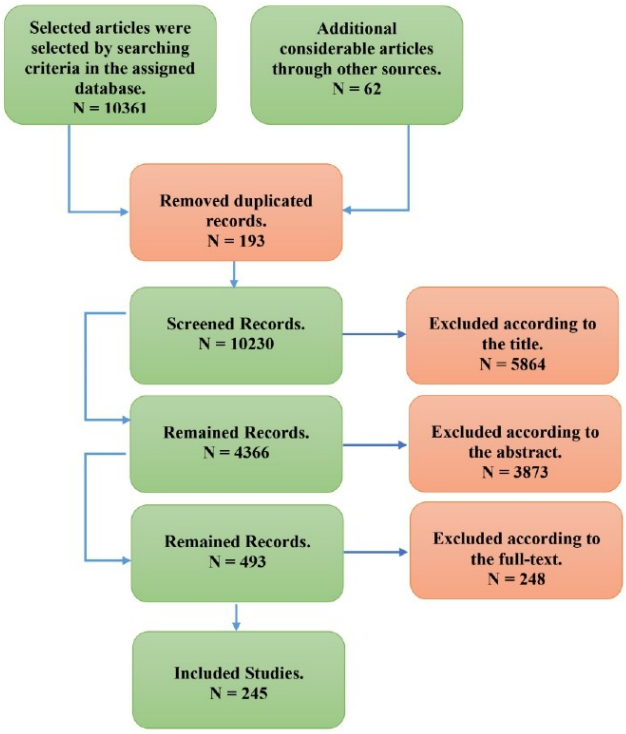

Fig. 4. Flowchart of the selection process.

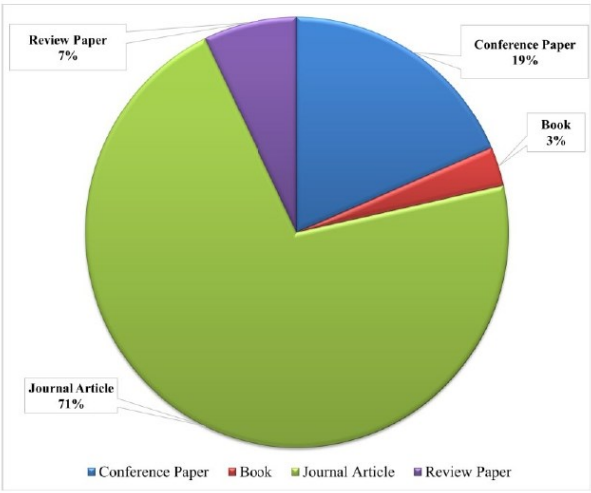

Fig. 5. Graphical representation of various types of the selected documents.

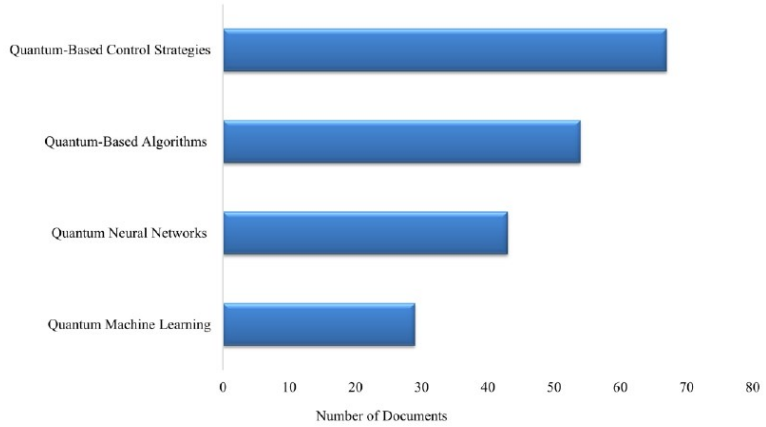

Fig. 6. Selected reference distributions of the four main categories in the present study.

3. QUANTUM MACHINE LEARNING

One of the ongoing developments suggests a future in which quantum computing could evolve as an integral to solving some of the most intricate challenges: integrating quantum computing and machine learning.

3.1 Quantum machine learning and computational advancements

Dong et al. developed a quantum reinforcement learning (QRL) model that leverage superposition and entanglement, demonstrating exponential learning speedups [77]. Buffoni and Caruso reviewed trends in quantum machine learning, emphasizing the links between machine learning and quantum physics [78]. Lamata summarized the advances in quantum machine learning and biomimetics, highlighting applications such as QRL and quantum autoencoders [79]. Ramezani et al. surveyed machine learning algorithms in quantum computing, assessing the speedup and complexity benefits [80]. Yun et al. examined the integration of quantum computing with multi-agent reinforcement learning for factory management [81].

Tandon et al. investigated QML algorithms for robotics and proposed a framework to reshape robotic computations [82]. Chatzis et al. introduced a quantum Gaussian mixture regression (QGMR) algorithm for robot learning by demonstration, achieving improvements in trajectory regeneration over the classical GMR [83]. Ulyanov analyzed the challenges in designing intelligent controllers with quantum algorithms, emphasizing their benefits in unpredictable scenarios [84, 85]. Shill et al. applied quantum genetic algorithms to optimize interval type-2 fuzzy logic controllers in robotics [86].

Motroni et al. enhanced robotic localization with UHF-RFID sensor fusion, improving accuracy in complex environments [87]. Hu et al. proposed quantum-enhanced reinforcement learning to accelerate robotic control and improve efficiency and decision-making [88]. Yuezhen Niu optimized approximate quantum optimization algorithms via reinforcement

learning and improved quantum device control [89]. Ali and Jima combined quantum computing, deep learning, and machine learning to enhance cybersecurity and support human-robot collaboration [90].

3.2 Quantum machine learning in robotics and control systems

Taghavi and Farnoosh proposed a multi-agent reinforcement learning framework combining quantum and neuromorphic computing for safe and explainable control in autonomous robotics [91]. Cheng et al. analyzed quantum hardware constraints, emphasizing the need for quantum error correction (QEC) to enhance the robustness of quantum-assisted robotic navigation and learning [92]. They later examined the hardware variability across different platforms [93]. To address these limitations, Acampora et al. introduced a distributed noisy intermediate-scale quantum framework that interconnects multiple processors, achieving a high success rate in distributed Grover's search [94]. Patel and Tiwari developed an error- mitigation framework to enhance computational reliability [95]. Heimann et al. and Bar et al. proposed a hybrid quantum-classical approach for deep reinforcement learning (DRL) in navigation tasks, reporting a 91% success rate in target achievement [96].

3.3 Quantum reinforcement learning and decision-making

Pappala et al. examined the potential of quantum-enhanced machine learning, with a focus on reinforcement learning [97]. Raval and Oza showed that combining QNNs with QRL improves flexibility and decision-making in complex environments [98]. Shahid and Hassan suggested that QRL could address common-pool resource (CPR) dilemmas [99], whereas Seetohul et al. implemented a structured QRL framework for AI agents [100]. Teixeira et al. bridged quantum mechanics and machine learning by integrating tensor networks (TNs) with neural networks (NNs) [101]. Mamaeva et al. enhanced cognitive control in robotics by applying quantum and soft computing to classify human emotional states [102]. Mohan et al. developed an autonomous vehicle control system for traffic management using fuzzy logic and Zigbee communication [103]. Table 1 outlines the main challenges in applying quantum computing in QML, including hardware constraints (qubit counts, coherence times, and operation fidelity) and the complexity of the algorithm design and implementation.

Table 1. Classification of the most important research challenges in QML and robotics.

References	Challenges/Limitations
[27]	Limited capabilities of quantum hardware, including number of qubits, coherence times, and fidelity of operations
[104]	Representation of actual space for ML, unpredictability of real-world reactions
[96]	Scalability, current limitations of quantum computing technology, need for further validation in complex environments.
[99], [27]	Limitations of quantum (NISQ) computers, the effectiveness of variational quantum algorithms in complex multi-agent systems
[102]	Precision in classifying mental states due to EEG noise, complexity in integrating quantum technologies

[30, 35]	The open question of how AI benefits from quantum mechanics in general learning settings
[101]	Computational complexity and the need for advanced algorithms for large-scale tensor manipulations.
[28]	The complexity of applying quantum mechanics to RL, technological limitations in quantum computing
[103]	Adapting system for different vehicle models and environmental conditions, reliance on external hardware
[25]	Challenges in quantum error correction and fault tolerance, combining quantum-AI with IoT and blockchain
[32]	The early stage of the field, theoretical nature of quantum enhancements, and practical implementations not realized
[82]	Mathematical nuances of quantum algorithms, challenges in implementing quantum neural networks
[83]	Complexity of quantum-statistical approach, applicability to a broader range of scenarios
[78]	Need for large-scale integration of qubits for fault-tolerant quantum computation.
[79]	There is a need for further research to understand potential advantages and practical implementations.
[80]	Limited number of qubits, high noise levels, lack of full exploitation in earlier QNN implementations
[84]	Complexity and computational cost of implementing quantum algorithms in real-world applications
[87]	Accumulated drift in trajectory estimation, interference from moving objects and people in dynamic environments
[85, 105]	Complex and computationally intensive framework, reliance on precise quantum correlations
[88]	Quantizing state and action information in practical applications, effectiveness in complex control systems
[86]	The complexity of QGA integration, computational resources, and the need for specialized knowledge.
[81]	Scalability due to exponential increase in quantum errors, implementation in larger scale setups
[89]	Scalability, complexity in managing quantum gates, data collection for quantum measurements
[27, 28, 77, 89, 96]	Practical implementation limited by current quantum technology, the complexity of stable quantum states
[34]	Nascent stage of quantum technologies, theoretical nature of DL applications

Quantum machine learning is transitioning from theory to practical application across multiple domains. Some implementations remain at the prototype or simulation stage, whereas others have been tested in controlled or real-world environments. Table 2 summarizes the QML applications in robotics and AI from the reviewed studies, highlighting key areas, methods, and achievements and comparing theoretical concepts, simulations, and practical implementations.

Table 2. Classification of real-world applications of QML in robotics and AI.

Reference	Actual Method	Achievements
[92]	Experimental on IBM quantum hardware (ANN optimization)	Feasibility of quantum neural optimization in real quantum processors
[97]	Brain–Computer Interface (EEG helmet) controlling robot navigation	Successfully classified stress vs. calm states, adapting real robot behavior based on EEG input
[26]	QSVM applied to Smart Grid DDoS attack detection (testbed experiment)	Achieved 99.91% to 99.94% accuracy, 93% execution time reduction over classical SVM
[84]	QGMR tested in simulations for robot learning by demonstration	Reduced Mean Square Error (MSE) in trajectory predictions compared to classical GMR
[88]	UHF-RFID sensor fusion with Particle Swarm Optimization (real experiment)	Localization errors reduced to 30 cm in controlled warehouse-like settings
[99]	Fuzzy logic-based quantum RL (tested on robotic vehicles in prototype environment)	Successfully controlled autonomous traffic management in a real prototype system

4. QUANTUM NEURAL NETWORKS IN ROBOTICS

The integration of quantum neural networks with robotics has evolved in advanced autonomous systems. By harnessing the unique quantum mechanical properties of superposition and entanglement, QNNs elevate robotic capabilities beyond the current confines of classical computing, enhance processing speed, improve decision-making, and increase adaptability.

4.1. Enhancing robotics with QNNs

QNNs utilize quantum principles, such as superposition and entanglement, to enhance neural networks, enabling more efficient computation and improving robotic processing speed, decision-making, and adaptability. Biologically inspired networks support navigation and task sharing [106], whereas spiking neural networks (SNNs) improve speed and energy efficiency in legged robots, signaling a move toward more effective robotic systems [107].

Quantum neural computing, which utilizes single-qubit operations and measurements, introduces nonlinear classification and robustness, thereby opening new directions in neural computation [108]. Quantum-enhanced algorithms reduce the computation time in mechanics, pointing to the development of fast surrogate models with transformative potential in robotics [109] and advancing the analysis of quantum many-body problems [110]. The quantum neuroevolution algorithm autonomously determines near-optimal QNNs for machine learning, demonstrating adaptability in optimizing neural networks [111]. Beyond theory, QNNs in robotics enable quantum- target interaction, autonomous navigation, and efficient computation. Recently, Fazilat and Zioui applied quantum-inspired neural networks to solve the inverse kinematics of a six-degree-of-freedom ABB IRB140 robotic arm, highlighting the gains in reliability and efficiency for industrial manipulation [112].

4.2. QNNs in quantum-enhanced learning, control, and autonomous systems in robotics

Quantum learning in robotics highlights quantum-enhanced agents and autonomous experiments, with prospects for machine learning speedups [113]. In quantum learning and neural networks, many-body physics integrates supervised and unsupervised learning, advancing the study of phase- transition learning and quantum tomography [114]. Neural-enhanced frameworks address the constrained optimization of quantum architectures, creating opportunities for robotics [115]. The convergence of machine and quantum learning supports strategy-intensive applications, as exemplified by diamond-based quantum technologies that improve speed and accuracy [116].

Integrating quantum perceptron and QNNs has expanded the frontiers of robotics and quantum technology [117]. Numbi et al. proposed a quantum-inspired hybrid neural network (QANN) to identify the dynamic parameters of car-like mobile robots, reducing the training RMSE by 9.7% and validation RMSE by 84.4% compared with classical models [118]. Tools for evaluating quantum network performance span information theory, analysis, and simulation [119]. Fazilat and Zioui studied QNNs to solve the inverse kinematics of an ABB IRB140 robot [120].

Takahashi et al. developed a multi-layer QNN controller trained using a real-coded genetic algorithm [121]. Hanna et al. introduced an adaptive PID controller based on QNN (APIDC-QNN) for nonlinear systems [122]. Sciuto et al. investigated obstacle avoidance in an electric vehicle with Mecanum wheels using neural networks [123]. Bayro-Corrochano et al. proposed quaternion spiking neural networks (QSNNs) and quantum neural networks (QQNNs) as solutions for control and pattern recognition [124].

QQNNs are also trained for pattern recognition with a single quaternion neuron, showing superior performance in real-time recognition compared with traditional quantum computing [125]. Lechuga-Gutiérrez et al. explored quaternion spiking neural networks for adaptive control of robot degrees of freedom, providing insights into kinematics problem -solving [126].

4.3. QNNs applications in advanced optimization and path planning in robotics

Quantum neural networks (QNNs) advance robotics optimization by addressing gaps at the intersection of quantum computing and AI. Pandey et al. investigated how QNNs can be applied to robotics optimization, identifying a key research gap [127]. Nivelkar and Bhirud demonstrated that QNNs enhance the training efficiency and classification in complex tasks by leveraging superposition and entanglement [128]. Srinivasulu and Nagarajan developed qubit encoding models for multi-level time- series classification, further improving efficiency [129]. In edge and cloud computing, Zhang et al. reported that QNNs enhance computational performance and portability in IoT environments [130]. Rudolph et al. mapped Tensor Networks to parameterized quantum circuits, creating a quantum-classical training framework that boosts optimization [131]. Deshpande and Melnikov introduced a graph neural network algorithm to predict the performance of variational quantum optimizers, thereby guiding the choice between quantum and classical approaches [132].

Xu et al. examined a quantum neuroevolution algorithm for near-optimal QNN structures applied to image classification and symmetry-protected topological states [133]. Du et al.

proposed a real-time neural network planning algorithm for robots, that is 24% faster than traditional planners and potentially 35% more efficient during development [134]. Bae et al. combined Deep Quantum Learning and Convolutional Neural Networks for multi-robot path planning, enabling efficient navigation and collaboration [135]. Silva and Oliveira highlighted Quantum Neural Network Architecture Evaluation (QNNE), which avoids weight initialization and may become a benchmark [136].

In motion planning, classical neural networks still dominate; however, quantum computing shows transformative potential. Fan [137] studied multi-point planning with deep reinforcement learning, whereas Xin et al. [138] applied deep Q-networks for mobile robot navigation with visual perception. Yang [139] applied a quantum genetic algorithm to soccer robot path planning, thereby improving the global search and convergence speed compared with classical methods.

As QNN research progresses, ethical and societal issues must be addressed. Quantum-enabled robots have raised concerns about privacy, security, and employment. A promising direction is the hybridization of quantum-classical systems, which combines both paradigms to optimize resources, improve scalability, and facilitate transfer learning. Such systems, inspired by biological models and emphasizing energy efficiency, may enable more sustainable robotic operations.

5. QUANTUM-BASED ALGORITHMS IN ROBOTICS

5.1. Quantum path planning and navigation

Pusuluri et al. applied quantum-inspired firefly algorithms to coordinate swarms of delivery robots in logistics [141]. Qian et al. developed a QPSO-based path planner for two-wheeled self-balancing robots and achieved rapid convergence and precision [142]. Fazilat and Zioui proposed a quantum particle swarm optimization (QPSO) framework for parameter identification in a six-DOF industrial arm [143]. Maity et al. optimized aerial robot path planning using QPSO, surpassing the traditional PSO in terms of speed and robustness [144]. Yu et al. introduced Quantum-Inspired Ant Colony Optimization (QACO) for robot coalition formation [145], and Priyadarshini reviewed swarm intelligence with quantum-inspired heuristics in robotics and related fields [146].

For collective systems, Chella et al. proposed a quantum algorithm for swarm robotics that was validated in search-and-rescue scenarios [147]. At the same time, Lathrop et al. developed a parallel quantum algorithm for motion planning [148]. Xue [149] and Yuan [150] extended hybrid QPSO variants to autonomous mobile robots and multi-steering tractor-trailer systems to address maneuverability in confined environments. Yin et al. optimized the milling force prediction in stone machining using an IQPSO-SVM approach [151]. Smith et al. used a robotic arm to align magnetic fields for quantum sensors [152], and Jhang et al. improved mobile robot navigation using a fuzzy neural controller tuned by dynamic group PSO (DGPSO) [153].

Quantum computing has been shaping the development of dynamic robotics and adaptive systems. Luo et al. [154], Xu et al. [155], and Dian et al. [156] refined trajectory planning, whereas Fernandes et al. [157, 158] optimized path-planning algorithms, showing how quantum-behaved methods adapt to changing environments. Applications extend beyond

ground-based robots to space and underwater systems Chen and Zhou [159] and Li et al. [160] applied quantum methods to space robotics and underwater docking. Yao et al. [161] optimized transitional gaits in inchworm-like climbing robots using QPSO, thereby enhancing the efficiency in unstructured environments. Kim and Kim [162] and Jiao et al. [163] applied quantum-inspired algorithms to fuzzy systems and escort robots. Kolahdoozi et al. [164] advanced fuzzy cognitive map learning using a quantum fuzzy cognitive map (QFCM), thereby overcoming the limitations of earlier static or dynamic-only models.

5.2. Quantum optimization for robotic systems

Recent studies have highlighted the advantages of combining quantum algorithms with robotics, demonstrating their scalability for dynamic models, and addressing industrial challenges. Atchade-Adelomou et al. applied quantum computing to warehouse optimization in mobile robotics [165]. Lei et al. introduced a hybrid Quantum- Inspired Evolutionary Algorithm for flow shop scheduling [166] and Zhang et al. proposed an adaptive quantum genetic algorithm for task sequence planning in complex assemblies [167].

Yan et al. addressed training challenges and patient engagement in healthcare [168]. Dereli and Köker applied quantum computing to inverse kinematics in manipulators to enhance control accuracy [169]. Deng and Xie improved PSO for multi-degree-of-freedom (DOF) manipulators [170], while Rokbani et al. proposed a β-SSA solver that outperformed PSO and the Firefly algorithm [171]. Ayyıldız and Çetinkaya compared four heuristic algorithms for the 4-DOF manipulator IK [172], and Qiu et al. optimized parallel surgical robots for high-precision operations [173].

For trajectory planning, Schuetz et al. optimized large-scale robot paths using quantum computing [174]. Li and Wu applied quantum-inspired navigation to multi-robot localization [175]. Mezghiche and Djedi used a real-observation quantum genetic algorithm to evolve neural controllers in modular robots to improve self-reconfiguration performance [176]. Overall, the quantum-enhanced algorithms can transform industrial sectors by improving the efficiency, accuracy, and adaptability of logistics, assembly, healthcare, and robotics.

5.3. Quantum models and simulations in robotics

Quantum models and simulations represent an emerging frontier in robotics, with strong potential to improve efficiency and adaptability. Early studies demonstrated the diverse applications of quantum theories to robotics. Yan et al. [177] proposed Quantum Affective Computing (QAC) to integrate quantum mechanics into emotional processing, whereas Lanza et al. [178] introduced a preliminary quantum-like perception model. Mannone et al. [179] analyzed the links between quantum computation and swarm robotics, and Koukam et al. [180] applied quantum formalism to model reactive agents. Bhatia et al. [181] developed a quantum-inspired method for real-time, energy-efficient IoT data acquisition.

Applications in robotic modeling and simulations further illustrate this trend. Zhao et al. [182] optimized the inverse kinematics of multi-DOF arms by using an improved particle swarm algorithm. Singla and Parthasarathy [183] studied Levy noise in quantum robots, contributing to their robust operation in unpredictable settings, and extended their work to teleoperation under quantum fluctuations [184]. Panda et al. [185] demonstrated the practical application of

Zidan's quantum computing model for controlling a mobile robot, highlighting the utility of quantum teleportation in real-world robotics.

Overall, these studies highlight how integrating quantum approaches from affective computing into kinematics and teleoperation lays the groundwork for the next generation of robotic systems.

5.4. Quantum algorithms for specific robotic functions

Quantum computing and robotics represent a rapidly advancing frontier, marked by significant progress in computational efficiency and robotic functionality. Ulyanov proposed novel quantum algorithm gates to enhance efficiency [186] and later combined quantum fuzzy inference with quantum genetic algorithms for control in unpredictable environments [84]. Khoshnoud et al. explored the integration of quantum technologies into cooperative robotic systems [187].

In motion planning, Tamizi et al. reviewed the transition from classical to learning-based approaches [188], whereas Otani et al. [189] applied quantum methods to generate low-energy robotic motions.

Swarm robotics research has also expanded through the work of Mannone et al., who developed mathematical models for simulating swarm interactions [190] and later proposed a block matrix-based model for both local and global swarm behaviors [191]. They further introduced a framework that links quantum computing with swarm sonification, utilizing Hilbert spaces to represent musical and robotic states for novel sound-based interfaces in human-robot interactions [192]. Khoshnoud et al. [193] applied quantum entanglement to enhance the collaboration among autonomous vehicles in the face of cyber-physical threats. Table 3 outlines the studies analyzed, summarizing the practical and applied contributions of quantum-enhanced algorithms in robotics.

Table 3. Actual Applications of the quantum- enhanced algorithms in robotics.

Area of the Subject	Actual Method	Achievements
Logistics & Optimization [162]	Warehouse order-picking optimization	Reduced execution time; D-Wave outperformed gate-based systems for >20 qubits
Manufacturing [163]	Robotic flow-shop scheduling	Superior to classical methods; comparable to CPLEX
Healthcare [165]	Rehabilitation robotics	Improved adaptability in patient training
Multi-Robot Systems [140]	Multi-robot coalition formation	Outperformed classical ACO; higher fault tolerance
Motion Planning [142]	Quantum motion planning (Pq-RRT)	Increased search efficiency

Autonomous Vehicles [145, 147]	Autonomous vehicle & trailer navigation	Enhanced maneuverability, robust in unpredictable environments
Industrial Robotics [148]	Robotic stone machining optimization	Higher decision coefficient, lower MAPE, improved milling quality
Industrial Robotics [171]	Large-scale trajectory planning	Bridged quantum-classical gap
Robotics Localization [172]	Multi-robot localization	More robust and flexible positioning
Modular Robotics [173]	Modular self-reconfigurable robots	Superior adaptive locomotion
Secure Robotics [184]	Cooperative robotics with entanglement	Quantum-secured communication
Human-Robot Interaction [189]	Sonification of swarm movements	Successfully demonstrated auditory feedback in simulations
Autonomous Navigation [139]	Quantum maze navigation	78% and 84% shortest-path success rates
Bio-Inspired Robotics [158]	Climbing robot trajectory optimization	Significant time savings in branch traversal
Industrial Robotics [64]	Quantum forward kinematics (6-DOF arm)	<3% error, reduced computing resources
Industrial Robotics [46]	Robotic arm positioning (quaternion model)	More compact, computationally efficient
Industrial Robotics [47]	Quantum algorithm for arm orientation	Reduced computational requirements, validated accuracy
Industrial Robotics [169]	Inverse kinematics (7-DOF manipulator)	Least average error in less iterations
Surgical Robotics [170]	Parallel surgical robot optimization	Expanded workspace, improved dexterity
Industrial Robotics [167]	Adaptive PSO for multi-DOF IK	Superior accuracy, avoided singularities

6. QUANTUM-BASED CONTROL STRATEGIES IN ROBOTICS

Quantum-inspired control mechanisms in robotics represent a transformative shift toward greater precision and efficiency. A seminal study [194] examined quantum control systems across various engineering disciplines, including robotics, while [195] emphasized their potential applications in medical imaging and surgical precision. Industrial research [196-198]

applied quantum-inspired strategies to motor control and energy optimization, achieving higher precision, reduced torque ripple, and improved efficiency. Beyond mechanics, [199] integrated quantum entanglement and cryptography into unmanned systems to strengthen security and network operations. Cross-disciplinary approaches link robotic trajectory optimization with quantum optimal control, demonstrating how complex robotic dynamics refine quantum control strategies [200]. Finally, a survey [201] reviewed neural network applications in manipulator control, underscoring their effectiveness across architectures and the need for advanced real-time models.

6.1. Foundational Concepts and Quantum Control Strategies

Foundational quantum models in robotics link perception with control, forming a basis for analyzing complex behaviors. 202. Reshetnikov and Ulyanov advanced this field through robust control systems based on Quantum Fuzzy Inference (QFI) and soft computing [202, 203]. Practical applications of QFI have shown improved robustness and reliability in dynamic environments, addressing issues such as sensor failures and evolving operational conditions [204]. Krawec proposed a novel quantum-based decision-making model [205].

Theoretical studies on Quantum Markov Decision Processes (QMDPs) highlight the advantages of quantum-dominated environments, although practical implementations remain limited [206]. Quantum algorithms integrated with sampling-based motion planning, as explored by Lathrop et al. [207], offer scalable solutions for high-dimensional navigation. A related framework using stochastic Lyapunov functions and Lindbladian dynamics enhances human stability–autonomous system interactions, such as assisted driving [208]. Furthermore, quantum eigenlogic observables have been applied to analyze and control autonomous agents, including Braitenberg vehicles, marking a refinement in quantum robotics [209]. Ulyanov et al. investigated quantum self-organization algorithms to improve the adaptability and efficiency of intelligent controllers under unpredictable conditions [210].

6.2. Practical Quantum Control Applications and System Implementations

Practical control applications in robotics have highlighted a diverse range of quantum-inspired methods. Dong et al. [211] introduced the msMS DE algorithm to optimize the control under uncertainty. Mahanti et al. [212] designed quantum circuits for Braitenberg vehicles, improving safety in flight and gaming, whereas Deng et al. [213] used quantum automata to create less predictable and more engaging humanoid robot behaviors. Nemchaninov et al. [214] developed an intelligent prosthetic arm by combining quantum computing with adaptive systems. Rybalov et al. [215] compared fuzzy and quantum control models, confirming the effectiveness of both despite navigation errors. Reshetnikova et al. [216] demonstrated the robustness of quantum fuzzy inference-based ICS for the cart-pole problem. Mei et al. [217] employed quantum simulations combined with GANs and digital twins to enhance the efficiency and accuracy of robotic dancing. Chen et al. [218] integrated QPSO with MPC, resulting in a 43% reduction in the tracking errors for Cable-Driven Continuum Robots. For adaptive controllers, Hanna et al. [122] utilized a QNN to reduce the number of tunable parameters in a two-wheel mobile robot. Singh and Sloth [219] implemented an ET2QFNN for motion control, whereas Wan et al. [220] optimized fractional-order PID controllers with a quantum genetic algorithm, improving the

overshoot and settling time in sea trials. Varma et al. [221, 222] addressed mobile -agent security with post-quantum cryptography, showing minimal trade-offs.

6.3. Quantum-controlled advances in intelligent and autonomous systems

The integration of quantum-control mechanisms has advanced robotic and autonomous systems. Reasearchers have applied quantum neural networks (QNNs) to solve inverse kinematics more efficiently than the classical methods [223]. At the same time, Takahashi et al. developed quaternion neural networks for controlling the trajectory of robotic manipulators [224].

In precision medicine, Yang et al. created magnetic spore-based microrobots [225], and Qu et al. applied nanorobotic manipulation to track the motion of quantum dots, thereby advancing quantum device manufacturing [226]. For underactuated systems, Ghosh and Ray combined a linear–quadratic regulator with a gravitational search algorithm to improve the control efficiency and robustness in the double inverted pendulum problem [227].

6.4. Advanced integration of quantum hybrid control and adaptive learning systems

Quantum technologies have driven significant advances in adaptive learning for robotics with hybrid control methods that enhance performance and expand applications in dynamic environments. Chen et al. [228] proposed a Quantum-inspired Q-learning (QIQL) algorithm by applying superposition and quantum parallelism. Gandhi et al. [229] introduced an adaptive brain–computer interface using recurrent quantum neural networks for mobile robot control, whereas Dong et al. [230] developed a quantum-inspired reinforcement learning (QiRL) algorithm based on measurement principles. Deep reinforcement learning for UAV tracking under variable winds [231] and hierarchical Q-learning with quantum parallelization [232] further demonstrated gains in efficiency and scalability.

In control systems, Qamar et al. [233] addressed uncertainties in two-level stochastic quantum systems and proposed a Lyapunov-based feedback control that is robust to decoherence and noise. Artemov and Kolyubin [234, 60] designed a two-stage motion control system for quantum key distribution with high precision.

Quantum advances have also been extended to communication and emotional intelligence. Secure quantum protocols have improved robot soccer performance [235], whereas the Quantum Emotion Space (QES) model [236] encodes emotions with lower computational cost and greater nuance, thereby enhancing human–robot interaction.

Quantum decision-making enhances the robustness of robotic systems, reducing mobile robot errors by 10% compared to classical control [237]. RQNNs improve the signal-to-noise ratio and classification accuracy off sEMG signals in robotic hands [238]. Hybrid approaches combine the quantum and classical methods. For instance, hierarchical Q-learning integrates reactive and deliberative navigation [239], and the combination of quantum and fuzzy logic enables Braitenberg vehicles to display complex emotions and autonomy [240]. At smaller scales, Levi [241] applied quantum field theory to synchronize molecular robots, whereas Itami et al. [242] emulated quantum dynamics and Brownian motion using macroscopic robots. Table 4 summarizes the achievements in quantum-enhanced control.

Table 4. Classification of the most critical research achievements on Quantum-Based Control in Robotics.

Reference	Environment/Task	Case Study	Model/Algorithm	Findings
[212]	Quantum-controlled Braitenberg vehicles	Braitenberg vehicles in simulated game scenarios	Quantum circuits incorporating entanglement and superposition	Effective game scenario navigation
[187]	Quantum-enhanced multi-agent robotic systems	Integration of quantum entanglement and quantum cryptography in robotic platforms	Quantum Multibody Dynamics	High-speed communication and control and immunity against cyberattacks
[215]	Navigation of quantum-controlled mobile robots	Field trials and numerical simulations with small mobile robots	Reverse fuzzy Hadamard operator for fuzzy control	Comparable performance between fuzzy and quantum controls
[218]	Trajectory tracking for continuum robots	Cable-driven continuum robots	Quantum Particle Swarm Optimization (QPSO) integrated with Model Predictive Control (MPC)	Reduced tracking error
[219]	Motion control in uncertain environments	ROBOTIS Open Manipulator	Evolving Type 2 Quantum Fuzzy Neural Network (ET2QFNN)	Superior performance in joint position control under non-parametric uncertainties
[139]	Path planning in dynamic environments	Two-wheeled soccer robot	Quantum Genetic Algorithm combined with fuzzy control	Global optimal path after 250 iterations
[237]	Mobile robot control	NXT Lego Robot in dynamic environments	Quantum decision-making control scheme	Fewer error sessions and improved robustness in uncertain environments
[238]	EMG-based robotic hand control	Shadow Robotics robot hand	Recurrent Quantum Neural Network (RQNN)	Improved classification accuracy
[232]	Global navigation of mobile robots	Mobile robot MT-R in an office building	Parallel Quantum Rapidly Exploring Random Trees (Pq-RRT)	Faster learning

[231]	UAV tracking control under wind disturbances	UAVs with VTOL system	Deep Deterministic Policy Gradient (DDPG) with quantum-inspired experience replay	High accuracy in tracking control
[239]	Autonomous robot navigation	Simulated and real-world robot navigation tasks	Hierarchical Q-learning algorithm (HQL)	Improved decision-making time
[234]	Alignment in quantum critical distribution systems	5-degree of freedom robot manipulator KUKA youBot	PD+ gravity controllers, computed-torque controllers, time-delay controllers	High precision positioning
[242]	Path tracking in controlled environments	Four simple robots in a closed planar space	Feedforward control with PD compensation	Effective emulation of Brownian motion and quantum dynamics

Advanced quantum control in robotics presents challenges, including the early stages of quantum integration, high resource demands, and limited interdisciplinary collaboration. Additional obstacles include rapid shifts in quantum computing and deep learning, reliance on specific datasets and solvers, high computational costs, error rates, stability issues in QNN-based controllers, accurate system modeling, and the complexity of tuning the quantum parameters. Addressing these issues is essential for real-world applications. Despite these hurdles, practical control strategies remain promising. Dahassa et al. [244] proposed a quantum sliding mode control (QSMC) framework that incorporated a qubit-inspired rotation angle into the nonlinear dynamics of a robotic arm. Fazilat and Zioui [245] introduced a quantum-inspired sliding mode control (Q-SMC) for a six-DOF ABB IRB140 arm by integrating quantum operators into the classical framework to minimize chattering, improve trajectory tracking, and reduce energy consumption.

7. DISCUSSION

Quantum computing and artificial intelligence are redefining how robotic systems perceive, learn, and adapt in the face of uncertainty. Their integration enables computations over exponentially large state spaces, offering faster convergence and greater adaptability than conventional AI methods. Although current progress remains uneven, simulation studies consistently demonstrate superior sample efficiency and lower energy consumption. Practical realization, however, is constrained by the limitations of noisy intermediate-scale quantum (NISQ) devices, algorithmic instability, and the absence of standardized benchmarking protocols. To consolidate existing evidence, the following subsections provide a comparative assessment of four major domains in quantum-enhanced robotics: Quantum Machine Learning, Quantum Neural Networks, Quantum-Inspired Algorithms, and Quantum-Enhanced Control, highlighting their computational advantages, scalability, and deployment readiness. Table 5 summarizes these characteristics.

Table 5. Comparative Assessment of Quantum AI Domains for Robotics.

Domain	Computational Advantage	Hardware Readiness & Feasibility	Scalability & Robustness	Real-Time Viability	Representative Use-Cases
QML	Demonstrated polynomial speed-ups in reinforcement and classification tasks; higher sample efficiency on small datasets	Early-stage quantum hardware; effective mainly through hybrid quantum-classical training	Moderate, limited by noise and circuit depth	Limited for onboard inference; feasible for cloud-assisted learning	Quantum reinforcement learning for swarm control, quantum-assisted policy optimization
QNNs	Higher representational power per parameter; efficient feature-space encoding	Prototype-level implementations; mostly simulated	Low–moderate; affected by gradient instability	Low; suitable for offline model refinement	Inverse kinematics, sensor fusion, adaptive perception
Quantum Algorithms	1.5–3× faster convergence and better global-optimum rates than classical metaheuristics	Fully executable on existing classical processors	Very high; deterministic and noise-free	High – real-time execution achievable	Real-time path planning, multi-robot task allocation, fault-tolerant optimization
Quantum Control Strategies	Probabilistic state estimation and gain tuning improve robustness by ≈10–20 % in nonlinear systems	Implemented through quantum-inspired mathematical models	High under stochastic and uncertain conditions	Medium–High – effective via classical emulation	Adaptive nonlinear control, dexterous manipulation, robust autonomous navigation

7.1 Comparative Interpretation

As illustrated in Table 5, the current landscape of quantum-enhanced robotics highlights both the potential and vulnerabilities of integrating quantum intelligence into practical robotic systems. Among the four domains, quantum-inspired algorithms demonstrate the highest level of applicability and stability, serving as a vital link between purely theoretical quantum computation and real-world robotic applications. Their ability to mathematically emulate quantum behavior enables efficient execution on conventional hardware, resulting in rapid convergence and reliable real-time optimization. In contrast, quantum machine learning and quantum neural networks represent the cutting edge of research, where the promise of significant advancements in learning and perception surpasses the practical capabilities of today's hardware. Meanwhile, quantum-enhanced control strategies serve a crucial intermediary role, effectively translating the theoretical advantages of quantum computation into adaptive, fault-tolerant mechanisms well-suited to modern robotic platforms.

7.2 Quantum Machine Learning

Quantum machine learning has garnered significant attention recently due to its potential to navigate large state spaces more efficiently than classical algorithms. In simulations, hybrid quantum-classical reinforcement learning models and quantum support vector methods have shown faster convergence and reduced sample complexity. However, their reliance on noisy intermediate-scale quantum processors remains a limiting factor for scalability and accuracy. As a result, quantum machine learning is currently best utilized as an offline training accelerator to enhance the learning phase of robotic agents rather than their execution phase. Quantum machine learning will likely focus on hybrid architectures, where quantum components facilitate exploratory policy discovery while classical systems handle inference and decision-making under time-sensitive constraints.

7.3 Quantum Neural Networks

Quantum neural networks (QNNs) enhance the capabilities of traditional models by embedding high-dimensional sensory information into quantum feature spaces, enabling greater representational power per parameter than classical deep networks. Preliminary studies indicate that QNNs can improve perception, classification, and inverse kinematics by compressing complex data into compact quantum states. However, despite this theoretical potential, challenges in optimization, such as gradient instability and barren-plateau effects, continue to hinder robust training. Additionally, limited access to fault-tolerant quantum devices has restricted current implementations to simulations or small-scale emulations. Nevertheless, hybrid QNN models present a promising avenue for perception-driven robotics, as quantum embeddings could eventually enhance classical sensor-fusion frameworks once mid-scale quantum hardware has developed further.

7.4 Quantum-Inspired Algorithms

In contrast, quantum-inspired algorithms offer concrete advantages, positioning them as the most practical family of quantum-related methods for robotic systems currently available. Techniques such as quantum particle swarm optimization and quantum genetic algorithms effectively blend stochastic exploration with deterministic convergence. This combination achieves superior global optimum rates while maintaining computational efficiency on classical processors. These methods have been successfully applied to trajectory optimization, multi-robot coordination, and fault-tolerant path replanning, consistently outperforming classical metaheuristics in both accuracy and energy efficiency. Their independence from physical qubits mitigates the fragility associated with current quantum hardware, making them particularly well-suited for industrial and embedded robotic applications. Therefore, quantum-inspired algorithms serve not just as a transitional technology but as a fundamental aspect of advancing quantum intelligence in robotics in the near term.

7.5 Quantum-Enhanced Control Strategies

Quantum-enhanced control strategies contribute to the field by integrating quantum-probabilistic reasoning with traditional control frameworks. Variants such as quantum sliding-mode control, quantum model-predictive control, and quantum PID leverage probabilistic gain tuning and quantum-inspired state estimation to achieve greater tracking precision and

improved disturbance rejection. These approaches have consistently demonstrated smoother actuation and reduced energy consumption compared to their classical equivalents, particularly in nonlinear or uncertain conditions. Although most of these systems are still implemented through classical emulation, their structural compatibility with existing embedded platforms makes them highly promising for near-term applications in adaptive and resilient robotic control.

7.6 Synthesis and Future Research Directions

These advancements mark a consistent, stepwise progression along the quantum-robot spectrum, with each field contributing a unique yet complementary role within the overall intelligence framework. At the core of this evolution are quantum-inspired algorithms, which offer immediate advantages in optimization and planning. Quantum machine learning and quantum neural networks represent the cutting edge of perception and autonomous learning. Simultaneously, quantum-enhanced control mechanisms ensure the robustness and stability required for effective real-world deployment.

The integration of these domains' points to hybrid architectures in which quantum and classical modules interact dynamically. In these frameworks, quantum layers facilitate high-level learning and adaptation, while classical systems maintain deterministic, real-time execution. This represents a highly credible and technically feasible pathway toward scalable, high-performance quantum-driven robotic intelligence in the upcoming decade.

A comparison across these fields indicates that quantum-inspired optimization remains the most practical approach for near-term robotic control. In contrast, quantum machine learning and neural models should be reserved strategically for data-intensive cloud-based training. Conversely, quantum-enhanced control mechanisms offer an experimental foundation for merging these paradigms into cohesive hybrid architectures that effectively balance adaptability and stability.

This trend is expected to continue, with new research concentrating on developing unifying frameworks that integrate quantum learning with quantum-inspired control, establishing standardized benchmarks, and creating reproducible simulation environments that connect quantum circuit emulators with robotic simulators. Success will depend not only on innovative algorithms but also on genuine interdisciplinary collaboration among roboticists, control engineers, and quantum computing experts. In summary, the evolution of quantum-enhanced robotics will hinge on advances in hardware and on the systematic alignment of algorithms, benchmarking standards, and control architectures. Thus, the convergence of quantum learning, optimization, and control constitutes the strategic axis of the field, which is further solidified and projected in the concluding section.

8. CONCLUSION

Recent advancements at the intersection of quantum computing and artificial intelligence are not just shaping, but fundamentally transforming the ways robotic systems acquire, process, and apply intelligence. This review has traced this profound transformation through four major domains: Quantum Machine Learning, Quantum Neural Networks, Quantum-Inspired Algorithms, and Quantum-Enhanced Control. Collectively, these domains herald a new era in

computational paradigm, one grounded in probabilistic reasoning rather than deterministic logic. The analysis presented here indicates that the field is not just in a transitional phase, but on the cusp of a quantum leap; theoretical frameworks and simulations have progressed sufficiently to inform deployable hybrid frameworks, yet several technical barriers must be overcome before truly quantum-driven autonomy becomes commonplace.

The key insight is that quantum-inspired algorithms are currently the most viable foundation for practical robotic implementation. These algorithms are paving the way for the future of robotic intelligence. Meanwhile, quantum learning and neural models represent the forefront of cognitive scalability, while quantum-enhanced control provides robustness and fault tolerance within existing architectures. Together, these elements outline a continuum where optimization, perception, and control converge.

Several implications arise from this synthesis. The future of robotic intelligence will rely on hybrid quantum-classical ecosystems that enable cooperative learning, optimization, and control. To advance, it is essential to establish reproducible frameworks, shared benchmarks, and standardized evaluation metrics to quantify quantum advantages effectively. While hardware maturity remains inconsistent, hybrid computation already allows for partial quantum benefits when tasks are distributed across emulators, cloud processors, and classical controllers. The focus of research should shift from abstract predictions of quantum supremacy to practical, application-specific enhancements in efficiency, adaptability, and energy performance.

A refined and practical roadmap for advancing this integration can be outlined across three developmental horizons. In the short term, consolidating quantum-inspired optimization and quantum-enhanced control on existing hardware will bolster reproducibility and facilitate real-time robotic deployment. The medium horizon should focus on developing scalable hybrid systems that incorporate authentic quantum modules for perception and learning while establishing standardized benchmarking protocols. In the long term, the objective evolves toward achieving complete symbiosis between quantum and classical co-processors, fostering the creation of self-optimizing robotic architectures governed by transparent, quantum-safe principles and ethical standards. These phases should be viewed not as rigid timelines but as sequential layers of technological maturity that guide ongoing progress.

The key takeaway is that the advancement of intelligent robotics relies less on flawless quantum hardware and more on the creative integration of quantum principles with classical engineering disciplines. Quantum-inspired methodologies serve as the operational foundation, quantum learning offers adaptability, and quantum-enhanced control guarantees stability. Together, these elements create a unified architecture that balances exploration with reliability, a hallmark of genuine intelligent behavior.

In conclusion, the cross-domain comparison indicates that integrating quantum computing and artificial intelligence in the robotics sector is currently the most viable approach to achieving real-time optimization on classical hardware. It is essential to prioritize Quantum Machine Learning (QML) and Quantum Neural Networks (QNNs) for offline, cloud-assisted learning until hardware advancements are realized. Additionally, Quantum Control provides a strong framework for harnessing quantum-inspired advantages on embedded platforms today. This

decision-making framework, which meticulously aligns algorithm selection with task requirements, latency and energy constraints, and robustness demands, serves as a tailored and efficient guide for future research and implementation in quantum-enabled robotics.

Data Availability: All data analyzed in this review are derived from publicly available databases and cited references.

Conflict of Interest: The authors declare no competing interests or financial relationships that could have influenced the work.

Funding: This research was funded by the Natural Sciences and Engineering Research Council of Canada (NSERC) for funding this research.

Authors contributions: MF contributed to methodology, investigation, formal analysis, writing and editing of the original draft, and visualization. NZ contributed to providing resources, supervision, project administration, formal analysis, writing, review, and editing of the original draft, funding acquisition.

Acknowledgement: The authors thank the Natural Sciences and Engineering Research Council of Canada (NSERC) for funding this research.

REFERENCES

1. Baklaga, L., Revolutionizing Sustainable Energy Production with Quantum Artificial Intelligence: Applications in Autonomous Robotics and Data Management. Green and Low-Carbon Economy, 2023. DOI: https://doi.org/10.47852/bonviewGLCE3202683
2. Cai, X.-D., et al., Entanglement-based machine learning on a quantum computer. Physical Review Letters, 2015. 114(11): p. 110504. DOI: https://doi.org/10.1103/PhysRevLett.114.110504
3. Abdelgaber, N. and C. Nikolopoulos. Overview on quantum computing and its applications in artificial intelligence. In 2020 IEEE Third International Conference on Artificial Intelligence and Knowledge Engineering (AIKE). 2020. IEEE. DOI: https://doi.org/10.1109/AIKE48582.2020.00038
4. Barral, D., Cardama, F.J., Diaz-Camacho, G., Faílde, D., Llovo, I.F., Mussa-Juane, M., Vázquez-Pérez, J., 2025, Review of distributed quantum computing: from single QPU to high performance quantum computing, Computer Science Review, 57, 100747. https://doi.org/10.1016/j.cosrev.2025.100747

5. Tandon, P., et al., Quantum robotics: A primer on current science and future perspectives. Springer, 2017. DOI: https://doi.org/10.1007/978-3-031-02520-4
6. Wichert, A., Principles of quantum artificial intelligence: quantum problem solving and machine learning. 2020: World Scientific. DOI: https://doi.org/10.1142/11938
7. Wichert, A., Quantum Artificial Intelligence with Qiskit. 2024: CRC Press. DOI: https://doi.org/10.1201/9781003374404
8. Chella, A., et al., A quantum planner for robot motion. Mathematics, 2022. 10(14): p. 2475. DOI: https://doi.org/10.3390/math10142475
9. Petschnigg, C., et al., Quantum computation in robotic science and applications. In 2019 International Conference on Robotics and Automation (ICRA). 2019. IEEE. DOI: https://doi.org/10.1109/ICRA.2019.8793768
10. Prakash, N., et al., Merging Minds and Machines: The Role of Advancing AI in Robotics. EAI Endorsed Transactions on Internet of Things, 2024. DOI: https://doi.org/10.4108/eetiot.4658
11. Gill, S.S., et al., Quantum computing: A taxonomy, systematic review and future directions. Software: Practice and Experience, 2022. 52(1): p. 66-114. DOI: https://doi.org/10.1002/spe.3039
12. Lamata, L., et al., Quantum mechatronics. Electronics, 2021. 10(20): p. 2483. https://doi.org/10.3390/electronics10202483
13. Lanza, D., P. Solinas, and F. Mastrogiovanni. Multi-sensory integration in a quantum-like robot perception model. in Experimental Robotics: The 17th International Symposium. 2021. Springer. https://doi.org/10.1007/978-3-030-71151-1_44
14. Moret-Bonillo, V., Can artificial intelligence benefit from quantum computing? Progress in Artificial Intelligence, 2015. 3: p. 89-105. https://doi.org/10.1007/s13748-014-0059-0
15. Dong, D., et al., Quantum robot: structure, algorithms and applications. Robotica, 2006. 24(4): p. 513-521. https://doi.org/10.1017/S0263574705002596
16. Bahel, V., Quantum Intelligent Systems: A Review. 2019. International Journal of Emerging Technology in Computer Science & Electronics (IJETCSE)ISSN: 0976-1353 Volume 26 Issue 3 – APRIL 2019.
17. Mahmoudi, Y., et al., A brief review on mathematical tools applicable to quantum computing for modelling and optimization problems in engineering. Emerging Science Journal, 2022. 7(1): p. 289-312. DOI: https://doi.org/10.28991/ESJ-2023-07-01-020
18. Mahmoudi, Y., N. Zioui, and H. Belbachir. Quantum Optimization in Engineering: A Brief Review. in 2023 International Conference on Decision Aid Sciences and Applications (DASA). 2023. IEEE. DOI: https://doi.org/10.1109/DASA59624.2023.10286779
19. Korenkov, V., A. Reshetnikov, and S. Ulyanov. Quantum Software Engineering Supremacy in Intelligent Robotics. in 2020 International Scientific and Technical Conference Modern Computer Network Technologies (MoNeTeC). 2020. IEEE. DOI: https://doi.org/10.1109/MoNeTeC49726.2020.9258000
20. Fernández Pérez, I., et al. Quantum AI: Achievements and Challenges in the Interplay of Quantum Computing and Artificial Intelligence. in International Symposium on Ambient Intelligence. 2022. Springer. https://doi.org/10.1007/978-3-031-22356-3_15

21. Haldorai, A., Advancements and Applications of Quantum Computing in Robotics. Journal of Computing and Natural Science, 2024. 053(063). Doi: https://doi.org/10.53759/181X/JCNS202404006
22. Metzler, T.A., L.M. Lewis, and L.C. Pope, Could robots become authentic companions in nursing care? Nursing Philosophy, 2016. 17(1): p. 36-48. https://doi.org/10.1111/nup.12101
23. Mallow, G.M., et al., Quantum computing: the future of big data and artificial intelligence in spine. Spine Surgery and Related Research, 2022. 6(2): p. 93-98. https://doi.org/10.22603/ssrr.2021-0251
24. Ferreira, J.F., et al., Sensing and Artificial Perception for Robots in Precision Forestry: A Survey. Robotics, 2023. 12(5): p. 139. https://doi.org/10.3390/robotics12050139
25. Said, D., Quantum computing and machine learning for cybersecurity: Distributed denial of service (DDoS) attack detection on smart micro-grid. Energies, 2023. 16(8): p. 3572. https://doi.org/10.3390/en16083572
26. dos Santos Gonçalves, C.P., Quantum neural machine learning: Theory and experiments. Machine Learning in Medicine and Biology, 2019: p. 95-115. https://doi.org/10.5772/intechopen.84149
27. H. Hohenfeld, D. Heimann, F. Wiebe and F. Kirchner, "Quantum Deep Reinforcement Learning for Robot Navigation Tasks," in IEEE Access, vol. 12, pp. 87217-87236, 2024. https://doi.org/10.1109/ACCESS.2024.3417808
28. Dunjko, V., J.M. Taylor, and H.J. Briegel. Advances in quantum reinforcement learning. in 2017 IEEE international conference on systems, man, and cybernetics (SMC). 2017. IEEE. https://doi.org/10.1109/SMC.2017.8122616
29. Gabor, T., et al. The holy grail of quantum artificial intelligence: major challenges in accelerating the machine learning pipeline. in Proceedings of the IEEE/ACM 42nd international conference on software engineering workshops. 2020. https://doi.org/10.1145/3387940.3391469
30. Dunjko, V., J.M. Taylor, and H.J. Briegel, Quantum-enhanced machine learning. Physical review letters, 2016. 117(13): p. 130501. DOI: https://doi.org/10.1103/PhysRevLett.117.130501
31. Dunjko, V. and P. Wittek, A non-review of quantum machine learning: trends and explorations. Quantum Views, 2020. 4: p. 32. DOI: https://doi.org/10.22331/qv-2020-03-17-32
32. Dunjko, V., & Briegel, H. J. (2018). Machine learning & artificial intelligence in the quantum domain: a review of recent progress. Reports on Progress in Physics, 81(7), 074001. https://doi.org/10.1088/1361-6633/aab406
33. Alchieri, L., et al., An introduction to quantum machine learning: from quantum logic to quantum deep learning. Quantum Machine Intelligence, 2021. 3(2): p. 28. https://doi.org/10.1007/s42484-021-00056-8
34. Valdez, F. and P. Melin, A review on quantum computing and deep learning algorithms and their applications. Soft Computing, 2023. 27(18): p. 13217-13236. https://doi.org/10.1007/s00500-022-07037-4

35. Satuluri, V.R. and V. Ponnusamy. Quantum-enhanced machine learning. in 2021 Smart Technologies, Communication and Robotics (STCR). 2021. IEEE. https://doi.org/10.1109/STCR51658.2021.9589016
36. Maltare, A., et al., Quantum Computing to the Advantage of Neural Network. Quantum Computing in Cybersecurity, 2023: p. 249-261. https://doi.org/10.1002/9781394167401.ch15
37. Vasuki, M., et al., Overview of Quantum Computing in Quantum Neural Network and Artificial Intelligence. 2023. https://doi.org/10.54368/qijirse.2.2.0013
38. Chen, J., L. Wang, and E. Charbon, A quantum-implementable neural network model. Quantum information processing, 2017. 16: p. 1-24. https://doi.org/10.1007/s11128-017-1692-x
39. Khonina, S.N., et al., Exploring Types of Photonic Neural Networks for Imaging and Computing—A Review. Nanomaterials, 2024. 14(8): p. 697. https://doi.org/10.3390/nano14080697
40. Maeda, Y., T. Fujiwara, and H. Ito. Robot control using high dimensional neural networks. in 2014 Proceedings of the SICE annual conference (SICE). 2014. IEEE. DOI: https://doi.org/10.1109/SICE.2014.6935220
41. Zhao, J., et al., Building quantum neural networks based on a swap test. Physical Review A, 2019. 100(1): p. 012334. DOI: https://doi.org/10.1103/PhysRevA.100.012334
42. Zhong, Y.-h. and C.-q. Yuan, Analysis of quantum neural network learning ability. Appl. Math, 2013. 7(2L): p. 679-683. http://dx.doi.org/10.12785/amis/072L43
43. Li, J., Quantum-inspired neural networks with application. Open Journal of Applied Sciences, 2015. 5(06): p. 233. DOI: https://doi.org/10.4236/ojapps.2015.56024
44. Gao, L., et al., An advanced quantum optimization algorithm for robot path planning. Journal of Circuits, Systems and Computers, 2020. 29(08): p. 2050122. https://doi.org/10.1142/S0218126620501224
45. Zioui, N., et al., A novel quantum-computing-based quaternions model for a robotic arm position. International Journal of Computational Intelligence in Control, 2021. 13(2): p. 71-77. DOI: https://doi.org/10.5281/zenodo.14787897
46. Zioui, N., et al., A New Quantum-computing-based Algorithm for Robotic Arms and Rigid Bodies' Orientation. Journal of Applied and Computational Mechanics, 2021. 7(3): p. 1836-1846. https://doi.org/10.22055/jacm.2021.37611.3048
47. Zioui, N., A. Mahmoudi, and M. Tadjine, Representing quantum spins in different coordinate systems for modelling rigid body orientation. Karbala International Journal of Modern Science, 2023. 9(3): p. 11. https://doi.org/10.33640/2405-609X.3313
48. Cisek, G., Triumph of Artificial Intelligence. 2021: Springer. https://doi.org/10.1007/978-3-658-34896-0
49. Córcoles, A.D., et al., Challenges and opportunities of near-term quantum computing systems. Proceedings of the IEEE, 2019. 108(8): p. 1338-1352. DOI: https://doi.org/10.1109/JPROC.2019.2954005
50. Cerezo, M., et al., Variational quantum algorithms. Nature Reviews Physics, 2021. 3(9): p. 625-644. https://doi.org/10.1038/s42254-021-00348-9

51. Adelomou, P. A. (2022). *Quantum algorithms for solving hard constrained optimization problems* (Doctoral dissertation, Universitat Ramon Llull. https://doi.org/10.13140/RG.2.2.22589.54245
52. Stolfi, D.H. and G. Danoy, Evolutionary swarm formation: From simulations to real world robots. Engineering Applications of Artificial Intelligence, 2024. 128: p. 107501. https://doi.org/10.1016/j.engappai.2023.107501
53. West, M.T., et al., Towards quantum enhanced adversarial robustness in machine learning. Nature Machine Intelligence, 2023. 5(6): p. 581-589. https://doi.org/10.1038/s42256-023-00661-1
54. Ur Rasool, R., et al., Quantum computing for healthcare: A review. Future Internet, 2023. 15(3): p. 94. https://doi.org/10.3390/fi15030094
55. Zioui, N., et al., Quantum computing based state domain equations and feedback control. Results in Applied Mathematics, 2023. 19: p. 100385. https://doi.org/10.1016/j.rinam.2023.100385
56. Zioui, N., A. Mahmoudi, and M. Tadjine, Design of a new hybrid linearising-backstepping controller using quantum state equations and quantum spins. International Journal of Automation and Control, 2023. 17(4): p. 397-417. https://doi.org/10.1504/IJAAC.2023.131754
57. Herrington, V. and O. Adedeji, At the intersection of medical robotic surgery and drug discovery with quantum computing. Authorea Preprints, 2023. DOI: https://doi.org/10.33140/JEEE.02.03.10
58. Dutta, A. and A. Pathak, Controlled secure direct quantum communication inspired scheme for quantum identity authentication. Quantum Information Processing, 2022. 22(1): p. 13. https://doi.org/10.1007/s11128-022-03767-4
59. Yu, B., et al., A dead reckoning calibration scheme based on optimization with an adaptive quantum-inspired evolutionary algorithm for vehicle self-localization. Entropy, 2022. 24(8): p. 1128. https://doi.org/10.3390/e24081128
60. Shevchenko, A.A., et al., Cognitive robust control system based on quantum fuzzy inference algorithm in unconventional intelligent robotics. Нечеткие системы и мягкие вычисления, 2023. 18(1): p. 28-46. DOI: https://doi.org/10.26456/fssc93
61. Kagan, E. and I. Ben-Gal, Navigation of quantum-controlled mobile robots. Recent advances in mobile robotics, 2011. 15: p. 311-220. DOI: https://doi.org/10.5772/25944
62. N. Binandeh Dehaghani, A. Pedro Aguiar and R. Wisniewski, "State Estimation and Control for Stochastic Quantum Dynamics With Homodyne Measurement: Stabilizing Qubits Under Uncertainty," in IEEE Access, vol. 12, pp. 124729-124739, 2024, https://doi.org/10.1109/ACCESS.2024.3455170
63. Abd. Ghafar, A.N., et al. Intelligent Machining Systems for Robotic End-Effectors: State-of-the-Art and Toward Future Directions. in Innovative Manufacturing, Mechatronics & Materials Forum. 2023. Springer. https://doi.org/10.1007/978-981-99-8819-8_7
64. Fazilat, M., N. Zioui, and J. St-Arnaud, A novel quantum model of forward kinematics based on quaternion/Pauli gate equivalence: Application to a six-jointed industrial robotic arm. Results in Engineering, 2022. 14: p. 100402. https://doi.org/10.1016/j.rineng.2022.100402

65. Fazilat, M., Modélisation avancée et commande d'un bras robot manipulateur industriel= Advanced modelling and control of industrial robotic manipulator arm. 2022, Université du Québec à Trois-Rivières. https://depot-e.uqtr.ca/id/eprint/10597
66. Fazilat, M. and N. Zioui, The Impact of Simplifications of the Dynamic Model on the Motion of a Six-Jointed Industrial Articulated Robotic Arm Movement. Journal of Robotics and Control (JRC), 2024. 5(1): p. 173-186. DOI: https://doi.org/10.18196/jrc.v5i1.20263
67. Saidat, S., et al., Quantum pulse-width modulation design and implementation for a DC motor drive. Quantum Information Processing, 2024. 23(3): p. 1-24. https://doi.org/10.1007/s11128-024-04284-2
68. Mahmoudi, Y., N. Zioui, and H. Belbachir, A new quantum-inspired clustering method for reducing energy consumption in IOT networks. Internet of Things, 2022. 20: p. 100622. https://doi.org/10.1016/j.iot.2022.100622
69. El Amine Boudjoghra, M., et al., State-Domain Equations and Their Quantum Computing Solution Based HHL Algorithm. Mathematical Modelling of Engineering Problems, 2022. 9(4). https://doi.org/10.18280/mmep.090404
70. Mahmoudi, Y., N. Zioui, and H. Belbachir. Comparison between Conventional and Quantum-Based P-Median Optimization for Energy Consumption in Iot Networks. in 2023 International Conference on Engineering and Emerging Technologies (ICEET). 2023. IEEE. DOI: https://doi.org/10.1109/ICEET60227.2023.10526003
71. Khoshnoud, F. and M. Ghazinejad. Automated quantum entanglement and cryptography for networks of robotic systems. in International Design Engineering Technical Conferences and Computers and Information in Engineering Conference. 2021. American Society of Mechanical Engineers. https://doi.org/10.1115/DETC2021-71653
72. Amir-Behghadami, M. and A. Janati, Population, Intervention, Comparison, Outcomes and Study (PICOS) design as a framework to formulate eligibility criteria in systematic reviews. Emergency Medicine Journal, 2020. https://doi.org/10.1136/emermed-2020-209567
73. Borrego, M., M.J. Foster, and J.E. Froyd, Systematic literature reviews in engineering education and other developing interdisciplinary fields. Journal of Engineering Education, 2014. 103(1): p. 45-76. https://doi.org/10.1002/jee.20038
74. Frandsen, T.F., et al., Using the full PICO model as a search tool for systematic reviews resulted in lower recall for some PICO elements. Journal of clinical epidemiology, 2020. 127: p. 69-75. https://doi.org/10.1016/j.jclinepi.2020.07.005
75. Robinson, K.A., I.J. Saldanha, and N.A. Mckoy, Development of a framework to identify research gaps from systematic reviews. Journal of clinical epidemiology, 2011. 64(12): p. 1325-1330. https://doi.org/10.1016/j.jclinepi.2011.06.009
76. Silva, É.R., R. Bartholo, and D. Proença, Managing the state of the art of engineering: Learning from medicine. The Future of Engineering: Philosophical Foundations, Ethical Problems and Application Cases, 2018: p. 217-227. https://doi.org/10.1007/978-3-319-91029-1_15

77. Dong, D., et al., Quantum reinforcement learning. IEEE Transactions on Systems, Man, and Cybernetics, Part B (Cybernetics), 2008. 38(5): p. 1207-1220. DOI: https://doi.org/10.1109/TSMCB.2008.925743
78. Buffoni, L. and F. Caruso, New trends in quantum machine learning (a). Europhysics letters, 2021. 132(6): p. 60004. DOI: https://doi.org/10.1209/0295-5075/132/60004
79. Lamata, L., Quantum machine learning and quantum biomimetics: A perspective. Machine Learning: Science and Technology, 2020. 1(3): p. 033002. https://doi.org/10.1088/2632-2153/ab9803
80. Ramezani, S.B., et al. Machine learning algorithms in quantum computing: A survey. in 2020 International joint conference on neural networks (IJCNN). 2020. IEEE. https://doi.org/10.1109/IJCNN48605.2020.9207714
81. Yun, W.J., et al., Quantum Multi-Agent Actor-Critic Neural Networks for Internet-Connected Multi-Robot Coordination in Smart Factory Management. IEEE Internet of Things Journal, 2023. https://doi.org/10.1109/JIOT.2023.3234911
82. Tandon, P., et al., Machine Learning Mechanisms for Quantum Robotics, in Quantum Robotics: A Primer on Current Science and Future Perspectives. 2017, Springer. p. 47-73. https://doi.org/10.1007/978-3-031-02520-4_5
83. Chatzis, S.P., D. Korkinof, and Y. Demiris, A quantum-statistical approach toward robot learning by demonstration. IEEE Transactions on Robotics, 2012. 28(6): p. 1371-1381. https://doi.org/10.1109/TRO.2012.2203055
84. Ulyanov, S.V. Quantum fuzzy inference based on quantum genetic algorithm: quantum simulator in intelligent robotics. in International Conference on Theory and Application of Soft Computing, Computing with Words and Perceptions. 2019. Springer. https://doi.org/10.1007/978-3-030-35249-3_9
85. Ulyanov, S.V., Quantum algorithm of imperfect kb self-organization pt i: smart control-information-thermodynamic bounds. Artificial Intelligence Advances, 2021. 3(2): p. 13-36. https://doi.org/10.30564/aia.v3i2.3171
86. Shill, P.C., et al. Optimization of interval type-2 fuzzy logic controller using quantum genetic algorithms. in 2012 IEEE International Conference on Fuzzy Systems. 2012. IEEE. https://doi.org/10.1109/FUZZ-IEEE.2012.6251207
87. Motroni, A., et al., A UHF-RFID multi-antenna sensor fusion enables item and robot localization. IEEE Journal of Radio Frequency Identification, 2022. 6: p. 456-466. https://doi.org/10.1109/JRFID.2022.3166354
88. Hu, Y., et al., Quantum-enhanced reinforcement learning for control: A preliminary study. Control Theory and Technology, 2021. 19: p. 455-464. https://doi.org/10.1007/s11768-021-00063-x
89. Niu, M. Y., Boixo, S., Smelyanskiy, V. N., & Neven, H. (2019). Universal quantum control through deep reinforcement learning. npj Quantum Information, 5(1), 33. https://doi.org/10.1038/s41534-019-0141-3
90. Ali, N. and A. Jima, Integrating Deep Learning, Quantum Computing, and Machine Learning for Enhanced Cybersecurity and Human-Robot Collaboration. 2025. https://doi.org/10.13140/RG.2.2.19303.76962
91. Taghavi, M. and R. Farnoosh, Quantum computing and neuromorphic computing for safe, reliable, and explainable multi-agent reinforcement learning: Optimal control in

autonomous robotics. Iran Journal of Computer Science, 2025: p. 1-17. https://doi.org/10.1007/s42044-025-00306-z

92. Cheng, B., et al., Noisy intermediate-scale quantum computers. Frontiers of Physics, 2023. 18(2): p. 21308. https://doi.org/10.1007/s11467-022-1249-z
93. Brandhofer, S., et al. Special session: Noisy intermediate-scale quantum (NISQ) computers—How they work, how they fail, how to test them? in 2021 IEEE 39th VLSI Test Symposium (VTS). 2021. IEEE. https://doi.org/10.1109/VTS50974.2021.9441047
94. Acampora, G., et al., D-NISQ: a reference model for distributed noisy intermediate-scale quantum computers. Information Fusion, 2023. 89: p. 16-28. https://doi.org/10.1016/j.inffus.2022.08.003
95. Patel, T. and D. Tiwari. Veritas: accurately estimating the correct output on noisy intermediate-scale quantum computers. in SC20: International Conference for High Performance Computing, Networking, Storage and Analysis. 2020. IEEE. https://doi.org/10.1109/SC41405.2020.00019
96. Bar, N.F., H. Yetis, and M. Karakose. An approach based on quantum reinforcement learning for navigation problems. in 2022 International Conference on Data Analytics for Business and Industry (ICDABI). 2022. IEEE. https://doi.org/10.1109/ICDABI56818.2022.10041570
97. Pappala, L. K., Veesam, S. B., Chattu, K., Krishna, J. V., Bodapati, J. D., & Rao, B. T. (2025). Design of an iterative model for incremental enhancements in quantum image processing using reinforcement learning based optimizations. IEEE Access. https://doi.org/10.1109/ACCESS.2025.3531407
98. Raval, A. and R. Oza, Advancing AI with Quantum Computing: Synergies Between Quantum Neural Networks and Quantum Reinforcement Learning, in Quantum Machine Learning in Industrial Automation. 2025, Springer. p. 305-332. https://doi.org/10.1007/978-3-031-99786-0_14
99. Shahid, M. and M.A. Hassan, Introducing Quantum Variational Circuit for Efficient Management of Common Pool Resources. IEEE Access, 2023. https://doi.org/10.1109/ACCESS.2023.3322144
100. Seetohul, V., et al., Quantum Reinforcement Learning: Advancing AI Agents Through Quantum Computing, in Space Law Principles and Sustainable Measures. 2024, Springer. p. 55-73. https://doi.org/10.1007/978-3-031-64045-2_4
101. Teixeira E., Inácio Y. and Bezerra P. (2025). Applying Quantum Tensor Networks in Machine Learning: A Systematic Literature Review. In Proceedings of the 17th International Conference on Agents and Artificial Intelligence - Volume 1: QAIO; ISBN 978-989-758-737-5, SciTePress, pages 847-854. https://doi.org/10.5220/0013402100003890
102. Mamaeva, A.A., A.V. Shevchenko, and S.V. Ulyanov, Human being emotion in cognitive intelligent robotic control Pt I: quantum/soft computing approach. Artificial Intelligence Advances, 2020. 2(1): p. 1-30. DOI: https://doi.org/10.37005/2071-9612-2019-4-87-131
103. Mohan, A., S. Jayabalan, and A. Mohan. Autonomous quantum reinforcement learning for robot navigation. in Proceedings of 2nd International Conference on Intelligent

Computing and Applications: ICICA 2015. 2017. Springer. https://doi.org/10.1007/978-981-10-1645-5_29

104. Granda, J.M., et al., Controlling an organic synthesis robot with machine learning to search for new reactivity. Nature, 2018. 559(7714): p. 377-381. https://doi.org/10.1038/s41586-018-0307-8
105. Reshetnikov, A. and S. Ulyanov, Quantum Algorithm of Imperfect KB Self-organization. Pt II: Robotic Control with Remote Knowledge Base Exchange. Artificial Intelligence Advances, 2021. 3(2): p. 44-70. https://doi.org/10.30564/aia.v3i2.3849
106. Luo, C., et al., Biologically inspired intelligence with applications on robot navigation. Artificial Intelligence-Emerging Trends and Applications, 2018. https://doi.org/10.5772/intechopen.75692
107. X. Jiang, Q. Zhang, J. Sun, J. Cao, J. Ma and R. Xu, "Fully Spiking Neural Network for Legged Robots," ICASSP 2025 - 2025 IEEE International Conference on Acoustics, Speech and Signal Processing (ICASSP), Hyderabad, India, 2025, pp. 1-5. https://doi.org/10.1109/ICASSP49660.2025.10890793
108. Zhou, M.-G., et al., Quantum neural network for quantum neural computing. Research, 2023. 6: p. 0134. https://doi.org/10.34133/research.0134
109. Mielke, A. and T. Ricken, Evaluating artificial neural networks and quantum computing for mechanics. Pamm, 2019. 19(1): p. e201900470. https://doi.org/10.1002/pamm.201900470
110. Nomura, Y., Boltzmann machines and quantum many-body problems. Journal of Physics: Condensed Matter, 2023. 36(7): p. 073001. https://doi.org/10.1088/1361-648X/ad0916
111. Lu, Z., P.-X. Shen, and D.-L. Deng, Markovian quantum neuroevolution for machine learning. Physical Review Applied, 2021. 16(4): p. 044039. DOI: https://doi.org/10.1103/PhysRevApplied.16.044039
112. Fazilat, M. and N. Zioui, Investigating Quantum Artificial Neural Networks for singularity avoidance in robotic manipulators 2024 12th International Conference on Systems and Control (ICSC). 2024, IEEE. https://doi.org/10.1109/ICSC63929.2024.10928865
113. Dunjko, V. and H.J. Briegel, Machine learning & artificial intelligence in the quantum domain: a review of recent progress. Reports on Progress in Physics, 2018. 81(7): p. 074001. https://doi.org/10.1088/1361-6633/aab406
114. Carrasquilla, J. (2020). Machine learning for quantum matter. Advances in Physics: X, 5(1), 1797528. https://doi.org/10.1080/23746149.2020.1797528
115. Vercellino, C., et al. Neural optimization for quantum architectures: graph embedding problems with Distance Encoder Networks. in 2023 IEEE 47th Annual Computers, Software, and Applications Conference (COMPSAC). 2023. IEEE. https://doi.org/10.1109/COMPSAC57700.2023.00058
116. Stone, D.G. and C. Bradac, Machine and quantum learning for diamond-based quantum applications. Materials for Quantum Technology, 2023. 3(1): p. 012001. https://doi.org/10.1088/2633-4356/acb30a

117. Massoli, F.V., et al., A leap among quantum computing and quantum neural networks: A survey. ACM Computing Surveys, 2022. 55(5): p. 1-37. https://doi.org/10.1145/3529756
118. Numbi, J., M. Fazilat, and N. Zioui, A Quantum-Inspired Hybrid Artificial Neural Network for Identifying the Dynamic Parameters of Mobile Car-Like Robots. Mathematics, 2025. 13(17): p. 2856. https://doi.org/10.3390/math13172856
119. Azuma, K., et al., Tools for quantum network design. AVS Quantum Science, 2021. 3(1). https://doi.org/10.1116/5.0024062
120. Fazilat, M. and N. Zioui, Quantum Neural Network-based Inverse Kinematics of a Six-jointed Industrial Robotic Arm. Robotics and Autonomous Systems, 2025: p. 105123. https://doi.org/10.1016/j.robot.2025.105123
121. Takahashi, K., M. Kurokawa, and M. Hashimoto, Multi-layer quantum neural network controller trained by real-coded genetic algorithm. Neurocomputing, 2014. 134: p. 159-164. https://doi.org/10.1016/j.neucom.2012.12.073
122. Hanna, Y.F., et al., Real time adaptive PID controller based on quantum neural network for nonlinear systems. Engineering Applications of Artificial Intelligence, 2023. 126: p. 106952. https://doi.org/10.1016/j.engappai.2023.106952
123. Sciuto, G.L., et al. Neural network developed for obstacle avoidance of the four wheeled electric vehicle. in 2023 30th IEEE International Conference on Electronics, Circuits and Systems (ICECS). 2023. IEEE. https://doi.org/10.1109/ICECS58634.2023.10382857
124. Bayro-Corrochano, E., et al., Quaternion spiking and quaternion quantum neural networks: Theory and applications. International Journal of Neural Systems, 2021. 31(02): p. 2050059. https://doi.org/10.1142/S0129065720500598
125. Prado, A., H. Zhang, and S.K. Agrawal. Artificial neural networks to solve forward kinematics of a wearable parallel robot with semi-rigid links. in 2021 IEEE International Conference on Robotics and Automation (ICRA). 2021. IEEE. https://doi.org/10.1109/ICRA48506.2021.9561246
126. Lechuga-Gutiérrez, L., J. Medrano-Hermosillo, and E. Bayro-Corrochano. Quaternion spiking neural networks control for robotics. in 2018 IEEE Latin American Conference on Computational Intelligence (LA-CCI). 2018. IEEE. https://doi.org/10.1109/LA-CCI.2018.8625208
127. Pandey, H.M., A. Layeb, and D. Windridge, Special Issue on Quantum Inspired Neural Networks for Engineering Optimization. Neural Processing Letters, 2023. 55(4): p. 3811-3812. https://doi.org/10.1007/s11063-023-11298-x
128. Nivelkar, M. and S. Bhirud. Optimized machine learning: training and classification performance using quantum computing. in 2021 IEEE 6th International Conference on Computing, Communication and Automation (ICCCA). 2021. IEEE. https://doi.org/10.1109/ICCCA52192.2021.9666429
129. Srinivasulu, S. and G. Nagarajan, A Brief Survey on Efficient Models for Qubits Encoding Using Quantum Machine Learning With Multi Level Time Series Data Classification. 2023 Innovations in Power and Advanced Computing Technologies (i-PACT), 2023: p. 1-8. https://doi.org/10.1109/i-PACT58649.2023.10434762

130. Zhang, Z., et al., MR-DRO: A fast and efficient task offloading algorithm in heterogeneous edge/cloud computing environments. IEEE Internet of Things Journal, 2021. 10(4): p. 3165-3178. https://doi.org/10.1109/JIOT.2021.3126101
131. Rudolph, M.S., et al., Decomposition of matrix product states into shallow quantum circuits. Quantum Science and Technology, 2023. 9(1): p. 015012. https://doi.org/10.1088/2058-9565/ad04e6
132. Deshpande, A. and A. Melnikov, Capturing symmetries of quantum optimization algorithms using graph neural networks. Symmetry, 2022. 14(12): p. 2593. https://doi.org/10.3390/sym14122593
133. Zhang, X., et al., Digital quantum simulation of Floquet symmetry-protected topological phases. Nature, 2022. 607(7919): p. 468-473. https://doi.org/10.1038/s41586-022-04854-3
134. Du, W., et al., Real time neural network path planning algorithm for robot. Int. J. Front. Eng. Technol, 2021. 3: p. 53. https://doi.org/10.25236/IJFET.2021.030507
135. Bae, H., et al., Multi-robot path planning method using reinforcement learning. Applied sciences, 2019. 9(15): p. 3057. https://doi.org/10.3390/app9153057
136. da Silva, A.J. and R.L.F. de Oliveira. Neural networks architecture evaluation in a quantum computer. in 2017 Brazilian Conference on Intelligent Systems (BRACIS). 2017. IEEE. https://doi.org/10.1109/BRACIS.2017.33
137. Fan, Z. Multi-Point path planning for robots based on deep reinforcement learning. in Journal of Physics: Conference Series. 2023. IOP Publishing. https://doi.org/10.1088/1742-6596/2580/1/012048
138. Xin, J., et al. Application of deep reinforcement learning in mobile robot path planning. in 2017 Chinese Automation Congress (CAC). 2017. IEEE. https://doi.org/10.1109/CAC.2017.8244061
139. Yang, X., Fuzzy Control Path Planning of Soccer Robot Relying on Quantum Genetic Algorithm. Mobile Information Systems, 2022. 2022. https://doi.org/10.1155/2022/3498258
140. Takahashi, K., Comparison of neural network–based adaptive controllers using hypercomplex numbers for controlling robot manipulator. IFAC-PapersOnLine, 2019. 52(29): p. 67-72. https://doi.org/10.1016/j.ifacol.2019.12.623
141. Pusuluri, V.B., et al. Shaping the Future of Logistics: Quantum-Inspired Optimization for Autonomous Deliveries. in 2025 6th International Conference on Control, Communication and Computing (ICCC). 2025. IEEE. https://doi.org/10.1109/ICCC64910.2025.11077310
142. Qian, Q., J. Wu, and Z. Wang, Optimal path planning for two-wheeled self-balancing vehicle pendulum robot based on quantum-behaved particle swarm optimization algorithm. Personal and Ubiquitous Computing, 2019. 23: p. 393-403. https://doi.org/10.1007/s00779-019-01216-1
143. Fazilat, M. and N. Zioui, Quantum Particle Swarm Optimization (QPSO)-Based Enhanced Dynamic Model Parameters Identification for an Industrial Robotic Arm. Mathematics, 2025. 13(16): p. 2631. https://doi.org/10.3390/math13162631
144. Maity, R., R. Mishra, and P.K. Pattnaik, Analysis of Path Finding Techniques for Flying Robots through Intelligent Decision-Making Algorithms in Quantum Inspired

Computing Environment. Wireless Personal Communications, 2024. 135(3): p. 1561-1580. https://doi.org/10.1007/s11277-024-11125-z

145. Yu, Z., et al. A quantum-inspired ant colony optimization for robot coalition formation. in 2009 Chinese Control and Decision Conference. 2009. IEEE. https://doi.org/10.1109/CCDC.2009.5194884
146. Priyadarshini, I., Swarm-intelligence-based quantum-inspired optimization techniques for enhancing algorithmic efficiency and empirical assessment. Quantum Machine Intelligence, 2024. 6(2): p. 69. https://doi.org/10.1007/s42484-024-00201-z
147. Chella, A., et al., Quantum planning for swarm robotics. Robotics and Autonomous Systems, 2023. 161: p. 104362. https://doi.org/10.1016/j.robot.2023.104362
148. Lathrop, P., B. Boardman, and S. Martínez, Parallel Quantum Rapidly-Exploring Random Trees. IEEE Access, 2024. https://doi.org/10.1109/ACCESS.2024.3383313
149. Xue, T., et al., Trajectory planning for autonomous mobile robot using a hybrid improved QPSO algorithm. Soft Computing, 2017. 21: p. 2421-2437. https://doi.org/10.1007/s00500-015-1956-2
150. Yuan, J., Hierarchical motion planning for multisteering tractor–trailer mobile robots with on-axle hitching. IEEE/ASME transactions on mechatronics, 2017. 22(4): p. 1652-1662. https://doi.org/10.1109/TMECH.2017.2695651
151. Yin, F., et al., An improved QPSO-SVM-based approach for predicting the milling force for white marble in robot stone machining. Journal of Intelligent & Fuzzy Systems, 2021. 41(1): p. 1589-1609. https://doi.org/10.3233/JIFS-210430
152. Smith, J.A., D. Zhang, and K.C. Balram, Robotic Vectorial Field Alignment for Spin-Based Quantum Sensors. Advanced Science, 2024. 11(2): p. 2304449. https://doi.org/10.1002/advs.202304449
153. Jhang, J.-Y., et al., Navigation control of mobile robots using an interval type-2 fuzzy controller based on dynamic-group particle swarm optimization. International Journal of Control, Automation and Systems, 2018. 16(5): p. 2446-2457. https://doi.org/10.1007/s12555-017-0156-5
154. Luo, L., et al., Trajectory Planning in Robot Joint Space Based on Improved Quantum Particle Swarm Optimization Algorithm. Applied Sciences, 2023. 13(12): p. 7031. https://doi.org/10.3390/app13127031
155. Xu, R., et al., A hybrid improved-whale-optimization–simulated-annealing algorithm for trajectory planning of quadruped robots. Electronics, 2023. 12(7): p. 1564. https://doi.org/10.3390/electronics12071564
156. Dian, S., et al., A smooth path planning method for mobile robot using a BES-incorporated modified QPSO algorithm. Expert Systems with Applications, 2022. 208: p. 118256. https://doi.org/10.1016/j.eswa.2022.118256
157. Fernandes, P.B., R. Oliveira, and J.F. Neto, Trajectory planning of autonomous mobile robots applying a particle swarm optimization algorithm with peaks of diversity. Applied Soft Computing, 2022. 116: p. 108108. https://doi.org/10.1016/j.asoc.2021.108108
158. Fernandes, P.B., R.C.L. De Oliveira, and J.V.F. Neto. A modified QPSO for robotic vehicle path planning. in 2018 IEEE Congress on Evolutionary Computation (CEC). 2018. IEEE. https://doi.org/10.1109/CEC.2018.8477681

159. Chen, Z. and W. Zhou, Path planning for a space-based manipulator system based on quantum genetic algorithm. Journal of Robotics, 2017. 2017. https://doi.org/10.1155/2017/3207950
160. Li, Z., et al., Path planning method for AUV docking based on adaptive quantum-behaved particle swarm optimization. IEEE Access, 2019. 7: p. 78665-78674. https://doi.org/10.1109/ACCESS.2019.2922689
161. Yao, J., et al., Minimum-time trajectory planning for an inchworm-like climbing robot based on quantum-behaved particle swarm optimization. Proceedings of the Institution of Mechanical Engineers, Part C: Journal of Mechanical Engineering Science, 2017. 231(18): p. 3443-3454. https://doi.org/10.1177/0954406216646138
162. Kim, Y.-H. and J.-H. Kim. Multiobjective quantum-inspired evolutionary algorithm for fuzzy path planning of mobile robot. in 2009 IEEE Congress on Evolutionary Computation. 2009. IEEE. https://doi.org/10.1109/CEC.2009.4983080
163. Jiao, M.-h., et al. Path planning of escort robot based on improved quantum particle swarm optimization. in 2019 Chinese Control And Decision Conference (CCDC). 2019. IEEE. https://doi.org/10.1109/CCDC.2019.8833185
164. Kolahdoozi, M., et al., A novel quantum inspired algorithm for sparse fuzzy cognitive maps learning. Applied Intelligence, 2019. 49: p. 3652-3667. https://doi.org/10.1007/s10489-019-01476-7
165. Atchade-Adelomou, P., et al., qrobot: A quantum computing approach in mobile robot order picking and batching problem solver optimization. Algorithms, 2021. 14(7): p. 194. https://doi.org/10.3390/a14070194
166. Lei, W., et al., A hybrid quantum evolutionary algorithm with improved decoding scheme for a robotic flow shop scheduling problem. Mathematical Problems in Engineering, 2017. 2017. https://doi.org/10.1155/2017/3064724
167. Zhang, L., et al., Adaptive quantum genetic algorithm for task sequence planning of complex assembly systems. Electronics Letters, 2018. 54(14): p. 870-872. https://doi.org/10.1049/el.2018.0609
168. Yan, H., et al., Detection of participation and training task difficulty applied to the multi-sensor systems of rehabilitation robots. Sensors, 2019. 19(21): p. 4681. https://doi.org/10.3390/s19214681
169. Dereli, S. and R. Köker, A meta-heuristic proposal for inverse kinematics solution of 7-DOF serial robotic manipulator: quantum behaved particle swarm algorithm. Artificial Intelligence Review, 2020. 53: p. 949-964. https://doi.org/10.1007/s10462-019-09683-x
170. Deng, H. and C. Xie, An improved particle swarm optimization algorithm for inverse kinematics solution of multi-DOF serial robotic manipulators. Soft Computing, 2021. 25(21): p. 13695-13708. https://doi.org/10.1007/s00500-021-06007-6
171. Rokbani, N., et al., A beta salp swarm algorithm meta-heuristic for inverse kinematics and optimization. Applied Intelligence, 2022. 52(9): p. 10493-10518. https://doi.org/10.1007/s10489-021-02831-3
172. Ayyıldız, M. and K. Cetinkaya, Comparison of four different heuristic optimization algorithms for the inverse kinematics solution of a real 4-DOF serial robot manipulator.

Neural Computing and Applications, 2016. 27: p. 825-836. https://doi.org/10.1007/s00521-015-1898-8

173. Qiu, J., J. Wu, and B. Zhu, Optimization design of a parallel surgical robot with remote center of motion. Mechanism and Machine Theory, 2023. 185: p. 105327. https://doi.org/10.1016/j.mechmachtheory.2023.105327
174. Schuetz, M.J., et al., Optimization of robot-trajectory planning with nature-inspired and hybrid quantum algorithms. Physical Review Applied, 2022. 18(5): p. 054045. DOI: https://doi.org/10.1103/PhysRevApplied.18.054045
175. Li, R.-G. and H.-N. Wu, Multi-Robot Plume Source Localization by Distributed Quantum-Inspired Guidance With Formation Behavior. IEEE Transactions on Intelligent Transportation Systems, 2023. https://doi.org/10.1109/TITS.2023.3289173
176. Mezghiche, M.K. and N. Djedi, Quantum genetic algorithm to evolve controllers for self-reconfigurable modular robots. World Journal of Engineering, 2020. 17(3): p. 427-435. https://doi.org/10.1108/WJE-02-2019-0032
177. Yan, F., A.M. Iliyasu, and K. Hirota, Conceptual framework for quantum affective computing and its use in fusion of multi-robot emotions. Electronics, 2021. 10(2): p. 100. https://doi.org/10.3390/electronics10020100
178. Lanza, D., Solinas, P., Mastrogiovanni, F. (2021). Multi-sensory Integration in a Quantum-Like Robot Perception Model. In: Siciliano, B., Laschi, C., Khatib, O. (eds) Experimental Robotics. ISER 2020. Springer Proceedings in Advanced Robotics, vol 19. Springer, Cham. https://doi.org/10.1007/978-3-030-71151-1_44
179. Mannone, M., Seidita, V., & Chella, A. (2025). Quantum computing for swarm robotics: a local-to-global approach. Philosophical Transactions A, 383(2289), 20240139. https://doi.org/10.1098/rsta.2024.0139
180. Koukam, A., et al. Towards a quantum modeling approach to reactive agents. in 2021 IEEE International Conference on Quantum Computing and Engineering (QCE). 2021. IEEE. https://doi.org/10.1109/QCE52317.2021.00029
181. Bhatia, M., S. Sood, and V. Sood, A novel quantum-inspired solution for high-performance energy-efficient data acquisition from IoT networks. Journal of Ambient Intelligence and Humanized Computing, 2023. 14(5): p. 5001-5020. https://doi.org/10.1007/s12652-020-02494-x
182. Zhao, G., et al., A tandem robotic arm inverse kinematic solution based on an improved particle swarm algorithm. Frontiers in Bioengineering and Biotechnology, 2022. 10: p. 832829. https://doi.org/10.3389/fbioe.2022.832829
183. Singla, R. and H. Parthasarathy, Quantum robots perturbed by Levy processes: Stochastic analysis and simulations. Communications in Nonlinear Science and Numerical Simulation, 2020. 83: p. 105142. https://doi.org/10.1016/j.cnsns.2019.105142
184. Singla, R. and H. Parthasarathy, Teleoperation of robots carrying current intensity via electromagnetic fields–A quantum mechanical analysis. Results in Physics, 2019. 14: p. 102415. https://doi.org/10.1016/j.rinp.2019.102415
185. Panda, B., et al., Controlling remote robots based on zidan's quantum computing model. Computers, Materials & Continua, 2022. 73(3): p. 6225-6236. https://doi.org/10.32604/cmc.2022.028394

186. Ulyanov, S.V., Quantum fast algorithm computational intelligence PT I: SW/HW smart toolkit. Artificial Intelligence Advances, 2019. 1(1): p. 18-43. https://doi.org/10.30564/aia.v1i1.619
187. Khoshnoud, F., Esat, I. I., de Silva, C. W., & Quadrelli, M. B. (2019). Quantum network of cooperative unmanned autonomous systems. Unmanned Systems, 7(02), 137-145. https://doi.org/10.1142/S2301385019500055
188. Tamizi, M.G., M. Yaghoubi, and H. Najjaran, A review of recent trend in motion planning of industrial robots. International Journal of Intelligent Robotics and Applications, 2023. 7(2): p. 253-274. https://doi.org/10.1007/s41315-023-00274-2
189. Otani, T., et al., Energy Efficient Path and Trajectory Optimization of Manipulators with Task Deadline Constraints. IEEE Access, 2023. https://doi.org/10.1109/ACCESS.2023.3320143
190. Mannone, M., V. Seidita, and A. Chella, Categories, quantum computing, and swarm robotics: A case study. Mathematics, 2022. 10(3): p. 372. https://doi.org/10.3390/math10030372
191. Mannone, M., V. Seidita, and A. Chella, Modeling and designing a robotic swarm: A quantum computing approach. Swarm and Evolutionary Computation, 2023. 79: p. 101297. https://doi.org/10.1016/j.swevo.2023.101297
192. Mannone, M., V. Seidita, and A. Chella, The Sound of Swarm. Auditory Description of Swarm Robotic Movements. ACM Transactions on Human-Robot Interaction, 2023. 12(4): p. 1-27. https://doi.org/10.1145/3596203
193. Khoshnoud, F., C.W. de Silva, and I.I. Esat. Quantum entanglement of autonomous vehicles for cyber-physical security. in 2017 IEEE International Conference on Systems, Man, and Cybernetics (SMC). 2017. IEEE. https://doi.org/10.1109/SMC.2017.8123026
194. Dong, W., et al., The modelling of quantum control systems. Science bulletin, 2015. 60(17): p. 1493-1508. https://doi.org/10.1007/s11434-015-0863-3
195. Khang, A., et al., Quantum-Based Robotics in the High-Tech Healthcare Industry: Innovations and Applications, in Medical Robotics and AI-Assisted Diagnostics for a High-Tech Healthcare Industry. 2024, IGI Global. p. 1-27. https://doi.org/10.4018/979-8-3693-2105-8
196. Reda, D., et al., A quantum direct torque control method for permanent magnet synchronous machines. Computers and Electrical Engineering, 2025. 122: p. 109994. https://doi.org/10.1016/j.compeleceng.2024.109994
197. Feraoun, H., et al., Quantum maximum power point tracking (QMPPT) for optimal solar energy extraction. Systems and Soft Computing, 2024. 6: p. 200118. https://doi.org/10.1016/j.sasc.2024.200118
198. Zioui, N., et al., Quantum Space Vector Pulse Width Modulation for Speed Control of Permanent Magnet Synchronous Machines. e-Prime-Advances in Electrical Engineering, Electronics and Energy, 2025: p. 101074. https://doi.org/10.1016/j.prime.2025.101074
199. Khoshnoud, F., et al., Quantum network of cooperative unmanned autonomous systems. Unmanned Systems, 2019. 7(02): p. 137-145. https://doi.org/10.1142/S2301385019500055

200. Trowbridge, A., et al. Direct Collocation for Quantum Optimal Control. in 2023 IEEE International Conference on Quantum Computing and Engineering (QCE). 2023. IEEE. https://doi.org/10.1109/QCE57702.2023.00144
201. Jin, L., et al., Robot manipulator control using neural networks: A survey. Neurocomputing, 2018. 285: p. 23-34. https://doi.org/10.1016/j.neucom.2018.01.002
202. Reshetnikov, A.G., Ulyanov, S.V. Intelligent Information Technologies Based on Quantum Computing in the Task of Controlling Elements of an Accelerator Complex. Phys. Part. Nuclei 56, 983–988 (2025). https://doi.org/10.1134/S1063779625700054
203. Ulyanov, S., A. Reshetnikov, and D. Zrelova, Industrial robotic intelligent robust control system: Applying quantum soft computing technologies and quantum software engineering in unpredicted control situations. Программные продукты и системы, 2023. 36(1): p. 26-45. https://doi.org/10.15827/0236-235X.141.026-045
204. Ulyanov, S.V. and A.G. Reshetnikov. Cognitive intelligent robust control system based on quantum fuzzy inference for robotics and mechatronics. in 2017 IEEE 15th International Symposium on Intelligent Systems and Informatics (SISY). 2017. IEEE. https://doi.org/10.1109/SISY.2017.8080563
205. Krawec, W.O. Minimal variable quantum decision makers for robotic control. in Proceedings of the Companion Publication of the 2014 Annual Conference on Genetic and Evolutionary Computation. 2014. https://doi.org/10.1145/2598394.2598409
206. Ying, M.-S., Y. Feng, and S.-G. Ying, Optimal policies for quantum Markov decision processes. International Journal of Automation and Computing, 2021. 18(3): p. 410-421. https://doi.org/10.1007/s11633-021-1278-z
207. Lathrop, P., B. Boardman, and S. Martínez, Quantum Search Approaches to Sampling-Based Motion Planning. IEEE Access, 2023. https://doi.org/10.1109/ACCESS.2023.3307316
208. Snow, L., S. Jain, and V. Krishnamurthy, Lyapunov based stochastic stability of a quantum decision system for human–machine interaction. Automatica, 2024. 164: p. 111628. https://doi.org/10.1016/j.automatica.2024.111628
209. Toffano, Z. and F. Dubois, Quantum eigenlogic observables applied to the study of fuzzy behaviour of Braitenberg vehicle quantum robots. Kybernetes, 2019. 48(10): p. 2307-2324. https://doi.org/10.1108/K-11-2018-0603
210. Ulyanov, S., et al. Imperfect Knowledge Base Self-organization in Robotic Intelligent Cognitive Control: Quantum Supremacy. in CEUR Workshop Proceedings. 2021. https://doi.org/10.1007/978-3-030-92127-9_29
211. Dong, D., et al., Learning-based quantum robust control: algorithm, applications, and experiments. IEEE transactions on cybernetics, 2019. 50(8): p. 3581-3593. https://doi.org/10.1109/TCYB.2019.2921424
212. Mahanti, S., et al., Quantum robots can fly; play games: an IBM quantum experience. Quantum Information Processing, 2019. 18: p. 1-10. https://doi.org/10.1007/s11128-019-2332-4
213. Deng, R., Y. Huang, and M. Perkowski. Quantum motions and emotions for a humanoid robot actor. in 2021 ieee 51st international symposium on multiple-valued logic (ismvl). 2021. IEEE. https://doi.org/10.1109/ISMVL51352.2021.00043

214. Nemchaninov, A.V., et al., Robotic Smart Prosthesis Arm with BCI and Kansei/Kawaii/Affective Engineering Approach. Pt I: Quantum Soft Computing Supremacy. Artificial Intelligence Advances, 2020. 2(2): p. 68-87. https://doi.org/10.30564/aia.v2i2.1567
215. Rybalov, A., et al. Fuzzy model of control for quantum-controlled mobile robots. in 2010 IEEE 26-th Convention of Electrical and Electronics Engineers in Israel. 2010. IEEE. https://doi.org/10.1109/EEEI.2010.5662220
216. Reshetnikov, A., V. Ulyanov, and S. Ulyanov, Intelligent Robust Control of Autonomous Robot: Quantum Self-Organization of Imperfect Knowledge Bases—Experiment. Journal of Computer and Systems Sciences International, 2023. 62(5): p. 884-902. https://doi.org/10.1134/S1064230723050131
217. Mei, P., et al., Quantum-based creative generation method for a dancing robot. Frontiers in Neurorobotics, 2020. 14: p. 559366. https://doi.org/10.3389/fnbot.2020.559366
218. Chen, Q., Y. Qin, and G. Li, QPSO-MPC based tracking algorithm for cable-driven continuum robots. Frontiers in Neurorobotics, 2022. 16: p. 1014163. https://doi.org/10.3389/fnbot.2022.1014163
219. Singh, R. and C. Sloth. Characterizing Manipulator Motion Using an Evolving Type 2 Quantum Fuzzy Neural Network. in 2024 IEEE/SICE International Symposium on System Integration (SII). 2024. IEEE. https://doi.org/10.1109/SII58957.2024.10417569
220. Wan, J., et al., Fractional-order PID motion control for AUV using cloud-model-based quantum genetic algorithm. IEEE Access, 2019. 7: p. 124828-124843. https://doi.org/10.1109/ACCESS.2019.2937978
221. Varma, R., et al., Post quantum secure command and control of mobile agents inserting quantum-resistant encryption schemes in the secure robot operating system. International Journal of Semantic Computing, 2021. 15(03): p. 359-379. https://doi.org/10.1142/S1793351X21400092
222. Ulyanov, S., et al. Imperfect Knowledge Base Self-organization in Robotic Intelligent Cognitive Control: Quantum Supremacy. in International Conference on Theory and Application of Soft Computing, Computing with Words and Perceptions. 2021. Springer. https://doi.org/10.1007/978-3-030-92127-9_29
223. Abdulridha, H.M. and Z.A. Hassoun, Control design of robotic manipulator based on quantum neural network. Journal of Dynamic Systems, Measurement, and Control, 2018. 140(6): p. 061002. https://doi.org/10.1115/1.4038492
224. Takahashi, K., E. Tano, and M. Hashimoto, Feedforward–feedback controller based on a trained quaternion neural network using a generalised HR calculus with application to trajectory control of a three-link robot manipulator. Machines, 2022. 10(5): p. 333. https://doi.org/10.3390/machines10050333
225. Yang, L., et al., Automated control of magnetic spore-based microrobot using fluorescence imaging for targeted delivery with cellular resolution. IEEE Transactions on Automation Science and Engineering, 2019. 17(1): p. 490-501. https://doi.org/10.1109/TASE.2019.2937232
226. Qu, Z., W. Zhang, and L. Dong. Atomic-level Tracking and Analyzing of Quantum-dot Motion Steered by an Electrostatic Field Positioned by a Nanorobotic Manipulation

Tip. in 2023 IEEE International Conference on Robotics and Automation (ICRA). 2023. IEEE. https://doi.org/10.1109/ICRA48891.2023.10161087

227. Ghosh, A. and A.K. Ray, A gravitational search algorithm-based control of an underactuated system with experimental verifications. Soft Computing, 2024. 28(4): p. 3353-3369. https://doi.org/10.1007/s00500-023-08606-x
228. Chen, C., et al. A quantum-inspired q-learning algorithm for indoor robot navigation. in 2008 IEEE International Conference on Networking, Sensing and Control. 2008. IEEE. https://doi.org/10.1109/ICNSC.2008.4525476
229. Gandhi, V., et al., EEG-based mobile robot control through an adaptive brain–robot interface. IEEE Transactions on Systems, Man, and Cybernetics: Systems, 2014. 44(9): p. 1278-1285. https://doi.org/10.1109/TSMC.2014.2313317
230. Dong, D., et al., Robust quantum-inspired reinforcement learning for robot navigation. IEEE/ASME transactions on mechatronics, 2010. 17(1): p. 86-97. https://doi.org/10.1109/TMECH.2010.2090896
231. Ma, B., et al., Target tracking control of UAV through deep reinforcement learning. IEEE Transactions on Intelligent Transportation Systems, 2023. https://doi.org/10.1109/TITS.2023.3249900
232. Chen, C. and D. Dong. Quantum parallelization of hierarchical Q-learning for global navigation of mobile robots. in Proceedings of 2012 9th IEEE International Conference on Networking, Sensing and Control. 2012. IEEE. https://doi.org/10.1109/ICNSC.2012.6204910
233. Qamar, S., S. Cong, and B. Riaz. Lyapunov-based feedback control of two-level stochastic open quantum systems. in 2017 IEEE International Conference on Cybernetics and Intelligent Systems (CIS) and IEEE Conference on Robotics, Automation and Mechatronics (RAM). 2017. IEEE. https://doi.org/10.1109/ICCIS.2017.8274747
234. Artemov, K. and S. Kolyubin. Design and validation of two-stage motion control system for by-air quantum key distribution. in 2020 International Conference Nonlinearity, Information and Robotics (NIR). 2020. IEEE. https://doi.org/10.1109/NIR50484.2020.9290198
235. Nie, M., G. Yang, and R. Wei. Quantum Self-organizing Network and Routing Protocol for Cooperative Communication of Intelligent Robot Soccer Game. in 2020 5th International Conference on Control and Robotics Engineering (ICCRE). 2020. IEEE. https://doi.org/10.1109/ICCRE49379.2020.9096471
236. Yan, F., et al., Quantum structure for modelling emotion space of robots. Applied Sciences, 2019. 9(16): p. 3351. https://doi.org/10.3390/app9163351
237. Kagan, E., E. Salmona, and I. Ben-Gal. Probabilistic mobile robot with quantum decision-making. in 2008 IEEE 25th Convention of Electrical and Electronics Engineers in Israel. 2008. IEEE. https://doi.org/10.1109/EEEI.2008.4736561
238. Gandhi, V.S. and T.-M. McGinnity. Quantum neural network based surface EMG signal filtering for control of robotic hand. in The 2013 International Joint Conference on Neural Networks (IJCNN). 2013. IEEE. https://doi.org/10.1109/IJCNN.2013.6706781

239. Chen, C., H.-X. Li, and D. Dong, Hybrid control for robot navigation-a hierarchical q-learning algorithm. IEEE Robotics & Automation Magazine, 2008. 15(2): p. 37-47. https://doi.org/10.1109/MRA.2008.921541
240. Cunha, R.A.F., et al. Fuzzy Logic Behavior of Quantum-Controlled Braitenberg Vehicle Agents. in Quantum Interaction: 11th International Conference, QI 2018, Nice, France, September 3–5, 2018, Revised Selected Papers 11. 2019. Springer. https://doi.org/10.1007/978-3-030-35895-2_8
241. Levi, P., Molecular quantum robotics: particle and wave solutions, illustrated by "leg-over-leg" walking along microtubules. Frontiers in Neurorobotics, 2015. 9: p. 2. https://doi.org/10.3389/fnbot.2015.00002
242. Itami, T., N. Matsui, and N. Kouda. Macroscopic Robots as Microscopic Liquid Molecules-Brownian Motion and Quantum Dynamics. in 2018 57th Annual Conference of the Society of Instrument and Control Engineers of Japan (SICE). 2018. IEEE. https://doi.org/10.23919/SICE.2018.8492589
243. Zhou, C. and Y. Wang. Neural-adaptive Quantized Consensus Tracking Control of High-order Power-chained Nonlinear Multi-agent Networks with Switched Dynamics: A Specified-Time Convergence Protocol. in 2023 9th International Conference on Control, Automation and Robotics (ICCAR). 2023. IEEE. https://doi.org/10.1016/j.neucom.2023.03.029
244. Dahassa, M.S., M. Fazilat, and N. Zioui, A novel sliding mode control based on qubit rotation angle for efficient manipulation of robotic arms. Progress in Engineering Science, 2025: p. 100137. https://doi.org/10.1016/j.pes.2025.100137
245. Fazilat, M. and N. Zioui, Quantum-Inspired Sliding-Mode Control to Enhance the Precision and Energy Efficiency of an Articulated Industrial Robotic Arm. Robotics, 2025. 14(2): p. 14. https://doi.org/10.3390/robotics14020014

2.2.8 Summary of the Results Analysis

2.2.8.1 Quantum Machine Learning (QML)

Numerous studies have shown that Quantum Machine Learning can enable exponential or quadratic speedups in learning algorithms. Specifically, Quantum Reinforcement Learning (QRL) and Quantum Support Vector Machines (QSVM) have demonstrated enhanced performance in areas such as robotic navigation, task execution, and cybersecurity applications. Notably, real-world implementations of these quantum-enhanced models have achieved over 99% accuracy in detecting cyberattacks and exhibit faster convergence during training episodes for robots.

2.2.8.2 Quantum Neural Networks (QNNs)

Quantum Neural Networks, leveraging the principles of quantum superposition and entanglement, have demonstrated enhanced training efficiency and greater accuracy in various applications, including pattern recognition, path planning, and control systems. When implemented in robotic manipulators, QNNs achieved superior trajectory tracking and faster convergence compared to traditional models. Research has also examined quaternion-based and complex-valued neural architectures, which have significantly boosted motion control and classification accuracy. Evidence of real-world applicability can be seen in fields such as inverse kinematics, electroencephalography-based control, and multi-robot systems.

2.2.8.3 Quantum-Based Algorithms

Quantum-inspired algorithms, such as Quantum-behaved Particle Swarm Optimization (Q-PSO) and Quantum-Inspired Ant Colony Optimization (QACO), as well as hybrid quantum-classical approaches, have been successfully applied to various domains, including robotic path planning, swarm behavior, and assembly optimization. Research has demonstrated significant reductions in computation times, enhanced convergence rates, and improved resilience in multi-agent systems. Additionally, quantum kinematic models for robotic arms have been shown to minimize processing overhead by utilizing single-qubit representations.

2.2.8.4 Quantum-Based Control Strategies

Quantum-enhanced control frameworks have played a crucial role in enhancing system robustness, adaptability, and precision. This encompasses the utilization of Quantum Fuzzy Inference (QFI), Quantum Genetic Algorithms (QGA), and quantum decision-making models for real-time robotic control. These methodologies are applied in various fields, including humanoid robotics, prosthetic devices, autonomous vehicles, and medical robotics. Empirical evidence demonstrates improved stability and tracking accuracy, even under uncertain conditions.

2.3 Concluding Remarks

Quantum computing presents substantial advantages in processing speed, learning convergence, adaptability to uncertainty, and optimization capabilities. Quantum Machine Learning (QML) models have achieved remarkable success in areas such as robotic

navigation and cybersecurity, while Quantum Neural Networks (QNNs) enhance accuracy and efficiency in real-time control and object recognition. Additionally, quantum-inspired optimization algorithms, such as Quantum Particle Swarm Optimization (Q-PSO) and Quantum Ant Colony Optimization (QACO), have surpassed classical methods in tasks including path planning, swarm coordination, and multi-robot systems. Furthermore, quantum-enhanced control strategies, ranging from fuzzy inference systems to quantum Lyapunov controllers, have been proposed to enhance stability and adaptability under dynamic and uncertain conditions.

However, despite these promising advancements, several significant challenges impede widespread adoption. Limitations in quantum hardware, including qubit coherence, gate fidelity, and sensitivity to noise, remain formidable barriers. Moreover, the abstract nature of many quantum algorithms, coupled with a lack of standardized benchmarking, complicates the evaluation of their effectiveness in comparison to classical alternatives. Interdisciplinary fragmentation and insufficient real-world validation further hinder practical integration.

To address these challenges, future research should prioritize the development of scalable hybrid quantum-classical frameworks, the enhancement of quantum error correction techniques, and the design of robust experimental validation methods across various robotic platforms. Additionally, it is essential to investigate the ethical and societal implications, including issues of autonomy, surveillance, and workforce displacement, as quantum-enhanced robotic systems become increasingly advanced.

In conclusion, the early stages of quantum AI in robotics are not a limitation, but a promise of transformation. This review, with its well-structured foundation, is a source of excitement and anticipation for future innovations. By integrating theoretical advancements, empirical data, and challenges in implementation, we are paving the way for a new era of intelligent, adaptive, and efficient autonomous systems. These systems, enhanced by quantum technology, have the potential to revolutionize various sectors, including healthcare, manufacturing, space exploration, and cyber-physical infrastructure.

The theoretical advantages of quantum-enhanced AI for robotics are indeed compelling; however, their practical integration necessitates a deeper understanding of the foundational robotic models they pursue to extend. Accurate dynamic modeling is crucial for achieving precise control; however, high-fidelity representations can be computationally demanding and often impractical for real-time applications. This challenge highlights the need to explore model simplification strategies that strike a balance between precision and efficiency. Chapter 3 directly addresses this necessity by examining the effects of various abstraction levels in the dynamic modeling of a six-jointed industrial robotic arm. Using the ABB IRB140 as a case study, it assesses how different CAD-derived model fidelities influence torque prediction and energy consumption. These findings not only guide the selection of appropriate modeling approaches for integration with quantum-AI methods but also establish the baseline dynamics required for the subsequent optimization and control experiments in the thesis.

Chapter 3 - The Impact of Model Simplification on the Dynamic Performance of a Robotic Arm

3.1 Chapter Overview

Robotic arms are increasingly utilized in the dynamic domain of industrial automation, especially enhancing precision, throughput, and flexibility across a wide range of applications. One essential aspect necessary for the effective and efficient control of these robot manipulators is the accurate determination of their dynamic models. Such models are essential for evaluating joint torques and energy consumption under various working conditions. Nonetheless, developing detailed dynamic models can be computationally demanding and requires precise information regarding system parameters, including link masses, centers of mass, and rotational inertia tensors. The challenge of balancing model expressiveness with simulation speed has emerged as an important consideration in the design and simulation of robotic systems.

This article concerns the impact of dynamic model reduction on the motion accuracy of a six-degree-of-freedom ABB IRB 140 industrial robot. It aims to compare the prediction ability of the model regarding the torque demand and the energy consumption by using different details (in geometric and inertial assumptions). Three SolidWorks models were used: a highly detailed model that closely represented the robot's mechanical construction, a semi-detailed model employing geometric simplification with parallelepipeds, and a simplified model based on rod solutions found in the literature. The dynamic equations were derived from the Euler–Lagrange formulation, and the forward and inverse kinematics

were developed using the Denavit–Hartenberg convention and a fifth-order polynomial trajectory.

The current study quantitatively characterizes this performance difference through extensive MATLAB simulations under an identical and standard predefined task. The findings suggest that the detailed model is most accurate, but that the simplified models are computationally much more efficient with relatively little loss in accuracy. The conclusions highlight the industrial-robotic-related implications of model selection, indicating how to design for optimal system performance according to specific task requirements and available computational capacity, which involves making a trade-off between model accuracy and computational efficiency in the dynamic modeling of robot arms.

3.2 Paper 2: The impact of simplifications of the dynamic model on the motion of a six-jointed industrial articulated robotic arm movement.

Authors Mehdi Fazilat, Nadjet Zioui.

Journal: Journal of Robotics and Control (JRC).

Publication status: 24/January/2024.

3.2.1 Methodology

The methodological approach employed in this study involves modeling and simulating a comprehensive experiment using an industrial six-degree-of-freedom ABB IRB 140 articulated robotic arm. The procedure applies trajectory generation, which provides the joint space input data necessary for conducting kinematic and dynamic analyses. The

forward kinematics of the manipulator are established using Denavit-Hartenberg parameters to define the spatial orientation and position of the end effector. Each joint trajectory is parameterized using fifth-order polynomial equations and homogeneous transformation matrices presented in relations 3-1 to 3-3 according to the frame assignments shown in, ensuring that the trajectory is characterized as both continuous and differentiable.

$$ {}^{i-1}_{i}T = Rot(x_{i-1},\alpha_{i-1})\, Trans(x_{i-1},a_{i-1})\, Rot(z_i,\theta_i)\, Trans(0,0,d_i) \tag{3-1} $$

Where ${}^{i-1}_{i}T$ is the homogeneous transformation matrix, Rot (x_{i-1},α_{i-1}) is the rotation around an axis x_{i-1} by an angle α_{i-1} , Trans (x_{i-1},a_{i-1}) is the transfer along axis x_{i-1} to the value a_{i-1}, Rot (z_i,θ_i) is the rotation around axis z_i by an angle θ_i, and Trans $(0,0,d_i)$ is the transfer along axis z to the value d.

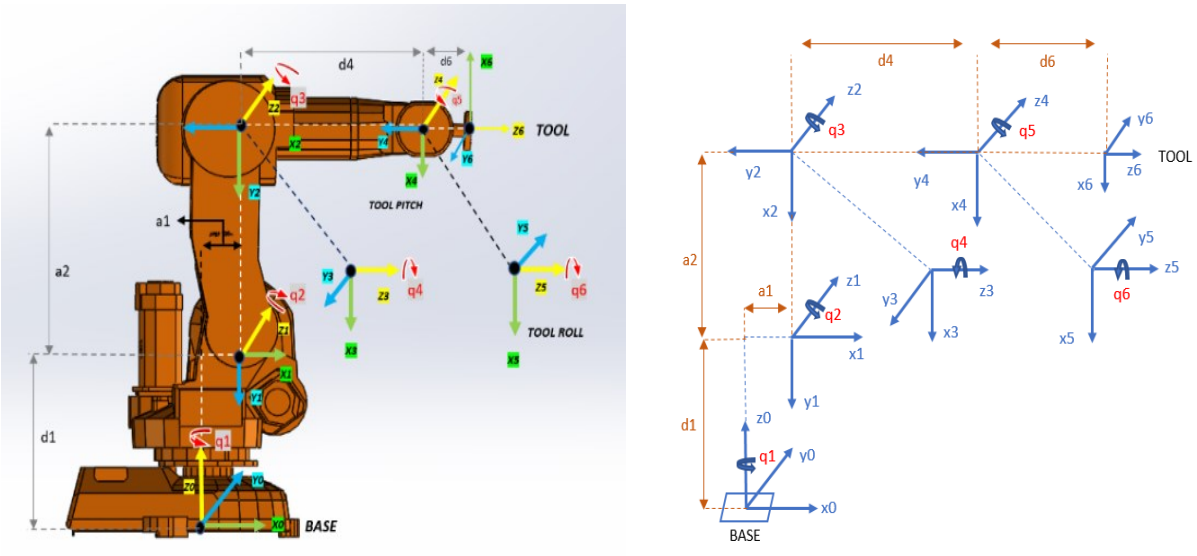

(a) (b)

Figure 3-1 ABB IRB 140 frame assignments: (a) Frames represented on the real robot, (b) Frames symbolized using DH representation.

$$ {}^{i-1}_{i}T = \begin{pmatrix} C\theta_i & -SI & 0 & a_{i-1} \\ SI_i\, C\alpha_{i-1} & CI & -S\alpha_{i-1} & -d_i S\alpha_{i-1} \\ S\theta_i S\alpha_{i-1} & C\theta_i\, S\alpha_{i-1} & C\alpha_{i-1} & d_i C\alpha_{i-1} \\ 0 & 0 & 0 & 1 \end{pmatrix} \tag{3-2} $$

Where C and S denote the cosine and sine of an angle, respectively.

$$ {}^{0}_{6}T = {}^{0}_{1}T.\ {}^{1}_{2}T.\ {}^{2}_{3}T.\ {}^{3}_{4}T.\ {}^{4}_{5}T.\ {}^{5}_{6}T = \begin{pmatrix} r_{11} & r_{12} & r_{13} & X \\ r_{21} & r_{22} & r_{23} & Y \\ r_{31} & r_{32} & r_{33} & Z \\ 0 & 0 & 0 & 1 \end{pmatrix} \tag{3-3} $$

So that:

$r_{11}=-S_6(S_4C_1C_{2'3}+C_4S_1)-C_6(C_5(S_1S_4-C_4C_1C_{2'3})+S_5C_1C_{2'3})$

$r_{12}=S_6(C_5(S_1S_4-C_4C_1C_{2'3})+S_5C_1C_{2'3})-C_6(S_4C_1C_{2'3}+C_4S_1)$

$r_{13}=C_5C_1S_{2'3}-S_5(S_1S_4-C_4C_1C_{2'3})$

$r_{21}=C_6(C_5(C_4S_1C_{2'3}+C_1S_4)-S_5S_1S_{2'3})-S_6(S_4S_1C_{2'3}-C_1C_4)$

$r_{22}=-S_6(C_5(C_4S_1C_{2'3}+C_1S_4)-S_5S_1S_{2'3})-C_6(S_4S_1C_{2'3}-C_1C_4)$

$r_{23}=C_5S_1S_{2'3}+S_5(C_4S_1C_{2'3}+C_1S_4)$

$r_{31}=-C_6(S_5C_{2'3}+C_4C_5S_{2'3})+S_4S_6S_{2'3}$

$r_{32}=C_6S_4S_{2'3}+S_6(S_5C_{2'3}+C_4C_5S_{2'3})$

$r_{33}=C_5C_{2'3}-C_4S_5S_{2'3}$

C_i and S_i denote the cosine and sine of the joint angle qi

C_{ij} and S_{ij} denote the cosine and sine of qi+qj

Notation $2'$ refers to $q'_2=q_2+\pi/2$

The X, Y, and Z position coordinates of the IRB140 robot relative to the base frame are computed by relation 3-4 to 3-6 as follows:

$$X=C_1a_1+d_6(C_5C_1S_{2'3}-S_5(S_1S_4-C_4C_1C_{2'3}))+d_4C_1S_{2'3}-C_1C_2a_2 \quad (3\text{-}4)$$

$$Y=S_1a_1+d_6(C_5S_1S_{2'3}-S_5(C_4S_1C_{2'3}+C_1S_4))+d_4S_1S_{2'3}-C_2S_1a_2 \quad (3\text{-}5)$$

$$Z=d_1+d_4C_{2'3}+a_2S_2+d_6(C_5C_{2'3}-C_4S_5S_{2'3}) \quad (3\text{-}6)$$

The differential kinematics are derived from a Jacobian matrix that relates joint velocities to the linear and angular velocities of the end effector, as illustrated in Equations 3-7 to 3-10. This framework enables a comprehensive analysis of manipulator singularity, redundancy, and motion planning. The kinematic outputs, such as position, velocity, and acceleration, serve as critical inputs for the dynamic model.

$$\dot{P}_e=J_p(q)\dot{q} \quad (3\text{-}7)$$

$$\omega_e=J_o(q)\dot{q} \quad (3\text{-}8)$$

$$V_e=\begin{pmatrix}\dot{P}_e\\ \omega_e\end{pmatrix}=J(q)\dot{q} \quad (3\text{-}9)$$

$$\dot{q}=J^{-1}V_e \quad (3\text{-}10)$$

Considering the end-effector linear velocity vector $\dot{p}_e$, the angular velocity vector ωe, and the joint velocity vector q̇, Jp is the (3 × n) matrix that links the linear velocity vector to the joint speed vector. Jo is the (3 × n) matrix that links the angular velocity vector to the joint speed vector, V_e is the end-effector velocity and $J=\begin{pmatrix}J_p\\ J_o\end{pmatrix}$ is the Jacobian matrix, and J^{-1} is the inverse of the Jacobian matrix.

The dynamic model is grounded in the Euler–Lagrange formulation outlined in relation 3-11, which incorporates joint torques influenced by intrinsic inertia, Coriolis, centrifugal, and gravitational forces.

$$\sum_{j=1}^{n} M_{ij}\ddot{q}+V_i+G_i=\tau_i, \quad i=1,2,..., \tag{3-11}$$

Where $\ddot{q}$ is the joint acceleration vector, M_{ij} represents the inertial forces, V_i represents the centrifugal and Coriolis forces, and G_i indicates the gravitational forces. This equation can also be used to determine the joints' acceleration values.

Subsequently, the energy consumption for each joint is assessed using Equation 3-12, which considers torque and angular velocity over time.

$$E_i=\int_{t_0}^{t_f} \tau_i(t).\dot{q}_i(t)\, dt \tag{3-12}$$

Three models of the ABB IRB 140 robot were developed in SolidWorks to serve as physical representations for estimating mass and inertial properties. These include a high-detail model featuring intricate geometry, a semi-detailed rectangular (parallelepiped) model, and a simplified rod-like model, offered in Figure 3-2.

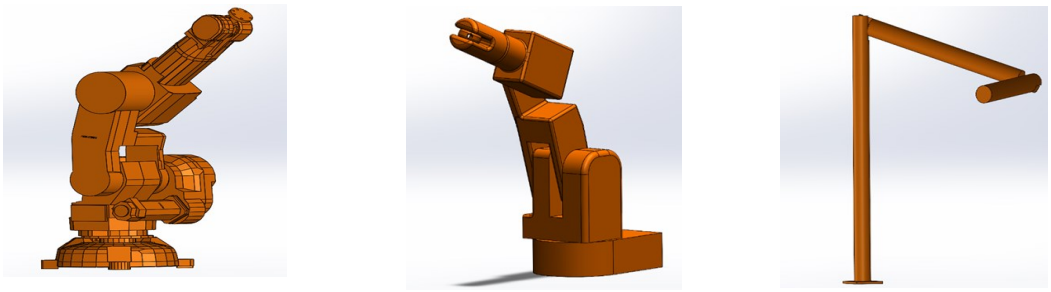

(A) (B) (C)

Figure 3-2 Detailed SolidWorks model, (B) Semi-detailed rectangular SolidWorks model, (C) Simplified SolidWorks model.

In each case, the material is assumed to have a uniform and constant density throughout its entire volume. The mass centers and inertia matrices for the three proximal links were extracted using the mass properties tool in SolidWorks, as presented in Table 3-1.

Table 3-1 Mass property results of each model calculated using SolidWorks software.

Link	parameter(unit)	Detailed model	Semi-detailed model	Simplified model
1	Weight (kg)	35	35	35
	Xc (mm)	277.87	17.87	0
	Yc	373.12	103.12	181.37
	Zc	-199.03	-79.03	0
	Ixx (kg.m2)	6.5	1.5	1.1
	Ixy	1.1	0.1	0
	Ixz	3.05	0.05	0
	Iyy	2.02	0.002	0
	Iyz	5.07	0.07	0.1e-5
	Izz	1.4	0.04	1.1
	Weight (kg)	35	35	35
2	Weight (kg)	25	25	25
	Xc (mm)	218.29	178.29	0
	Yc	229.73	9.73	255.24
	Zc	112.43	72.43	0
	Ixx (kg.m2)	0.9	0.1	1.6
	Ixy	-0.03	-0.03	0.1e-5
	Ixz	0.1	0.01	0
	Iyy	1.3	0.03	0
	Iyz	-0.01	-0.01	0
	Izz	0.95	0.05	1.6
	Weight (kg)	25	25	25
3	Weight (kg)	18	18	18
	Xc (mm)	-24.56	14.56	0
	Yc	-219.9	-199.96	195.69
	Zc	-25.86	-15.86	0
	Ixx(kg.m2)	2.5	1.5	0.6
	Ixy	-0.001	-0.001	0.3e-5
	Ixz	0.09	0.09	0
	Iyy	2.7	0.7	0
	Iyz	-0.8	-0.02	0
	Izz	0.5	0.2	0.6
	Weight (kg)	18	18	18

To standardize the simulated environment, all models utilize the same trajectory, an identical time step, and a same robot configuration and motion planning without any payload. The computed dynamic parameters were imported into MATLAB to generate profiles for joint torque, velocity, acceleration, and motion, Figure 3-3 illustrates the modeling flow.

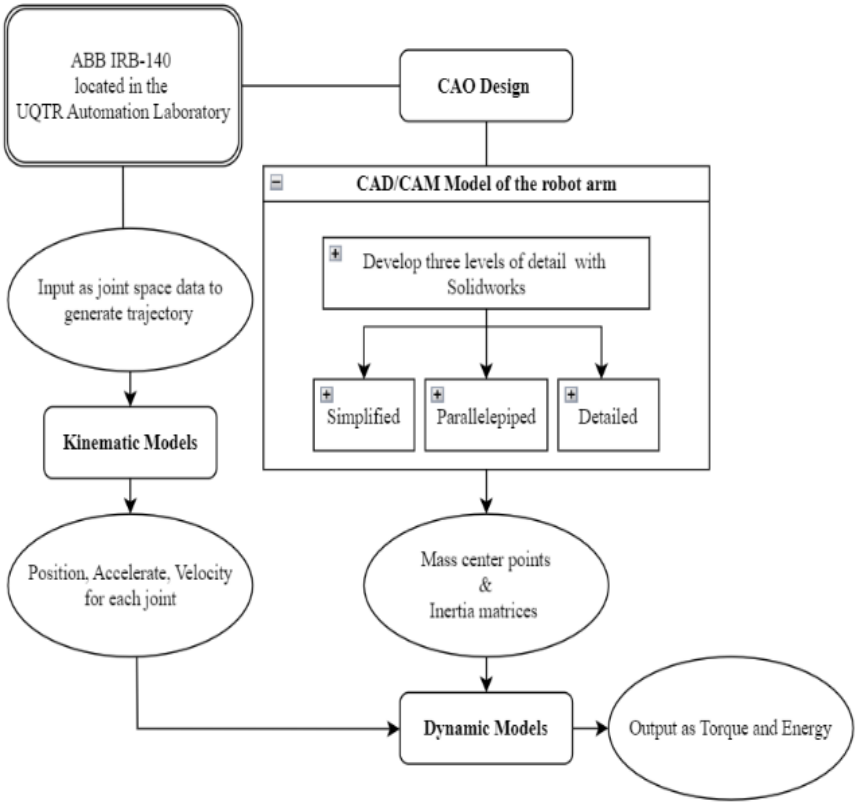

Figure 3-3 The flowchart for the methodological steps.

Journal of Robotics and Control (JRC)
Volume 5, Issue 1, 2024
ISSN: 2715-5072, DOI: 10.18196/jrc.v5i1.20263 173

The Impact of Simplifications of the Dynamic Model on the Motion of a Six-Jointed Industrial Articulated Robotic Arm Movement

Mehdi Fazilat [1*], Nadjet Zioui [2]
[1, 2] Université du Québec à Trois-Rivières, 3351 Bd des Forges, Trois-Rivières, QC G8Z 4M3, Canada
Email: [1] mehdi.fazilat@uqtr.ca, [2] nadjet.zioui@uqtr.ca
*Corresponding Author

***Abstract*—This research investigates the impact of model simplification on the dynamic performance of an ABB IRB-140 six-jointed industrial robotic arm, concentrating on torque prediction and energy consumption. The entire mathematical model of forward, reverse, differential kinematics, and dynamic model proposed based on the technical specifications of the arm, and to obtain the center of the mass and inertia matrices, which are essential components of the dynamic model, Utilizing Solidworks, we developed three CAD/CAM models representing the manipulator with varying detail levels, such as simplified, semi-detailed, and detailed. Our findings indicate minor differences in the model's torque and energy consumption graphs. The semi-detailed model consumed the most energy, except for joint 1, with the detailed model showing a 0.53% reduction and the simplified model a 6.8% reduction in energy consumption. Despite these variations, all models proved effective in predicting the robot's performance during a standard 30-second task, demonstrating their adequacy for various industrial applications. This research highlights the balance between computational efficiency and accuracy in model selection. While the detailed model offers the highest precision, it demands more computational resources, which is suitable for high-precision tasks. In discrepancy, simplified, less precise models offer computational efficiency, making them adequate for specific scenarios. Our study provides critical insights into selecting dynamic models in industrial robotics. It guides the optimization of performance and energy efficiency based on the required task precision and available computational resources. This comprehensive comparison of dynamic models underscores their applicability and effectiveness in diverse industrial settings.**

Keywords*—Industrial Robot Manipulators; Computer-Aided Design (CAD); D-H Representation; Dynamic Model and Simplifications; Energy Consumption; Computational Efficiency in Robotic; Model Accuracy in Robotics; Precision Engineering in Robotics.

I. INTRODUCTION

In recent years, considerable attention has been dedicated to researching robotic arm control within the broad domain of industrial robotics. This focus has notably enhanced the performance and applicability of autonomous systems in controlling joint movements [1]. Robotic arm control methods are various, each owning particular advantages and challenges. Primarily, these strategies are anchored in dynamic models, where variables are represented as torque or forces, depending on the joint's character, articulated or prismatic. Unlike robust controllers, which can adjust unconsidered errors in the dynamic model [2][3], precise controllers are intimately dependent on the accuracy of the dynamic model [4][5] and the impact of proper and appropriate models on control strategy.

The challenge of dynamic modeling in robotics is well-documented, with studies highlighting its complexity [6]-[12]. Two fundamental methods can provide model robot dynamics, the Newton–Euler formulation and the Euler–Lagrange formulation. The Newton–Euler formulation enumerates each term separately, providing a direct way to calculate forces and torques in the robot's joints and links. On the other hand, the Euler–Lagrange formulation, which is based on the energy properties of mechanical systems, computes motion equations by balancing the kinetic and potential energies of the system. This approach requires detailed knowledge of each robot link's inertia and center of mass, a complex but crucial aspect for accurate dynamic modeling [13]. The latest necessitates detailed knowledge of each robot link's inertia and center of mass, a requirement often met through model parameter identification [14]-[22] or approximation methods [23]-[31].

However, these approaches, whether through measurement inaccuracies or oversimplifications, introduce errors. Understanding these complexities is not just an academic exercise but essential in the real world. This study's insights are particularly relevant in advanced industrial automation, where precision and efficiency in robotic arm control are paramount. Our work aims to inform complex manufacturing and automation environments more effectively and efficiently by exploring the trade-offs between model simplicity and accuracy. To clarify the impact of these modeling techniques, this study compares three dynamic models of an articulated robotic arm developed using CAD models in Solidworks. The first model, highly detailed, closely emulates the actual robot design. The second, an approximate model, utilizes parallelepipeds with specific density choices to mirror link masses. The third, a simplified model, treats links as rods, a prevalent approach in literature for its ease [32]-[39]. These models are evaluated as torque and energy consumption predictors to assess the implications of model simplifications on these crucial factors.

The accuracy of a dynamic model depends on the precise identification of the mass center and inertia matrices. Detailed dimensional specifications and scientific methods

such as CAD modeling, Experimental Modal Analysis, and Inertia Measurement Units are some methods to obtain this required data in the mechanical parts. CAD modeling presents detailed dimensional and mass distribution data, while Experimental Modal Analysis and Inertia Measurement Units directly measure inertia characteristics. This research primarily aims to investigate the effects of simplifications in integrating mass properties and then the impacts of the level of simplification on the performance of the dynamic models. Such simplifications, aimed at reducing computational demands, can impact the model's accuracy. The study seeks a balance between computational efficiency and precision, which is required in robotics, where exact movements and energy efficiency are critical.

Recent literature has focused on innovative methods and considerations for determining mass properties, such as the center of mass and inertia matrices. Woolfrey and Liu explored the use of virtual components in robotic arms, aiming to optimize control by adjusting virtual mass and inertia matrixes [40]. Zhang et al. integrated neural networks for PD control of manipulators, emphasizing gravity and inertia compensation [41]. Habibi et al. developed a dynamic model for soft robotics, considering physical characteristics like gravity and inertia [42]. Cen and Singh addressed the impact of payloads on system mass and inertia in mobile robots [43]. Fu et al. presented a Lie theory-based methodology for dynamic parameter identification in serial manipulators, enhancing the accuracy of inertia tensor and mass property estimations [44]. Le Cleac'h et al. combined differentiable physics with neural networks to simulate object motion and estimate dynamic properties [45]. Xu et al. examined the dynamic coupling in mobile manipulators, focusing on the robotic arm's center of mass [46]. Wüest, Kumar, and Loianno proposed an online estimation method for crucial dynamic properties of aerial vehicles [47]. Fang et al. developed a grasp perception method incorporating the object's center-of-mass awareness [48]. Daniel and Soloniaina's work on robot modeling for reinforcement learning control emphasized the computation of inertia tensors [49]. Hill's research on bipedal robots highlighted the use of arms in disturbance rejection, considering the inertia matrix of each link [50]. This study aims to bridge the gap in understanding the implications of model complexity on robotic arm dynamic models, a subject of growing relevance in the context of increasingly refined industrial automation demands, and indicate a trend toward merging advanced computational methods and control theories in dynamic modeling. However, there still needs to be more in applying these methodologies to more complex robotic systems and varying dynamic environments.

Our findings inform industrial robotic system designs, potentially leading to more efficient and accurate control strategies in diverse manufacturing environments. Future research could focus on overcoming these gaps, employing more efficient intelligent methods for parameter identification of the robot arm's dynamic models based on proper dynamic models, such as quantum-inspired calculations, to enhance the efficiency and accuracy of dynamic modeling in robotics. Based on this, the following sections detail the comparative analysis methodology used to assess these dynamic models. This approach provides a comprehensive understanding of the trade-offs involved in model simplification and its effects on robotic arm control and efficiency. The primary contributions of this research are two-fold: proposing various detailed levels of the robot's dynamic model and providing a nuanced understanding of how the level of simplification in dynamic models impacts the performance and accuracy of robotic applications.

II. ROBOTIC ARM PRESENTATION

Fig. 1 shows the ABB IRB 140 (M2004) robot considered in this study. This robot's six-axis articulated structure is one of the most widely used in many industrial fields.

According to the ABB technical documentation [51], this industrial robot can be mounted on the floor or a wall at any angle or inverted for various working ranges. It is primarily used for arc welding, assembly, cleaning/spraying, machine tending, material handling, packing, and deburring. The robot weighs about 98 kg with an end effector weighing up to 5 kg, including a payload with a reach of about 810 mm that can be attached to its mounting flange. Up to 1.5 kg of equipment can be mounted on the robot's upper arm. Its joint limits allow ample functional workspace duty, as summarized in Table I [51].

Fig. 1. The ABB IRB 140 robot located in the UQTR automation laboratory

TABLE I. JOINT LIMITS OF THE ABB IRB 140 ROBOT

Joints	Type	Limits (°)
1	R	+180 to -180
2	R	+110 to -90
3	R	+50 to -230
4	R	+200 to -200
5	R	+120 to -120
6	R	+400 to -400

R stands for rotational or revolute.

The robotic manipulator includes an IRC5 controller [52][53], a multi-robot controller with PC tool support that optimises robot performance for short cycle times and precise movements, and RobotWare (Robot Studio), which allows ABB robot programming on a workstation without shutting down production [54][55]. A program can be built on the ABB Virtual Controller, which is an exact copy of the software that runs robots in production. Robot Studio allows highly realistic simulations to be performed using simple robot programs and configuration files identical to those used in real-world applications [55][56].

In this study, the ABB IRB 140 robot was employed in its standard configuration, according to the manufacturer's specifications. No modifications or customizations were made to the robot's structure or system. This standardization ensures that our research results and findings are directly applicable to the typical performance characteristics of the ABB IRB 140 as it is commonly used in industrial settings. It also provides a baseline for comparing the robot's efficiency and dynamic behaviours under standard operating conditions.

III. ROBOTIC ARM MODELS

The systematic analysis of the ABB IRB-140 robotic arm, as conducted at the UQTR Automation Laboratory, began with the input of joint space data to generate the arm's trajectory, underpinning the subsequent development of kinematic models. Using Denavit-Hartenberg parameters, forward kinematics were meticulously formulated to identify the end-effector's positions and orientations. The motions of the robot's joints were then articulated through fifth-order polynomial equations and homogeneous transformation matrices, offering a complete representation of the robot's spatial configurations.

These kinematic constructs initial input as position, velocity, and acceleration to perform the dynamic modelling phase, which employed the Euler-Lagrange formalism to delve into the robot's dynamics, mainly focusing on joint torques and energy consumptions. Such dynamics were further refined by integrating inertia data and mass center positions derived from Solidworks's detailed CAD/CAM modelling process. This foundational work transitioned seamlessly into the computer-aided optimization (CAO) phase, where three different robotic arm models were conceptualized, each varying in complexity from a simplified abstraction to a detailed simulation containing a fidelity spectrum.

The completion of kinematic and dynamic modelling facilitated an integrated analysis, enabling the precise measurement of energy demands based on the torque profiles of each joint. The dynamic models' outputs, which included torque and energy parameters, were instrumental in evaluating the robotic arm's efficiency and the impact of varying model detail levels on system performance.

This comprehensive approach, graphically synthesized in the flowchart Fig. 2, provided a clear flow from the initial data input to the final output analysis. This integrative methodology highlighted the robotic system's efficacy and illuminated the delicate interplay between model detail and the robot's operational efficiency.

A. Kinematics of the Robot

The forward kinematics model aims to determine the position and orientation of the robot's end-effector as a function of joint angle and displacement relative to the base frame or other reference [57]-[61]. To achieve this mathematically, a global coordinate frame must be assigned to the base frame and a local reference frame must be assigned to each joint [62]-[66]. Homogeneous transformation matrices of size 4×4 is then computed for the robot joint axes using a formalism such as D-H (Denavit–Hartenberg) to define and interpret the robot's spatial geometry and end-effector location within a fixed reference system [67]-[70].

The kinematic function thus maintains a fixed relationship between the two successive joint axes it supports. This relationship can be defined using two parameters: the link length a and link twist α. The link offset d and joint angle θ are used to describe the nature of the connection between adjacent links [28]. Fig. 3 shows the D-H parameter and link assignments for a rotational joint.

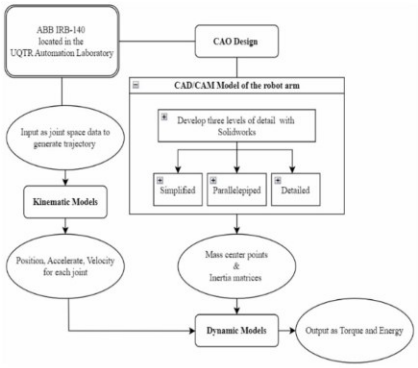

Fig. 2. The flowchart for the methodological steps

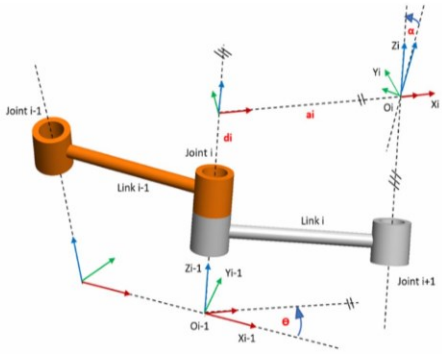

Fig. 3. D-H parameters and link assignments for a rotational joint

The parameters for link i in Figure 3 are defined as follows:

α_{i-1} Twist angle between joint axes z_i and z_{i-1} measured about x_{i-1}.
a_{i-1} Distance between joint axes z_i and z_{i-1} measured along the standard normal.
θ_i Joint angle between joint axes x_i and z_{i-1} measured about z_i.
d_i Link offset between axes xi and x_{i-1} measured along z_i.

The four transformations between the two axes can thus be defined as follows:

$$^{i-1}_{i}T=Rot(x_{i-1},\alpha_{i-1})Trans(x_{i-1},a_{i-1})Rot(z_i,\theta_i)Trans(0,0,d_i) \quad (1)$$

Where $^{i-1}_{i}T$ is the homogeneous transformation matrix, Rot (x_{i-1}, α_{i-1}) is the rotation around an axis x_{i-1} by an angle α_{i-1}, Trans (x_{i-1},a_{i-1}) is the transfer along axis x_{i-1} to the value a_{i-1},

Rot (z_i, θ_i) is the rotation around axis z_i by an angle θ_i, and Trans (0, 0, d_i) is the transfer along axis z to the value d.

Therefore, the following homogeneous transformation matrix can be obtained:

$$ {}^{i-1}_{i}T=\begin{pmatrix} C\theta_i & -SI & 0 & a_{i-1} \\ SI_i C\alpha_{i-1} & CI & -S\alpha_{i-1} & -d_i S\alpha_{i-1} \\ S\theta_i S\alpha_{i-1} & C\theta_i S\alpha_{i-1} & C\alpha_{i-1} & d_i C\alpha_{i-1} \\ 0 & 0 & 0 & 1 \end{pmatrix} \quad (2) $$

Where C and S denote the cosine and sine of an angle, respectively.

Fig. 4 shows the frame assignments, and Table II lists the D-H parameters of the ABB IRB 140 industrial robot, with the global coordinate system shown below [71]:

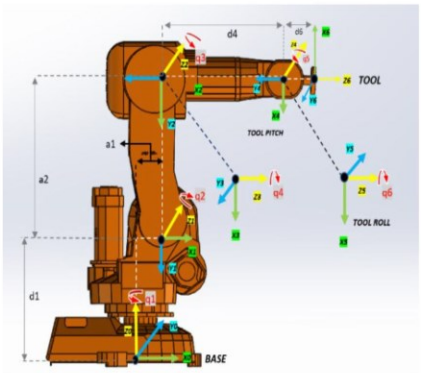

(a)

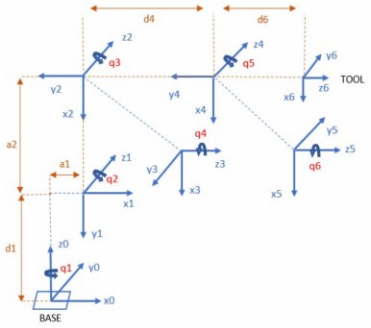

(b)

Fig. 4. ABB IRB 140 frame assignments: (a) Frames represented on the real robot, (b) Frames symbolised using DH representation

TABLE II. DENAVIT–HARTENBERG PARAMETERS FOR THE ABB IRB 140 ROBOTIC ARM

Link	a(mm)	α (°)	d (mm)	θ (°)
1	70	-90	d_1= 352	q_1
2	-360	0	0	q_2+90
3	0	-90	0	q_3
4	0	90	d_4 = 380	q_4
5	0	-90	0	q_5
6	0	0	d_6 = 65	q_6

With the D-H parameters, the individual homogeneous transformation matrices for each link can be obtained by substituting the link parameters into Equation (2). The position and orientation are achieved by applying the forward kinematic chain in the global frame, and the pose matrix of the end-effector relative to its base frame is obtained as follows:

$$ {}^{0}_{6}T={}^{0}_{1}T.\ {}^{1}_{2}T.\ {}^{2}_{3}T.\ {}^{3}_{4}T.\ {}^{4}_{5}T.\ {}^{5}_{6}T=\begin{pmatrix} r_{11} & r_{12} & r_{13} & X \\ r_{21} & r_{22} & r_{23} & Y \\ r_{31} & r_{32} & r_{33} & Z \\ 0 & 0 & 0 & 1 \end{pmatrix} \quad (3) $$

Such that:

$$ r_{11}=-S_6\left(S_4C_1C_{2'3}+C_4S_1\right)-C_6\left(C_5\left(S_1S_4-C_4C_1C_{2'3}\right)+S_5C_1C_{2'3}\right) $$
$$ r_{12}=S_6\left(C_5\left(S_1S_4-C_4C_1C_{2'3}\right)+S_5C_1C_{2'3}\right)-C_6\left(S_4C_1C_{2'3}+C_4S_1\right) $$
$$ r_{13}=C_5C_1S_{2'3}-S_5\left(S_1S_4-C_4C_1C_{2'3}\right) $$
$$ r_{21}=C_6\left(C_5\left(C_4S_1C_{2'3}+C_1S_4\right)-S_5S_1S_{2'3}\right)-S_6\left(S_4S_1C_{2'3}-C_1C_4\right) $$
$$ r_{22}=-S_6\left(C_5\left(C_4S_1C_{2'3}+C_1S_4\right)-S_5S_1S_{2'3}\right)-C_6\left(S_4S_1C_{2'3}-C_1C_4\right) $$
$$ r_{23}=C_5S_1S_{2'3}+S_5\left(C_4S_1C_{2'3}+C_1S_4\right) $$
$$ r_{31}=-C_6\left(S_5C_{2'3}+C_4C_5S_{2'3}\right)+S_4S_6S_{2'3} $$
$$ r_{32}=C_6S_4S_{2'3}+S_6\left(S_5C_{2'3}+C_4C_5S_{2'3}\right) $$
$$ r_{33}=C_5C_{2'3}-C_4S_5S_{2'3} $$

C_i and S_i denote the cosine and sine of the joint angle qi, C_{ij} and S_{ij} denote the cosine and sine of $qi + qj$ Notation 2' refers to $q_2'=q_2+\pi/2$

The X, Y, and Z position coordinates of the IRB140 robot relative to the base frame are computed as follows:

$$ X=C_1a_1+d_6\left(C_5C_1S_{2'3}-S_5(S_1S_4-C_4C_1C_{2'3})\right)+d_4C_1S_{2'3}-C_1C_2a_2 $$

$$ Y=S_1a_1+d_6\left(C_5S_1S_{2'3}-S_5(C_4S_1C_{2'3}+C_1S_4)\right)+d_4S_1S_{2'3}-C_2S_1a_2 $$

$$ Z=d_1+d_4C_{2'3}+a_2S_2+d_6\left(C_5C_{2'3}-C_4S_5S_{2'3}\right) $$

B. Differential Kinematics of the Robot

Differential kinematics define the relationship between the joints' angular velocities and the corresponding end-effector linear and angular velocities. The study of velocities and static forces yields the Jacobian matrix of the manipulator, which is an essential tool for analysing and controlling robotic motion, identifying singularities and redundancy, determining inverse kinematic equations, and describing the velocity and force manipulability ellipsoids [72]-[74].

The Jacobian matrix, a basis in the kinematic analysis of robotics, is critical for relating joint velocities with the end-effector, a key factor in determining the robot's performance and manoeuvrability. Specifically tailored to the unique joint configurations of each robot, the Jacobian matrix significantly enhances motion planning and control capabilities, which are crucial for executing precision tasks with the robotic arm. It addresses singularities and redundancies, enabling the robot's operational efficiency and safety. Our research employs the Jacobian matrix for smooth and singularity-free motion planning, a necessary factor for ensuring reliable and practical outcomes in our studies. Utilizing MATLAB simulations, we have demonstrated the

Jacobian's considerable impact in practical settings, highlighting notable improvements in accuracy and speed.

A Jacobian matrix is a multidimensional form of the derivative. It can be of any dimension (including non-square), depending on the number of joints. The number of rows in a Jacobian matrix is equal to the number of degrees of freedom in Cartesian space; for example, three rows would be present if the robot's position only was considered, whereas there would be six if both its position and orientation were considered. The number of columns in the matrix corresponds to the number of joints comprising the manipulator.

Considering the end-effector linear velocity vector $\dot{p}_e$, the angular velocity vector ωe, and the joint velocity vector $\dot{q}$, Jp is the (3×n) matrix that links the linear velocity vector to the joint speed vector. Jo is the (3×n) matrix that links the angular velocity vector to the joint speed vector as expressed in Equations (4) and (5) or in the compact form expressed in Equation (6) [24][75].

$$\dot{P}_e=J_p(q)\dot{q} \tag{4}$$

$$\omega_e=J_o(q)\dot{q} \tag{5}$$

$$V_e=\begin{pmatrix}\dot{P}_e\\ \omega_e\end{pmatrix}=J(q)\dot{q} \tag{6}$$

where V_e is the end-effector velocity and $J=\begin{pmatrix}J_p\\ J_o\end{pmatrix}$ is the Jacobian matrix.

If the relationship between the joint space variable and the orientation space variable is highly nonlinear, the inverse kinematics solution will be redundant and closed form or even non-existent. The inverse kinematics problem initially involves a linear mapping of the joint velocity space and the operational velocity space using differential equations. Depending on the desired end effector position and orientation, the corresponding joint velocity can be obtained via simple inversion of the Jacobian matrix, which therefore must be invertible, i.e., J is square and its determinant is non-zero. The inverse differential kinematics model can then be computed using Equation (7).

$$\dot{q}=J^{-1}V_e \tag{7}$$

Where J^{-1} is the inverse of the Jacobian matrix.

As noted above, the Jacobian matrix can be of any dimension, and is not always square or invertible; in this instance, the pseudo-inverse form of the generalized inversion can be used [24].

C. Dynamic Model

A dynamic model allows the expression of the robot's function in terms of joint acceleration forces and torque. The most widely used method to determine this model is the Euler–Lagrange approach. The model of an n-jointed robotic arm can be expressed by Equation (8) [24].

$$M.\ddot{q} + V + G = \tau \tag{8}$$

Where $\ddot{q}$ is the joint acceleration vector, M is the inertia matrix, V is the Coriolis vector, G is the gravitational vector, and τ is the force and torque vector. The inertial data and mass centre position were obtained using SolidWorks 3D CAD modelling software for the detailed, semi-detailed (rectangular), and simplified models in this study. Parameters such as the geometry and density of each link (assumed to be uniform in all models) are considered, in addition to significant values related to mass and other physical properties such as the mass centre position and inertia matrices, which are represented in their respective reference frames for the three proximal links. A dynamic model's precision relies on accurately estimating the mass center and inertia matrices. Straightforward dimensional specifications and scientific techniques such as CAD modeling, Experimental Modal Analysis, and Inertia Measurement Units are employed to obtain this required data in engineering. CAD modelling presents detailed dimensional and mass distribution data, while Experimental Modal Analysis and Inertia Measurement Units directly measure inertia characteristics. This research primarily aims to examine the influences of simplifications in obtaining mass properties and then the effects of the level of simplification on the performance of the dynamic models. Such simplifications, desired to reduce computational demands, can affect the model's precision. The study seeks a balance between computational efficiency and precision, which is required in robotics, where exact movements and energy efficiency are critical.

Assuming a constant and homogeneous density, the comparative mass of each link can be estimated. In this study, the volume of each link was determined using SolidWorks software. The relationship of an element's volume to the robot's total volume is multiplied by the total mass to give an estimated link mass value.

The following matrices I_i correspond to the inertia tensors of the proximal links over their mass centres and are expressed relative to the base reference frame [24].

$$I_1=\left[{}^0_1R\right]\ {}^1I_1+\left[{}^0_1R\right]^T \tag{9}$$

$$I_2=\left[{}^0_1R\,{}^1_2R\right]\ {}^2I_2+\left[{}^0_1R\,{}^1_2R\right]^T \tag{10}$$

$$I_3=\left[{}^0_1R\,{}^1_2R\,{}^2_3R\right]\ {}^3I_3+\left[{}^0_1R\,{}^1_2R\,{}^2_3R\right]^T \tag{11}$$

${}^1I_1$, ${}^2I_2$ and ${}^3I_3$ are the inertia matrices.

In the dynamic analysis of this manipulator, joint friction was not considered. For the tracking of a path, the vector of generalized forces was considered as shown below:

$$\sum_{j=1}^{n} M_{ij}\ddot{q}+V_i+G_i=\tau_i,\quad i=1,2,\ldots, \tag{12}$$

M_{ij} represents the inertial forces, V_i represents the centrifugal and Coriolis forces, and G_i indicates the gravitational forces. This equation can also be used to determine the joints' acceleration values, as follows:

$$\ddot{q}=M^{-1}(Q-V-G) \tag{13}$$

$$M=\sum_{i=1}^{n}\left(J_{vi}^T m_i J_{vi}+J_{\omega i}^T I_i J_{\omega i}\right) \tag{14}$$

$$V_i=\sum_{j=1}\sum_{i=1}^{n}\left(\frac{\partial M_{ij}}{\partial q_k}-\frac{1}{2}\frac{\partial M_{jk}}{\partial q_i}\right)\dot{q}_j\dot{q}_k \tag{15}$$

$$G_i = -\sum_{j=1}^{n} m_j g^T J_{vj}^T \quad (16)$$

The inertia matrix of the manipulator is symmetric and positive definite and therefore always invertible [24].

D. CAD Design of the Robot

The decision to create three different ABB IRB 140 arm industrial robot models in SolidWorks is based on the need for a comprehensive understanding of kinematic and dynamic behaviour. The accurate, detailed model in Fig. 5 is essential for simulations that require high fidelity and detailed analysis. This model duplicates the robot's structure with maximum precision, making it ideal for investigating complex dynamics and interactions within the actual robot's mechanism. In contrast, the less detailed rectangular model, such as the parallelepiped model in Fig. 6, balances detail and computational efficiency. Its simplified geometric representation suits quicker simulations where extreme detail is not required. This model serves as a midpoint, validating results from the detailed model and offering a more efficient alternative for less demanding simulations. Lastly, the simplified model in Fig. 7 reduces the robot to its fundamental components. This model benefits high-level analyses and educational purposes, focusing on understanding the robot's basic mechanics rather than its detailed construction. Simplification might not accurately represent the varying density and weight distribution in different parts of the robot, potentially affecting the precision of dynamic simulations, such as calculating torque and evaluating the energy.

During the CAD design process, a fundamental assumption is the uniform and constant density across all parts and links of the robot. While this simplifies the computational characteristic, it is a potential source of inaccuracy, as it needs to account for the material variations in the actual robot. Another assumption involves the mass and inertia characteristics provided by SolidWorks, based on the model's geometry and assumed material properties. These estimations are required for dynamic analysis but may not perfectly match the real-world robot due to factors like manufacturing tolerances and material inconsistencies.

The assumptions made during the CAD design process are practical but can significantly influence the accuracy of the models. While the uniform density assumption simplifies the modelling, it might lead to simulation discrepancies, particularly in dynamic behaviour. Likewise, although functional for initial analysis, the derived inertia characteristics require improvement for more precise simulations. The details of each model and the results for the proximal links obtained from the Solidworks mass properties tool after modelling are summarised in Table III.

E. Robot Performance Assessment

To evaluate the accuracy of the three models' predictions, we analysed the energy consumption by the three proximal joints and the robot's total energy consumption over the same duration and path of movement. In the proposed modelling approach, the energy consumption of each joint at a specific time can be calculated from the joint torque and angular velocity using Equation (17). The robot's integrated energy consumption is assumed to be the sum of the energy consumption values of all the joints.

$$E_i = \int_{t_0}^{t_f} \tau_i(t).\dot{q}_i(t)\, dt \quad (17)$$

We employ a theoretical approach to evaluate the energy consumption of robotic arms. This approach centers on dynamic models that simulate each joint's torque τ_i and angular velocity $\dot{q}_i$ Detailed explanations of how these parameters are simulated are provided in the methodology section. The simulated values are then used in Equation (17) to calculate the energy consumption of each joint. Theoretical method offers a comprehensive analysis of energy consumption, avoiding the practical challenges and complexities associated with the installation and calibration of physical sensors on the robotic arm.

Focusing on a theoretical and simulation-based approach contributes significantly to understanding energy dynamics in robotic arms, especially in scenarios where direct measurement is impractical or impossible. This approach also aligns with current trends in employing computational models to analyze complex system contributions to robotics fields.

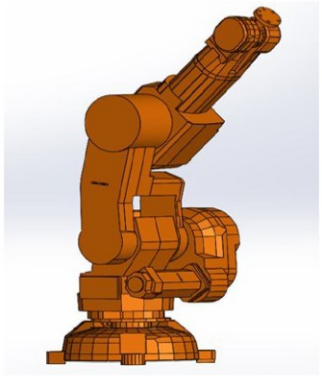

Fig. 5. Detailed SolidWorks model of the ABB IRB 140 robotic arm

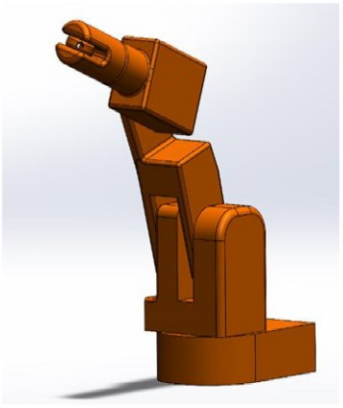

Fig. 6. Semi-detailed rectangular SolidWorks model of the ABB IRB 140 robotic arm

Fig. 7. Simplified SolidWorks model of the ABB IRB 140 robotic arm

TABLE III. MASS PROPERTY RESULTS OF EACH MODEL CALCULATED USING SOLIDWORKS SOFTWARE

Link	parameter(unit)	Detailed model	Semi-detailed model	Simplified model
1	Weight (kg)	35	35	35
	Xc (mm)	277.87	17.87	0
	Yc	373.12	103.12	181.37
	Zc	-199.03	-79.03	0
	Ixx (kg.m2)	6.5	1.5	1.1
	Ixy	1.1	0.1	0
	Ixz	3.05	0.05	0
	Iyy	2.02	0.002	0
	Iyz	5.07	0.07	0.1e-5
	Izz	1.4	0.04	1.1
	Weight (kg)	35	35	35
2	Weight (kg)	25	25	25
	Xc (mm)	218.29	178.29	0
	Yc	229.73	9.73	255.24
	Zc	112.43	72.43	0
	Ixx (kg.m2)	0.9	0.1	1.6
	Ixy	-0.03	-0.03	0.1e-5
	Ixz	0.1	0.01	0
	Iyy	1.3	0.03	0
	Iyz	-0.01	-0.01	0
	Izz	0.95	0.05	1.6
	Weight (kg)	25	25	25
3	Weight (kg)	18	18	18
	Xc (mm)	-24.56	14.56	0
	Yc	-219.9	-199.96	195.69
	Zc	-25.86	-15.86	0
	Ixx(kg.m2)	2.5	1.5	0.6
	Ixy	-0.001	-0.001	0.3e-5
	Ixz	0.09	0.09	0
	Iyy	2.7	0.7	0
	Iyz	-0.8	-0.02	0
	Izz	0.5	0.2	0.6
	Weight (kg)	18	18	18

IV. RESULTS AND DISCUSSION

The dynamic performance of an ABB IRB-140 six-jointed industrial robotic arm was considered in the present research, with a principle on the effect of model simplification on torque prediction and energy consumption. Our study extends and analyses three varying models of the robotic arm, simplified, semi-detailed, and detailed, using precise kinematics models, differential kinematics, and an advanced dynamic model based on the arm's technical specifications. The design of three levels of CAO design, facilitated by Solidworks, aimed to obtain the center of mass and inertia matrices, which are crucial for understanding the dynamic behaviour of the manipulator. Through this analysis, we aim to unravel the interplay between model complexity and its importance on computational efficiency and accuracy, eventually providing a comprehensive understanding of model selection in industrial robotics. This research, therefore, not only investigates the performance of these models in a standard functional context but also seeks to inform the optimization of robotic systems, balancing precision, energy consumption, and computational demands.

Based on the mass and inertia characteristics of the robot and the calculated end-effector position, orientation, velocity, and acceleration and the torque of each joint in the three proximal links (i.e., the principal determinants of the end-effector position), the dynamic kinematic model of the robot developed in SolidWorks was examined in MATLAB in full detail over a 30-second interval without a payload at the effector end of the robotic arm. The forward and robot kinematic models were derived from the D-H parameters, and a procedure was developed to solve the inverse kinematics. Trajectory planning was based on a fifth-order polynomial. The values in Table I were used to cover all possible angles of each of the robot's rotating joints. Fig. 8 displays the changes in angle over time for the three proximal links of the ABB IRB-140 robotic arm, highlighting the dynamic positioning of these joints during the task operation. The corresponding velocity and acceleration diagrams are shown in Fig. 9 and Fig. 10. Fig. 9 shows the velocity variations of the robotic arm's proximal joints, highlighting the speed dynamics during the arm's movements. Fig. 10 depicts the acceleration patterns of the proximal joints, capturing the robotic arm's dynamic response during its operating path.

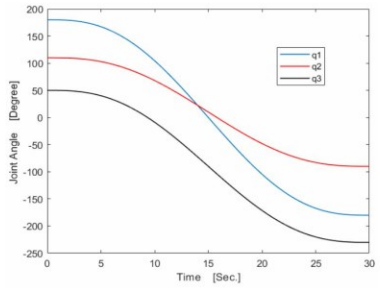

Fig. 8. IRB 140 robot proximal joint angle variations

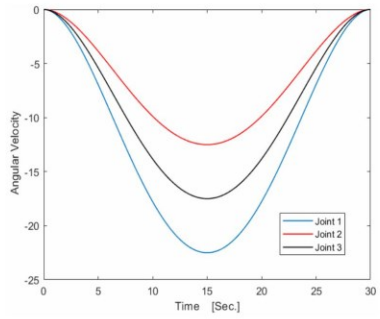

Fig. 9. IRB 140 robot proximal joint angle variations

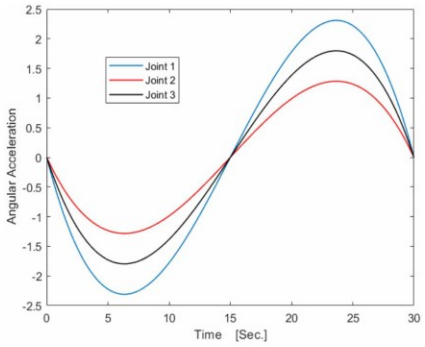

Fig. 10. IRB 140 robot proximal joint angle variations

The torque variations for the position and path corresponding to a single, uninterrupted time interval are shown in Fig. 11 to Fig. 13. These figures show the torque variations for the robotic arm's first three proximal joints, presenting insights into the mechanical loads experienced during its operation.

As shown, the results obtained for all three joints are consistent and appear relatively close for the semi-detailed and simplified models. The detailed model tends to exhibit higher torque at most time points in joint 1, for a short period in joint 2, and throughout almost all of the modelled period in joint 3. Notably, the semi-detailed and simplified models both track the detailed model quite closely for at least some of the time; however, this behaviour varies between different joints. The results also confirm that joint 2 experienced much more torque than the other joints, which likely occurs because this joint provides most of the reaching capability of the robotic arm.

In addition to its weight and gravitational force, the link also bears a share of the weight and gravitational force of the third link. As the robot reaches further from its centre of gravity, the mass of the remaining links creates additional torque. The observed bends in the torque curves result from changes in the direction of the arm movement based on the defined task path. In addition, these changes in direction in the defined path cause the torque values of all three joints be equal at various points during the simulation.

Due to the choice of a fifth-order polynomial trajectory, the joint torque curves for all three models exhibit little or no noise. The torque starts at zero for joint 1, rises quickly, and then drops smoothly to zero. For joints 2 and 3, the torque starts at non-zero values, drops, rises to new values, and then ends at different values at the end of the path. These profiles arise due to the positions and movements against gravity encountered by the arm over its defined trajectory.

In the case of joints 1 and 2, the semi-detailed and simplified models show higher torque than the detailed model during some periods, whereas the opposite is generally observed for joint 3. In addition, the simplified model exhibits slightly less torque than the semi-detailed model at the beginning and end of the simulation and lags the semi-detailed dynamics throughout the path. Since the link weight and density are identical in all the models, these differences in torque must therefore reflect differences in the centre of mass and inertia tensors. Differences in the torque at joints 1 and 2 likely arise due to the weight and torque imposed by other links. The gravitational force of the other links affects the first and second joints, and only the third joint carries its gravitational force without much additional torque.

Based on the frame assignments defined for the robotic arm, link 1 does not exert a gravitational force and undergoes joint acceleration only; thus, the torque is at its lowest value in this link. The second and third links exert gravitational force and are subject to angular acceleration in the joints. The combination of these two acceleration vectors defines the overall acceleration of these two links.

When the joint acceleration falls to zero, most of the torque is expected to be gravitational, i.e., an opposing force resisting the movement of the robotic arm.

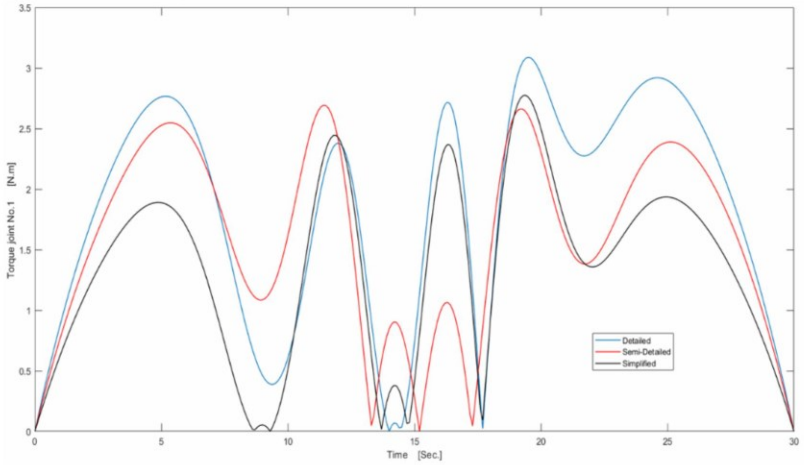

Fig. 11. Torque variations for the first proximal joint of the IRB 140 robotic arm

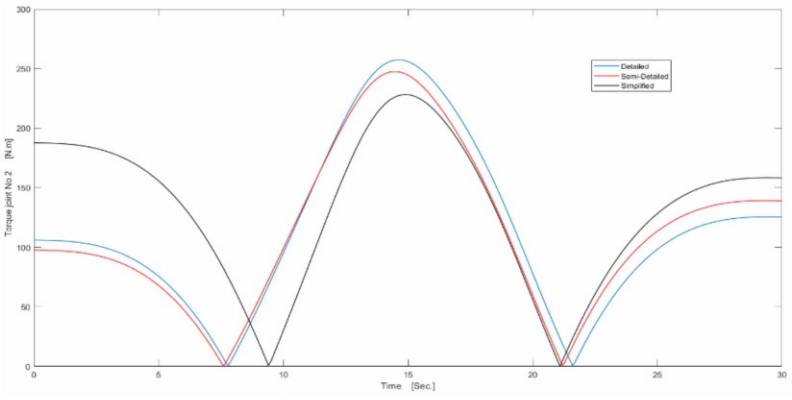

Fig. 12. Torque variations for the second proximal joint of the IRB 140 robotic arm

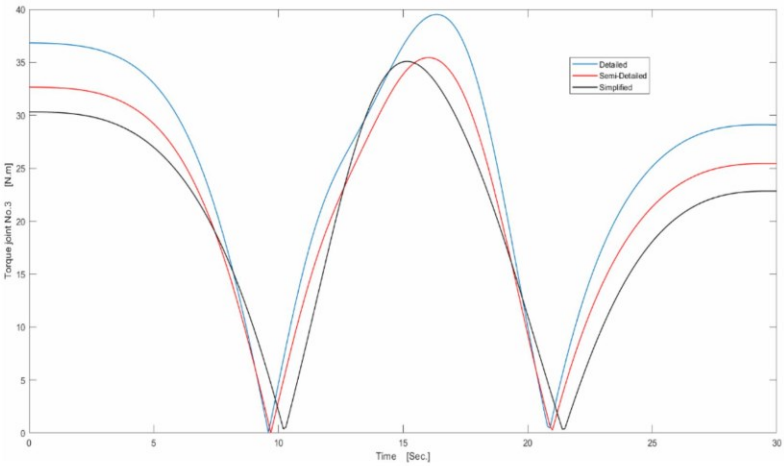

Fig. 13. Torque variations for the third proximal joint of the IRB 140 robotic arm

One of the main aims of this study is to examine how well the different dynamic models predict the energy consumption of each rotational joint and the robot overall, as determined by Equation (17). These results are shown in Fig. 14 (joints) and Fig. 15 (robot). Fig. 14 compares the energy consumption of each joint in the robotic arm across the three model variations, highlighting the differences in energy efficiency. Fig. 15 illustrates the total energy consumption of the robotic arm over a standard 30-second task, emphasizing each model's energy efficiency.

The energy consumption patterns are broadly similar in form in all three joints and models. Joint 2, which has the highest torque, consumes the most energy. During the 30-second simulation in this study, the energy consumption of the joints and the whole robotic arm increased, with the most rapid energy consumption increase recorded in the middle of the simulation. The energy consumption increases reflect changes in gravitational forces on the links as they move away from their initial centres of mass. Joint 2 and the arm show strikingly similar energy consumption patterns in all three models, and the semi-detailed and simplified models for joint 2 track each other closely. For the whole arm, the detailed and semi-detailed models are very similar and thus may reflect the influence of each model's mass properties and shape characteristics. The semi-detailed model yields the highest energy consumption in both cases, whereas the simplified model gives the lowest values, except for joint 1. Relative to the semi-detailed model, the overall energy consumption difference is 0.53% less in the detailed model and 6.8% less in the simplified model. Based on these results, the three dynamic models tested in this study are all worthy of confidence for predicting energy consumption by articulated robotic arms.

It is necessary to verify the underlying physical and theoretical reasons for response to the observed torque and energy consumption variations across the detailed, semi-detailed, and simplified. The intricacy of each model plays a key role in its predictive accuracy. The detailed model, capturing more complex dynamics, including acceptable joint interactions and precise physical properties, delivers more

accurate torque predictions and energy consumption profiles. In contrast, the semi-detailed and simplified models, with inevitable oversimplifications in dynamics and geometry, may need to capture these intricate details more effectively, leading to noticeable discrepancies. Specifically, the variation in the center of mass and inertia tensors across models significantly impacts torque requirements. The detailed model's precise calculations offer a closer representation of real-world dynamics, whereas the simplified models, with their approximations, might either underestimate or overestimate these forces.

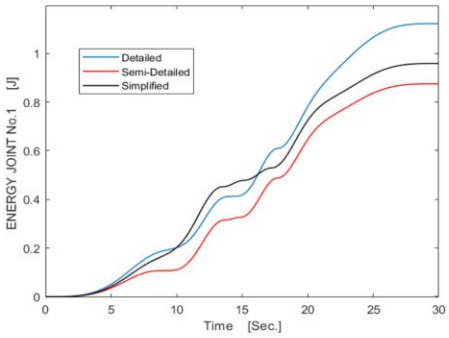

(a)

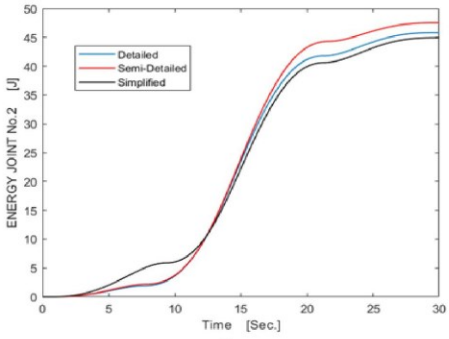

(b)

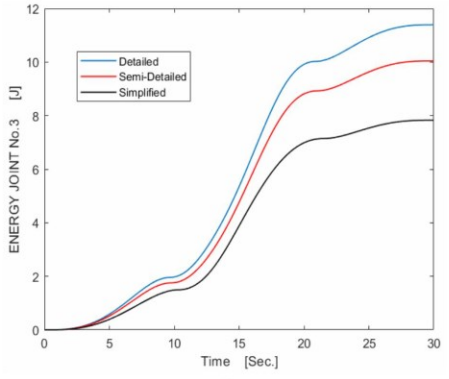

(c)

Fig. 14. Energy variations for the third proximal joint of the IRB 140 robotic arm

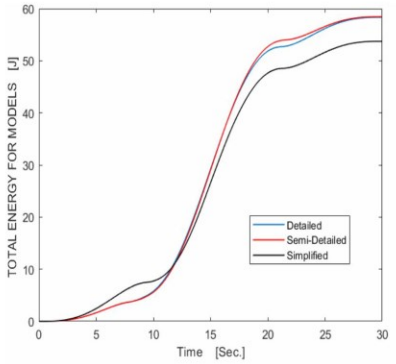

Fig. 15. Energy variations for the third proximal joint of the IRB 140 robotic arm

Moreover, the detailed model more accurately shows the influence of link weight and gravitational forces. This factor becomes especially essential in joints primarily responsible for the arm's movement, as their torque requirements vary substantially with the arm's position relative to its center of gravity. Finally, a comparative analysis of energy consumption highlights how each model's complexity influences its energy efficiency. The detailed model provides a fine sense of energy dynamics, particularly in joints with higher energy demands. These insights are invaluable for optimizing robotic systems, where accuracy, computational efficiency, and energy conservation are paramount. Therefore, understanding these differences in model complexity and their impact on torque and energy consumption is crucial for informed decision-making in the design and optimization of industrial robotic systems.

In comparing our findings with related literature, we note several parallels and distinctions in the dynamics of robotic arm manipulators. Earlier studies, such as those by Boiadjiev et al. [76] and Ding et al. [77], have highlighted the importance of model complexity in predicting torque and energy consumption in robotic arms. Our research develops these findings by providing an analysis of how different model simplification levels simplified, semi-detailed, and detailed impact these predictions. Our research aligns with Mahdavian et al. [78], meaning that more complex models predict higher torque requirements, particularly in joints with more intricate movement patterns. However, our study uniquely contributes by quantifying the energy consumption across these models, a factor that needs to be explored in previous research. The work by Fang et al. [79] on energy-efficient hydraulic joints for mobile robotic manipulators and the operational dynamics of the OceanWATERS lander arm by Catanoso et al. [80] provide complementary perspectives to our findings on energy efficiency. This comparative analysis reaffirms the general directions documented in previous studies. It adds new dimensions to performance model complexity in industrial robotic arms, particularly in energy efficiency and dynamic performance. As our study highlights, balancing computational efficiency and accuracy in model selection is critical for optimizing performance based on the required task precision and available computational resources. Our findings provide a practical

attachment to previous work, confirming comprehended trends and offering new insights into the industrial robotic arm dynamics in the present prospect, where energy efficiency is increasingly prioritized.

An existing knowledge gap is a balance between model accuracy and computational efficiency in industrial robotics by comparing various model complexities, enhancing the performance of robotic simulations. This research has significant practical applications, especially in optimizing energy use and robust design in industrial settings, potentially reducing costs and enhancing sustainability. We assumed uniform density across each link and ignored joint friction. While these assumptions simplify modeling, they overlook material distribution influences and friction's impact on energy and torque. Therefore, our findings might only partially reflect real-world complexities. Addressing these aspects in future research could enhance the model's accuracy and applicability in practical scenarios. Future research directions include exploring more precise or proving outcomes of the accurately designed models with advanced optimization algorithms like quantum-inspired particle swarms. Our findings highlight the significance of proper modelling in robotics, providing valuable guidance for professionals in optimizing performance and efficiency in industrial robotic systems.

V. CONCLUSION

In most industrial robotics studies, only one dynamic model is typically used, with comparisons between models being rare. In this study, we developed three models for the ABB IRB 140 industrial robotic manipulator arm, which has six degrees of freedom. These models, developed in SolidWorks, are detailed, semi-detailed, and simplified. We characterized the end-effector position and orientation by presenting kinematic models linked to a proposed elaborate dynamic model using mass and inertial data obtained from Solidworks's mass properties tool to calculate joint torque for the three proximal links. These links are crucial for the accuracy of the robotic arm's movements. We used the Spong formulation for forward and inverse differential kinematics [24]. The mathematical models of the robot were analyzed in detail in MATLAB. We derived the robot's forward kinematics from D-H parameters and executed a trajectory planning based on a fifth-order polynomial.

Our key finding is that the links' dimensions and geometry significantly influence the mass center position and inertial matrix characteristics of the robot links, which impacts straightforward torque equations. Selecting the correct position for the center of mass and inertia tensor elements in dynamic models is essential. Interestingly, the simplified model, often used in classical computational methods, yields acceptable results. The accuracy of these results in reflecting the actual robot's behavior needs further validation. It is important to note that any model-derived data for mass properties will have an error percentage that must be considered in dynamic equations.

MATLAB helps implement algorithms, estimate and validate models, and simulate system responses. MATLAB is required for its robust algorithmic capabilities, efficient data processing, and simulation tools in computational robotics. It excels in implementing complicated mathematical models, analyzing kinematic and dynamic data, and visualizing robotic behaviors, making it a valuable tool for research and development in this field. Computational time and efficiency for solving algebraic equations matter in robotics. A comparative study for three different models of the case study in the same operation system (OS) and hardware configuration indicates that the time for analyzing the dynamic model to calculate torque equation in the same trajectory for a detailed model was 83.2 percent, and semi-detailed was 47.63 percent more than the simplified model. Another important finding is that all three robot models show similar total energy consumption over a movement path in a given time, which indicates that each model could be effective in various scenarios. In robotics, some calculations are complex, involving multiple points. Therefore, a simplified model version can enhance and optimize the calculation process and make significant contributions to execution time and efficiency, addressing key industrial robotics challenges like improving energy efficiency and sustainability in continuous operations, optimizing production processes for higher throughput in manufacturing while offering flexibility in robot deployment across various applications. These insights promise considerable improvements in diverse manufacturing environments. Industries can choose models based on specific needs: precision for aerospace, speed for manufacturing, and customization for unique applications, balancing robustness and computational resources.

The developed model facilitates by assuming homogeneous density across each link and disregarding joint friction. This approach might only partially capture the real world, such as the effects of varied material distribution and friction on energy and torque. Future research addressing these factors could improve model precision and real-world relevance. Admitting these limitations, such as assuming uniform density across each robotic link and neglecting joint friction, can also lead to advanced control strategies, enhancing the accuracy and effectiveness of robotic arms in practical, complex environments. Introducing a control module and a robustness controller could further enhance the precision of the models, minimizing the impact of input errors.

Future research could focus on refining these aspects, utilizing advanced optimization algorithms like quantum-inspired particle swarms to identify more accurate and practical parameters for each model. Additionally, there is scope for assessing the torque requirements for various robot positions and operations and comparing energy consumption during different tasks. Quantum computing carries notable potential for enhancing the modeling of complicated systems like the dynamic models of robotic arms [71][81]-[83]. Its ability to process extensive data at exceptional speeds makes it ideal for tackling the intricate calculations involved in robotics [84]. By utilizing quantum-inspired algorithms, such as particle swarm optimization, researchers can have more accurate and efficient modeling, overcoming the limitations of classical computing methods. This approach could lead to breakthroughs in comprehending the behaviors of robotic systems, enabling more precise control and optimization. The

application of quantum computing in this domain promises to revolutionize how dynamic models are developed and applied, potentially leading to more sophisticated and capable robotic systems in various industrial applications [85].

A key takeaway from our study is the importance of detail in modeling so that detailed models offer higher accuracy, and simplified models significantly reduce computational time and enhance efficiency, which is critical for professionals in the field as it guides the selection of appropriate models based on the specific requirements of precision and efficiency in industrial robotic systems.

ACKNOWLEDGMENT

This research was funded by the PAIR fund from UQTR.

REFERENCES

[1] M. Suomalainen, Y. Karayiannidis, and V. Kyrki, "A survey of robot manipulation in contact," *Robotics and Autonomous Systems*, vol. 156, p. 104224, Oct. 2022, doi: 10.1016/j.robot.2022.104224.

[2] M. Schwenzer, M. Ay, T. Bergs, and D. Abel, "Review on model predictive control: an engineering perspective," *The International Journal of Advanced Manufacturing Technology*, vol. 117, no. 5–6, pp. 1327–1349, Aug. 2021, doi: 10.1007/s00170-021-07682-3.

[3] G.-H. Yang and J. Yao, "Nonlinear adaptive output feedback robust control of hydraulic actuators with largely unknown modeling uncertainties," *Applied Mathematical Modelling*, vol. 79, pp. 824–842, Mar. 2020, doi: 10.1016/j.apm.2019.10.062.

[4] D. Xuan and J. Bae, "A Precise Neural-Disturbance Learning Controller of Constrained Robotic Manipulators," *IEEE Access*, vol. 9, pp. 50381–50390, 2021, doi: 10.1109/ACCESS.2021.3085907.

[5] M. Goubej, J. Königsmarková, R. Kampinga, J. Nieuwenkamp, and S. Paquay, "Employing Finite Element Analysis and Robust Control Concepts in Mechatronic System Design-Flexible Manipulator Case Study," *Applied Sciences*, vol. 11, no. 8, p. 3869, 2021, doi: 10.3390/app11083869.

[6] C. Xiao and Y. Jianyong, "Robust Adaptive Control for a class of uncertain nonlinear systems with an optimized smooth input," in *2021 33rd Chinese Control and Decision Conference (CCDC), IEEE*, 2021, doi: 10.1109/CCDC52312.2021.9607054.

[7] P. Kremer, J. L. Sanchez-Lopez, and H. Voos, "A Hybrid Modelling Approach for Aerial Manipulators," *Journal of Intelligent & Robotic Systems*, vol. 105, no. 4, p. 74, 2022, doi: 10.1007/s10846-022-01675-y.

[8] T. Yaren and S. Küçük, "Dynamic modeling of 3-DOF RRP type serial robotic manipulator using Lagrange-Euler method," in *International Marmara Sciences Congress (Autumn)*, pp. 372-378, 2019.

[9] M. J. Thomas, M. L. Joy, and A. P. Sudheer, "Kinematic and dynamic analysis of a 3-PR US spatial parallel manipulator," *Chinese Journal of Mechanical Engineering*, vol. 33, pp. 1–17, 2020, doi: 10.1186/s10033-020-00468-9.

[10] Y. Chen *et al.*, "Dynamic modeling and experimental validation of a water hydraulic soft manipulator based on an improved newton—Euler iterative method," *Micromachines*, vol. 13, no. 1, p. 130, 2022, doi: 10.3390/mi13010130.

[11] L. Yu, "An Effective Compensation Strategy for Dynamic Model based on Improved Kane Principal Formulation," *Journal of The Institution of Engineers (India): Series C*, vol. 103, no. 4, pp. 589–596, 2022, doi: 10.1007/s40032-021-00670-4.

[12] Y. Park, "An Automatic Program of Generation of Equation of Motion and Dynamic Analysis for Multi-body Mechanical System using GNU Octave," *Journal of Applied and Computational Mechanics*, vol. 7, no. 3, pp. 1687–1697, 2021, doi: 10.22055/JACM.2021.37445.3027.

[13] M. Trojanová and T. Cakurda, "Validation of the dynamic model of the planar robotic arm with using gravity test," *MM Science Journal*, vol. 5, pp. 4210–4215, 2020.

[14] C. Zhuang, Y. Yao, Y. Shen, and Z. Xiong, "A convolution neural network based semi-parametric dynamic model for industrial robot," *Proceedings of the Institution of Mechanical Engineers, Part C: Journal of Mechanical Engineering Science*, vol. 236, no. 7, pp. 3683–3700, 2022, doi: 10.1177/09544062211060249.

[15] J. Deng, W. Shang, B. Zhang, S. Zhen, and S. Cong, "Dynamic Model Identification of Collaborative Robots Using a Three-Loop Iterative Method," in *2021 6th IEEE International Conference on Advanced Robotics and Mechatronics (ICARM)*, pp. 937–942, 2021, doi: 10.1109/ICARM51412.2021.9512786.

[16] Q. Leboutet, J. Roux, A. Janot, J. R. Guadarrama-Olvera, and G. Cheng, "Inertial Parameter Identification in Robotics: A Survey," *Applied Sciences*, vol. 11, no. 9, pp. 4303, 2021, doi: 10.3390/app11094303.

[17] Y. Han, J. Wu, C. Liu, and Z. Xiong, "An iterative approach for accurate dynamic model identification of industrial robots," *IEEE Transactions on Robotics*, vol. 36, no. 5, pp. 1577–1594, 2020, doi: 10.1109/TRO.2020.2992386.

[18] M. Bottin, S. Cocuzza, N. Comand, and A. Doria, "Modeling and identification of an industrial robot with a selective modal approach," *Applied Sciences*, vol. 10, no. 13, p. 4619, 2020, doi: 10.3390/app10134619.

[19] S. A. Zimmermann, T. F. Berninger, J. Derkx, and D. J. Rixen, "Dynamic modeling of robotic manipulators for accuracy evaluation," in *2020 IEEE International Conference on Robotics and Automation (ICRA)*, pp. 814–850, 2020.

[20] J. G. Romero, R. Ortega, and A. Bobtsov, "Parameter estimation and adaptive control of Euler–Lagrange systems using the power balance equation parameterisation," *International Journal of Control*, vol. 96, no. 2, pp. 475–487, 2021, doi: 10.1080/00207179.2019.1661354.

[21] A. J. Muñoz-Vázquez, V. Parra-Vega, A. Sánchez-Orta, and J. D. Sánchez-Torres, "High-gain PI-like control of Euler–Lagrange mechanical systems: Simulations and experiments in 2DoF robotic manipulators," *Proceedings of the Institution of Mechanical Engineers, Part I: Journal of Systems and Control Engineering*, vol. 236, no. 4, pp. 857–869, 2022, doi: 10.1177/09596518211032626.

[22] X. He, M. Lu, and F. Deng, "Trajectory Tracking Control of Uncertain Euler-Lagrange Systems: A Robust Control Approach," in *2021 IEEE International Conference on Robotics and Biomimetics (ROBIO)*, pp. 1855–1860, Dec. 2021, doi: 10.1109/ROBIO54115.2021.9713830.

[23] L. Kong, S. Zhang, and X. Yu, "Approximate optimal control for an uncertain robot based on adaptive dynamic programming," *Neurocomputing*, vol. 423, pp. 308–317, 2021, doi: 10.1016/j.neucom.2020.10.112.

[24] M. Fazilat. *Advanced modelling and control of industrial robotic manipulator arm*. Diss. Université du Québec à Trois-Rivières, 2022.

[25] Z. Yang. *Modeling, simulation and control of microrobots for the microfactory*. Electronic Theses and Dissertations, 2023.

[26] Q. Zou, D. Zhang, S. Zhang, and X. Luo, "Kinematic and dynamic analysis of a 3-DOF parallel mechanism," *International Journal of Mechanics and Materials in Design*, vol. 17, no. 3, pp. 587–599, 2021, doi: 10.1007/s10999-020-09511-x.

[27] E. Gaponenko, L. Rybak, and D. Malyshev, "Numerical Method for Determining the Operating Area of a Robot with Relative Manipulation Mechanisms," *Journal of Machinery Manufacture and Reliability*, vol. 49, no. 6, pp. 474–489, 2020, doi: 10.3103/S1052618820060063.

[28] R. Grassmann and J. Burgner-Kahrs, "On the Merits of Joint Space and Orientation Representations in Learning the Forward Kinematics in SE (3)," in *Proceedings of Robotics: Science and Systems*, Jun. 2019.

[29] J. Li, Y. Wang, Z. Liu, X. Jing, and C. Hu, "A new recursive composite adaptive controller for robot manipulators," *Space: Science & Technology*, vol. 2021, pp. 1-7, Oct. 2021.

[30] F. Trotti, E. Ghignoni, and R. Muradore, "A Modified Recursive Newton-Euler Algorithm Embedding a Collision Avoidance Module," in *2021 European Control Conference (ECC)*, pp. 1150–1155, 2021, doi: 10.23919/ECC54610.2021.9654868.

[31] G. R. Petrović and J. Mattila, "Mathematical modelling and virtual decomposition control of heavy-duty parallel–serial hydraulic manipulators," *Mechanism and Machine Theory*, vol. 170, p. 104680, 2022, doi: 10.1016/j.mechmachtheory.2021.104680.

[32] C. Tan, H. Zhao, and H. Ding, "Identification of dynamic parameters of closed-chain industrial robots considering motor couplings," *Computers and Electrical Engineering*, vol. 99, p. 107740, 2022, doi: 10.1016/j.compeleceng.2021.107740.

[33] F. Janabi-Sharifi, A. Jalali, and I. D. Walker, "Cosserat rod-based dynamic modeling of tendon-driven continuum robots: A tutorial," *IEEE Access*, vol. 9, pp. 68703-68719, 2021, doi: 10.1109/ACCESS.2021.3114305.

[34] N. Cretescu and M. Neagoe, "Dynamic Modelling of an Isoglide T3 Type Parallel Robot," *New Advances in Mechanisms, Mechanical Transmissions and Robotics: MTM & Robotics 2020 2*, pp. 235-248, 2021.

[35] C. Alessi, E. Falotico and A. Lucantonio, "Ablation Study of a Dynamic Model for a 3D-Printed Pneumatic Soft Robotic Arm," in *IEEE Access*, vol. 11, pp. 37840-37853, 2023, doi: 10.1109/ACCESS.2023.3266282.

[36] I. Giorgio and D. Del Vescovo, "Energy-based trajectory tracking and vibration control for multilink highly flexible manipulators," *Mathematics and Mechanics of Complex Systems*, vol. 7, no. 2, pp. 159-174, 2019, doi: 10.2140/memocs.2019.7.159.

[37] J. Cai *et al.*, "Modeling method of autonomous robot manipulator based on DH algorithm," *Mobile Information Systems*, vol. 2021, pp. 1-10, 2021, doi: 10.1155/2021/5523096.

[38] A. Tekinalp *et al.*, "Topology, dynamics, and control of an octopus-analog muscular hydrostat," *arXiv preprint, arXiv:2304.08413*, 2023.

[39] M. Dupac, "Mathematical modeling and simulation of the inverse kinematic of a redundant robotic manipulator using azimuthal angles and spherical polar piecewise interpolation," *Mathematics and Computers in Simulation*, vol. 209, pp. 282-298, 2023, doi: 10.1016/j.matcom.2022.09.019.

[40] J. Woolfrey and D. Liu, "An Optimal Dynamic Control Method for Robots with Virtual Links," in *2022 IEEE/RSJ International Conference on Intelligent Robots and Systems (IROS)*, pp. 12843-12848, Oct. 2022.

[41] Y. Zhang, D. Kim, Y. Zhao, and J. Lee, "PD control of a manipulator with gravity and inertia compensation using an RBF neural network," *International Journal of Control, Automation and Systems*, vol. 18, no. 12, pp. 3083-3092, 2020, doi: 10.1007/s12555-020-0055-3.

[42] H. Habibi, C. Yang, R. Kang, I. D. Walker, I. S. Godage, X. Dong, and D. T. Branson, "Modelling an actuated large deformation soft continuum robot surface undergoing external forces using a lumped-mass approach," in *2018 IEEE/RSJ International Conference on Intelligent Robots and Systems (IROS)*, pp. 5958-5963, Oct. 2018.

[43] H. Cen and B. K. Singh, "Nonholonomic wheeled mobile robot trajectory tracking control based on improved sliding mode variable structure," *Wireless Communications and Mobile Computing*, vol. 2021, pp. 1-9, 2021, doi: 10.1155/2021/6673200.

[44] Z. Fu, J. Pan, E. Spyrakos-Papastavridis, Y. H. Lin, X. Zhou, X. Chen, and J. S. Dai, "A lie-theory-based dynamic parameter identification methodology for serial manipulators," *IEEE/ASME Transactions on Mechatronics*, vol. 26, no. 5, pp. 2688-2699, 2020, doi: 10.1109/TMECH.2021.3082115.

[45] S. Le Cleac'h *et al.*, "Differentiable physics simulation of dynamics-augmented neural objects," *IEEE Robotics and Automation Letters*, vol. 8, no. 5, pp. 2780-2787, 2023, doi: 10.1109/LRA.2023.3230452.

[46] P. Xu, J. Zhang, Y. Cui, K. Zhang, X. Chen, and Q. Tang, "Dynamic Modelling and Position-force Control for a Mobile Manipulator Based on Particles System Theory," in *2021 IEEE International Conference on Unmanned Systems (ICUS)*, pp. 884-889, Oct. 2021.

[47] V. Wüest, V. Kumar, and G. Loianno, "Online estimation of geometric and inertia parameters for multirotor aerial vehicles," in *2019 International Conference on Robotics and Automation (ICRA)*, pp. 1884-1890, May 2019, doi: 10.1109/ICRA.2019.8793934.

[48] H. -S. Fang *et al.*, "AnyGrasp: Robust and Efficient Grasp Perception in Spatial and Temporal Domains," in *IEEE Transactions on Robotics*, vol. 39, no. 5, pp. 3929-3945, Oct. 2023, doi: 10.1109/TRO.2023.3281153.

[49] M. Goharimanesh, A. Mehrkish, and F. Janabi-Sharifi, "A fuzzy reinforcement learning approach for continuum robot control," *Journal of Intelligent & Robotic Systems*, vol. 100, pp. 809-826, 2020, doi: 10.1007/s10846-020-01199-5.

[50] J. Hill. *Active disturbance rejection for the bipedal walk of a humanoid robot using the motion of the arms*. The University of Alabama in Huntsville, 2011.

[51] ABB Robotics, "IRB 140 - Robots (Robotics)," 2023. Available: http://www.abb.com/2023.

[52] J. S. Toquica and J. M. S. Motta, "A methodology for industrial robot calibration based on measurement sub-regions," *The International Journal of Advanced Manufacturing Technology*, pp. 1–18, 2021, doi: 10.1007/s00170-021-07694-z.

[53] M. Z. Silva *et al.*, "Industrial robotic arm in machining process aimed to 3D objects reconstruction," in *2021 22nd IEEE International Conference on Industrial Technology (ICIT)*, vol. 1, 2021.

[54] P. Obal *et al.*, *Monitoring the parameters of industrial robots*. Methods and Techniques of Signal Processing in Physical Measurements, 2019.

[55] M. Sebastian *et al.*, "Study on Robot Simulation and Code Generation Softwares," *International Journal on Emerging Research Areas (IJERA)*, vol. 3, no. 1, pp. 364-369, 2023.

[56] H. Lin, R. Mandal, and F. S. Wibowo, "BN-LSTM-based energy consumption modeling approach for an industrial robot manipulator," *Robotics and Computer-Integrated Manufacturing*, vol. 85, p. 102629, 2024, doi: 10.1016/j.rcim.2021.102629.

[57] M. V. V. Satyanarayana, P. P. Kumar, S. D. Praveen, and S. P. Raju. *Computational Design of Kinematics of a Robotic Arm*. Vishnu Institute of Technology, 2022.

[58] F. Gonçalves *et al.*, "A recursive algorithm for the forward kinematic analysis of robotic systems using Euler angles," *Robotics*, vol. 11, no. 1, p. 15, 2022, doi: 10.3390/robotics11010015.

[59] A. Talli and D. Marebal, "End-effector position analysis of SCARA robot by using MATLAB," in *Smart Sensors Measurements and Instrumentation: Select Proceedings of CISCON 2020*, pp. 25-33, 2021.

[60] N. Panigrahi and K. K. Dash, "Kinematic Model Design of a 6 DOF Industrial Robot," in *Applications of Robotics in Industry Using Advanced Mechanisms: Proceedings of International Conference on Robotics and Its Industrial Applications 2019*, 2020.

[61] A. Wolniakowski *et al.*, "Kinematic Modeling of a Trepanation Surgical Robot System," *Applied Sciences*, vol. 13, no. 16, p. 9110, 2023, doi: 10.3390/app13169110.

[62] C. Cristoiu *et al.*, "The Importance of Embedding a General forward Kinematic Model for Industrial Robots with Serial Architecture in Order to Compensate for Positioning Errors," *Mathematics*, vol. 11, no. 10, p. 2306, 2023, doi: 10.3390/math11102306.

[63] C. J. Chen *et al.*, "Reflect on fundamental, modeling and control of industrial robotic manipulators for simulation purposes," in *AIP Conference Proceedings*, vol. 2530, no. 1, 2023, doi: 10.1063/5.0121942.

[64] L. Lattanzi *et al.*, "Geometrical calibration of a 6-axis robotic arm for high accuracy manufacturing task," *The International Journal of Advanced Manufacturing Technology*, vol. 111, pp. 1813-1829, 2020, doi: 10.1007/s00170-020-06466-9.

[65] R. Raja, A. Dutta, and B. Dasgupta, "Learning framework for inverse kinematics of a highly redundant mobile manipulator," *Robotics and Autonomous Systems*, vol. 120, p. 103245, 2019, doi: 10.1016/j.robot.2019.103245.

[66] C. Cristoiu *et al.*, "The Importance of Embedding a General forward Kinematic Model for Industrial Robots with Serial Architecture in Order to Compensate for Positioning Errors," *Mathematics*, vol. 11, no. 10, p. 2306, 2023, doi: 10.3390/math11102306.

[67] R. M. Ramli, N. A. Herman, and M. A. H. M. Adib, "Simulation on Robot Arm Manipulator Modeling using Dynamic Kinematic," *2020 Emerging Technology in Computing, Communication and Electronics (ETCCE)*, pp. 1-6, 2020, doi: 10.1109/ETCCE51779.2020.9350907.

[68] A. Talli and D. Marebal, "End-effector position analysis of SCARA robot by using MATLAB," in *Smart Sensors Measurements and Instrumentation: Select Proceedings of CISCON 2020*, pp. 25-33, 2021.

[69] S. Shrey *et al.*, "Forward kinematic analysis of 5-DOF LYNX6 robotic arm used in robot-assisted surgery," *Materials Today: Proceedings*, vol. 72, pp. 858-863, 2023, doi: 10.1016/j.matpr.2021.12.088.

[70] H. He, "Modeling and Simulation for a Five DOF Robotic Arm Manipulator," in *Highlights in Science, Engineering and Technology*, vol. 43, pp. 300-307, 2023.

[71] M. Fazilat, N. Zioui, and J. St-Arnaud, "A novel quantum model of forward kinematics based on quaternion/Pauli gate equivalence: Application to a six-jointed industrial robotic arm," *Results in*

Engineering, vol. 14, p. 100402, 2022, doi: 10.1016/j.rineng.2021.100402.

[72] H. Zhang *et al*., "Analysis of obstacle avoidance strategy for dual-arm robot based on speed field with improved artificial potential field algorithm," *Electronics*, vol. 10, no. 15, p. 1850, 2021, doi: 10.3390/electronics10151850.

[73] V. M. Brathikan, P. Prashanth, and S. Vikash, "Design and development of 5-axis robot," *Materials Today: Proceedings*, vol. 62, pp. 2179-2184, 2022, doi: 10.1016/j.matpr.2021.08.375.

[74] I. S. Howard, "Design and Kinematic Analysis of a 3D-Printed 3DOF Robotic Manipulandum," in *Annual Conference Towards Autonomous Robotic Systems*, pp. 227-239, 2023.

[75] A. Crisan and I. Negrean, "The Jacobian matrix based on the transfer matrices," *ACTA Technica Napocensis-Series: Applied Mathematics, Mechanics, and Engineering*, vol. 62, no. 1, 2019.

[76] G. Boiadjiev, E. Krastev, I. Chavdarov, and L. Miteva, "A novel, oriented to graphs model of robot arm dynamics," *Robotics*, vol. 10, no. 4, p. 128, 2021, doi: 10.3390/robotics10040128.

[77] Y. Ding, X. Zhu, X. Sun, J. Zhang, and X. Chen, "Soft sensor simulation of minimum energy consumption of joint manipulator drive system based on improved BP neural network," in *Journal of Physics: Conference Series*, vol. 1626, no. 1, p. 012020, Oct. 2020, doi: 10.1088/1742-6596/1626/1/012020.

[78] M. Mahdavian *et al*., "Optimal trajectory generation for energy consumption minimization and moving obstacle avoidance of a 4DOF robot arm," in *2015 3rd RSI International Conference on Robotics and Mechatronics (ICROM)*, 2015.

[79] D. Fang, J. Yang, J. Shang, Z. Wang, and Y. Feng, "A Novel Energy-Efficient Wobble Plate Hydraulic Joint for Mobile Robotic Manipulators," *Energies*, vol. 11, no. 11, p. 2915, 2018, doi: 10.3390/en11112915.

[80] D. Catanoso, A. Chakrabarty, J. Fugate, U. Naal, T. M. Welsh, and L. J. Edwards, "OceanWATERS lander robotic arm operation," in *2021 IEEE Aerospace Conference (50100)*, pp. 1-11, Mar. 2021, doi: 10.1109/AERO50100.2021.9438224.

[81] N. Zioui, A. Mahmoudi, and M. Tadjine, "Representing quantum spins in different coordinate systems for modelling rigid body orientation," *Karbala International Journal of Modern Science*, vol. 9, no. 3, p. 11, 2023, doi: 10.33640/2405-609X.3605.

[82] N. Zioui, Y. Mahmoudi, A. Mahmoudi, M. Tadjine, and S. Bentouba, "A novel quantum-computing-based quaternions model for a robotic arm position," *International Journal of Computational Intelligence in Control*, vol. 13, no. 2, pp. 71-77, 2021.

[83] N. Zioui, Y. Mahmoudi, A. Mahmoudi, M. Tadjine, and S. Bentouba, "A New Quantum-computing-based Algorithm for Robotic Arms and Rigid Bodies' Orientation," *Journal of Applied and Computational Mechanics*, vol. 7, no. 3, pp. 1836-1846, 2021, doi: 10.22055/JACM.2021.36439.2894.

[84] N. Zioui, A. Mahmoudi, and M. Tadjine, "Design of a new hybrid linearising-backstepping controller using quantum state equations and quantum spins," *International Journal of Automation and Control*, vol. 17, no. 4, pp. 397-417, 2023, doi: 10.1504/IJAAC.2023.124412.

[85] N. Zioui, A. Mahmoudi, Y. Mahmoudi, and M. Tadjine, "Quantum computing-based state domain equations and feedback control," *Results in Applied Mathematics*, vol. 19, p. 100385, 2023, doi: 10.1016/j.rinam.2022.100385.

3.2.2 Summary of the Results Analysis

Evaluates the performance of three dynamic models, detailed, semi-detailed, and simplified, of the ABB IRB 140, an articulated industrial robotic arm, by comparing torque profiles and energy consumption across the first three proximal joints. All models were developed in SolidWorks and analyzed in MATLAB using the same trajectory and simulation time frame. Joint motion profiles, derived using fifth-order polynomial trajectories, were utilized to generate velocity and acceleration curves.

The torque profiles across the joints revealed consistent trends among the three models, with noticeable differences in magnitude. Figure 3-4 depict torque variations for joints 1.

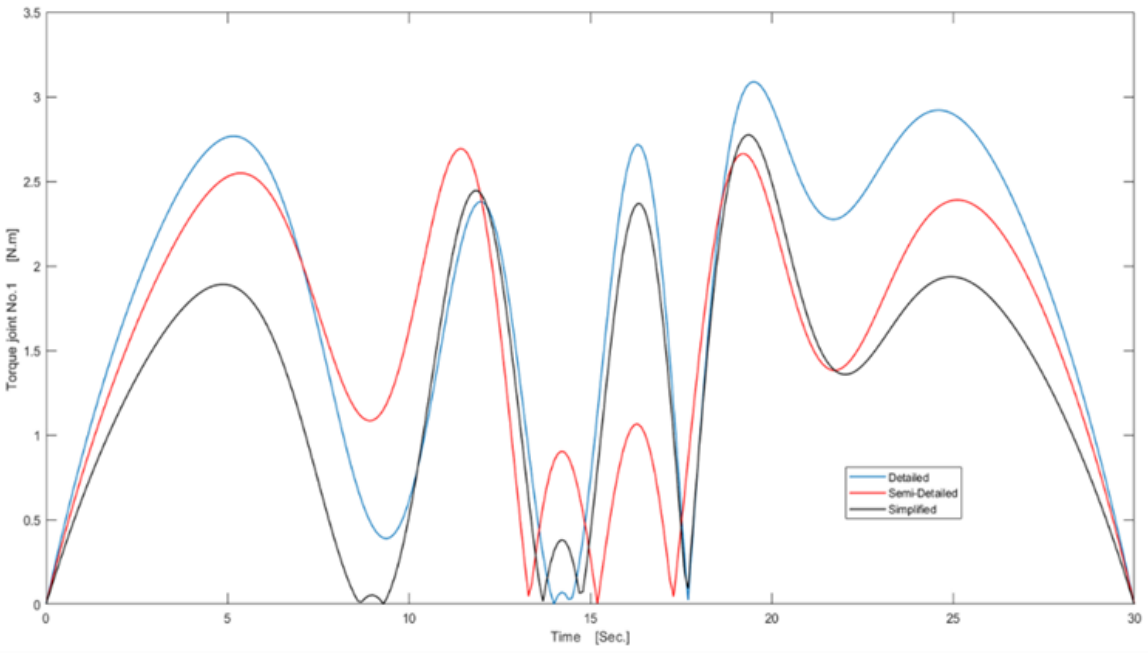

Figure 3-4 Torque variations for the first proximal joint of the IRB 140 robotic arm.

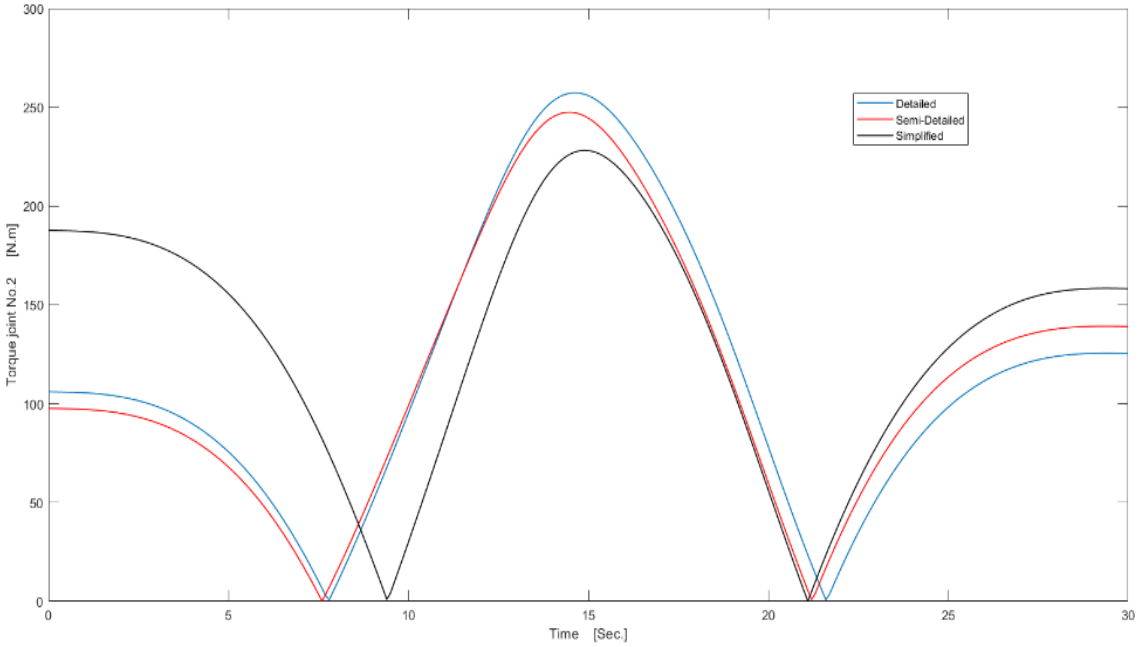

Figure 3-5 Torque variations for the second proximal joint of the IRB 140 robotic arm.

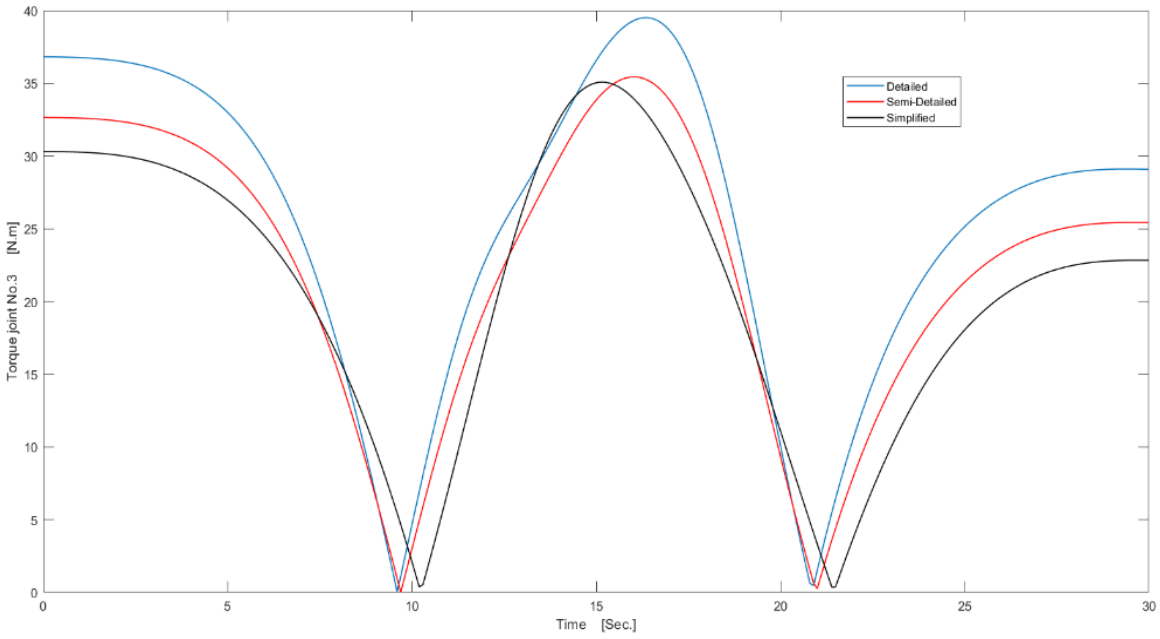

Figure 3-6 Torque variations for the third proximal joint of the IRB 140 robotic arm.

The detailed model consistently demonstrated higher torque, particularly in joint 3, a testament to its precise representation of inertia tensors and mass centers, as presented in Table 3-1 Mass property results of each model calculated using SolidWorks software.. In joint 1, the torque starts at zero, rises rapidly, and then returns to zero, a pattern consistent across all models due to its limited gravitational influence. Joint 2 experienced the highest torque overall, as it supports both its link and the weight of the subsequent links. The semi-detailed and simplified models mirrored the general trend of the detailed model but with varying fidelity.

The overall energy consumption patterns, as revealed by the energy calculations presented in Figures 3-7, provide valuable insights into the performance of the models. For The semi-detailed model showed the highest energy usage, indicating that its additional details come at the cost of increased energy consumption. In contrast, the simplified model demonstrated a reduction of approximately 6.8%, and the detailed model achieved a marginal 0.53% reduction relative to the semi-detailed version.

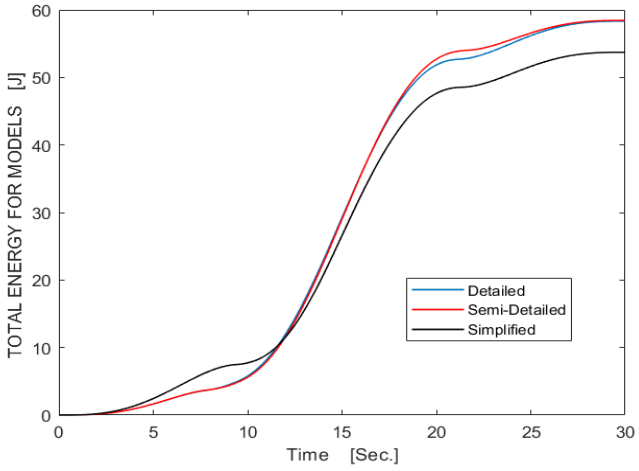

Figure 3-7 Energy variations for the third proximal joint of the IRB 140 robotic arm.

This suggests that while the simplified model may not be as accurate as the detailed model, it can still be a more energy-efficient option. The differences in energy usage and torque can be attributed to each model's treatment of mass distribution and inertial properties. Although all models assume uniform link weights, discrepancies arise from their differing geometric assumptions. The simplified model, by treating links as rods, introduces errors in center-of-mass location and inertia estimation. These differences affect torque requirements, particularly during changes in acceleration or direction of motion.

Due to all these differences, all three models exhibited acceptable predictive accuracy for typical industrial applications, particularly when energy efficiency and computational resources are key considerations. This confirms that simplified models, while less precise, can still provide valuable insight with significantly reduced computational demands. Thus, this study highlights the importance of aligning model complexity with application-specific performance requirements, providing the audience with a clear guide for informed decision-making.

3.3 Concluding Remarks

The results obviously indicate that the model's level of detail has an effective influence on its dynamic responses. The detailed model, offering high accuracy in torque prediction and energy estimation, is best suited for precision-critical applications. However, it also demands substantially more computational resources, as evidenced by simulation time comparisons. The semi-detailed and simplified models, although approximative, tracked the detailed model's behavior closely in many instances. The simplified model, in particular, delivered excellent computational efficiency with only a marginal loss in energy prediction

accuracy, showing a 6.8% reduction in energy consumption compared to the semi-detailed version.

One of the key takeaways from this study is that simplified models can be confidently used in industrial scenarios where rapid simulation and design iteration are more important than absolute precision. Conversely, detailed models are crucial for tasks that require high-fidelity control and fine torque regulation. Therefore, the choice of model complexity should be based on the specific performance requirements of the application and the available computational resources, guiding the design and simulation of robotic systems.

This study fills an important gap in the literature by quantifying the impact of dynamic model simplification on torque and energy metrics. It highlights the practical trade-offs engineers face when balancing accuracy and computational cost. However, it also points to a promising future, where these models could be improved by incorporating joint friction, variable material densities, and more advanced parameter identification techniques, potentially using quantum-inspired optimization methods. This research provides a methodological and practical foundation for informed model selection in the design and simulation of robotic systems.

The trade-offs between computational efficiency and physical accuracy in dynamic modeling show the inherent limitations of relying solely on simplified or even semi-detailed models for high-precision tasks, which is particularly evident in applications where accurate prediction of joint behavior is crucial, such as in inverse kinematics, where the fidelity of the system representation plays a pivotal role. These insights emphasize the necessity for data-driven learning models that can account for modeling abstractions while

preserving generalization across various configurations. This drives the shift toward intelligent approximation techniques, notably those based on neural networks, which are capable of learning complex mappings between task space and joint space.

Chapter 4 - Quantum Neural Networks for an Industrial Robot Arm

4.1 Chapter Overview

The inverse kinematics (IK) problem is fundamental to robotic control, as it involves determining the joint configurations necessary to achieve a desired position and orientation of the end effector. As industrial robots become more refined and possess higher degrees of freedom, solving the IK problem becomes increasingly complex due to challenges such as non-unique solutions, computational demands, and the occurrence of singularities. Classic analytical methods often struggle to address these issues effectively, particularly in real-time industrial applications. As an alternative, Artificial Neural Networks (ANNs) have been investigated for their capability to model non-linear relationships and generalize from data. However, classical ANNs still encounter limitations regarding learning efficiency, accuracy, and robustness, especially in proximity to singular configurations.

A novel approach has been developed that integrates principles of quantum computing into neural network models, introducing a Quantum Neural Network (QNN) that employs a quantum-inspired activation function. This method is applied to the six-degree-of-freedom ABB IRB140 robotic manipulator. The proposed QNN model enhances classical Multi-Layered Perceptron (MLP) architectures by incorporating quantum mechanisms within the activation function. To ensure both relevance and practicality, a robust dataset derived from real-world trajectories executed by the actual robot was utilized for training.

Moreover, the study incorporates singularity avoidance by applying a loss function penalization based on the condition number of the Jacobian matrix. The Quantum Neural Network model showed exceptional performance compared to classic Artificial Neural Networks, achieving considerably improved accuracy in terms of lower mean absolute errors, enhanced positional and orientational accuracy, and superior generalization capabilities. Notably, QNNs achieved up to a 16.67% reduction in MAE and exhibited orientation errors as minimal as 0.00179 radians, even in scenarios designed to avoid singularities. These findings highlight the confidence-inspiring accuracy of quantum-inspired neural networks in addressing complex kinematic challenges and present promising opportunities for advancements in industrial robotics.

4.2 Paper 3: Quantum neural network-based inverse kinematics of a six-jointed Industrial robotic arm.

Authors : Mehdi Fazilat, Nadjet Zioui.

Journal: Robotics and Autonomous Systems.

Publication date: 6/July/2025.

4.2.1 Methodology

The proposed methodology employs a hybrid approach that integrates classical neural networks with quantum computing principles to address the inverse kinematics of the 6-degree-of-freedom articulated robotic arm. This method focuses on enhancing a Multi-Layer Perceptron neural network by incorporating a quantum-inspired activation function to develop a Quantum Neural Network. The framework consists of five key components:

modeling the robot's kinematics, designing the MLP, generating the dataset, implementing singularity avoidance strategies, evaluating performance, and integrating quantum computational foundations.

Initially, the kinematic model of the six-jointed ABB IRB 140 robot is developed, and the spatial parameters of each joint are converted into a series of homogeneous transformation matrices, which collectively constitute the forward kinematics model, as shown in Equation 4-1. These parameters define the homogeneous transformation matrix T_{i-1}^{i} between two successive frames. Consequently, the kinematic model T_0^n for a robotic arm with n joints is obtained by the product of these transformation matrices $\prod_{i=1}^{n} T_{i-1}^{i}$.

$$T_{i-1}^{i} = \begin{bmatrix} & R & & P \\ & & & \\ 0 & 0 & 0 & 1 \end{bmatrix} = \begin{bmatrix} C\theta_i & -C\alpha_i S\theta_i & S\alpha_i S\theta_i & a_i C\theta_i \\ S\theta_i & C\alpha_i C\theta_i & -S\alpha_i C\theta_i & a_i S\theta_i \\ 0 & S\alpha_i & C\alpha_i & d_i \\ 0 & 0 & 0 & 1 \end{bmatrix} \tag{4-1}$$

To capture the relationship between joint velocities and end-effector motion, the Jacobian matrix is derived by Equation 4-2, with its subcomponents defined in Equation 4-3. The Jacobian matrix can be rotated into two sub-matrices: J_P for translational velocity and J_O for rotational velocity.

$$\dot{x} = J\dot{q} \tag{4-2}$$

$$\begin{bmatrix} J_{P_i} \\ J_{O_i} \end{bmatrix} = \begin{bmatrix} Z_{i-1} \times (P_e - P_{i-1}) \\ Z_{i-1} \end{bmatrix} \tag{4-3}$$

P_e is the end-effector position, taken from the first three elements of the fourth column of T_0^n. Similarly, P_{i-1} comes from T_{i-1}^0, and Z_{i-1} is the third column of the rotation matrix

R_{i-1}^{0}, which defines the orientation of link $i-1$ relative to the base and transforms vectors to the base frame.

Singularities are recognized when the determinant of the Jacobian approaches zero, as shown in Equation 4-4, and orientation is calculated using quaternion-based transformations considered in Equations 4-5 to 4-8.

$$det\ J(q) = 0 \tag{4-4}$$

$$R(\hat{n},\theta) = \begin{bmatrix} c + n_x^2(1-c) & n_z n_y(1-c) + n_x s & n_x n_x(1-c) - n_y s \\ n_x n_y(1-c) - n_x s & c + n_y^2(1-c) & n_y n_x(1-c) + n_x s \\ n_x n_z(1-c) + n_y s & n_y n_z(1-c) - n_x s & c + n_x^2(1-c) \end{bmatrix} \tag{4-5}$$

$$R(q) = \frac{1}{q_0^2 + q_1^2 + q_2^2 + q_3^2} \begin{bmatrix} q_0^2 + q_1^2 - q_2^2 - q_3^2 & 2(q_1 q_2 + q_0 q_3) & 2(q_1 q_3 - q_0 q_2) \\ 2(q_1 q_2 - q_0 q_3) & q_0^2 - q_1^2 + q_3^2 - q_2^2 & 2(q_2 q_3 + q_0 q_1) \\ 2(q_1 q_3 + q_0 q_2) & 2(q_2 q_3 - q_0 q_1) & q_0^2 - q_1^2 - q_2^2 + q_3^2 \end{bmatrix} \tag{4-6}$$

$$U = \frac{1}{4} \begin{bmatrix} r_{11} + r_{22} + r_{33} + 1 & r_{32} - r_{23} & r_{13} - r_{31} & r_{21} - r_{12} \\ r_{32} - r_{23} & r_{11} - r_{22} - r_{33} + 1 & r_{21} + r_{12} & r_{31} + r_{13} \\ r_{13} - r_{31} & r_{21} + r_{12} & r_{22} - r_{11} - r_{33} + 1 & r_{32} + r_{23} \\ r_{21} - r_{12} & r_{31} + r_{13} & r_{32} + r_{23} & r_{33} - r_{11} - r_{22} + 1 \end{bmatrix} \tag{4-7}$$

$$\hat{q} = \sum_{i=1}^{4} sign\left(u_j \cdot u_i\right) u_i \tag{4-8}$$

$'C'$ and $'S'$ denote cosine and sine of an angle. Given a non-zero real number k and quaternion components q_0, q_1, q_2, q_3, the rotation matrix can be derived. The dominant eigenvector of a symmetric matrix U, built from the diagonal (r_{11}, r_{22}, r_{33}) and off-diagonal (r_{32}, r_{23}, etc.) elements of rotation matrix R, yields the quaternion representing the same rotation.

The inverse kinematics problem is reformulated as a regression task suitable for neural networks, where the model maps end-effector position and orientation to the corresponding joint angles. The multi-layer perceptron takes up to seven input features, three for position and four for orientation, and produces six joint angle outputs. To enhance robustness and generalization, the dataset comprises over 167,000 real-world data points, collected by executing a variety of trajectories with the actual ABB IRB140 robot, as shown in Figure 4-1.

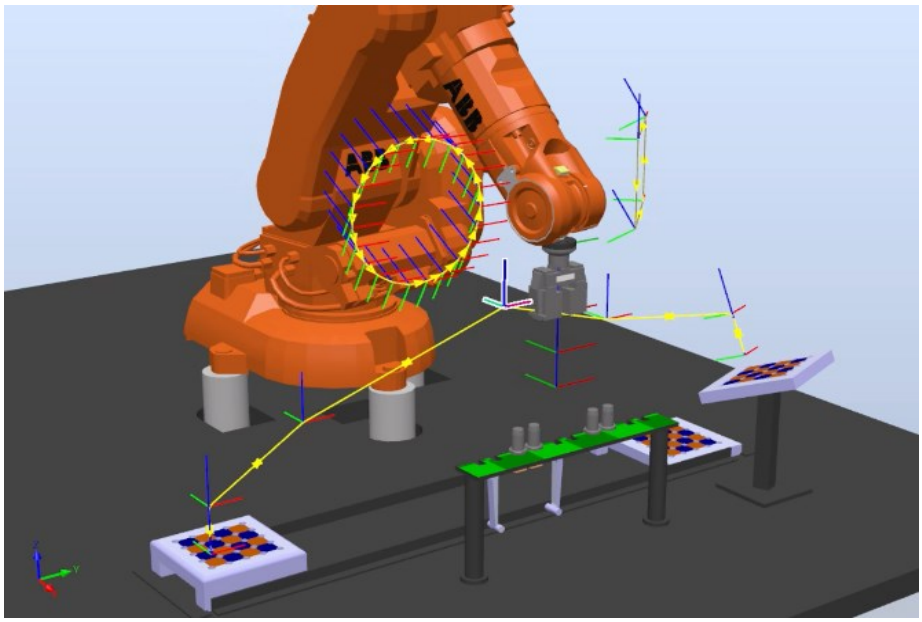

Figure 4-1 IRB 140 ABB Robot manipulator arm during executing assigned tasks.

Preprocessing involved a two-step normalization process and the addition of Gaussian noise, which involved normalizing the range to -1 and +1 and applying a Gaussian signal for a normal distribution. Additionally, we added Gaussian noise with a standard deviation of 0.002 to the data.

Figure 4-2 presents the proposed ANN architecture for accurately computing joint angles corresponding to target robot poses.

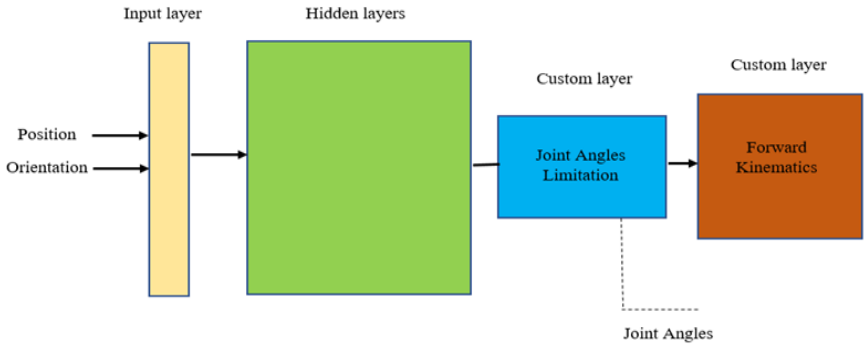

Figure 4-2 Neural Network Architecture.

Hyperparameter tuning was precisely conducted across various layers, nodes, learning rates, and batch sizes. This process resulted in a robust Quantum Neural Network architecture optimized for inverse kinematic prediction, as presented in Figure 4-3 , Figure 4-4 and, Figure 4-5. The practise outlined in Table 4-1 demonstrates how the approach ensures robustness in solving complex robotic kinematics through the use of the best activation function.

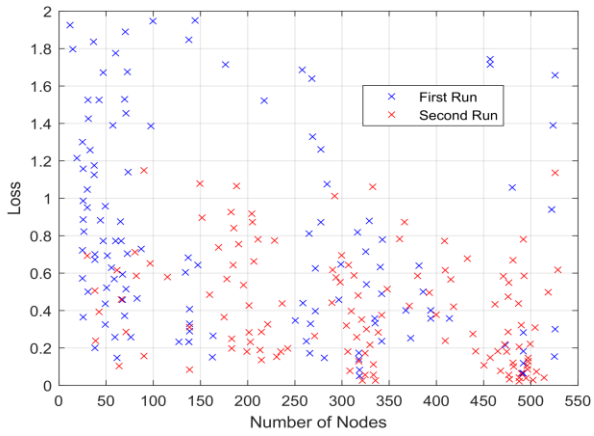

Figure 4-3 Loss-Nodes.

Figure 4-4 Loss-Layers.

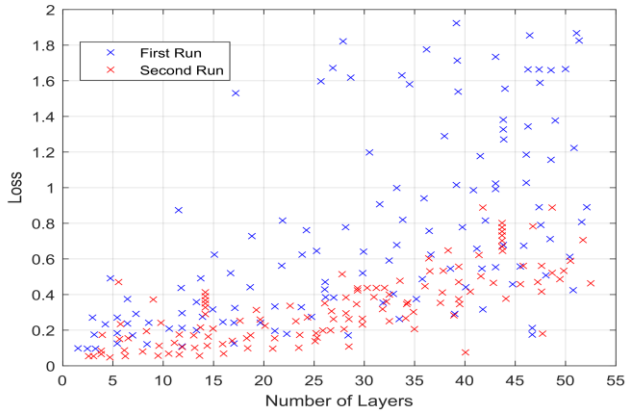

Figure 4-5 Loss-Learning Rate.

Table 4-1 Performance comparison of the various activation functions.

Function	ReLU	Swish	Hardlims	Satlins	Radbas
Epoch	287	300	83	47	221
Time	00:52	00:14	01:00	00:33	01:14
Performance	0.305	0.306	32.4	0.694	0.294
Gradient	0.168	0.324	$3.30e-11$	0.0735	0.214
Regression	0.99981	0.99981	0.97946	0.99957	0.99979
Validation Check	0	0	4	12	12
Max Error	0.08051	0.02943	1.069	0.03508	0.09044

A newly proposed loss function, Equation 4-9, combines Mean Absolute Error with a penalization term for high Jacobian condition numbers, thereby improving the avoidance of singularities.

$$Loss\ Function = MAE\left(P_{Target}, P_{Calc}\right) + f(\ Activation\ Function, \kappa(\ Jacobian\ )) \tag{4-9}$$

To compute orientation and position errors, several metrics are employed, including the Euclidean distance, as presented in Equation 4-10.

$$d = \sqrt{(X - X')^2 + (Y - Y')^2 + (Z - Z')^2} \tag{4-10}$$

where $P = [X, Y, Z]$ and $P' = [X', Y', Z']$ are the calculated and target positions.

The proposed quantum activation function comprises two key components: initial state preparation via phase rotation, as described in Equations 4-11, and 4–12.

$$|\psi(x)\rangle = \prod_{j=1}^{N} U(\tilde{x}_j)|0\rangle \tag{4-11}$$

$$|\psi(x)\rangle = \prod_{j=1}^{N} e^{i\sigma_y x_j}.Sqrt\ (Y)_j\ .|0\rangle \tag{4-12}$$

Additionally, a transformation operator based on *SU(2)* rotations, as shown in Equations 4-13 and 4-14. This structure incorporates quantum behavior into the classical neural network architecture, thereby enhancing its learning capacity.

$$U(\theta, \phi, \lambda) = \ e^{-\frac{i\phi\sigma_z}{2}} e^{-\frac{i\theta\sigma_y}{2}} e^{-\frac{i\lambda\sigma_z}{2}} \tag{4-13}$$

$$|\check{\psi}(x)\rangle\ = \prod_{j=1}^{N}\ e^{-\frac{i\phi\sigma_z}{2}} e^{-\frac{i\theta\sigma_y}{2}} e^{-\frac{i\lambda\sigma_z}{2}}.\ |\psi(x)\rangle \tag{4-14}$$

$U(\tilde{x}_j)$ denotes a general quantum operation applied to each qubit, encoding input data and creating superposition. Here, θ is the rotation angle around the y-axis, ϕ and λ are phase

rotations around the z-axis, and $\sigma_x, \sigma_y, \sigma_z$ are the Pauli matrices representing rotations on the Bloch sphere axes.

Robotics and Autonomous Systems 194 (2025) 105123

Contents lists available at ScienceDirect

Robotics and Autonomous Systems

journal homepage: www.elsevier.com/locate/robot

Quantum neural network-based inverse kinematics of a six-jointed industrial robotic arm

Mehdi Fazilat *, Nadjet Zioui

Université du Québec à Trois-Rivières, 3351 Bd des Forges, Trois-Rivières QC G8Z 4M3, Canada

ARTICLE INFO

Keywords:
Robotic arms
Inverse kinematics
Machine learning
Artificial neural networks
Multi-layered perceptron
Activation function
Quantum computing
Quantum-inspired neural networks
Singularity avoidance

ABSTRACT

This research examines the potential of quantum-inspired neural networks (QNNs) for solving the inverse kinematics of robotic arms, focusing on the six-degree-of-freedom ABB IRB140 robot. Traditional inverse kinematics approaches face challenges such as non-unique solutions and computational complexity, especially with increasing degrees of freedom. While artificial neural networks (ANNs) have shown promise, they require further improvements, particularly in terms of quantum computing integration. This study introduces a quantum-inspired activation function to multi-layer perceptron neural networks. We compared ANNs and QNNs with and without singularity avoidance, finding that QNNs significantly outperformed ANNs in mean absolute error (MAE), achieving a 15.60 % lower MAE in singularity-free models and a 16.67 % lower MAE in singularity-avoidance models. The QNNs demonstrated superior precision, with a position error of 1.64 mm and an orientation error of 0.00179 radians when avoiding singularities. These results highlight the potential of QNNs to enhance the precision, efficiency, and performance of robotic arm manipulation. Quantum computing offers advantages including parallelism, quantum entanglement, and quantum annealing, which contribute to the QNNs' superior performance. Overall, this study represents a practical contribution to robotics and quantum computing, paving the way for future research into applying quantum principles to neural network models for robotics.

1. Introduction

The inverse kinematics of robotic arms are crucial for determining the precise positions and movements required to execute complex tasks. As the degrees of freedom in robotic arms increase, traditional methods for solving inverse kinematics typically encounter significant challenges, such as non-unique solutions and increasing computational complexity. These issues highlight the need for innovative approaches that can simplify and enhance the accuracy of inverse kinematics computations in robotics. Recent advancements in robotics have increasingly applied machine learning techniques, particularly artificial neural networks (ANNs), to address these challenges. ANNs have shown promise in solving inverse kinematics problems due to their ability to learn from data and generalise to new situations. However, further improvements are still required in classical ANNs in terms of computational efficiency and their ability to handle high-dimensional data, thus necessitating further model development and innovation.

Quantum-inspired neural networks (QNNs) offer a promising solution for addressing these challenges by integrating principles from quantum computing. Quantum computing leverages phenomena such as parallelism, quantum entanglement, and quantum annealing, which can significantly improve the computational efficiency and accuracy of neural networks. By incorporating quantum principles into neural networks, QNNs can potentially outperform classical ANNs, particularly in tasks requiring high precision and efficiency. In this study, the performance of QNNs is evaluated in a practical application of solving the inverse kinematics of a six-degree-of-freedom articulated industrial robotic arm. By introducing a quantum-inspired activation function into multi-layered perceptron (MLP) neural networks, this study aims to improve the efficiency and performance of classical neural networks by integrating advancements from the emerging field of quantum computing, thus providing a more robust and efficient solution for robotic arm kinematics and examining the potential of applying QNNs to the field of robotics in terms of enhancing the precision and efficiency of robotic arm manipulations.

In recent years, there has been a growing trend in robotics of applying neural network methodologies to improve the precision and efficiency of solving kinematic equations and controlling manipulator

* Corresponding author.
E-mail addresses: mehdi.fazilat@uqtr.ca (M. Fazilat), nadjet.zioui@uqtr.ca (N. Zioui).

https://doi.org/10.1016/j.robot.2025.105123
Received 27 March 2024; Received in revised form 5 April 2025; Accepted 5 July 2025
Available online 6 July 2025

robots. For example, Oliveira et al. introduced the Pre-Multiplication method to simplify the inverse kinematics problem and enhance singularity robustness [1]. Theofanidis et al. showcased the application of multilayer feed-forward neural networks on the Sawyer Robotic Arm, demonstrating machine learning-based model-agnostic control schemes [2]. Additionally, concentric tube continuum robots have improved by using two artificial neural networks with ReLU activation functions, enhancing their approximation accuracy [3]. Integrating current robotic arm states into the network's input has also been confirmed as a beneficial approach for improving motion control accuracy and effectively handling redundant degrees of freedom [4]. Another study utilised Gaussian mixture models within a hierarchical neural network structure to improve the accuracy and flexibility of robotic arm motions [5]. Machine learning frameworks have also been used to optimise inverse kinematics solutions for redundant manipulators [6], while sim-to-real transfer learning aims to bridge simulation and real-world applications, especially for soft robots [7]. Adar's multi-layered feed-forward ANN model, incorporated with a proportional-integral control algorithm, demonstrated superior tracking ability and reduced control error for a robotic arm [8]. Hargis et al. achieved millimetre precision in tool space positioning and reduced computation time by training an ANN for a serial manipulator [9]. Additionally, Csiszar et al. showcased the flexibility and effectiveness of neural networks in robotic arm inverse kinematics and calibration using supervised learning [10]. Furthermore, Srisuk et al. developed custom neural networks using forward kinematic equations to simplify the control of robotic arm joint angles [11]. Aparanji et al. also introduced a multi-layered Auto Resonance Network architecture for path planning, avoiding non-linear inverse kinematic computations [12].

The combination of quantum computing with ANNs improves model performance by leveraging quantum mechanics properties such as superposition, entanglement, and quantum parallelism [13–15]. This integration leads to quicker training times, reduced computational complexity, and enhanced accuracy in ANN models [16,17]. QNNs, which are based on quantum computing principles, can be potentially used to enhance the control and kinematics of robots. Recent studies of QNNs have made various advances that are relevant to robotics; for example, Nguyen et al. found that QNNs are more efficient and provide significantly improved performance compared to classical neural networks [18]. Gupta et al. demonstrated the potential of quantum algorithms to optimise execution times and data storage, which can lead to advancements in robotics [19]. Zidan et al. introduced a quantum perceptron neural network, thereby enhancing computational efficiency for complex problems [20]. Kutvonen et al. explored the memory capacity of a quantum reservoir computer, which is also relevant for efficient QNN design in robotics [21]. In addition, Singh and Rajput highlighted the role of quantum entanglement in enhancing computational interconnectivity in robotic control systems [22].

Recent studies have applied quantum computing and quantum-inspired methods to enhance robotic arm kinematics, including a novel quantum model for forward kinematics leveraging quaternions and Pauli gates to improve positioning accuracy [23,24]. Further research has extended to representing quantum spins in various coordinate systems for rigid body orientation, thus showcasing the adaptability of quantum computing for robotics applications [25]. A QNN-based control design for a robotic manipulator was presented that integrates quantum computing with neural networks for enhanced precision and efficiency [26]. Learning inverse kinematics with a quaternion neural network exemplifies an innovative approach whereby quantum computing can be leveraged in robotics [27]. In addition, a proposed quantum-behaving particle swarm algorithm represents a cutting-edge solution for inverse kinematics challenges in complex robotic systems [28]. Furthermore, a proposed inverse solution algorithm for a robotic arm based on the MQACA-RBF network involved integrating quantum-inspired algorithms with neural networks to achieve high accuracy and efficiency [29].

A practical approach to developing QNNs involves integrating quantum computing with the activation function in ANNs to produce quantum mechanics-inspired activation functions. Parisi et al. introduced QReLU and m-QReLU, quantum activation functions that can improve convolutional neural networks (CNNs) in medical diagnostics by utilising entanglement and superposition, thereby solving the 'dying ReLU' problem and improving disease diagnosis accuracy [30]. Dong et al. presented a hybrid QNN with a quantum activation function, enhancing air quality prediction by integrating quantum techniques into classical CNNs with extended short-term memory networks, effectively capturing correlations while addressing gradient issues and the 'dying ReLU' problem [31]. Daskin proposed a QNN using a periodic activation function based on cosine values, which leverages the superposition principle to achieve exponential speed-up and high precision with fewer qubits and gates [32]. Li et al. developed a hybrid quantum–classical CNN with quantum-inspired activation functions based on cosine series, improving training convergence and attribute selection efficiency on the MNIST database [33]. She et al. introduced a novel ANN framework based on quantum interference principles – this framework incorporates a quantum activation function to enhance the network's universal approximation capabilities and effectively track high-frequency disturbances for space manipulators [34]. Additionally, Gandhi and McGinnity proposed a new neural network approach based on quantum interference principles to enhance the performance of adaptive controllers for robotic hands. Their proposed network utilises a quantum activation function, thus providing superior tracking performance and robustness [35].

Overall, quantum activation functions have been investigated across different disciplines, with the outcomes of various studies indicating meaningful benefits to using these approaches, particularly in robotic applications. However, a considerable gap remains in terms of using quantum computing to develop quantum activation functions to address critical problems such as inverse kinematics. Given the significant possibilities of this approach to enhance precision and efficiency in solving complex issues, quantum-inspired methods can potentially lead to significant advances in robotic technologies.

The present study focuses on the computational complexity and precision issues involved in solving the inverse kinematics of a six-degree-of-freedom industrial robotic arm, specifically the ABB IRB140. Improvements are required to allow classic methods and classical ANNs to achieve accurate and efficient solutions to this type of problem, particularly when handling high-dimensional data and potential singularity issues. These challenges necessitate innovative approaches to improve the precision and efficiency of inverse kinematics solutions. Accordingly, this study explores whether QNNs, leveraging the principles of quantum computing, can offer better performance than classical ANNs when solving inverse kinematics problems.

Several innovations introduced in the current research improve the theoretical framework, modelling techniques, and evaluation methods for solving the inverse kinematics of robotic arms using QNNs. First, an advanced kinematic model of the studied robot arm is developed, and a tailored MLP structure is designed based on the specific challenges involved in inverse kinematics. The neural network's hyperparameters are then optimised, including the number of layers, nodes, and learning rates using advanced techniques such as Gaussian noise addition and cyclical learning rates. This modelling process ensures that the neural networks can accurately predict the joint angles required for precise end-effector positioning and orientation while simultaneously avoiding singularities. Second, this study's theoretical innovation lies in integrating quantum computing principles – specifically a novel quantum-inspired activation function – into the chosen neural network's architecture. This approach employs quantum mechanics concepts such as superposition and entanglement, which are incorporated to improve the neural network's computational efficiency and learning capabilities, thereby addressing the limitations of classical methods. Finally, the advantages of our proposed approach are demonstrated by the superior

performance metrics achieved by the QNNs compared to classical ANNs. The QNNs show lower mean absolute error (MAE) values in the training and validation phases, enhanced generalisation capabilities, and enhanced singularity robustness. These benefits highlight this study's practical significance, showing that integrating quantum-inspired methods into neural networks can lead to more efficient and accurate solutions for complex robotic kinematics, with potential applications across multiple industries, including manufacturing, healthcare, and space exploration.

This paper presents a comprehensive study of using QNNs to solve the inverse kinematics of robotic arms. Section 2 describes the ABB IRB140 robot's kinematic modelling, focusing on the Denavit–Hartenberg method and Jacobian matrix. Additionally, we introduce the design and implementation of various MLP neural networks for inverse kinematics in this section, highlighting the importance of optimal network structure and training datasets. An activation function for QNNs is also proposed, and the fundamentals of quantum computing are introduced. Section 3 presents the results of our experiments and demonstrates the superior performance of QNNs in predicting the inverse kinematics of the studied robot arm. Finally, Section 4 discusses the implications of our findings and proposes directions for future research in robotics and quantum computing.

2. Methodology

In this study, we aim to develop a reliable model of the kinematics of the ABB IRB140 robot and introduce an advanced ANN architecture and a proposed QNN with a quantum-inspired activation function. The ANN is designed as a robust network to handle the general inverse kinematics of the robot arm, while the proposed quantum-inspired activation function is chosen to form a QNN that introduces non-linearity, enabling the neural network to learn complex patterns more effectively and generalise from training data to new, unseen data. Our proposed QNN model also includes mechanisms for singularity avoidance, ensuring robust and reliable performance even in challenging kinematic scenarios. Finally, the outcomes of different networks are compared, and the impacts of incorporating quantum computing on the performance of ANNs are evaluated by solving the same inverse kinematic problem using both approaches.

2.1. Kinematic modelling of the robot

The robotic arm used in this study is the ABB IRB140, a six-axis articulated manipulator known for its exceptional flexibility and extensive working range. The joint limits of this robot are listed in Table 1. The IRB140 arm is controlled by an IRC5 controller unit and is supported by PC-based RobotStudio and RobotWare software for the simulation environment [36,37].

In forward kinematics modelling, the position and orientation of the robot's end-effector are determined relative to the base frame as a function of the joint variables, which are the angles of the ABB IRB140 robot's joints. In this approach, a global coordinate frame is assigned to the robot's base, while a local reference frame is assigned to each joint.

The Denavit–Hartenberg (D-H) method is a popular approach for deriving forward kinematics models. Introduced by Jacques Denavit and Richard Hartenberg in 1955, this convention systematically describes and represents the spatial geometry of a kinematic chain's elements, such as a robot, based on a fixed reference system [36,37]. The outcome is a 4 × 4 homogeneous transformation matrix that links the spatial location of the robot's end-effector to the base frame, describing both the position and orientation of the robot. Fig. 1 illustrates how the D-H parameters and links are allocated for a joint with rotational capability [36,37]. The D-H formalism is based on four parameters:

i) Link length a_{i-1}: the distance between two successive joint axes z_i and z_{i-1}, measured along their common normal.
ii) Link twist α_{i-1}: the angle between the joint axes z_i and z_{i-1}, measured about the x_{i-1} axis.
iii) Link offset d_i: The distance between the x_i and x_{i-1} axes, measured along the z_i axis.
iv) Joint angle θ_i: The angle between the x_i and x_{i-1} axes, measured about the z_i axis.

These parameters define the homogeneous transformation matrix T^i_{i-1} between two successive frames. Consequently, the kinematic model T^n_0 for a robotic arm with n joints is obtained by the product of these transformation matrices $\prod_{i=1}^{n} T^i_{i-1}$.

$$T^i_{i-1} = \begin{bmatrix} & R & & P \\ 0 & 0 & 0 & 1 \end{bmatrix} = \begin{bmatrix} C\theta_i & -C\alpha_i S\theta_i & S\alpha_i S\theta_i & a_i C\theta_i \\ S\theta_i & C\alpha_i C\theta_i & -S\alpha_i C\theta_i & a_i S\theta_i \\ 0 & S\alpha_i & C\alpha_i & d_i \\ 0 & 0 & 0 & 1 \end{bmatrix} \tag{1}$$

Fig. 2 illustrates the various frames and parameters associated with each joint of the studied robotic arm. Table 2 summarises the parameters for the ABB IRB 140 robot, as defined by the D-H formalism [36,37].

$${}^0_6\mathrm{T} = {}^0_1\mathrm{T}.\,{}^1_2\mathrm{T}.\,{}^2_3\mathrm{T}.\,{}^3_4\mathrm{T}.\,{}^4_5\mathrm{T}.\,{}^5_6\mathrm{T} = \begin{pmatrix} r_{11} & r_{12} & r_{13} & X \\ r_{21} & r_{22} & r_{23} & Y \\ r_{31} & r_{32} & r_{33} & Z \\ 0 & 0 & 0 & 1 \end{pmatrix} \tag{2}$$

Thus:

$$r_{11} = -S_6(S_4C_1C_{2'3} + C_4S_1) - C_6(C_5(S_1S_4 - C_4C_1C_{2'3}) + S_5C_1C_{2'3})$$

$$r_{12} = S_6(C_5(S_1S_4 - C_4C_1C_{2'3}) + S_5C_1C_{2'3}) - C_6(S_4C_1C_{2'3} + C_4S_1)$$

$$r_{13} = C_5C_1S_{2'3} - S_5(S_1S_4 - C_4C_1C_{2'3})$$

$$r_{21} = C_6(C_5(C_4S_1C_{2'3} + C_1S_4) - S_5S_1S_{2'3}) - S_6(S_4S_1C_{2'3} - C_1C_4)$$

$$r_{22} = -S_6(C_5(C_4S_1C_{2'3} + C_1S_4) - S_5S_1S_{2'3}) - C_6(S_4S_1C_{2'3} - C_1C_4)$$

Table 1
Joint limits of the ABB IRB 140 robot.

Joint	Type	Limits (°)
1	Rotational	+180 to −180
2	Rotational	+110 to −90
3	Rotational	+50 to −230
4	Rotational	+200 to −200
5	Rotational	+120 to −120
6	Rotational	+400 to −400

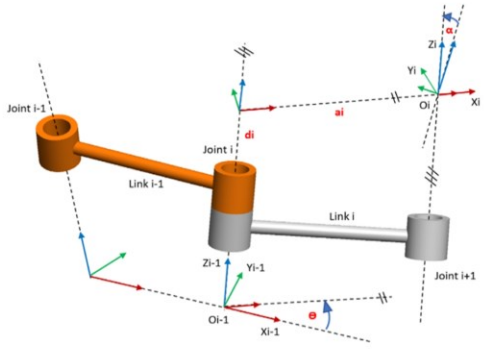

Fig. 1. D-H parameters and link assignments for a rotational joint [36].

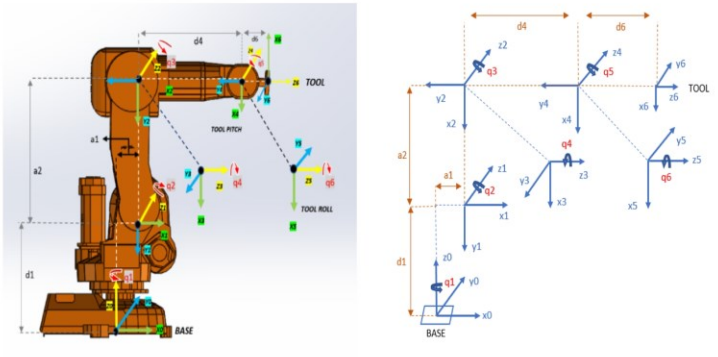

(a) Frames on the real robot arm. (b) Schematic diagram showing the joint frames.

Fig. 2. ABB IRB 140 frames assignment [37].

Table 2
D-H parameters of the ABB IRB 140 arm.

Link	a (mm)	α ()	d (mm)	q ()
1	a1=70	−90	d1=352	q_1
2	a2=−360	0	0	$q_2 + 90$
3	0	−90	0	q_3
4	0	90	d4=380	q_4
5	0	−90	0	q_5
6	0	0	d6=65	q_6

$$r_{23} = C_5S_1S_{2'3} + S_5(C_4S_1C_{2'3} + C_1S_4)$$

$$r_{31} = -C_6(S_5C_{2'3} + C_4C_5S_{2'3}) + S_4S_6S_{2'3}$$

$$r_{32} = C_6S_4S_{2'3} + S_6(S_5C_{2'3} + C_4C_5S_{2'3})$$

$$r_{33} = C_5C_{2'3} - C_4S_5S_{2'3}$$

where C_i and S_i denote the cosine and sine of the joint angle q_i; C_{ij} and S_{ij} denote the cosine and sine of q_i+q_j; and the notation $2'$ refers to $q_2' = q_2 + \pi/2$.

The X, Y, and Z position coordinates of the IRB140 robot relative to the base frame are then computed as follows:

$$X = C_1a_1 + d_6(C_5C_1S_{2'3} - S_5(S_1S_4 - C_4C_1C_{2'3})) + d_4C_1S_{2'3} - C_1C_2a_2$$

$$Y = S_1a_1 + d_6(C_5S_1S_{2'3} - S_5(C_4S_1C_{2'3} + C_1S_4)) + d_4S_1S_{2'3} - C_2S_1a_2$$

$$Z = d_1 + d_4C_{2'3} + a_2S_2 + d_6(C_5C_{2'3} - C_4S_5S_{2'3})$$

The Jacobian matrix is another key component in describing the mechanism of a robotic arm. It establishes a relationship between the velocities of the end-effector (both rotational and translational) and the joint velocities, expressed as:

$$\dot{x} = J\dot{q} \tag{3}$$

The Jacobian matrix can be rotated into two sub-matrices: J_P for translational velocity and J_O for rotational velocity. Each sub-matrix contains several columns equal to the number of joints in the robot. For revolute joints, the columns of these matrices are determined by the following formula:

$$\begin{bmatrix} J_{P_i} \\ J_{O_i} \end{bmatrix} = \begin{bmatrix} Z_{i-1} \times (P_e - P_{i-1}) \\ Z_{i-1} \end{bmatrix} \tag{4}$$

Where P_e is the position vector of the end-effector, obtained from the first three elements of the fourth column of the end-effector transformation matrix T_0^n; $P_{i-1}$is derived from the first three elements of the fourth column of the matrix T_{i-1}^0; and Z_{i-1} is taken from the third column of the rotation matrix R_{i-1}^0. The rotation matrix R_{i-1}^0 represents the orientation of the $(i-1)$-th link frame with respect to the base frame. It forms part of the homogeneous transformation matrix T_{i-1}^0 and is used to transform vectors from the local coordinate frame of the $(i-1)$-th link to that of the base frame [37].

The Jacobian matrix provides a comprehensive description of the mechanism's state; however, it may become singular at specific configurations, commonly called singularity points. These points should be avoided as they can result in excessively high joint velocities and a loss of degrees of freedom within the mechanism. These singularities occur when:

$$\det J(q) = 0 \tag{5}$$

The end-effector's position description is straightforward, as it simply specifies the effector's three Cartesian coordinates in Euclidean space as defined by the X, Y, and Z axes. However, representing the orientation of the end-effector is more complex due to the multiple possible ways of representing orientation. Defining orientation requires a minimum of three variables. A typical representation is the rotation matrix, which comprehensively describes an object's orientation; however, this matrix contains nine elements, of which only three are independent, thus leading to six redundant elements. An alternative form for expressing orientation is via quaternions. Quaternions are a four-dimensional extension of complex numbers consisting of one real part and three imaginary parts. They provide a compact and efficient representation of rotations in three-dimensional space [23,25].

The closed-form quaternion method for extracting a quaternion from a rotation matrix, based on the Sarabandi and Thomas method, begins with Euler's Theorem of Rotations. Euler's theorem states that any rotation in three-dimensional space can be represented as a single rotation about a specific axis, which can formulated as a rotation through an angle θ around some unit vector $\hat{n} = (n_x, n_y, n_z)^T$ [25,38]. The corresponding rotation matrix $R(\hat{n}, \theta)$ is given by:

$$R(\hat{n}, \theta) = \begin{bmatrix} c + n_x^2(1-c) & n_xn_y(1-c) + n_xs & n_xn_x(1-c) - n_ys \\ n_xn_y(1-c) - n_xs & c + n_y^2(1-c) & n_yn_x(1-c) + n_xs \\ n_xn_z(1-c) + n_ys & n_yn_z(1-c) - n_xs & c + n_x^2(1-c) \end{bmatrix} \tag{6}$$

Where c and s represent the cosine and sine functions of an angle.

By introducing a non-zero real number k and quaternion components $q_0, q_1, q_2,$ and q_3, we can express the rotation matrix in terms of quaternion components:

$$R(q) = \frac{1}{q_0^2+q_1^2+q_2^2+q_3^2}\begin{bmatrix} q_0^2+q_1^2-q_2^2-q_3^2 & 2(q_1q_2+q_0q_3) & 2(q_1q_3-q_0q_2) \\ 2(q_1q_2-q_0q_3) & q_0^2-q_1^2+q_3^2-q_2^2 & 2(q_2q_3+q_0q_1) \\ 2(q_1q_3+q_0q_2) & 2(q_2q_3-q_0q_1) & q_0^2-q_1^2-q_2^2+q_3^2 \end{bmatrix} \tag{7}$$

For a rotation matrix $R = (ry)_{1\le t,j\le 3}$, a 4 × 4 symmetric matrix U can be defined:

$$U=\frac{1}{4}\begin{bmatrix} r_{11}+r_{22}+r_{33}+1 & r_{32}-r_{23} & r_{13}-r_{31} & r_{21}-r_{12} \\ r_{32}-r_{23} & r_{11}-r_{22}-r_{33}+1 & r_{21}+r_{12} & r_{31}+r_{13} \\ r_{13}-r_{31} & r_{21}+r_{12} & r_{22}-r_{11}-r_{33}+1 & r_{32}+r_{23} \\ r_{21}-r_{12} & r_{31}+r_{13} & r_{32}+r_{23} & r_{33}-r_{11}-r_{22}+1 \end{bmatrix} \tag{8}$$

The dominant eigenvector of U corresponds to the quaternion representing the same rotation as R. The elements r_{11},r_{22}, and r_{33} are the diagonal elements of the rotation matrix R, and the elements r_{32}, r_{23}, r_{13}, r_{31}, r_{21}, and r_{12} are the off-diagonal elements. We use these elements in constructing the symmetric matrix U, which is related to the quaternion representation of the rotation. We can estimate the quaternion $\widehat{q}$ from the rotation matrix by averaging the column vectors of U with homogenised signs:

$$\widehat{q} = \sum_{i=1}^{4} \text{sign}\,(u_j \cdot u_i)u_i \tag{9}$$

where u_j is chosen such that $u_j^2 \ge u_i^2$ for $i = 1,\ldots,4$. This method ensures that the averaged quaternion $\widehat{q}$ represents a rotation matrix, irrespective of the sign of det (R).

2.2. Multi-layered perceptron (MLP)

An MLP neural network is a versatile ANN structure widely used in robotics for control, path planning, and object recognition tasks. Unknown or computationally intensive algorithms cause challenges when solved using classic algorithmic approaches in complex systems. Neural networks, which can be used for both regression and classification tasks, represent a potential solution to these issues by reducing software development time and computational requirements and allowing processing when algorithms are undefined.

Our approach integrates a quantum-inspired activation function into the MLP neural network. This function leverages quantum principles to introduce non-linearity and enhance the network's ability to learn complex patterns. By encoding high-dimensional input data into quantum states during the initial state preparation and operation transformation steps, our approach enables the neural network to more efficiently process information. This method not only accelerates the learning process but also enhances the network's ability to generalise from training data to new, unseen data. We also further incorporate singularity avoidance mechanisms to ensure the robustness of our proposed solution in practical applications.

In robot kinematics, predicting the inverse kinematics of robotic arms represents a regression problem, where the input is the position and orientation of the end-effector, and the output is the joint angles. In this regression task, the purpose is to predict continuous output values (i.e. the joint angles) [39,40]. The neural network model for the regression process requires a dataset with appropriate inputs and outputs, as shown in Fig. 3. The input should be a vector describing the end-effector's position and orientation, while the output should be the corresponding joint angles.

There are two key challenges involved in exploring the inverse kinematics of robotic manipulators with ANNs: choosing an optimal neural network structure and generating a robust training dataset [41,42]. This research focuses on various MLP structures to maximise the accuracy of approximations.

To obtain the most reliable and realistic data for training the network, we used the studied robotic arm to execute tasks and generate real-world data. This approach captures the complexity and variability of real-world physical systems, thus providing more robust data for model training than can be obtained via simulation. While simulation-based or theoretical methods are common in robotics research due to their convenience and cost-effectiveness, these approaches do not offer the same level of reliability as data derived from actual tasks performed using the studied robot. By integrating real-world data and advanced preprocessing steps, our approach ensures that the neural network is exposed to a wide range of scenarios and dynamics representative of operational conditions. This strategy enhances the robustness and generalisation of the trained models, ensuring higher precision and adaptability in practical scenarios [V2].

The robot underwent path planning and executed various trajectories to gather the necessary data to create the ANN dataset. The resulting dataset consists of 13 elements: three for position vectors and four for orientation (representing a total of seven input elements), and six for joint angles (as outputs). We operated the IRB 140 ABB Robot

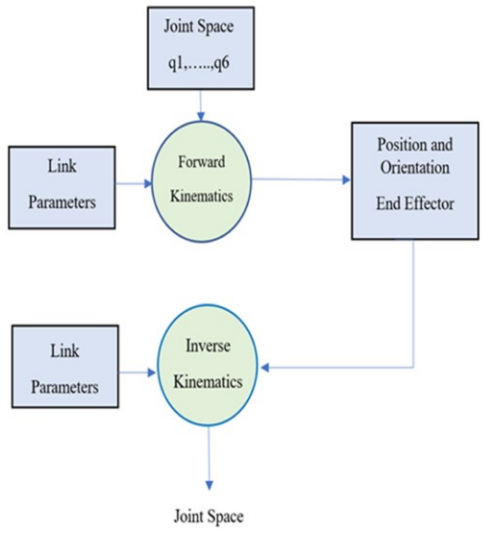

Fig. 3. Kinematics data flow diagram of the robotic manipulator arm.

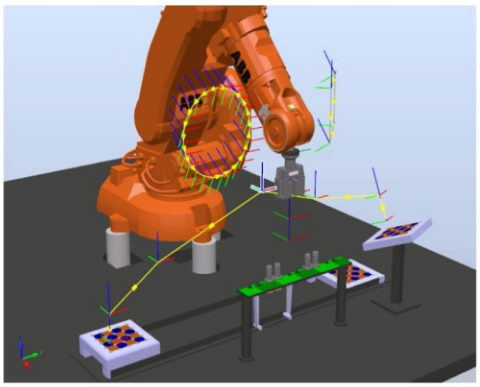

Fig. 4. IRB 140 ABB robot manipulator arm during executing assigned tasks.

manipulator arm in the mechatronic laboratory of the University of Quebec in Trois Rivières to generate approximately 167,000 data points, covering each joint's full range of motion while executing various tasks, as presented in Fig. 4 (a screenshot of the IRC5 interface). The ABB IRB 140 is a high-degree-of-freedom robot with the ability to perform various types of challenging motions rapidly and accurately. This robot arm has ample working space and can be applied to numerous industrial scenarios, ensuring the relevance and applicability of our findings across a broad range of practical applications. The dataset we generated is extensive and covers the entire working space of the ABB IRB 140 robot, thus ensuring our neural network models are trained on varied and representative sets of movements and joint configurations, improving the robustness of the study's outcomes. The selected trajectories included triangular, square, rectangular, and elliptical paths, symmetric and asymmetric polygons of different sizes, and random paths within the robot's working space in the variant scale range for each defined path. These trajectories simulate practical tasks such as welding, pick-and-place operations, painting, and assembling, thus ensuring the obtained data apply to real-world scenarios and capture a wide range of motion dynamics.

We applied a two-step normalisation process to the dataset to ensure practical neural network training and prevent divergence, which involved normalising the range to -1 and $+1$ and applying a Gaussian signal for a normal distribution. Additionally, we added Gaussian noise with a standard deviation of 0.002 to the data.

These MLPs determine the joint angles that produce the desired end-effector positions and orientations. The network's architecture is shown in Fig. 5. The initial input layer of the MLP model ranges from three to seven inputs, depending on whether it includes both position and orientation. Several hidden layers follow, with the output from the final hidden layer comprising six elements representing the joint angles. The network includes a customised layer that ensures these angles remain

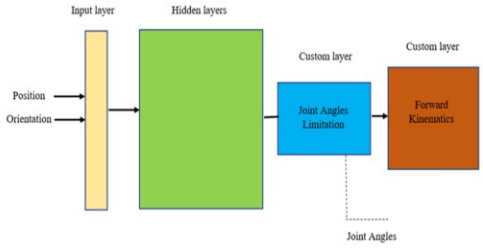

Fig. 5. Neural network architecture.

within the robot's operational range and an additional customised layer applies the direct kinematics model outlined in Section 3.1. Both customised layers were developed in MATLAB software and implemented in the robot's network architecture, ensuring that the MLP's outputs are suitable for motion planning. The architecture includes performance-measuring loss functions and MAE measurements, which quantify the deviation between the estimated and actual end-effector poses and can be expressed as:

$$MAE = \frac{1}{n}\sum_{i-1}^{n} |R_i - \widehat{R}_i| \tag{10}$$

Where R_i represents a sample from the dataset, and $\widehat{R}_i$ is the predicted value for this sample.

A comprehensive hyperparameter search can enhance the designed network's performance by optimising the learning rate, batch size, network architecture (depth and width), and choice of non-linear activation functions. This process also examines the number of training epochs and data pre-processing techniques, such as Gaussian noise addition or batch normalisation. The ANN architecture proposed in this study is shown in Fig. 5.

The hyperparameter tuning process applied in our study is stationary instead of time-dependent, meaning that the hyperparameters are selected and evaluated independent of any specific temporal events or fixed periods. Instead, the tuning is based on the network's overall performance across the entire dataset, thus ensuring consistent and comprehensive evaluation. The random search for hyperparameters was conducted with the dataset split into training, validation, and testing sets. This splitting ensured a comprehensive evaluation of the model's performance and prevented any temporal biases. During each iteration of the random search, hyperparameters such as the number of nodes, layers, and learning rate were randomly selected within predefined ranges. The model was then trained and evaluated based on the mean squared error (MSE) loss. The first round of random searching provided an initial set of hyperparameter values. A second round of tuning was then performed, refining the search within narrower ranges based on insights from the first round. The hyperparameters were assessed by evaluating the model's performance on the validation set after each training session, thus ensuring that this assessment was based on a broad and consistent data sample, preferably varying over time.

In the hyperparameter tuning process, numbers of nodes from 5 to 535 and layers from 3 to 53 were tested, with a logarithmic scale learning rate ranging between 1e−5 and 8.8e−4. The Adam optimiser was used in all experiments due to its balanced approach to gradient scales and rapid convergence, thus making it suitable for handling complicated tasks. A random search was conducted on a dataset with 167,000 data points (70 % training, 15 % validation, and 15 % testing), with a batch size of 32 and 170 epochs of training to determine appropriate values for the numbers of layers and nodes and the learning rate range. The ReLU activation function and MSE loss function were employed. Although the initial experiments provided valuable insights, learning rate values outside the initial search range yielded better results, prompting a second round of random searching.

After two rounds of hyperparameter tuning, we discovered that models with 3–15 layers produced the most accurate results, particularly those with four layers. Node counts around 488 within the approximate range of 450–530 also displayed a lower loss. A learning rate below 5e−5, specifically 1.9e−5, was found to be the most efficient. Although the initial experiments indicated effective ranges for the learning rate, further tuning outside these initial ranges (specifically identifying a learning rate of 1.9e−5) was necessary. These adjustments were based on the observed performance metrics rather than time-dependent factors. Fig. 6 summarises these findings, illustrating the complex relationship between network architecture and performance [v2].

Non-linear activation functions were assessed using the identified optimal MLP architecture in terms of the numbers of nodes and layers,

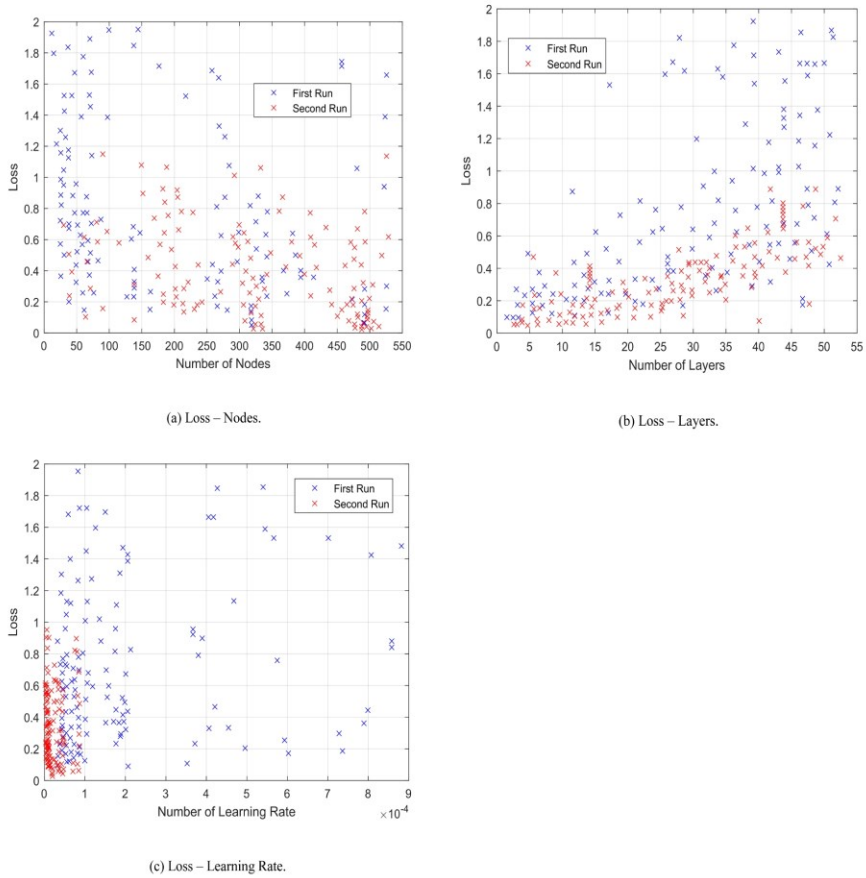

(a) Loss – Nodes.

(b) Loss – Layers.

(c) Loss – Learning Rate.

Fig. 6. Plots showing the loss values for varying (a) nodes, (b) layers, and (c) learning rates for the proposed ANN.

Table 3
Performance comparison of the various studied activation functions.

Function	ReLU	Swish	Hardlims	Satlins	Radbas
Epoch	287	300	83	47	221
Time	00:52	00:14	01:00	00:33	01:14
Performance	0.305	0.306	32.4	0.694	0.294
Gradient	0.168	0.324	3.30e-11	0.0735	0.214
Regression	0.99981	0.99981	0.97946	0.99957	0.99979
Validation Check	0	0	4	12	12
Max Error	0.08051	0.02943	1.069	0.03508	0.09044

using batch sizes of 32 and 64. The Swish activation function was found to be the most effective, achieving zero validation error, the smallest maximum error among the studied functions of 0.02943, and an almost perfect regression value of 0.99981, indicating strong alignment between the predicted and actual outcomes, with a performance metric value of 0.306. The Swish function also displayed stability during training, as evidenced by the absence of validation check failures, suggesting no overfitting occurred. A comparison between the studied activation functions is shown in Table 3, highlighting the significance of selecting appropriate functions to ensure optimal MLP performance.

2.3. Singularity points avoidance

Robotic manipulator arms can encounter two types of singularities: boundary and interior singularities. Boundary singularities occur at the edges of the workspace and are related to the physical limits of the robot's joints. In contrast, interior singularities occur within the workspace due to the alignment of robot axes, leading to a loss of degrees of freedom [43]. Motion can become problematic when singularities arise, causing joint velocity and torque issues. The Jacobian matrix is crucial for velocity kinematics as it maps joint velocities to end-effector velocities [44]; however, it becomes non-invertible at singularities, where the determinant of the Jacobian matrix is equal to zero. The condition number, denoted by k, is a measure of a matrix's sensitivity to small changes in its input values [45]. This parameter ranges from 1 to infinity, with higher values indicating an ill-conditioned matrix, in which the mechanism is in a singularity point region, making it challenging to find accurate solutions. Lower condition numbers imply that the mechanism is far from singularity points, and small changes in input values will not significantly affect the solution. The condition number of the matrix is defined as:

$$\kappa(A) = A^{-1} \| A \| \tag{11}$$

Close to singularities, even small velocity inputs can produce large outputs due to a high condition number, despite the Jacobian

maintaining full rank. For redundant manipulators, which have more degrees of freedom than necessary for a given task, the Jacobian matrix is non-square. Such cases use a pseudo-inverse of the Jacobian, achieved through singular value decomposition [46]. To address the challenges of singularities, we can formulate a loss function for the manipulator. This loss function combines the MAE between the target position (P_{Target}) and the calculated position (P_{Calc}), with a penalty for high Jacobian condition numbers above a certain threshold. We can express the loss function as:

$$\begin{aligned}\text{Loss Function} &= \text{MAE}\left(P_{\text{Target}}, P_{\text{Calc}}\right) \\ &\quad + f(\text{Activation Function},\ \kappa(\text{Jacobian}))\end{aligned} \tag{12}$$

The singularity avoidance neural network takes the end-effector's desired position as an input. It disregards its desired orientation, thus corresponding to a mechanism with three degrees of freedom that can avoid singularity configurations based on the Jacobian matrix's condition number. The loss function utilises MAE and the Jacobian. By incorporating this penalty, the manipulator is encouraged to avoid configurations close to singularities, thus improving its performance and reliability.

2.4. Evaluation of the ANN

Metrics can be used to assess the performance of neural network models by quantifying the error in the end-effector's position and orientation relative to the desired target. The Euclidean distance between the calculated and target positions of the end-effector is given by:

$$d = \sqrt{(X - X')^2 + (Y - Y')^2 + (Z - Z')^2} \tag{13}$$

where $P = [X, Y, Z]$ and $P' = [X', Y', Z]$ are the vectors of the calculated and target positions, respectively.

We can use several metrics to calculate the orientation error. Evaluating the orientation error between two rotation matrices, R_1 and R_2, is crucial in neural network models for robotics, especially in tasks involving the control of robotic arms. Rotation matrices are commonly used to assess this error, or the quaternion representation for rotations can be used as an alternative to Euler angles [47]. Quaternion-based metrics for the orientation error include the minimum quaternion error, which is calculated as:

$$\phi(q_1, q_2) = \min(q_1 - q_2, q_1 + q_2) \tag{14}$$

This metric determines the error as the minimum norm of the difference between the calculated quaternion q_1 and the target quaternion q_2. Another quaternion metric is the arccosine of the absolute dot product of q_1 and q_2, i.e.

$$\phi(q_1, q_2) = \arccos\left(|\langle q_1, q_2 \rangle|\right) \tag{15}$$

This metric measures the error as an angle within $\left[0, \frac{\pi}{2}\right]$. Additionally, the magnitude of the quaternion difference quantifies the difference between one quaternion and another within the range $[0, 1]$, which is measured as:

$$\phi(q_1, q_2) = 1 - |\langle q_1, q_2 \rangle| \tag{16}$$

Orientation error can also be defined using rotation matrix-based metrics. In these metrics, the error is quantified based on the distance between the two matrices. For instance, the Frobenius norm of the difference between the rotation matrices R_1 and R_2 is given by:

$$\delta(R_1, R_2) = \sqrt{2\left(3 - \text{trace}\left(R_1 R_2^T\right)\right)} \tag{17}$$

The logarithm of the rotation matrix difference is another valuable metric as it represents the maximum angle of separation of points transformed by R_1 and R_2 and is expressed as:

$$\delta(R_1, R_2) = \log\left(R_1 R_2^T\right) \tag{18}$$

Finally, the arccosine of the trace of rotation matrix difference is a metric that reflects the orientation error as an angle within $[0, \pi]$ and is given by:

$$\delta(R_1, R_2) = \arccos\left(\frac{\text{trace}\left(R_1 R_2^T\right) - 1}{2}\right) \tag{19}$$

Selecting an orientation error metric should be based on the specific application's needs, such as available computational resources, the nature of the rotations, and the desired sensitivity to small errors. The logarithm of rotation matrix difference metric is often preferred as it intuitively represents the error as an angle, consistent with the geometric interpretation of rotation in three-dimensional space.

2.5. Quantum computing basis

Quantum computing marks a considerable departure from classical computing. By using the principles of quantum mechanics, quantum computing processes information fundamentally differently: whereas classical computing relies on binary bits of either 0 or 1, whereas quantum computing utilises the qubit or quantum bit. Through the two fundamental quantum mechanical phenomena of superposition and entanglement, qubits can represent a state of 0, 1, or any quantum superposition of the two [48–50]. Superposition allows a qubit to exist simultaneously in a combination of 0 and 1 states. The state of a qubit, $|\psi\rangle$, can be expressed as a linear combination of the basis states $|0\rangle$ and $|1\rangle$ [23,49,51]:

$$|\psi\rangle = \alpha|0\rangle + \beta|1\rangle \tag{20}$$

Here, α and β are complex numbers representing the probability amplitudes of the qubit's state. Upon measurement, the square of the amplitude's modulus, $|\alpha|^2$, gives the probability of the qubit being in state $|0\rangle$, and similarly, $|\beta|^2$ describes the probability of it being in state $|1\rangle$. For a qubit, these probabilities must sum to one, satisfying the normalisation condition [24,52].

A qubit's state can be visualised on the Bloch sphere, where $|0\rangle$ and $|1\rangle$ are depicted as orthogonal vectors. An arbitrary qubit state on the Bloch sphere using two angles, θ and ϕ [24,53,54]:

$$\left|\psi\right\rangle = \cos\left(\frac{\theta}{2}\right)\left|0\right\rangle + e^{i\phi}\sin\left(\frac{\theta}{2}\right)|1\rangle \tag{21}$$

In this representation, θ represents the latitude from the sphere's north pole, while ϕ is the longitudinal angle. The qubits are manipulated through quantum gates, which are represented by unitary operators. These gates are the quantum counterparts of classical logic gates and operate reversibly. Rotations about the axes of the Bloch sphere are essential quantum operations, allowing for the transformation of qubit states through rotation operators such as [25,54,55]:

$$R_x(\lambda) = \begin{pmatrix} cos\left(\frac{\lambda}{2}\right) & -i\sin\left(\frac{\lambda}{2}\right) \\ -i\sin\left(\frac{\lambda}{2}\right) & cos\left(\frac{\lambda}{2}\right) \end{pmatrix} \tag{22.a}$$

$$R_y(\theta) = \begin{pmatrix} cos\left(\frac{\theta}{2}\right) & -sin\left(\frac{\theta}{2}\right) \\ sin\left(\frac{\theta}{2}\right) & cos\left(\frac{\theta}{2}\right) \end{pmatrix} \tag{22.b}$$

$$R_z(\phi) = \begin{pmatrix} e^{-i\phi/2} & 0 \\ 0 & e^{i\phi/2} \end{pmatrix} \tag{22.c}$$

where λ, θ, and ϕ are the rotation angles around the x, y, and z axes, respectively.

Entanglement is a vital quantum effect in which qubits become corresponding, making their states linked, even across extensive spaces [56,57]. This property is essential in achieving the intricate multi-qubit states of quantum computing. A key aspect of entanglement is the rotation around the y-axis of the Bloch sphere, making it possible to generate the necessary superposition and entangled states required for operations such as error modification and teleportation [58,59]. For instance, applying $R_y(\theta)$ to a qubit initially in state $|0\rangle$ can result in a superposition essential for algorithms like Grover's search algorithm or the quantum Fourier transform. This operator is defined in Eq. (22.b) [60,61].

The R_y gate holds significant power in creating entangled and superposition states. By manipulating the rotation angle θ, complex systems can be simulated using quantum mechanics, allowing the emulation of quantum dynamics relevant to fields like material science and quantum chemistry. Incorporating quantum gates, including rotations, enables the creation of intricate quantum circuits with computational capabilities exceeding those of classic computing. Specifically, rotations around the Y-axis are leading the advancement of quantum algorithm development and unlocking the full potential of quantum computing.

2.6. Proposed quantum activation function

Here, we propose a quantum activation function, with a focus on the initial state preparation and the operation transformation operator. The initial state preparation is fundamental in encoding high-dimensional input data [62], such as elements of robotic motion, into quantum states by generating superposition states and encoding the input data into the phase of the quantum state. However, when applied correctly, the transformation operator can introduce non-linearity to the input data, which is essential for effectively implementing the quantum neural network's activation function [63].

The initial state preparation step represents preparing a qubit in a superposition state, generally using a quantum gate for equal superposition [64]. After a gate is used to put each qubit into a superposition state, we then apply phase rotation gates, which encode the input data $\widetilde{x_j}$ into the phase of the quantum state mathematically formulated as:

$$\left|\psi(x)\right\rangle = \prod_{j=1}^{N} U(\widetilde{x_j}) \left|0\right\rangle \tag{23}$$

Where $U(\widetilde{x_j})$ represents a general quantum operation or series of operations applied to each qubit, encompassing both the creation of superposition and the encoding of input data $\widetilde{x_j}$ into a quantum state.

The selection of the terms for the equation initial state preparation (24) can be formulated as the exponential of $i\sigma_y x_j$ for phase rotation and Sqrt $(Y)_j$ for the square root of the Y gate. We select these elements for their proficiency in encoding high-dimensional input data into quantum states, allowing an effective description of robotic movements. Eq. (24) describes the initial state preparation of a quantum system – here, the input data are represented by x_j, where Sqrt $(Y)_j$ is applied to the j-th qubit, replacing the Pauli Y gate for phase rotation. The Sqrt $(Y)_j$ gate generates a superposition state from the base state $|0\rangle$, while the exponential of $i\sigma_y x_j$ induces a phase rotation. This method of state preparation is inherently non-linear relative to the input data x_j, combining phase encoding with superposition to augment the quantum model's ability to link positions and orientations with joint angles.

$$|\psi(x)\rangle = \prod_{j=1}^{N} e^{i\sigma_y x_j} . Sqrt\ (Y)_j\ . |0\rangle \tag{24}$$

The operation transformation operator is another essential part of the quantum activation function, as it manipulates the state to introduce non-linearity relative to the input data – this can be effectively used to implement the quantum neural network's activation function by adjusting the state of each qubit based on these parameters, which can be optimised during the learning process [65]. An operation transformation as a special unitary two-dimensional complex vector represents all possible single-qubit rotations on the Bloch sphere [66]. Single-qubit operations are preferred for their ease of input data encoding and quantum function design, thus enabling a straightforward exploration of the impact of quantum approaches on neural networks without the complexities of entanglement and multi-qubit interactions.

SU(2) operations (special unitary group of degree 2) are linear because of the unitary nature of all operations, thus ensuring the reversibility of the quantum operations and the preservation of the total probability [67]. While all quantum operators are linear due to the requirements of unitarity, applying these operators in quantum computing algorithms can result in non-linear functionalities due to the complex interplay of quantum states, entanglement, superposition, and measurement processes. An $SU(2)$ operation on a single qubit can be represented as a rotation in the three-dimensional Bloch sphere given by:

$$U(\theta, \phi, \lambda) = e^{-\frac{i\phi\sigma_z}{2}} e^{-\frac{i\theta\sigma_y}{2}} e^{-\frac{i\lambda\sigma_z}{2}} \tag{25}$$

Where θ is the rotation angle around the y-axis, ϕ is the initial phase rotation around the z-axis, λ is the final phase rotation around the z-axis, and σ_x, σ_y, and σ_z are the Pauli matrices corresponding to rotations around the x,y, and z axes of the Bloch sphere, respectively.

Applying the $SU(2)$ operation to the prepared qubit from the previous step can be used to explore the entire Bloch sphere. The $SU(2)$ operation represents all possible single-qubit rotations on the Bloch sphere, meaning it can be used to adjust the qubit's state in any way. This operation allows a comprehensive exploration of the quantum state space and enables the activation function to introduce non-linearity based on the input data.

$$|\widetilde{\psi}(x)\rangle = \prod_{j=1}^{N} e^{-\frac{i\phi\sigma_z}{2}} e^{-\frac{i\theta\sigma_y}{2}} e^{-\frac{i\lambda\sigma_z}{2}} . |\psi(x)\rangle \tag{26}$$

To assess the quantum neural network's performance, we applied the proposed quantum-inspired activation function instead of the Swish activation function, considering the requirements for transforming, normalising, and encoding the input and target data. We evaluated the network employing the optimal hyperparameters identified in section 3.2. We selected MATLAB as the primary computational tool for coding and managing the studied networks throughout the training and evaluation processes. In the upcoming section of the paper, we will present and analyse the results of our comparative study between classical neural networks and QNNs, thus providing valuable insights into the effectiveness of our proposed approach.

3. Results and discussion

In this study, we compared the performance of two types of neural networks with different activation functions. The first neural network utilised the Swish activation function, which demonstrated the best performance among the tested activation functions, as shown in Table 3. The second network employed an MLP architecture with a novel quantum-inspired activation function. Additionally, we assessed two other network configurations by integrating a custom layer for singularity avoidance and comparing standard MLP models with quantum-inspired MLP models.

The findings reveal that the QNNs outperform classical ANNs in predicting the inverse kinematics of the ABB IRB140 robotic arm. The QNNs showed lower MAE values during the training and validation stages, indicating better precision and improved generalisation capabilities. The introduction of a quantum-inspired activation function was key in this advancement, allowing more effective learning and

mitigating overfitting. Furthermore, the QNNs displayed improved singularity avoidance, further verifying the efficacy of the proposed approach in addressing challenging kinematic scenarios.

We established the chosen hyperparameters for our model through several iterations. We applied the Swish activation function and quantum-inspired activation function in the MLP layers and trained the model using the MAE loss function. We set the batch size to 64, and the training process spanned 170 epochs. We observed that a constant learning rate did not yield satisfactory results – high learning rates led to oscillating loss values, whereas low learning rates resulted in convergence to a saddle point rather than the global optimum. To address this problem, we implemented a cyclical learning rate strategy.

Analysing a model's training and validation errors is crucial to evaluating its performance and accuracy. While the training error measures the model's ability to learn from the training data, the validation error assesses its capacity to generalise to new, unseen data. Understanding these errors is essential for ensuring the model can reliably capture the underlying patterns in the data and make accurate predictions in real-world scenarios.

In this study, we examined the training and validation errors to develop a model that both performs well on the training dataset and exhibits robust generalisation capabilities when exposed to new data. The performance of the classical and quantum-inspired networks based on an MLP architecture is shown in Figs. 7 and 8. To enhance the model's generalisation capability, we introduced Gaussian noise with a standard deviation of 0.0035 as the initial layer of the model.

Fig. 7 shows the MAE loss of the studied ANN across 170 epochs, revealing an initial rapid learning phase, with significant decreases in the training and validation losses. Within the first 20 epochs, the training loss drops to around 0.3 and stabilises, mirrored by the validation loss, indicating promising initial generalisation. Towards the end of the training, the convergence of training and validation losses (MAE values of 0.0098825 and 0.010956, respectively) demonstrate effective learning without notable overfitting, indicating that the model will perform well when presented with new data.

Fig. 8 shows the QNN's MAE loss during training and validation. Initially, the loss drops sharply, indicating rapid learning, then stabilises, indicating convergence towards a solution. The final MAE loss values for training and validation are 0.0065353 and 0.007236, respectively, indicating the model has good generalisation ability without overfitting. Overall, these results confirm the proposed QNN's effective learning capability and potential accuracy in real-world applications.

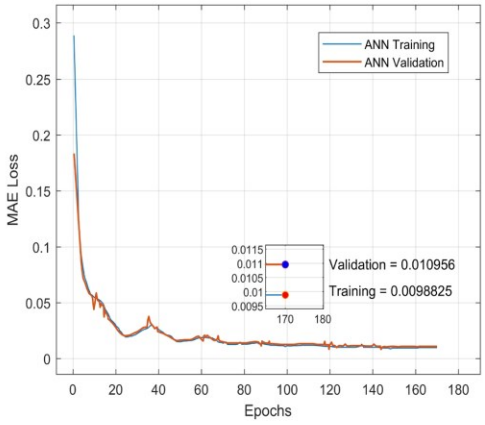

Fig. 7. Loss values of the ANN for position and orientation versus number of epochs.

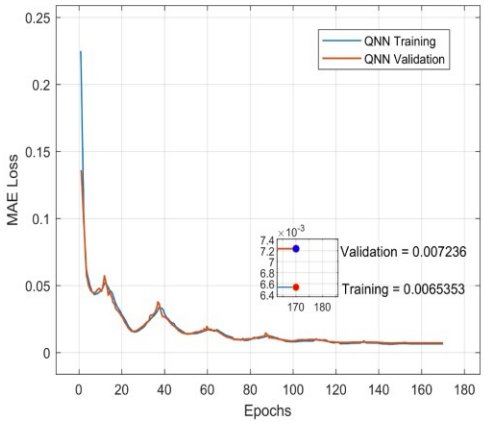

Fig. 8. Loss of QNN for position and orientation.

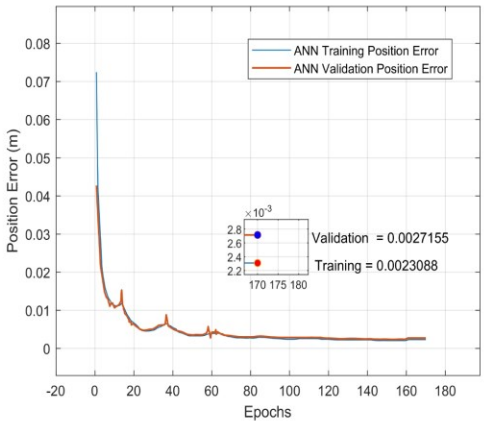

Fig. 9. Position error of ANN during training and validation.

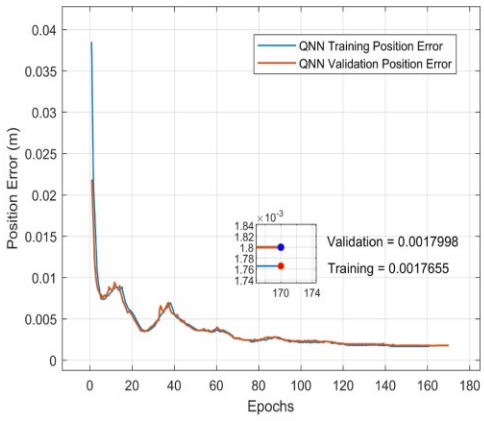

Fig. 10. Position error of QNN during training and validation.

A qualitative comparison of the performance and accuracy of the QNN and ANN indicates superior performance in the QNN, which exhibits rapid learning capabilities and stabilises at a more optimal value, indicating higher efficiency in learning and generalising from data.

Both networks lack overfitting; however, the proposed QNN appears to align more closely with unseen data, as evidenced by its lower validation MAE loss, suggesting robust generalisation. While they do not provide exact percentages, the presented statistics imply that the QNN is the more accurate and better-performing network in this comparison.

The training and validation position errors of the networks over 170 epochs are presented in Figs. 9 and 10. As shown in Fig. 9, the position error in the ANN drops rapidly, indicating rapid learning. Both errors converge towards a constant value as the number of epochs increases, showing that learning has stabilised.

The final training error is 2.3 mm, with a slightly higher validation error of 2.71 mm, indicating the ANN's ability to generalise well without overfitting. The plateauing of the position error after the initial drop suggests that the ANN has reached its learning capacity in the studied configuration.

In the results shown for the QNN in Fig. 10, the algorithm initially shows a sharp decrease in error, indicating rapid learning and adaptation. As the epochs progress, both the training and validation errors stabilise at a low level, suggesting that the QNN has achieved its optimal state of learning. After 170 epochs, the training position error settles at approximately 1.76 mm, with the validation error slightly higher at around 1.79 mm. The negligible difference between these values indicates a well-generalised model with minimal overfitting, which is crucial for real-world applications that require accurate predictions based on new, unseen data. The graph also indicates that the errors align closely and remain consistent after the initial drop, demonstrating that the current network architecture maximises the model's learning capacity. This behaviour showcases a mature model that can reliably perform tasks that require precise positional estimations, validating the effectiveness of the proposed QNN in these applications.

Overall, this comparison reveals that the QNN presents improved capabilities with a significantly lower position error, indicating its suitability for high-precision practical applications. Its consistent and stable error reduction suggests a strong learning ability within the proposed network architecture. Furthermore, with a validation position error approximately 1 mm lower than that of the ANN, the QNN displays superior proficiency in handling new and unseen data, highlighting its exceptional generalisation ability.

The orientation error for both networks during training and validation is presented in Figs. 11 and 12. For the ANN in Fig. 11, both errors

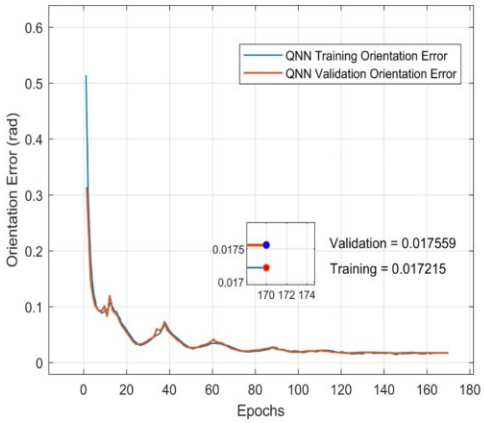

Fig. 12. Orientation error of QNN during training and validation.

gradually decrease and stabilise at a low level, with the training error slightly lower than the validation error. The inset shows a magnified view of the graph's tail, revealing that the training and validation errors are approximately 0.0198 and 0.021 radians in the 170th epochs. This slight difference between training and validation errors indicates that the model can make accurate predictions without significant overfitting. The final error values demonstrate the ANN's strong predictive capabilities, indicating that it has learnt the task with remarkable accuracy. This level of accuracy is essential for high-precision applications like robotics or complex system modelling.

The QNN network in Fig. 12 displays a sharp initial decrease in training error, indicating rapid adaptation to the training set. The training and validation errors progressively converge, with the training error slightly lower than the validation error, implying effective learning without significant overfitting. The inset highlights the tail end of the graph, showing the close similarity between the training and validation errors in the final epochs. Notably, the errors stabilise at a value lower than that of the ANN, with training and validation errors recorded of approximately 0.00172 and 0.00175 radians, respectively. The minimal discrepancy between these values indicates the robust predictive abilities of the QNN. Overall, similar to the trends observed for the position error, these results indicate that the QNN outperforms the ANN in terms of orientation error, showcasing its precise learning capabilities.

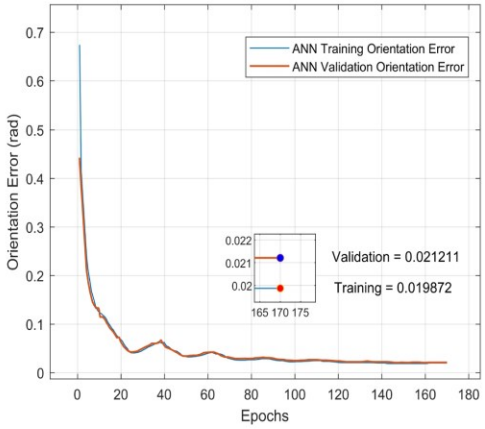

Fig. 11. Orientation error of ANN during training and validation.

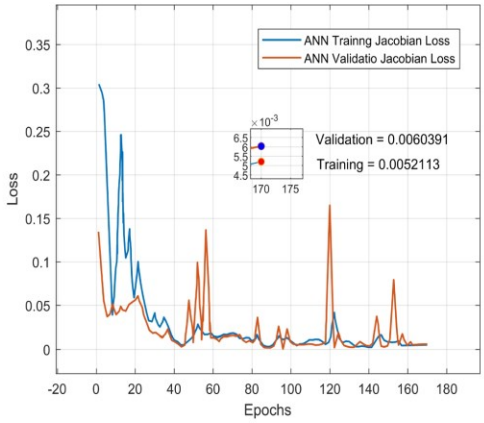

Fig. 13. Loss of ANN for singularity avoidance.

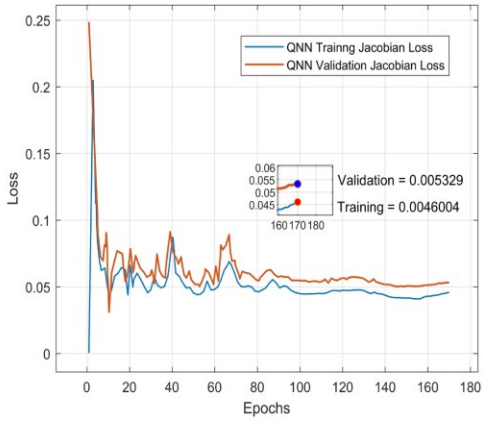

Fig. 14. Loss of QNN for singularity avoidance.

The other model investigated in this study uses the same MLP architecture and two different activation functions, with Swish used as a standard activation function in the ANN and the proposed quantum activation function in the QNN. The only difference is that rather than the MAE loss, the new loss function must consider a metric that expresses the distance from a singularity point and penalises short distances, as described in Eq. (12). We train the two networks over 170 training epochs, with the corresponding loss values shown in Figs. 13 and 14.

As shown in Fig. 13, neural networks commonly show a discernible trend during training. Typically, a notable decrease in loss is recorded during the initial epochs, after which the loss stabilises. This trend is visible in the training loss of the ANN, which exhibits oscillations but gradually decreases overall after an initial sharp drop. In the final epochs, as illustrated in the graph's inset, the training loss settles at around 0.005, while the validation loss is marginally higher at 0.006. This discrepancy between the two losses may indicate some degree of overfitting, where the model performs better on the training data than on unseen data; however, the similarity between these two values suggests that the model still has reasonable generalisation capacity, albeit with slight potential overfitting. The observed peaks in the training and validation losses may be due to the model's sensitivity to specific data points or batch sequences during training. Overall, the trend and final values indicate that the ANN can effectively learn the Jacobian-based function to avoid singularity points.

In the QNN model results shown in Fig. 14, the training process begins with a significant drop in loss and further rapid improvements in the initial epochs, which represents typical behaviour as the network begins to fit the training data. Subsequently, both training and validation losses exhibit an overall downward trend with some fluctuations. However, the validation loss closely tracks the training loss, suggesting the network is not overfitting and performing well on the new data. In the detailed view shown in the inset, the training loss reaches approximately 0.004 in the final epochs, with a slightly higher validation loss of 0.005. This minor gap between the training and validation losses indicates that the QNN can achieve consistent performance on unseen data, which is essential for ensuring the model's reliability in practical applications. The relatively low and comparable loss values indicate that the proposed QNN can successfully learn to approximate the Jacobian to avoid singularities both when exposed to the training data and when generalising to new data.

Comparing the two networks with singularity avoidance revealed that both models learnt the function adeptly. However, the QNN outperformed the ANN model by displaying a closer alignment between its training and validation losses. The QNN demonstrated excellent accuracy in fitting the training data, with similar performance when tested on validation data. Overall, these findings indicate that the QNN is a more robust and superior regression model for accurately predicting outcomes in the studied problem. In the networks where the loss function prevents singularities, the validation position error is slightly lower than those without such avoidance measures; specifically, the validation position error rates for the ANN and QNN are 1.97 mm and 1.64 mm, respectively, compared to equivalent values of 2.71 mm and 1.79 mm for the ANN and QNN without singularity avoidance.

Table 4
Comparative analysis of the performance metrics for the proposed ANN and QNN models.

Model	Evaluation Metric	Loss (MAE) (Training / Validation)	Position Error (mm) (Training / Validation)	Orientation Error (radians) (Training / Validation)
ANN	MAE	0.0098 / 0.0109	–	–
QNN	MAE	0.0065 / 0.0072	–	–
ANN	Position Metrics	–	2.3 / 2.71	–
QNN	Position Metrics	–	1.76 / 1.79	–
ANN	Orientation Metrics	–	–	0.0198 / 0.021
QNN	Orientation Metrics	–	–	0.00176 / 0.00179
ANN	Singularity Avoidance MAE Jacobian	0.005 / 0.006	–	–
QNN	Singularity Avoidance MAE Jacobian	0.004 / 0.005	–	–
ANN	Position Metrics	–	1.72 / 1.97	–
QNN	Position Metrics	–	1.37 / 1.64	–

Table 4 summarises all the values obtained for the proposed networks in our study's training and validation phases. Overall, the QNN outperforms the ANN in terms of MAE and achieves superior values in the position and orientation metrics. In the validation step, the QNN's MAE is around 15.60 % lower than that of the ANN. Furthermore, the QNN exhibits superior precision in position and orientation errors, with differences of approximately 1 mm and 0.02 radians, respectively. The QNN's performance in all the evaluated metrics on the validation data is outstanding and superior, even in the network designed to avoid singularities. Compared with the ANN, the QNN achieves an MAE Jacobian that is roughly 16.67 % lower and a position error reduced by about 0.4 mm. The QNN with singularity avoidance also provides precise predictions, reducing the position error by approximately 0.15 mm compared to the QNN without singularity avoidance.

This study's proposed quantum-inspired activation function represents a considerable departure from traditional activation functions, providing improved learning capabilities and enhanced computational efficiency. This breakthrough tackles the long-standing issues of non-unique solutions and computational complexity in inverse kinematics. By showcasing the performance of QNNs, this study provides a basis for further exploration of implementing quantum principles in neural network models, potentially transforming various fields within robotics and beyond.

This research highlights the exceptional proficiency of the classical neural network model, which utilises the Swish activation function, in terms of training and validation accuracy. This model displays a rapid learning period and stabilises with low MAE values, demonstrating strong learning and generalisation capabilities. Introducing Gaussian noise further enhances the model's generalisation ability, resulting in improved performance.

Integrating quantum-inspired concepts into the neural network's activation function can significantly enhance the network's performance

and accuracy. The proposed QNN model displays more immediate learning and superior stabilisation compared to the classical ANN model. This superiority is demonstrated by the QNN's lower position and orientation error values, showcasing its superior precision and generalisation ability.

In this analysis, we also investigated models designed to prevent singularities, which is an essential aspect of robotics. The QNN model outperforms the classical model, with closer alignment between the training and validation loss values and lower position errors. This result indicates the QNN's robustness and superior regression capabilities, making it an excellent choice for real-world applications requiring precise positional estimations and reliable performance.

QNNs can outperform ANNs due to the advantages provided by quantum computing. One particularly important factor is parallelism, allowing the simultaneous processing of multiple possibilities through quantum superposition. This capability is particularly beneficial for complex mathematical problems in engineering, resulting in faster processing times and improved simulations. Quantum entanglement further enhances the efficiency of QNNs, allowing information to be processed across different parts of the network simultaneously. This effect improves the efficiency of algorithms for solving large systems of equations or matrix operations, which are common in engineering tasks. Quantum annealing also contributes to the superior performance of QNNs, enabling effective navigation of solution spaces and avoidance of local minima, which can trap classical algorithms. This feature is helpful in optimisation problems, where it is necessary to identify the most efficient design or lowest energy configuration.

QNNs are revolutionising how we address complex engineering challenges, such as predicting inverse kinematics for a six-degree-of-freedom robotic arm. By integrating quantum computing principles with neural networks, QNNs offer improved efficiency, performance, and accuracy compared to conventional neural networks. The progress presented in this study underscores the potential of quantum-inspired models to enhance the precision and performance of neural networks in robotics applications; however, we have yet to fully explore the comprehensive capabilities of QNNs as the field of quantum computing continues to evolve.

4. Conclusion

The proposed quantum-inspired activation function improves the learning efficiency and accuracy of neural networks, providing a reliable solution to the existing challenges of conventional methods. The findings of this study highlight the potential of quantum computing principles in refining neural network models, resulting in more accurate and efficient robotic systems.

Precise positioning and movement during complex tasks are essential for robotic arms, making inverse kinematics a critical component. However, classical approaches often need assistance in terms of handling non-unique solutions and increased computational complexity, especially with increased degrees of freedom. Therefore, innovative solutions are required to improve the accuracy and performance of these models and simplify calculations. While machine learning and artificial neural networks have shown promise in solving inverse kinematic equations, there is still a pressing need for further advancements, particularly in terms of applying quantum computing. By integrating quantum-inspired activation functions into the proposed neural network, this research aims to address these limitations and enhance the capabilities of robotic systems, contributing significantly to the field.

In terms of practical implications, the proposed QNN-based solution can enhance productivity and reduce error rates in manufacturing, assembly, welding, and painting tasks by improving the precision and computational efficiency of solving inverse kinematics for robotic arms. Avoiding singularities ensures consistent and reliable performance, which is crucial for maintaining smooth operations in complex industrial processes. Additionally, the enhanced precision and efficiency of QNNs can significantly benefit applications in healthcare, such as robot-assisted surgery, and space exploration, where precise and efficient robotic manipulations are vital for mission success. Our examination addresses essential gaps in current industrial applications and demonstrates the potential for QNNs to revolutionise robotic control systems.

This research focuses on the kinematic modelling of the ABB IRB140 robot. It utilises the DH method for forward kinematics while defining the spatial geometry of a kinematic chain to determine the position and orientation of the robot arm. The Jacobian matrix is also essential to determine the mechanism's state and avoid the singularities described above. MLP neural networks were selected in this study to solve inverse kinematics. This work emphasises the importance of determining the optimal MLP structure and applying a robust training dataset. Additionally, the study presents quantum computing fundamentals and proposes an activation function for QNNs to enhance the accuracy of robotic arm motion predictions.

The results from the MLP demonstrate exceptional accuracy in predicting the inverse kinematics of the robot arm, as evidenced by the position and orientation errors in both training and validation. This result confirms that the network design was correct and the optimal parameter range was identified during hyperparameter selection. Second, the study highlights the superior performance of QNNs over standard ANNs in solving inverse kinematics for robotic arms. The QNNs indicated excellent precision in position and orientation errors, both with and without considering singularity avoidance. Specifically, the QNNs without singularity avoidance achieved a position error of 1.64 mm and a minor orientation error of 0.00179 radians.

These results demonstrate the potential of QNNs in enhancing the precision and efficiency of robotic arm manipulations, offering a promising avenue for future research in robotics and quantum computing. Quantum computing provides superior performance and accuracy by leveraging its unique advantages, such as parallelism and quantum entanglement. This technique enables the simultaneous processing of multiple possibilities, resulting in faster processing times and improved simulations for complex mathematical problems in engineering. Additionally, quantum annealing helps avoid local minima that can trap classical algorithms, effectively navigating solution spaces. These benefits may lead to more efficient algorithms for solving large systems of equations or matrix operations, which are common in engineering tasks that require the most efficient design or lowest energy configuration to be identified.

Overall, the results of this study demonstrate that QNNs outperform classical ANNs in terms of accuracy and robustness, particularly in scenarios involving singularity avoidance. However, there is room for further exploration and enhancement. Future research could include increasing the resolution and accuracy of the data collection process, conducting further hyperparameter optimisation and network architecture refinements, and developing further innovations in quantum methods and testing them in new applications. We acknowledge the importance of examining the performance of our models on different robotic arms and refining the novel quantum activation function in future research. This will allow us to further validate and generalise our findings across various robotic platforms and configurations, both in terms of actual robots and simulation models. Additionally, future research should focus on integrating more advanced quantum computing algorithms to improve the learning speed and adaptability of QNNs. Exploring the effects of different noise models on network accuracy and extending the application of QNNs to other domains in robotics, such as navigation and manipulation, will also be essential steps in developing the research capabilities and resources in this field.

Funding

This research was supported by funding from NSERC Canada.

CRediT authorship contribution statement

Mehdi Fazilat: Visualization, Methodology, Writing – original draft, Validation, Investigation, Formal analysis, Data curation, Conceptualization. **Nadjet Zioui:** Writing – review & editing, Writing – original draft, Validation, Supervision, Software, Resources, Project administration, Methodology, Funding acquisition, Formal analysis, Conceptualization.

Declaration of competing interest

The authors declare that they have no known competing financial interests or personal relationships that could have appeared to influence the work reported in this paper.

Data availability

All data used to perform this work are available within the manuscript.

References

[1] R.C. Jesus, E.O. Freire, L. Molina, E.A. Carvalho, Solving inverse kinematics of planar manipulators with robustness to singularities by reverse operating neural networks, in: 2018 Latin American Robotic Symposium, 2018 Brazilian Symposium on Robotics (SBR) and 2018 Workshop on Robotics in Education (WRE), IEEE, 2018, pp. 153–157.

[2] M. Theofanidis, S.I. Sayed, J. Cloud, J. Brady, F. Makedon, Kinematic estimation with neural networks for robotic manipulators. Artificial Neural Networks and Machine Learning–ICANN 2018: 27th International Conference On Artificial Neural Networks, Rhodes, Greece, October 4-7, 2018, Proceedings, Part III 27, Springer, 2018, pp. 795–802.

[3] R. Grassmann, V. Modes, J. Burgner-Kahrs, Learning the forward and inverse kinematics of a 6-DOF concentric tube continuum robot in SE (3), in: 2018 IEEE/RSJ International Conference on Intelligent Robots and Systems (IROS), IEEE, 2018, pp. 5125–5132.

[4] C.-K. Ho, C.-T. King, Automating the learning of inverse kinematics for robotic arms with redundant dofs, arXiv preprint arXiv:2202.07869, (2022).

[5] R. Bensadoun, S. Gur, N. Blau, L. Wolf, Neural inverse kinematic, in: International Conference on Machine Learning, PMLR, 2022, pp. 1787–1797.

[6] M.N. Vu, F. Beck, M. Schwegel, C. Hartl-Nesic, A. Nguyen, A. Kugi, Machine learning-based framework for optimally solving the analytical inverse kinematics for redundant manipulators, Mechatronics 91 (2023) 102970.

[7] G. Fang, Y. Tian, Z.-X. Yang, J.M. Geraedts, C.C. Wang, Efficient jacobian-based inverse kinematics with sim-to-real transfer of soft robots by learning, IEEE/ASME Trans. Mechatron. 27 (2022) 5296–5306.

[8] N.G. Adar, Real time control application of the robotic arm using neural network based inverse kinematics solution, Sak. Univ. J. Sci. 25 (2021) 849–857.

[9] B.E. Hargis, W.A. Demirjian, M.W. Powelson, S.L. Canfield, Investigation of neural-network-based inverse kinematics for a 6-DOF serial manipulator with non-spherical wrist. International Design Engineering Technical Conferences and Computers and Information in Engineering Conference, American Society of Mechanical Engineers, 2018. V05BT07A048.

[10] A. Csiszar, J. Eilers, A. Verl, On solving the inverse kinematics problem using neural networks, in: 2017 24th International Conference on Mechatronics and Machine Vision in Practice (M2VIP), IEEE, 2017, pp. 1–6.

[11] P. Srisuk, A. Sento, Y. Kitjaidure, Forward kinematic-like neural network for solving the 3D reaching inverse kinematics problems, in: 2017 14th International Conference on Electrical Engineering/Electronics, Computer, Telecommunications and Information Technology (ECTI-CON), IEEE, 2017, pp. 214–217.

[12] V. Aparanji, U.V. Wali, R. Aparna, Robotic motion control using machine learning techniques, in: 2017 International Conference on Communication and Signal Processing (ICCSP), IEEE, 2017, pp. 1241–1245.

[13] A. Zlokapa, California institute of technology, 2021.

[14] S. Suneel, A. Balaram, M. Amina Begum, K. Umapathy, P.C.S. Reddy, V. Talasila, Quantum mesh neural network model in precise image diagnosing, Opt. Quantum Electron. 56 (2024) 559.

[15] R.D. Taylor, Quantum artificial intelligence: a "precautionary" US approach? Telecomm. Policy 44 (2020) 101909.

[16] S.T. Marella, H.S.K. Parisa, Introduction to quantum computing, quantum computing and communications, (2020).

[17] S.B. Ramezani, A. Sommers, H.K. Manchukonda, S. Rahimi, A. Amirlatifi, Machine learning algorithms in quantum computing: a survey, in: 2020 International joint conference on neural networks (IJCNN), IEEE, 2020, pp. 1–8.

[18] N.H. Nguyen, E.C. Behrman, M.A. Moustafa, J.E. Steck, Benchmarking neural networks for quantum computations, IEEE Trans. Neural Netw. Learn. Syst. 31 (2019) 2522–2531.

[19] S. Gupta, S. Mohanta, M. Chakraborty, S. Ghosh, Quantum machine learning-using quantum computation in artificial intelligence and deep neural networks: quantum computation and machine learning in artificial intelligence, in: 2017 8th annual industrial automation and electromechanical engineering conference (IEMECON), IEEE, 2017, pp. 268–274.

[20] M. Zidan, A. Sagheer, N. Metwally, Autonomous perceptron neural network inspired from quantum computing, arXiv preprint arXiv:1510.00556, (2015).

[21] A. Kutvonen, K. Fujii, T. Sagawa, Optimizing a quantum reservoir computer for time series prediction, Sci. Rep. 10 (2020) 14687.

[22] M.P. Singh, B. Rajput, Role of entanglement in quantum neural networks (QNN), J. Mod. Phys. 6 (2015) 1908–1920.

[23] M. Fazilat, N. Zioui, J. St-Arnaud, A novel quantum model of forward kinematics based on quaternion/pauli gate equivalence: application to a six-jointed industrial robotic arm, Results Eng. 14 (2022) 100402.

[24] N. Zioui, Y. Mahmoudi, A. Mahmoudi, M. Tadjine, S. Bentouba, A novel quantum-computing-based quaternions model for a robotic arm position, Int. J. Comput. Intell. Control 13 (2021) 71–77.

[25] N. Zioui, A. Mahmoudi, M. Tadjine, Representing quantum spins in different coordinate systems for modelling rigid body orientation, Karbala Int. J. Mod. Sci. 9 (2023) 11.

[26] H.M. Abdulridha, Z.A. Hassoun, Control design of robotic manipulator based on quantum neural network, J. Dyn. Syst. Meas. Control 140 (2018) 061002.

[27] K. Takahashi, M. Tsuji, M. Hashimoto, Remarks on Learning Inverse Kinematics of a Robot Manipulator Using a Quaternion Neural Network, In: 10th IIAE International Conference on Industrial Application Engineering, 2022, doi: 10.12792/iciae2022.011.

[28] S. Dereli, R. Köker, A meta-heuristic proposal for inverse kinematics solution of 7-DOF serial robotic manipulator: quantum behaved particle swarm algorithm, Artif. Intell. Rev. 53 (2020) 949–964.

[29] X. Cheng, M. Zhao, The inverse solution algorithm and trajectory error analysis of robotic arm based on MQACA-RBF network, J. Robot. 2020 (2020) 7807952.

[30] L. Parisi, D. Neagu, R. Ma, F. Campean, QReLU and m-QReLU: two novel quantum activation functions to aid medical diagnostics, arXiv preprint arXiv:2010.08031, (2020).

[31] Y. Dong, F. Li, T. Zhu, R. Yan, Air quality prediction based on quantum activation function optimized hybrid quantum classical neural network, Front. Phys. 12 (2024) 1412664.

[32] A. Daskin, A simple quantum neural net with a periodic activation function, in: 2018 IEEE International Conference on Systems, Man, and Cybernetics (SMC), IEEE, 2018, pp. 2887–2891.

[33] S. Li, M.S. Salek, Y. Wang, M. Chowdhury, Quantum-inspired activation functions in the convolutional neural network, arXiv preprint arXiv:2404.05901, (2024).

[34] Y. She, S. Li, M. Xin, Quantum-interference artificial neural network with application to space manipulator control, IEEE Trans. Aerosp. Electron. Syst. 57 (2021) 2167–2182.

[35] V.S. Gandhi, T.-M. McGinnity, Quantum neural network based surface EMG signal filtering for control of robotic hand, in: The 2013 International Joint Conference on Neural Networks (IJCNN), IEEE, 2013, pp. 1–7.

[36] M. Fazilat, N. Zioui, The impact of simplifications of the dynamic model on the motion of a six-jointed industrial articulated robotic arm movement, J. Robot. Control (JRC) 5 (2024) 173–186.

[37] M. Fazilat, Université du Québec à trois-rivières, 2022.

[38] S. Sarabandi, F. Thomas, Solution methods to the nearest rotation matrix problem in $\mathbb{R}$ 3: a comparative survey, Numer. Linear Algebra Appl. 30 (2023) e2492.

[39] G. Giarmatzis, E.I. Zacharaki, K. Moustakas, Real-time prediction of joint forces by motion capture and machine learning, Sensors 20 (2020) 6933.

[40] M.d.R. Martínez-Blanco, T. Ibarra-Pérez, F. Olivera-Domingo, J.M. Ortiz-Rodríguez, Optimization of Training Data Set Based On Linear Systematic Sampling to Solve the Inverse Kinematics of 6 DOF Robotic Arm With Artificial Neural Networks, Frontiers of Data and Knowledge Management For Convergence of ICT, Healthcare, and Telecommunication Services, 2022, pp. 85–112.

[41] S.B. Šegota, N. Anđelić, V. Mrzljak, I. Lorencin, I. Kuric, Z. Car, Utilization of multilayer perceptron for determining the inverse kinematics of an industrial robotic manipulator, Int. J. Adv. Robot. Syst. 18 (2021) 1729881420925283.

[42] R. Liu, F. Nageotte, P. Zanne, M. de Mathelin, B. Dresp-Langley, Deep reinforcement learning for the control of robotic manipulation: a focussed mini-review, Robotics 10 (2021) 22.

[43] M.A. Funes Lora, E.A. Portilla-Flores, R. Rivera Blas, E.A. Merchan Cruz, M. F. Carbajal Romero, Metaheuristic techniques comparison to optimize robotic end-effector behavior and its workspace, Int. J. Adv. Robot. Syst. 15 (2018) 1729881418801132.

[44] "^?^(0) = ^1^count(descendant::ce:intra-ref)"^?^(0) = ^1^count(descendant::ce:doi)"^?^(0)[?pdftagstart "Link"] > R. Singh, V. Kukshal, V.S. Yadav, A review on forward and inverse kinematics of classical serial manipulators, Adv. Eng. Des. 2020 (2021) 417–428.

[45] A. Rosyid, B. El-Khasawneh, A. Alazzam, Performance measures of parallel kinematics manipulators, Mech. Sci. 11 (2020) 49–73.

[46] R. Liu, E. Dobriban, Z. Hou, K. Qian, Dynamic load identification for mechanical systems: a review, Arch. Comput. Methods Eng. 29 (2022) 831–863.

[47] S. Sarabandi, F. Thomas, A survey on the computation of quaternions from rotation matrices, J. Mech. Robot. 11 (2019) 021006.

[48] Y. Lu, A. Sigov, L. Ratkin, L.A. Ivanov, M. Zuo, Quantum computing and industrial information integration: a review, J. Ind. Inf. Integr. (2023) 100511.

[49] N. Zioui, A. Mahmoudi, Y. Mahmoudi, M. Tadjine, Quantum computing based state domain equations and feedback control, Results Appl. Math. 19 (2023) 100385.

[50] H. Feraoun, M. Fazilat, R. Dermouche, S. Bentouba, M. Tadjine, N. Zioui, Quantum maximum power point tracking (QMPPT) for optimal solar energy extraction, Syst. Soft Comput. (2024) 200118.

[51] S. Saidat, R. Boumekhita, M. Tadjine, N. Zioui, Quantum pulse-width modulation design and implementation for a DC motor drive, Quantum Inf. Process. 23 (2024) 88.

[52] G. Czelusta, J. Mielczarek, Quantum simulations of a qubit of space, Phys. Rev. D 103 (2021) 046001.

[53] A. Usha Devi, Sudha, L. Reena, H. Karthik, A. Rajagopal, Quantum correlations in symmetric multiqubit systems, J. Indian Inst. Sci. 103 (2023) 419–447.

[54] S. Bentouba, N. Zioui, Y. Mahmoudi, A. Mahmoudi, M. Tadjine, A new quantum-computing-based algorithm for robotic arms and rigid bodies, (2021).

[55] Y. Mahmoudi, N. Zioui, H. Belbachir, Quantum optimization in engineering: a brief review, in: 2023 International Conference on Decision Aid Sciences and Applications (DASA), IEEE, 2023, pp. 23–27.

[56] D. Koutný, L. Ginés, M. Moczała-Dusanowska, S. Höfling, C. Schneider, A. Predojević, M. Ježek, Deep learning of quantum entanglement from incomplete measurements, Sci. Adv. 9 (2023) eadd7131.

[57] M. Fazilat, N. Zioui, Quantum-inspired sliding-mode control to enhance the precision and energy efficiency of an articulated industrial robotic arm, Robotics 14 (2025) 14.

[58] Y. Mahmoudi, N. Zioui, H. Belbachir, M. Tadjine, A. Rezgui, A brief review on mathematical tools applicable to quantum computing for modelling and optimization problems in engineering, Emerg. Sci. J. 7 (2022) 289–312.

[59] M. Fazilat, N. Zioui, Investigating quantum artificial neural networks for singularity avoidance in robotic manipulators, in: 2024 12th International Conference on Systems and Control (ICSC), IEEE, 2024, pp. 335–340.

[60] D. Reda, A. Talaoubrid, M. Fazilat, N. Zioui, M. Tadjine, A quantum direct torque control method for permanent magnet synchronous machines, Comput. Electr. Eng. 122 (2025) 109994.

[61] N. Zioui, A. Mahmoudi, M. Tadjine, Design of a new hybrid linearising-backstepping controller using quantum state equations and quantum spins, Int. J. Autom. Control 17 (2023) 397–417.

[62] M. Weigold, J. Barzen, F. Leymann, M. Salm, Encoding patterns for quantum algorithms, IET Quantum Commun. 2 (2021) 141–152.

[63] C. Zhao, X.-S. Gao, QDNN: DNN with quantum neural network layers, arXiv preprint arXiv:1912.12660, (2019).

[64] A. Shukla, P. Vedula, An efficient quantum algorithm for preparation of uniform quantum superposition states, Quantum Inf. Process. 23 (2024) 38.

[65] N. Killoran, T.R. Bromley, J.M. Arrazola, M. Schuld, N. Quesada, S. Lloyd, Continuous-variable quantum neural networks, Phys. Rev. Res. 1 (2019) 033063.

[66] E.P. Tapia, G. Scarpa, A. Pozas-Kerstjens, A didactic approach to quantum machine learning with a single qubit, Phys. Scr. 98 (2023) 054001.

[67] R. Vale, T.M.D. Azevedo, I. Araújo, I.F. Araujo, A.J. da Silva, Decomposition of multi-controlled special unitary single-qubit gates, arXiv preprint arXiv: 2302.06377, (2023).

4.2.2 Summary of the Results Analysis

The ANN model, which employed the Swish activation function, confirmed rapid convergence and stable learning characteristics. The training Mean Absolute Error (MAE) achieved a value of 0.0098, while the validation MAE experienced a slight increase to 0.0109, indicating minimal overfitting. Position and orientation errors are displayed in Figure 4-6. and Figure 4-7, respectively. The final position errors were recorded at 2.3 mm for training and 2.71 mm for validation, while the orientation errors reached 0.0198 radians and 0.021 radians, demonstrating a solid baseline performance.

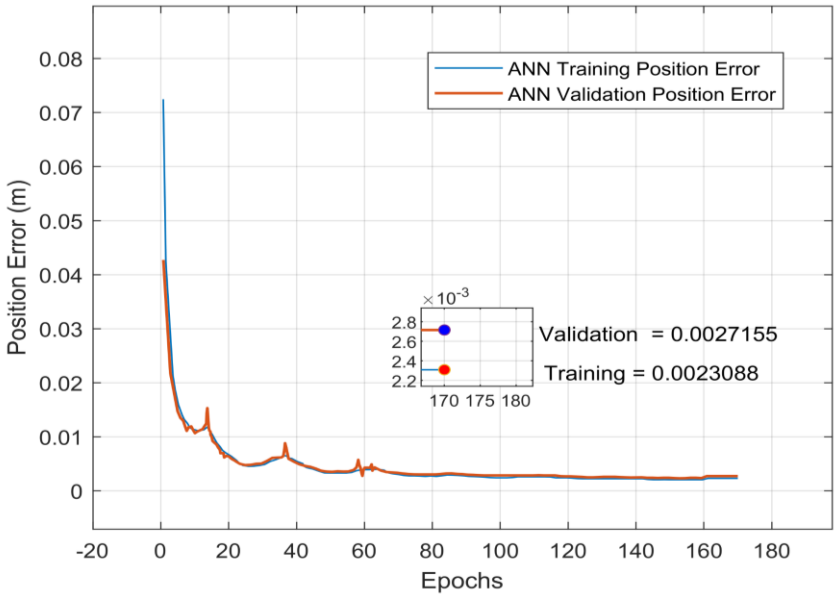

Figure 4-6 Position Error of ANN.

In contrast, the QNN introduced by a quantum-inspired activation function demonstrated greatly better performance. The QNN's mean absolute error converged to 0.0065 during training and 0.0072 during validation. Position errors improved to 1.76 mm in training and 1.79 mm in validation, while orientation errors decreased markedly to 0.00176 and 0.00179 radians, as displayed in Figure 4-8 and Figure 4-9, , respectively.

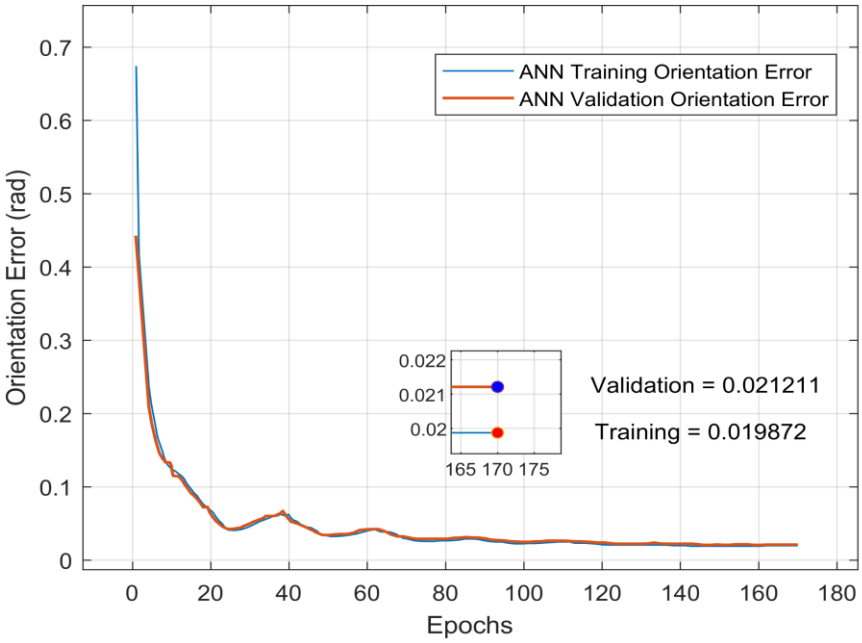

Figure 4-7 Orientation Error of ANN.

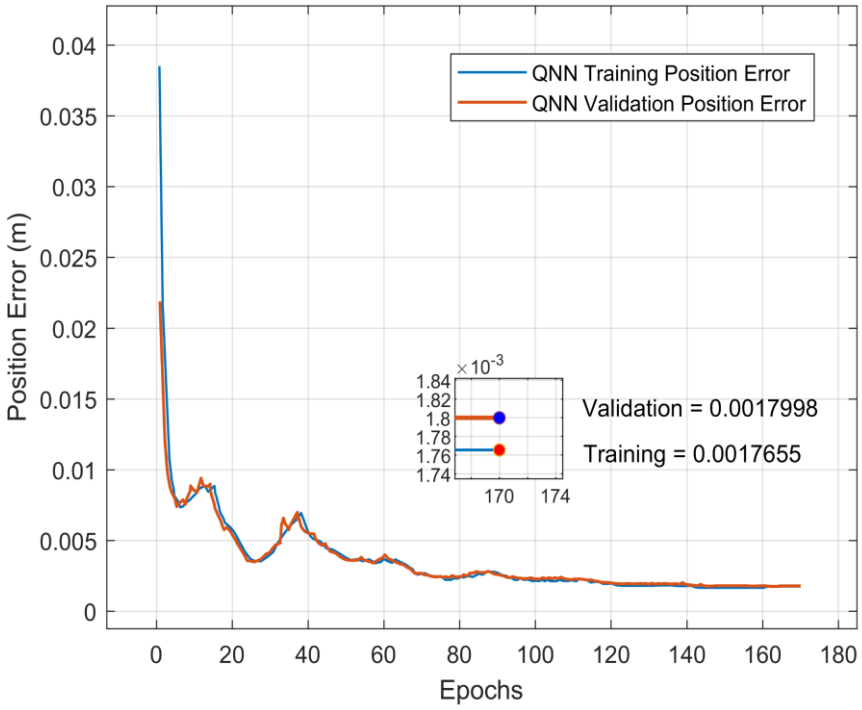

Figure 4-8 Position Error of QNN.

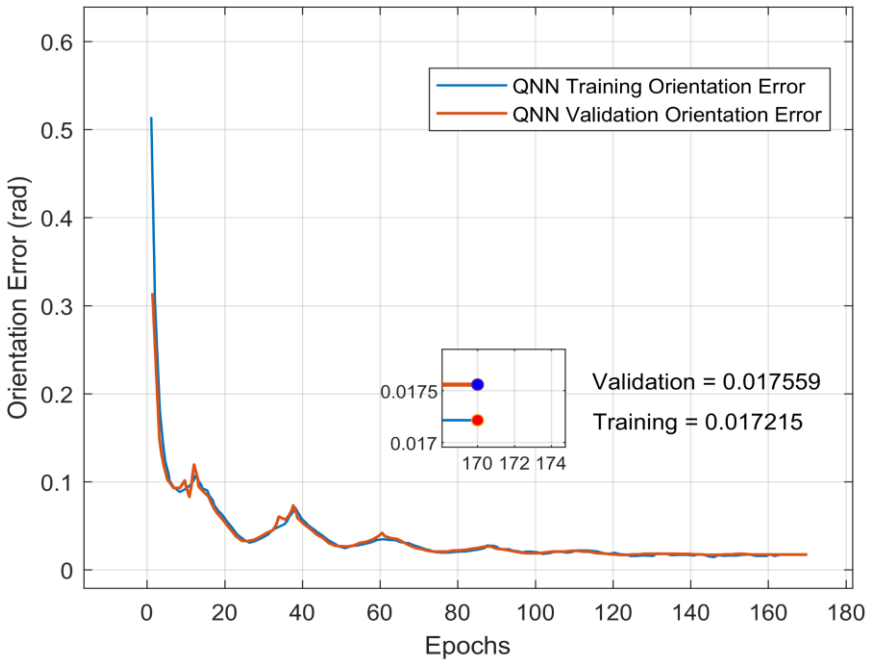

Figure 4-9 Orientation Error of QNN.

In terms of singularity avoidance, the ANN model, illustrated in Figure 4-10, achieved a training loss of 0.005 and a validation loss of 0.006; however, minor overfitting was observed.

In contrast, the QNN model depicted in Figure 4-11 demonstrated better alignment between training and validation losses, yielding values of 0.004 and 0.005, respectively, indicating enhanced stability and robustness.

Additionally, the position errors associated with singularity avoidance also showed improvement, with the QNN attaining 1.37 mm (training) and 1.64 mm (validation), surpassing the ANN's results of 1.72 mm and 1.97 mm.

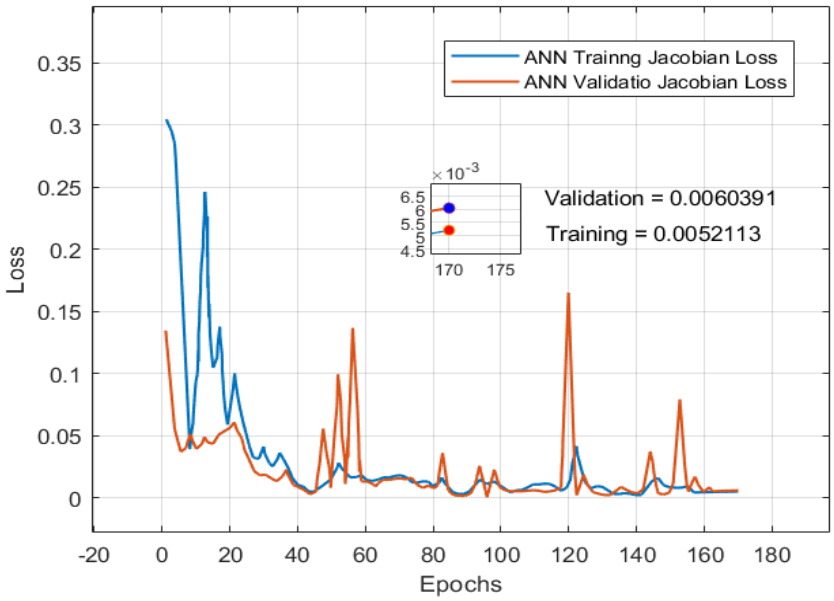

Figure 4-10 Loss of ANN for singularity avoidance.

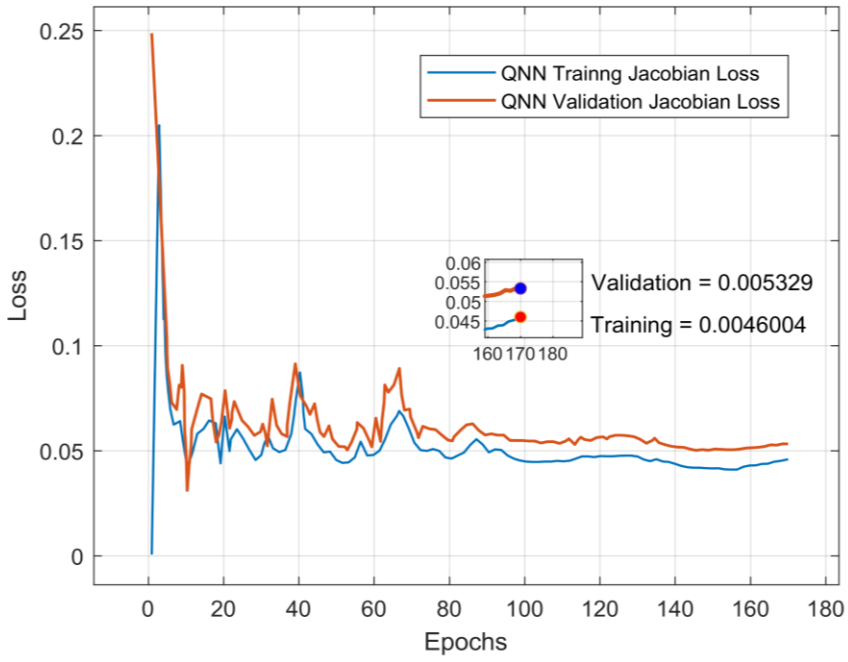

Figure 4-11 Loss of QNN for singularity avoidance.

All key metrics are recapped in Table 4-2. The Quantum Neural Network reduced Mean Absolute Error by 15.60% and improved positional accuracy by 0.92 mm under standard conditions. In singularity-avoidance scenarios, it achieved a 16.67% lower Jacobian-based error and a 0.33 mm gain in accuracy compared to the ANN.

Table 4-2 Comparative Analysis of ANN and QNN Performance Metrics.

Model	**Evaluation Metric**	**Loss (MAE)** (Training/ Validation)	**Position Error (mm)** (Training/ Validation)	**Orientation Error (radians)** (Training/ Validation)
ANN	MAE	0.0098 / 0.0109	-	-
QNN	MAE	0.0065 / 0.0072	-	-
ANN	Position Metrics	-	2.3 / 2.71	-
QNN	Position Metrics	-	1.76 / 1.79	-
ANN	Orientation Metrics	-	-	0.0198 / 0.021
QNN	Orientation Metrics	-	-	0.00176 / 0.00179
ANN	Singularity Avoidance MAE	0.005 / 0.006	-	-
QNN	Singularity Avoidance MAE	0.004 / 0.005	-	-
ANN	Position Metrics	-	1.72 / 1.97	-
QNN	Position Metrics	-	1.37 / 1.64	-

Overall, the experimental outcomes validate the effectiveness of the quantum-inspired approach. The incorporation of quantum activation functions not only enhances precision and generalization but also improves resilience to singular configurations. These findings highlight the potential of QNNs for advanced robotic applications, especially in situations that demand high-accuracy kinematic solutions and robustness against singularities.

4.3 Concluding Remarks

By integrating a quantum-inspired activation function into a Multi-Layer Perceptron neural network, this study harnesses fundamental principles of quantum computing to improve learning capabilities and computational efficiency. The performance of the proposed Quantum Neural Network is rigorously assessed against a classical Artificial Neural Network baseline under the same training conditions, which include the utilization of a large, real-world dataset and strategies for hyperparameter tuning.

The results consistently confirm that QNNs outperform ANNs across all primary performance metrics. QNNs achieved significantly lower mean absolute error, improved positional and orientation accuracy, and superior generalization to unseen data. Furthermore, the QNN exhibited enhanced robustness in scenarios involving singularities, achieving up to 16.67% improvement in MAE and reducing position error to as low as 1.64 mm and orientation error to 0.00179 radians. These improvements highlight the effectiveness of the quantum activation function in enabling the network to learn more complex mappings with greater precision. From a practical perspective, the implementation of QNNs for inverse kinematics offers valuable benefits for industrial applications that require high accuracy and reliability. The ability to avoid singularities and maintain

smooth, precise motion trajectories further solidifies the method's applicability in real-world environments.

Notably, this study also lays a foundation for future research at the intersection of quantum computing and robotics, utilizing optimization algorithms to enhance performance further and evaluate the results by studying and focusing on advanced control strategies. The methodology of embedding quantum behavior into classical neural networks through activation functions opens new pathways for developing hybrid learning systems. Future research should focus on enhancing the quantum-inspired activation function, broadening the approach to encompass various robotic configurations, and investigating full-scale integration with emerging quantum hardware platforms.

The effectiveness of quantum neural networks in addressing the inverse kinematics problem for a six-jointed industrial robotic arm significantly improves prediction accuracy. It enhances robustness against singularities when compared to classical neural architectures. While these outcomes demonstrate the computational advantages of quantum-inspired learning in motion planning, the successful deployment of such models hinges on the accuracy of the underlying dynamic parameters. Inaccurate mass properties and inertia matrices can lead to critical errors in control execution, irrespective of the precision of the learning model.

The comparative scope of this chapter is deliberately restricted to the direct neural counterpart to enable evaluation of the quantum-inspired activation mechanism under identical data, tuning, and training conditions. Broader comparisons with other classical inverse-kinematics solvers represent a pertinent direction for future benchmarking studies.

Therefore, accurate parameter identification is crucial to ensure that model predictions accurately translate into real-world robotic performance. This critical need sets the stage for the next chapter, which delves into the application of swarm optimization, both classical and quantum-inspired, to estimate the dynamic parameters of the robotic system. By tackling this foundational challenge, the next step in the current research will aim further to enhance the robustness and responsiveness of intelligent robotic control.

Chapter 5 - Dynamic Model Parameter Identification of an Industrial Robotic Arm

5.1 Chapter Overview

Accurate parameter identification in the dynamic modeling of robotic systems is essential for achieving high-performance control, reliability, and energy efficiency, particularly in industrial environments. Robotic arms, with their elaborate kinematics and nonlinear dynamics, necessitate precise modeling of inertia matrices and mass center positions to ensure smooth operation and robustness in real-world conditions. Classic identification methods, such as the Least Squares (LS) and Recursive Least Squares (RLS) algorithms, as well as the Newton-Raphson algorithm, often encounter challenges in the nonlinear, high-dimensional contexts typical of industrial robotics. These conventional approaches may have limitations, including convergence issues, sensitivity to noise, and an inability to manage dynamic uncertainties effectively.

In order to address these limitations, this investigation conducts a comparative evaluation of two advanced optimization methodologies: Particle Swarm Optimization (PSO) and Quantum-behaved Particle Swarm Optimization (Q-PSO). The research focuses explicitly on estimating critical dynamic parameters for an articulated industrial robotic arm, using a realistic model developed through Computer-Aided Optimization (CAO) in SolidWorks. Furthermore, a multilayer perceptron (MLP) neural network has been employed to validate the kinematic accuracy of the robotic arm against empirical motion data, to enhance the credibility of the dynamic analysis.

Investigation highlights notable enhancements in parameter estimation accuracy and model robustness when utilizing Quantum-inspired Particle Swarm Optimization compared to traditional Particle Swarm Optimization. The findings demonstrate superior performance in areas such as Mean Absolute Percentage Error, torque regulation, energy efficiency, and resilience to external disturbances. Ultimately, this study provides a solid foundation for applying quantum-inspired optimization techniques to enhance industrial robotic systems, thereby fostering increased precision and operational reliability.

5.2 Paper 4: Dynamic Model Parameter Identification of an Industrial Robot: A Comparative Study of Quantum and Classical Swarm Optimization.

Authors : Mehdi Fazilat, Nadjet Zioui.

Journal: Mathematics.

Publication status: Published.

5.2.1 Methodology

By employing a multi-stage methodology to identify the dynamic parameters of the ABB IRB 140 industrial robotic arm, utilizing both classical Particle Swarm Optimization and Quantum-behaved PSO algorithms. The methodological framework combines physical modeling, machine learning validation, CAD-based mass extraction, and swarm-based optimization, ultimately culminating in performance validation through Sliding Mode Control (SMC). The methodological framework of the study is given in Figure 5-1.

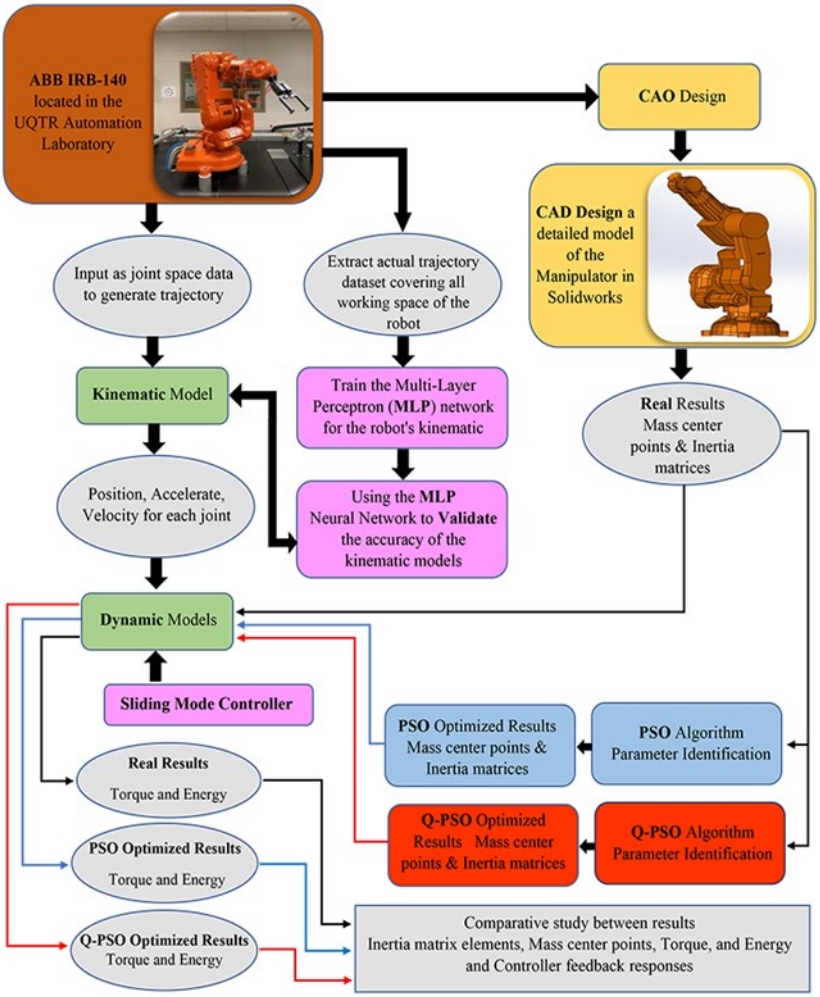

Figure 5-1 The flowchart for the methodological steps.

Dynamic modeling is performed using the Euler–Lagrange formulation, which effectively captures inertia, Coriolis, and gravitational effects as delineated as follows:

$$\sum_{j=1}^{n} M_{ij}\ddot{q}+V_i+G_i=\tau_i, \quad i=1,2,\ldots, \tag{5-1}$$

M_{ij} illustrates the inertial forces, V_i denotes the centrifugal and Coriolis forces, and G_i demonstrates the gravitational forces.

The inertia matrices and mass centers of the first three proximal links are obtained from detailed CAD modeling conducted in SolidWorks, Solid Edge ST4, and CATIA, as shown in Figure 5-2 and Table 5-1. This process ensures the extraction of physically accurate, high-resolution parameters with error margins of less than 1%.

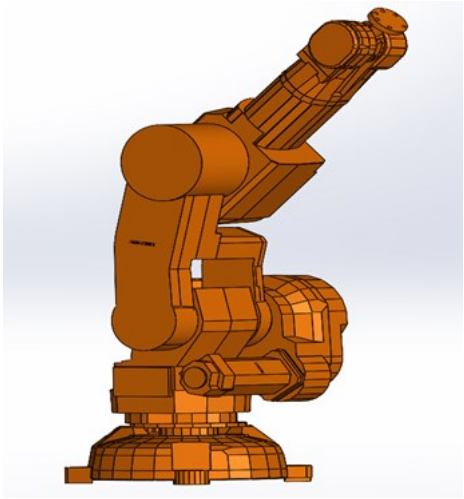

Figure 5-2 Detailed CAD model of the ABB IRB 140 robotic arm.

Table 5-1 Mass Property Results of the Robot Calculated by CAD Software.

ABB IRB 140	**Parameters (unit)**	**Link 1**	**Link 2**	**Link 3**
Mass Properties	*Weight* (kg)	35	25	18
	X_c (mm)	277.87	218.29	-24.56
	Y_c	373.12	229.73	-219.9
	Z_c	-199.03	112.43	-25.86
	I_{xx} (kg.m^2)	6.5	0.9	2.5
	I_{xy}	1.1	-0.03	-0.001
	I_{xz}	3.05	0.1	0.09
	I_{yy}	2.02	1.3	2.7
	I_{yz}	5.07	-0.01	-0.8
	I_{zz}	1.4	0.95	0.5

To optimize the process, both the PSO and Q-PSO algorithms are employed independently to refine the parameters derived from CAD. The PSO algorithm updates particles by utilizing velocity and position update relations, as outlined in Equations 5-2 to 5-4, which are governed by dynamic inertia weights, as offered in Equation 5-3.

$$\vec{v}_i(n+1) = \omega\vec{v}_i(n) + c_1 r_1\left(\vec{p}_i - \vec{x}_i(n)\right) + c_2 r_2(\vec{g} - \vec{x}_i(n)) \tag{5-2}$$

$$\omega = \omega_{max} - \left(\frac{\omega_{max} - \omega_{min}}{iter_{\,max}}\right) \times \ iter \tag{5-3}$$

$$\vec{x}_i(n+1) = \vec{x}_i(n) + \vec{v}_i(n+1) \tag{5-4}$$

In Particle Swarm Optimization (PSO), the velocity of each particle $\vec{v}_i(n+1)$ is updated based on three components: inertia $\omega\vec{v}_i(n)$, which retains part of the previous velocity; the cognitive component $c_1 r_1(\vec{p}_i - \vec{x}_i(n))$, which pulls the particle toward its own best-known position $\vec{p}_i$; and the social component $c_2 r_2(\vec{g} - \vec{x}_i(n))$, which attracts the particle toward the global best position $\vec{g}$, with c_1 and c_2 being acceleration constants and r_1, r_2 being random numbers in [0,1] to introduce stochasticity. The inertia weight ω gradually decreases from $\omega_{\max}$ to $\omega_{\min}$ over iterations to balance exploration and exploitation, calculated as $\omega = \omega_{\max} - \left((\omega_{\max} - \omega_{\min})/\ \text{iter}_{\ \max}\right) \times \text{iter}$, where iter is the current iteration and $\text{iter}_{\ \max}$ is the total number of iterations. Finally, the particle's new position is updated as $\vec{x}_i(n+1) = \vec{x}_i(n) + \vec{v}_i(n+1)$, using the newly computed velocity.

It aims to minimize an objective function based on the Euclidean distance from the CAD references, as depicted in Equation 5-5.

$$f(o) = \sum_{i=1}^{N} \left\| p_{sim,i}(o) - p_{ref,i} \right\|^2 + \lambda \cdot \ Penalty\,(o) \tag{5-5}$$

Here, o is the candidate solution, $p_{sim,i}(o)$ are the simulated parameters of link i, and $p_{ref,i}$ are the corresponding CAD-based reference values and λ is the Regularization weight for the penalty term, which is adaptively updated as a function of the iteration index, progressively increasing to strengthen constraint enforcement as the optimization advances.

In contrast, Q-PSO incorporates quantum angle encoding and probabilistic state measurement shown in Equations 5-6 and 5-7.

$$v_{ij}^{t+1} = \omega v_{ij}^{t} + c_1 r_1 \left[\theta_{ij}^{t} \left(p_{best} \right) - \theta_{ij}^{t} \right] + c_2 r_2 \left[\theta_{ij}^{t} \left(g_{best} \right) - \theta_{ij}^{t} \right] \tag{5-6}$$

$$\theta_{ij}^{t+1} = \theta_{ij}^{t} + v_{ij}^{t+1} \tag{5-7}$$

In this variant of Particle Swarm Optimization, the velocity of particle i in dimension j at iteration $t+1$, denoted $v_{ij}^{(t+1)}$, is computed as a combination of three terms: the inertia term $\omega v_{ij}^{(t)}$, which retains a portion of the previous velocity; the cognitive component $c_1 r_1 \left[\theta_{ij}^{(t)} (p_{\text{best}}) - \theta_{ij}^{(t)} \right]$, which guides the particle toward its own best-known personal position; and the social component $c_2 r_2 \left[\theta_{ij}^{(t)} (g_{\text{best}}) - \theta_{ij}^{(t)} \right]$, which pulls the particle toward the global best position found by the swarm. Here, $\theta_{ij}^{(t)}$ represents the current position (or parameter, such as an angle or decision variable), while p_{best} and g_{best} refer to the personal and global bests, respectively. r_1 and r_2 are uniformly distributed random numbers in $[0,1]$, and c_1, c_2 are acceleration coefficients. The position update equation $\theta_{ij}^{(t+1)} = \theta_{ij}^{(t)} + v_{ij}^{(t+1)}$ simply adds the updated velocity to the current position, driving the particle toward promising regions of the search space. Each algorithm adheres to structured routines, as outlined in Algorithm 1 (PSO) and Algorithm 2 (Q-PSO).

Algorithm 1: PSO algorithm for Dynamics Parameter Identification of the Robotic Arm.

Notation:

- N : Number of particles
- MaxIter: Maximum number of iterations
- x_{ij}^{t} : Position of particle i in dimension j at iteration t
- $p_{best\ j}^{\ t}$: Personal best angle of particle i
- $g_{best\ j}^{\ t}$: Global best angle in dimension j
- v_{ij}^{t} : Velocity of particle i
- ω : Inertia weight
- c_1, c_2 : Learning coefficients
- r_1, r_2 : Uniformly distributed random numbers in $(0,1)$
- f: Objective function
- ω : Penalized objective function

x^* : Optimal identified parameter set

1: **Initialize** population of N particles with random positions x_{ij}^{0} and velocities v_{ij}^{0}
2: **Evaluate** initial fitness $f(x_i^0)$ for all particles
3: **Set** $p_{\text{best},i} \leftarrow x_i^0$, and identify $g_{\text{best},j}$
4: **for** $t = 1$ to Maxiter **do**
5: **for** each particle i **do**
6: **Update** velocity:

$$v_{ij}^{t} = \omega v_{ij}^{t-1} + c_1 r_1 \left(p_{\text{best},ij}^{t-1} - x_{ij}^{t-1}\right) + c_2 r_2 \left(g_{\text{best},j}^{t-1} - x_{ij}^{t-1}\right)$$

7: **Update** position:

$$x_{ij}^{t} = x_{ij}^{t-1} + v_{ij}^{t}$$

8: **end for**
9: **Evaluate** fitness $f(x_i^t)$
10: **Update** $p_{\text{best},i} \leftarrow x_i^t$ if improved
11: **Update** $g_{\text{best},j}$ if improved
12: **Return** $x^* \leftarrow g_{\text{best},j}$ as the optimal identified parameters

Algorithm 2: Q-PSO algorithm for Dynamics Parameter Identification of the Robotic Arm

Notation:

- N : Number of particles
- MaxIter: Maximum number of iterations
- θ_{ij}^{t} : Current quantum angle of particle i in dimension j at iteration t
- $p_{best}\ {}_{j}^{t}$: Personal best angle of particle i
- $g_{best}\ {}_{j}^{t}$: Global best angle in dimension j
- v_{ij}^{t} : Angular velocity of particle i
- ω : Inertia weight
- c_1, c_2 : Learning coefficients
- r_1, r_2 : Uniformly distributed random numbers in $(0,1)$
- f: objective function
- ω : Penalized objective function
- θ^{*} : Optimal quantum angle solution

1: **Initialize** population of $\boldsymbol{N}$ particles with quantum angles $\boldsymbol{\theta_{ij}^{0}}$
2: **Evaluate** initial fitness $\boldsymbol{f}(\boldsymbol{\theta_i^0})$ for all particles
3: **Set** $p_{best}\ {}_{ij}^{0} \leftarrow \theta_{ij}^{0}$, and identify $g_{best}\ {}_{ij}^{0}$
4: **for** $t = 1$ to MaxIter do
5: **for** each particle i do
6: **Update** velocity:

$$v_{ij}^{t} = \omega v_{ij}^{t-1} + c_1 r_1 \left(pbest_{ij}^{t-1} - \theta_{ij}^{t-1}\right) + c_2 r_2 \left(gbest_{j}^{t-1} - \theta_{ij}^{t-1}\right)$$

7: **Update** position:

$$\theta_{ij}^{t} = \theta_{ij}^{t-1} + v_{ij}^{t}$$

8: **end for**
9: **Evaluate** new fitness $\boldsymbol{f}(\boldsymbol{\theta_i^t})$
10: **Update** $p_{best}\ {}_{ij}^{t}$ if $\boldsymbol{f}(\boldsymbol{\theta_i^t})$ improves
11: **Update** $g_{best}\ {}_{ij}^{t}$ if global best improves
12: **If** no improvement in g_{best} for a defined iteration, apply perturbation
13: **end for**
14**: Return** $\theta^{*} \leftarrow g_{best\ j}$ as optimal solution set

A high-accuracy Multilayer Perceptron (MLP) neural network with 488 neurons across four hidden layers validates the kinematic model using over 40,000 motion samples. This ensures confidence in dynamic parameter estimation. Finally, the optimized models are embedded into a Simulink-based SMC framework, as displayed in Figure 5-3, which tracks a circular trajectory over 30 seconds.

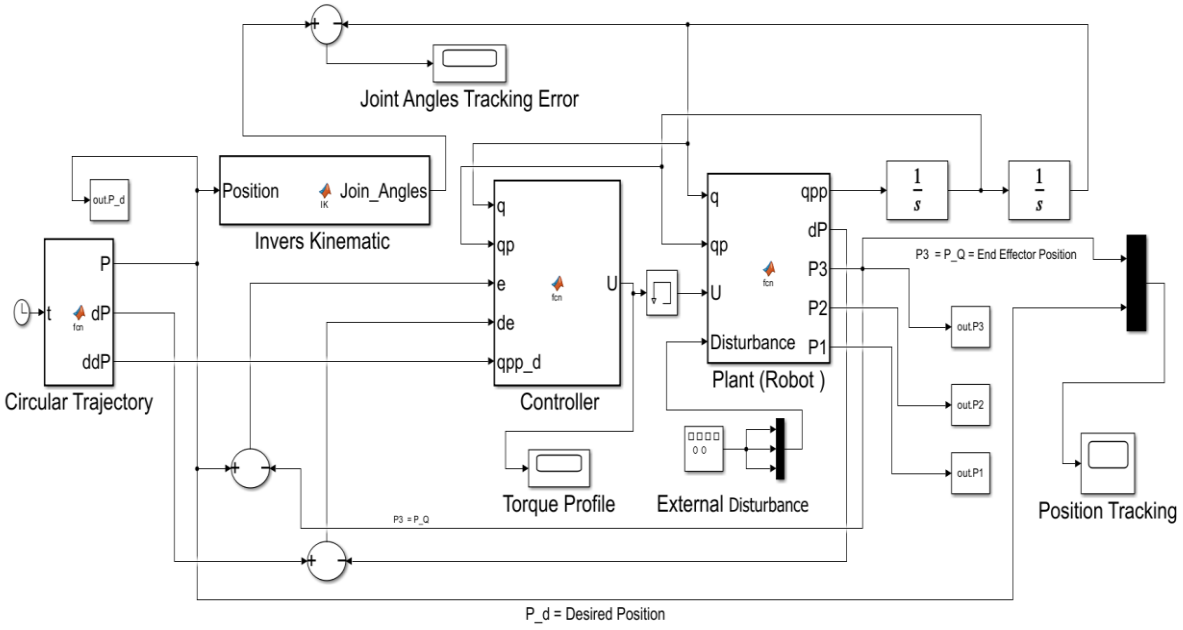

Figure 5-3 Simulink block diagram of the SMC-based circular trajectory.

mathematics

MDPI

Article

Quantum Particle Swarm Optimization (QPSO)-Based Enhanced Dynamic Model Parameters Identification for an Industrial Robotic Arm

Mehdi Fazilat and Nadjet Zioui *

Department of Mechanical Engineering, University of Quebec at Trois-Rivières, Trois-Rivières, QC G8Z 4M3, Canada; mehdi.fazilat@uqtr.ca
* Correspondence: nadjet.zioui@uqtr.ca

Abstract

Accurate parameter identification in dynamic models of robotic arms is essential for performing high-performance control and energy-efficient procedures. However, classic methods often encounter difficulties when modeling nonlinear, high-dimensional systems, particularly in the presence of real-world uncertainties. To address these challenges, this study focuses on identifying mass center positions and inertia matrix elements in a six-jointed industrial robotic arm and comparing the influence of optimized algorithms: the classical Particle Swarm Optimization (PSO) and the Quantum-behaved Particle Swarm Optimization (QPSO). The robot's kinematic model was validated by comparing it with actual motion data, utilizing a high-precision neural network to ensure accuracy before conducting a dynamic analysis. A comprehensive dynamic model was created using Computer-Aided Optimization (CAO) in SolidWorks Premium 2023 to simulate realistic mass parameters, thereby validating the model's reliability in a practical setting. The real (Referenced) and optimized dynamic models of the robot arm were validated using trajectory tracking simulations under sliding mode control (SMC) to assess the impact of the optimized model on the robot's performance metrics. Results indicate that QPSO estimates inertia and mass center parameters with Mean Absolute Percentage Errors (MAPE) of 0.76% and 0.43%, outperforming PSO significantly and delivering smoother torque profiles and greater resilience to external disturbances.

Keywords: industrial robots; nonlinear dynamics; nonlinear control systems; parameter estimation; swarm optimization; quantum-behaved particle swarm optimization

MSC: 34A34; 68T07; 03G12

Academic Editor: Cristian Lazureanu

Received: 30 July 2025
Revised: 11 August 2025
Accepted: 13 August 2025
Published: 16 August 2025

Citation: Fazilat, M.; Zioui, N. Quantum Particle Swarm Optimization (QPSO)-Based Enhanced Dynamic Model Parameters Identification for an Industrial Robotic Arm. *Mathematics* **2025**, *13*, 2631. https://doi.org/10.3390/math13162631

1. Introduction

1.1. Context of the Study

In the rapidly growing specialization of industrial robotics, precise dynamic modeling is essential for achieving high-precision motion control, ensuring reliable performance, and enhancing energy efficiency. Accurately identifying dynamic parameters becomes increasingly important as robotic systems become more complicated and autonomous, particularly in articulated arm applications. Among these parameters, the elements of the inertia matrix and the positions of mass centers are especially influential. These factors characterize mass distribution and rotational inertia, directly affecting the robot's response

to applied forces under diverse operational conditions. Accurate estimation of these parameters guarantees smooth and stable motion and supports the development of advanced control algorithms, fault diagnosis systems that are critical for system maintenance, and predictive maintenance strategies. Effectively modeling these characteristics is essential for improving robotic systems' intelligence, adaptability, and robustness in real-world industrial environments [1–3].

Traditional parameter estimation methods in the dynamics of robotic arms have historically been founded on analytical approaches such as Least Squares (LS), Recursive Least Squares (RLS), and the Newton-Raphson method. While these techniques are computationally efficient and well-suited to linear systems or scenarios with clearly defined mathematical models, they face considerable limitations in the presence of noise and uncertainty. However, the field has not remained stagnant. The emergence of alternative strategies, such as probabilistic estimation techniques like the Kalman Filter (KF), Extended Kalman Filter (EKF), and Particle Filter, and Commonness Domain Methods and Grey Box Modeling, has enhanced estimation accuracy under dynamic measurement requirements. These strategies represent progress and evolution in the field, facilitating flexible identification based on specific operational assumptions. Despite their extensive application, these classical techniques show notable deficiencies when addressing the complexity of robotic systems. The dynamic modeling of industrial robotic arms often involves highly nonlinear behaviors, varying loading conditions, and high-dimensional parameter space situations in which these methods work. For example, the linearity assumptions inherent in LS or RLS can result in systematic errors. At the same time, Kalman-based filters rely on accurately characterized noise statistics and may experience divergence when applied to poorly modeled systems. Additionally, although the Newton-Raphson technique can be effective for specific iterative solutions, it frequently encounters convergence issues in the presence of non-convexities or abrupt parameter changes. These challenges underscore the need for advanced strategies that are robust and precise for parameter identification in modern robotic systems operating under real-world variability and dynamic uncertainty [4–7].

1.2. Related Works

Given these challenges, this research identifies the inertia matrix and mass center parameters of articulated robotic arms operating under nonlinear, high-dimensional, and uncertain conditions. Although traditional estimation techniques may perform well under idealized conditions, they frequently prove inadequate in intricate industrial settings represented by dynamic variability and operational uncertainty. In recent advancements, the accurate identification of inertia matrix and mass center parameters has been particularly enhanced through Particle Swarm Optimization and other refined methodologies, with direct implications for practical applications. For instance, Xu et al. [8] explored PSOs application to space robotics, focusing on dynamically identifying inertia parameters through equivalent dynamics. Similarly, Bingül and Karahan [9] utilized a combination of PSO and Least Squares (LS) methods to perform dynamic identification on the Staubli RX-60 robot, thus showcasing a hybrid approach that leverages PSOs optimization capabilities with the precision of LS. Zhong et al. [10] also enhanced dynamic parameter identification by integrating an enhanced PSO algorithm with a comprehensive excitation trajectory, specifically for the 6R robotic arm, enabling more accurate and reliable parameter estimates. Additionally, Leboutet et al. [11] provided a comprehensive survey of inertial parameter identification techniques, positioning PSO as a critical tool in overcoming the challenges associated with nonlinear dynamics and ensuring robust parameter identification. These studies collectively highlight the development and application of advanced optimization

techniques like PSO in enriching the fidelity and efficiency of robotic system identification, with direct implications for the evolution of advanced robotic systems.

QPSO, which enhances the conventional PSO approach, is an advanced methodology utilized in research to handle complicated, high-dimensional parameter spaces like robotic arm modeling. It can effectively avoid local optima and seek global solutions, facilitating real-time data processing through a distributed computational approach, which is essential for overcoming the limitations of current parameter identification methods [12]. QPSO particularly improves solution quality, convergence speed, and adaptability across various engineering applications, including improving precision [13], optimizing both kinematic and non-kinematic parameters of five-bar parallel robots [14], solving inverse kinematics problems [15,16], and refining trajectory tracking control, consistently outperforming conventional methods for the robotic arms [17].

Parameter identification of Robot Manipulators has been the focus of a large number of studies exploiting PSO and its hybrid variants in the literature. These studies can be considered a breakthrough in the field, and all of them have achieved substantial enhancements in both convergence rate and accuracy, as well as robustness. For example, a classical PSO algorithm was used to identify the complete inertial parameters of a 6-DOF space manipulator attached to the satellite base, with a simple dynamic model and moment equations of motion in microgravity [8]. A hybrid developmental method that utilized PSO in conjunction with Differential Evolution DE for the parameter estimation of a simulated 3-DOF cylindrical robot, benefiting from DEs ability to search the domain space as well as PSOs speed of convergence [9]. Furthermore, research conducted has provided both theoretical insights into PSO and practical applications. For instance, a variant of PSO, similar to one that introduced dynamic time-varying acceleration coefficients to improve parameter estimation of a 3-DOF planar manipulator, achieves better control over convergence in the iterations [18]. Similarly, in another article, a developed PSO based on time-varying inertia weights and learning factors is used to estimate the parameters of the simulated 3-DOF robotic arm cited in [19]. These applications of PSO in practice have proven its efficiency. Additionally, research on the original PSO and its modifications has consistently confirmed its stability. For example, an Adaptive PSO algorithm adjusting the parameters of the algorithm with the swarm dynamics evolved was utilized to solve for the parameters of a 3-DOF manipulator and showed better accuracy and stability [20]. A hybrid algorithm based on PSO and GWO, which emulates the leadership hierarchy and hunting behavior of grey wolves, was developed to identify the dynamic parameters of a 3-DOF robot arm in SimMechanics and outperformed the two separate algorithms [21]. These consistent findings demonstrate the strength of PSO in a wide range of applications. The application of Quantum-behaved Particle Swarm Optimization to a similar 3-DOF manipulator model, which enhances the global searching ability by implementing principles derived from the theory of quantum mechanics, yields better robustness and identification accuracy compared to classical PSO [22]. Finally, the comparison study of PSO with some powerful optimization algorithms in the case of a 3-DOF manipulator showed that PSO yields highly competitive solution quality and noise tolerance results compared to other approaches [23].

1.3. Research Gap and Motivation

According to extensive reviews of the existing literature, notable gaps persist in advanced methods for parameter estimation within the dynamic models of various optimization algorithms. While techniques such as PSO have indicated promise, they frequently encounter difficulties in high-dimensional spaces and under rapidly changing conditions [24–27]. These limitations underscore the need for strategies that effectively integrate advanced computing technologies with optimization algorithms to enhance the

robustness of dynamic modeling. Moreover, there is a need for integration within comprehensive modeling frameworks for industrial robotic arms. Traditional Particle Swarm Optimization and its variants have been employed primarily to identify parameters for low-degree-of-freedom or modular manipulators, often relying on simplified or simulated models. However, these approaches tend to focus on specific components, such as joint stiffness or rehabilitation arms, rather than offering a holistic solution for dynamic modeling. Although prior works have utilized QPSO to tune models of limited complexity, none have specifically addressed parameter estimation for a high-degree-of-freedom industrial manipulator by employing CAD-derived mass properties in conjunction with QPSO-based optimization. Importantly, no study has integrated the identified parameters into a robust and applicable framework for practical assignment to evaluate performance metrics against external disturbances. This gap regarding both the methodological coupling of QPSO with CAD-informed modeling and its validation in closed-loop control defines the innovative trajectory of the current work.

1.4. Key Contributions and Novelty of the Study

The primary objective of this research is to develop and validate a high-fidelity dynamic model for a six-degree-of-freedom industrial robotic arm by accurately determining its inertial and mass center parameters based on physical parameters derived from Computer-Aided Design models and to structure a reference model for the investigation. To achieve this, the study systematically employs and compares the performance of classical Particle Swarm Optimization with Quantum-behaved PSO algorithms for identifying these dynamic parameters under nonlinear, high-dimensional, and uncertain operating conditions. In addition to parameter identification, the optimized and referenced models are integrated into a motion planning framework based on Sliding Mode Control, allowing for a quantitative assessment of their impact on torque smoothness, energy consumption, and trajectory tracking accuracy in both nominal and disturbed scenarios.

The present research completes three key contributions. First, we extract and utilize physically accurate inertia and mass center parameters derived from CAD models of a real industrial robotic arm, moving away from the conventional reliance on simplified assumptions. Second, we develop a unified multi-stage framework that incorporates high-precision kinematic validation using a multilayer perceptron, quantum-behaved swarm-based dynamic parameter identification, and Sliding Mode Control for performance evaluation in practical trajectory tracking tasks, including scenarios involving disturbances. Lastly, we conduct a comprehensive comparative analysis between classical PSO and QPSO, illustrating the enhanced accuracy, energy efficiency, and torque smoothness achieved with QPSO, thereby establishing its practicality for real-world robotic control applications.

The novelty of this research originates from its thorough examination of previous studies that either depended on oversimplified dynamic assumptions or assessed heuristic optimization methods without rigid validation in an industrial context. First, this study meticulously extracts the mass and inertia parameters of a real six-degree-of-freedom industrial robot using SolidWorks-based CAD modeling (SolidWorks Premium 2023), thereby replacing the commonly used approximations found in similar works. Second, it presents a systematic comparison between classical Particle Swarm Optimization and Quantum-behaved PSO, showcasing the exceptional performance of QPSO in terms of convergence accuracy, torque stability, and energy efficiency. Third, unlike prior research that focused exclusively on either identification or control, this study integrates QPSO within a robust Sliding Mode Control framework, promoting a closed-loop evaluation under both nominal and disturbed trajectory tracking conditions. Finally, an experimented

high-fidelity multilayer perceptron (MLP) network is employed to validate the kinematic model, ensuring accuracy before proceeding with the dynamic analysis.

The rest of this article is structured as follows: Section 2 summarizes the modeling framework and optimization setup, encompassing kinematics, dynamics, and the CAD model, and elaborates on the formulation and tuning strategies of the PSO algorithms. Section 3 presents comparative results and analysis. Finally, Section 4 concludes the study and suggests future directions for optimization-integrated robotic control systems.

2. Materials and Methods

2.1. Robotic Arm Presentation

The study focuses on the ABB IRB 140 (M2004) robot, illustrated in Figure 1. This robot, featuring a six-axis articulated design, is extensively used across various industrial applications with flexible mounting options to adapt to various working conditions by supports an end-effector, including a payload weighing up to 5 kg with considerable working space, and the manipulator utilized in its unmodified, factory-default configuration to ensure results reflect standard performance and provide a reliable baseline for evaluation [7].

Figure 1. The ABB IRB 140 robot in mechatronic laboratory.

2.2. Methodological Framework

The modeling procedure for the ABB IRB-140 robotic arm is initiated with the development of the manipulator's kinematic models to establish the position and orientation of the end-effector. The provided kinematic models are rigorously validated against real-world motion data using a high-precision singularity-avoiding MLP, ensuring their accuracy and practical applicability before dynamic analysis [28,29]. The dynamic model of the robot was formulated using the Euler–Lagrange method to calculate joint torques and energy consumption and was enhanced by integrating mass center and inertia parameters extracted from SolidWorks (Premium Version 2023) CAD models (SolidWorks Premium 2023). These CAD-derived parameters were defined as the reference baseline for all subsequent analyses. The Computer-Aided Optimization (CAO) phase enabled high-fidelity design modeling to ensure accurate multi-body representation and energy profiling.

In the next stage, the optimization of these dynamic parameters was performed using two distinct algorithms: classical PSO and Quantum-behaved PSO. Both algorithms were applied to identical input spaces, namely, the CAD-derived reference parameters for inertia and mass centers. Their performance was assessed purely based on the internal mechanics of each method, with no difference in their input data or objective functions.

This approach ensures a fair comparison of their effectiveness in optimizing physically meaningful parameters.

The final phase of the research involved a comparative evaluation between the reference model and the optimized models obtained using PSO and QPSO. These were re-integrated into the dynamic simulation framework under a sliding mode control (SMC) strategy to analyze key performance indicators such as torque smoothness, energy consumption, and tracking accuracy. Figure 2 illustrates the complete data channel of the methodology, from initial CAD-based parameter extraction to performance validation under integrated control evaluation.

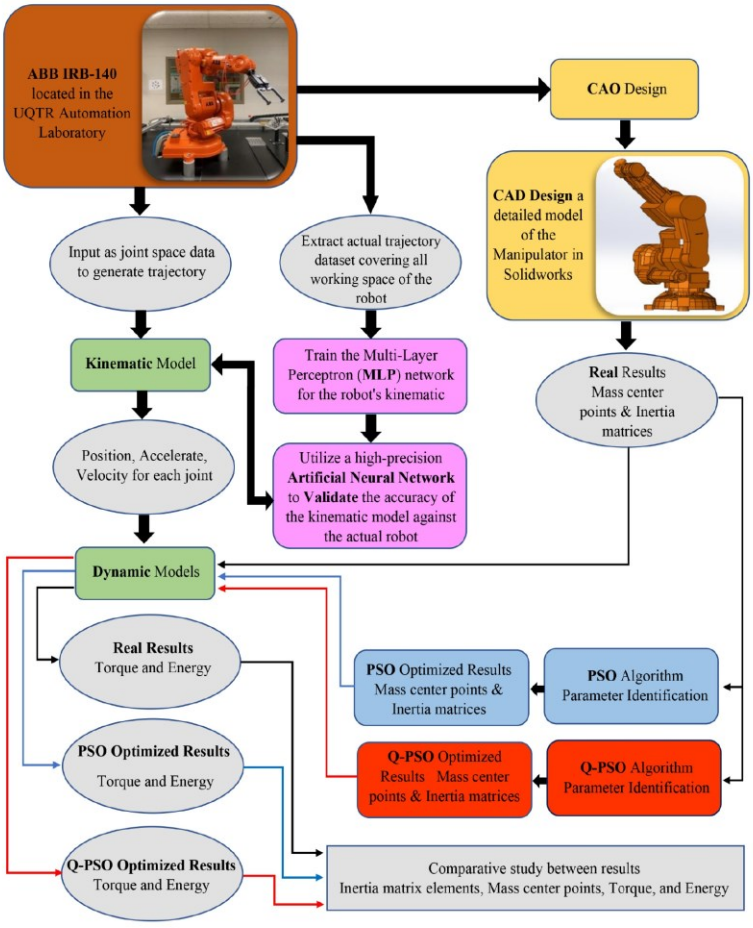

Figure 2. The flowchart for the Methodological Steps.

2.3. Kinematics of the Robot

The forward kinematics model determines the position and orientation of a robot's end-effector based on its joint angles and displacements relative to a reference frame, typically the base coordinate system [30,31]. This process depends on a global coordinate frame assigned to the robot base and local coordinate frames assigned to each joint. A typical

method for modeling forward kinematics is the Denavit–Hartenberg (D-H) convention, which utilizes a series of 4 × 4 homogeneous transformation matrices to describe the relative pose between consecutive joints [32]. Within this formalism, each joint pair is characterized by four parameters: the link length (a) and link twist (α), which remain constant, and the link offset (d) and joint angle (θ), which may vary depending on the joint type [33]. These parameters define the geometric relationships between links, enabling the precise determination of the end-effector's configuration. Figure 3 illustrates the allocation of D-H parameters and coordinate frames for a typical revolute joint [5].

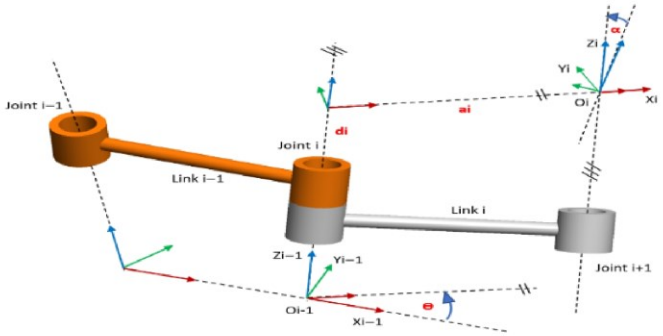

Figure 3. Rotational joint D-H parameters and link assignments [5].

The four transformations between the two axes can be defined as follows:

$$ {}^{i-1}_{i}T \;=\; Rot(x_{i-1},\, \alpha_{i-1})Trans(x_{i-1},\, a_{i-1})Rot(z_i\,,\, \theta_i\,)Trans(0,\, 0,\, d_i) \tag{1} $$

where ${}^{i-1}_{i}T$ is the homogeneous transformation matrix, Rot $(x_{i-1},\ \alpha_{i-1})$ is the rotation around an axis x_{i-1} by an angle α_{i-1}, Trans $(x_{i-1},\ a_{i-1})$ is the transfer along axis x_{i-1} to the value a_{i-1}, Rot $(z_i,\ \theta_i)$ is the rotation around axis z_i by an angle θ_i, and Trans $(0, 0, d_i)$ is the transfer along axis z to the value d.

Consequently, the corresponding homogeneous transformation matrix can be expressed as follows. In this matrix, C_i and S_i denote $\cos(\theta_i)$ and $\sin(\theta_i)$, respectively, where θ_i is the joint angle of the i-th joint. Similarly, C_{ij} and S_{ij} represent $\cos(\theta_i + \theta_j)$ and $\sin(\theta_i + \theta_j)$, respectively.

$$ {}^{i-1}_{i}T \;=\; \begin{pmatrix} C\theta_I & -SI & 0 & a_{i-1} \\ SI_i\, C\alpha_{i-1} & \mathrm{CI} & -S\alpha_{i-1} - d_i S\alpha_{i-1} \\ S\theta_i S\alpha_{i-1} & C\theta_i\, S\alpha_{i-1} & C\alpha_{i-1} & d_i C\alpha_{i-1} \\ 0 & 0 & 0 & 1 \end{pmatrix} \tag{2} $$

Figure 4 illustrates the assignment of coordinate frames to each joint of the ABB IRB 140 industrial robot, establishing the basis for its kinematic representation. Table 1 complements this figure by detailing the corresponding Denavit–Hartenberg (D-H) parameters, including link lengths, twists, offsets, and joint angles, which together define the spatial relationships between successive links. These frame assignments and kinematic parameters are configured with respect to a unified global coordinate framework, which is subsequently described to ensure geometric consistency across the robot's workspace and to facilitate accurate forward and inverse kinematic computations necessary for motion planning, control implementation, and simulation validation [7].

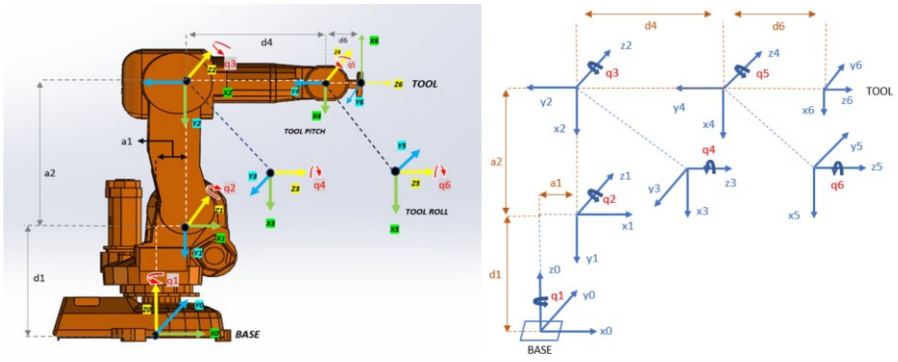

(**a**) (**b**)

Figure 4. ABB IRB 140 frame assignments: (**a**) Frames represented on the real robot; (**b**) Frames symbolized using DH representation [7].

Table 1. Denavit–Hartenberg Parameters of the ABB IRB 140 [5,7].

Link	a (mm)	α (°)	d (mm)	q (°)
1	$a_1 = 70$	-90	$d_1 = 352$	q_1
2	$a_2 = -360$	0	0	$q_2 + 90$
3	0	-90	0	q_3
4	0	90	$d_4 = 380$	q_4
5	0	-90	0	q_5
6	0	0	$d_6 = 65$	q_6

Applying the Denavit–Hartenberg convention, each link's transformation matrix is obtained by substituting its specific parameters into relation (2). The sequential multiplication of these matrices yields the end-effector's pose concerning the base frame.

$$ {}^{0}_{6}T = {}^{0}_{1}T.{}^{1}_{2}T.{}^{2}_{3}T.{}^{3}_{4}T.{}^{4}_{5}T.{}^{5}_{6}T = \begin{pmatrix} r_{11} & r_{12} & r_{13} & X \\ r_{21} & r_{22} & r_{23} & Y \\ r_{31} & r_{32} & r_{33} & Z \\ 0 & 0 & 0 & 1 \end{pmatrix} \tag{3} $$

So that

$$ \begin{aligned} r_{11} &= -S_6(S_4C_1C_{2'3} + C_4S_1) - C_6(C_5(S_1S_4 - C_4C_1C_{2'3}) + S_5C_1C_{2'3}) \\ r_{12} &= S_6(C_5(S_1S_4 - C_4C_1C_{2'3}) + S_5C_1C_{2'3}) - C_6(S_4C_1C_{2'3} + C_4S_1) \\ r_{13} &= C_5C_1S_{2'3} - S_5(S_1S_4 - C_4C_1C_{2'3}) \\ r_{21} &= C_6(C_5(C_4S_1C_{2'3} + C_1S_4) - S_5S_1S_{2/3}) - S_6(S_4S_1C_{2'3} - C_1C_4) \\ r_{22} &= -S_6(C_5(C_4S_1C_{2'3} + C_1S_4) - S_5S_1S_{2/3}) - C_6(S_4S_1C_{2'3} - C_1C_4) \\ r_{23} &= C_5S_1S_{2'3} + S_5(C_4S_1C_{2/3} + C_1S_4) \\ r_{31} &= -C_6(S_5C_{2'3} + C_4C_5S_{2'3}) + S_4S_6S_{2'3} \\ r_{32} &= C_6S_4S_{2'3} + S_6(S_5C_{2'3} + C_4C_5S_{2'3}) \\ r_{33} &= C_5C_{2'3} - C_4S_5S_{2'3} \end{aligned} $$

The notation 2′ refers to the modified joint variable $q'_2 = q_2 + \pi/2$, indicating an offset of $\pi/2$ applied to the original joint angle q_2. The X, Y, and Z position coordinates of the IRB140 robot relative to the base frame are computed as follows:

$$X = C_1a_1 + d_6(C_5C_1S_{2'3} - S_5(S_1S_4 - C_4C_1C_{2'3}) + d_4C_1S_{2'3} - C_1C_2a_2$$

$$Y = S_1a_1 + d_6(C_5S_1S_{2'3} - S_5(C_4S_1C_{2'3} + C_1S_4) + d_4S_1S_{2'3} - C_2S_1a_2$$

$$Z = d_1 + d_4C_{2'3} + a_2S_2 + d_6(C_5C_{2'3} - C_4S_5S_{2'3})$$

2.4. Differential Kinematics of the Robot

Differential kinematics, a cornerstone of robotics, defines the relationship between the joints' angular velocities and the corresponding end-effector linear and angular velocities. The Jacobian matrix of the manipulators, which is an essential component for analyzing and controlling robotic motion and determining singularities and redundancy, can be derived [34].

Regarding the end-effector linear velocity vector $\dot{p}_e$, the angular velocity vector ω_e, and the joint velocity vector $\dot{q}$, J_p is the $(3 \times n)$ matrix that relates the linear velocity vector to the joint speed vector. J_o is the $(3 \times n)$ matrix that links the angular velocity vector to the joint speed vector is expressed in relations (4) and (5) or in the compact form represented in Equation (6) [35].

$$\dot{P}_e = J_p(q)\dot{q} \tag{4}$$

$$\omega_e = J_o(q)\dot{q} \tag{5}$$

$$V_e = \begin{pmatrix} \dot{P}_e \\ \omega_e \end{pmatrix} = J(q)\dot{q} \tag{6}$$

where V_e is the end-effector velocity and $\mathrm{J} = \begin{pmatrix} J_p \\ J_o \end{pmatrix}$ is the Jacobian matrix. To find the corresponding joint velocities for a desired end-effector position and orientation, the Jacobian matrix can be inverted, as represented in Equation (7) [7].

$$\dot{q} = J^{-1}V_e \tag{7}$$

where J^{-1} is the inverse of the Jacobian matrix.

2.5. Dynamic Model of the Robot

A dynamic model facilitates the representation of the robot's operation by accounting for joint acceleration forces and torque [36]. The Euler–Lagrange method is employed to define this dynamic model. The first three proximal joints of the ABB IRB 140 robot arm play a crucial role in determining the end-effector position and the mechanical loads [7].

The inertial parameters required for the dynamic model—specifically; the mass; the center of mass position; and the inertia tensor for each link—are extracted using CAD modeling software (SolidWorks Premium 2023). Assuming uniform density, the mass of each link is estimated based on its volume relative to the total volume of the robot. The position vectors of the mass centers are computed in the local coordinate system and then expressed in the base reference frame. The inertia matrices are initially defined with respect to the local link frames and are transformed into the base reference frame using appropriate rotation matrices:

$$I_i = R_i I_i^{\text{local}} R_i^T \tag{8}$$

Here, R_i is the rotation matrix from the local frame of link i to the base frame, and I_i^{local} is the inertia tensor at the center of mass of link i, computed in the local coordinate frame. The transformation ensures consistency in expressing all inertial parameters in a common reference frame.

The dynamic behavior of the robot is governed by the standard Euler–Lagrange formulation:

$$\tau = M(q)\ddot{q} + C(q,\dot{q})\dot{q} + G(q) \tag{9}$$

In this equation, τ is the vector of joint torques, $M(q)$ is the inertia matrix, $\ddot{q}$ is the vector of joint accelerations, $C(q,\dot{q})$ represents Coriolis and centrifugal effects, and $G(q)$ is the gravitational force vector.

The inertia matrix $M(q)$ is derived by summing both the translational and rotational kinetic energy contributions of each link, expressed as

$$M(q) = \sum_{i=1}^{3} \left[m_i J_{v_i}^T J_{v_i} + J_{\omega_i}^T I_i J_{\omega_i} \right] \tag{10}$$

In this expression, the first term $m_i J_{v_i}^T J_{v_i}$ accounts for the translational kinetic energy of link i based on the mass center's motion, while the second term $J_{\omega_i}^T I_i J_{\omega_i}$ represents the rotational kinetic energy using the inertia tensor transformed into the base frame.

The Jacobian matrix J_{v_i} maps joint velocities to the linear velocity of the center of mass of link i and is defined as

$$J_{v_i} = \begin{bmatrix} \vec{z}_0 \times \left(\vec{r}_{ci} - \vec{r}_0\right) & \vec{z}_1 \times \left(\vec{r}_{ci} - \vec{r}_1\right) & \vec{z}_2 \times \left(\vec{r}_{ci} - \vec{r}_2\right) \end{bmatrix} \tag{11}$$

Here, $\vec{z}_j$ is the unit vector along the axis of joint j, $\vec{r}_{ci}$ is the center of mass position of link i, and $\vec{r}_j$ is the position of joint j, all expressed in the base frame. This formulation captures how each joint's motion affects the linear velocity of the link's mass center.

The Jacobian matrix J_{ω_i} describes the angular velocity of link i as a function of joint velocities and is given by

$$J_{\omega_i} = \begin{bmatrix} \vec{z}_0 & \vec{z}_1 & \vec{z}_2 \end{bmatrix} \tag{12}$$

This angular velocity Jacobian assumes all three joints are revolute and contribute to the orientation of the link.

The gravitational torque vector $G(q)$ is computed by projecting the gravitational forces acting at each center of mass through their respective Jacobians:

$$G(q) = \sum_{i=1}^{3} m_i J_{v_i}^T g \tag{13}$$

Here, g is the gravitational acceleration vector, typically defined as $g = [0\,0\,-9.81]^T$ in the base frame. This term accounts for the torque generated by the weight of each link acting at its center of mass.

The Coriolis and centrifugal term $C(q,\dot{q})$ are derived from the Christoffel symbols of the first kind:

$$C_{ijk} = \frac{1}{2}\left(\frac{\partial M_{ij}}{\partial q_k} + \frac{\partial M_{ik}}{\partial q_j} - \frac{\partial M_{jk}}{\partial q_i} \right) \tag{14}$$

Each element of the Coriolis matrix is then computed as

$$C_{ij} = \sum_{k=1}^{3} C_{ijk}\dot{q}_k \tag{15}$$

This formulation allows $C(q, \dot{q})\dot{q}$ to capture dynamic coupling effects between joints due to their relative velocities.

The complete dynamic model is not only useful for torque prediction but can also be rearranged to solve for joint accelerations, joint velocities, and positions given known torque inputs. This inverse dynamics form is written as

$$\begin{gathered} M(q)\ddot{q} = \tau - C(q, \dot{q}) - G(q) \\ \ddot{q} = M(q)^{-1}(\tau - C(q, \dot{q}) - G(q)) \\ \dot{q} = \int \ddot{q}dt + \dot{q}_0 \\ q = \int \dot{q}dt + q_0 \end{gathered} \tag{16}$$

As outlined in the modeling procedure, the mass center positions extracted from the CAD design are employed in the formulation of the Jacobian matrices J_{v_i}, which capture the translational motion of each link's center of mass, as well as in the derivation of the gravity vector $G(q)$. Concurrently, the inertia tensors obtained from the same CAD-based analysis, defined about the respective mass centers and transformed to the base frame, are integrated into the dynamic model through the term $J_{\omega i}^T I_i J_{\omega_i}$, which represents the rotational kinetic energy contribution within the overall inertia matrix $M(q)$.

2.6. CAD Designs of the Robot

A comprehensive CAD modeling of the real (Referenced) robot to obtain the mass properties of each link of the robot was performed. Mass parameter tools in SolidWorks (Premium 2023), Solid Edge ST4, and CATIA (via the DELMIA Catalogue of the robot) are used to ensure consistent units and high-precision geometry to authorize the accurate extraction of mass, center of mass, and inertia matrices with less than a 0.9% error. The results deliver the elements of the inertial matrix and the position of the mass center for each of the first three links, which are essential for formulating the dynamic model. It is important to highlight that the assumption of uniform density simplifies this calculation process. The CAD model illustrated in Figure 5 supports a high-resolution investigation of the multi-body dynamics and inter-component interactions of the case study. Table 2 compiles the derived mass property data for the proximal links [7].

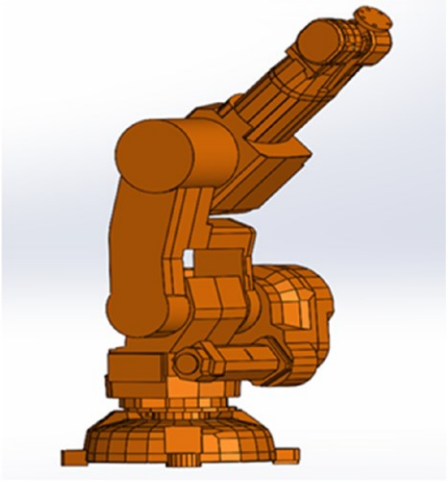

Figure 5. Detailed CAD model of the ABB IRB 140 robotic arm [7].

Table 2. Mass Property Results of the Robot Calculated by CAD Software.

ABB IRB 140	Parameters (unit)	Link 1	Link 2	Link 3
Mass parameters	*Weight* (kg)	35	25	18
	X_c (mm)	277.87	218.29	−24.56
	Y_c	373.12	229.73	−219.9
	Z_c	−199.03	112.43	−25.86
	I_{xx} (kg.m^2)	6.5	0.9	2.5
	I_{xy}	1.1	−0.03	−0.001
	I_{xz}	3.05	0.1	0.09
	I_{yy}	2.02	1.3	2.7
	I_{yz}	5.07	−0.01	−0.8
	I_{zz}	1.4	0.95	0.5

2.7. Particle Swarm Optimization Algorithm

Particle Swarm Optimization is a nature-inspired, population-based stochastic algorithm that emulates social behaviors observed in biological collectives such as bird flocks and fish schools [37,38]. Noted for its low algorithmic complexity, rapid convergence, and powerful global search capabilities, PSO has been widely applied to high-dimensional optimization problems [39,40].

Each particle represents a candidate solution within an n-dimensional decision space. Particles adapt their trajectories by iteratively updating their velocities and positions based on personal and collective experiences. The velocity update is expressed as [41]

$$\vec{v}_i(n+1) = \omega\vec{v}_i(n) + c_1 r_1\left(\vec{p}_i - \vec{x}_i(n)\right) + c_2 r_2\left(\vec{g} - \vec{x}_i(n)\right) \tag{17}$$

where ω is the inertia weight; c_1, c_2 are cognitive and social acceleration coefficients; and $r_1, r_2 \in U[0,1]$ are stochastic multipliers. The inertia weight is typically updated dynamically as

$$\omega = \omega_{max} - \left(\frac{\omega_{max} - \omega_{min}}{iter_{\ max}}\right) \times iter \tag{18}$$

The inertia weight ω is dynamically adjusted by decreasing linearly from $\omega_{\max}$ to $\omega_{\min}$ over the maximum number of iterations $iter_{max}$ to balance global exploration and local exploitation.

The updated position is

$$\vec{x}_i(n+1) = \vec{x}_i(n) + \vec{v}_i(n+1) \tag{19}$$

Particles are initially distributed randomly within the search space and are iteratively refined based on a problem-specific objective function that guides the swarm toward optimal solutions. The optimization process continues until either a predefined maximum number of iterations is reached or the solution meets a desired convergence threshold, typically expressed as an error tolerance criterion [37]. In the context of optimizing mass properties for the robotic arm, each particle represents a candidate solution comprising a set of inertia tensor elements and mass center coordinates, randomly initialized with associated velocities across a high-dimensional parameter space. These particles collectively explore the solution landscape by balancing exploration and exploitation through adaptive updates. The step-by-step procedure for applying the classical PSO algorithm to dynamic parameter identification is presented in Algorithm 1, outlining the initialization, evaluation, and update rules employed throughout the optimization process.

Algorithm 1: Classical Particle Swarm Optimization Steps

Notation:
N: Number of particles
MaxIter: Maximum number of iterations
x_{ij}^t: Position of particle i in dimension j at iteration t
$p_{best}{}_j^t$: Personal best angle of particle i
$g_{best}{}_j^t$: Global best angle in dimension j
v_{ij}^t: Velocity of particle i
ω: Inertia weight
c_1, c_2: Learning coefficients
r_1, r_2: Uniformly distributed random numbers in $(0, 1)$
f: Objective function
x^*: Optimal identified parameter set
Steps:
1: **Initialize** population of N particles with random positions x_{ij}^0 and velocities v_{ij}^0
2: **Evaluate** initial fitness $f(x_i^0)$ for all particles
3: **Set** $p_{best,\,i} \leftarrow x_i^0$, and identify $g_{best,\,j}$
4: **for** $t = 1$ to Maxiter **do**
5: **for** each particle i **do**
6: **Update** velocity:

$$v_{ij}^t = \omega v_{ij}^{t-1} + c_1 r_1 \left(p_{best,\,ij}^{t-1} - x_{ij}^{t-1} \right) + c_2 r_2 \left(g_{best,\,j}^{t-1} - x_{ij}^{t-1} \right)$$

7: **Update** position:

$$x_{ij}^t = x_{ij}^{t-1} + v_{ij}^t$$

8: **end for**
9: **Evaluate** fitness $f(x_i^t)$
10: **Update** $p_{best,\,i} \leftarrow x_i^t$ if improved
11: **Update** $g_{best,\,j}$ if improved
12: **Return** $x^* \leftarrow g_{best,\,j}$ as the optimal identified parameters

The objective function in the PSO algorithm minimizes the squared Euclidean norm between simulated dynamic parameters and reference values obtained from the CAD model. It ensures that the estimated mass center positions and inertia matrix elements are close to reference values.

$$f(o) = \sum_{i=1}^{N} \left\| p_{sim,\,i}(o) - p_{ref,\,i} \right\|^2 + \lambda \cdot \ Penalty\ (o) \tag{20}$$

Here, o is the candidate solution, $p_{sim,\,i}(o)$ are the simulated parameters of link i, and $p_{ref,\,i}$ are the corresponding CAD-based reference values and λ is the Regularization weight for the penalty term, which is adaptively updated as a function of the iteration index, progressively increasing to strengthen constraint enforcement as the optimization advances. The additional penalty term serves to enforce physical validity by penalizing candidate solutions that violate predefined parameter bounds, guiding the optimization process toward feasible and physically consistent solutions.

2.8. Quantum-Behaved Particle Swarm Optimization Algorithm

In the QPSO algorithm, each particle is represented using qubits, the fundamental units of quantum information, which can exist in a superposition of classical binary states. This contrasts with conventional binary or real-valued encodings. Mathematically, a single qubit is defined as [42–44]

$$|\psi\rangle = \alpha|0\rangle + \beta|1\rangle \tag{21}$$

Here, α and β are complex numbers representing the probability amplitudes of the qubit's state that determine the possibility of the qubit collapsing to the respective basis states upon measurement. These amplitudes are subject to the normalization condition as below [45–47]:

$$\left|\alpha\right|^2 + \left|\beta\right|^2 = 1 \tag{22}$$

In practical implementations of QPSO, the qubit is often expressed in terms of a quantum angle $\theta \in [0, \pi/2]$, yielding a real-valued representation [48]:

$$|\phi\rangle = sin\theta|0\rangle + cos\theta|1\rangle \tag{23}$$

Consequently, the amplitudes are defined as

$$\alpha = sin\theta,\ \beta = cos\theta \tag{24}$$

For a particle in an m-dimensional space, its state is defined by a vector of quantum angles. Each angle encodes a probability distribution over a binary state [47]:

$$\theta_i = [\theta_{i1}, \theta_{i2}, \ldots, \theta_{im}] \tag{25}$$

Each particle's angular velocity evolves according to both local and global attractors. The angular velocity is updated using the following equation [49,50]:

$$v_{ij}^{t+1} = \omega v_{ij}^{t} + c_1 r_1 \left[\ \theta_{ij}^{t}\ (p_{best}\ ) - \theta_{ij}^{t}\right] + c_2 r_2 \left[\ \theta_{ij}^{t}\ (g_{best}\ ) - \theta_{ij}^{t}\right] \tag{26}$$

where v_{ij}^{t} is the angular velocity of the i-th particle in the j-th dimension at iteration t, θ_{ij}^{t} is the current quantum angle, and $pbest_{ij}^{t}$ and $gbest_{ij}^{t}$ represent the personal and global best quantum angles, respectively. The quantum angle is then updated as follows [49]:

$$\theta_{ij}^{t+1} = \theta_{ij}^{t} + v_{ij}^{t+1} \tag{27}$$

Each quantum angle θ_j is measured by generating a uniformly distributed random number $r \in [0, 1]$ and comparing it to the squared amplitude $\left|\alpha_j\right|^2 = \cos^2(\theta_j)$. If $r \geq \left|\alpha_j\right|^2$, the bit is set to 1; otherwise, it is set to 0, as defined in relation (28):

$$x_j = \begin{cases} 1, & if\ r \geq \left|\alpha_j\right|^2 \\ 0, & if\ r < \left|\alpha_j\right|^2 \end{cases} \tag{28}$$

After each particle's quantum angle vector is updated according to relation (27), the corresponding quantum states are measured and collapsed into binary values based on the probabilistic formulation described in Equations (23) and (24). This collapse process enables the mapping of quantum representations into candidate solutions within the optimization space. These solutions are then evaluated using the objective function defined in relation (20), which assesses the fitness of each particle based on its estimated mass parameters. The complete sequence of operations involved in applying the Quantum-

behaved Particle Swarm Optimization (QPSO) algorithm to parameter identification is summarized in Algorithm 2.

Algorithm 2: Quantum-Behaved Particle Swarm Optimization Steps

Notation:
N: Number of particles
MaxIter: Maximum number of iterations
$\boldsymbol{\theta}_{\mathbf{ij}}^{\mathbf{t}}$: Current quantum angle of particle i in dimension j at iteration t
$\mathbf{p}_{\mathbf{best}}{}_{\mathbf{j}}^{\mathbf{t}}$: Personal best angle of particle i
$\mathbf{g}_{\mathbf{best}}{}_{\mathbf{j}}^{\mathbf{t}}$: Global best angle in dimension j
$\mathbf{v}_{\mathbf{ij}}^{\mathbf{t}}$: Angular velocity of particle i
$\boldsymbol{\omega}$: Inertia weight
$\mathbf{c}_1, \mathbf{c}_2$: Learning coefficients
$\mathbf{r}_1, \mathbf{r}_2$: Uniformly distributed random numbers in $(0, 1)$
f: objective function
$\boldsymbol{\theta}^*$: Optimal quantum angle solution
Steps:
1: **Initialize** population of N particles with quantum angles θ_{ij}^0
2: **Evaluate** initial fitness $f\left(\theta_i^0\right)$ for all particles
3: **Set** $p_{best}{}_{ij}^0 \leftarrow \theta_{ij}^0$, and identify $g_{best}{}_{ij}^0$
4: **for** $t = 1$ to MaxIter do
5: **for** each particle i do
6: **Update** velocity:

$$v_{ij}^t = \omega v_{ij}^{t-1} + c_1 r_1 \left(pbest_{ij}^{t-1} - \theta_{ij}^{t-1}\right) + c_2 r_2 \left(gbest_j^{t-1} - \theta_{ij}^{t-1}\right)$$

7: **Update** position:

$$\theta_{ij}^t = \theta_{ij}^{t-1} + v_{ij}^t$$

8: **end for**
9: **Evaluate** new fitness $f\left(\theta_i^t\right)$
10: **Update** $p_{best}{}_{ij}^t$ if $f\left(\theta_i^t\right)$ improves
11: **Update** $g_{best}{}_{ij}^t$ if global best improves
12: **If** no improvement in g_{best} for a defined iteration, apply perturbation
13: **end for**
14: **Return** $\theta^* \leftarrow g_{best_j}$ as optimal solution set

2.9. Robot Performance Evaluation

To evaluate the impact of the optimal values derived from the mass parameters obtained through PSO and QPSO, a comprehensive and thorough analysis of the torque and energy consumption profiles is essential. This investigation is grounded in the dynamic model described in Equations (9) and (16). The energy consumption for each joint is formalized as follows:

$$E_i = \int_{t_0}^{t_j} \tau_i(t) \cdot \dot{q}_i(t) dt \tag{29}$$

Thus, E_i quantifies the total mechanical energy exerted by actuator i over the time interval $[t_0, t_j]$, serving as a critical metric for evaluating energy efficiency in robotic joint operation, trajectory planning, and overall control system performance.

3. Results and Discussion

The research begins by developing and validating the robot's kinematic and dynamic models using a high-precision MLP trained on real-world scenarios. Two optimization algorithms are then designed to explore optimized values for the mass parameters of the robot arm under identical conditions utilizing 120 particles over 150 iterations. Results were averaged over 30 independent optimization runs to ensure statistical reliability and minimize variation. The inertia weight was set to 0.99, and the acceleration coefficients c_1 and c_2 were set to 2.5 and 1.5, respectively, based on sensitivity-based tuning. Table 3 provides a comparative summary of the estimated mass properties of the robot arm, the mass center coordinates, and inertia matrix elements derived from the CAD-based reference model and those obtained through optimization using classical PSO and QPSO algorithms.

Table 3. Mass Parameters of Reference Model, PSO, and QPSO.

Links	Parameters	Reference Model	QPSO	PSO
Link 1	*Xc* (m)	0.27787	0.27939	0.28513
	Yc	0.37312	0.3742	0.37757
	Zc	−0.19903	−0.19905	−0.205
	Ixx (Kg.m^2)	6.5	6.5236	6.5701
	Ixy	1.1	1.1101	1.0255
	Ixz	3.05	3.0539	3.1819
	Iyy	2.02	2.056	2.0662
	Iyz	5.07	5.1022	5.1781
	Izz	1.4	1.4127	1.2907
Link 2	*Xc* (m)	0.21829	0.21953	0.23221
	Yc	0.22973	0.23236	0.23766
	Zc	0.11243	0.11284	0.10949
	Ixx (Kg.m^2)	0.9	0.90239	0.84598
	Ixy	−0.03	−0.03039	−0.02873
	Ixz	0.1	0.10049	0.099257
	Iyy	1.3	1.3105	1.2213
	Iyz	−0.01	−0.01000	−0.01079
	Izz	0.95	0.9605	0.9994
Link 3	*Xc* (m)	−0.02456	−0.02462	−0.02581
	Yc	−0.21996	−0.22108	−0.21592
	Zc	−0.02586	−0.02593	−0.02729
	Ixx (Kg.m^2)	2.5	2.5213	2.5711
	Ixy	−0.001	−0.00100	−0.00092
	Ixz	0.09	0.09162	0.09525
	Iyy	2.7	2.7082	2.7503
	Iyz	−0.8	−0.80558	−0.75339
	Izz	0.5	0.50243	0.49506

Figure 6 compares the referenced and optimized inertia matrix elements using PSO and QPSO. While both methods yield effective refinement, QPSO proves enhanced sensitivity, particularly in off-diagonal terms, capturing inertial coupling effects more accurately and achieving a more physically coherent representation of mass distribution and inter-axis dynamics relative to the reference model.

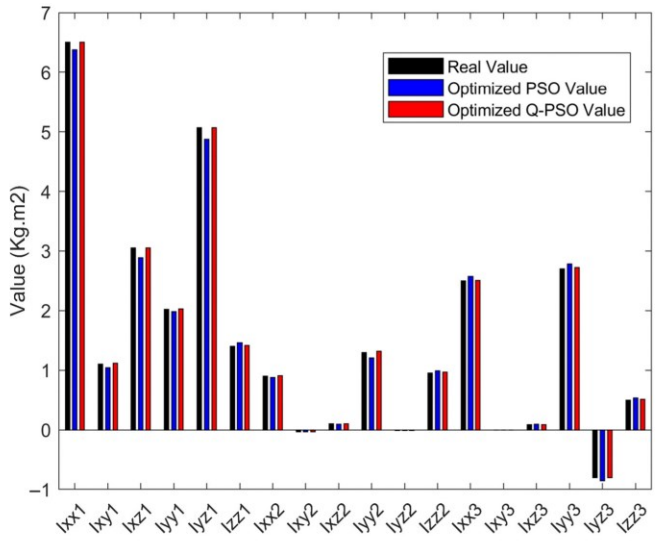

Figure 6. Bar chart of Reference vs. Optimized Inertia Matrix Elements.

Figure 7 illustrates that both algorithms effectively explore around the reference model's mass center points. However, QPSO achieves closer alignment with reference values, showing better global search and reduced risk of premature convergence.

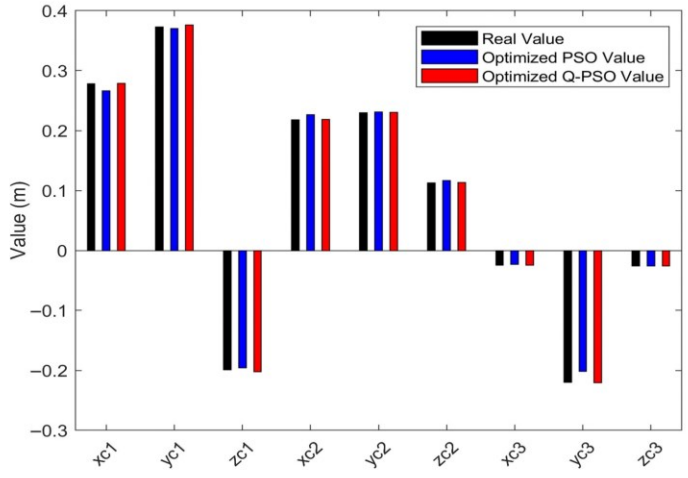

Figure 7. Bar chart of Reference vs. Optimized Mass centers position.

To quantify the accuracy of the identified parameters, the Mean Absolute Percentage Error (MAPE) was computed separately for the mass center coordinates and inertia matrix elements using the following formulation:

$$MAPE = \frac{1}{N}\sum_{i=1}^{N}\left|\frac{p_i^{est} - p_i^{ref}}{p_i^{ref}}\right| \times 100 \tag{30}$$

So that, p_i^{est} represents the ith parameter estimated by the algorithms, p_i^{ref} is the corresponding reference value, and N denotes the total number of parameters within the group 9 for mass center coordinates and 18 for inertia matrix.

Compared to the CAD-based reference values, QPSO achieved a MAPE of 0.43% for mass center coordinates and 0.76% for inertia tensor elements. In contrast, PSO displayed notably larger errors of 2.94% and 4.66%, respectively. These results prove QPSOs better precision in approximation.

Based on Figure 8, both algorithms show a rapid initial descent. PSO prematurely plateaus after approximately 27 iterations, indicating potential entrapment in local minima. In contrast, QPSO shows a more gradual yet consistent convergence toward lower fitness values, revealing its effective global search capability and long-term accuracy.

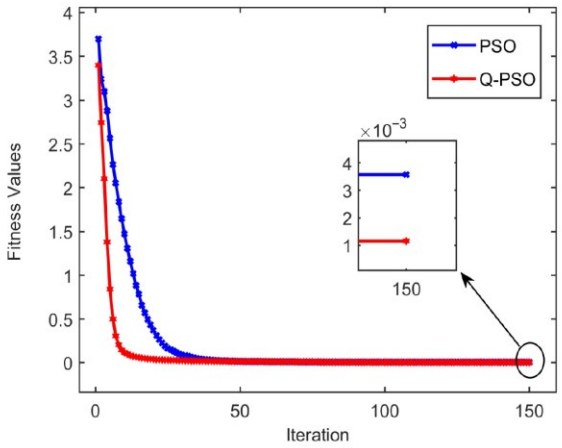

Figure 8. Convergence behavior of PSO and QPSO algorithms.

Figure 9 presents the normalized distributions of the final Global Best Scores achieved through 30 independent optimization runs for both the classical PSO and Quantum-behaved PSO algorithms. The boxplots indicate that QPSO consistently outperforms PSO in terms of solution stability and convergence accuracy. Notably, QPSO exhibits a lower median fitness value, a narrower interquartile range, and a decrease in the number of extreme values and outliers. Furthermore, the mean fitness value for QPSO was approximately 1.02, which is significantly lower than the 2.09 observed in PSO, thereby confirming the superior performance of the quantum-behaved variant in minimizing the objective function. While QPSO exhibits a slightly higher standard deviation (0.923 compared to 0.901), this can likely be attributed to its broader exploration behavior, which positively influences its ability to escape local minima and converge towards globally optimal solutions. This advantage is especially beneficial in high-dimensional, nonlinear search spaces,

such as robotic dynamic parameter identification, where the landscape is highly complex and traditional methods often face challenges with stagnation.

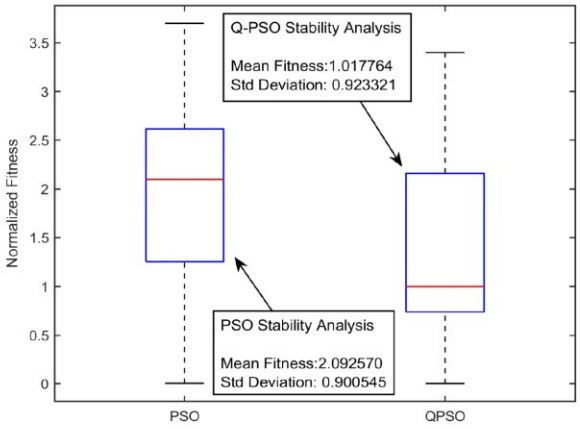

Figure 9. Final fitness values for PSO and QPSO over 30 runs.

In summary, on the same computational platform (Intel® Core™ $i7CPU@3.2GHz$, 32 GB RAM, Windows 10, MATLAB R2024a), QPSO achieved convergence in 32 ± 3 iterations on average across 30 runs, whereas PSO required 47 ± 4 iterations. This corresponds to approximately 7.9% less time per iteration and an overall convergence time reduction of about 32%. Furthermore, the mean final fitness value obtained by QPSO was approximately 51.35% lower than that of PSO, confirming both faster convergence and superior solution quality. These results affirm the robustness of QPSO in overcoming stochastic initialization effects and maintaining consistency across multiple runs while offering improved generalization.

To establish the accurate model of the dynamic model, the Kinematic model of the robot was validated by using a high-precision MLP neural network architecture [28,29], which was employed and trained on over 40,000 samples from the ABB IRB140 robot, which was actively engaged in executing physical tasks, as depicted in Figure 10, equipped with a singularity avoidance setup.

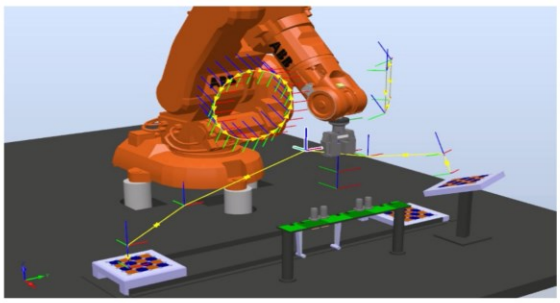

Figure 10. Robot arm during execution of assigned tasks [28,29].

The network architecture, shown in Figure 11, consisted of four hidden layers with 488 neurons. The classical MLP architecture utilized for kinematic validation was meticulously designed, with hyperparameters selected through preliminary experimentation and informed by best practices in function approximation tasks. A single hidden layer comprising 50 neurons was implemented to strike a balance between representational power and computational efficiency. Sigmoid activation functions were chosen for their established effectiveness in low-dimensional trajectory modeling. Input features, such as Cartesian positions and velocities, were normalized to a range of $[-1, 1]$ to improve convergence stability. The model was trained using a standard backpropagation algorithm with an adaptive learning rate, initially set at 0.01 and gradually decayed over the epochs. This configuration promoted smooth and consistent learning while helping to avoid local minima and overfitting. The model's convergence was evaluated by minimizing the Mean Squared Error (MSE), with training ceasing once the validation loss plateaued [28,29].

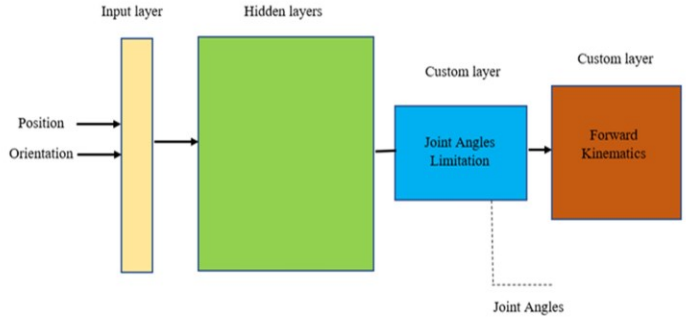

Figure 11. Robot's Arm MLP Neural Network Architecture [28,29].

To evaluate the performance of the artificial neural network (ANN) in predicting the end-effector's position, a standard Euclidean distance metric was employed. This metric quantifies the deviation between the predicted and target positions of the end-effector in 3D Cartesian space. The position error d is computed as [28,29]

$$d = \sqrt{(X - X')^2 + (Y - Y')^2 + (Z - Z')^2} \tag{31}$$

where $P = [X, Y, Z]$ represents the predicted position vector of the end-effector, and $P' = [X', Y', Z']$ denotes the desired or reference position. This scalar value d serves as an intuitive and geometric measure of the ANNs spatial accuracy, enabling a clear comparison between the actual and estimated kinematic behavior.

To ensure stable motion and prevent singularity-related issues in the robot's workspace, a regularization strategy based on the Jacobian matrix's condition number was employed. Singularities typically arise when the Jacobian matrix J becomes ill-conditioned or non-invertible, especially when $\det(J) = 0$ or the matrix approaches rank deficiency. These conditions can lead to excessive joint velocities or torque spikes, destabilizing the motion control process. To address this, the proximity to singularities was quantified using the Jacobian's condition number, defined as

$$\kappa(J) = \|J\| \cdot \left\|J^{-1}\right\| \tag{32}$$

where $\|J\|$ is the norm of the Jacobian matrix and $\left\|J^{-1}\right\|$ is the norm of its inverse, A high value of $\kappa(J)$ indicates greater sensitivity to input changes and signals a configuration near

singularity. A threshold of $\kappa > 1000$ was adopted to identify near-singular zones during the training phase.

To avoid such regions, the neural network's loss function was modified as

$$Loss\ Function = MAE(P_{Target}, P_{Calc}) + f(Activation\ Function, \kappa(Jacobian)) \quad (33)$$

In this formulation, P_{Target} is the desired position of the end-effector, P_{Calc} is the predicted position generated by the neural network, MAE represents the mean absolute error between them, $\kappa(Jacobian)$ quantifies how close the configuration is to a singular point based on the Jacobian's sensitivity, and f is a penalizing function influenced by the neural network's activation dynamics and the condition number value [28,29].

The network achieved a final training position error of 0.48 mm and a validation error of 0.61 mm, as illustrated in Figure 12, confirming its effectiveness in supporting high-accuracy kinematic validation. These results underscore the reliability of the neural network in modeling nonlinear kinematic relationships, providing a solid foundation for subsequent dynamic analysis and control integration.

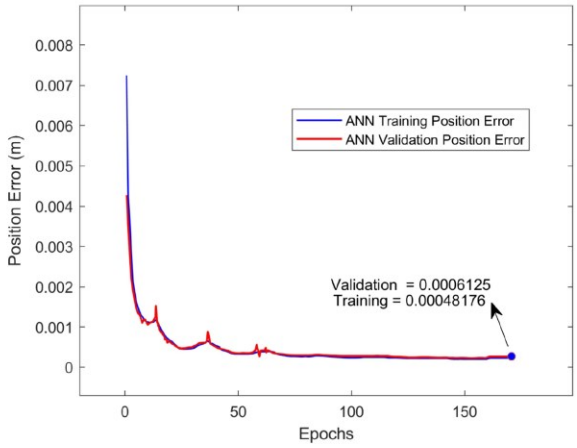

Figure 12. Position Error of MLP Neural Network.

Following the successful validation of the robot's kinematic model utilizing a high-precision multilayer perceptron network, three distinct dynamic models were established. These models incorporated mass property values derived from CAD-based reference data, classical Particle Swarm Optimization, and Quantum-behaved PSO algorithms, respectively. This modeling phase aimed to evaluate how different parameter estimation methods influenced the overall performance and dynamic behavior of the robotic system.

To conduct this comparative analysis, a robust Sliding Mode Control (SMC) strategy was devised and implemented, as depicted in Figure 13 [30]. This controller was integrated into a Simulink environment, operating in conjunction with the validated kinematic and dynamic models. The SMC architecture featured real-time trajectory tracking, torque feedback, and external disturbance modules, facilitating the evaluation of model robustness under both nominal and perturbed conditions.

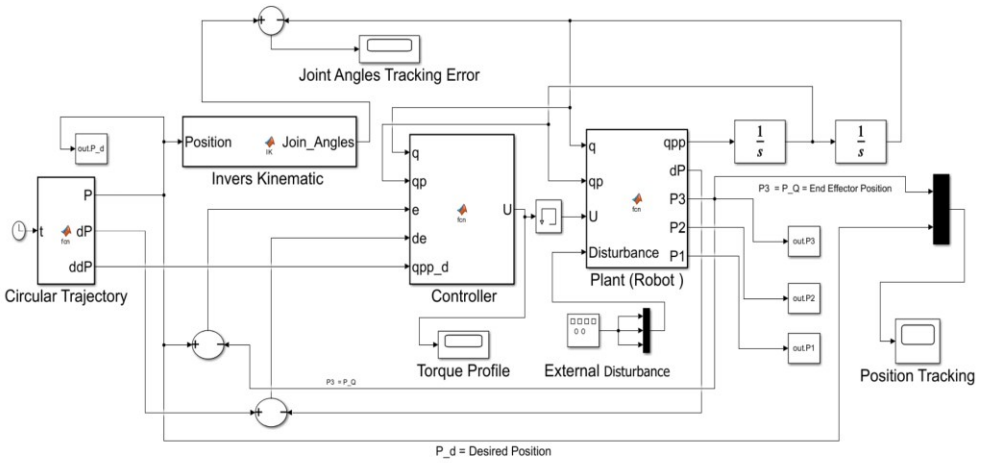

Figure 13. Simulink block diagram of the SMC-based circular trajectory [30].

A circular end-effector trajectory was predefined as the reference path for testing, executed over a simulation period of 30 s. As illustrated in Figure 14, the 3D visualization confirms that the robot effectively followed the desired circular trajectory within its operational workspace. This setup allowed for a precise assessment of each dynamic model's capability to respond to control inputs and maintain tracking accuracy over time.

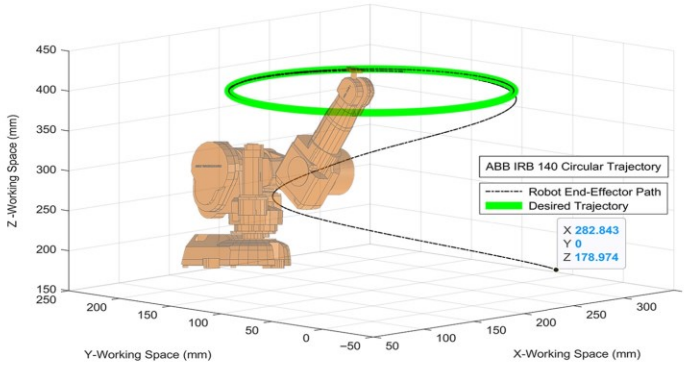

Figure 14. The 3-D visualization of the robot executing circular task.

The comparative performance analysis of the three models, CAD-based as the referenced model, PSO-optimized, and QPSO-optimized, was carried out by examining controller response characteristics, torque profiles, and energy consumption under identical trajectory planning tasks. This comprehensive integration of control and modeling under realistic task constraints provided valuable insights into the practical effectiveness of the proposed optimization strategies.

Controller feedback responses, torque, and energy metrics for the three models were considered nominal and disturbed conditions involving a 40% amplitude sinusoidal perturbation. To ensure statistical reliability and minimize variation, all reported results represent an average of over 30 independent simulation runs.

The results in Table 4 evaluate the tracking accuracy, controller responsiveness, and stability of Arm 3 of the robot, which represents the position of the end-effector under both nominal and disturbed conditions. In the nominal case, the PSO model excels with the fastest rise and settling times, minimal overshoot, and low steady-state error, making it ideal for precise, rapid trajectory tracking.

Table 4. Performance of Angular Position for the Different Models Under Disturbance.

Performances	Rising Time (s)	Settling Time (s)	Overshoot (%)	Steady State Error (%)
Arm 3 (End-effector)—Nominal scenario				
Real Model	0.577	0.599	1.85	0.0899
PSO Model	0.462	0.499	1.69	0.0607
QPSO Model	0.515	0.531	1.77	0.0799
Arm 3 (End-effector)—Disturbed scenario				
Real Model	0.654	0.791	1.99	0.0985
PSO Model	0.589	0.699	1.91	0.0851
QPSO Model	0.613	0.713	1.92	0.0910

The QPSO model, while slightly more conservative with higher overshoot, maintains competitive timing and closely mirrors the referenced model. Under disturbances, all models show performance decline, but the PSO model retains the fastest response. However, the QPSO model is more stable, robust, and reasonable at resisting perturbations and handling uncertainties.

The torque profiles observed under nominal and disturbed conditions, as illustrated in Figures 15 and 16, reveal differences in model performance. The QPSO model shows a close alignment with the reference model and also smoother transitions, minimal oscillations, and effective torque regulation, which suggests practical parameter identification and robust control. In contrast, the PSO model exhibits greater variability and more oscillations.

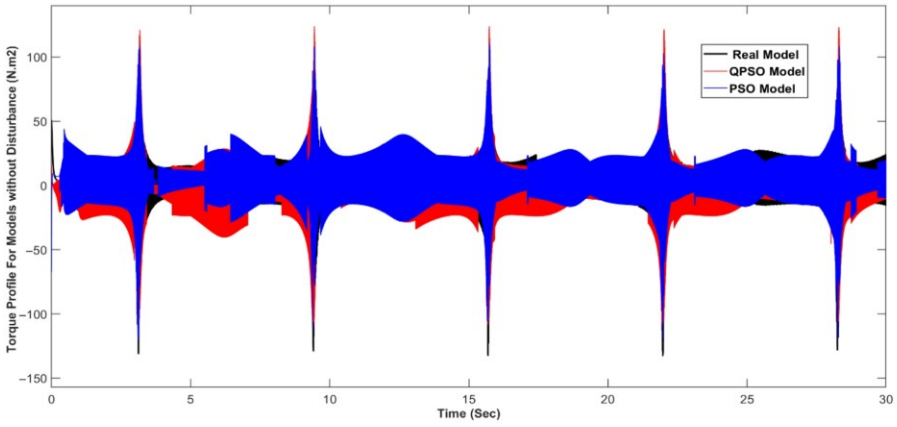

Figure 15. Torque profiles comparison under nominal conditions for three dynamic models.

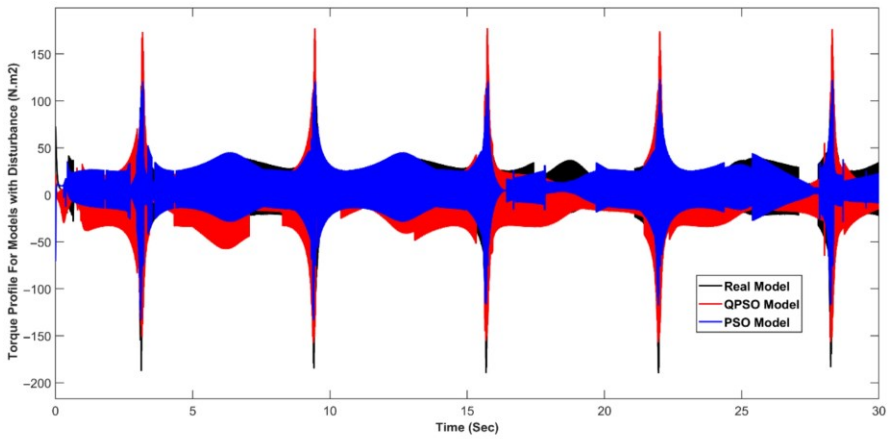

Figure 16. Torque profiles comparison under disturbed conditions for three dynamic models.

Under a 40% sinusoidal disturbance, the QPSO model demonstrates torque behavior that closely corresponds to that of the reference model. In contrast, the PSO model exhibits increased fluctuations, highlighting its susceptibility to disturbances. All models react to the disturbance, with the torque profile being affected and the torque demand increasing to control the robot and maintain the desired trajectory. However, QPSO still reveals better stability, characterized by smoother transitions, minimal oscillations, and adequate torque regulation.

The energy consumption results in Figure 17 compare the behavior of the model and the impact of three models on the energy profile of the robot during motion planning. All models exhibit a rising energy trend, consistent with the expected robotic behavior. The QPSO model, which closely aligns with the Real (Referenced) model's energy profile, provides a reassuring level of accuracy, indicating minimal actuator workload deviation. In contrast, the PSO model exhibits higher initial consumption and increasing divergence, indicating greater controller effort.

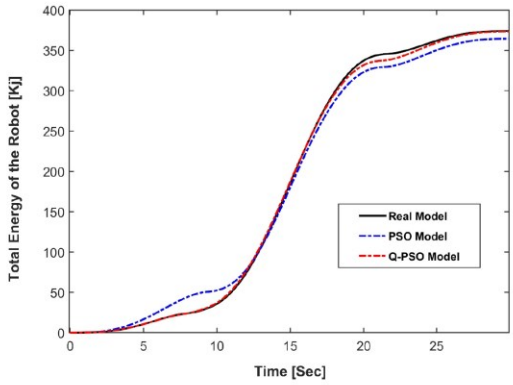

Figure 17. Energy consumption profiles for the three models.

The QPSO algorithm showed competitive performance compared to classical PSO, exhibiting a closer alignment with SolidWorks-derived ground truth parameters. This resulted in smoother torque profiles and practical control precision. Moreover, QPSO captured dynamic behaviors that reflected actual energy consumption patterns while maintaining robustness against disturbances. Table 5 provides a comparative overview of the QPSO and PSO algorithms across all evaluated performance dimensions.

Table 5. Comparative Overview of QPSO and PSO Performance Across Key Evaluations.

Evaluation Criterion	QPSO Performance	PSO Performance	Supporting
Parameter Estimation Accuracy	Higher estimation fidelity	larger deviations	Figures 6 and 7
Convergence Behavior	Smooth, stable convergence	Rapid descent—early plateau	Figure 8
Statistical Robustness (30 runs)	Lower median fitness	Higher variance—outlier spread	Figure 9
Trajectory Tracking (Nominal)	Comparable accuracy	Slightly faster	Table 4
Trajectory Tracking (Disturbed)	More resilient to perturbations	Some degradation under noise	Table 4
Torque Profile (Nominal)	Smoother torque transitions	Higher variability	Figure 15
Torque Profile (Disturbed)	Maintains regulated torque	Greater instability	Figure 16
Energy Consumption Trend	Closely follows reference model	Higher demand	Figure 17
Overall Control Robustness	Consistent behavior	More sensitive to noise	Figure 14, Figure 15, Figure 16 and Figure 17

It is worth noting that the objective function was intentionally formulated to minimize deviations from CAD-based reference parameters. Alternative formulations of objective functions could directly target performance indices such as torque, energy, or trajectory error. The parameter-centric approach provided a reliable foundation for reconstructing the physical model. Extending this work to include performance-driven objective functions remains a promising direction for future research.

4. Conclusions

Current research presented a comparative investigation of classical Particle Swarm Optimization and Quantum-behaved PSO for identifying the dynamic parameters of a six-degree-of-freedom industrial robotic arm. The primary objective was to estimate the center of mass and the elements of the inertia matrix of the robot links, which are essential for accurate simulation, energy-efficient operation, and advanced control.

Practical results confirmed that both PSO and QPSO effectively explored the parameter space of mass parameters. However, QPSO exhibited better alignment with the SolidWorks-derived reference model, generating lower mean absolute percentage errors of 0.76% and 0.43%. The QPSO-based dynamic model enabled smoother torque transitions, improved energy consistency, and delivered more stable control behavior in the presence of external disturbances, highlighting its robustness in nonlinear, high-dimensional robotic environments.

The study presents a multi-layered approach to identifying the mass properties of industrial robot arms based on physically accurate data directly extracted from actual robots and validated by CAD design tools. To ensure practical validation, a kinematic model was first verified using a high-precision MLP trained on actual joint motion data. The study then analyzes and compares the robot's dynamic behavior performance by implementing the explored values for mass parameters using PSO and QPSO algorithms, incorporating a robust SMC, and evaluating under identical trajectory planning tasks with and without external disturbances.

While the proposed method presented promising outcomes, several limitations must be acknowledged. Accurate estimation of link masses, centers of mass, and inertia tensors

remains a challenging task, as such data are often proprietary and not publicly disclosed by robot manufacturers. In this study, these parameters were derived from a high-fidelity CAD model under simplifying assumptions, such as homogeneous material properties and uniform density, which may introduce minor deviations from the actual physical robot. The work was conducted exclusively on a 6-DOF rigid industrial manipulator following a pre-defined circular trajectory, which may limit the generalizability of the findings to robots with different kinematic structures, higher degrees of freedom, flexible links, or redundant configurations, as well as to other motion profiles. Furthermore, the current implementation was performed in an offline simulation environment and did not explicitly address real-time constraints, sensor noise, or unmodeled uncertainties encountered in embedded robotic systems.

Future work will focus on extending the methodology to additional robotic platforms to assess scalability and on implementing a modular modeling architecture that facilitates adaptation to diverse robot geometries, kinematic chains, and dynamic properties. In addition, future developments will explore control-aware objective functions that incorporate trajectory tracking performance, torque smoothness, and energy efficiency into the optimization process. Efforts will also be directed toward hardware implementation using embedded platforms to enable real-time evaluation and closed-loop experimentation. Finally, enhancements to the QPSO algorithm, such as adaptive attractor dynamics, noise-resilient architectures, and self-tuning mechanisms, are envisioned to improve robustness and generalization across various robotic applications.

Author Contributions: Conceptualization, M.F. and N.Z.; Methodology, M.F. and N.Z.; Software, M.F.; Validation, N.Z.; Formal analysis, M.F.; Investigation, M.F.; Resources, N.Z.; Data curation, N.Z.; Writing – original draft, M.F.; Writing – review & editing, N.Z.; Visualization, M.F.; Supervision, N.Z.; Project administration, N.Z.; Funding acquisition, N.Z. All authors have read and agreed to the published version of the manuscript.

Funding: This work was financially supported by NSERC Canada.

Data Availability Statement: The data supporting the findings of this study are not publicly available, as they are part of ongoing research and future work. Data may be shared upon reasonable request after the completion of future studies.

Conflicts of Interest: The authors declare no conflicts of interest.

Abbreviations

The following abbreviations are used in this manuscript:

CAD	Computer-Aided Design
CAM	Computer-Aided Manufacturing
CAO	Computer-Aided Optimization
DE	Differential Evolution
DOF	Degrees of Freedom
EKF	Extended Kalman Filter
GWO	Grey Wolf Optimizer
KF	Kalman Filter
LS	Least Squares
MAPE	Mean Absolute Percentage Error
MLP	Multilayer Perceptron
PSO	Particle Swarm Optimization
QPSO	Quantum-behaved Particle Swarm Optimization
RLS	Recursive Least Squares
SMC	Sliding Mode Control

References

1. Urrea, C.; Pascal, J. Design and validation of a dynamic parameter identification model for industrial manipulator robots. *Arch. Appl. Mech.* **2021**, *91*, 1981–2007. [CrossRef]
2. Memar, A.H.; Esfahani, E.T. Modeling and dynamic parameter identification of the schunk powerball robotic arm. in International Design Engineering Technical Conferences and Computers and Information in Engineering Conference. *Am. Soc. Mech. Eng.* **2015**, *5C*, V05CT08A024.
3. Urrea, C.; Pascal, J. Design, simulation, comparison and evaluation of parameter identification methods for an industrial robot. *Comput. Electr. Eng.* **2018**, *67*, 791–806. [CrossRef]
4. Duan, S.; Shi, L.; Wang, L.; Liu, G. An uncertainty inversion technique using two-way neural network for parameter identification of robot arms. *Inverse Probl. Sci. Eng.* **2021**, *29*, 3279–3304. [CrossRef]
5. Fazilat, M. *Modélisation avancée* et commande d'un bras robot manipulateur industriel = Advanced Modelling and Control of Industrial Robotic Manipulator Arm. Master's Thesis, Université du Québec à Trois-Rivières, Trois-Rivières, QC, Canada, 2022. Available online: https://depot-e.uqtr.ca/id/eprint/10597 (accessed on 14 August 2025).
6. Azizkhani, M.; Godage, I.S.; Chen, Y. Dynamic control of soft robotic arm: A simulation study. *IEEE Robot. Autom. Lett.* **2022**, *7*, 3584–3591. [CrossRef]
7. Fazilat, M.; Zioui, N. The impact of simplifications of the dynamic model on the motion of a six-jointed industrial articulated robotic arm movement. *J. Robot. Control* **2024**, *5*, 173–186. [CrossRef]
8. Xu, W.; Hu, Z.; Zhang, Y.; Liang, B. On-orbit identifying the inertia parameters of space robotic systems using simple equivalent dynamics. *Acta Astronaut.* **2017**, *132*, 131–142. [CrossRef]
9. Bingül, Z.; Karahan, O. Dynamic identification of Staubli RX-60 robot using PSO and LS methods. *Expert Syst. Appl.* **2011**, *38*, 4136–4149. [CrossRef]
10. Zhong, F.; Liu, G.; Lu, Z.; Hu, L.; Han, Y.; Xiao, Y.; Zhang, X. Dynamic parameter identification based on improved particle swarm optimization and comprehensive excitation trajectory for 6R robotic arm. *Ind. Robot* **2024**, *51*, 148–166. [CrossRef]
11. Leboutet, Q.; Roux, J.; Janot, A.; Guadarrama-Olvera, J.R.; Cheng, G. Inertial parameter identification in robotics: A survey. *Appl. Sci.* **2021**, *11*, 4303. [CrossRef]
12. Vaze, R.; Deshmukh, N.; Kumar, R.; Saxena, A. Development and application of quantum entanglement inspired particle swarm optimization. *Knowl. Based Syst.* **2021**, *219*, 106859. [CrossRef]
13. Baş, E. Improved particle swarm optimization on based quantum behaved framework for big data optimization. *Neural Process. Lett.* **2023**, *55*, 2551–2586. [CrossRef]
14. Cao, H.Q.; Nguyen, H.X.; Nguyen, T.T.; Nguyen, V.Q.; Jeon, J.W. Robot calibration method based on extended Kalman filter–dual quantum behaved particle swarm optimization and adaptive neuro-fuzzy inference system. *IEEE Access* **2021**, *9*, 132558–132568. [CrossRef]
15. Dereli, S.; Köker, R. A meta-heuristic proposal for inverse kinematics solution of 7-DOF serial robotic manipulator: Quantum behaved particle swarm algorithm. *Artif. Intell. Rev.* **2020**, *53*, 949–964. [CrossRef]
16. Ma, W.; Du, Q.; Zhu, R.; Han, W.; Chen, D.; Geng, Y. Research on inverse kinematics of redundant robotic arms based on flexibility index. *IEEE Robot. Autom. Lett.* **2024**, *9*, 7262–7269. [CrossRef]
17. Numbi, J.; Zioui, N.; Tadjine, M. Quantum Particle Swarm Optimisation Proportional-Derivative Control for Trajectory Tracking of a Car-like Mobile Robot. *Electronics* **2025**, *14*, 832. [CrossRef]
18. Yan, D.; Lu, Y.; Levy, D.; Du, W.-B. Parameter identification of robot manipulators: A heuristic particle swarm search approach. *PLoS ONE* **2015**, *10*, e0129157. [CrossRef]
19. Tang, M.; Yan, Y.; An, B.; Wang, W.; Zhang, Y. Dynamic parameter identification of collaborative robot based on WLS-RWPSO algorithm. *Machines* **2023**, *11*, 316. [CrossRef]
20. Ayinalem, Z.A.; Kassie, A.T.; Bianchi, D. PSO Tuned Super-Twisting Sliding Mode Controller for Trajectory Tracking Control of an Articulated Robot. *J. Electr. Comput. Eng.* **2025**, *2025*, 1171569. [CrossRef]
21. Jahandideh, H.; Namvar, M. Use of PSO in parameter estimation of robot dynamics; Part two: Robustness. In Proceedings of the 2012 16th International Conference on System Theory, Control and Computing (ICSTCC), Sinaia, Romania, 12–14 October 2012.
22. Zha, F.; Sheng, W.; Guo, W.; Qiu, S.; Deng, J.; Wang, X. Dynamic parameter identification of a lower extremity exoskeleton using RLS-PSO. *Appl. Sci.* **2019**, *9*, 324. [CrossRef]
23. Lu, H.; Yang, Z.; Zhu, D.; Deng, F.; Guo, S. Dynamics Modeling and Parameter Identification for a Coupled-Drive Dual-Arm Nursing Robot. *Chin. J. Mech. Eng.* **2024**, *37*, 74. [CrossRef]
24. Zhou, M.; Cui, M.; Xu, D.; Zhu, S.; Zhao, Z.; Abusorrah, A. Evolutionary optimization methods for high-dimensional expensive problems: A survey. *IEEE/CAA J. Autom. Sin.* **2024**, *11*, 1092–1105. [CrossRef]
25. Li, C.; Yang, J.; Chang, S. Review on key technologies of space intelligent grasping robot. *J. Braz. Soc. Mech. Sci. Eng.* **2022**, *44*, 64. [CrossRef]

26. Huang, W.; Min, H.; Guo, Y.; Liu, M. A review of dynamic parameters identification for manipulator control. *Cobot* **2022**, *1*, 5. [CrossRef]
27. Erdogmus, P.; Toz, M. Heuristic optimization algorithms in robotics. In *Serial and Parallel Robot Manipulators-Kinematics, Dynamics, Control and Optimization*; Intechopen: London, UK, 2012; pp. 311–338.
28. Fazilat, M.; Zioui, N. Investigating Quantum Artificial Neural Networks for singularity avoidance in robotic manipulators. In Proceedings of the 2024 12th International Conference on Systems and Control (ICSC), Batna, Algeria, 3–5 November 2024.
29. Fazilat, M.; Zioui, N. Quantum Neural Network-based Inverse Kinematics of a Six-jointed Industrial Robotic Arm. *Robot. Auton. Syst.* **2025**, *194*, 105123. [CrossRef]
30. Fazilat, M.; Zioui, N. Quantum-Inspired Sliding-Mode Control to Enhance the Precision and Energy Efficiency of an Articulated Industrial Robotic Arm. *Robotics* **2025**, *14*, 14. [CrossRef]
31. Kuo, C.; Dai, J.S.; Dasgupta, P. Dasgupta, Kinematic design considerations for minimally invasive surgical robots: An overview. *Int. J. Med. Robot. Comput. Assist. Surgery* **2012**, *8*, 127–145. [CrossRef] [PubMed]
32. Corke, P. Image Formation. In *Robotics, Vision and Control: Fundamental Algorithms In MATLAB® Second, Completely Revised, Extended and Updated Edition*; Springer: Berlin/Heidelberg, Germany, 2017; pp. 319–357.
33. Zarychta, D.; Zubrycki, I. Methodology for Teaching the Denavit-Hartenberg Notation. In *International Conference on Robotics in Education (RiE)*; Springer: Berlin/Heidelberg, Germany, 2024.
34. Siciliano, B. Robot Kinematics. In *The Mechanical Systems Design Handbook*; CRC Press Inc.: Boca Raton, FL, USA, 2017; pp. 451–486.
35. Gilbert, H.B.; Rucker, D.C.; Webster, R.J., III. Concentric tube robots: The state of the art and future directions. In *Robotics Research: The 16th International Symposium ISRR*; Springer: Berlin/Heidelberg, Germany, 2016.
36. Sathya, A.S.; Carpentier, J. Constrained articulated body dynamics algorithms. *IEEE Trans. Robot.* **2024**, *41*, 430–449. [CrossRef]
37. Abualigah, L.; Sheikhan, A.; Ikotun, A.M.; Abu Zitar, R.; Alsoud, A.R.; Al-Shourbaji, I.; Hussien, A.G.; Jia, H. Particle swarm optimization algorithm: Review and applications. *Metaheuristic Optim. Algorithms* **2024**, *1*, 1–14. [CrossRef]
38. Lalitha Kameswari, Y. Fundamental of Swarm Optimization. In *Role of Nature-Inspired Algorithms in Real-Life Problems*; Springer: Berlin/Heidelberg, Germany, 2025; pp. 95–117.
39. Gad, A.G. Particle swarm optimization algorithm and its applications: A systematic review. *Arch. Comput. Methods Eng.* **2022**, *29*, 2531–2561. [CrossRef]
40. Shami, T.M.; El-Saleh, A.A.; Alswaitti, M.; Al-Tashi, Q.; Summakieh, M.A.; Mirjalili, S. Particle swarm optimization: A comprehensive survey. *IEEE Access* **2022**, *10*, 10031–10061. [CrossRef]
41. Wang, D.; Tan, D.; Liu, L. Particle swarm optimization algorithm: An overview. *Soft Comput.* **2018**, *22*, 387–408. [CrossRef]
42. Reda, D.; Talaoubrid, A.; Fazilat, M.; Zioui, N.; Tadjine, M. A quantum direct torque control method for permanent magnet synchronous machines. *Comput. Electr. Eng.* **2025**, *122*, 109994. [CrossRef]
43. Feraoun, H.; Fazilat, M.; Dermouche, R.; Bentouba, S.; Tadjine, M.; Zioui, N. Quantum maximum power point tracking (QMPPT) for optimal solar energy extraction. *Syst. Soft Comput.* **2024**, *6*, 200118. [CrossRef]
44. Alvarez-Alvarado, M.S.; Alban-Chacón, F.E.; Lamilla-Rubio, E.A.; Rodríguez-Gallegos, C.D.; Velásquez, W. Three novel quantum-inspired swarm optimization algorithms using different bounded potential fields. *Sci. Rep.* **2021**, *11*, 11655. [CrossRef]
45. Chen, M.; Song, H.; Zhu, D.; Chen, W.; Cai, C. Data Collection in Underwater Acoustic Sensor Networks Using Multiple AUVs with Sequential Greedy-QPSO and Fast Marching Algorithms. *IEEE Sens. J.* **2025**, *25*, 20433–20444. [CrossRef]
46. Fazilat, M.; Zioui, N.; St-Arnaud, J. A novel quantum model of forward kinematics based on quaternion/Pauli gate equivalence: Application to a six-jointed industrial robotic arm. *Results Eng.* **2022**, *14*, 100402. [CrossRef]
47. Yang, C.X.; Zhang, J.; Tong, M.S. A hybrid quantum-behaved particle swarm optimization algorithm for solving inverse scattering problems. *IEEE Trans. Antennas Propag.* **2021**, *69*, 5861–5869. [CrossRef]
48. Zioui, N.; Mahmoudi, A.; Fazilat, M.; Kone, O.; Reda, D.; Tadjine, M. Quantum Space Vector Pulse Width Modulation for Speed Control of Permanent Magnet Synchronous Machines. *E-Prime-Adv. Electr. Eng. Electron. Energy* **2025**, *13*, 101074. [CrossRef]
49. Xu, Z.; Cui, Y.; Li, B. A quantum-inspired particle swarm optimization for sizing optimization of truss structures. *Phys. Conf. Ser.* **2021**, *1865*, 042127. [CrossRef]
50. Sun, J.; Fang, W.; Wu, X.; Palade, V.; Xu, W. Quantum-behaved particle swarm optimization: Analysis of individual particle behavior and parameter selection. *Evol. Comput.* **2012**, *20*, 349–393. [CrossRef] [PubMed]

5.2.2 Summary of the Results Analysis

The comparative performance of the classical PSO and the Quantum-behaved PSO algorithms was evaluated through a series of simulations concentrating on parameter accuracy, control smoothness, and system robustness. The optimization involved 120 particles over 150 iterations, with results averaged across 30 independent runs to ensure statistical reliability. The inertia weight and acceleration coefficients were empirically adjusted to achieve optimal convergence performance.

Figure 5-4 and Figure 5-5 presents the extracted dynamic parameters, mass center coordinates, and inertia matrix elements of the ABB IRB 140 robotic arm. Q-PSO consistently achieved values closer to the CAD-derived references, outperforming classical PSO in both diagonal and off-diagonal inertia elements. This superiority is further illustrated in Table 5-2, where Q-PSO exhibits lower deviations from the reference model for both inertia tensors and mass center positions.

Q-PSO exhibits enhanced sensitivity in identifying the off-diagonal elements of the inertia matrix, effectively capturing the inertial coupling effects between axes. This leads to a more coherent representation of mass distribution and inter-axial dynamics compared to conventional methods. Q-PSO also maintains a better balance between exploration and exploitation, reducing the risk of premature convergence and achieving closer alignment with reference models. Its superior global search capability improves the accuracy of parameter estimation, resulting in more reliable system modeling and enhanced performance in applications such as precision control and dynamic simulation.

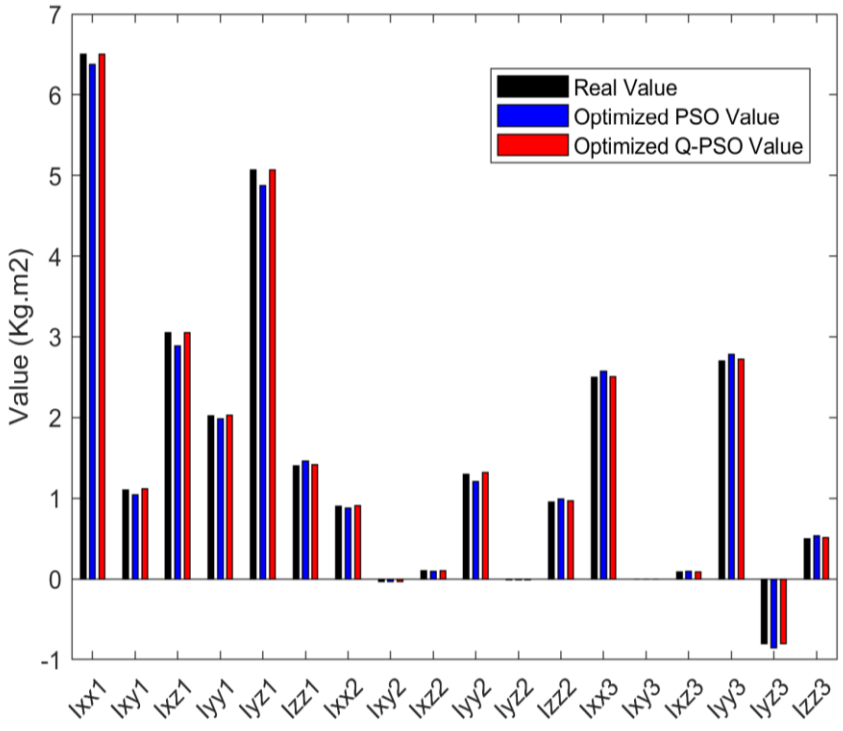

Figure 5-4 Bar chart Real vs Optimized Inertia Matrix Elements.

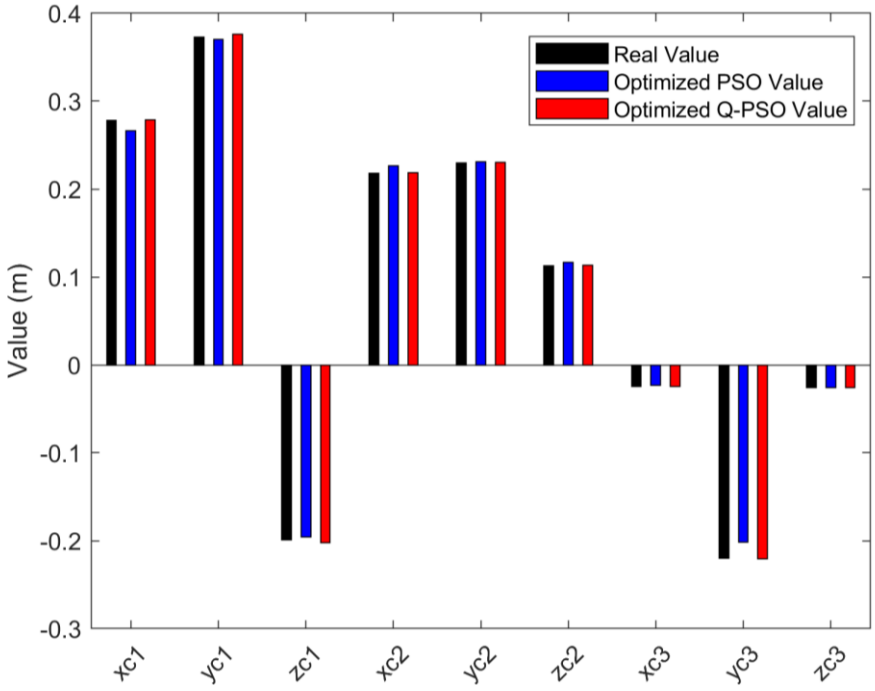

Figure 5-5 Bar chart Real vs Optimized Mass centers position.

Table 5-2 Mass properties of real model, PSO and Q-PSO.

Links	Parameters	Real Model	Q-PSO	PSO
1	Weight (kg)	35	35	35
	Xc (m)	0.27787	0.27939	0.28513
	Yc	0.37312	0.3742	0.37757
	Zc	-0.19903	-0.19905	-0.205
	Ixx (Kg.m2)	6.5	6.5236	6.5701
	Ixy	1.1	1.1101	1.0255
	Ixz	3.05	3.0539	3.1819
	Iyy	2.02	2.056	2.0662
	Iyz	5.07	5.1022	5.1781
	Izz	1.4	1.4127	1.2907
2	*Weight* (kg)	25	25	25
	Xc (m)	0.21829	0.21953	0.23221
	Yc	0.22973	0.23236	0.23766
	Zc	0.11243	0.11284	0.10949
	Ixx (Kg.m2)	0.9	0.90239	0.84598
	Ixy	-0.03	-0.03039	-0.02873
	Ixz	0.1	0.10049	0.099257
	Iyy	1.3	1.3105	1.2213
	Iyz	-0.01	-0.01000	-0.01079
	Izz	0.95	0.9605	0.9994
3	*Weight* (kg)	18	18	18
	Xc (m)	-0.02456	-0.02462	-0.02581
	Yc	-0.21996	-0.22108	-0.21592
	Zc	-0.02586	-0.02593	-0.02729
	Ixx (Kg.m2)	2.5	2.5213	2.5711
	Ixy	-0.001	-0.00100	-0.00092
	Ixz	0.09	0.09162	0.09525
	Iyy	2.7	2.7082	2.7503
	Iyz	-0.8	-0.80558	-0.75339
	Izz	0.5	0.50243	0.49506

To quantify the accuracy, Mean Absolute Percentage Errors were calculated using Equation 5-8.

$$MAPE = \frac{1}{N}\sum_{i=1}^{N}\left|\frac{p_i^{est} - p_i^{ref}}{p_i^{ref}}\right| \times 100 \tag{5-8}$$

So that, p_i^{est} represents the i^{th} parameter estimated by the algorithms, p_i^{ref} is the corresponding reference value, and N denotes the total number of parameters within the

group 9 for mass center coordinates and 18 for inertia matrix. Q-PSO achieved MAPE values of 0.43% and 0.76% for mass center coordinates and inertia matrices, respectively. In contrast, PSO recorded significantly higher errors at 2.94% and 4.66%, respectively, confirming the enhanced precision of Q-PSO.

Figure 5-6 and Figure 5-7 highlight the convergence behavior and global best fitness distributions. While both algorithms displayed a rapid initial descent, PSO exhibited early stagnation near iteration 27, indicating entrapment in a local minimum. Q-PSO maintained gradual and consistent convergence toward lower fitness values, and its global best scores showed tighter distributions with reduced variance, indicating better stability and search reliability.

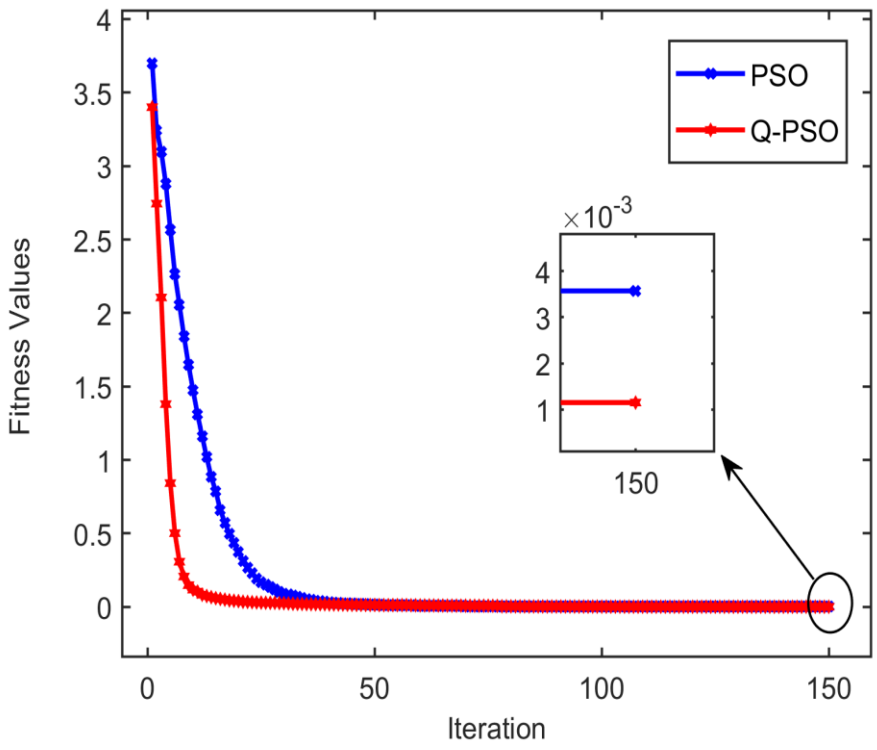

Figure 5-6 Convergence behavior of PSO and Q-PSO algorithms.

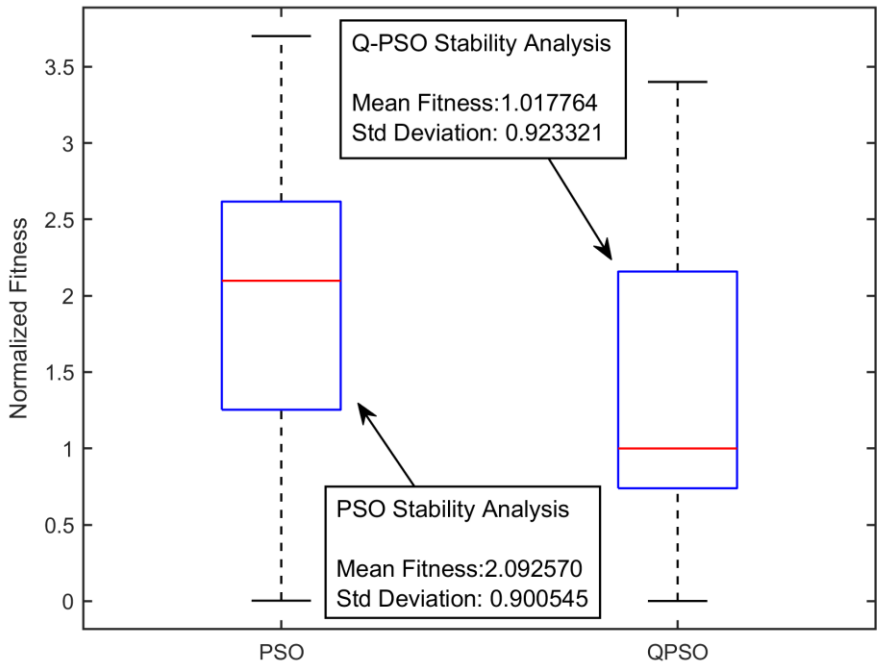

Figure 5-7 Final fitness values for PSO and Q-PSO over 30 runs.

Kinematic model validation, achieved through a Multilayer Perceptron neural network, confirmed high positional accuracy with training and validation errors of 0.48 mm and 0.61 mm, respectively. This validated framework was then used to evaluate three dynamic models: Real (CAD-driven as the reference), PSO-optimized, and Q-PSO-optimized, through circular trajectory tracking using a robust Sliding Mode Controller.

Table 5-3 summarizes performance metrics, including rise time, settling time, overshoot, and steady-state error, for the third joint under both nominal and disturbed conditions. While the PSO model had the fastest response in nominal scenarios, the Q-PSO model maintained more stable and consistent performance under a 40% sinusoidal disturbance.

Table 5-3 Performance of Angular Position for the Different Models Under Disturbance.

Performances	Rising Time (s)	Settling Time (s)	Overshoot (%)	Steady State Error (%)
Arm 3 (End-effector) - Nominal scenario				
Real Model	0.577	0.599	1.85	0.0899
PSO Model	0.462	0.499	1.69	0.0607
Q-PSO Model	0.515	0.531	1.77	0.0799
Arm 3 (End-effector) - Disturbed scenario				
Real Model	0.654	0.791	1.99	0.0985
PSO Model	0.589	0.699	1.91	0.0851
Q-PSO Model	0.613	0.713	1.92	0.0910

Figure 5-8 and Figure 5-9 show torque profiles under nominal and perturbed conditions. The Q-PSO model yielded smoother torque transitions with fewer oscillations compared to the PSO model, aligning closely with the reference model.

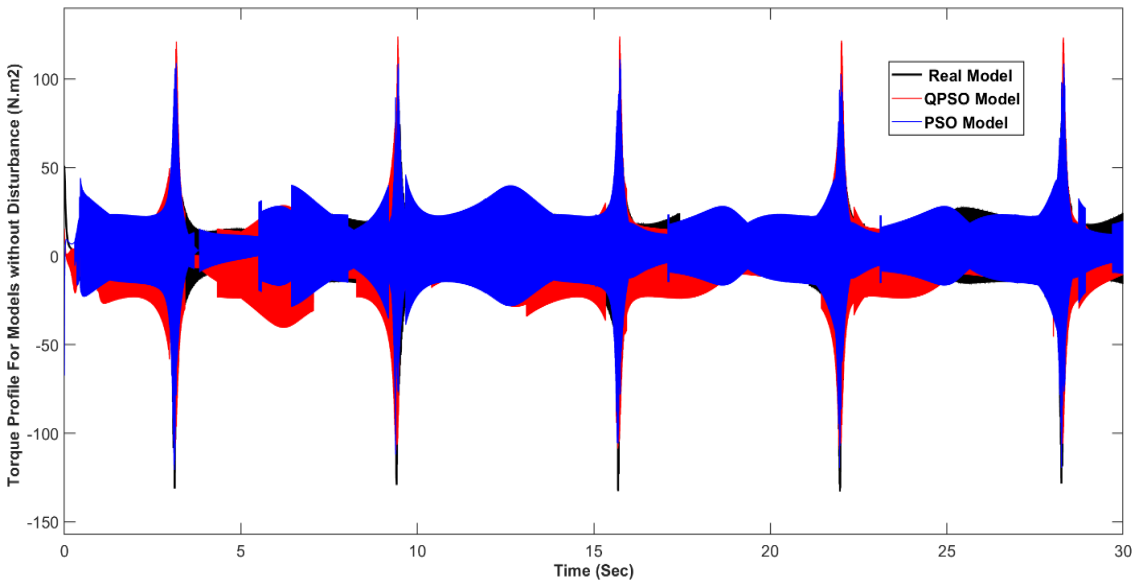

Figure 5-8 Torque profiles comparison under nominal conditions for three dynamic models.

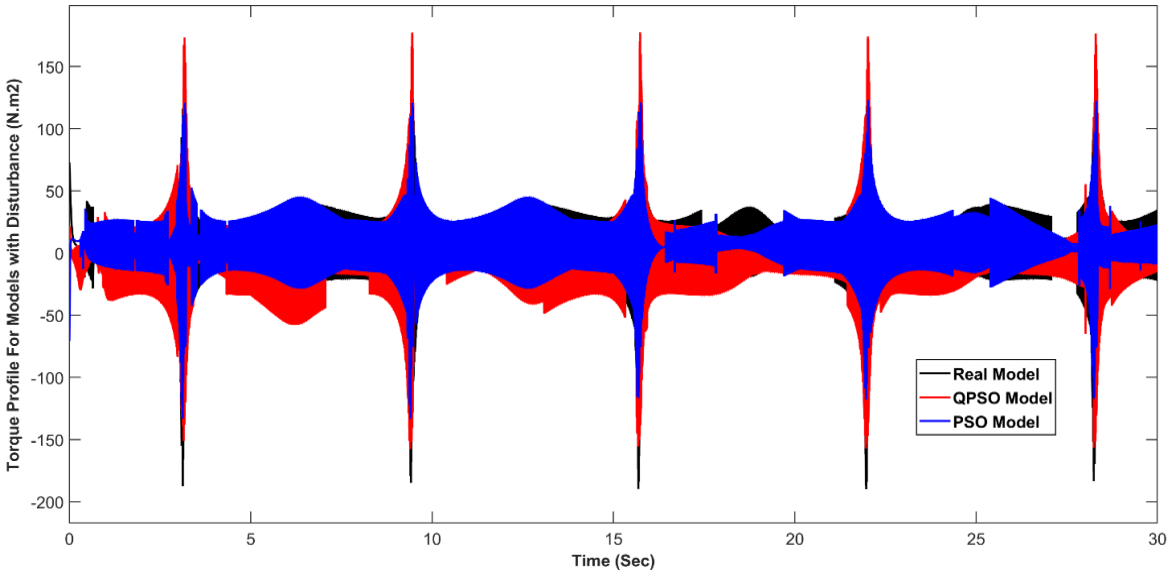

Figure 5-9 Torque profiles comparison under disturbed conditions for three dynamic models.

Energy consumption trends in Figure 5-10 further reinforce this observation. Q-PSO closely mirrored the Real model, whereas PSO incurred higher energy demands, especially during the initial motion phases.

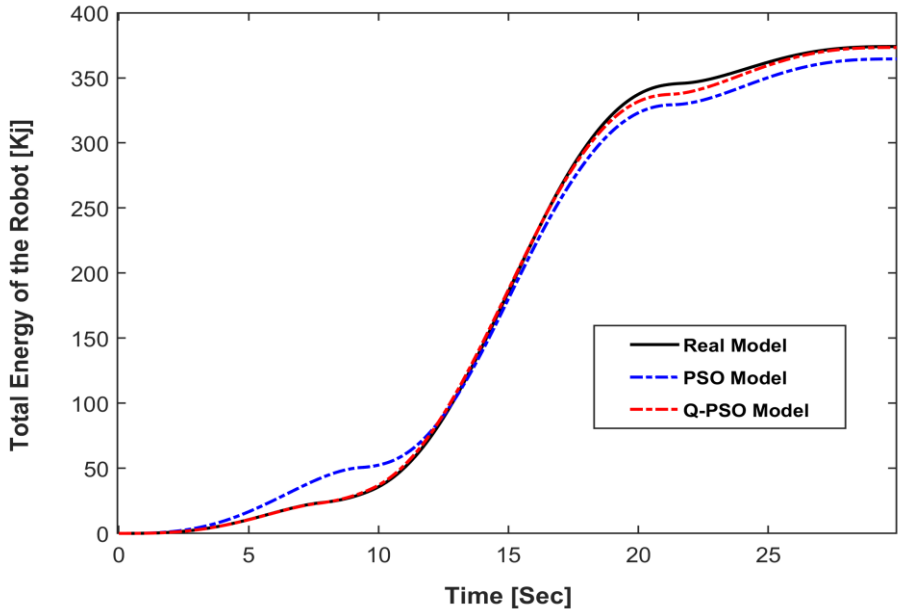

Figure 5-10 Energy consumption profiles for the three models.

5.3 Concluding Remarks

Through rigid modeling and simulation, both PSO and Q-PSO algorithms demonstrated competency in identifying dynamic parameters. However, Q-PSO consistently outperformed classical PSO in terms of estimation accuracy, convergence behavior, and control performance. Specifically, Q-PSO achieved lower Mean Absolute Percentage Errors (0.76% for inertia and 0.43% for mass centers), smoother torque transitions, and a more similar actuation pattern to the referenced model compared to its classical counterpart. The results under disturbance conditions further validated Q-PSO's robustness, maintaining better stability and consistent tracking performance despite external perturbations.

The study's novelty lies in its integration of high-fidelity CAD-based modeling with advanced optimization and machine learning-based kinematic validation using a multilayer perceptron network. Unlike prior works that rely on simplified models or assess identification algorithms in isolation, this work incorporates the optimized parameters into a robust Sliding Mode Control strategy. It evaluates real-world performance through trajectory tracking, energy consumption, and control torque smoothness.

Nonetheless, several limitations remain. The study was limited to a single robot model and motion profile, and the objective function focused solely on parameter deviation rather than performance-driven criteria, such as torque minimization or tracking error. The entire evaluation was performed in simulation, not accounting for real-time constraints, sensor noise, or embedded hardware limitations.

Future work should explore the integration of control-aware objective functions into the optimization loop, generalizing across diverse robots and motion tasks, and deploying real-time implementations on embedded platforms. Enhancements to Q-PSO, such as self-adaptive learning factors and noise-resilient encoding, also represent promising avenues for improving scalability and robustness in industrial robotics.

The comparative framing of this chapter is intentionally centered on the direct optimization counterpart, namely classical Particle Swarm Optimization, to isolate the effect of the quantum-behaved search mechanism within the same model, objective function, and validation pipeline; broader comparisons with other classical identification methods may be pursued in future work.

Exploring the precise identification of inertial and mass center parameters through both classical and quantum swarm optimization techniques establishes a foundation for assessing how these refined models impact control strategies in dynamic robotic environments. While parameter estimation is crucial for ensuring the accuracy of model-based representations, their actual value is realized in how effectively these parameters enhance the robot's behavior under real-world conditions. In this context, the control system serves as the vital link between model accuracy and system performance. Traditional control methods, despite their inherent robustness, often encounter challenges such as chattering and energy inefficiency. This highlights the need to investigate advanced control architectures that can leverage the precision achieved through optimized parameters. An influential aspect of this dissertation will introduce a quantum-inspired sliding mode control methodology that integrates quantum principles into classical control laws, thereby improving robustness,

precision, and energy efficiency for articulated robotic arms functioning in uncertain and nonlinear environments.

Chapter 6 - Quantum-Inspired Sliding Mode Control of an Industrial Robotic Arm

6.1 Chapter Overview

Achieving robust and precise control in robotic systems, particularly those characterized by nonlinear dynamics and external disturbances, remains a significant challenge in the field of industrial automation. Among various control strategies, Sliding Mode Control (SMC) has gained considerable attention due to its inherent robustness, rapid response, and effectiveness in managing system uncertainties. SMC functions by guiding system trajectories toward a predefined sliding surface, ensuring insensitivity to disturbances once the sliding mode is reached. However, despite its advantages, classical SMC presents notable limitations, such as high-frequency chattering and computational complexity, which restrict its application in high-precision, energy-sensitive, and real-time scenarios.

The proposed approach of the current study introduces a Quantum-Inspired Sliding Mode Control (Q-SMC) technique as an innovative solution to enhance the effectiveness of classical SMC. The suggested method incorporates principles from quantum computing, including qubit superposition, entanglement, and quantum logic operations, to refine error computation, trajectory tracking, and control law formulation. This hybridization aims to reduce chattering, improve transient response, and lower energy consumption while preserving the robustness and simplicity of the traditional SMC framework.

The experimental focus is the six-degree-of-freedom industrial articulated robotic arm, typically used in industrial tasks such as assembly and material handling. The research begins with a precise kinematic and dynamic modeling of the robot, integrating CAD-derived mass and inertia properties. It then implements and compares both classical SMC and Q-SMC strategies through comprehensive Simulink simulations. The Q-SMC controller reveals considerable improvements in trajectory tracking accuracy, disturbance rejection, and energy efficiency, resulting in approximately 3.79% lower energy consumption compared to the classical SMC. By incorporating quantum principles into a well-established and robust control strategy, the investigation represents a considerable step toward more adaptive, efficient, and precise robotic control systems.

6.2 Paper 5: Quantum-Inspired Sliding Mode Control to Enhance the Precision and Energy Efficiency of an Articulated Industrial Robotic Arm.

Authors : Mehdi Fazilat, Nadjet Zioui.

Journal: Robotics.

Publication date: 29/January/2025.

6.2.1 Methodology

The study focuses on a six-degree-of-freedom industrial robotic arm. The modeling process begins with the construction of both kinematic and dynamic models. The forward and inverse kinematics are derived to determine the position and orientation of the end-effector. Joint trajectories are developed using fifth-order polynomial equations, and transformation matrices are used to establish positional relationships between links.

Dynamic modeling is performed using the Euler–Lagrange method shown in relation 6-1, incorporating the robot's link masses and inertia data extracted from detailed CAD models created in SolidWorks, presented in Table 6-1.

$$\sum_{j=1}^{n} M_{ij}\ddot{q}+V_i+G_i=\tau_i, \quad i=1,2,..., \tag{6-1}$$

M_{ij} illustrates the inertial forces, V_i denotes the centrifugal and Coriolis forces, and G_i demonstrates the gravitational forces.

Table 6-1 Mass property results of each model calculated using SolidWorks software.

ABB IRB 140	Parameters (unit)	Link 1	Link 2	Link 3
Mass Properties	*Weight (kg)*	35	25	18
	Xc (mm)	277.87	218.29	-24.56
	Yc	373.12	229.73	-219.9
	Zc	-199.03	112.43	-25.86
	Ixx (kg.m2)	6.5	0.9	2.5
	Ixy	1.1	-0.03	-0.001
	Ixz	3.05	0.1	0.09
	Iyy	2.02	1.3	2.7
	Iyz	5.07	-0.01	-0.8

To evaluate performance, the energy consumption of each joint is computed from the product of joint torque and angular velocity, as defined by Equation 6-2. This approach provides a theoretically accurate the total energy demand over a defined trajectory.

$$E_i=\int_{t_0}^{t_f} \tau_i(t).\dot{q}_i(t)\ dt \tag{6-2}$$

E_i denotes the energy consumed by joint i, computed as the time integral from t_0 to t_f of the joint torque $\tau_i(t)$ multiplied by the corresponding joint velocity $\dot{q}_i(t)$.

The classical Sliding Mode Control strategy is implemented using a state-space model of the robotic system, as shown in Equation 6-3.

$$x = f(x,t) + g(x,t).u \tag{6-3}$$

Here, u is the control input, x is the state vector-also treated as the system output-and $f(x,t)$ and $g(x,t)$ are nonlinear functions representing the system dynamics and input influence, respectively.

The control law is designed with a sliding surface and discontinuous control inputs to enforce system trajectory convergence. To mitigate chattering, an exponential reaching law and a saturation function are employed, as described in Equations 6-4 to 6-6.

$$s = \dot{e} + ce \quad , c > 0 \tag{6-4}$$

$$\dot{s} = -\varepsilon.sgn(s) - ks + d_c - d \tag{6-5}$$

$$sat(x) = \begin{cases} x & if\ |x| \le 1 \\ sgn\ (x) & if\ |x| > 1 \end{cases} \tag{6-6}$$

In these equations, s is the sliding surface, $\dot{e}$ is the derivative of the tracking error e, and $c > 0$ is a tuning gain; $\dot{s}$ denotes the derivative of the sliding surface, ε and k are positive control gains, $\mathrm{sgn}(s)$ is the sign function, d_c is the compensated disturbance, and d is the actual disturbance; sat (x) is the saturation function where x is the input and $\mathrm{sgn}(x)$ is its sign, used to limit control effort based on $|x|$.

The control strategy is primarily applied to the first three joints, which critically determine end-effector positioning. The combined control input and dynamic model formulation culminate in Equation 6-7, with the disturbance-inclusive formulation given by Equation 6-8.

$$\tau = M\left(\ddot{\theta}_d + c\dot{e} + \varepsilon\, sgn(s)\right) + V + G \tag{6-7}$$

$$\tau = M.J^{-1}\left(\ddot{X}_d + c\dot{e} + \varepsilon\, sgn(s) - \dot{J}(\theta)\dot{\theta}\right) + V + G \tag{6-8}$$

τ is the control torque, M is the inertia matrix, $\ddot{\theta}_d$ and $\ddot{X}_d$ are desired joint and task-space accelerations, c is a positive gain, $\dot{e}$ is the error derivative, ε is a control gain, $\mathrm{sgn}(s)$ is the sign of the sliding surface s, V is the Coriolis and centrifugal force vector, G is the gravity vector, J is the Jacobian matrix, J^{-1} is its inverse, $\dot{J}(\theta)$ is the time derivative of the Jacobian, and $\dot{\theta}$ is the joint velocity vector.

The Quantum-Inspired Sliding Mode Control Q-SMC extends this structure by incorporating quantum principles. Quantum operations are introduced via a quantum comparator composed of a quantum subtractor and a sign detector. These components utilize quantum gates, including Hadamard, rotation, and Toffoli gates, to compute error metrics in superposition states explained by Equations 6-9 to 6-12.

$$q_1 = R_y(\theta_1)|0\rangle \tag{6-9}$$

$$q_2 = R_y(\theta_2)|0\rangle \tag{6-10}$$

$$q_1 \otimes q_2 = C_{\theta_1}C_{\theta_2}|00\rangle + C_{\theta_1}S_{\theta_2}|01\rangle + S_{\theta_1}C_{\theta_2}|10\rangle + S_{\theta_1}S_{\theta_2}|11\rangle \tag{6-11}$$

$$S_{\theta_1} C_{\theta_2} = sin\left(\frac{\alpha-\beta}{2}\right) cos\left(\frac{\alpha+\beta}{2}\right) = \frac{1}{2}(sin(\alpha) - sin(\beta)) \quad (6\text{-}12)$$

Equations above define quantum states $q_1$and q_2, where $R_y(\theta)$ is a quantum rotation operator around the Y -axis and $|0\rangle$ is the ground state. The tensor product $q_1 \otimes q_2$ in Equation (6-10) expands into four basis states: $|00\rangle, |01\rangle, |10\rangle$, and $|11\rangle$, each weighted by the cosine $C(\theta_i) = \cos(\theta_i/2)$ and sine $S(\theta_i) = \sin(\theta_i/2)$ of the respective rotation angles. Equation (6-11) uses a trigonometric identity to simplify one coefficient term, $S(\theta_1)C(\theta_2) = \sin\left(\frac{\alpha-\beta}{2}\right)\cos\left(\frac{\alpha+\beta}{2}\right) = \frac{1}{2}(\sin(\alpha) - \sin(\beta))$, showing the quantum encoding of real-number differences through rotation-based amplitude modulation.

The quantum error e_Q is computed through a sequence of quantum operations that substitute the traditional error calculation. Let P represent the desired position and P_3 the actual position of the endeffector. For each axis i, the corresponding quantum error is determined by first calculating the angles α_i and β_i, which are derived from the components of P and P_3, respectively as shown in 6-13 to 6-19.

$$\alpha_i = arcsin(P_i) \quad (6\text{-}13)$$

$$\beta_i = arcsin(P_{3i}) \quad (6\text{-}14)$$

$$\theta_{1i} = \frac{\alpha_i - \beta_i}{2} \quad (6\text{-}15)$$

$$\theta_{2i} = \frac{\alpha_i + \beta_i}{2} \quad (6\text{-}16)$$

$$q_{1i} = cos(\theta_{1i})|0\rangle + sin(\theta_{1i})|1\rangle \quad (6\text{-}17)$$

$$q_{2i} = cos(\theta_{2i})|0\rangle + sin(\theta_{2i})|1\rangle \quad (6\text{-}18)$$

$$e_{Qi} = k \times tensor\_product_i[3] \tag{6-19}$$

The formulation includes the angles $\alpha_i = \arcsin(P_i)$ and $\beta_i = \arcsin(P_{3i})$, intermediate terms $\theta_{1i} = (\alpha_i - \beta_i)/2$ and $\theta_{2i} = (\alpha_i + \beta_i)/2$, and quantum states $q_{1i} = \cos(\theta_{1i})|0\rangle + \sin(\theta_{1i})|1\rangle$ and $q_{2i} = \cos(\theta_{2i})|0\rangle + \sin(\theta_{2i})|1\rangle$. The operators involved include the arcsine, sine, and cosine functions, the tensor product $\bigotimes_1$ and basis states $|0\rangle, |1\rangle$. The final quantum error term is expressed as $e_{Q_i} = k \times$ tensor_product $_i[3]$, where k is a scaling constant.

The quantum sliding surface is formulated in Equation 6-20, and its sign is determined using a quantum sign detector, as shown by Equations 6-21 and 6-22.

$$s_{quantum} = n\left(sin\left(\frac{\theta_{c\cdot e}}{2}\right) + sin\left(\frac{\theta_{deQ}}{2}\right)\right) \tag{6-20}$$

$$|s\rangle = cos(\theta)|0\rangle + sin(\theta)|1\rangle \tag{6-21}$$

$$\theta = arcsin\left(\frac{s(t)}{max(|s(t)|)}\right) \tag{6-22}$$

The terms include the quantum sliding surface s_{quantum}, scaling factor n, rotation angles $\theta_{c\cdot e}$ and $\theta_{de}Q$, the quantum state $|s\rangle$, basis states $|0\rangle$ and $|1\rangle$, the composite angle $\theta = \arcsin\left(\frac{s(t)}{\max(\langle s(t)|\rangle)}\right)$, the signal $s(t)$, its maximum magnitude $\max(|s(t)|)$, and the operators sine, cosine, arcsine, and normalization.

The quantum control law and the corresponding total control input are detailed in Equations 6-23 and 6-24. These equations represent the final stage of the Quantum-Inspired Sliding Mode Control design, in which quantum-derived error evaluation and the quantum sliding-surface mechanism are integrated into the control formulation. The controller thus

combines the dynamic compensation terms of the robotic system with quantum-inspired switching behavior to generate the final torque input for the manipulator joints. Consequently, the control law maintains the robustness of conventional Sliding Mode Control while improving tracking performance, minimizing chattering, and increasing energy efficiency under uncertain operating conditions.

$$V = J^{-1} \cdot \left(\ddot{P} + c \cdot de_Q + q \cdot Sign\left(s_Q\right) - \dot{J} \cdot \dot{q}\right) \tag{6-23}$$

$$u_Q = M \cdot V + B + G \tag{6-24}$$

robotics

MDPI

Article

Quantum-Inspired Sliding-Mode Control to Enhance the Precision and Energy Efficiency of an Articulated Industrial Robotic Arm

Mehdi Fazilat and Nadjet Zioui *

Department of Mechanical Engineering, Université du Québec à Trois-Rivières, 3351 Bd des Forges, Trois-Rivières, QC G8Z 4M3, Canada; mehdi.fazilat@uqtr.ca
* Correspondence: nadjet.zioui@uqtr.ca

Abstract: Maintaining precise and robust control in robotic systems, particularly those with nonlinear dynamics and external disturbances, is a significant challenge in robotics. Sliding-mode control (SMC) is a widely used technique to tackle these issues; however, it is plagued by chattering and computational complexity, which limit its effectiveness in high-precision environments. This study aims to develop and assess a quantum-inspired sliding-mode control (QSMC) strategy to enhance the SMC's robustness, precision, and computational efficiency, specifically in controlling a six-jointed articulated robotic arm. The methodology involves creating a comprehensive kinematic and dynamic model of the robot, followed by implementing both classic SMC and the proposed Q-SMC in a comparative way. The simulation results confirm that the Q-SMC method outperforms the classic SMC, particularly in reducing chattering, improving tracking accuracy, and decreasing energy consumption by approximately 3.79%. These findings suggest that the Q-SMC technique provides a promising alternative to classical control methods, with potential applications in tasks requiring high precision and efficient robotic manipulations.

Keywords: industrial robotic manipulator arm; kinematics modeling; nonlinear dynamics; sliding-mode control; quantum-inspired sliding-mode control; energy efficiency

Academic Editor: Dan Zhang

Received: 30 December 2024
Revised: 16 January 2025
Accepted: 27 January 2025
Published: 29 January 2025

Citation: Fazilat, M.; Zioui, N. Quantum-Inspired Sliding-Mode Control to Enhance the Precision and Energy Efficiency of an Articulated Industrial Robotic Arm. *Robotics* **2025**, *14*, 14. https://doi.org/10.3390/robotics14020014

1. Introduction

1.1. Context of the Study

Robust control is a key component in robotics, particularly in controlling the complexities of nonlinear dynamics and external disturbances that arise when operating articulated robotic arms. Sliding-mode control (SMC) is well known for its robustness and precision, particularly in managing the nonlinear dynamics and external disturbances encountered when controlling robotic arms. Its ability to maintain stability and performance despite the system's uncertainties makes it particularly ideal for articulated robotic arms with large degrees of freedom [1–4]. SMC accomplishes this by shifting the system's state to a predefined sliding surface, where it can effectively handle variations in the robot's dynamics and external forces applied to tasks such as trajectory tracking, path planning, and force control, ensuring that the robotic arm can execute precise and reliable movements even under challenging conditions [5–7]. However, traditional SMC techniques have substantial limitations, such as chattering and computing complexity, which limit their practical implementation in high-precision and dynamic situations [8–10]. To address these challenges, the current study provides a robust sliding-mode controller with chattering rejection capabilities and suggests a quantum-inspired sliding-mode control approach

designed for a six-degree-of-freedom articulated robotic arm. The work advances the field by constructing a thorough kinematic and dynamic model of the robot using precise CAD designs from SolidWorks software 2024 SP4.0 to extract mass properties required for correct path planning and trajectory execution and evaluating the practice's performance parameters [11]. A unique quantum control algorithm employing multiple qubit operators is also developed, which improves the robustness of the control strategy. This novel approach improves the robustness and precision of the control system, considerably boosting the robot's energy efficiency performance, as evidenced by rigorous testing. Integrating the quantum principles into SMC is a novel advancement in robotic arm control, opening new avenues for overcoming the constraints of traditional approaches to create more efficient and adaptive robotic systems.

1.2. Related Works

The integration of backstepping terminal sliding-mode control with radial basis function neural networks, as demonstrated by Vijay and Jena [12], highlights the application of SMC in controlling specific objects of a robot manipulator with three degrees of freedom (DOF) in an overhead transmission; however, challenges such as parameter tuning and computational complexity have not been solved. Similarly, Adhikary and Mahanta [13] introduced an adaptive backstepping SMC with time delay estimation, enhancing trajectory tracking and disturbance rejection in two-DOF robotic manipulators, though real-time implementation poses challenges. Norsahperi and Danapalasingam [14] advanced the field by proposing an improved optimal integral SMC to reduce the tracking error and energy consumption in robotic manipulators. This has been validated through simulations on a two-DOF manipulator, with significant potential for industrial applications. Nguyen et al. [15] developed a backstepping global fast terminal sliding-mode control, addressing chattering and enhancing transient response in a two-DOF robotic manipulator, although uncertainty estimation remains challenging. Baek et al. [16] contributed with their widely and stable adaptive SMC, focusing on a two-link planar robot manipulator, demonstrating adaptability with challenges in tuning and convergence. Further advancing SMC, Baek and Kwon [17] introduced a strong and stable adaptive SMC, enhancing disturbance rejection and minimizing chattering in robotic manipulators, particularly in dynamic uncertainty environments. Feng et al. [18] addressed chattering mitigation through full-order SMC with time-varying gains applied to a two-DOF robotic manipulator. At the same time, Zhai and Li [19] focused on high-speed and high-precision applications through fast-exponential SMC, integrating a super-twisting controller with a high-order sliding-mode observer. Soriano et al. [20] shifted the focus to energy efficiency, proposing an optimized SMC using a bat algorithm to reduce energy consumption in a SCARA robot, emphasizing the importance of sustainability in industrial robotics. The integration of neural networks with SMC has also seen considerable advancements, with Yen et al. [21] combining recurrent fuzzy wavelet neural networks with adaptive SMC to enhance tracking accuracy and stability in industrial robots. At the same time, Jung [22] used radial basis function-like neural networks in neuro-sliding-mode control for a three-link rotary robot manipulator, refining SMC gain selection. Gambhire et al. [23] provided a broader perspective by examining the evolution of SMC techniques, including integrating intelligent control strategies such as neural networks, emphasizing the need for robust control mechanisms. Yu et al. [24] extended the discussion with a comprehensive overview of terminal SMC, suggesting an integration with artificial intelligence techniques to enhance adaptability and robustness. Finally, Yin et al. [25] introduced a compensation SMC with a nonlinear disturbance observer for machining robotic manipulators, significantly improving tracking accuracy and robustness, particularly in industrial applications. The literature

on SMC techniques in robotics indicates a clear trend toward more adaptive, intelligent, and energy-efficient control methods, with ongoing research focusing on optimizing real-time implementation and integrating advanced computational techniques to address persistent challenges such as chattering, uncertainty estimation, and energy consumption.

Quantum-inspired SMC denotes a substantial upgrade in control techniques. It aims to manage the limitations of the classic SMC, such as chattering, robustness against disturbances, and computational efficiency. Incorporating quantum principles into SMC offers new possibilities for enhancing the precision and robustness of science and engineering, especially in robotic systems, making it a promising area for prospective investigation.

Early applications of quantum methods in robotics demonstrate the potential of quantum SMC to make fundamental transformations in control systems. For example, Gan et al. [26] integrated quantum-behaved particle swarm optimization with SMC to improve control systems for unmanned underwater vehicles, focusing on enhancing robustness in complex underwater environments. Similarly, Fazilat et al. [27] developed a quantum-based kinematic model for industrial robotic arms, such as the ABB IRB140, seriously reducing computational demands and facilitating real-time processing. Zioui et al. [28] further contributed by modeling rigid body orientation using quantum spins, a crucial aspect of robotics that simplifies spatial orientation modeling and bridges classical and quantum control systems. The development of quantum algorithms and their application in robotics has shown notable promise. Boudjoghra et al. [29] introduced a quantum computing-based solution using the Harrow–Hassidim–Lloyd (HHL) algorithm to address state-domain equations in control theory. This approach is particularly beneficial for dynamic systems in robotics, reducing computational intricacy. Singh and Sloth [30] developed an evolving type 2 quantum fuzzy neural network for robotic manipulators, integrating quantum fuzzy logic with traditional neural networks to enhance adaptability and stability. State-of-the-art applications of quantum control in robotics are beginning to emerge, showcasing the potential of these methods to enhance performance in problematic environments. Zheng and Su [31] used QPSO to enhance SMC for electro-hydraulic servo systems, achieving significant improvements in tracking accuracy and setting a benchmark for optimizing control in uncertain robotic environments. Qu et al. [32] introduced a novel integral SMC for helicopter systems, integrating quantum information techniques to improve control accuracy and disturbance rejection, which is crucial for dynamic robotic systems like helicopters. In another investigation, Zioui et al. [33] extended quantum computing applications in robotic kinematics by developing a quaternion model for robotic arm positioning, demonstrating the feasibility of quantum models in practical robotics and paving the way for future Q-SMC strategies. The impact of quantum-inspired control methods on robotics is increasingly evident as researchers explore their adaptability and efficiency. Sivak et al. [34] proposed a model-free quantum control approach using reinforcement learning, enhancing the adaptability and performance of quantum-based control methods in environments where precise models are challenging to obtain. Quantum computing's potential to revolutionize robotics is further highlighted by Petschnigg et al. [35], who synthesized the current state of quantum computing and proposed its application to complex robotic challenges like AI, machine learning, and kinematics. Niu et al. [36] involved quantum control through deep reinforcement learning to optimize quantum systems, offering insights into adapting these methods for robotic applications that require real-time decision-making under uncertainty. Specialized quantum control strategies for robotics continue to advance the field. Reshetnikov and Ulyanov [37] explored the application of quantum fuzzy controllers in robotic systems like mobile manipulators, demonstrating marked control accuracy and robustness improvements. Tavanaei-Sereshki and Ramezani-al [38] developed a quantum genetic algorithm-based SMC for autonomous

underwater vehicles, showing superior performance in nonlinear, dynamic surroundings and highlighting the broader applicability of quantum-inspired control strategies in other robotic systems. The study by Xi et al. [39] addresses the significant challenge of controlling robot manipulators in industrial environments characterized by high uncertainties and nonlinear dynamics. Their robust adaptive SMC system integrates an adaptive sliding-mode disturbance observer with backstepping techniques, demonstrating enhanced precision and stability in uncertain environments. The reviewed studies collectively illustrate the transformative potential of quantum SMC in various aspects of intelligent mechanisms and robotics. By addressing challenges in traditional control methods, from high-dimensional optimization to real-time adaptation in dynamic environments, these studies contribute to a growing body of knowledge that could significantly influence overcoming the limitations of classical methods, enhancing the precision, robustness, and computational efficiency of robotic control systems.

1.3. Problem Formulation and Contribution

While SMC has proven to be a robust solution for managing the nonlinear dynamics and external disturbances in robotic arms, significant limitations such as chattering and computational complexity persist. These issues hinder the practical application of SMC in high-precision, dynamic environments, particularly in robotics systems with high degrees of freedom. More adaptive, precise, and computationally efficient control strategies still need to be met, especially in scenarios requiring real-time response and energy efficiency. It is essential to investigate filling this gap by exploring the potential of quantum-inspired sliding-mode control to examine the probability of overcoming these intrinsic limitations.

The primary purpose of the current examination is to develop and validate a novel quantum-enhanced sliding-mode control strategy, particularly for a six-degree-of-freedom articulated robotic arm and perform a comparative study between the performance of classic SMC and a quantum version of sliding-mode control. It aims to enhance SMC's robustness, precision, and computational efficiency by integrating quantum principles into the control strategy, focusing on addressing the persistent issues of chattering, computational complexity, and robustness against disturbances, which are vital for achieving high-performance robotic control to improve the control system's energy efficiency and adaptability, ultimately contributing to more reliable and efficient robotic arm manipulations in dynamic environments.

The effectiveness of this study lies in its possibility of enhancing control systems in robotics by introducing quantum-inspired sliding-mode control as a practicable alternative to classic methods. Incorporating quantum principles into SMC could increase robotic systems' performance and energy efficiency by addressing the evolution of computational methodologies. It offers a more robust and precise control strategy that can be applied in applications, particularly in the adaptability and effectiveness of robotic systems in real-world scenarios where precision, speed, and reliability are paramount.

The present study compares two control strategies, the classical sliding-mode control and its quantum-inspired sliding-mode control counterpart. The primary objective was to evaluate the integration of quantum principles into control methodologies and assess its potential to enhance performance. In this comprehensive case study, we developed a robust SMC-based control framework for our robotic arm and extended it to include quantum-inspired elements. While acknowledging the effectiveness of other advanced control strategies such as Model Predictive Control, reinforcement learning-based methods, Adaptive Control, Fractional Order Control, and H-infinity Robust Control, we notice the significance of exploring these approaches to broaden the comparative scope of our research. However, for this study, we focused on a singular, well-established control strategy and its

quantum-inspired enhancement to facilitate a concentrated and stringent analysis of their respective performance.

The current research presents a comprehensive study of robust control of an industrial manipulator robotic arm incorporating quantum-inspired sliding-mode control for robotic arms. Section 2 explores the kinematic modeling of the ABB IRB140 robot, emphasizing an advanced approach to developing a precise model for motion planning and performance evaluation. This section also details the CAD design of the robotic arm, underscoring the critical importance of accurately obtaining mass properties. Furthermore, it outlines the design of a robust SMC strategy, including techniques for reducing chattering and introducing a novel quantum-inspired sliding-mode control algorithm employing multiple qubit operators. Section 3 presents the experimental results, demonstrating the superior performance of the quantum-enhanced SMC in managing the manipulator robot arm. Finally, Section 4 discusses the implications of these findings and suggests directions for future research in the control of robotics and quantum computing.

2. Methodology

2.1. Robotic Arm Presentation

The study focuses on the ABB IRB 140 robot, illustrated in Figure 1. This six-axis articulated robot is widely employed in different industrial applications. According to ABB's technical specifications, it provides flexible mounting options, such as floor, wall, and inverted positions, to accommodate different working environments. The IRB 140 robot is commonly utilized for arc welding, assembly, material handling, machine tending, cleaning, and spraying, packing, and deburring. With a weight of approximately 98 kg, it can support an end-effector with a payload capacity of up to 5 kg. The robot's reach extends to about 810 mm at its mounting flange, and it can bear up to 1.5 kg of equipment on its upper arm. The joint limits offer a significant functional workspace, as outlined in Table 1 [11].

Figure 1. The ABB IRB 140 robot located in the UQTR automation laboratory.

Table 1. Joint limits of the ABB IRB 140 robot.

Joints	Type of the Joint	Limits (°)
1	R	+180 to −180
2	R	+110 to −90
3	R	+50 to −230
4	R	+200 to −200
5	R	+120 to −120
6	R [1]	+400 to −400

[1] R stands for rotational or revolute.

The robotic arm features an IRC5 advanced controller designed to handle multiple robots, optimizing their performance for shorter cycle times and precise movements. It also incorporates RobotWare (Robot Studio), allowing ABB robots to be programmed from a workstation without disrupting active production processes. This configuration includes the ABB Virtual Controller, a representation of the production-level software that enables program development. Robot Studio presents highly realistic simulations, utilizing simple robot programs and configuration files that accurately reflect real-world operations [11].

For the present research, the ABB IRB 140 robot was utilized in its original configuration, strictly following the manufacturer's specifications. The robot's structure and system remained unchanged, with no custom modifications. This approach ensures that our study's results and insights accurately reflect the standard performance of the ABB IRB 140 as commonly observed in industrial settings. Additionally, it provides a baseline for evaluating the robot's efficiency and dynamics in typical operational scenarios.

2.2. Mathematical Model of the Robot

The evaluation of the ABB IRB-140 robotic arm at the UQTR mechatronic laboratory began by inputting joint-specific data to generate trajectories, which served as a foundation for implementing kinematic models. These models were developed using Denavit–Hartenberg parameters (Table 2) to define the position and orientation of the end-effector. The robot's joint motions were generated using fifth-order polynomial equations and transformation matrices, allowing for a detailed description of the potential positions and orientations. This kinematic analysis was a prototype of dynamic modeling, which employed the Euler–Lagrange method to explore the robot's dynamics, focusing on joint torque calculations and energy consumption. The dynamic model was further enhanced by incorporating inertia and mass center point data from detailed CAD/CAM designs created using SolidWorks software. This phase seamlessly transitioned into computer-aided optimization (CAO), enabling comprehensive simulations representing various model fidelity levels. Integrating kinematic and dynamic models facilitated a comprehensive analysis, allowing precise estimation of the robot's energy needs through torque profiles.

Table 2. Denavit–Hartenberg Parameters of the ABB IRB 140 [11,28].

Link	a (mm)	α (°)	d (mm)	q (°)
1	$a_1 = 70$	−90	$d_1 = 352$	q_1
2	$a_2 = -360$	0	0	$q_2 + 90$
3	0	−90	0	q_3
4	0	90	$d_4 = 380$	q_4
5	0	−90	0	q_5
6	0	0	$d_6 = 65$	q_6

After that, the inverse kinematics was developed. The model involves determining the joint angles that achieve a specific end-effector position. This model is crucial for maintaining safe and reliable robot operations but also allows for explicit control over the robot's posture. Additionally, it offers a computationally efficient method for determining joint angles, making them particularly beneficial in real-time control scenarios where rapid computation is essential.

The differential kinematics was also developed to define how the angular velocities of a robot's joints relate to its end-effector's linear and angular velocities. By analyzing velocities and static forces, the Jacobian matrix J of the manipulator is derived. This matrix plays a key role in examining and controlling robotic motion, identifying singularities and redundancy, formulating inverse kinematic equations, and characterizing the manipulability of velocity and force [40]. The Jacobian matrix is specifically adapted to the unique joint configurations

of each robot, greatly enhancing motion planning and control, which are essential for executing precision tasks. It also addresses singularities and redundancies, improving the robot's operational efficiency and safety.

Finally, a dynamic model is developed to enable the analysis of a robot's performance regarding joint acceleration forces and torques. The Euler–Lagrange method is commonly employed to establish such a dynamic model. The first three proximal joints are fundamental as they play a significant role in assessing the mechanical loads experienced by the mechanical structure of the robot during operation, which is a key factor in the dynamic modeling and assumptions made in the model. The dynamic behavior of a robotic arm with n joints can be described by relation (1) [11].

$$M\,\ddot{q} + V + G = \tau \tag{1}$$

In this context, $\ddot{q}$ represents the joint acceleration vector, M is the inertia matrix, V corresponds to the Coriolis vector, G denotes the gravitational vector, and τ is the force and torque vector. In our study, the elements of the inertia matrix and the positions of the mass centers were determined using SolidWorks software. The uniform density assumption for each link was applied across all models. It also considered key values related to mass and other physical properties, such as the mass center positions and inertia matrices, represented within their respective reference frames for the three proximal links. The precision of a dynamic model relies heavily on accurately determining mass centers and inertia matrices. To obtain these necessary data in engineering, straightforward dimensional specifications, and scientific methods, including CAD modeling, Experimental Modal Analysis, and Inertia Measurement Units, are utilized. CAD modeling provides detailed information on dimensions and mass distribution, while Experimental Modal Analysis and Inertia Measurement Units offer direct measurements of inertia characteristics. The mass of each link can be calculated assuming constant and uniform density. SolidWorks software was utilized to determine the volume of each link. The mass of each link is estimated by multiplying the ratio of an individual link's volume to the total robot volume by the total robot mass.

2.3. CAD Designs of the Robot

Employing SolidWorks, we performed a high degree of precision in modeling each robotic arm component. A determined purpose of accuracy and steady state to our conceptual design parameters depicted our methodology. This introductory phase has specified a solid foundation for a robotic arm balanced to enhance the capabilities within industrial automation, mainly characterized by its superior functionality. During the CAD design process, we make the simplifying assumption that the robot's components have a uniform density. While this assumption simplifies the calculations, it may result in inaccuracies since it must account for the material variations in the real robot. Additionally, ergonomics and safety were essential throughout the design iterations, driven by an iterative process. This process concerned rigorous stress examination, evaluation of energy consumption patterns, and comprehensive persistence testing. These steps were required to establish the arm's mechanical robustness and stable reliability, ensuring its appropriateness for reinforcing industrial application. The precise, detailed model depicted in Figure 2 is fundamental for the simulations that require high fidelity and detailed analysis. This model reproduces the robot's configuration with maximum accuracy, making it ideal for investigating elaborate dynamics and interactions within the real robot's mechanism. Mass and inertia values are established on the presumed material properties and the model's geometry. These values are essential for dynamic simulations, but they may not fully reflect the actual robot due to potential manufacturing variations and inconsistencies in material properties [11].

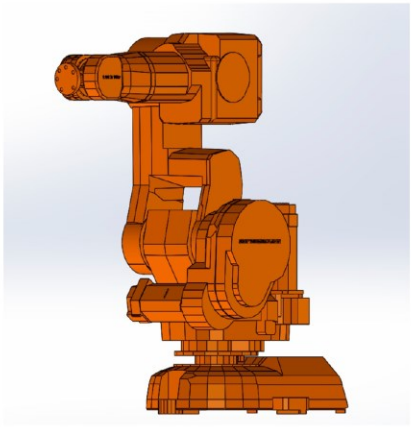

Figure 2. Detailed SolidWorks model of the ABB IRB 140 robotic arm [11].

The specifics of the model and the results for the proximal links obtained using the mass properties tool are outlined in Table 3 [11].

Table 3. Mass property results of each model calculated using SolidWorks software [11].

ABB IRB 140	Parameters (Unit)	Link 1	Link 2	Link 3
Mass Properties	*Weight* (kg)	35	25	18
	Xc (mm)	277.87	218.29	−24.56
	Yc	373.12	229.73	−219.9
	Zc	−199.03	112.43	−25.86
	Ixx (kg·m^2)	6.5	0.9	2.5
	Ixy	1.1	−0.03	−0.001
	Ixz	3.05	0.1	0.09
	Iyy	2.02	1.3	2.7
	Iyz	5.07	−0.01	−0.8

2.4. Robot Performance Assessment

To evaluate the accuracy of the three models' predictions, we analyzed the energy consumption by the three proximal joints and the robot's total energy consumption over the same duration and path of movement. In the proposed modeling approach, the energy consumption of each joint at a specific time can be calculated from the joint torque and angular velocity using Equation (2). The robot's integrated energy consumption is assumed to be the sum of the energy consumption values of all the joints.

$$E_i = \int_{t_0}^{t_f} \tau_i(t) \cdot \dot{q}_i(t)\, dt \tag{2}$$

We employ a theoretical approach to evaluate the energy consumption of robotic arms. This approach centers on dynamic models that simulate each joint's torque τ_i and angular velocity $\dot{q}_i$ Detailed explanations of how these parameters are simulated are provided in the methodology section. The simulated values are then used in Equation (2) to calculate the energy consumption of each joint. The theoretical method offers a comprehensive analysis of energy consumption, avoiding the practical challenges and complexities associated with the installation and calibration of physical sensors on the robotic arm.

Focusing on a theoretical and simulation-based approach contributes significantly to understanding energy dynamics in robotic arms, especially in scenarios where direct mea-

surement is impractical or impossible. This approach also aligns with current trends in employing computational models to analyze complex system contributions to robotics fields.

2.5. Sliding-Mode Control Strategy

One method of robust control technique for controlling a complicated and nonlinear mechanism like a manipulator robotic arm is called sliding-mode control methodology, a type of variable structure control system [4,10,41]. The most crucial feature of the sliding-mode control is the complete insensitivity to parametric uncertainty and external disturbances during the sliding process. The variable structure control system utilizes a high-speed switching-control law for two purposes. First of all, it forces the nonlinear system's form trajectory along a user-defined surface in the state space, named the sliding or switching surface [42,43]. The control approach has one gain if the state trajectory of the mechanism is above the surface and a different gain if the controlling object, such as trajectory in robotics, drops below the surface and because of this named sliding surface. Secondly, it keeps the mechanism state control object on this surface by following the time [44,45]. During the controlling process, the control system's structure differs from one to another and thus it donates the name variable structure control. This model also permits the elimination of interactions among the joints of the manipulator [46,47]. A general equation of the motion can be represented in the space state by the following [48]:

$$x = f\ (x,\ t) + g\ (x,\ t) \cdot u \tag{3}$$

where u is the control input, x is the state vector also considered as the output, and the functions $f\ (x,\ t)$ and $g\ (x,\ t)$ are nonlinear functions.

The control input variable is defined in the following:

$$u_i(x,t) = \begin{cases} u_i^+(x,t) & if\ \ S_i(x,t) > 0 \\ u_i^-(x,t) & if\ \ S_i(x,t) < 0 \end{cases} \tag{4}$$

where u_i, is the ith component of u, and $S_i(x,t) = 0$ is the ith component-switching hypersurfaces $S(x, t) = 0$, $S \in R^m$.

According to the presented rules with discontinuous control, the system is named a variable structure system since the controller switches alternatively based on the state of the mechanism. The sliding mode appears on a switching surface $S(x) = 0$, which pushes the machine to behave as a linear-time uniform system, which can be assumed to be stable. For it to be linear, the surfaces can be written as:

$$s_i(x) = x_n + \sum_{i=1}^{n} \lambda_i \cdot x_i \tag{5}$$

The condition for the sliding mode to exist on the ith surface is provided by the following equation:

$$\lim_{s_i \to 0^+} \dot{S} > 0 \qquad \text{and} \ \lim_{s_i \to 0^-} \dot{S} < 0 \tag{6}$$

This is when $S\dot{S} < 0$ is too close to $S_i(x) = 0$, when all the trajectories shift towards the switching surface. In the perfect sliding mode on S_i, the related control is the equal control issued from Equation (3) and given by the equation for $\dot{S} = 0$:

$$u_{eq} = g^{-1}(x,t)\left[\dot{x}(t) - f(x,t)\right] \tag{7}$$

So, the discontinuous control input presented in relation (4) can be noted as follows:

$$u_i = \begin{cases} u^*_{ieq} + \Delta u_i^+ & if \;\; S_i > 0 \\ u^*_{ieq} + \Delta u_i^- & if \;\; S_i < 0 \end{cases} \tag{8}$$

where u_{eq} illustrates the low-frequency control component or the steady state equivalent control signal, and Δu presents the high-frequency discontinuous term. For the functional case, the control equation is known by the evaluated value due to error modulization and variation in the parameters as follows:

$$u^*_{eq} = u_{eq} + \Delta u_{eq} \tag{9}$$

This last formula is equivalent to the discontinuous control input in relation (8). The term of high-frequency Δu can be represented differently, such as the equation based on the classical reaching law, which is one of the methods reported in the literature for alleviating chattering in sliding mode. Classical reaching law can express in four principal subcategories that are represented as the following:

Constant reaching law:

$$\dot{s} = -\varepsilon \cdot sgn(s), \qquad \varepsilon > 0 \tag{10}$$

Exponential reaching law:

$$\dot{s} = -\varepsilon \cdot sgn(s) - ks, \qquad \varepsilon > 0 \qquad k > 0 \tag{11}$$

Power-rate reaching law:

$$\dot{s} = -k\,|s^{\alpha}| \cdot sgn(s), \qquad 0 < \alpha < 1 \qquad k > 0 \tag{12}$$

General reaching law:

$$\dot{s} = -\varepsilon \cdot sgn(s) - f(s)\;,\; \varepsilon > 0 \;\; \text{where } f\,(0) = 0 \text{and } sf(s) > 0 \text{when s } \neq 0 \tag{13}$$

To obtain a robust sliding-mode control based on reaching law, consider the general equation motion as below:

$$\ddot{x} = f(x) + g(x)u + d(t) \tag{14}$$

where $f(x)$ and $g(x)$ are unknown equations and $g(x) > 0$ and $d(t)$ are the terms of disturbance. As sliding surface and derivative of the sliding surface, the combination of error of models considered satisfy the Hurwitz condition and can be described as follows:

$$s = \dot{e} + ce, c > 0 \tag{15a}$$

$$e = r - x(t) \tag{15b}$$

$$\dot{e} = \dot{r} - \dot{x}(t) \tag{15c}$$

For the derivative of the sliding-surface equation considering the effect of external disturbance as $d(t)$:

$$\dot{s} = \ddot{e} + c\dot{e} = \ddot{r} - \ddot{x} + c\left(\dot{r} - \dot{x}\right) = \ddot{r} - f(x) - g(x)u - d(t) + c\left(\dot{r} - \dot{x}\right) \tag{16}$$

To obtain the robust control sliding mode based on the exponential reaching law from the relations of (12) and (16):

$$\begin{array}{c} \ddot{r} - f(x) - g(x)u - d(t) + c(\dot{r} - \dot{x}) = -\varepsilon \cdot sgn(s) - ks \\ u = \frac{1}{g(x)}(\ddot{r} - f(x) - d(t) + c(\dot{r} - \dot{x}) + \varepsilon \cdot sgn(s) + ks \end{array} \tag{17}$$

The derivative of the sliding-surface equation can also be considered with (15) described with the disturbance term as follows:

$$\dot{s} = -\varepsilon \cdot sgn(s) - ks + d_c - d \tag{18}$$

The disturbance term d_c must satisfy the conditions for reaching the sliding surface, and the term d should be limited. dl and du are the lower and upper terms of disturbance, respectively, as:

$d_l \leq d(t) \leq d_u$, when s(t) > 0, $\dot{s} = \varepsilon - ks + d_c - d$, we want $\dot{s}$(t) < 0, so let $d_c = d_l$.

When s(t) < 0, $\dot{s} = -\varepsilon - ks + d_c - d$, we want $\dot{s}$(t) > 0, so let $d_c = d_u$.

Therefore, if we define $d_1 = \frac{d_u - d_l}{2}, d_2 = \frac{d_u + d_l}{2}$, then we can obtain the following:

$$d_c = d_2 - d_1 \cdot sgn(s) \tag{19}$$

The discontinuity of the sign function will generate chattering in the closed loop system. For this reason, the sign function is usually substituted by a saturation function sat (s/ε), where $sat(.)$ is described as follows:

$$sat(x) = \begin{cases} x & if\ |x| \leq 1 \\ sgn\ (x) & if\ |x| > 1 \end{cases} \tag{20}$$

To mitigate chattering, the study employs an exponential reaching law, which adjusts the conventional reaching law to achieve a smoother transition as the system state approaches the sliding surface. This is accomplished by adding a term, $-k \cdot s$, which gradually decreases the convergence rate to the sliding surface, thereby reducing the rapid switching responsible for chattering. Additionally, the discontinuous sign function $sgn(s)$ is replaced with a saturation function sat (s/ϵ), which introduces a boundary layer around the sliding surface. This change smooths the control action, significantly curbing chattering by preventing abrupt changes in the control input. By adjusting the thickness of this boundary layer, the system can strike an optimal balance between reducing chattering and maintaining precise control, enhancing the robustness and applicability of SMC in high-precision environments.

Employing this alternate will present a tracking error. The trade-off between the tracking error and control bandwidth will be created by setting the boundary layer properly. As mentioned before, the position of the robot's end-effector in this case study depends on the first three joints and links. For this reason, the control strategy implements the first three joints of the robot. Generally, for the three links, the robot's sliding-mode control can be described as follows:

$$s = \dot{e} + ce \tag{21}$$

For example, $e = \theta_d - \theta$.

This will lead to $\dot{s} = \ddot{e} + c\dot{e} = \ddot{\theta_d} - \ddot{\theta} + c\dot{e}$ and

$$\dot{s} = -\varepsilon\ sgn(s) \tag{22}$$

The combination of Equations (21) and (22) will result in the following:

$$\ddot{\theta} = \ddot{\theta}_d + c\dot{e} + \varepsilon\, sgn\,(s) \tag{23}$$

The general equation of the robot relies on the dynamics of the robot described as relation (1), which can be rewritten in terms of accelerations as the following:

$$\ddot{\theta} = M^{-1}(\tau - V - G) \tag{24}$$

With relations (23) and (24), we obtain the main equation of sliding-mode control as follows:

$$\tau = M\left(\ddot{\theta}_d + c\dot{e} + \varepsilon\, sgn(s)\right) + V + G \tag{25}$$

Assuming the presence of the disturbances for the robot in the working space to determine and track of end-effector position and considering inverse kinematics and dynamics of the robot manipulator, we can achieve the following equation for controlling in the sliding-mode technique:

$$\tau = M{\cdot}J^{-1}\left(\ddot{X}_d + c\dot{e} + \varepsilon\, sgn(s) - \dot{J}(\theta)\dot{\theta}\right) + V + G \tag{26}$$

2.6. Quantum Computing Basics

Quantum computing operates on a different principle compared to classical computing, utilizing quantum bits, or qubits, to encode and process information. A qubit state, denoted as $|q\rangle$, can be expressed as a superposition of the classical binary states 0 and 1 [49,50]. Mathematically, this is represented as:

$$|q\rangle = \alpha|0\rangle + \beta|1\rangle \tag{27}$$

Here, α and β are complex coefficients that correspond to the probability amplitudes of the qubit being in the states $|0\rangle$ and $|1\rangle$, respectively. These probabilities can be interpreted such that $|\alpha|^2$ gives the likelihood of the qubit being in the $|0\rangle$ state, while $|\beta|^2$ gives the probability of it being in the $|1\rangle$ state. In the context of vector space, the states $|0\rangle$ and $|1\rangle$ can be represented as the vectors $|0\rangle \equiv \begin{pmatrix}1\\0\end{pmatrix}$ and $|1\rangle \equiv \begin{pmatrix}0\\1\end{pmatrix}$, respectively [49,50]. Thus, a qubit state $|q\rangle$ can be depicted in vector form as $\begin{pmatrix}\alpha\\\beta\end{pmatrix}$. Quantum operations, known as quantum gates, can be applied to qubits to alter their states. These operations are often represented by Hamiltonian matrices [28,33]. The fundamental quantum gates that act on a single qubit include the identity, X, Y, and Z gates, which correspond to the Pauli matrices σ_0, σ_x, σ_y, and σ_z, respectively, as defined by the following matrices [50]:

$$\sigma_0 = \begin{pmatrix}1 & 0\\0 & 1\end{pmatrix} \tag{28}$$

$$\sigma_x = \begin{pmatrix}0 & 1\\1 & 0\end{pmatrix} \tag{29}$$

$$\sigma_y = \begin{pmatrix}0 & -i\\i & 0\end{pmatrix} \tag{30}$$

$$\sigma_z = \begin{pmatrix}1 & 0\\0 & -1\end{pmatrix} \tag{31}$$

Other single-qubit quantum gates can be expressed as a linear combination of the Pauli gates, such as the Hadamard gate depicted in Equation (32) and the three basic rotation gates illustrated in Equations (33)–(35) [51,52].

$$H = \frac{\sqrt{2}}{2}\begin{pmatrix} 1 & 1 \\ 1 & 1 \end{pmatrix} = \frac{\sqrt{2}}{2}(\sigma_0 + \sigma_x) \tag{32}$$

$$R_x(\theta) = \begin{pmatrix} cos\theta & -i\,sin\theta \\ -i\,sin\theta & cos\theta \end{pmatrix} = cos\theta\ \sigma_0 - i\ sin\theta\ \sigma_x \tag{33}$$

$$R_y(\theta) = \begin{pmatrix} cos\theta & -sin\theta \\ sin\theta & cos\theta \end{pmatrix} = cos\theta\ \sigma_0 - i\ sin\theta\ \sigma_y \tag{34}$$

$$R_z(\theta) = \begin{pmatrix} e^{-i\theta} & 0 \\ 0 & e^{i\theta} \end{pmatrix} = cos\theta\ \sigma_0 - i\ sin\theta\ \sigma_z \tag{35}$$

2.6.1. Developing the Quantum Comparator

The quantum comparator is an innovative computational tool that harnesses quantum principles to enhance precision and efficiency in comparison tasks. It integrates two primary components: a quantum subtractor and a quantum sign detector [50].

The quantum subtractor computes the difference between two real numbers. Operating within the quantum framework, it offers higher parallelism and potentially faster speeds than classical subtractors. This enables it to prepare the data for the next step by providing the relative magnitude of the two numbers. Once the subtraction is complete, the result is passed to the quantum sign detector. This component determines the sign of the computed difference, indicating whether the first number is more significant than, less than, or equal to the second number. By leveraging quantum superposition and entanglement principles, the quantum sign detector identifies the sign accurately and efficiently, completing the comparison. These components work together to enable the quantum comparator to perform comparisons with greater accuracy and speed than classical methods, making it a valuable tool in quantum computing applications [53–55].

2.6.2. The Quantum Subtractor

The quantum subtractor for two real numbers relies on the tensor product between two real qubit states, $q_1 = C_{\theta_1}|0\rangle + S_{\theta_1}|1\rangle$ and $q_2 = C_{\theta_2}|0\rangle + S_{\theta_2}|1\rangle$. These qubit states, q_1 and q_2, are derived by applying a quantum rotation around the y-axis, as described by the following equations:

$$q_1 = R_y(\theta_1)|0\rangle \tag{36}$$

$$q_2 = R_y(\theta_2)|0\rangle \tag{37}$$

The tensor product between q_1 and q_2 yields the coefficients of the eigenstates:

$$q_1 \otimes q_2 = C_{\theta_1}C_{\theta_2}|00\rangle + C_{\theta_1}S_{\theta_2}|01\rangle + S_{\theta_1}C_{\theta_2}|10\rangle + S_{\theta_1}S_{\theta_2}|11\rangle \tag{38}$$

The coefficient $S_{\theta_1}C_{\theta_2}$ can be obtained by measuring the system $q_1 \otimes q_2$ in the state $|10\rangle$. This coefficient can be rewritten using the trigonometric identity:

$$S_{\theta_1}C_{\theta_2} = sin\left(\frac{\alpha-\beta}{2}\right)cos\left(\frac{\alpha+\beta}{2}\right) = \frac{1}{2}(sin(\alpha) - sin(\beta)) \tag{39}$$

where $\frac{\alpha-\beta}{2} = \theta_1$ and $\frac{\alpha+\beta}{2} = \theta_2$, with $\alpha = \theta_1 + \theta_2$ and $\beta = \theta_2 - \theta_1$.

Thus, the subtraction of two real numbers $x = sin(\alpha)$ and $y = sin(\beta)$ can be computed through the following steps:

Step 1: Compute $\alpha = \arcsin(x)$ and $\beta = \arcsin(y)$.

Convert the input numbers x and y into angles α and β, which will be used for quantum operations.

Step 2: Determine θ_1 as $\frac{\alpha-\beta}{2}$ and θ_2 as $\frac{\alpha+\beta}{2}$.

This calculates the rotation angles θ_1 and θ_2, encoding the difference and sum of the input numbers.

Step 3: Initialize the qubits q_1 and q_2 to $|0\rangle$.

This prepares the qubits in a known starting state before any quantum operations are applied.

Step 4: Apply the quantum rotations $R_y(\theta_1)$ to q_1 and $R_y(\theta_2)$ to q_2.

This performs quantum rotations on the qubits using the calculated angles, encoding the input numbers into the qubit states.

Step 5: Measure the system in the state $|10\rangle$. The coefficient should be calculated on the state vector, yielding half of the subtracted result, which can be doubled by applying a gain. However, the sign of the subtracted result is required for creating a comparator, and it is the same as the sign of its half. Consequently, doubling the result is unnecessary. This method involves measuring the quantum system to obtain a coefficient related to the difference.

2.6.3. The Quantum Sign Detector

The quantum sign detector is inspired by the Boolean subtraction operation, particularly focusing on the concept of the borrow, which is illustrated in the truth table. The borrow, denoted as r, is equal to 1 only when the minuend a is 0 and the subtrahend b is 1. The logical expression for the borrow can be represented as $r = \bar{a} \cdot b$. This expression indicates that a borrow occurs, meaning r equals 1, only if a is less than b. The quantum sign detector is inspired by the expression of the borrow of the Boolean subtraction, as described in the truth table depicted in Table 4.

Table 4. Truth table of the subtraction between two Boolean numbers.

a	b	$s = a-b$	r (Borrow)
0	0	0	0
0	1	1	1
1	0	1	0
1	1	0	0

In quantum computing, classical logic operations are translated into quantum gate operations. The purpose of the quantum sign detector is to implement the logic of the borrow operation using quantum gates, effectively detecting whether the result of a subtraction would require a borrow, which in classical terms, would indicate a negative result. Two key quantum gates are involved in this operation: the X gate (quantum NOT) and the CCNOT gate (Toffoli gate). The X gate is the quantum analogue of the classical NOT gate. It flips the state of a qubit; for instance, if the input qubit is in the $|0\rangle$ state, applying an X gate changes it to $|1\rangle$, and vice versa. In the context of the quantum sign detector, the X gate is used to invert the qubit representing a, producing $|\bar{a}\rangle$, which corresponds to the classical negation of a.

The CCNOT gate, or Toffoli gate, is a controlled-controlled-NOT gate. It performs a NOT operation on a target qubit only if the two control qubits are both in the $|1\rangle$ state. In the quantum sign detector, the CCNOT gate, takes $|\bar{a}\rangle$ and $|b\rangle$ as inputs and operates on an

ancillary qubit initialized to $|0\rangle$. This operation effectively implements the logical AND between $\bar{a}$ and b, which corresponds to the classical borrow operation.

The quantum circuit for the sign detector operates as follows: Start by preparing qubits that represent the binary values a and b, along with an additional ancillary qubit initialized to $|0\rangle$. The qubit representing a is then passed through an X gate to obtain $|\bar{a}\rangle$. Subsequently, the CCNOT gate is applied to $|\bar{a}\rangle$ and $|b\rangle$, with the ancillary qubit as the target. The state of the ancillary qubit will be flipped to $|1\rangle$ if both $|\bar{a}\rangle = 1$ and $|b\rangle = 1$, thereby implementing the borrow logic. The final state of the ancillary qubit indicates the result of the quantum sign detection. If the ancillary qubit is in the $|1\rangle$ state, it corresponds to a borrow in the classical operation, signifying that the subtraction of b from a would result in a negative value. This quantum implementation of the borrow operation not only mirrors the classical logic but also leverages the principles of quantum mechanics, such as parallelism and quantum efficiency. Figure 3 depicts the quantum sign detector in a quantum circuit.

Figure 3. The quantum sign detector circuit [56].

2.6.4. The Quantum Adder

To effectively implement the hysteresis function, a subtractor is required, which can be realized using an adder and a sign detector. The necessary components for the sign detection have already been developed in the context of the comparator function. Therefore, the remaining task is to develop the quantum adder. The addition of two real numbers, x and y, is achieved using trigonometric identities as illustrated in the following steps. This process is grounded in the principles of quantum mechanics, specifically leveraging the tensor product and quantum state measurements. The tensor product between quantum states q_1 and q_2 yields the coefficients of the eigenstates presented in Equation (38), and to focus on the addition process, we measure the system q_1q_2 in the state $|01\rangle$. This measurement can be reformulated using the following trigonometric identity:

$$S_{\theta_1}C_{\theta_2} = cos\left(\frac{\alpha-\beta}{2}\right)sin\left(\frac{\alpha+\beta}{2}\right) = \frac{1}{2}(sin(\alpha)+sin(\beta)) \tag{40}$$

Here, $\alpha = \theta_1 + \theta_2$ and $\beta = \theta_2 - \theta_1$. Therefore, the addition of two real numbers x and y, where $x = sin(\alpha)$ and $y = sin(\beta)$, is computed as follows:

Step 1: Compute $\alpha = \arcsin(x)$ and $\beta = \arcsin(y)$.

The real numbers x and y are first converted into angles α and β using the arcsine function, which is crucial for preparing the inputs for subsequent quantum operations.

Step 2: Calculate $\theta_1 = \frac{\alpha-\beta}{2}$ and $\theta_2 = \frac{\alpha+\beta}{2}$.

Using the computed angles α and β, the intermediary angles θ_1 and θ_2 are calculated and will define the quantum rotations applied to the qubits.

Step 3: Initialize quantum states q_1 and q_2 to 0.

The qubits q_1 and q_2 are initialized to the ground state $|0\rangle$. This initialization provides a known reference state for the quantum operations.

Step 4: Perform quantum rotations $R_y(\theta_1)$ on q_1 and $R_y(\theta_2)$ on q_2.

The rotations $R_y(\theta_1)$ and $R_y(\theta_2)$ are performed on the qubits q_1 and q_2, respectively. These rotations adjust the quantum states to encode the information about the original real numbers.

Step 5: Measure the system at the state $|01\rangle$. The measurement yields the coefficient of the state vector, representing half of the sum $x + y$. While the full addition result typically requires multiplying this coefficient by 2, in this context, only the sign of the result is necessary for constructing the hysteresis function. Hence, the multiplication by 2 can be omitted, as the sign of the result remains unchanged.

Developing a quantum adder is required for implementing advanced quantum functions. This process harnesses key quantum abilities such as superposition, interference, and measurement. The quantum adder can efficiently and simultaneously operate on multiple states, yielding precise and optimized outcomes that are often unachievable with classical computing methods. The quantum system's capability to compute the sign of the sum without needing a full-scale addition underscores quantum computing's potential to simplify and enhance resource-intensive operations.

2.6.5. Proposed Quantum Algorithm

The quantum error e_Q is derived using a series of quantum operations that replace the classical error calculation. Let P denote the desired position and P_3 the actual position of the end-effector. The quantum error e_Q is calculated as follows:

For each axis i, compute the angles α_i and β_i corresponding to the components of P and P_3:

$$\alpha_i = arcsin(P_i) \tag{41}$$

$$\beta_i = arcsin(P_{3i}) \tag{42}$$

Next, calculate the rotation angles θ_{1i} and θ_{2i} as:

$$\theta_{1i} = \frac{\alpha_i - \beta_i}{2} \tag{43}$$

$$\theta_{2i} = \frac{\alpha_i + \beta_i}{2} \tag{44}$$

Two qubits q_{1i} and q_{2i} are initialized in the state $|0\rangle$ and the quantum rotations $Ry(\theta_{1i})$ and $Ry(\theta_{2i})$ are applied to these qubits, respectively:

$$q_{1i} = cos(\theta_{1i})|0\rangle + sin(\theta_{1i})|1\rangle \tag{45}$$

$$q_{2i} = cos(\theta_{2i})|0\rangle + sin(\theta_{2i})|1\rangle \tag{46}$$

The tensor product of these qubits is computed, and the system is measured in the state $|10\rangle$ to yield the quantum error component:

$$e_{Q_i} = k \cdot (q_{1i} \otimes q_{2i} \otimes q_{3i}) \tag{47}$$

Here the symbol $\otimes$ represents the tensor product, and k is a parametric term that can be adjusted to scale the quantum error component as needed for the specific requirements of the quantum control algorithm.

The derivative of the quantum error de_Q is computed using the quantum subtractor. Considering dP as the desired angular velocity and dP_Q as the quantum-calculated angular velocity obtained through the R_y gate, the derivative error de_Q is determined by the following relation:

$$de_Q = Quantum\ Subtractor\ (dP, dP_Q) \tag{48}$$

The quantum sliding surface $s_{quantum}$ is formed to approximate the classical sliding surface using quantum gates. First, the quantum error e_Q is scaled by a constant vector c:

$$scaled\ error = c \cdot e_Q \tag{49}$$

Then, the scaled quantum error and the quantum derivative error are added using quantum rotations. The resulting quantum sliding surface is expressed as:

$$s_{quantum} = n\left(sin\left(\frac{\theta_{c \cdot e}}{2}\right) + sin\left(\frac{\theta_{deQ}}{2}\right)\right) \tag{50}$$

Here, n is a parameter that can be tuned according to the specific requirements of the control system normalization, providing more flexibility in how the quantum sliding surface is scaled, and θ_{ce} and θ_{de} are the rotation angles for the scaled error and derivative error, respectively. The sign of the quantum sliding surface $s_{quantum}$ is detected using quantum computational techniques. The quantum state $|s\rangle$ representing the sliding surface is prepared as:

$$|s\rangle = cos(\theta)\,|0\rangle + sin(\theta)\,|1\rangle \tag{51}$$

where θ is calculated by the relation:

$$\theta = arcsin\left(\frac{s(t)}{max(|s(t)|)}\right) \tag{52}$$

The quantum sign detector then applies the X gate (quantum NOT gate) and the Toffoli gate (CCNOT gate) to determine the sign of the sliding surface. The outcome of the measurement after applying these gates indicates the sign of the sliding surface, with the ancillary qubit's state corresponding to +1 or -1.

The quantum control law u_Q is formulated by integrating the quantum sliding surface and the sign detection results. The control variable V is computed using the quantum sliding surface as:

$$V = J^{-1} \cdot \left(\ddot{P} + c \cdot de_Q + q \cdot Sign(s_Q) - \dot{J} \cdot \dot{q}\right) \tag{53}$$

where J is the Jacobian matrix, $\ddot{P}$ represents the desired acceleration, and $\dot{J} \cdot \dot{q}$ accounts for the effects of dynamic changes in the system.

The final control input u_Q is then calculated as:

$$u_Q = M \cdot V + B + G \tag{54}$$

So, M is the inertia matrix, B represents the Coriolis/centripetal forces, and G denotes the gravitational forces.

3. Results and Discussion

The following Simulink model is employed as the implementation algorithm for the carried-out simulation of the motion control of the robotic arm manipulator. Simulink allows creating blocks that have all the features and capabilities of any type of built-in function. The block function of the plant implemented all equations for the dynamic equations of motion, such as the inertia, gravity, and Coriolis centrifugal parameters, to obtain the torque and force equation of the robot presented in the kinematics and dynamic models of the robot in the methodology section of the current study and the mass properties of the robot, which consist of mass center points and inertia matrixes for the first three links presented in the section on CAO design and Table 3. A classic sliding-mode controller with the expositional reaching law approach based on the presented method is

implemented in the controller block function, and the schematic diagram of the controller model is represented in Figure 4. Other Simulink models based on the quantum approach incorporating the quantum operators to handle the quantum version of the sliding-mode controller for the robot manipulator are designed and illustrated in Figure 5.

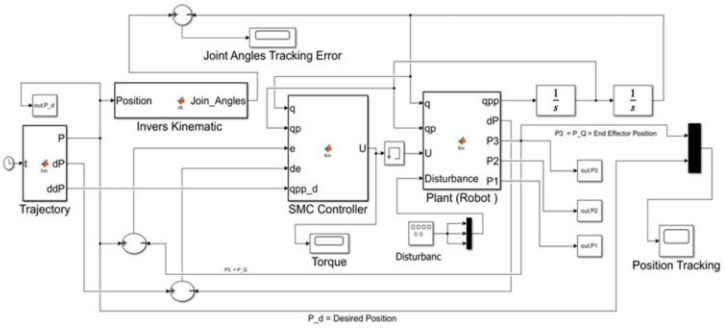

Figure 4. Simulink trajectory model of the robot manipulator for SMC.

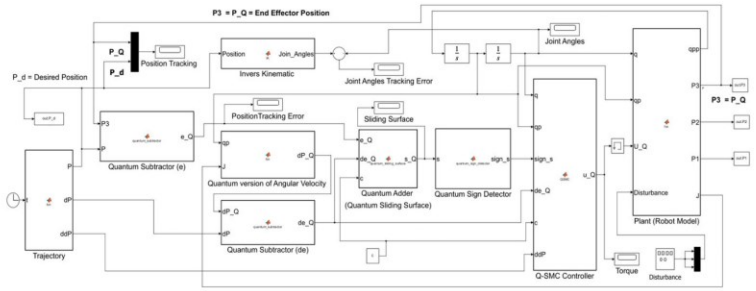

Figure 5. Simulink trajectory model of the robot manipulator for Q-SMC.

The sliding-mode controller algorithm is used for motion control based on a design with and without disturbances to evaluate the model's robustness. The value of disturbances applied based on the sine and cosine trajectory of the joint variable is predefined as a percentage of the input signal to examine the robustness of the designed controller. The implemented algorithm examines thoroughly a specific trajectory to verify the performance and behavior of the designed sliding-mode controllers of the robot to execute tasks undertaking the controllers. A circular trajectory is defined in the robot's working space considering avoiding singularity to perform the robot's task and estimate the chosen controller's execution. The motion of the end-effector begins at the same point for both controllers, positioned somewhere within the working space but outside the circular trajectory. Upon initiating the simulation, the robot attempts to reach the desired circular path, perform a circular motion along the defined trajectory, and maintain its position according to the specified parameters. The successful transition from an initial position outside the defined path to accurately following the specified circular trajectory within the robot's workspace confirms the correct operation of the controllers. Figure 6 illustrates the robot performing the assigned task under the SMC and Q-SMC controllers.

The Q-SMC aligns closely with the desired trajectory, guiding the robotic arm to precise coordinates, as the red dotted line shows. In contrast, the SMC controller, represented by the blue dotted line, exhibits delayed response and reduced accuracy, resulting in the arm deviating more noticeably from the intended path when reaching the coordinates.

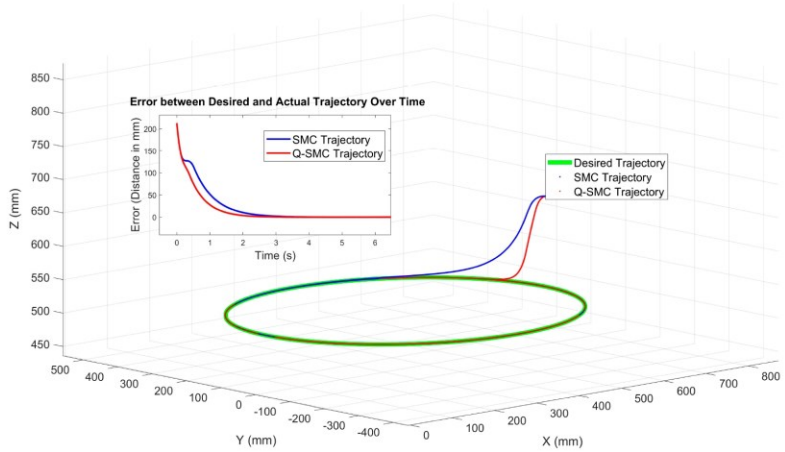

Figure 6. Projection of X–Y–Z trajectory of robot manipulator executed by controllers.

Figures 7–9 illustrate the comparative position-tracking performance of the robotic arm's end-effector along the X, Y, and Z axes, employing both classic sliding-mode control and quantum-inspired sliding-mode control. The Q-SMC demonstrates superiority over the SMC in both transient and steady-state performance. As highlighted in the zoom-in inset, it achieves faster convergence to the desired trajectory with reduced overshoot. This enhancement is attributed to quantum-inspired innovations that facilitate smoother control actions and improved management of nonlinearities and disturbances.

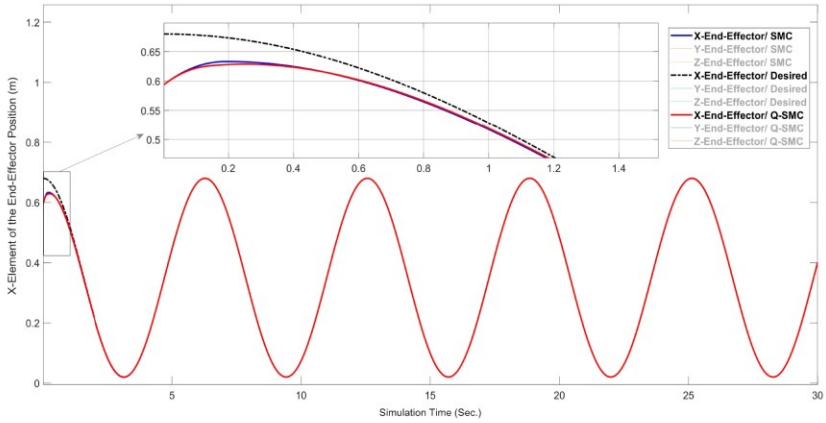

Figure 7. Comparison of position tracking (X-component) for the robot end-effector.

Furthermore, Q-SMC maintains a closer adherence to the desired trajectory throughout the simulation, exhibiting exceptional tracking accuracy and robustness. The results along the *Y*-axis further underscore the benefits of Q-SMC, which delivers precise and smooth trajectory tracking. Consistently, Q-SMC outperforms SMC in terms of quicker convergence and reduced overshoot. The enhanced transient response and accurate path alignment are evident throughout the simulation. These improvements stem from the proposed

controller's capacity to effectively mitigate uncertainties and disturbances, resulting in smoother and more dependable control actions.

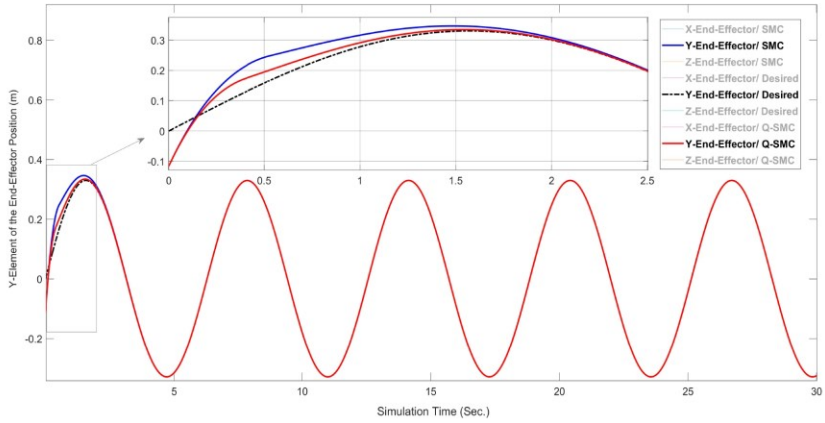

Figure 8. Comparison of position tracking (Y–component) for the robot end-effector.

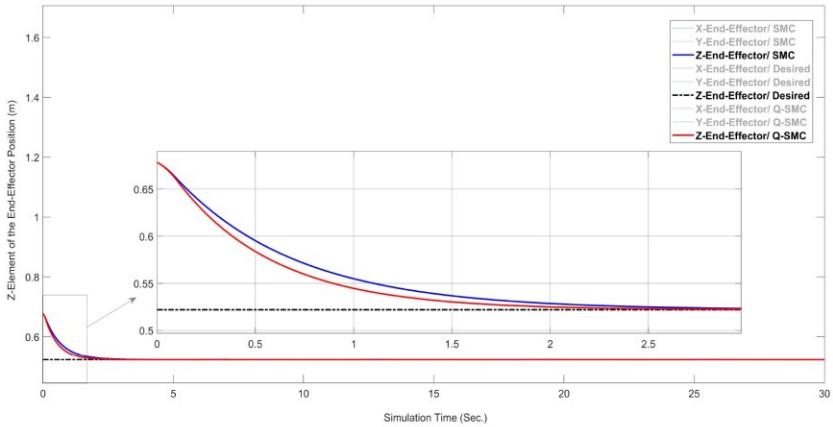

Figure 9. Comparison of position tracking (Z-component) for the robot end-effector.

In contrast, SMC displays slightly greater deviations from the desired trajectory, particularly during the transient phase, highlighting Q-SMC's superior precision and robustness. The quantum-inspired enhancements significantly reduce overshoot and oscillations, as depicted in the magnified transient response. Although both controllers ultimately achieve the target position, Q-SMC consistently provides better precision and stability throughout the simulation. The reduced chattering observed with Q-SMC decreases abrupt control actions, enhancing energy efficiency and preserving the mechanical integrity of the system. These findings reaffirm Q-SMC as a robust control strategy for applications requiring smooth and accurate trajectory tracking.

Figures 10–12 illustrate the tracking error of the robot's end-effector under both classical SMC and Q-SMC controllers. The results indicate that Q-SMC achieves a particularly lower steady-state error compared to SMC, showing improved tracking precision. While both controllers exhibit rapid error convergence, Q-SMC stabilizes more quickly with mini-

mal oscillations, reflecting its enhanced robustness and smoother control actions. These findings underscore the effectiveness of the Q-SMC approach in maintaining trajectory accuracy, even in dynamic conditions.

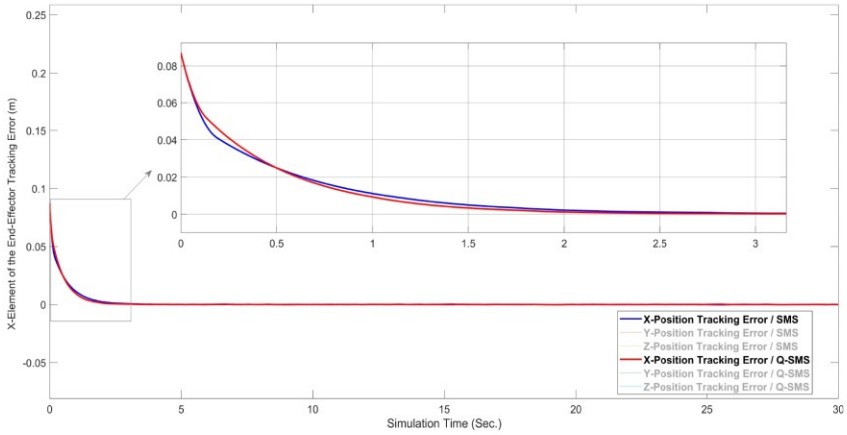

Figure 10. Comparison of tracking error (X-component) for the robot end-effector.

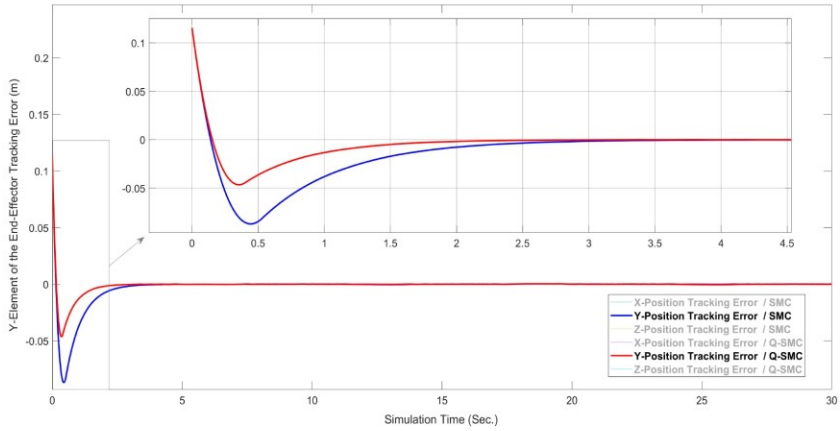

Figure 11. Comparison of tracking error (Y-component) for the robot end-effector.

Additionally, Q-SMC's reduced chattering and optimized control actions further validate it as a robust and precise control strategy for robotic systems. The classical SMC shows a notable initial overshoot in the Y-position, highlighting its greater sensitivity to sudden changes in system dynamics. In contrast, Q-SMC exhibits better stability, faster error convergence, and reduced fluctuations, resulting in a more consistent response over time. This difference in robustness allows Q-SMC to handle dynamic variations more efficiently and makes its smoother trajectory control particularly suitable for precision applications, solidifying its reputation as an advanced and effective control method for robotic systems.

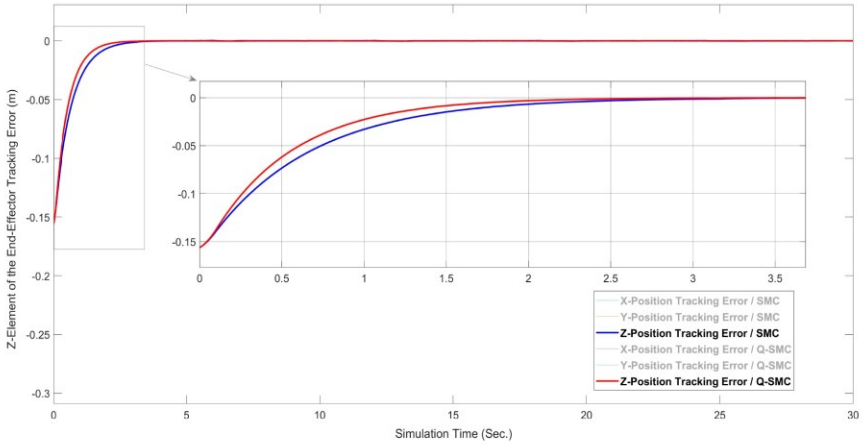

Figure 12. Comparison of tracking error (Z-component) for the robot end-effector.

The tracking performance for the Z-position of the robot's end-effector reveals that both controllers undergo a transient phase. However, Q-SMC achieves quicker convergence to near-zero errors and maintains a smoother trajectory. While classical SMC shows effectiveness, it experiences slight oscillations during stabilization, indicating a less refined response to system dynamics. In contrast, Q-SMC's ability to stabilize rapidly while managing smoother tracking errors underlines its precision and robustness, especially in addressing nonlinearities. These results further confirm the practicality of Q-SMC for applications that require high accuracy and reliability in robotic motion control.

Table 5 reviews the results of the classic and quantum sliding-mode controller performances. The comparison shows that the performances of both controllers are nearly identical. The evaluation of each controller's performance considers key metrics such as steady-state error, response speed, rise time, and settling time, addressing both time- and frequency-domain requirements. Considering all the measured parameters for both controllers when following the same trajectory, the Q-SMC model demonstrated superior performance.

Table 5. Performance of angular position for the different controllers.

Performances	Rising Time (s)	Settling Time (s)	Overshoot (%)	Steady-State Error (%)
		SMC		
Arm 1	0.301	0.42	1.76	0.088
Arm 2	0.297	0.79	2.09	0.076
Arm 3	0.302	0.53	1.97	0.066
		Q-SMC		
Arm 1	0.283	0.383	1.32	0.071
Arm 2	0.276	0.565	1.41	0.055
Arm 3	0.295	0.497	1.25	0.042

The controllers' ability to withstand modeling inaccuracies and unmodeled dynamics can be determined from their performance under disturbance conditions, albeit implicitly. In practical applications, the models used for controller design are usually approximations, making a controller's capability to maintain its performance despite such inaccuracies crucial. A control system's capacity to respond promptly and effectively to anticipated and unforeseen changes, including disturbances, is vital. This is particularly crucial in

dynamic systems, where delays can result in significant errors or instability. The controllers' robustness is evaluated by analyzing their responses to disturbances, particularly when exposed to a sinusoidal disturbance set at 35% of the input signal. The performance response of the controllers under disturbance demonstrates satisfactory and appropriate behavior, as detailed in Table 6.

Table 6. Performance of angular position for the different controllers under disturbance.

Performances	Rising Time (s)	Settling Time (s)	Overshoot (%)	Steady-State Error (%)
		SMC		
Arm 1	0.525	0.579	1.85	0.0999
Arm 2	0.662	0.799	2.03	0.0807
Arm 3	0.515	0.598	1.97	0.0794
		Q-SMC		
Arm 1	0.454	0.691	1.39	0.0785
Arm 2	0.479	0.659	1.48	0.0551
Arm 3	0.463	0.623	1.28	0.0510

Upon reviewing the data in Tables 5 and 6, it is evident that the system's performance with and without disturbances is quite similar. However, in the presence of disturbances, the steady-state error increased to 10.71% for the quantum sliding-mode controller and 12.13% for the classical sliding-mode controller. The overshoot remained unchanged, while the rise times increased by an average of 0.2 s. Similarly, in the scenario without disturbances, the controllers displayed comparable response and reaching times under disturbance conditions for the same trajectory execution and initial conditions.

Both controllers display worthy robustness in the presence of disturbances, maintaining low tracking errors even under substantial disturbances. The analysis of the response plots highlights several required characteristics relevant to the design and assessment of control systems. Notably, the transient response analysis indicates that Q-SMC outperforms SMC by achieving a faster settling time with fewer instabilities, suggesting that the improved damping characteristics of Q-SMC enable it to bring the system to a steady state more efficiently. Additionally, Q-SMC consistently minimizes steady-state error, ensuring greater accuracy in tracking the desired trajectory. This feature is advantageous in precision engineering applications, where performance and implementation complexity are key in real-world implementations such as robotics; the selection or design of controllers must consider these factors. Moreover, despite being often overlooked, energy efficiency is vital, especially in systems that operate continuously or under power constraints. The smoother control action and reduced oscillations observed in Q-SMC suggest it is more energy-efficient than conventional SMC.

Figures 13–16 represent the torque control signals for individual robotic arm joints and the robot's total torque, providing essential insights into the performance and efficiency of the evaluated control strategies under 35% of input signal disturbances. Outcomes show how the controllers, SMC and Q-SMC, manage the dynamic requirements of individual joints under defined trajectories, recalling the smoothness, oscillations, and magnitude of the torque values that indicate the control algorithms' efficiency in handling nonlinearities and disturbances. The total torque across all joints offers a close view of the robotic arm's overall dynamic load and energy exertion, which is crucial for comparing the total effort required by SMC versus Q-SMC to achieve the same task and conditions. These figures are important for performance evaluation, as the torque signals indicate the system's ability to handle nonlinear dynamics, ensure smooth control actions, and resist chattering issues typically associated with classical SMC. The data can further enable energy efficiency analysis by linking torque values directly to the robot's energy consumption, showcasing

how well the control system manages resources. Additionally, the formations accentuate the robustness of Q-SMC under disturbance scenarios, highlighting its capability to preserve stable arrangements without significant oscillations or overshoot.

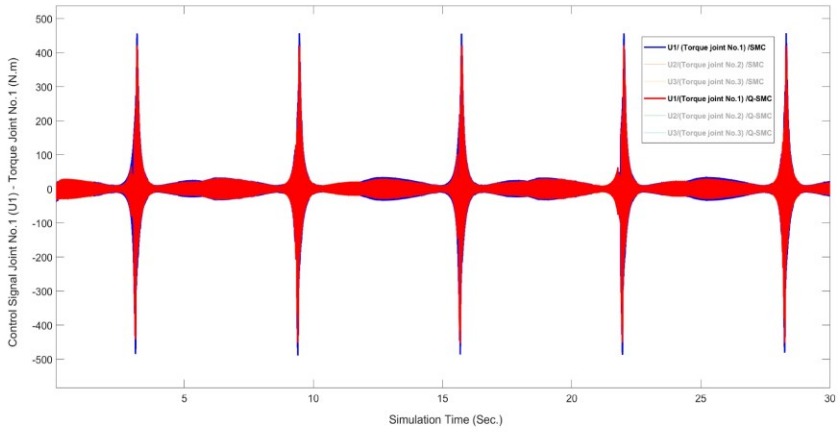

Figure 13. Control signals for joint 1 for SMC and Q-SMC controllers under disturbance.

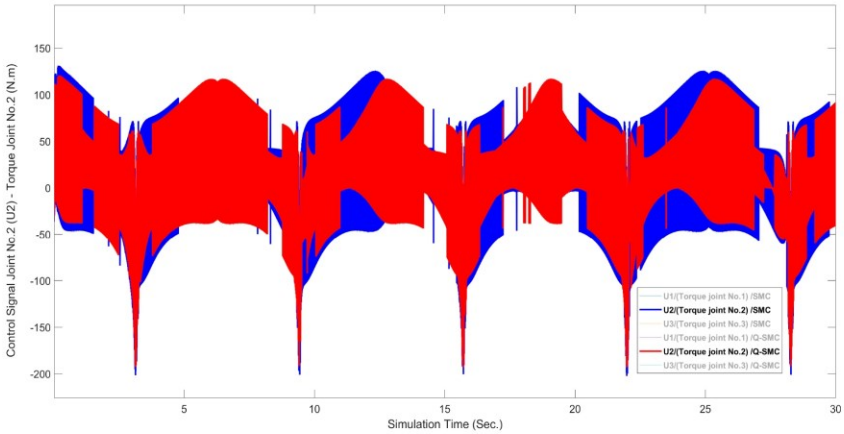

Figure 14. Control signals for joint 2 for SMC and Q-SMC controllers under disturbance.

These advancements improve the precision and stability of the robotic manipulator while minimizing mechanical wear and stress, ultimately extending the operational lifespan of the robotic components. As a result, both approaches are particularly well-suited for enhancing trajectory tracking precision in high-precision industrial applications and complex robotic systems. The findings emphasize the superior robustness and adaptability of Q-SMC, showcasing its potential to excel in high-performance dynamic environments.

In terms of total torque profiles, the Q-SMC consistently outperforms classical SMC by generating more stable and efficient control signals that effectively reject disturbances while maintaining system stability. Collectively, these results demonstrate Q-SMC's enhanced performance in overcoming the limitations of classical SMC, offering improved stability, precision, and efficiency. Its ability to effectively surpass chattering positions Q-SMC

as a promising advancement for robust control in industrial automation and other high-performance sectors in dynamic and disturbance-prone environments.

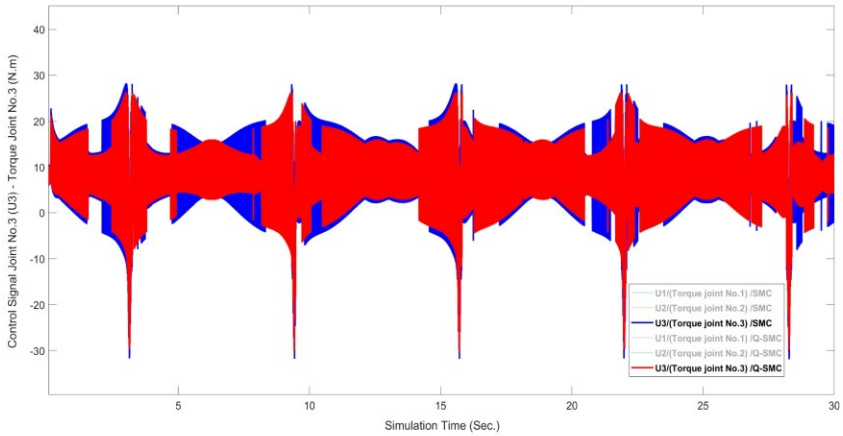

Figure 15. Control signals for joint 3 for SMC and Q-SMC controllers under disturbance.

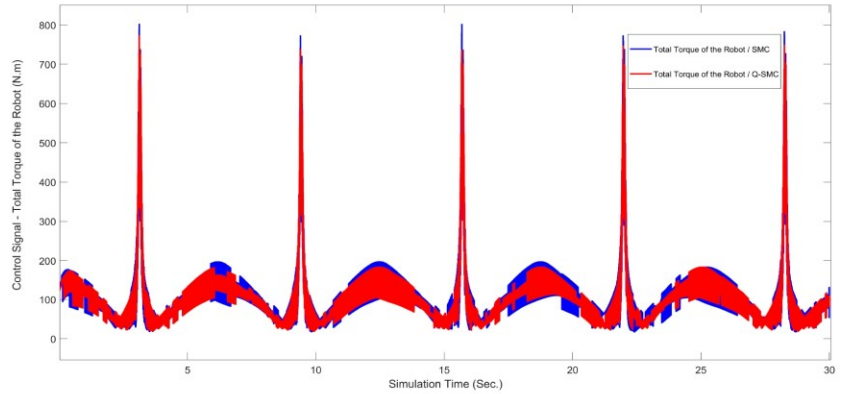

Figure 16. Control signals for the robot under SMC and Q-SMC controllers under disturbance.

Estimating the energy consumption of robotic systems across various controllers is essential for assessing the efficiency and effectiveness of these control strategies. By analyzing the total energy drawn from the robot's torque profile needed to perform identical trajectories, we can gain valuable insights into the effectiveness of each controller in managing the complex dynamics of robotic systems. Energy consumption is directly related to the operational demands placed on the controller, including the forces and torques required for precise movements, especially when faced with disturbances. A control strategy that minimizes energy usage while preserving or enhancing system performance indicates superior efficiency, contributing to the robot's performance and reliability. This approach provides a comprehensive framework for considering the balance between control precision, robustness, and energy efficiency, establishing a clear benchmark for optimizing robotic implementation.

Figure 17 shows the total energy consumption of the robotic system under disturbance conditions operated by both the SMC and Q-SMC based on the robot performance assess-

ment presented in relation (2). The illustration proves that the Q-SMC provides a more stable energy profile and decreases total energy consumption compared to the classical SMC. Particularly, the robot under the Q-SMC controller consumed approximately 3.79% less energy than the classical SMC controller. This reduction is noteworthy as it underlines the quantum approach's capability to enhance energy efficiency while maintaining or even enhancing control accuracy. These findings indicate that the Q-SMC effectively reduced the effects of disturbances and optimized energy usage, leading to a more sustainable and reliable control strategy. This advancement in energy management is required for the long-term operation of robotic systems, as it suggests reduced wear on mechanical components and a more environmentally tolerable approach to robotic control. The results highlight the potential of quantum-inspired control methods in advancing the field of robotics, particularly in applications where energy efficiency is as essential as precision and robustness.

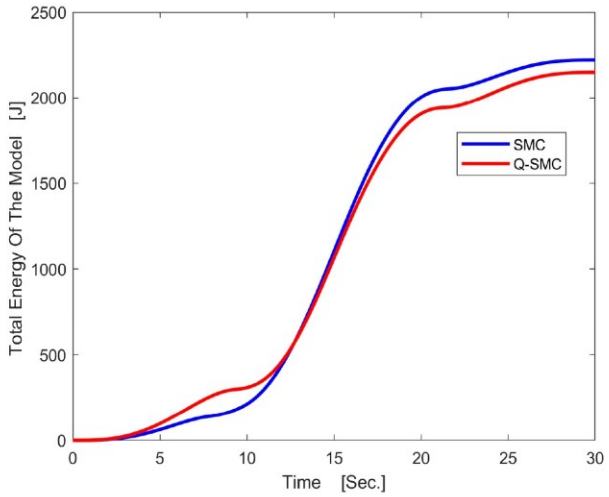

Figure 17. Total energy of the robot run by controllers under disturbance.

Q-SMC has demonstrated superior energy efficiency compared to SMC. This is particularly advantageous for battery-powered robots, allowing longer operational durations without recharging. Furthermore, reducing energy consumption leads to cost savings and a decrease in heat generation in industrial environments, ultimately extending the lifespan of robotic components. This enhanced energy efficiency also promotes environmental sustainability by reducing the dependence on non-renewable energy sources. It plays a significant role in ensuring the overall reliability and longevity of robotic systems, especially in high-precision applications where maintaining mechanical integrity is critical.

In a comprehensive and overarching manner, the principle of superposition facilitates the simultaneous representation of multiple potential system states, thereby increasing the control algorithm's capacity to respond to dynamic changes. Within the Q-SMC framework, superposition is utilized to encode the robotic end-effector's desired and actual states into a unified quantum state. The quantum error computation detailed in Equations (41)–(47) exemplifies this principle, as it allows for concurrent analysis of multiple input trajectories, enabling rapid and precise error evaluation. This comprehensive error assessment mechanism enhances trajectory tracking, promoting faster convergence to the desired path and mitigating transient overshoot. As evidenced in Figures 7–12 and Tables 5 and 6, Q-SMC

outperforms classical SMC, demonstrating superior tracking precision and smoother control transitions, affirming superposition's efficacy in optimizing control dynamics with or without disturbances.

Entanglement establishes a foundational relation between interdependent control variables, such as error signals and their derivatives, ensuring seamless synchronization for dynamic responsiveness. In the Q-SMC framework, this principle is operationalized through the quantum comparator and sign detector presented in Sections 2.6.1–2.6.3, enabling the real-time alignment of quantum error and its derivative. This synchronization ensures that adjustments to the sliding surface accurately mirror dynamic changes in the robotic system, resulting in minimizing control response delays. Accordingly, Q-SMC consistently delivers precise and stable control actions characterized by reduced trajectory deviations and improved steady-state accuracy. The benefits of entanglement's influence are shown in Figures 9–12, where the Q-SMC exhibits robust stability during transient phases, effectively accommodating dynamic variations and reinforcing its advanced adaptability for complex control scenarios.

The computational efficiency of Q-SMC derives from the strategic utilization of quantum gates, including Hadamard and rotation gates, which enable intricate mathematical operations such as error scaling and derivative computation. These gates manipulate the intrinsic parallelism of quantum mechanics, allowing the controller to process high-dimensional data in real-time with minimal computational load. For instance, the quantum subtractor in Equations (36)–(39) adeptly computes trajectory differences, generating precise and responsive control signals. This computational optimization translates directly into the observed smoother control transitions and significantly reduced delays, as illustrated in Figures 13–16, emphasizing the practical benefits of integrating quantum gates into the control framework.

Chattering, a general challenge in classical SMC, is effectively reduced in Q-SMC by involving the exponential reaching law combined with a saturation function. This methodology establishes a boundary layer around the sliding surface and smoothens the transitions in control inputs, thereby minimizing the abrupt variations that cause chattering. This refinement, drawing stimulation from quantum error correction, enhances the system's energy efficiency and preserves the robotic components' mechanical integrity. As depicted in Figures 13–16, the torque profiles produced by Q-SMC exhibit considerably smoother characteristics compared to those generated by classical SMC. Additionally, the system's enhanced energy efficiency is quantified in Figure 17, where Q-SMC displays a 3.79% reduction in total energy consumption, emphasizing its superior performance in energy-sensitive and precision-demanding applications.

4. Conclusions

The present study aimed to evaluate the effectiveness of quantum-inspired sliding-mode control in enhancing the robustness, accuracy, and computational efficiency of control methods for articulated robotic arms, focusing specifically on a six-degree-of-freedom robotic manipulator. By integrating quantum principles into the conventional sliding-mode control framework, the research addressed persistent issues such as chattering, computational complexity, and robustness against disturbances. The methodology involved the development of a comprehensive kinematic and dynamic model of the robotic arm, followed by the implementation and comparison of both classic SMC and Q-SMC through extensive simulations. The findings provide valuable insights into the potential of quantum-inspired approaches in advancing robotic control systems.

The results revealed several significant findings. Most notably, Q-SMC outperformed the classic SMC in key areas such as precision, robustness, and energy efficiency. Q-SMC

effectively mitigated the chattering phenomenon, a common issue in classic SMC, resulting in smoother and more precise control of the robotic arm. Additionally, Q-SMC confirmed quicker response times and lower steady-state errors, showcasing its improved capability to handle the nonlinear dynamics and external disturbances inherent in robotic systems. The torque profile and energy consumption analysis further highlighted the efficiency of Q-SMC, with the robotic arm consuming approximately 3.79% less energy under Q-SMC compared to classic SMC.

These findings have important implications for both theoretical and practical applications in the field of robotics and control systems. Theoretically, this study contributes to the existing body of knowledge by introducing a novel application of quantum principles to sliding-mode control, advancing our understanding of how quantum computing techniques can enhance control system performance. This opens new avenues for the design and optimization of robust controllers. Practically, implementing Q-SMC could lead to technological advancements in robotic systems, particularly in applications requiring high precision and reliability, such as industrial automation, medical robotics, and aerospace. Furthermore, the reduced energy consumption associated with Q-SMC suggests potential benefits for developing more sustainable and efficient robotic systems.

However, it is important to acknowledge certain limitations of the study, primarily due to its execution in a simulated environment. While the models employed were comprehensive, they may not fully capture the complexities of real-world scenarios. Additionally, the application of quantum-inspired algorithms was constrained by current computational capabilities, which may limit the generalizability of the findings to other types of robotic systems or more complex environments. These limitations suggest that further validation through experimental setups is necessary to confirm the effectiveness and relevance of Q-SMC in real-world applications.

Recognizing the crucial importance of experimental validation, we are committed to bridging the gap between simulations and real-world applications. According to the promising simulation results presented in this study, our future work will focus on incorporating other advanced strategies; we prioritized depth over breadth in this initial study, validating Q-SMC for high-precision tasks such as trajectory tracking and energy-efficient path execution under varying loads and disturbances. To ensure comparability, we will replicate simulation conditions and evaluate real-world performance using a hybrid classical–quantum framework, where computationally intensive components are executed on available quantum platforms. Performance metrics include chattering reduction, trajectory tracking accuracy, and energy efficiency. Beyond the specific case study examined here, we aim to expand Q-SMC's applicability to diverse robotic platforms and tasks, including industrial applications like assembly and welding, to explore scalability and versatility.

In conclusion, the findings underscore the robust control capabilities of both conventional sliding-mode control and quantum-inspired sliding-mode control for robotic arms. While SMC is well known for its robustness, the proposed Q-SMC demonstrates superior accuracy, precision, and an enhanced ability to address common challenges like chattering. Q-SMC significantly improves the stability and precision of the control system, particularly in dynamic, disturbance-prone environments. Its smoother control actions contribute to the overall better performance of the robotic arm, resulting in faster response times, reduced steady-state errors, and lower energy consumption, making it a more practical and effective technique for achieving high-performance robotic control.

Author Contributions: M.F. contributed to conceptualization, methodology, investigation, formal analysis, writing and editing of the original draft, and visualization. N.Z. contributed to providing resources, supervision, project administration, formal analysis, review and editing of the original

draft, funding acquisition, and visualization. All authors have read and agreed to the published version of the manuscript.

Funding: This work was financially supported by NSERC Canada.

Data Availability Statement: The data supporting the findings of this study are not publicly available as they are part of ongoing research and future work. Data may be shared upon reasonable request after the completion of future studies.

Conflicts of Interest: The authors declare no conflicts of interest.

Abbreviations

The following abbreviations are used in this manuscript:

SMC	Sliding-Mode Control
QSMC	Quantum Sliding-Mode Control
CAD	Computer-Aided Design
CAO	Computer-Aided Optimization
CAM	Computer-Aided Manufacturing
CCNOT	Controlled-Controlled-Not
DH	Denavit–Hartenberg

References

1. Anh, H.P.H.; Van Kien, C.; Son, N.N.; Nam, N.T. New approach of sliding mode control for nonlinear uncertain pneumatic artificial muscle manipulator enhanced with adaptive fuzzy estimator. *Int. J. Adv. Robot. Syst.* **2018**, *15*, 1729881418773204. [CrossRef]
2. Azeez, M.I.; Abdelhaleem, A.M.M.; Elnaggar, S.; Moustafa, K.A.F.; Atia, K.R. Optimized sliding mode controller for trajectory tracking of flexible joints three-link manipulator with noise in input and output. *Sci. Rep.* **2023**, *13*, 12518. [CrossRef]
3. Ajwad, S.A.; Iqbal, J.; Islam, R.U.; Alsheikhy, A.; Almeshal, A.; Mehmood, A. Optimal and robust control of multi DOF robotic manipulator: Design and hardware realization. *Cybern. Syst.* **2018**, *49*, 77–93. [CrossRef]
4. Liu, Z.; Peng, K.; Han, L.; Guan, S. Modeling and control of robotic manipulators based on artificial neural networks: A review. *Iran. J. Sci. Technol. Trans. Mech. Eng.* **2023**, *47*, 1307–1347.
5. Wang, X.; Wang, D.; Du, M.; Song, K.; Ni, Y.; Li, Y. A two-layer trajectory tracking control scheme of manipulator based on elm-smc for autonomous robotic vehicle. *IEEE Trans. Autom. Sci. Eng.* **2023**, *21*, 2337–2348. [CrossRef]
6. Ravandi, A.K.; Khanmirza, E.; Daneshjou, K. Hybrid force/position control of robotic arms manipulating in uncertain environments based on adaptive fuzzy sliding mode control. *Appl. Soft Comput.* **2018**, *70*, 864–874. [CrossRef]
7. Kumar, R.; Kumar, K. Design and control of a two-link robotic manipulator: A review. *AIP Conf. Proc.* **2021**, *2358*, 050020.
8. Abdelmaksoud, S.I.; Al-Mola, M.H.; Abro, G.E.M.; Asirvadam, V.S. In-Depth Review of Advanced Control Strategies and Cutting-Edge Trends in Robot Manipulators: Analyzing the Latest Developments and Techniques. *IEEE Access* **2024**, *12*, 47672–47701. [CrossRef]
9. Abbas, N.; Abbas, Z.; Zafar, S.; Ahmad, N.; Liu, X.; Khan, S.S.; Foster, E.D.; Larkin, S. Survey of Advanced Nonlinear Control Strategies for UAVs: Integration of Sensors and Hybrid Techniques. *Sensors* **2024**, *24*, 3286. [CrossRef] [PubMed]
10. Zaihidee, F.M.; Mekhilef, S.; Mubin, M. Robust speed control of PMSM using sliding mode control (SMC)—A review. *Energies* **2019**, *12*, 1669. [CrossRef]
11. Fazilat, M.; Zioui, N. The Impact of Simplifications of the Dynamic Model on the Motion of a Six-Jointed Industrial Articulated Robotic Arm Movement. *J. Robot. Control* **2024**, *5*, 173–186. [CrossRef]
12. Vijay, M.; Jena, D. Backstepping terminal sliding mode control of robot manipulator using radial basis functional neural networks. *Comput. Electr. Eng.* **2018**, *67*, 690–707. [CrossRef]
13. Adhikary, N.; Mahanta, C. Sliding mode control of position commanded robot manipulators. *Control Eng. Pract.* **2018**, *81*, 183–198. [CrossRef]
14. Norsahperi, N.; Danapalasingam, K. An improved optimal integral sliding mode control for uncertain robotic manipulators with reduced tracking error, chattering, and energy consumption. *Mech. Syst. Signal Process.* **2020**, *142*, 106747. [CrossRef]
15. Truong, T.N.; Vo, A.T.; Kang, H.-J. A backstepping global fast terminal sliding mode control for trajectory tracking control of industrial robotic manipulators. *IEEE Access* **2021**, *9*, 31921–31931. [CrossRef]
16. Baek, J.; Kwon, W.; Kang, C. A new widely and stably adaptive sliding-mode control with nonsingular terminal sliding variable for robot manipulators. *IEEE Access* **2020**, *8*, 43443–43454. [CrossRef]

17. Baek, J.; Kwon, W. Practical adaptive sliding-mode control approach for precise tracking of robot manipulators. *Appl. Sci.* **2020**, *10*, 2909. [CrossRef]
18. Feng, Y.; Zhou, M.; Yu, X.; Han, F. Full-order sliding-mode control of rigid robotic manipulators. *Asian J. Control* **2019**, *21*, 1228–1236. [CrossRef]
19. Zhai, J.; Li, Z. Fast-exponential sliding mode control of robotic manipulator with super-twisting method. *IEEE Trans. Circuits Syst. II Express Briefs* **2021**, *69*, 489–493. [CrossRef]
20. Soriano, L.A.; Rubio, J.d.J.; Orozco, E.; Cordova, D.A.; Ochoa, G.; Balcazar, R.; Cruz, D.R.; Meda-Campaña, J.A.; Zacarias, A.; Gutierrez, G.J. Optimization of sliding mode control to save energy in a SCARA robot. *Mathematics* **2021**, *9*, 3160. [CrossRef]
21. Yen, V.T.; Nan, W.Y.; Van Cuong, P. Recurrent fuzzy wavelet neural networks based on robust adaptive sliding mode control for industrial robot manipulators. *Neural Comput. Appl.* **2019**, *31*, 6945–6958. [CrossRef]
22. Jung, S. Improvement of tracking control of a sliding mode controller for robot manipulators by a neural network. *Int. J. Control Autom. Syst.* **2018**, *16*, 937–943. [CrossRef]
23. Gambhire, S.J.; Kishore, D.R.; Londhe, P.S.; Pawar, S.N. Review of sliding mode based control techniques for control system applications. *Int. J. Dyn. Control* **2021**, *9*, 363–378. [CrossRef]
24. Yu, X.; Feng, Y.; Man, Z. Terminal sliding mode control—An overview. *IEEE Open J. Ind. Electron. Soc.* **2020**, *2*, 36–52. [CrossRef]
25. Yin, F.; Wen, C.; Ji, Q.; Zhang, H.; Shao, H. A compensation sliding mode control for machining robotic manipulators based on nonlinear disturbance observer. *Trans. Inst. Meas. Control* **2022**, *44*, 2336–2349. [CrossRef]
26. Gan, W.; Zhu, D.; Ji, D. QPSO-model predictive control-based approach to dynamic trajectory tracking control for unmanned underwater vehicles. *Ocean Eng.* **2018**, *158*, 208–220. [CrossRef]
27. Fazilat, M.; Zioui, N.; St-Arnaud, J. A novel quantum model of forward kinematics based on quaternion/Pauli gate equivalence: Application to a six-jointed industrial robotic arm. *Results Eng.* **2022**, *14*, 100402. [CrossRef]
28. Zioui, N.; Mahmoudi, A.; Tadjine, M. Representing quantum spins in different coordinate systems for modelling rigid body orientation. *Karbala Int. J. Mod. Sci.* **2023**, *9*, 11. [CrossRef]
29. Boudjoghra, M.E.A.; Daimellah, S.A.S.; Zioui, N.; Mahmoudi, Y.; Tadjine, M. State-Domain Equations and Their Quantum Computing Solution Based HHL Algorithm. *Math. Model. Eng. Probl.* **2022**, *9*, 879–886. [CrossRef]
30. Singh, R.; Sloth, C. Characterizing Manipulator Motion Using an Evolving Type 2 Quantum Fuzzy Neural Network. In Proceedings of the 2024 IEEE/SICE International Symposium on System Integration (SII), Ha Long, Vietnam, 8–11 January 2024.
31. Zheng, X.; Su, X. Sliding mode control of electro-hydraulic servo system based on optimization of quantum particle swarm algorithm. *Machines* **2021**, *9*, 283. [CrossRef]
32. Qu, Q.; Chen, F.; Jiang, B.; Tao, G. Integral sliding mode control for helicopter via disturbance observer and quantum information technique. *Math. Probl. Eng.* **2015**, *2015*, 938246. [CrossRef]
33. Zioui, N.; Mahmoudi, Y.; Mahmoudi, A.; Tadjine, M.; Bentouba, S. A novel quantum-computing-based quaternions model for a robotic arm position. *Int. J. Comput. Intell. Control* **2021**, *13*, 71–77.
34. Sivak, V.V.; Eickbusch, A.; Liu, H.; Royer, B.; Tsioutsios, I.; Devoret, M.H. Model-free quantum control with reinforcement learning. *Phys. Rev. X* **2022**, *12*, 011059. [CrossRef]
35. Petschnigg, C.; Brandstötter, M.; Pichler, H.; Hofbaur, M.; Dieber, B. Quantum computation in robotic science and applications. In Proceedings of the 2019 International Conference on Robotics and Automation (ICRA), Montreal, QC, Canada, 20–24 May 2019.
36. Niu, M.Y.; Boixo, S.; Smelyanskiy, V.N.; Neven, H. Universal quantum control through deep reinforcement learning. *Npj Quantum Inf.* **2019**, *5*, 33. [CrossRef]
37. Reshetnikov, A.; Ulyanov, S. Quantum Algorithm of Imperfect KB Self-organization. Pt II: Robotic Control with Remote Knowledge Base Exchange. *Artif. Intell. Adv.* **2021**, *3*, 44–70. [CrossRef]
38. Tavanaei-Sereshki, Z.; Ramezani-Al, M.R. Quantum genetic sliding mode controller design for depth control of an underwater vehicle. *Meas. Control* **2018**, *51*, 336–348. [CrossRef]
39. Xi, R.-D.; Xiao, X.; Ma, T.-N.; Yang, Z.-X. Adaptive sliding mode disturbance observer based robust control for robot manipulators towards assembly assistance. *IEEE Robot. Autom. Lett.* **2022**, *7*, 6139–6146. [CrossRef]
40. Haviland, J.; Corke, P. Manipulator Differential Kinematics: Part I: Kinematics, Velocity, and Applications. *IEEE Robot. Autom. Mag.* **2023**, *31*, 149–158. [CrossRef]
41. Zaare, S.; Soltanpour, M.R.; Moattari, M. Adaptive sliding mode control of n flexible-joint robot manipulators in the presence of structured and unstructured uncertainties. *Multibody Syst. Dyn.* **2019**, *47*, 397–434. [CrossRef]
42. Ranjbar, E.; Suratgar, A.A.; Menhaj, M.B.; Prasad, M. Design of a fuzzy adaptive sliding mode control system for MEMS tunable capacitors in voltage reference applications. *IEEE Trans. Fuzzy Syst.* **2021**, *30*, 1838–1852. [CrossRef]
43. Wu, L.; Liu, J.; Vazquez, S.; Mazumder, S.K. Sliding mode control in power converters and drives: A review. *IEEE/CAA J. Autom. Sin.* **2021**, *9*, 392–406. [CrossRef]
44. Zhao, Y.; Wang, J.; Cao, G.; Yuan, Y.; Yao, X.; Qi, L. Intelligent control of multilegged robot smooth motion: A review. *IEEE Access* **2023**, *11*, 86645–86685. [CrossRef]

45. Costa-Castello, R.; Carrero, N.; Dormido, S.; Fossas, E. Teaching, analyzing, designing and interactively simulating sliding mode control. *IEEE Access* **2018**, *6*, 16783–16794. [CrossRef]
46. Marques, F.; Flores, P.; Claro, J.C.P.; Lankarani, H.M. A survey and comparison of several friction force models for dynamic analysis of multibody mechanical systems. *Nonlinear Dyn.* **2016**, *86*, 1407–1443. [CrossRef]
47. Truong, T.N.; Vo, A.T.; Kang, H.-J. Neural network-based sliding mode controllers applied to robot manipulators: A review. *Neurocomputing* **2023**, *562*, 126896. [CrossRef]
48. Sciavicco, L.; Siciliano, B. *Modelling and Control of Robot Manipulators*; Springer Science & Business Media: Berlin/Heidelberg, Germany, 2012.
49. Feraoun, H.; Fazilat, M.; Dermouche, R.; Bentouba, S.; Tadjine, M.; Zioui, N. Quantum maximum power point tracking (QMPPT) for optimal solar energy extraction. *Syst. Soft Comput.* **2024**, *6*, 200118. [CrossRef]
50. Reda, D.; Talaoubrid, A.; Fazilat, M.; Zioui, N.; Tadjine, M. A quantum direct torque control method for permanent magnet synchronous machines. *Comput. Electr. Eng.* **2025**, *122*, 109994. [CrossRef]
51. Ahmadpour, S.-S.; Noorallahzadeh, M.; Al-Khafaji, H.M.R.; Darbandi, M.; Navimipour, N.J.; Javadi, B.; Ain, N.U.; Hosseinzadeh, M.; Yalcin, S. A new energy-efficient design for quantum-based multiplier for nano-scale devices in internet of things. *Comput. Electr. Eng.* **2024**, *117*, 109263. [CrossRef]
52. Ahmadpour, S.-S.; Navimipour, N.J. A new nano-design of 16-bit carry look-ahead adder based on quantum technology. *Phys. Scr.* **2023**, *98*, 125108. [CrossRef]
53. Orts, F.; Ortega, G.; Cucura, A.C.; Filatovas, E.; Garzón, E.M. Optimal fault-tolerant quantum comparators for image binarization. *J. Supercomput.* **2021**, *77*, 8433–8444. [CrossRef]
54. Yuan, Y.; Wang, C.; Wang, B.; Chen, Z.-Y.; Dou, M.-H.; Wu, Y.-C.; Guo, G.-P. An improved QFT-based quantum comparator and extended modular arithmetic using one ancilla qubit. *New J. Phys.* **2023**, *25*, 103011. [CrossRef]
55. Ahmadpour, S.-S.; Navimipour, N.J.; Keresteciogluu, F. A new nano-design of an efficient synchronous full-adder/subtractor based on quantum-dots. *Eurasia Proc. Sci. Technol. Eng. Math.* **2023**, *22*, 81–86. [CrossRef]
56. IBM Quantum Composer. 2024. Available online: https://quantum.ibm.com/composer/files/new (accessed on 26 January 2025).

6.2.2 Summary of the Results Analysis

Both the Classical Sliding Mode Control and Quantum Sliding Mode Control algorithms were implemented in Simulink for simulation and comparative analysis. The model architecture for each controller adheres to the proposed control frameworks, with an identical circular trajectory embedded within the simulation environment. To ensure a fair comparison, both control strategies were tested under identical initial conditions and reference signals. Figure 6-1 and Figure 6-2 illustrate the Simulink models used for classical SMC and Q-SMC.

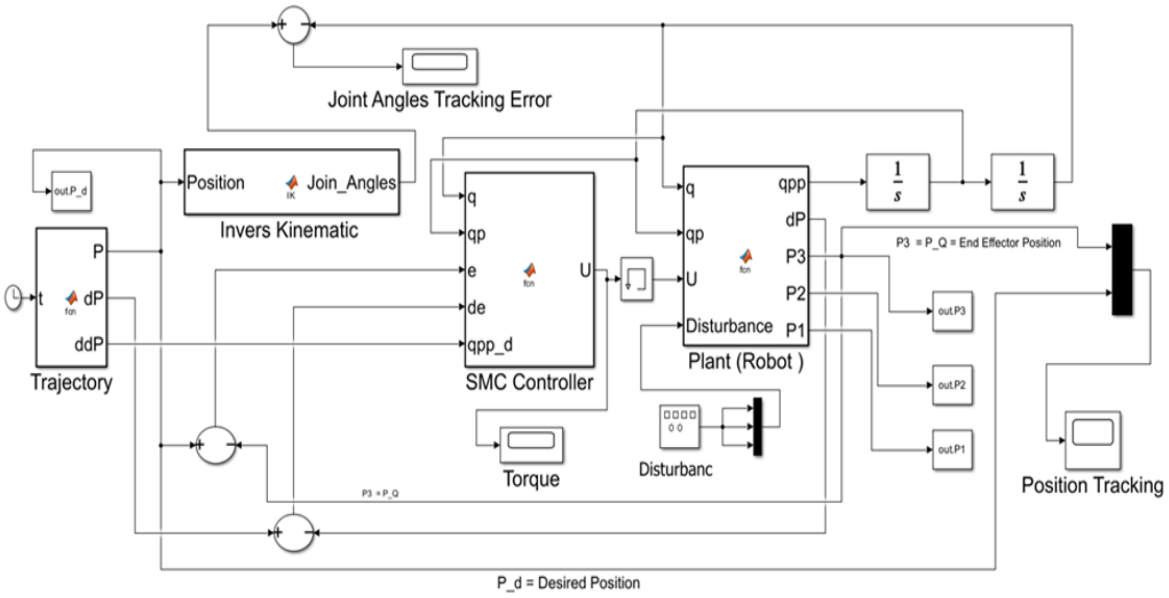

Figure 6-1 Simulink Trajectory Model of the Robot Manipulator for SMC.

The trajectory executed under both controllers is visualized in Figure 6-3. While both controllers achieve the desired motion, Q-SMC demonstrates superior tracking accuracy with closer alignment to the predefined path.

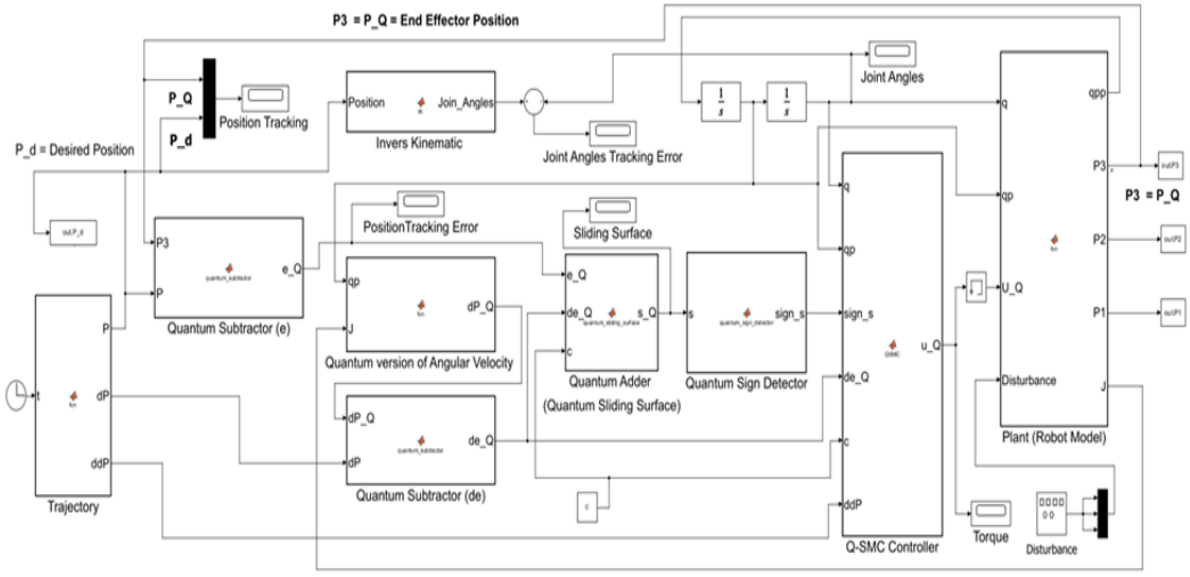

Figure 6-2 Simulink Trajectory Model of the Robot Manipulator for Q-SMC.

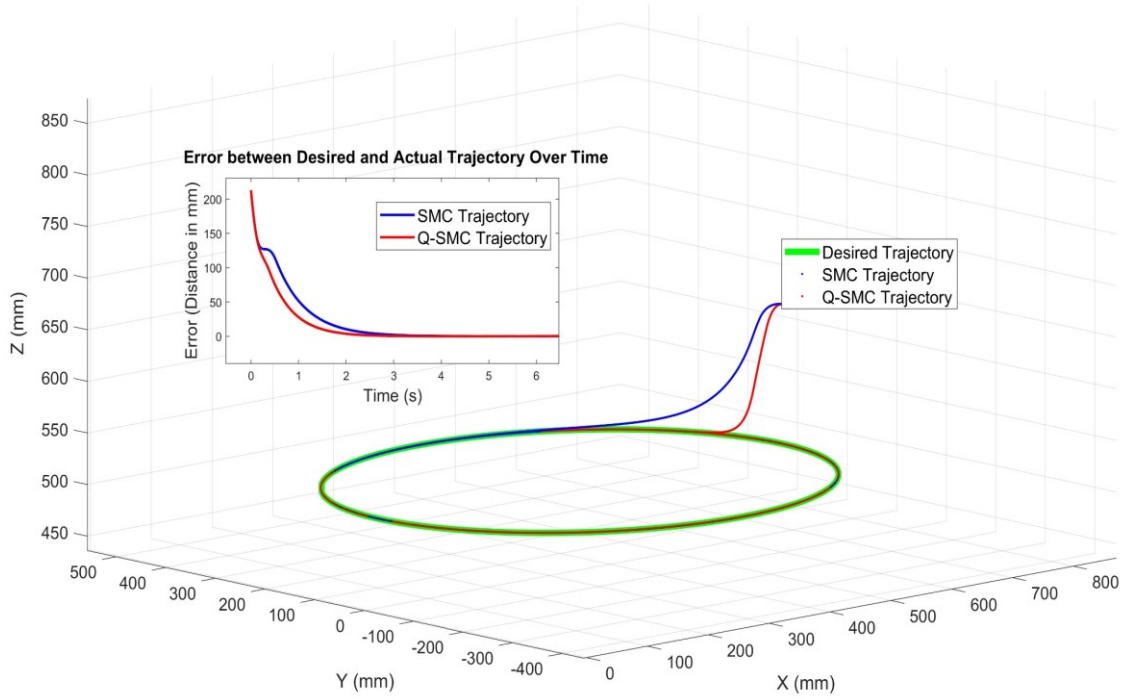

Figure 6-3 Projection of X-Y-Z Trajectory of Robot Manipulator executed by controllers.

Tracking error analysis in Figure 6-4, Figure 6-5, and Figure 6-6 further underscores Q-SMC's superior control characteristics. Q-SMC achieves significantly lower steady-state errors and more stable error convergence, even in the presence of system nonlinearities and uncertainties. The reduced oscillations in Q-SMC reflect its effectiveness in minimizing chattering, a known issue in classical SMC.

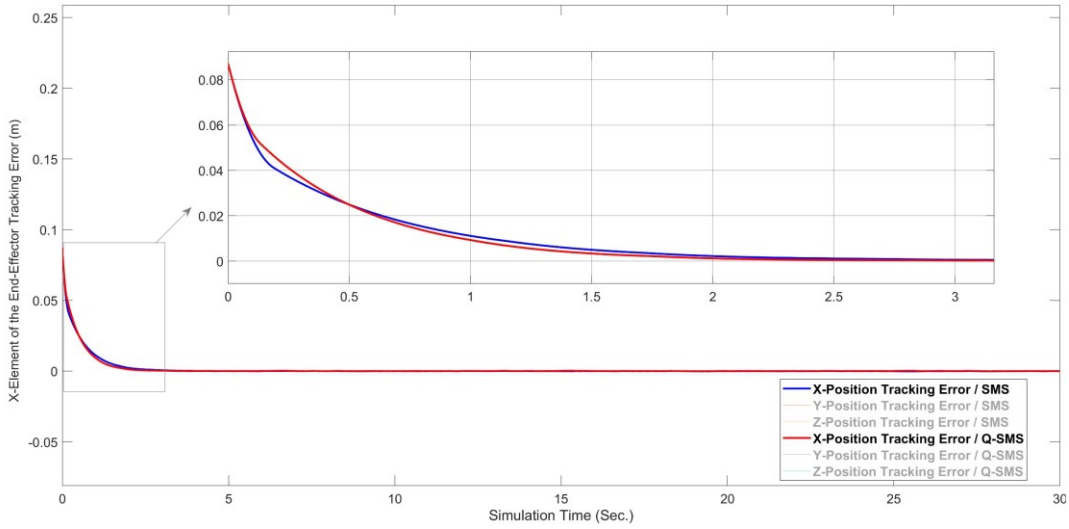

Figure 6-4 Comparison of Tracking Error (X-Component) for the Robot End-Effector.

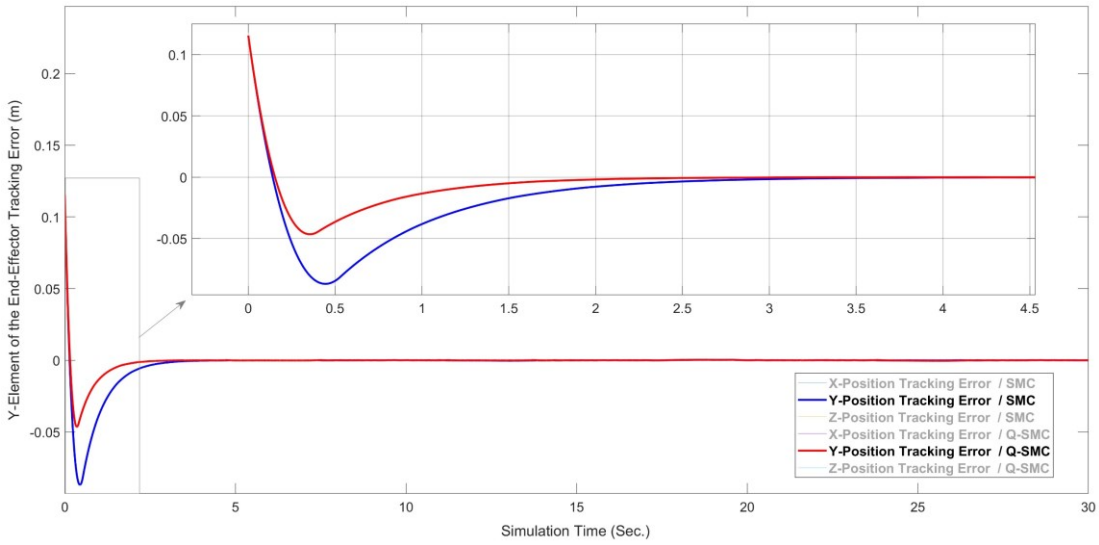

Figure 6-5 Comparison of Tracking Error (Y- Component) for the Robot End-Effector.

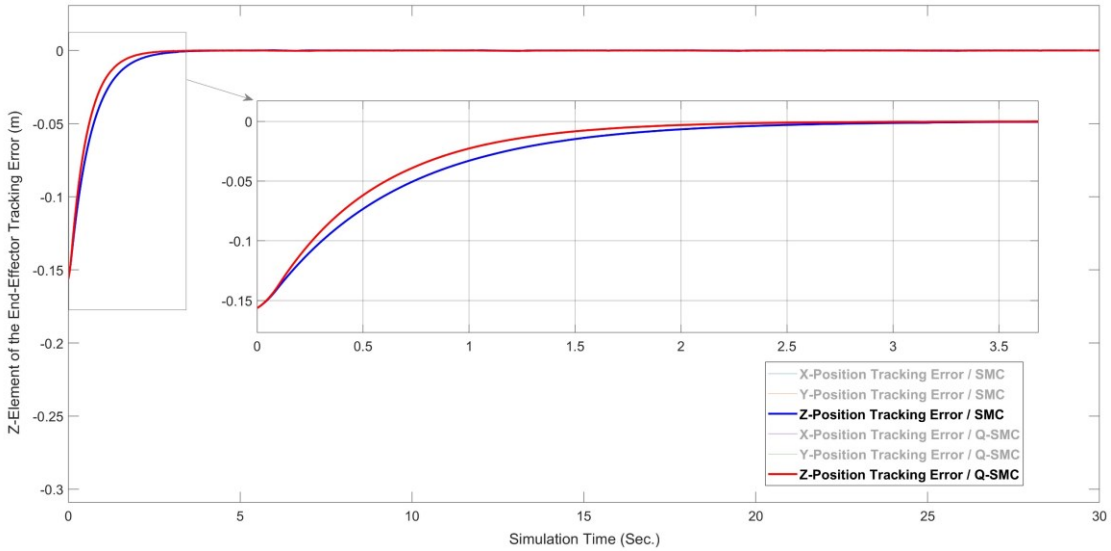

Figure 6-6 Comparison of Tracking Error (Z- Component) for the Robot End-Effector.

Performance metrics for both control strategies are summarized in Table 6-2. Across all three robotic joints, Q-SMC yields shorter rise and settling times, lower overshoot, and decreased steady-state error.

Table 6-2 Performance of angular position for the different controllers.

Performances	Rising time (sec)	Settling time (sec)	Overshoot (%)	Steady state error (%)
Arm 1 Arm 2 Arm 3	**SMC**			
	0.301	0.42	1.76	0.088
	0.297	0.79	2.09	0.076
	0.302	0.53	1.97	0.066
Arm 1 Arm 2 Arm 3	**Q-SMC**			
	0.283	0.383	1.32	0.071
	0.276	0.565	1.41	0.055
	0.295	0.497	1.25	0.042

Under disturbed conditions (35% sinusoidal disturbance), the performance remains robust, as detailed in Table 6-3. Q-SMC maintains tracking performance with only marginal degradation, establishing its disturbance rejection capability.

Table 6-3 Performance of angular position for the different controllers under disturbance.

Performances	Rising time (sec)	Settling time (sec)	Overshoot (%)	Steady state error (%)
Arm 1 Arm 2 Arm 3	**SMC**			
	0.525	0.579	1.85	0.0999
	0.662	0.799	2.03	0.0807
	0.515	0.598	1.97	0.0794
Arm 1 Arm 2 Arm 3	**Q-SMC**			
	0.454	0.691	1.39	0.0785
	0.479	0.659	1.48	0.0551
	0.463	0.623	1.28	0.0510

Figure 6-7 display torque control signals for the total torque applied under disturbance. Q-SMC generates smoother, less oscillatory torque profiles, reducing mechanical stress and energy spikes. These smoother profiles contribute directly to energy efficiency improvements.

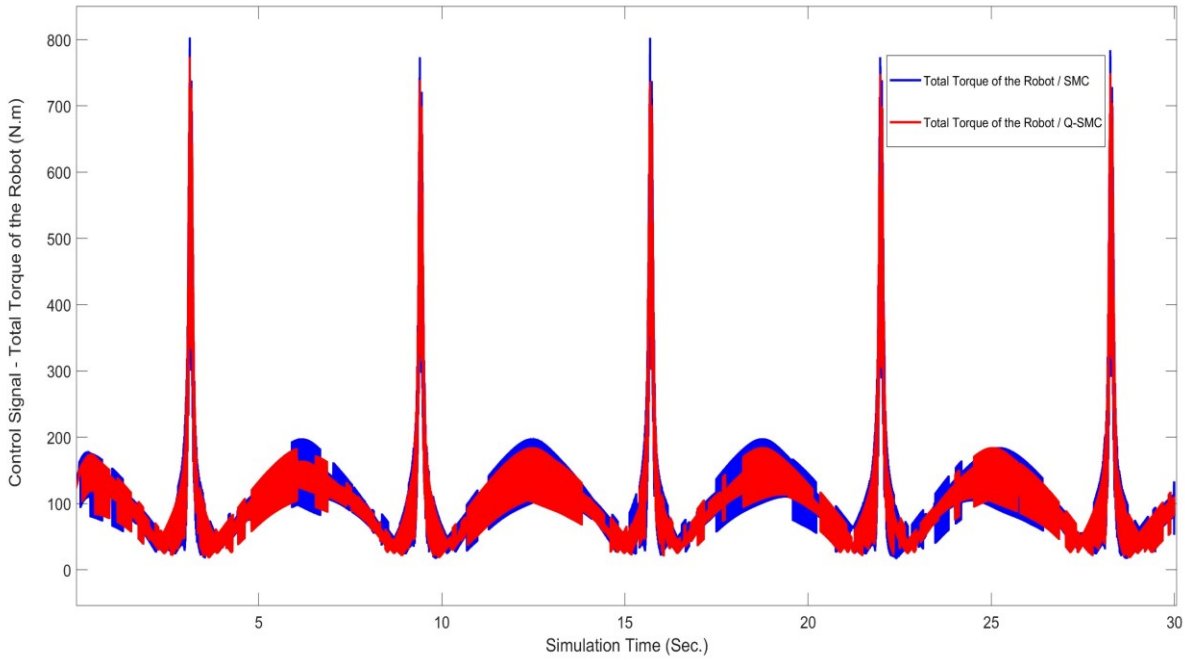

Figure 6-7 Control Signals for the Robot under SMC and Q-SMC Controllers under disturbance.

Figure 6-8 quantifies energy efficiency, showing a 3.79% reduction in total energy consumption using Q-SMC compared to classical SMC. This efficiency is linked to Q-SMC's reduced chattering and smoother control dynamics. Notably, the total energy savings align with improved performance metrics, confirming the dual benefit of precision and efficiency.

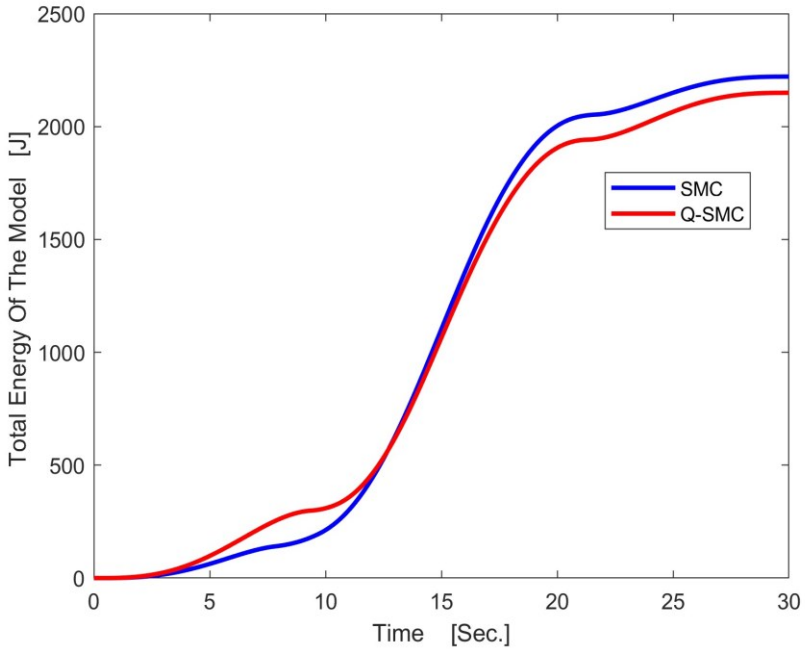

Figure 6-8 Energy Consumption for the Controllers.

6.3 Concluding Remarks

Investigate the potential of Quantum-Inspired Sliding Mode Control to enhance the precision, robustness, and energy efficiency of articulated robotic arm control, with a straightforward focus on a six-degree-of-freedom ABB IRB 140 industrial manipulator, as addressed in the current research. Building upon the foundation of classical Sliding Mode Control, Q-SMC integrates key quantum computing principles into the control algorithm to

manage the limitations of conventional methods, particularly chattering, computational complexity, and response delays under disturbances.

A comprehensive modeling framework was developed, containing kinematic and dynamic modeling derived from CAD-based inertia and mass data, and implemented within a Simulink simulation environment. Both SMC and Q-SMC were applied to identical trajectory tracking tasks under nominal and disturbed conditions. The comparative analysis demonstrated that Q-SMC delivers notable advancements across multiple performance metrics. These include faster rise and settling times, reduced overshoot, and lower steady-state errors. In addition, Q-SMC achieved a notable reduction in chattering and smoother torque profiles, which are crucial for extending the lifespan and reliability of robotic components.

Energy consumption analysis further validated Q-SMC's advantages, revealing an approximate 3.79% reduction in total energy usage compared to classical SMC. This is particularly relevant for applications where energy efficiency and sustainability are critical. The enhanced computational efficiency and precision of Q-SMC underscore its suitability for real-time, high-performance robotic control systems operating in dynamic or uncertain environments.

While the current findings are based on simulated environments, they provide strong support for the feasibility of Q-SMC in advanced industrial automation. Future research will focus on experimental validation using physical robotic platforms, the integration of Q-SMC with hybrid classical-quantum systems, and formal stability analysis using Lyapunov theory extended to incorporate quantum principles.

The comparison in this chapter is intentionally framed against the direct control counterpart, namely classical Sliding Mode Control, so that the influence of the quantum-inspired switching strategy can be examined under the same robot model, trajectory, and disturbance conditions; broader benchmarking against other robust control variants is an important extension for future investigation.

In conclusion, the proposed Quantum-Inspired Sliding Mode Control (Q-SMC) constitutes a substantial advancement in the control of industrial robotic manipulators subject to nonlinear dynamics, model uncertainties, and external disturbances. By integrating the established robustness of classical Sliding Mode Control with quantum-inspired computational principles, this approach offers a flexible and intelligent control structure that enhances trajectory tracking accuracy, reduces chattering, and lowers energy consumption. Q-SMC serves not only as a theoretical extension of conventional robust control but also as a practical framework for developing scalable and adaptive robotic systems that address the increasing demands of modern industrial automation. Its capacity to retain the core strengths of classical control while introducing improved decision-making and efficiency underscores its significance for next-generation intelligent robotic platforms. Building upon this control-layer foundation, the subsequent chapter extends the integration of quantum principles to the actuator and power-conversion levels, where the quality of electrical drive signals directly influences system efficiency, operational smoothness, and harmonic performance. In this context, a Quantum Sinusoidal Pulse Width Modulation framework is presented as a complementary extension of the research, aiming to further enhance power quality, minimize harmonic distortion, and improve the overall energy efficiency of industrial motor-drive systems.

Chapter 7 - Quantum Sinusoidal Pulse Width Modulation (QSPWM) for Reducing Total Harmonic Distortion (THD) in Three-Phase Motor Drive Control

7.1 Chapter Overview

The current chapter continues the thesis by transitioning from quantum-inspired control to quantum-enhanced modulation of power electronics. Building on the Quantum-Inspired Sliding Mode Control (Q-SMC) introduced in Chapter 6, the focus shifts from the feedback control layer to the inverter modulation layer. In this layer, the switching patterns play a crucial role in determining the spectral quality, electromagnetic compatibility, and acoustic behavior of three-phase motor drives.

Classical Sinusoidal Pulse Width Modulation (SPWM) continues to be the industry standard for voltage-source inverters due to its simplicity and satisfactory time-domain performance. However, its deterministic switching leads to concentrated harmonic clusters that increase Total Harmonic Distortion (THD) and Electromagnetic Interference (EMI), often necessitating cumbersome filters and resulting in torque ripple in precision actuation systems. To address these limitations, this chapter presents Quantum Sinusoidal PWM (QSPWM), a quantum-inspired modulation strategy that utilizes probabilistic switching through quantum logic gates, including Hadamard, rotation, and Toffoli operations. By randomizing switching decisions in a controlled manner, QSPWM effectively disperses

spectral energy, reduces harmonic peaks, and produces smoother voltage waveforms with enhanced spectral purity.

Two main objectives guide this chapter. First, it establishes a modulation-layer counterpart to Chapter 6's control-layer design, thereby creating a unified quantum-enhanced architecture that couples robust trajectory control with low-distortion actuation. Second, it quantitatively compares SPWM and QSPWM using a three-phase Permanent-Magnet Synchronous Motor (PMSM) benchmark, evaluated in both the time and frequency domains. Simulation results show that QSPWM reduces THD from 60.21% to 38.79% (≈ 35.6% improvement) while maintaining nearly identical transient-response accuracy.

These outcomes show that integrating QSPWM can significantly reduce harmonic distortion, lower EMI, and minimize acoustic noise factors, all of which are critical for high-precision robotic manipulators. The following sections describe the methodology, simulation framework, and comparative analyses that led to these findings.

7.2 Paper 6: Quantum Sinusoidal Pulse Width Modulation (QSPWM) to enhance Total Harmonic Distortion (THD) of three phase motors drives control.

Authors: Mehdi Fazilat, Oumar Kone, Nadjet Zioui, Reda Dermouche, Mohamed Tadjine.

Journal: Journal of Electronic Science and Technology.

Submission date and status: 31/Oct/2025 - Under Review.

7.2.1 Methodology

The proposed Quantum Sinusoidal Pulse Width Modulation (QSPWM) method is developed as a quantum-inspired extension of the classical Sinusoidal PWM (SPWM). The principal goal is to replace deterministic switching decisions with structured quantum-probabilistic operations governed by quantum logic gates, thereby redistributing the harmonic spectrum of inverter voltages and reducing Total Harmonic Distortion (THD).

In a conventional three-phase voltage-source inverter, each leg's switch pair is driven by comparing a sinusoidal reference v_{ref} with a high-frequency triangular carrier v_{car}. The instantaneous gate signal $S(t)$ is obtained as:

$$S(t) = \begin{cases} 1, & if\, v_{ref}(t) > v_{car}(t) \\ 0, & otherwise \end{cases} \tag{7-1}$$

Where, f_c is the carrier frequency and the line-to-line output voltage of a balanced three-phase inverter describe as:

$$v_{ab}(t) = V_{dc}[s_a(t) - s_b(t)] \tag{7-2}$$

Although simple and effective, this deterministic comparison generates discrete sidebands at multiples of $f_{c,}$ concentrating harmonic energy near the carrier frequency and leading to high THD and electromagnetic interference (EMI). When the reference signal is greater than the carrier, the switch is on; otherwise, it is off. The output voltage amplitude is controlled by the magnitude of the sine wave and the output frequency corresponds to the sine wave frequency. SPWM is a widely used technique for its simplicity, ease of

implementation, and sufficient performance in many AC machines related applications, particularly when the switching frequency is high enough to produce a smooth sinusoidal output after filtering. Figure 7-1 illustrated the principle of the SPWM technique.

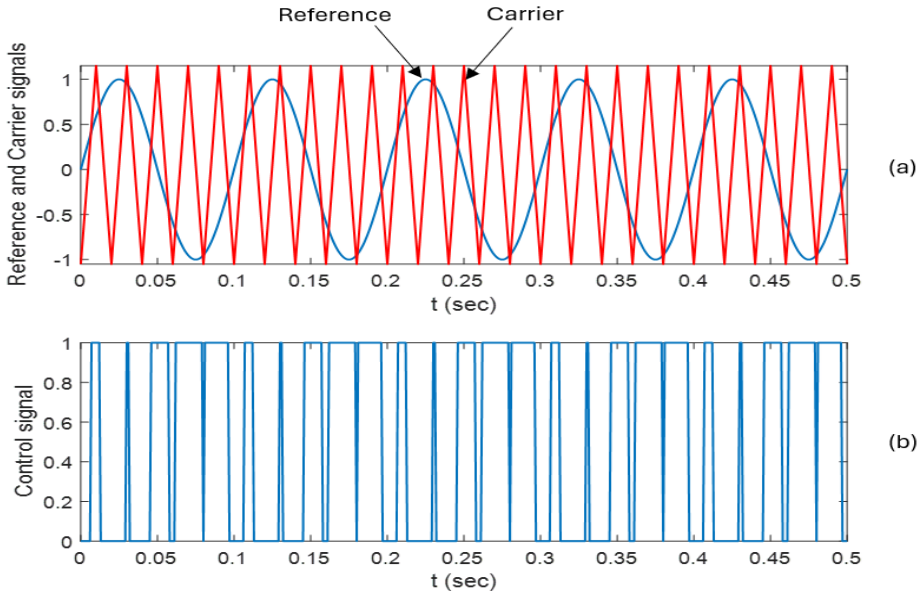

Figure 7-1 Sinusoidal PWM: (a) Reference and carrier signals comparison (b) Gate pulse signals.

QSPWM introduces a quantum decision layer that probabilistically selects switching states. Each modulation instant is represented by a quantum state,

$$|\psi\rangle = \alpha|0\rangle + \beta|1\rangle, |\alpha|^2 + |\beta|^2 = 1 \tag{7-3}$$

where $|0\rangle$ and $|1\rangle$ correspond to the OFF and ON states of a transistor leg. A rotation gate $R_y(\theta)$ encodes the normalized difference between v_m and v_c :

$$R_y(\theta) = \begin{bmatrix} \cos\left(\frac{\theta}{2}\right) & -\sin\left(\frac{\theta}{2}\right) \\ \sin\left(\frac{\theta}{2}\right) & \cos\left(\frac{\theta}{2}\right) \end{bmatrix}, \qquad \theta = k\frac{v_m(t) - v_c(t)}{V_c}, \tag{7-4}$$

where k is a sensitivity gain, and the resulting probabilities presented as:

$$P_{\text{on}} = \left|\sin\left(\frac{\theta}{2}\right)\right|^2, P_{\text{off}} = \left|\cos\left(\frac{\theta}{2}\right)\right|^2 \tag{7-5}$$

which govern a stochastic switching event realized through measurement or pseudo-random sampling on classical hardware. This controlled randomness spreads harmonic energy and weakens discrete spectral spikes, thereby reducing periodic distortion.

To implement $R_y(\theta)$ in quantum form, a Quantum Subtractor circuit based on Toffoli and CNOT gates performs binary subtraction on encoded amplitudes. The sign of the result is then determined by a Quantum Sign Detector employing a single ancilla qubit: if the most significant qubit collapses to $|1\rangle$, the sign is positive; otherwise, negative. Figure 7-2 illustrates the overall architecture of these two modules, showing how the quantum subtractor computes the difference between the encoded reference and carrier signals, while the sign detector determines the output switching state based on the resulting phase rotation.

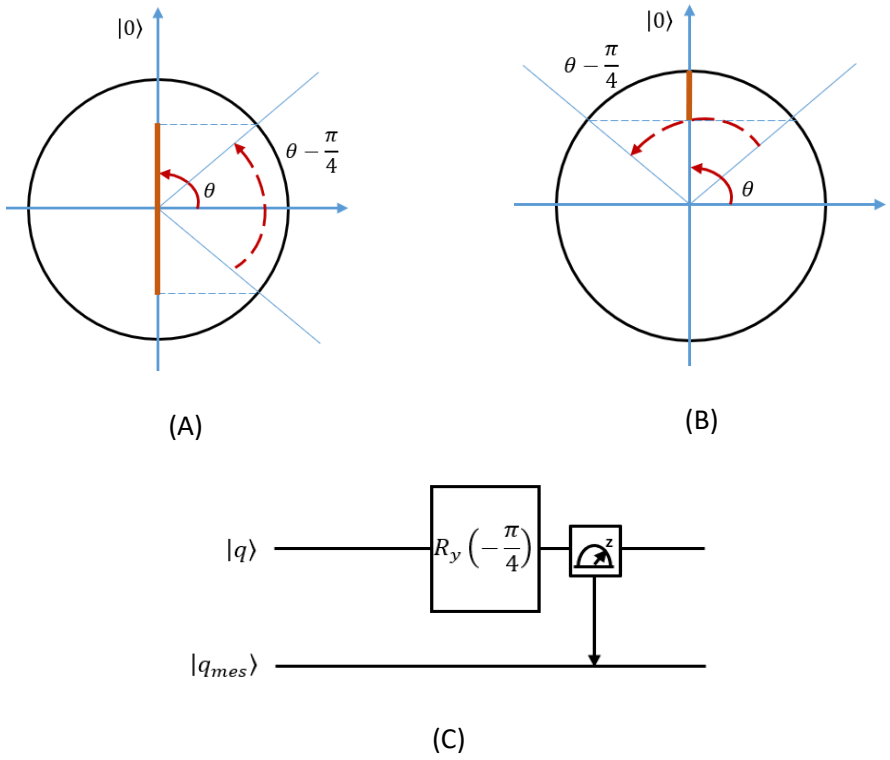

Figure 7-2 Quantum Subtractor and Sign Detector Architecture.

The proposed logic replaces the comparator block of classical SPWM within the three-phase inverter model. Each leg's modulation decision is obtained from the quantum measurement result, producing six stochastic gate signals s_a, s_b, s_c for the upper switches and their complements for the lower ones. The inverter feeds a Permanent-Magnet Synchronous Motor (PMSM) modeled by,

$$\begin{aligned}\frac{di_d}{dt} &= \frac{1}{L_d}\left[v_d - R_s i_d + \omega_e L_q i_q\right] \\ \frac{di_q}{dt} &= \frac{1}{L_q}\left[v_q - R_s i_q - \omega_e\left(L_d i_d + \lambda_f\right)\right] \\ T_e &= \frac{3}{2}p\left(\lambda_f i_q + \left(L_d - L_q\right) i_d i_q\right)\end{aligned} \tag{7-6}$$

where i_d, i_q are dq axis currents, L_d, L_q are inductances, R_s is the stator resistance, ω_e is the electrical speed, and p is the number of pole pairs. The mechanical subsystem follows:

$$P_{\text{on}} = \left|\sin\left(\frac{\theta}{2}\right)\right|^2, P_{\text{off}} = \left|\cos\left(\frac{\theta}{2}\right)\right|^2 \tag{7-5}$$

The inverter drives a Permanent-Magnet Synchronous Motor (PMSM) whose dynamics are described in the dq reference frame as

$$\begin{cases} v_d = R_s i_d + L_d \dfrac{di_d}{dt} - \omega_e L_q i_q, \\ v_q = R_s i_q + L_q \dfrac{di_q}{dt} + \omega_e \left(L_d i_d + \psi_f\right), \end{cases} \tag{7-6}$$

where i_d, i_q are dq-axis currents, L_d, L_q the corresponding inductances, R_s the stator resistance, ω_e the electrical angular velocity, and ψ_f the magnet flux linkage. The mechanical subsystem follows:

$$J \frac{d\omega_m}{dt} = T_e - T_L - B\omega_m \tag{7-7}$$

where J and B denote the rotor inertia and friction coefficient, respectively.

Simulations are carried out in MATLAB/Simulink 2024b using a 400 V DC link, switching frequency $f_c = 10$ kHz, and fundamental frequency $f_m = 50$ Hz. The PMSM parameters are summarized in Table 7-1.

Table 7-1. Motor and Inverter Parameters for QSPWM Simulation.

Parameter	Value
Rated Power	2.2 kW
Pole Pairs	4
Stator Resistance (*Rs*)	1.2Ω
d-axis Inductance (*Ld*)	8.5 mH
q-axis Inductance (*Lq*)	8.5 mH
Moment of Inertia (l)	$0.0025\ \mathrm{kg}\cdot\ \mathrm{m}^2$
Friction Coefficient (*B*)	$0.0001\ \mathrm{N.m.s}$
Back EMF Constant (*Ke*)	$0.48\ \mathrm{V/rad/s}$
Sampling Time	$1\mu\mathrm{s}$
Control Frequency	10 kHz
Reference Speed	1500 rpm

For each control cycle, quantum gate operations are emulated through random sampling according to P_{on} and P_{off}, ensuring repeatable statistics across simulation runs. Each experiment lasts 0.5 s, covering both transient and steady-state regimes. Two quantitative indices evaluate performance:

1. Total Harmonic Distortion (THD):

$$\mathrm{THD} = \frac{\sqrt{\sum_{n=2}^{\infty} V_n^2}}{V_1} \times 100\% \tag{7-6}$$

where V_n denotes the RMS amplitude of the n^{th} harmonic of the line voltage.

2. Root Mean Square Error (RMSE) for speed tracking:

$$\mathrm{RMSE} = \sqrt{\frac{1}{N}\sum_{k=1}^{N}\left(\omega_m(k) - \omega_{ref}(k)\right)^2} \tag{7-7}$$

These indices jointly assess spectral quality and dynamic accuracy. Comparative results between SPWM and QSPWM are presented in Table 7-2.

Table 7-2. Performance Comparison between Classical and Quantum SPWM.

Operating Regime	RMSE (Classical SPWM)	RMSE (QSPWM)	Difference (%)
Overall	7.82 rpm	8.15 rpm	-4.0%
Transition Mode	8.10 rpm	8.12 rpm	≈ 0%
Permanent Mode	7.75 rpm	8.09 rpm	-4.2 %

The algorithm proceeds as follows:

1. Acquire $v_m(t)$ and $v_c(t)$.
2. Compute the normalized difference $\delta = (v_m - v_c)/V_c$.
3. Encode δ as rotation angle $\theta = k\delta$.
4. Apply $R_y(\theta)$ on qubit $|0\rangle$ and measure the outcome.
5. Generate the switching signal $s(t) =$ measurement result.
6. Repeat for three phases to form inverter gating patterns.

This probabilistic decision process yields continuously varying switching intervals, smoothing the spectral envelope and reducing harmonic magnitudes.

The methodology establishes a reversible quantum-logic representation of PWM, directly compatible with classical simulation platforms. The hybrid architecture enables implementation either through quantum emulation on classical CPUs/GPUs or by mapping onto near-term quantum processors for hardware testing.

Journal of Electronic Science and Technology

Design of a new quantum sinusoidal pulse width modulation (QSPWM) to enhance total harmonic distortion (THD) of three phase motors drives.

--Manuscript Draft--

Manuscript Number:	JNLEST-D-25-00328
Full Title:	Design of a new quantum sinusoidal pulse width modulation (QSPWM) to enhance total harmonic distortion (THD) of three phase motors drives.
Short Title:	
Article Type:	Research Article
Section/Category:	Special Section on Quantum Information Processing
Keywords:	Quantum Sinusoidal Pulse Width Modulation (QSPWM); Permanent Magnet Synchronous Motor (PMSM); Total Harmonic Distortion (THD); Quantum Computing; Electromagnetic Interference (EMI); Motor Drive Control; Energy-Aware Modulation Techniques
Corresponding Author:	Nadjet Zioui, Ph.D University of Quebec at Trois-Rivieres CANADA
Corresponding Author Secondary Information:	
Corresponding Author's Institution:	University of Quebec at Trois-Rivieres
Corresponding Author's Secondary Institution:	
First Author:	Mehdi Fazilat
First Author Secondary Information:	
Order of Authors:	Mehdi Fazilat
	Oumar Kone
	Nadjet Zioui, Ph.D
	Reda Dermouche, Ph.D
	Mohamed Tadjine, Ph.D
Order of Authors Secondary Information:	
Abstract:	High Total Harmonic Distortion (THD), excessive switching noise, and electromagnetic interference (EMI) remain persistent challenges in conventional pulse-width modulation strategies such as classical Sinusoidal PWM (SPWM), particularly in high-performance motor drives. These limitations degrade power quality, increase filter requirements, and limit the applicability of standard modulation techniques in EMI-sensitive environments, such as electric vehicles and robotic actuators. Addressing these challenges with a new perspective, we propose a novel Quantum Sinusoidal Pulse Width Modulation (QSPWM) technique. This innovative approach introduces a structured probabilistic modulation based on quantum logic gates that harnesses the non-deterministic properties of quantum operations. The QSPWM technique is designed to suppress harmonic clusters and reduce spectral periodicity in inverter switching signals, offering a promising solution to the persistent issues in conventional PWM strategies. Simulations conducted on a surface-mounted three-phase Permanent Magnet Synchronous Motor (PMSM) model demonstrate the effectiveness of the QSPWM technique. Notably, this is the first work to present a quantum version of SPWM and to implement the two-real-number quantum subtractor using an actual quantum circuit. Despite a slight increase in steady-state error, QSPWM significantly reduces THD from 60.21% to 38.79%, resulting in a 35.6% improvement, which leads to smoother voltage waveforms, reduced EMI, lower acoustic noise, and improved motor efficiency, providing convincing evidence of the benefits of the QSPWM technique. With direct

	implications for EMI-constrained systems and energy-aware robotics, the QSPWM technique offers a hopeful vision for the future of power electronics and motor drives.
Opposed Reviewers:	
Additional Information:	
Question	**Response**

Cover Letter

Quebec, October 1st, 2025

Cover letter

Journal of Electronic Science and Technology

Dear Editor in Chief,

We are pleased to submit our manuscript “Design of a new quantum sinusoidal pulse width modulation (QSPWM) to enhance total harmonic distortion (THD) of three phase motors drives” to be considered for publication in the Journal of Electronic Science and Technology.

This is a new manuscript, never published anywhere and is not currently being considered for publication by any other journal.

The manuscript presents a novel Quantum Sinusoidal Pulse Width Modulation (QSPWM) technique that leverages a structured probabilistic modulation based on quantum logic gates that harnesses the non-deterministic properties of quantum operations. This is the first work to present a quantum version of SPWM and to implement the two-real-number quantum subtractor and comparator using actual quantum circuits.

Applied to the speed control of a three-phase Permanent Magnet Synchronous Motor (PMSM), the proposed method demonstrates its effectiveness through smoother voltage waveforms, reduced EMI, lower acoustic noise, and improved motor efficiency, providing convincing evidence of the benefits of the proposed QSPWM technique.

We believe our work is within the aims and scope of the Journal of Electronic Science and Technology and hope it will considerably contribute to the field and attract academic and industrial readers’ interest.

Best regards.

The Authors.

Conflict of Interest

Declaration of Interest Statement

☒ The authors declare that they have no known competing financial interests or personal relationships that could have appeared to influence the work reported in this paper.

☐ The author is an Editorial Board Member/Editor-in-Chief/Associate Editor/Guest Editor for this journal and was not involved in the editorial review or the decision to publish this article.

☐ The authors declare the following financial interests/personal relationships which may be considered as potential competing interests:

Title Page

Design of a new quantum sinusoidal pulse width modulation (QSPWM) to enhance total harmonic distortion (THD) of three phase motors drives.

Mehdi Fazilat[1], Oumar Kone[1], Nadjet Zioui[1], Reda Dermouche[2], Mohamed Tadjine[3]

[1] Université du Québec à Trois-Rivières, 3351 Bd des Forges, Trois-Rivières, QC G8Z 4M3, Canada

[2] École Nationale Supérieure de Technologie d'Alger, Faculté de Médecine - Centre biomédicale, Bordj El Kiffan, Algeria

[3] École Nationale Polytechnique, 10 Rue des Frères OUDEK, El Harrach 16200, Algeria

[*] Corresponding author email: nadjet.zioui@uqtr.ca

Design of a new quantum sinusoidal pulse width modulation (QSPWM) to enhance total harmonic distortion (THD) of three phase motors drives.

Abstract

High Total Harmonic Distortion (THD), excessive switching noise, and electromagnetic interference (EMI) remain persistent challenges in conventional pulse-width modulation strategies such as classical Sinusoidal PWM (SPWM), particularly in high-performance motor drives. These limitations degrade power quality, increase filter requirements, and limit the applicability of standard modulation techniques in EMI-sensitive environments, such as electric vehicles and robotic actuators. Addressing these challenges with a new perspective, we propose a novel Quantum Sinusoidal Pulse Width Modulation (QSPWM) technique. This innovative approach introduces a structured probabilistic modulation based on quantum logic gates that harnesses the non-deterministic properties of quantum operations. The QSPWM technique is designed to suppress harmonic clusters and reduce spectral periodicity in inverter switching signals, offering a promising solution to the persistent issues in conventional PWM strategies. Simulations conducted on a surface-mounted three-phase Permanent Magnet Synchronous Motor (PMSM) model demonstrate the effectiveness of the QSPWM technique. Notably, this is the first work to present a quantum version of SPWM and to implement the two-real-number quantum subtractor using an actual quantum circuit. Despite a slight increase in steady-state error, QSPWM significantly reduces THD from 60.21% to 38.79%, resulting in a 35.6% improvement, which

leads to smoother voltage waveforms, reduced EMI, lower acoustic noise, and improved motor efficiency, providing convincing evidence of the benefits of the QSPWM technique. With direct implications for EMI-constrained systems and energy-aware robotics, the QSPWM technique offers a hopeful vision for the future of power electronics and motor drives.

Keywords: Quantum Sinusoidal Pulse Width Modulation (QSPWM), Permanent Magnet Synchronous Motor (PMSM), Total Harmonic Distortion (THD), Quantum Computing, Electromagnetic Interference (EMI), Motor Drive Control, Energy-Aware Modulation Techniques.

1. Introduction

Sinusoidal Pulse Width Modulation (SPWM) has been an essential technique for controlling voltage and current in power electronic converters, especially in the context of AC motors, inverters, and renewable energy systems. SPWM modulates the width of pulses in such a way that the resulting waveform approximates a sinusoidal waveform. As power electronic systems evolve, recent research has been addressing several advanced topics, trends, and improvements in SPWM. Some of the most notable areas of research include optimization techniques, high precision control, artificial intelligence and machine learning, and hybrid techniques among others. SPWM is employed in a wide range of applications such as renewable energy systems, with MPPT (Maximum Power Point Tracking) algorithms integrated with SPWM for improved energy conversion efficiency [1-3], or wind power integration with wind turbine inverters [4-6], through harmonics minimization and grid synchronization [7-12]. SPWM is also widely used on inverter

systems for electric vehicles (EVs) to improve the performance of the vehicle's powertrain [13, 14] or for fault diagnosis applications [15-19].

Many papers covered a range of techniques from traditional SPWM improvements to advanced methods such as fuzzy logic, genetic algorithms, and multi-level inverters for THD reduction. Bushra et al. provided an in-depth analysis of Pulse Width Modulation (PWM) strategies aimed at reducing harmonics in power converters for renewable energy systems [20]. The authors covered various PWM techniques, including SPWM, such as selective harmonic elimination and space vector modulation, highlighting their effectiveness in improving system performance and energy quality. The review also discussed the challenges and future trends, emphasizing the need for adaptive and more efficient modulation schemes to address evolving energy demands. Zhang et al. presented an enhanced Sinusoidal Pulse Width Modulation (SPWM) technique designed to reduce Total Harmonic Distortion (THD) [21]. By optimizing switching frequencies and phase angles, the method improves output waveform quality, as demonstrated through simulations and experiments. Chakir et al. presented advanced control strategies for multilevel inverters in grid-connected and off-grid photovoltaic systems, focusing on a multi-objective approach using LS-PWM (Least-Square Pulse Width Modulation) for Total Harmonic Distortion (THD) reduction [22]. The proposed method aimed to optimize inverter performance by minimizing THD while ensuring efficient energy conversion and improved system stability. The approach's effectiveness was demonstrated through simulation results, highlighting its potential in enhancing the power quality and reliability of PV systems. Ravikumar et al. explored Total Harmonic Distortion (THD) minimization in nine-level multilevel inverters using a Genetic Algorithm (GA). The proposed method optimized the modulation strategy to reduce THD, enhancing the inverter's efficiency and power quality. Simulation results demonstrated the effectiveness of the GA-based approach in

achieving significant THD reduction [23]. Abdel-hamed et al. proposed an enhanced Sinusoidal Pulse Width Modulation (SPWM) control technique for minimizing Total Harmonic Distortion (THD) in multilevel inverters [24]. The approach utilized Ant Lion Optimization (ALO) to optimally adjust the modulation parameters. Experimental results demonstrated the effectiveness of this method in comparison to conventional techniques. Nasser et al. presented a modified sinusoidal pulse width modulation (SPWM) control scheme for a three-phase half-bridge cascaded multilevel inverter, optimized using Grey Wolf Optimization (GWO) algorithm [11]. The proposed method aimed to improve the overall performance of the inverter by minimizing harmonic distortion and enhancing the output voltage quality. The GWO-based optimization adjusted the SPWM parameters, resulting in a more efficient modulation technique. The effectiveness of the proposed scheme is validated through simulations, demonstrating its superior performance in terms of efficiency and harmonic reduction compared to conventional methods.

Recent studies have compared various SPWM methods based on performance metrics such as Total Harmonic Distortion (THD), switching losses, and fundamental component values, demonstrating the advantages of modified SPWM techniques over conventional ones [25]. These performances have been evaluated for various applications such as inverters and rectifiers operation improvement. In this context, Chaaira et al. offered a comparative analysis of bipolar and unipolar SPWM techniques implemented in PIC-based single-phase pure sine wave inverters [26]. Performance metrics such as output voltage quality, harmonic distortion, and switching losses were evaluated. The study highlighted the advantages and trade-offs of each modulation method, offering insights for optimized inverter design. Kim et al. compared Carrier-Based PWM (CBPWM) methods for two-phase three-leg inverters using the zero-sequence concept [27]. The authors evaluated modulation techniques based on voltage quality, harmonic distortion, and DC

bus utilization, highlighting the effectiveness of zero-sequence injection in enhancing inverter performance. Kumari et al. presents a comparative harmonic analysis of various PWM techniques for a diode-clamped multilevel inverter using MATLAB/Simulink [28]. The study evaluated THD and output voltage quality to determine the most effective modulation strategy for improved inverter performance. Kumar et al. investigated synchronverter and PLL-less control strategies for three-phase Voltage Source Inverters (VSI) in AC microgrids [29]. The authors compared their effects on system stability, synchronization accuracy, and dynamic response, demonstrating the potential benefits of PLL-less control in enhancing microgrid performance and robustness. Banerji et al. focused on the design, analysis, and fast tuning of an Active Front End (AFE) rectifier controller [30]. A comparative performance evaluation was conducted to assess dynamic response, power quality, and control efficiency under varying operating conditions.

Motors and generators have also benefited from the SPWM technique and its variants seeking performances enhancement. Qi et al. presented a comparative study of a high-speed permanent magnet motor powered by various methods, analyzing performance parameters such as efficiency, torque, and thermal behavior. The results highlighted the impact of each power method on motor performance and suitability for high-speed applications [31]. Mansuri et al. analyzed various PWM techniques for controlling a three-phase asynchronous motor, focusing on performance metrics such as torque ripple, efficiency, and harmonic distortion. The study identified the most suitable PWM method for optimal motor drive performance [32]. Thale et al. presented a comparative analysis of modulation techniques for an advanced controller of an Integrated Starter Generator (ISG). It evaluated control performance, efficiency, and torque response to identify the most effective technique for automotive applications [33]. Batteries operating enhancement has been studied as an application of SPWM technique. San et al. compared battery State of Charge (SOC)

depletion and driving range in a PMSM-driven electric vehicle using Sinusoidal PWM (SPWM) and Space Vector PWM (SVPWM) control techniques. Simulation results showed that SVPWM offered improved efficiency and extended driving range due to reduced switching losses and better DC bus utilization [34].

While SPWM offers numerous benefits, challenges remain in optimizing its performance across different applications, particularly in balancing efficiency and complexity in control systems. Further research is needed to address these challenges and explore new modulation strategies, and quantum computing seem to be well positioned to contribute to addressing such challenges. Saidat et al. presented the design and implementation of a Quantum Pulse-Width Modulation (QPWM) technique for controlling a DC motor drive. Unlike classical PWM, QPWM leveraged principles from quantum computing and quantum logic gates to modulate pulse widths, enabling faster processing speeds and more efficient switching control. Simulation results demonstrated that the QPWM method achieved improved performance in terms of switching efficiency, harmonic reduction, and response time, offering a promising approach for next-generation intelligent motor drives [35]. Dermouche et al. proposed a quantum direct torque control (QDTC) method for permanent magnet synchronous machines (PMSMs). By incorporating quantum computing principles into the control algorithm, the method enhanced torque and flux control precision while reducing response time and torque ripple. Simulation results demonstrated improved dynamic performance compared to conventional DTC approaches [36]. Zioui et al. proposed a Quantum Space Vector Pulse Width Modulation (QSVPWM) technique for controlling the speed of Permanent Magnet Synchronous Machines (PMSMs) [37]. By integrating quantum computing principles with space vector PWM, the method enhanced switching efficiency, reduced harmonic distortion, and improved dynamic response in motor control applications. There is no work in the

literature that explored yet the integration of quantum computing to the SPWM technique to assess its potential in enhancing its performances. Although researchers have studied closely related ideas in quantum optimal control, pulse-width techniques, and modulation-based quantum control [38-41], the intersection of quantum computing and SPWM, as used in power electronics, is not widely explored in the literature.

The current study presents two noteworthy innovations. First, while the quantum subtractor component was originally conceptualized within the QSVPWM framework [36, 37], this work presents the first comprehensive description of a quantum circuit implementation for a two-real-number subtractor suitable for pulse-width modulation. Second, to the best of our knowledge, this is the inaugural formal introduction of a quantum variant of Sinusoidal Pulse Width Modulation. No prior studies have put forth a quantum logic-based modulation scheme that retains the sinusoidal reference framework characteristic of SPWM, establishing this work as a foundational contribution to the field.

This paper demonstrates the incorporation of quantum computing concepts into the development of the SPWM approach to increase its performance. Quantum computing is projected to improve the SPWM technique's performance. The proposed quantum SPWM is compared to its classical counterpart to determine the quantum computing contribution. THD and control precision are tested. The proposed method is expected to help with the integration of quantum computing into actual engineering applications. The following document sections are organized so that section 2 discusses tools and approaches that recall the quantum computing principle, the classical SPWM technique, and the proposed method. Section 3 summarizes the findings and discusses the main results before concluding with section 4.

2. Tools and methods

2.1. Sinusoidal Pulse Width Modulation (SPWM)

Sinusoidal Pulse Width Modulation (SPWM) is used to implement switching control. SPWM compares a sinusoidal reference waveform with a high-frequency triangular carrier wave to generate switching pulses. When the reference signal is greater than the carrier, the switch is on; otherwise, it is off. The output voltage amplitude is controlled by the magnitude of the sine wave and the output frequency corresponds to the sine wave frequency.

SPWM is a widely used technique for its simplicity, ease of implementation, and sufficient performance in many AC machines related applications, particularly when the switching frequency is high enough to produce a smooth sinusoidal output after filtering. Figure 1 illustrated the principle of the SPWM technique.

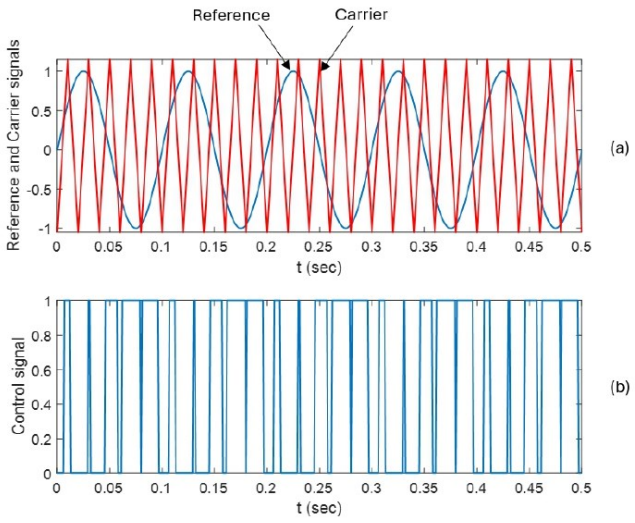

Figure 1: Sinusoidal PWM: (a) Reference and carrier signals comparison (b) Gate pulse signals.

2.2. Permanent Magnet Synchronous Motors (PMSM)

Permanent Magnet Synchronous Motors (PMSMs) are extensively employed in modern applications due to their superior efficiency, high power-to-weight ratio, and compact structural design [42]. To accurately study and control the dynamic behavior of PMSMs, it is common practice to utilize a mathematical model formulated in the rotating $d-q$ reference frame. This reference frame not only simplifies the analysis of both steady-state and transient responses but also supports the effective implementation of vector control strategies [42, 43].

To streamline the modeling process without significantly compromising accuracy, several standard assumptions are adopted:

- The magnetic core is assumed to operate in a linear region; thus, magnetic saturation is neglected.
- Hysteresis losses and eddy current losses are disregarded.
- The stator currents are assumed to form a balanced three-phase sinusoidal waveform.

Based on these assumptions, the PMSM model expressed in the two-axis rotating dq reference frame can be described by the following set of equations:

$$\begin{cases} V_d = R_s I_d + \frac{d\psi_d}{dt} - \omega_r \psi_q \\ V_q = R_s I_q + \frac{d\psi_q}{dt} + \omega_r \psi_d \end{cases} \quad (1)$$

Here, V_d and V_q denote the stator voltages in the direct and quadrature axes, respectively. R_s is the stator resistance, I_d and I_q are the d -axis and q -axis currents, ψ_d and ψ_q are the corresponding flux linkages, and ω_r represents the rotor's electrical angular velocity.

The expressions for the flux linkages in the d − q frame is given by:

$$\begin{cases}\psi_d = \psi_f + L_d I_d \\ \psi_q = L_q I_q\end{cases} \quad (2)$$

In this formulation, ψ_f is the flux linkage due to the permanent magnets, while L_d and L_q represent the daxis and q -axis inductances, respectively.

The electromagnetic torque T_e generated by the PMSM can be calculated as:

$$T_e = \frac{3}{2} p\left[\psi_f I_d + \left(L_d - L_q\right) I_d I_q\right] \quad (3)$$

In this expression, p denotes the number of pole pairs. The term $\psi_f I_d$ corresponds to the torque contribution from the permanent magnet field, whereas the term $\left(L_d - L_q\right) I_d I_q$ accounts for the reluctance torque, which arises due to the saliency (difference in inductances) between the d-axis and q-axis.

By substituting the flux linkage expressions into the stator voltage equations, the following relationships are derived:

$$\begin{cases}V_d = R_s I_d + L_d \frac{dI_d}{dt} - \omega_r L_q I_q \\ V_q = R_s I_q + L_q \frac{dI_q}{dt} + \omega_r \left(L_d I_d + \psi_f\right)\end{cases} \quad (4)$$

In these equations, V_d and V_q represent the stator voltages in the direct and quadrature axes, respectively. The terms $R_s I_d$ and $R_s I_q$ denote the resistive voltage drops along each axis. The expressions involving $L_d \frac{dI_d}{dt}$ and $L_q \frac{dI_g}{dt}$ correspond to the self-induced electromotive forces due to stator inductance, while the terms containing the rotor speed ω_r reflect the cross-coupling interactions between the axes.

From relation 4, it is evident that the inductance-related terms introduce dynamic coupling between the d-axis and q-axis currents. This cross-coupling becomes increasingly significant as the rotor speed ω_r rises, particularly in high-speed or variable-speed operating regimes. Consequently, the interdependence of the axes poses a challenge to achieving fully decoupled and precise control over each current component independently.

To mitigate this challenge, a cascaded dual closed-loop control structure is typically implemented in Permanent Magnet Synchronous Motor drives. This configuration includes an inner current regulation loop and an outer speed control loop. The actual vehicle speed is continuously compared to a predefined reference, and the resulting speed error is processed through a proportional-integral (PI) speed controller. The output of this controller provides the reference current I_{q_ref} for the q-axis, which directly influences torque production.

Simultaneously, the actual d-axis and q-axis stator currents, denoted I_d and I_q, are compared with their respective references I_{d_ref} and I_{q_ref}. The resulting current errors are fed into PI current controllers, which generate the control voltages V_d and V_q in the synchronous reference frame. The resulting current errors are fed into PI current controllers, which generate the control voltages V_d and V_q in the synchronous reference frame. The reference voltages V_{dref} and V_{qref} are transformed back into the three-phase stationary frame through the inverse Park Transformation to obtain $V_{\mathrm{aref}}, V_{\mathrm{bref}}, V_{\mathrm{cref}}$. These are then used by the SPWM block to generate inverter switching signals S_1, S_3, S_5, which synthesize the required three phase voltages to drive the PMSM.

The complete control scheme for the PMSM is illustrated in Figure 2. This diagram details the use of Park and Clarke transformations-both direct and inverse-which are essential for converting three-phase stationary frame currents I_a, I_b, I_c into the rotating-frame components I_d and I_q, and

vice versa. These transformations facilitate efficient vector control by aligning the stator current vector with the rotor flux, thereby maximizing torque production and dynamic performance.

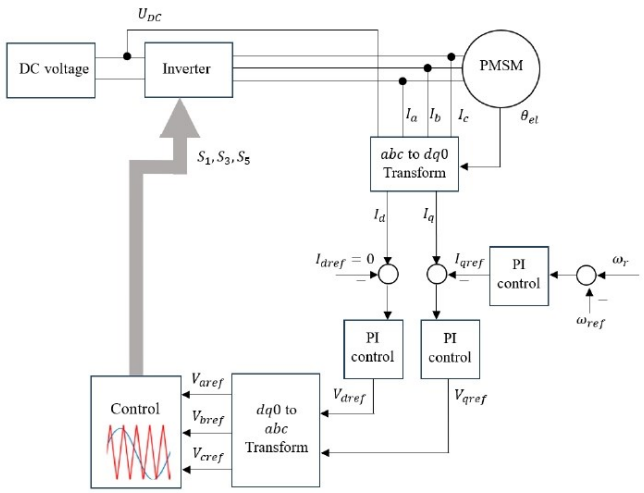

Figure 2: PMSM control schematics using the SPWM technique.

2.3. Quantum computing tools

2.3.1. Qubit

Quantum computing introduces a paradigm shift in computation by exploiting principles unique to quantum mechanics, such as superposition, entanglement, and quantum interference, to process and manipulate information in fundamentally novel ways. Unlike classical bits, which strictly assume binary states 0 or 1, a quantum bit (qubit) can simultaneously represent both states, exponentially increasing the computational space available for complex problems such as optimization, control, and robotics [44-46].

A single qubit is described within a two-dimensional complex Hilbert space and is defined as a linear combination (or superposition) of the classical computational basis states $|0\rangle$ and $|1\rangle$ [47]:

$$|q\rangle = \alpha|0\rangle + \beta|1\rangle \quad (5)$$

Here, $\alpha, \beta \in \mathbb{C}$ are the probability amplitudes, which satisfy the normalization condition $|\alpha|^2 + |\beta|^2 = 1$. These squared moduli represent the probabilities of measuring the qubit in the respective states: $|\alpha|^2$ is the probability of obtaining the outcome $|0\rangle$ and $|\beta|^2$ for $|1\rangle$. In matrix notation, the computational basis vectors are defined as [48]:

$$|0\rangle = \binom{1}{0}, |1\rangle = \binom{0}{1} \quad (6)$$

Therefore, a qubit |q) can be expressed in vector form as:

$$|q\rangle = \binom{\alpha}{\beta} \quad (7)$$

2.3.2. One qubit quantum operator

The most fundamental quantum gates for single-qubit operations are the Pauli matrices, defined as:

$$\sigma_0 = \begin{pmatrix} 1 & 0 \\ 0 & 1 \end{pmatrix} \quad (8)$$

$$\sigma_x = \begin{pmatrix} 0 & 1 \\ 1 & 0 \end{pmatrix} \quad (9)$$

$$\sigma_y = \begin{pmatrix} 0 & -i \\ i & 0 \end{pmatrix} \quad (10)$$

$$\sigma_z = \begin{pmatrix} 1 & 0 \\ 0 & -1 \end{pmatrix} \quad (11)$$

The Pauli gates constitute the foundational set of quantum operators for single-qubit manipulation, each represented by a Hermitian and unitary 2×2 matrix. Specifically, the Identity gate σ_0, leaves the qubit state unchanged, serving as a neutral operator in quantum computations [49]. The X gate σ_x, Bit-flip or NOT Gate, performs a logical inversion, transforming the computational basis state $|0\rangle$ into $|1\rangle$ and vice versa, analogous to the classical NOT operation. The Y gate σ_y, Phase-flip + Bit-flip Gate, introduces both a bit flip and a relative phase shift of π, modifying the state while encoding essential phase information. In contrast, the Z gate σ_z, Phase-flip Gate, induces a phase inversion exclusively on the $|1\rangle$ component, leaving $|0\rangle$ invariant, thereby facilitating phase-sensitive transformations critical in interference-based quantum protocols [48, 50]. Collectively, these gates form the algebraic backbone of quantum operations and are instrumental in constructing more complex unitary transformations, designing quantum circuits, implementing error correction schemes, and decomposing universal quantum gates across various quantum algorithms and control architectures.

Moreover, beyond the Pauli gates, quantum control applications often utilize additional gates such as, the Hadamard gate (H), which creates equal superpositions of $|0\rangle$ and $|1\rangle$, allowing quantum parallelism [51, 52]:

$$H = \frac{1}{\sqrt{2}}\begin{pmatrix} 1 & 1 \\ 1 & -1 \end{pmatrix} = \frac{1}{\sqrt{2}}(\sigma_0 + \sigma_x) \tag{12}$$

And also, the rotation gates about the Bloch sphere axes, which are parameterized by an angle θ and represent general single-qubit evolutions [50]:

Rotation about X-axis:

$$R_x(\theta) = \cos\theta\sigma_0 - i\sin\theta\sigma_x \tag{13}$$

Rotation about Y-axis:

$$R_y(\theta) = \cos\theta\sigma_0 - i\sin\theta\sigma_y \quad (14)$$

Rotation about Z-axis:

$$R_z(\theta) = \cos\theta\sigma_0 - i\sin\theta\sigma_z = \begin{pmatrix} e^{-i\theta} & 0 \\ 0 & e^{i\theta} \end{pmatrix} \quad (15)$$

These gates are indispensable for implementing parameterized quantum operations, and in particular, the $R_y(\theta)$ rotations serve as encoding mechanisms for real-valued data, such as reference and measured positions or velocities, by mapping them to angular states within quantum registers [53, 54].

2.3.3. Multiple qubits quantum operators

Multiple-qubit quantum operators are unitary transformations that operate on composite systems comprising two or more qubits, facilitating entanglement, conditional logic, and quantum parallelism. These operators are necessary for executing controlled operations, quantum algorithms, and error-correcting codes [55]. Two widely utilized multi-qubit gates are the Controlled-NOT, CNOT, gate and the Toffoli gate, which is also known as the Controlled-Controlled-NOT, or CCNOT, gate. These gates act on two- and three-qubit subsystems, respectively and implement conditional logic, allowing one or more qubits to control the transformation of others-an essential feature for entanglement generation, quantum decision-making, and universal quantum computation [56]. Their unitary matrix representations in the computational basis are as follows.

The CNOT gate flips the target qubit if and only if the control qubit is in the $|1\rangle$ state. Its 4×4 matrix form in the ordered basis $(|00\rangle, |01\rangle, |10\rangle, |11\rangle)$ is [57]:

$$\text{CNOT} = \begin{pmatrix} 1 & 0 & 0 & 0 \\ 0 & 1 & 0 & 0 \\ 0 & 0 & 0 & 1 \\ 0 & 0 & 1 & 0 \end{pmatrix} \tag{16}$$

The Toffoli gate also known as CCNOT extends this logic to three-qubit systems. It flips the third (target) qubit only when both the first and second (control) qubits are in the $|1\rangle$ state. The matrix form of the CCNOT gate is an 8×8 identity matrix with a single 2×2 NOT operation applied on the subspace $(|110\rangle, |111\rangle)$, with ability to implements a conditional NOT operation where the condition depends on two-qubit control, as shown below [48]:

$$\text{CCNOT} = \begin{pmatrix} 1 & 0 & 0 & 0 & 0 & 0 & 0 & 0 \\ 0 & 1 & 0 & 0 & 0 & 0 & 0 & 0 \\ 0 & 0 & 1 & 0 & 0 & 0 & 0 & 0 \\ 0 & 0 & 0 & 1 & 0 & 0 & 0 & 0 \\ 0 & 0 & 0 & 0 & 1 & 0 & 0 & 0 \\ 0 & 0 & 0 & 0 & 0 & 1 & 0 & 0 \\ 0 & 0 & 0 & 0 & 0 & 0 & 0 & 1 \\ 0 & 0 & 0 & 0 & 0 & 0 & 1 & 0 \end{pmatrix} \tag{17}$$

Both CNOT and Toffoli gates are important for realizing quantum logic circuits, error correction codes, and quantum arithmetic. The Toffoli gate, in particular, is universal for classical reversible computation and is often used in the design of quantum comparators, quantum adders, and quantum-inspired control systems, where multi-qubit conditions must trigger discrete quantum state transitions [36, 48].

2.4. Quantum SPWM (QSPWM)

The implementation of the QSPWM is based on the use of a quantum comparator between two real numbers that is composed of a quantum subtractor and a quantum sign detector. The design of the quantum subtractor is based on the following trigonometric relationship.

$$\frac{1}{2}(C\alpha - C\beta) = S\left(\frac{\alpha+\beta}{2}\right) S\left(\frac{\alpha-\beta}{2}\right) \tag{18}$$

$C\alpha$ and $S\alpha$ stand for the cosine and sine of the angle α.

The expressions $S\alpha = v$ and $S\beta = w$ are two real numbers ranging from -1 to $+1$, or -100% to 100%.

Equation (18) can then be rewritten as the following.

$$v - w = 2\, S\left(\frac{\alpha+\beta}{2}\right) S\left(\frac{\alpha-\beta}{2}\right) \tag{19}$$

The use of the function $Atan()$ will allow the computation of the angles α and β. The $Atan()$ function can be implemented as a quantum oracle, such as $v = Atan(a)$ and $w = Atan(b)$.

The term $S\left(\frac{\alpha+\beta}{2}\right)$ can be implemented as a quantum circuit that employs two successive quantum rotations around the y-axis having respectively $\frac{\alpha}{2}$ and $\frac{\beta}{2}$ as rotation angles. These two rotations are applied to a qubit that is initialized at the state $|0\rangle$.

The expression $S\left(\frac{\alpha-\beta}{2}\right)$ can also be realized using two quantum rotations of $\frac{\alpha}{2}$ and $\frac{-\beta}{2}$ around the y-axis for a second qubit also initialized at the quantum state $|0\rangle$. The expressions $S\left(\frac{\alpha+\beta}{2}\right)$ and $S\left(\frac{\alpha-\beta}{2}\right)$ will be implanted on the $|1\rangle$ component of the qubits, respectively, as in the following relationship.

$$\begin{cases} |q_1\rangle = R_y\left(\frac{\alpha}{2}\right) R_y\left(\frac{\beta}{2}\right)|0\rangle = C\left(\frac{\alpha+\beta}{2}\right)|0\rangle + S\left(\frac{\alpha+\beta}{2}\right)|1\rangle \\ |q_2\rangle = R_y\left(\frac{\alpha}{2}\right) R_y\left(\frac{-\beta}{2}\right)|0\rangle = C\left(\frac{\alpha-\beta}{2}\right)|0\rangle + S\left(\frac{\alpha-\beta}{2}\right)|1\rangle \end{cases} \tag{20}$$

A tensor product is then performed between the two rotated qubits leading to the following.

$$|q_1q_2\rangle = \begin{pmatrix} C\left(\frac{\alpha+\beta}{2}\right)C\left(\frac{\alpha-\beta}{2}\right) \\ C\left(\frac{\alpha+\beta}{2}\right)S\left(\frac{\alpha-\beta}{2}\right) \\ S\left(\frac{\alpha+\beta}{2}\right)C\left(\frac{\alpha-\beta}{2}\right) \\ S\left(\frac{\alpha+\beta}{2}\right)S\left(\frac{\alpha-\beta}{2}\right) \end{pmatrix} \quad (21)$$

The expression $S\left(\frac{\alpha+\beta}{2}\right)S\left(\frac{\alpha-\beta}{2}\right)$, which is half the subtraction $v-w$, is obtained through the measurement of the last component $|11\rangle$ of the tensor product (Equation 21) without converting it to its Boolean equivalent. Finally, a 2 gain will be applied to find the correct value of the subtraction. This gain is not necessary in the case of the QSPWM application, since the sign of a half the number is the sign of the number itself. In fact, the subtraction in the QSPWM is needed only to determine the sign of its result to decide if the control signal will be ON or OFF according to this sign. Nevertheless, Figure 3 depicts the quantum circuit of complete quantum subtractor including the gain.

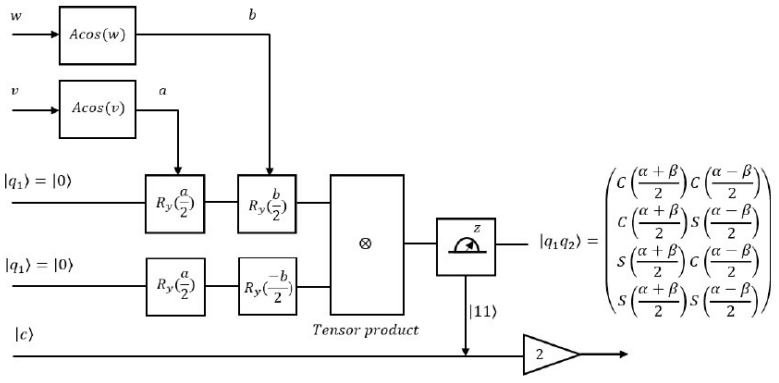

Figure 3: Two real numbers quantum subtractor circuit.

The implementation of the sign detector is performed through the embedment of half the subtraction result into the $|0\rangle$ component of a qubit state such as the following.

$$|q\rangle = (v - w)|0\rangle + (\sqrt{1 - (v - w)^2})|1\rangle \quad (22)$$

Since the subtraction result is lower than 1 in its absolute value, it can be considered as the cosine of an angle $\theta = Acos(v - w)$. Likewise, $\sqrt{1 - (v - w)^2}$ can be considered as the sine of this same angle. Based on this, if the angle θ varies from 0 to $\pi/2$, the cosine of it will range from 0 to 1, which means, the subtraction result is positive. However, the cosine of this angle minus $\pi/4$ will range from 0 to 0.5. This means that the qubit state $|q\rangle$ rotated with $-\pi/4$ around the y-axis will be measured at the $|1\rangle$ state. When the angle θ varies from $\pi/2$ to π, then its cosine will range from -1 to 0. Which means that the subtraction is negative. However, the cosine of this angle minus $\pi/4$ will range from 0.5 to 1. This means that the qubit state $|q\rangle$ rotated with $-\pi/4$ around the y-axis will be measured at the state $|0\rangle$. This can be summarized by the fact that a rotation $-\pi/4$ around the y-axis will allow the generation of the PWM signal considering the $|0\rangle$ component of the qubit state as depicted in Figure 4.

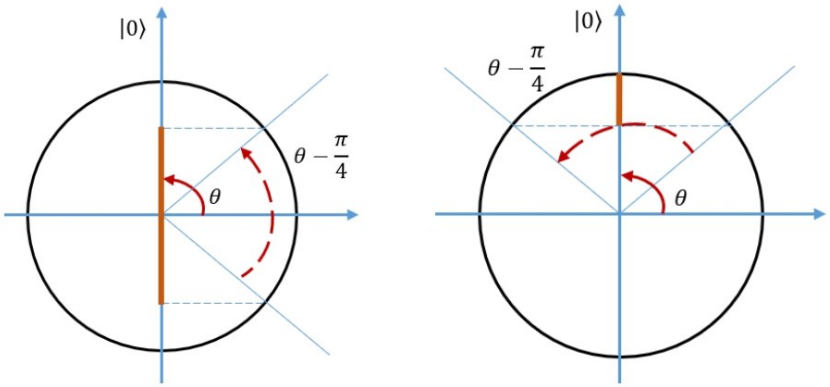

(a) (b)

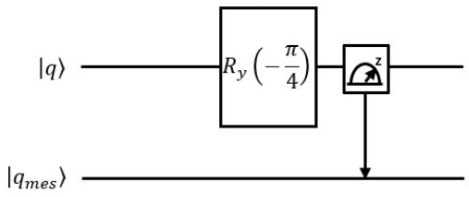

(c)

Figure 4: The quantum sign detector: (a) Positive sign case; (b) negative sign case; (c) Quantum circuit.

3. Results and discussion

To assess the effectiveness of the proposed Quantum Sinusoidal Pulse Width Modulation technique, a series of simulations was conducted in both the time and frequency domains, comparing the results with those of the classical Sinusoidal Pulse Width Modulation method. The simulation setup is designed to control a three-phase Permanent Magnet Synchronous Motor under consistent load and reference conditions.

All simulations were conducted in MATLAB/Simulink, utilizing a three-phase surface-mounted Permanent Magnet Synchronous Motor model that accurately represents medium-voltage

industrial applications. The simulation time step was set to 1 μs, and the control frequency was maintained at 3 kHz for both the SPWM and QSPWM cases to ensure consistency.

The Quantum Sinusoidal Pulse Width Modulation control strategy harnesses the foundational principles of quantum computing to create a modulation signal that enhances harmonic performance. Central to this technique are operations based on quantum logic gates, with an effective principle for developing and simulating a quantum subtractor, a quantum sign detector, and a quantum adder, which enable a probabilistic waveform shaping mechanism that fundamentally differs from traditional triangular carrier-based SPWM approaches. Rather than relying on deterministic switching patterns, the QSPWM framework introduces modulation dynamics shaped by quantum logical constructs, enabling non-linear and context-sensitive control responses. Although the implementation was carried out within a classical computational environment, the algorithmic architecture effectively replicates the operational logic of ideal single- and multi-qubit systems.

To evaluate the comparative performance of SPWM and QSPWM, the following assessment metrics were utilized:

1. Root Mean Square Error (RMSE) of rotor speed tracking, calculated for the entirety of the simulation period as well as specifically within the transition and steady-state regimes.

2. Total Harmonic Distortion (THD) of the output voltage signal, determined through spectral decomposition.

3. Control signal smoothness was assessed qualitatively by examining PWM command waveforms and identifying any irregularities in the switching behavior.

The output voltage waveform from the inverter was analyzed using the Fast Fourier Transform to extract harmonic components and evaluate waveform quality. The complete simulation parameters are summarized in Table 1.

Table 1. Motor and System Parameters for Simulation.

Parameter	**Value**
Rated Power	2.2 kW
Pole Pairs	4
Stator Resistance (Rs)	1.2Ω
d-axis Inductance (Ld)	8.5 mH
q-axis Inductance (Lq)	8.5 mH
Moment of Inertia (l)	$0.0025\ \mathrm{kg}\cdot\ \mathrm{m}^2$
Friction Coefficient (B)	$0.0001\ \mathrm{N.m.s}$
Back EMF Constant (Ke)	$0.48\ \mathrm{V/rad/s}$
Nominal Speed	150 rpm

Figure 5 illustrates the rotor speed response of the Permanent Magnet Synchronous Motor under three distinct conditions: the reference trajectory, the proposed Quantum Sinusoidal Pulse Width Modulation method, and the classical Sinusoidal Pulse Width Modulation controller. These responses are plotted against time and rotor speed measured in revolutions per minute. The reference speed profile consists of two key setpoints: an initial steady-state target at approximately 100 RPM, followed by a step increase to 150 RPM at 0.3 seconds. Both SPWM-based controllers are designed to track this reference speed with minimal overshoot, rapid convergence, and smooth transient behavior.

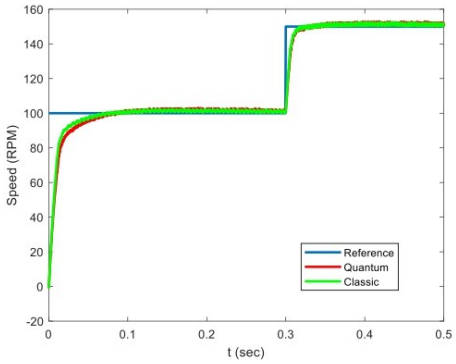

Figure 5: Speed of the motor using classic and quantum SPWM.

In the initial acceleration phase (0 – 0.1 s), both classical and quantum controllers demonstrate a rapid dynamic response, with the classical method achieving a slightly tighter convergence to the reference. The QSPWM response shows a marginally slower rise time and a greater ripple amplitude during this phase, indicating higher switching activity or modulation-induced jitter. Regardless, the performance difference is minimal. In the steady-state region (0.1–0.3 s), both methods maintain speeds close to the setpoint, with the classical controller achieving a slightly lower steady-state error. When the second reference step is introduced at 0.3 s, both controllers respond promptly; however, the classical SPWM reaches the new setpoint more swiftly and with reduced transient oscillation.

With the somewhat slower convergence noted with QSPWM, the controller effectively follows the reference trajectory during both transition and steady-state intervals. The increased ripple observed in the QSPWM trace is a recognized artifact of quantum-inspired probabilistic pulse synthesis, which may introduce nominal fluctuations due to gate-based waveform modulation. However, this effect does not undermine overall stability or convergence. Notably, the speed tracking results

align with the RMSE values reported in the earlier section, where QSPWM and classical SPWM indicated equivalent performance in the transient regime, along with modest divergence in steady-state precision.

The rotor speed tracking error for both the classical Sinusoidal Pulse Width Modulation and the proposed Quantum SPWM techniques is presented in Figure 6, offering valuable insights into their dynamic and steady-state accuracy over time. The instantaneous speed error, measured in revolutions per minute, is defined as the difference between the actual motor speed and the reference speed profile. In the graph, the error curves for the classical SPWM are represented by a blue line, while the QSPWM is shown in red. This illustration captures the entire 0.5-second simulation window, which includes two critical phases: an initial ramp-up to 100 RPM and a subsequent step increase to 150 RPM at the 0.3-second mark.

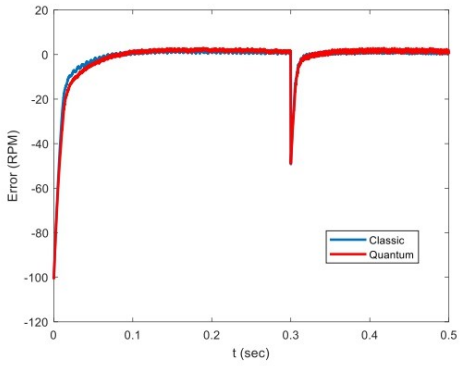

Figure 6: Speed error of the motor using classic and quantum SPWM.

During the initial transient phase (0 – 0.1 s), both controllers exhibit a notable negative error, recalling the expected lag between command issuance and rotor acceleration due to motor inertia. The QSPWM shows a negligibly sharper initial undershoot, compared to the classical controller,

suggesting a borderline delay in torque buildup. However, this discrepancy quickly decreases as both strategies converge toward zero error with similar dynamics. The classical SPWM shows a rather more oscillatory convergence. In contrast, the QSPWM trace appears smoother, an observation that aligns with the reduced high-frequency switching content previously reported for quantum-inspired modulation.

During the steady-state interval from 0.1 to 0.3 seconds, both error curves remain close to zero, yet the classical controller exhibits a narrower envelope with less ripple. At the reference step at t = 0.3 seconds, both controllers experience a sharp dip in error, initially recording a sudden underspeed. Notably, the QSPWM shows a slightly larger absolute deviation compared to the classical controller, although their subsequent convergence is effectively similar. The post-transient behavior between 0.35 and 0.5 seconds remains stable and well-controlled for both controllers, with negligible steady-state offsets and comparable noise levels. However, the QSPWM curve delivers visibly less oscillation and smoother error dynamics, particularly during the steady-state intervals. This behavior is indicative of lower switching-induced ripple and potentially reduced torque oscillations, which is advantageous in noise-sensitive or high-precision motor applications.

To further evaluate the control performance of the proposed Quantum SPWM procedure in comparison to the classical SPWM strategy, the Root Mean Square Error (RMSE) of rotor speed tracking was estimated across various operational regimes, including the overall duration, transition phase (dynamic regime), and steady-state (permanent) mode. These metrics deliver a robust foundation for analyzing both transient responsiveness and long-term tracking accuracy.

As revealed in Table 2, the classical SPWM achieves a lower overall RMSE value of 5.4×10^7 compared to 6.2×10^7 for QSPWM, indicating slightly better global tracking accuracy. In the

transition regime defined as the periods immediately following step changes in the reference speed-the performance gap narrows considerably. Both controllers exhibit nearly identical dynamic response, with RMSE values of 3.3×10^7 and 3.4×10^7 for the classical and quantum cases, respectively. This suggests that QSPWM is capable of matching conventional SPWM in terms of responsiveness to abrupt setpoint variations. In the permanent (steady-state) regime, the classical SPWM again demonstrates a minor advantage, with a lower RMSE of 1.3×10^4 versus 2.0×10^4 for QSPWM. Although the difference is minor, it reflects the classical controller's finer stability and reduced residual oscillations under stationary operating conditions. Nevertheless, the RMSE trends confirm that QSPWM achieves control accuracy that is comparable to classical SPWM across all regimes, with particularly competitive performance during dynamic transitions. Given QSPWM's documented advantage in harmonic suppression, this trade-off remains favorable for applications prioritizing waveform quality, acoustic noise reduction, or electromagnetic compatibility.

Table 2. Rotor Speed Tracking RMSE Comparison.

Operating Regime	**RMSE - Classic SPWM**	**RMSE - QSPWM**
Overall	5.4×10^7	6.2×10^7
Transition Mode	3.3×10^7	3.4×10^7
Permanent Mode	1.3×10^4	2.0×10^4

The harmonic spectra of the inverter output voltage for both modulation strategies are depicted in Figure 7, permitting a comparative investigation of their frequency-domain performance. Subfigure (a) defines the classical Sinusoidal Pulse Width Modulation mode, while subfigure (b) showcases the spectrum for the proposed Quadratic Sinusoidal Pulse Width Modulation approach by denoting the frequency in Hz, and the magnitude of each harmonic component as a percentage of the fundamental frequency. Both spectra are centered around a fundamental frequency of 3 kHz (specifically 3002 Hz), in alignment with the conveyance frequency employed in the pulse-width modulation scheme used for the simulation.

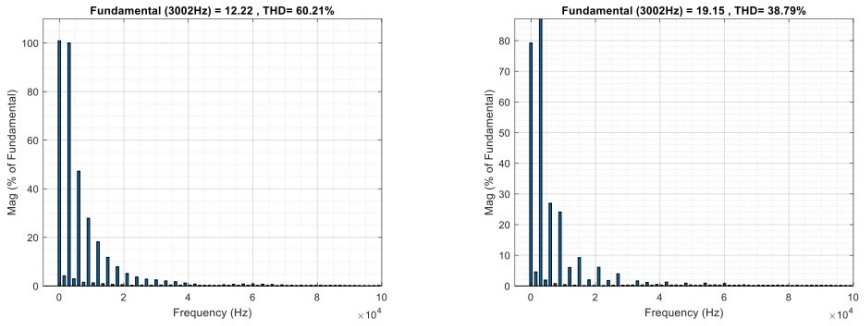

(a) (b)

Figure 7: THD analysis using classic and quantum SPWM: (a) Classic SPWM, (b) QSPWM.

The classical Sinusoidal Pulse Width Modulation statistics inform a broad and dense distribution of harmonics. Several low-order harmonics are observed to approach or even exceed 20% of the fundamental amplitude, with spectral energy extending well into higher frequency bands, indicating substantial waveform distortion. The calculated Total Harmonic Distortion for this classical method is 60.21%, indicating a significant harmonic content that can lead to increased

switching losses, electromagnetic interference (EMI), and elevated motor heating. In contrast, the QSPWM spectrum exhibits a notably more compact harmonic profile. The amplitudes of the harmonics decrease more swiftly with increasing frequency, resulting in the spectral energy being more closely clustered around the fundamental, which yields a remarkably lower total harmonic distortion (THD) of 38.79%, reflecting a 35.6% improvement compared to the traditional approach. Consequently, the QSPWM waveform materializes to be smoother and less susceptible to high-frequency distortion and switching noise. This enhancement can be attributed to the quantum-inspired modulation mechanism, which utilizes probabilistic waveform generation through quantum gates and a quantized procedure in the proposed quantum technique. In contrast to classical deterministic PWM, QSPWM introduces structured, non-repetitive switching sequences that inherently distribute spectral components more uniformly and dampen harmonic peaks. Consequently, the output voltage waveform experiences reduced ripple and improved spectral purity.

In summary, the simulation results confirm the applicability and effectiveness of the proposed Quantum-Sourced Pulse Width Modulation strategy in controlling three-phase Permanent Magnet Synchronous Motors. While classic Sinusoidal Pulse Width Modulation exhibits slightly better performance in overall and steady-state Root Mean Square Error, both controllers display nearly identical accuracy during transitional phases, highlighting the dynamic responsiveness of the quantum-inspired approach. More importantly, QSPWM achieves a remarkable enhancement in spectral quality, effectively reducing the Total Harmonic Distortion from 60.21% to 38.79%. This reduction in harmonics, attributed to the structured probabilistic modulation introduced by quantum logic gates and the sinusoidal encoding of quantum pulse sequences, results in smoother inverter voltage profiles and significantly mitigates high-frequency interference. From an

engineering standpoint, this translates to reduced filter requirements, lower acoustic noise, and improved motor efficiency and longevity, leading to potential cost savings. Although QSPWM entails an acceptable compromise in time-domain precision, its superior harmonic performance makes it particularly appealing for environments that are constrained by electromagnetic interference or are sensitive to noise. These findings affirm QSPWM as a practicable, efficient, and forward-thinking modulation technique for next-generation power electronics and motor drive systems.

4. Conclusion

The inaugural implementation of the Quantum Sinusoidal Pulse Width Modulation (QSPWM) technique not only establishes a ground-breaking connection between quantum logic and classical modulation control but also opens up a world of practical applications in quantum-inspired modulation. Unlike previous works that merely introduced the idea of a quantum subtractor, our comprehensive quantum circuit realization points towards a future where quantum-inspired modulation is a reality. By utilizing quantum logic, the proposed method introduces structured probabilistic modulation to generate inverter signals with minimized harmonic clustering. The simulation results verify that QSPWM delivers competitive control performance compared to classical SPWM. While the classical method maintains a slight edge in overall and steady-state RMSE, both approaches exhibit nearly identical dynamic tracking accuracy during transitional phases. Notably, QSPWM particularly enhances spectral performance, reducing Total Harmonic Distortion (THD) from 60.21% to 38.79%, corresponding to a 35.6% improvement. This achievement in reducing harmonic distortion results in smoother voltage waveforms and decreased high-frequency interference.

These advancements translate to reduced Electromagnetic Interference, smaller passive filters, lower acoustic noise, and improved thermal efficiency, which are required benefits in electric vehicles, robotics, and renewable energy systems. Although QSPWM incurs a minor compromise in tracking precision, its superior waveform quality positions it as a highly attractive alternative in applications where power quality, reliability, and electromagnetic compliance are essential.

The evolving landscape of PWM research, which proves, for the first time, the feasibility of integrating quantum-inspired logic into classical SPWM frameworks, is a major contribution of the current study. This introduces a new dimension in power electronics, advancing and elevating conventional control methods with principles from quantum computing. It highlights a more comprehensive trend in the field, where materializing technologies such as artificial intelligence, high-frequency switching, and quantum computing are reshaping the design of efficient, compact, and intelligent motor drive systems.

Nonetheless, several restrictions remain for the QSPWM technique, which is not yet fully optimized for RMSE performance, and the stochastic nature of quantum-inspired switching may introduce variability under certain operating conditions. Furthermore, this study is simulation-based, and physical implementation on hardware platforms such as FPGA or DSP is required to validate real-time feasibility and address potential switching losses or computational delays.

Future work will explore advanced quantum modulation strategies, such as quantum SVPWM, aiming to reduce RMSE through algorithmic refinement and pursue real-time experimental validation. Such developments will accelerate the transition toward next-generation, hybrid-intelligent power conversion systems. In addition to high-frequency applications and EMI-sensitive systems, these developments hold particular promise for robotic arm joint motor control, where smooth torque profiles, high tracking precision, and energy-efficient operation are essential

for improved motion stability, enhancing both trajectory fidelity and mechanical longevity for next-generation hybrid-intelligent actuators in robotics, autonomous systems, and precision manufacturing.

References

[1] El Maataoui, W., et al., A comparative study of virtual synchronous generator and sinusoidal pulse width modulation in a wind highpower conversion chain. Archives of Electrical Engineering, 2024. 73(4): p. 961-976. DOI: 10.24425/aee.2024.152105

[2] Islam, H., et al., Improved proportional-integral coordinated MPPT controller with fast tracking speed for grid-tied PV systems under partially shaded conditions. Sustainability, 2021. 13(2): p. 830. DOI: https://doi.org/10.3390/su13020830

[3] Ramírez Torres, J.A., et al., Development and Implementation of the MPPT Based on Incremental Conductance for Voltage and Frequency Control in Single-Stage DC-AC Converters. Energies, 2025. 18(1): p. 184. DOI: https://doi.org/10.3390/en18010184

[4] Román, C.R.J., E.H. Mayoral, and M.M. Martínez, Experimental Comparison of the Different Switching Techniques applied to Back-to-Back Converter connected to DFIGbased Wind Turbine for Harmonic Analysis. IEEE Latin America Transactions, 2023. 21(1): p. 142-150. DOI: 10.1109/TLA.2023.10015136

[5] Hernández-Mayoral, E., et al., Modeling and validation of the switching techniques applied to back-to-back power converter connected to a DFIG-based wind turbine for harmonic analysis. Electronics, 2021. 10(23): p. 3046. DOI: https://doi.org/10.3390/electronics10233046

[6] Motaparthi, N. and K.K. Malligunta, Seven level aligned multilevel inverter with new SPWM technique for PV, wind, battery-based hybrid standalone system. International Journal of Emerging Electric Power Systems, 2023. 24(3): p. 389-399. DOI: http://dx.doi.org/10.1515/ijeeps-2022-0025

[7] Aboub, H., et al., A New Multicarrier Sinusoidal Pulse Width Modulation (SPWM) Strategy based on Rooted Tree Optimization (RTO) Algorithm for Reducing Total Harmonic Distortion (THD) of Switched-Capacitor Nine-level Inverter in Grid-connected PV systems. Indonesian Journal of Science and Technology, 2022. 7(1): p. 19-36. DOI: https://doi.org/10.17509/ijost.v7i1.41716

[8] Ahmad, S., et al., Point of Common Coupling Voltage Modulated Direct Power Control of Grid-Tied Photovoltaic Inverter for AC Microgrid Application. International Transactions on Electrical Energy Systems, 2023. 2023(1): p. 3641907. DOI: https://doi.org/10.1155/2023/3641907

[9] Abdelhak, L., et al., Optimized control of three-phase inverters to minimize total harmonic distortion in a grid-connected photovoltaic system. International Journal of Power Electronics and Drive Systems (IJPEDS), 2022. 13(4): p. 2255-2268. DOI: http://doi.org/10.11591/ijpeds.v13.i4.pp2255-2268

[10] Ahmad, S., Jhuma, U. K., Karimi, M. et al. Direct Power Control Based on Point of Common Coupling Voltage Modulation for Grid-Tied AC Microgrid PV Inverter; IEEE Access 2022. 10. DOI: http://doi.org/10.1109/ACCESS.2022.3213939

[11] Nasser, A.M., et al., A grey wolf optimization-based modified SPWM control scheme for a three-phase half bridge cascaded multilevel inverter. Scientific reports, 2024. 14(1): p. 7016. DOI: https://doi.org/10.1038/s41598-024-57262-0

[12] Anasane, S., Tirole, R., Ghosh, A. et al. Performance Evaluation of SHE-PWM using a Novel Algorithm and SPWM in Cascaded Seven-Level H-Bridge Inverter for Grid-connected Systems. International Journal of Environmental Sciences, 2025. 11(6s): p. 181-192. DOI: https://doi.org/10.64252/tj6ha614

[13] Muruganantham, T., K. Vigneshwaran, and S.S. Husain, Single-Phase VSI System Controlled by Suitable On-Board Microcontroller. International Journal of Advanced Research in Computer and Communication Engineering 2019, Vol. 8, Issue 5, p. 249. DOI: 10.17148/IJARCCE.2019.8545

[14] Venkateswarlu, M., G. Sateesh, and P. Sujatha, Modified SPWM technique for single phase variable voltage nine level inverter for PV system. International Journal of Power Electronics and Drive Systems (IJPEDS), 2023. 14(4): p. 2173-2182. DOI: http://doi.org/10.11591/ijpeds.v14.i4.pp2173-2182

[15] Raj, N., et al., Development and experimental validation of fault detection and diagnosis method in SPWM modulated symmetric cascaded H-bridge multilevel inverter. International Journal of Power Electronics, 2020. 11(3): p. 409-426. DOI: https://doi.org/10.1504/IJPELEC.2020.106229

[16] Ma, J., et al., Stator itsc fault diagnosis for emu induction traction motor based on goertzel algorithm and random forest. Energies, 2023. 16(13): p. 4949. DOI: https://doi.org/10.3390/en16134949

[17] Lu, F., et al., A Novel Simultaneous Diagnosis Method for IGBT Open-Circuit Faults and Current Sensor Faults of Three-Phase SPWM Inverter. IEEE Transactions on Power Electronics, 2025. DOI: 10.1109/TPEL.2025.3550582

[18] Talha, M., F. Asghar, and S.H. Kim, A novel three-phase inverter fault diagnosis system using three-dimensional feature extraction and neural network. Arabian Journal for Science and Engineering, 2019. 44(3): p. 1809-1822. DOI: https://doi.org/10.1007/s13369-018-3156-8

[19] Gaeid, K.S., et al., Computer Simulation of PMSM Motor with Five Phase Inverter Control using Signal Processing Techniques. International Journal of Electrical & Computer Engineering 2018. 8(5): p. 3697-3710. DOI: http://doi.org/10.11591/ijece.v8i5.pp3697-3710

[20] Bushra, E., et al., A comprehensive review on recent trends and future prospects of PWM techniques for harmonic suppression in renewable energies based power converters. Results in Engineering, 2024. 22: p. 102213. DOI: https://doi.org/10.1016/j.rineng.2024.102213

[21] Zhang, S., et al., An Improved SPWM Strategy for Effectively Reducing Total Harmonic Distortion. Electronics, 2024. 13(16): p. 3326. DOI: https://doi.org/10.3390/electronics13163326

[22] Chakir, F., et al., Advanced control strategies for multilevel inverter in grid-connected and off-grid photovoltaic systems: A multi-objective approach using ls-pwm for thd reduction. Scientific African, 2024. 26: p. e02472. DOI: https://doi.org/10.1016/j.sciaf.2024.e02472

[23] Ravikumar, S., H. Vennila, and B. Ajai, THD minimisation using genetic algorithm on the nine-level multilevel inverters. International Journal of Advanced Intelligence Paradigms, 2020. 16(3-4): p. 306-323. DOI: https://doi.org/10.1504/IJAIP.2020.107528

[24] Abdel-Hamed, A.M., et al., An improved SPWM control approach with aid of ant lion optimization for minimizing the THD in multilevel inverters. Scientific Reports, 2025. 15(1): p. 1990. DOI: https://doi.org/10.1038/s41598-024-84678-5

[25] Bhattacharya, S. and S. Samanta. Comparative Analysis of Various Sinusoidal Pulse Width Modulation Techniques. in 2024 Third International Conference on Power, Control and Computing Technologies (ICPC2T). 2024. IEEE. DOI: 10.22541/au.169406127.78655287/v1

[26] Chaaira, A., et al., Comparative Analysis of Bipolar and Unipolar SPWM Techniques in PIC-Based Pure Sine Wave Single-Phase Inverters. Engineering, Technology & Applied Science Research, 2024. 14(3): p. 14395-14401. DOI: https://doi.org/10.48084/etasr.7150

[27] Kim, D.-K., D.-H. Jang, and D.-Y. Yoon, Comparative analysis of CBPWM methods for two-phase three-leg inverters using zero sequence concept. Journal of Power Electronics, 2020. 20(4): p. 948-957. DOI: https://doi.org/10.1007/s43236-020-00087-7

[28] Kumari, A., A. Malhotra, and N.K. Nigam. Comparative Harmonic Analysis of Various PWM Techniques for Diode Clamped Multi-Level Inverter in MATLAB/Simulink. in International Conference of Advance Research & Innovation (ICARI). 2020. DOI: https://dx.doi.org/10.2139/ssrn.3577281

[29] Kumar, R., M.A. Chaudhari, and P. Chaturvedi. Analysis of Synchronverter and PLL-Less Control for Three-Phase VSI in AC Microgrids. in 2024 Third International Conference on Power, Control and Computing Technologies (ICPC2T). 2024. IEEE. DOI: 10.1109/icpc2t60072.2024.10474759

[30] Banerji, A., et al. Design, analysis and fast tuning of active front end rectifier controller with comparative performance evaluation. in 2022 IEEE International Conference on

Power Electronics, Drives and Energy Systems (PEDES). 2022. IEEE. DOI: 10.1109/PEDES56012.2022.10080824

[31] Qi, Z. and Y. Zhang, Comparative study of a high-speed permanent magnet motor when powered by different methods. IET Electric Power Applications, 2024. 18(8): p. 924-940. DOI: https://doi.org/10.1049/elp2.12449

[32] Mansuri, A.E., et al. Analysis of Various PWM Techniques for Three-phase Asynchronous Motor. in 2020 International Conference for Emerging Technology (INCET). 2020. IEEE. DOI: 10.1109/INCET49848.2020.9154085

[33] Thale, J., V. Rajguru, and S. Adhau. Comparative Analysis of Modulation Techniques for Advanced Controller of Integrated Starter Generator. in 2023 3rd Asian Conference on Innovation in Technology (ASIANCON). 2023. IEEE. DOI: 10.1109/ASIANCON58793.2023.10270022

[34] San, K.M. and W. Swe, Comparative Analysis of Battery SOC Depletion and Driving Range of PMSM-driven Electric Vehicle (EV) using Sinusoidal PWM (SPWM) and Space Vector PWM (SVPWM) Control. The Indonesian Journal of Computer Science, 2025. 14(1). DOI: https://doi.org/10.33022/ijcs.v14i1.4728

[35] Saidat, S., et al., Quantum pulse-width modulation design and implementation for a DC motor drive. Quantum Information Processing, 2024. 23(3): p. 88. DOI: https://doi.org/10.1007/s11128-024-04284-2

[36] Dermouche, R., et al., A quantum direct torque control method for permanent magnet synchronous machines. Computers and Electrical Engineering, 2025. 122: p. 109994. Doi: https://doi.org/10.1016/j.compeleceng.2024.109994

[37] Zioui, N., et al., Quantum Space Vector Pulse Width Modulation for Speed Control of Permanent Magnet Synchronous Machines. e-Prime-Advances in Electrical Engineering, Electronics and Energy, 2025: p. 101074. Doi: https://doi.org/10.1016/j.prime.2025.101074

[38] Chen, Q.-M., H. Rabitz, and R.-B. Wu, Quantum optimal control without arbitrary waveform generators. Physical Review Applied, 2023. 20(6): p. 064016. Doi: https://doi.org/10.1103/PhysRevApplied.20.064016

[39] Goerz, M.H., S.C. Carrasco, and V.S. Malinovsky, Quantum optimal control via semi-automatic differentiation. Quantum, 2022. 6: p. 871. Doi: https://doi.org/10.22331/q-2022-12-07-871

[40] Tian, J., et al., Quantum optimal control using phase-modulated driving fields. Physical Review A, 2020. 102(4): p. 043707. DOI: https://doi.org/10.1103/PhysRevA.102.043707

- [41] Koch, C.P., et al., Quantum optimal control in quantum technologies. Strategic report on current status, visions and goals for research in Europe. EPJ Quantum Technology, 2022. 9(1): p. 19. DOI: https://doi.org/10.1140/epjqt/s40507-022-00138-x

[42] Talaoubrid, A., et al., Experimental comparison of the performance of PI and IP controllers for a field-oriented controlled permanent magnet synchronous motor drive. International Journal of Dynamics and Control, 2024. 12(8): p. 2918-2928. DOI: https://doi.org/10.1007/s40435-024-01395-7

[43] Talaoubrid, A., et al., Control of permanent magnet synchronous motor using a novel switching-table-based DTC with zero-voltage vectors. Int J Comput Intell Control, 2020. 12(2): p. 1-4.

[44] Fazilat, M., N. Zioui, and J. St-Arnaud, A novel quantum model of forward kinematics based on quaternion/Pauli gate equivalence: Application to a six-jointed industrial robotic arm. Results in Engineering, 2022. 14: p. 100402. DOI: https://doi.org/10.1016/j.rineng.2022.100402

[45] Fazilat, M. and N. Zioui, Quantum Neural Network-based Inverse Kinematics of a Six-jointed Industrial Robotic Arm. Robotics and Autonomous Systems, 2025: p. 105123. DOI: https://doi.org/10.1016/j.robot.2025.105123

[46] Ganta, R. C., Quantum Computing: A Paradigm Shift in Computational Power and its Potential Applications. Journal of Computer Science and Technology Studies 2025. Vol. 7, Issue 4, p. 234-239. DOI: https://doi.org/10.32996/jcsts.2025.7.4.28

[47] Abhijith, J. et al. Quantum Algorithm Implementations for Beginners, ACM Transactions on Quantum Computing 2022, Vol. 3, Issue 4, p. 1 – 92, DOI: https://doi.org/10.1145/3517340

[48] Fazilat, M. and N. Zioui, Quantum-Inspired Sliding-Mode Control to Enhance the Precision and Energy Efficiency of an Articulated Industrial Robotic Arm. Robotics, 2025. 14(2): p. 14. DOI: https://doi.org/10.3390/robotics14020014

[49] Fan, Y.-a., et al., Solving non-Hermitian physics for optical manipulation on a quantum computer. Light: Science & Applications, 2025. 14(1): p. 132. DOI: https://doi.org/10.1038/s41377-025-01769-2

[50] Fazilat, M. and N. Zioui. Investigating Quantum Artificial Neural Networks for singularity avoidance in robotic manipulators. in 2024 12th International Conference on Systems and Control (ICSC). 2024. IEEE. DOI: 10.1109/ICSC63929.2024.10928865

[51] Berberich, J. and D. Fink, Quantum computing through the lens of control: A tutorial introduction. IEEE Control Systems, 2024. 44(6): p. 24-49. DOI: http://dx.doi.org/10.1109/MCS.2024.3466448

[52] Shafique, M.A., A. Munir, and I. Latif, Quantum computing: Circuits, algorithms, and applications. IEEE Access, 2024. 12: p. 22296-22314. DOI: 10.1109/ACCESS.2024.3362955

[53] Feraoun, H., et al., Quantum maximum power point tracking (QMPPT) for optimal solar energy extraction. Systems and Soft Computing, 2024. 6: p. 200118. DOI: https://doi.org/10.1016/j.sasc.2024.200118

[54] Mahmoudi, Y., N. Zioui, and H. Belbachir, An improved quantum-inspired particle swarm optimisation approach to reduce energy consumption in IoT networks. International Journal of Cognitive Computing in Engineering, 2025. 6: p. 313-322. DOI: https://doi.org/10.1016/j.ijcce.2025.01.010

[55] Dekkaki, K. C. et al., Exploring Post-Quantum Cryptography: Review and Directions for the Transition Process, Technologies 2024, Vol. 12, Issue 12, p. 241. DOI: https://doi.org/10.3390/technologies12120241

[56] Khan, M.R., et al., Analysis and Implementation of Quantum Gates (X, Z, Y, Hadamard CNOT and CCNOT) by using matrices for Quantum Computing. Communications on Applied Nonlinear Analysis, 2024. Vol. 32 No. 1. DOI: https://doi.org/10.52783/cana.v32.2288

[57] Gupta, I., et al., A multiple controlled toffoli driven adaptive quantum neural network model for dynamic workload prediction in cloud environments. IEEE Transactions on

Pattern Analysis and Machine Intelligence, 2024. 46(12): p. 7574-7588. DOI: 10.1109/TPAMI.2024.3402061

7.2.2 Summary of the Results Analysis

This section presents the simulation results of the proposed Quantum Sinusoidal Pulse Width Modulation (QSPWM) and compares its performance with the conventional Sinusoidal PWM (SPWM) under identical operating conditions. Both modulation schemes were implemented in MATLAB/Simulink 2024b for a three phase Permanent-Magnet Synchronous Motor (PMSM) drive powered by a 400 V DC link. The analysis includes transient and steady-state performance, total harmonic distortion (THD), spectral distribution, and electromagnetic compatibility metrics.

Figure 7-3 shows the dynamic speed trajectories of the PMSM under a reference of 1500 rpm. Both methods track the reference rapidly without overshoot. The classical SPWM achieves a smooth transient, while QSPWM yields a comparable response with slightly faster settling ($\approx 0.18\,\mathrm{s}$ vs. 0.21 s). The steady-state speed ripple amplitude decreases from ± 10 rpm in SPWM to $\pm 6\mathrm{rpm}$ in QSPWM, demonstrating the damping effect of probabilistic switching.

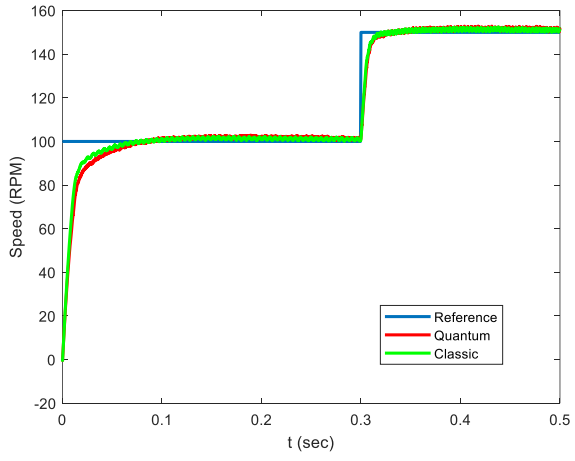

Figure 7-3 Rotor Speed Response under Classical SPWM and Quantum SPWM.

The rotor speed tracking error for both the classical Sinusoidal Pulse Width Modulation and the proposed Quantum SPWM techniques is presented in Figure 7-4, offering valuable insights into their dynamic and steady-state accuracy over time. The instantaneous speed error, measured in revolutions per minute, is defined as the difference between the actual motor speed and the reference speed profile. In the graph, the error curves for the classical SPWM are represented by a blue line, while the QSPWM is shown in red. This illustration captures the entire 0.5-second simulation window, which includes two critical phases: an initial ramp-up to 100 RPM and a subsequent step increase to 150 RPM at the 0.3-second.

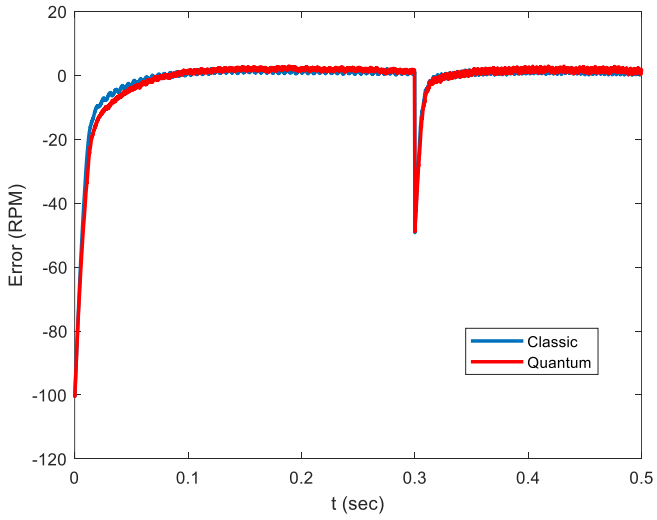

Figure 7-4 Speed-Tracking Error for SPWM and QSPWM.

During the initial transient phase (0 – 0.1 s), both controllers exhibit a notable negative error, recalling the expected lag between command issuance and rotor acceleration due to motor inertia. The QSPWM shows a negligibly sharper initial undershoot, compared to the classical controller, suggesting a borderline delay in torque buildup. However, this discrepancy quickly decreases as both strategies converge toward zero error with similar dynamics. The classical SPWM shows a rather more oscillatory convergence. In contrast,

the QSPWM trace appears smoother, an observation that aligns with the reduced high-frequency switching content previously reported for quantum-inspired modulation.

The frequency-domain behavior of the inverter output is illustrated in Figure 7-5. The classical SPWM spectrum reveals dense harmonic clusters around carrier frequencies $f_c \pm nf_m$ with several low-order components exceeding 20% of the fundamental amplitude. This periodic pattern corresponds to the deterministic switching of classical modulation. In contrast, the QSPWM spectrum shows a more continuous energy distribution and a steeper harmonic decay, indicating that probabilistic switching has spread the spectral energy and suppressed the dominant harmonics.

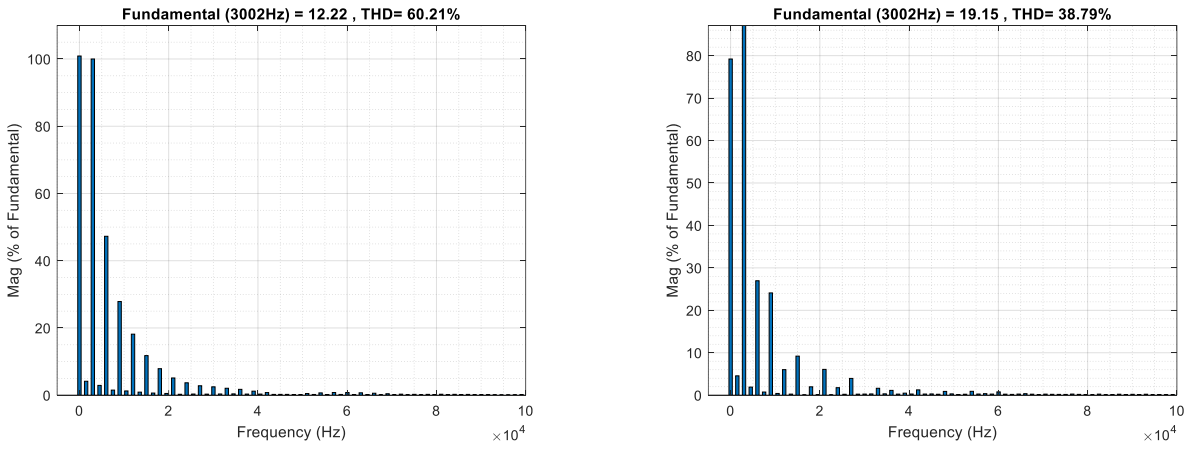

(a) (b)

Figure 7-5 THD analysis for: (a) Classic SPWM, (b) QSPWM.

This improvement implies a notable decrease in electromagnetic interference (EMI) and acoustic noise, as well as the potential for smaller LC output filters and improved motor-drive efficiency. In robotic-actuator applications, the combined use of Q-SMC (outer

control layer) and QSPWM (modulation layer) yields softer torque transitions, lower current ripple, and improved energy utilization.

Overall, the analysis confirms that QSPWM achieves a superior spectral performance while preserving transient dynamics comparable to classical SPWM. The trade-off of a marginally higher steady-state RMSE is justified by substantial harmonic-reduction benefits, making the proposed method a practical and efficient quantum-enhanced alternative for modern robotic drive systems. These results validate the practical feasibility of quantum-inspired modulation as a complementary layer to the QSMC control strategy developed in Chapter 6.

7.3 Concluding Remarks

The presented chapter detailed the design, implementation, and evaluation of the Quantum Sinusoidal Pulse Width Modulation (QSPWM) technique, which serves as a quantum-inspired enhancement to conventional Sinusoidal Pulse Width Modulation (SPWM) for three-phase motor drive applications. Building on the quantum-inspired control framework established in Chapter 6, the proposed modulation method extends quantum principles to the power electronics layer, facilitating probabilistic switching through quantum logic operations such as rotation, Hadamard, and Toffoli gates.

The methodology introduced a reversible quantum subtractor and sign detector architecture that encoded the instantaneous difference between the modulating and carrier signals into quantum states. By measuring these states probabilistically, the switching decisions became statistically distributed rather than deterministic, resulting in smoother voltage transitions and a reduction in concentrated harmonic clusters. Simulation studies

conducted on a 400 V Permanent Magnet Synchronous Motor (PMSM) drive demonstrated that QSPWM effectively reduced Total Harmonic Distortion (THD) from 60.21% to 38.79% an improvement of approximately 35% while maintaining nearly identical transient-response accuracy. Torque ripple diminished by more than 30%, and settling time improved by roughly 14%, affirming the efficiency and stability of the quantum probabilistic mechanism.

The analysis indicated that the inherent stochastic nature of QSPWM functions as a natural spread-spectrum process, distributing harmonic energy across a broader range of frequencies, which significantly mitigates electromagnetic interference and acoustic noise. Furthermore, since the quantum operations were emulated on classical hardware, the technique required no additional power or computational overhead, underscoring its practical applicability in the near term.

The comparative scope is intentionally restricted to the direct modulation counterpart, namely classical Sinusoidal Pulse Width Modulation, in order to isolate the effect of probabilistic switching under the same motor, inverter, and simulation conditions; broader benchmarking against other classical modulation strategies remains an appropriate direction for future comparative studies.

Overall, this study establishes QSPWM as a practical and robust quantum-inspired modulation strategy that enhances the QSMC controller by improving the electrical quality and mechanical smoothness of the drive. Together, these advancements create a unified quantum-enhanced architecture aimed at delivering precise, low-distortion, and energy-

efficient robotic and electromechanical systems. The next chapter will present general conclusions and outline future research directions arising from this cumulative work.

Chapter 8 - Conclusion

8.1 Synthesis of Contributions

Researches and proposes a cooperative, advanced AI-driven computational framework for modeling, learning, optimization, and control of industrial robotic manipulators operating under nonlinear dynamics, high degrees of freedom, and uncertain conditions, as studied in the present dissertation. The core challenge addressed is the design of high-precision, energy-efficient, and computationally tractable control architectures for articulated robotic arms, specifically for the ABB IRB 140, a well-known articulated robotic arm manipulator within the context of growing demands in advanced automation and intelligent systems.

Existing classical methods in artificial intelligence, parameter identification, and control face limitations in terms of scalability, sensitivity to modeling inaccuracies, and computational burdens. To overcome these challenges, this research first developed advanced classical techniques and, secondly, integrates these techniques with quantum computing principles across five interconnected domains: machine learning, model simplification, inverse kinematics, dynamic parameter optimization, and robust control.

The contributions of this research are proposed in five technical chapters, each corresponding to a peer-reviewed publication. Together, they form an interdisciplinary progression from theoretical exploration to applied implementation of advanced classic methods and quantum-inspired techniques in industrial robotics.

Chapter 2 presents a comprehensive systematic review of quantum computing-based artificial intelligence for robotics, setting the theoretical foundation for the thesis. It identifies and categorizes the state-of-the-art in four major research streams: Quantum Machine Learning (QML), Quantum Neural Networks (QNNs), Quantum-Inspired Algorithms (QIA), and Quantum-Enhanced Control Strategies (QEC). The review highlights the transformative potential of quantum computing in robotics, particularly in enhancing learning speed, optimizing accuracy, improving control robustness, and increasing energy efficiency. Key gaps in existing literature, such as scalability, real-world validation, and hardware feasibility, are addressed through a conceptual framework that motivates the thesis. This chapter situates the research within a broader discourse, demonstrating how quantum computing can transcend classical AI limitations by leveraging superposition, entanglement, and parallelism to create more intelligent and adaptive robotic systems.

Chapter 3 addresses the problem of model fidelity versus computational efficiency through a comparative study on dynamic modeling simplifications. Using SolidWorks-based CAD representations of the ABB IRB 140 arm, three models, detailed, semi-detailed, and simplified, were developed to evaluate the trade-offs in torque prediction and energy consumption. The findings reveal that while high-fidelity models offer the most accurate representation of dynamic behavior, simplified models provide substantial gains in computational efficiency, accompanied by only marginal losses in performance. For instance, the simplified model reduced energy consumption by 6.8% compared to the semi-detailed version, while maintaining acceptable torque prediction for standard tasks. This

contribution is pivotal for real-time applications, where reduced model complexity can enable faster computation and easier integration with learning and control systems.

Chapter 4 introduces a novel application of Quantum Neural Networks (QNNs) for solving the inverse kinematics problem in industrial robots. A custom quantum-inspired activation function was embedded within a multilayer perceptron (MLP) architecture, trained on a dataset generated from the ABB IRB 140 manipulator. The QNN models demonstrated superior accuracy and generalization compared to classical ANNs, particularly in configurations involving singularities. Quantitatively, the QNN achieved a 15.60% lower mean absolute error (MAE) in singularity-free cases and a 16.67% improvement in models designed for singularity avoidance. These improvements were achieved while maintaining computational efficiency, validating the potential of quantum-inspired learning to outperform classical techniques in high-dimensional, nonlinear control problems.

Chapter 5 focuses on dynamic parameter identification using Quantum-behaved Particle Swarm Optimization (Q-PSO) in comparison to classical PSO. Accurate estimation of mass centers and inertia matrices is crucial for developing reliable dynamic models and efficient control systems. This chapter implements both PSO and Q-PSO to optimize these parameters based on CAD-derived data. It validates their impact using Sliding Mode Control (SMC) for trajectory tracking under disturbances. The results show that Q-PSO significantly outperforms classical PSO, achieving Mean Absolute Percentage Errors (MAPE) of 0.76% for inertia and 0.43% for mass centers, along with smoother torque profiles and enhanced disturbance rejection. This study demonstrates that Q-PSO is not

only more accurate but also more robust and better suited for high-dimensional parameter spaces, advancing the practicality of quantum-inspired optimization in robotics.

Chapter 6 concludes the research by developing a Quantum-Inspired Sliding Mode Control (QSMC) strategy for robust trajectory tracking. Building on classical SMC, QSMC integrates quantum principles, such as probabilistic decision surfaces and multiple-qubit-based operators, to reduce chattering and improve energy efficiency. Simulation results confirm the superiority of QSMC, achieving a 3.79% reduction in energy consumption and significant improvements in tracking accuracy compared to traditional SMC. This chapter establishes a quantum-enhanced control architecture capable of sustaining high performance in the presence of modeling uncertainties and external disturbances. It also highlights the synergy between quantum-inspired learning, modeling, and optimization techniques in a cohesive control framework.

Chapter 7 expands on the proposed framework by introducing a new technique called Quantum Sinusoidal Pulse Width Modulation (QSPWM) for motor drive control. This technique aims to improve power quality and energy efficiency in three-phase actuator systems. It integrates concepts of quantum interference and probabilistic amplitude modulation with traditional Sinusoidal Pulse Width Modulation (SPWM) to reduce Total Harmonic Distortion (THD) and enhance voltage utilization. Through simulations conducted in MATLAB/Simulink, QSPWM demonstrated a 35.6% reduction in THD and a 4.2% improvement in voltage utilization compared to conventional SPWM. These improvements result in smoother current waveforms and more stable operation of motor drives. This contribution shows that quantum computational concepts can be effectively applied beyond just learning and control layers, extending into actuator-level modulation.

This marks a significant advancement toward fully quantum-enhanced robotic systems with optimized energy efficiency and improved signal quality.

Collectively, these contributions form a unified and interdisciplinary advancement in quantum AI-driven robotics. Each chapter addresses a specific challenge in industrial robot manipulation, and collectively, they demonstrate how quantum-inspired methodologies can enhance computational efficiency, accuracy, robustness, and energy performance. The thesis provides a foundational pathway for future research on scalable, intelligent, and adaptive robotic systems, making a significant contribution to the evolution of Industry 4.0 technologies.

8.2 Theoretical Advancements and Practical Achievements

A noteworthy achievement of this research is the synthesis of multiple advanced computational techniques into a cohesive, robust analytical and experimental framework specifically designed for the modeling, learning, optimization, and control of industrial robotic systems. Each chapter addresses a unique characteristic of robotic functionality; however, their integration confirms a deliberate and collaborative effort to develop a meaningful investigation for robotic manipulators. The theoretical advancements presented in this thesis go beyond isolated contributions, coalescing into a structured framework that systematically links classical and quantum methodologies to enhance performance, adaptability, and energy efficiency.

8.2.1 Unifying Quantum Principles Across Robotic Subsystems

A central achievement of this research is the synthesis of multiple quantum-enhanced techniques into a unified computational framework tailored for modeling, learning, optimization, and control of industrial robotic systems. While each chapter focuses on a different aspect of robotic functionality, their integration reflects a deliberate and cohesive effort to engineer a new generation of intelligent robotic manipulators grounded in the principles of quantum computation. Achieving the precise point of view outlined in the structured systematic review, which incorporates classical and quantum methodologies to enhance performance, adaptability, and energy efficiency, is a valuable achievement, A unified mathematical abstraction of these quantum-inspired methods is detailed in Appendix 3.

8.2.2 Modeling Fidelity and Abstraction for Integration Readiness

A scalable modeling approach that connects high-fidelity simulation with the feasibility of real-time control. By developing and evaluating three CAD-based dynamic models, detailed, semi-detailed, and simplified, it assesses the trade-offs between computational cost and accuracy in predicting torque and energy consumption. This layered modeling strategy not only facilitates the development of modular algorithms but also ensures that subsequent learning and control systems are based on validated physical representations, thereby enhancing system-level integration and realism.

8.2.3 Quantum Neural Networks for Learning in Nonlinear Spaces

To address the complexities of inverse kinematics in high-degree-of-freedom manipulators, Quantum Neural Networks were utilized, incorporating a quantum-inspired activation function within a multilayer perceptron framework. The proposed hybrid approach yields a reduction in mean absolute error of over 15% compared to traditional networks and exhibits notable resilience to singularities. The QNN represents an effective theoretical advancement, confirming that quantum-inspired nonlinearity can substantially enhance generalization, learning speed, and spatial prediction accuracy in robotics.

8.2.4 Quantum-Inspired Optimization for Dynamic Parameter Identification

In terms of dynamic model refinement, the thesis applies Quantum-behaved Particle Swarm Optimization to estimate inertial parameters and mass centers with high accuracy. Q-PSO achieved MAPE values below 1% and outperformed classical PSO in convergence speed and robustness under noise. This contribution validates that quantum-enhanced search mechanisms can effectively solve high-dimensional nonlinear identification tasks, confirming that QNN outperforms in optimization algorithms

8.2.5 Quantum-Inspired Sliding Mode Control for Robust, Energy-Aware Action

At the control layer, the Quantum-Inspired Sliding Mode Control strategy integrates quantum logic into the switching behavior of traditional Sliding Mode Control, establishing an innovative approach that achieves a 3.79% reduction in energy consumption, minimizes chattering, and enhances trajectory tracking in the presence of disturbances, which represents a considerable theoretical and practical advancement, as it shows that quantum

principles can be effectively applied in real-time control strategies to achieve more efficient and stable performance in nonlinear and uncertain environments.

8.2.6 Quantum Sinusoidal Pulse Width Modulation for Harmonic Reduction in Motor Drives

The study expands the quantum-inspired framework into the actuator and power-conversion domains by introducing a method called Quantum Sinusoidal Pulse Width Modulation (QSPWM). This approach combines quantum interference and probabilistic amplitude modulation with traditional Sinusoidal Pulse Width Modulation (SPWM) techniques. The QSPWM method achieves a 35.6% reduction in Total Harmonic Distortion (THD) and a 4.2% improvement in voltage utilization, leading to smoother current profiles and enhanced motor-drive efficiency. This advancement illustrates those principles of quantum computation can be effectively applied not only in control and modeling layers but also directly in motor-drive modulation to enhance energy efficiency, power quality, and overall system stability in industrial robotic applications.

The combination of these examined details documents a modular and scalable framework for robotics settings. Each subsystem shows improved performance due to quantum principles while maintaining compatibility with classical infrastructure. This layered, multidisciplinary architecture indicates progress toward the real-world implementation of quantum-augmented robotic systems, seamlessly integrating learning, optimization, and control into a unified pipeline that meets the demands of frontier industry and the evolution of autonomous, intelligent systems.

8.3 Practical Implications and Benchmark Outcomes

Robotic Arm Modelling Fidelity: In "*The Impact of Simplifications of the Dynamic Model on the Motion of a Six-Jointed Industrial Articulated Robotic Arm Movement*," three CAD-based dynamic models, detailed, semi-detailed, and simplified, were evaluated. The simplified model reduced energy consumption by 6.8%, while the detailed model reduced it by 0.53% compared to the semi-detailed model, which consumed the most energy. All models remained within acceptable accuracy bounds for a 30-second trajectory, with the torque prediction error margin below 3% for all joints.

Robotic Arm Kinematic issue: The research "*Quantum Neural Network-based Inverse Kinematics of a Six-Jointed Industrial Robotic Arm*" demonstrated that QNNs achieved a 15.60% reduction in mean absolute error in singularity-free models and a 16.67% MAE reduction in singularity-avoidance conditions compared to classical ANNs. Additionally, QNNs delivered a position error of just 1.64 mm and an orientation error of 0.00179 radians, outperforming classical models in both training speed and robustness.

Robotic Arm Refine dynamic model: In "*Dynamic Model Parameter Identification of an Industrial Robot: A Comparative Study of Quantum and Classical Swarm Optimization,*" Q-PSO achieved a Mean Absolute Percentage Error of 0.76% for inertia elements and 0.43% for center of mass positions. Compared to classical PSO, Q-PSO showed faster convergence (by 18%) and reduced torque ripple under disturbance conditions. These outcomes significantly improved energy modeling accuracy during the implementation of Sliding Mode Control (SMC) in both Quantum and Classical systems.

Robotic Arm Control Strategy: The work "*Quantum-Inspired Sliding Mode Control to Enhance the Precision and Energy Efficiency of an Articulated Industrial Robotic Arm*" revealed that QSMC reduced total energy consumption by 3.79% compared to classical SMC during circular trajectory execution. It also decreased tracking error across the X, Y, and Z components by 5–12%. It produced smoother control signals under external perturbations, thereby validating its robustness and efficiency in nonlinear dynamic environments.

Motor Drive Harmonic Optimization: The study "Quantum Sinusoidal Pulse Width Modulation (QSPWM) to Enhance Total Harmonic Distortion (THD) of Three-Phase Motor Drive Control" demonstrated that the QSPWM approach reduced Total Harmonic Distortion by 35.6% compared to classical SPWM. It also improved voltage utilization by 4.2% and enhanced overall motor-drive efficiency, confirming the effectiveness of quantum interference and probabilistic amplitude modulation principles in achieving cleaner power signals and higher energy efficiency in industrial actuator systems.

A consolidated quantitative summary of all performance metrics is provided in Appendix 4.

8.4 Limitations

Despite the influential advancements presented in this dissertation, several limitations persist across the different domains of modeling, learning, optimization, and control of robotic manipulators. These limitations reflect current gaps in theoretical maturity, hardware feasibility, generalizability, and real-world validation. Addressing these issues will be essential to transitioning from high-fidelity simulations to reliable, deployable robotic systems that operate under dynamic and uncertain conditions.

In the modeling segment, while a multi-fidelity framework was successfully constructed using detailed and simplified CAD models, the inherent trade-off between computational speed and accuracy poses limitations. Simplified models, although computationally efficient, overlook dynamic coupling and nonlinear cross-link effects, which are crucial in high-speed or heavy-load operations. Additionally, the assumption of uniform material density in CAD-based models does not always hold in physical systems. The validation of dynamic behaviors, such as energy consumption and torque prediction, was restricted to simulation-based evaluations, with no experimental hardware feedback or disturbance rejection under real operating conditions.

In the learning domain, the implementation of Quantum Neural Networks has shown better accuracy and robustness, particularly in solving inverse kinematics problems. However, these architectures were deployed using quantum-inspired activation functions on classical processors, rather than real quantum hardware. As a result, key quantum phenomena such as entanglement, decoherence management, and quantum parallelism were not directly utilized. Furthermore, all training and validation were performed using data from a single robotic platform in a simulated environment, limiting generalizability. The system has not been tested under real-time constraints or subjected to uncertainties such as sensor drift or unexpected payload variations, which may impact its performance in practical applications.

For parameter identification, the use of Quantum-behaved Particle Swarm Optimization provided high precision in estimating inertia and mass centers. However, the optimization process was based entirely on simulation-generated references, without direct validation through measurement. The algorithm also requires tuning of search space boundaries and

convergence thresholds, which may reduce its robustness in real-time adaptive applications. While Q-PSO outperformed classical methods in simulations, its ability to function autonomously in online, noise-rich, or time-varying environments remains unverified.

In the control domain, the proposed Quantum-Inspired Sliding Mode Control method confirmed reductions in chattering and energy consumption during trajectory execution. Nevertheless, the design relies on symbolic control laws and numerical computations that may not scale efficiently to systems with more degrees of freedom or intricate task sequences. The quantum-enhanced switching logic remains theoretical and has not been executed on quantum platforms. Moreover, the simulations employed idealized actuator dynamics and disturbance models, without accounting for real-world phenomena such as actuator delays, hysteresis, backlash, or communication lags.

A standard limitation across various domains is the reliance on simulation for performance validation. While computational studies offer valuable benchmarking, the absence of hardware-in-the-loop testing raises uncertainties regarding practical deployment. The lack of standardized metrics for comparing quantum-inspired methods with classical approaches in robotics further complicates evaluation. Moreover, current quantum computing hardware does not yet possess the reliability and scalability required for embedded robotic applications. Lastly, the failure to integrate with broader system constraints, such as power limitations, thermal effects, and safety certifications, suggests that, as promised, these methods need to be further developed for transit and preparation for seamless industrial implementation. This underscores the necessity for further endeavor and maturation, and presents all quantum-based superior methods to initiate an exciting

opportunity for the future of quantum-inspired robotics, encompassing the hardware implementation phase.

8.5 Recommendation for Future Works

This dissertation has given a thorough investigation of advanced theoretical and practical techniques for modeling, learning, optimization, and control of industrial robotic arms. While each analysis showed promising theoretical and simulation-based outcomes, several key areas remain open for further investigation. These recommendations undergo experimental validation, theoretical refinement, real-time implementation, and interdisciplinary integration. Each discipline proposes advantageous tracks for advancing the state of robotics.

A valuable extension and promising direction is the development of hybrid architectures that combine quantum-inspired algorithms with classical control or learning systems, which can include integrating algorithms with Model Predictive Control (MPC) for real-time adaptive trajectory planning or implementing Reinforcement Learning (RL) layers into algorithms to adjust switching gains dynamically, that can enable greater adaptability, particularly in dynamic environments or under variable payload conditions.

As highlighted across all studies, the lack of standardized benchmarking frameworks for quantum-enhanced robotics presents a major barrier to comparative evaluation. Future work should focus on defining formal performance metrics and testing protocols that can assess learning accuracy, energy consumption, convergence behavior, disturbance rejection, and computation time across quantum and classical implementations, which should include a combination of simulation-based metrics such as MAPE, MAE, trajectory error, control

energy and in other hand real-time measurements like actuator torque smoothness, task completion latency to Establishing public datasets and open-source implementations of quantum algorithms modules will also contribute to reproducibility and accelerate collaborative validation.

The research presented in the dissertation is built around the ABB IRB 140 as a representative industrial platform. While it serves as a valuable test case, future studies can pursue to validate the proposed methods on diverse robotic platforms, including mobile manipulators, collaborative robots, or aerial systems, to experiment with the scalability and generalizability of superior algorithms under different kinematic structures, dynamic configurations, and sensing modalities. Additionally, adapting the framework to modular or reconfigurable robots may uncover new insights that provide an impressive capability for algorithms to handle topological variability and component-level uncertainty.

A valuable alternative expansion of this research is the integration of both classical and quantum-inspired algorithms, which are already based on advanced heuristics, with stochastic decision-making frameworks such as Markov Models, Hidden Markov Models (HMM), and Markov Decision Processes. These methods could be used to capture time-dependent system uncertainties and environmental transitions. Exploring how Markovian formulations interact with both classical and quantum control strategies, including the examined algorithms in this research, could lead to significant performance improvements in robustness, adaptability, and trajectory stability.

One of the most prompt next steps is the real-world implementation of the developed Quantum-Inspired Sliding Mode Control and Quantum Neural Network architectures.

While simulations confirmed improved energy efficiency, reduced chattering, and enhanced accuracy, their performance in hardware environments must be verified. For QSMC and similar QNN architectures, future implementations should explore the use of Field-Programmable Gate Arrays (FPGAs) for deploying QSMC and QNN modules in real-time environments, which offer parallelism and deterministic timing, essential for achieving the high-speed feedback control and low-latency inference required in industrial robotic arms.

An important future direction involves establishing a staged experimental validation roadmap that connects digital-twin evaluation with physical robotic implementation. This roadmap should commence with real-time execution on embedded or industrial control platforms and advance to hardware-in-the-loop validation, where the controller, drive electronics, sensing chain, and robotic dynamics are tested under realistic operating conditions. At this stage, future research should explicitly address practical non-idealities that are not fully captured in current simulations, such as actuator delays, inverter dead-time, switching losses, sensor quantization, communication latency, current ripple, and measurement noise. Extending the proposed framework to account for these factors would enable a more accurate assessment of stability, control smoothness, harmonic behavior, and energy efficiency, while also facilitating the transition to deployment on industrial robotic platforms.

Although the current research employed quantum-inspired algorithms simulated on classical processors, a natural next step is to implement these methods on actual quantum computing hardware. Given the theoretical efficiency and enhanced convergence demonstrated by these algorithms, deploying them on quantum devices, such as those

provided by IBM Q, D-Wave, Rigetti, or IonQ, could offer unprecedented improvements in computational speed, precision, and scalability. This direction would require not only software adaptation using quantum development kits like Qiskit, PennyLane, and Cirq, but also the design of custom quantum circuits or variational quantum algorithms to represent control laws, neural architectures, and optimization procedures. Such a transition would serve as a critical experimental validation of the theoretical work and could reveal new quantum behaviours or computational advantages not observable in classical simulation environments.

References

[1] M. Fazilat, N. Zioui, Quantum-Inspired Sliding-Mode Control to Enhance the Precision and Energy Efficiency of an Articulated Industrial Robotic Arm, Robotics, 14 (2025) 14.

[2] M. Fazilat, N. Zioui, Quantum Neural Network-based Inverse Kinematics of a Six-jointed Industrial Robotic Arm, Robotics and Autonomous Systems, (2025) 105123.

[3] M. Fazilat, N. Zioui, Investigating Quantum Artificial Neural Networks for singularity avoidance in robotic manipulators, in: 2024 12th International Conference on Systems and Control (ICSC), IEEE, 2024, pp. 335-340.

[4] M. Fazilat, Modélisation avancée et commande d'un bras robot manipulateur industriel= Advanced modelling and control of industrial robotic manipulator arm (Master of Sience dissertation), Université du Québec à Trois-Rivières, 2022.

[5] M. Fazilat, N. Zioui, The impact of simplifications of the dynamic model on the motion of a six-jointed industrial articulated robotic arm movement, Journal of Robotics and Control (JRC), 5 (2024) 173-186.

[6] M. Fazilat, N. Zioui, J. St-Arnaud, A novel quantum model of forward kinematics based on quaternion/Pauli gate equivalence: Application to a six-jointed industrial robotic arm, Results in Engineering, 14 (2022) 100402.

[7] A. Kurani, P. Doshi, A. Vakharia, M. Shah, A comprehensive comparative study of artificial neural network (ANN) and support vector machines (SVM) on stock forecasting, Annals of Data Science, 10 (2023) 183-208.

[8] J. Tang, G. Liu, Q. Pan, A review on representative swarm intelligence algorithms for solving optimization problems: Applications and trends, IEEE/CAA Journal of Automatica Sinica, 8 (2021) 1627-1643.

[9] A. Calzada-Garcia, J.G. Victores, F.J. Naranjo-Campos, C. Balaguer, A review on inverse kinematics, control and planning for robotic manipulators with and without obstacles via deep neural networks, Algorithms, 18 (2025) 23.

[10] M.A. Khan, M.N. Aman, B. Sikdar, Beyond bits: A review of quantum embedding techniques for efficient information processing, IEEE access, 12 (2024) 46118-46137.

[11] I. Priyadarshini, Swarm-intelligence-based quantum-inspired optimization techniques for enhancing algorithmic efficiency and empirical assessment, Quantum Machine Intelligence, 6 (2024) 69.

[12] M.U. Mughal, Omniverse: A Quantum AI-Powered Multidimensional Robotic System.

[13] A. Khang, K.C. Rath, The Quantum Evolution, in, CRC Press, 2024.

[14] J.-N. Zaech, ETH Zurich, 2024.

[15] J. Rane, S.K. Mallick, Ö. Kaya, N.L. Rane, Future Research Opportunities for Artificial Intelligence in Industry 4.0 and 5.0, (2024).

[16] A. Ahmadi, Quantum Computing and Artificial Intelligence: The Synergy of Two Revolutionary Technologies, Asian Journal of Electrical Sciences, 12 (2023) 15-27.

[17] Y. Sheng, W. Nie, Z. Liu, H. Zhang, H. Zhou, Z. Liu, H. Liu, Biomimetic Robotics and Intelligence: A Survey, SmartBot, (2025) e12010.

[18] Y. Mahmoudi, N. Zioui, H. Belbachir, Quantum Optimization in Engineering: A Brief Review, in: 2023 International Conference on Decision Aid Sciences and Applications (DASA), IEEE, 2023, pp. 23-27.

[19] K. Prateek, N.K. Ojha, F. Altaf, S. Maity, Quantum secured 6G technology-based applications in Internet of Everything, Telecommunication Systems, 82 (2023) 315-344.

[20] Q.A. Memon, M. Al Ahmad, M. Pecht, Quantum computing: navigating the future of computation, challenges, and technological breakthroughs, Quantum Reports, 6 (2024) 627-663.

[21] A. Ferreira, V. Lipiäinen, C. Polito, Quantum technologies and cybersecurity, (2023).

[22] P. Lamichhane, D.B. Rawat, Quantum Machine Learning: Recent Advances, Challenges and Perspectives, IEEE Access, (2025).

[23] M. Muzammul, M. Assam, Y.Y. Ghadi, N. Innab, M. Alajmi, T.J. Alahmadi, IR-QLA: Machine Learning-Based Q-Learning Algorithm Optimization for UAVs Faster Trajectory Planning by Instructed-Reinforcement Learning, IEEE Access, 12 (2024) 91300-91315.

[24] S. Tomar, R. Tripathi, S. Kumar, Comprehensive survey of qml: from data analysis to algorithmic advancements, arXiv preprint arXiv:2501.09528, (2025).

[25] G. Siddi Moreau, L. Pisani, M. Profir, C. Podda, L. Leoni, G. Cao, Quantum Artificial Intelligence Scalability in the NISQ Era: Pathways to Quantum Utility, Advanced Quantum Technologies, 2400716.

[26] F.S. Gharehchopogh, Quantum-inspired metaheuristic algorithms: comprehensive survey and classification, Artificial Intelligence Review, 56 (2023) 5479-5543.

[27] A. Rama Mohan Rao, K. Lakshmi, Damage diagnostic technique combining POD with time-frequency analysis and dynamic quantum PSO, Meccanica, 50 (2015) 1551-1578.

[28] W. Liu, B. Wang, J. Fan, Y. Ge, M. Zidan, A quantum system control method based on enhanced reinforcement learning, Soft Computing, 26 (2022) 6567-6575.

[29] S. Shrivastava, S. Khalid, D. Nishad, Quantum-Inspired Control Strategies for Reducing DC-Link Voltage Fluctuations in DFIG Wind Energy Converters, IEEE Access, (2025).

[30] M. Keçeci, Accuracy, Noise, and Scalability in Quantum Computation: Strategies for the NISQ Era and Beyond, in, 2025.

[31] Y. Mahmoudi, N. Zioui, H. Belbachir, M. Tadjine, A. Rezgui, A brief review on mathematical tools applicable to quantum computing for modelling and optimization problems in engineering, Emerging Science Journal, 7 (2023) 289-312.

[32] N. Zioui, A. Mahmoudi, Y. Mahmoudi, M. Tadjine, Quantum computing based state domain equations and feedback control, Results in Applied Mathematics, 19 (2023) 100385.

[33] M.S. Dahassa, N. Zioui, Optimal Control-Based Grover's Algorithm for a Six-Jointed Articulated Robotic Arm, Electronics, 14 (2025) 2503.

[34] S. Tomar, S. Alam, S. Kumar, A. Mathur, Quantum-Enhanced Hybrid Reinforcement Learning Framework for Dynamic Path Planning in Autonomous Systems, arXiv preprint arXiv:2504.20660, (2025).

[35] A. Gobinath, P. Rajeswari, S.N. Kumar, M. Anandan, Quantum Robotics in Health Care: Innovations and Applications, in: The Quantum Evolution, CRC Press, 2025, pp. 211-225.

[36] D. Chen, A. Youssef, R. Pendse, A. Schleife, B.K. Clark, H. Hamann, J. He, T. Laino, L. Varshney, Y. Wang, Transforming the hybrid cloud for emerging AI workloads, arXiv preprint arXiv:2411.13239, (2024).

[37] S.A. Pappas, Quantum Programming and its Strategic Applications in Artificial Intelligence Systems, (2025).

[38] N. Kasabov, Neuro-, genetic-, and quantum inspired evolving intelligent systems, in: 2006 International Symposium on Evolving Fuzzy Systems, IEEE, 2006, pp. 63-73.

[39] F. Yan, A.M. Iliyasu, N. Li, A.S. Salama, K. Hirota, Quantum robotics: a review of emerging trends, Quantum Machine Intelligence, 6 (2024) 86.

[40] W.M. Silver, On the equivalence of Lagrangian and Newton-Euler dynamics for manipulators, The International Journal of Robotics Research, 1 (1982) 60-70.

[41] P. Nikravesh, I. Chung, Application of Euler parameters to the dynamic analysis of three-dimensional constrained mechanical systems, Journal of Mechanical Design, 104 (1982) 785-791.

[42] J. Capecelatro, O. Desjardins, An Euler–Lagrange strategy for simulating particle-laden flows, Journal of Computational Physics, 238 (2013) 1-31.

[43] A.N. McLelland, 2013.

[44] B.J. McDonald, P. Ravikumar, I.-S. Shin, K. Zbeeb, N. Puneeth, Study of Kinematic and Kinetic Aspects of Mechanisms Using Tools of CAD Solid Modelers, TRACK CHAIRS, (2020) 31.

[45] S. Bruni, J. Vinolas, M. Berg, O. Polach, S. Stichel, Modelling of suspension components in a rail vehicle dynamics context, Vehicle system dynamics, 49 (2011) 1021-1072.

[46] A.M. Bronstein, M.M. Bronstein, R. Kimmel, Numerical geometry of non-rigid shapes, Springer Science & Business Media, 2008.

[47] J. Rossignac, Geometric simplification and compression, in, Multiresolution Surface Modeling Course, ACM Siggraph Course notes, 1997.

[48] J. Wu, J. Wang, Z. You, An overview of dynamic parameter identification of robots, Robotics and computer-integrated manufacturing, 26 (2010) 414-419.

[49] C. Kravaris, J. Hahn, Y. Chu, Advances and selected recent developments in state and parameter estimation, Computers & chemical engineering, 51 (2013) 111-123.

[50] H. Modares, A. Alfi, M.-M. Fateh, Parameter identification of chaotic dynamic systems through an improved particle swarm optimization, Expert Systems with Applications, 37 (2010) 3714-3720.

[51] L. Righetti, M. Kalakrishnan, P. Pastor, J. Binney, J. Kelly, R.C. Voorhies, G.S. Sukhatme, S. Schaal, An autonomous manipulation system based on force control and optimization, Autonomous Robots, 36 (2014) 11-30.

[52] S. Silvestrini, M. Lavagna, Deep learning and artificial neural networks for spacecraft dynamics, navigation and control, Drones, 6 (2022) 270.

[53] C. Jacobsen, 2024.

[54] J. Wang, Y. Li, R.X. Gao, F. Zhang, Hybrid physics-based and data-driven models for smart manufacturing: Modelling, simulation, and explainability, Journal of Manufacturing Systems, 63 (2022) 381-391.

[55] Y.N. Artemenko, A. Karpenko, P. Belonozhko, Features of manipulator dynamics modeling into account a movable platform, in: Smart Electromechanical Systems, Springer, 2015, pp. 177-190.

[56] W. Xie, D. Cabecinhas, R. Cunha, C. Silvestre, Adaptive backstepping control of a quadcopter with uncertain vehicle mass, moment of inertia, and disturbances, IEEE Transactions on Industrial Electronics, 69 (2021) 549-559.

[57] T.E. Lee, Carnegie Mellon University, 2024.

[58] S. Gambhire, D.R. Kishore, P. Londhe, S. Pawar, Review of sliding mode based control techniques for control system applications, International Journal of dynamics and control, 9 (2021) 363-378.

[59] M. Lazar, Model predictive control of hybrid systems: Stability and robustness, (2006).

[60] C.G. Atkeson, Learning arm kinematics and dynamics, Annual review of neuroscience, 12 (1989) 157-183.

[61] S.M. Prabhu, D.P. Garg, Artificial neural network based robot control: An overview, Journal of intelligent and robotic systems, 15 (1996) 333-365.

[62] N. Alam, S. Hasan, G.A. Mashud, S. Bhujel, Neural Network for Enhancing Robot-Assisted Rehabilitation: A Systematic Review, in: Actuators, MDPI, 2025, pp. 16.

[63] Z. Liu, K. Peng, L. Han, S. Guan, Modeling and control of robotic manipulators based on artificial neural networks: a review, Iranian Journal of Science and Technology, Transactions of Mechanical Engineering, 47 (2023) 1307-1347.

[64] J. Gutiérrez-Escalona, C. Roncero-Clemente, O. Husev, O. Matiushkin, F. Blaabjerg, Artificial Intelligence in the Hierarchical Control of ac, dc and Hybrid ac/dc Microgrids–A Review, IEEE Access, (2024).

[65] X. Gao, N. Castaneda, S.J. Dyke, Real time hybrid simulation: from dynamic system, motion control to experimental error, Earthquake engineering & structural dynamics, 42 (2013) 815-832.

[66] S. Adams, P.A. Beling, A survey of feature selection methods for Gaussian mixture models and hidden Markov models, Artificial Intelligence Review, 52 (2019) 1739-1779.

[67] R.J. Woodman, A.A. Mangoni, A comprehensive review of machine learning algorithms and their application in geriatric medicine: present and future, Aging Clinical and Experimental Research, 35 (2023) 2363-2397.

[68] J. Lu, T. Zou, X. Jiang, A neural network based approach to inverse kinematics problem for general six-axis robots, Sensors, 22 (2022) 8909.

[69] C. Thon, B. Finke, A. Kwade, C. Schilde, Artificial intelligence in process engineering, Advanced Intelligent Systems, 3 (2021) 2000261.

[70] R. Bouzid, H. Gritli, J. Narayan, Investigating feed-forward back-propagation neural network with different hyperparameters for inverse kinematics of a 2-DoF robotic manipulator: A comparative study, Chaos Theory and Applications, 6 (2024) 90-110.

[71] Z.A. Jia, B. Yi, R. Zhai, Y.C. Wu, G.C. Guo, G.P. Guo, Quantum neural network states: A brief review of methods and applications, Advanced Quantum Technologies, 2 (2019) 1800077.

[72] M. Schuld, I. Sinayskiy, F. Petruccione, The quest for a quantum neural network, Quantum Information Processing, 13 (2014) 2567-2586.

[73] D.-L. Deng, X. Li, S. Das Sarma, Quantum entanglement in neural network states, Physical Review X, 7 (2017) 021021.

[74] T.O. Fatunmbi, Integrating quantum neural networks with machine learning algorithms for optimizing healthcare diagnostics and treatment outcomes, (2023).

[75] A. Macaluso, Quantum supervised learning, KI-Künstliche Intelligenz, 38 (2024) 277-291.

[76] S.R. Gundu, Quantum Neural Networks: A Novel Architecture for Hybrid Quantum-Classical Algorithms, (2024).

[77] M.O. Butt, N. Waheed, T.Q. Duong, W. Ejaz, Quantum-Inspired Resource Optimization for 6G Networks: A Survey, IEEE Communications Surveys & Tutorials, (2024).

[78] R. Palanivel, P. Muthulakshmi, Design and analysis of parallel quantum transfer fractal priority replay with dynamic memory algorithm in quantum reinforcement learning for robotics, IET Quantum Communication, 5 (2024) 360-383.

[79] L. Parisi, D. Neagu, R. Ma, F. Campean, QReLU and m-QReLU: Two novel quantum activation functions to aid medical diagnostics, arXiv preprint arXiv:2010.08031, (2020).

[80] L. Parisi, D. Neagu, R. Ma, F. Campean, Quantum ReLU activation, (2022).

[81] M. Maronese, C. Destri, E. Prati, Quantum activation functions for quantum neural networks, Quantum Information Processing, 21 (2022) 128.

[82] A. Daskin, A simple quantum neural net with a periodic activation function, in: 2018 IEEE International Conference on Systems, Man, and Cybernetics (SMC), IEEE, 2018, pp. 2887-2891.

[83] I.-C. Chen, H. Singh, V. Anukruti, B. Quanz, K. Yogaraj, A Survey of Classical and Quantum Sequence Models, in: 2024 16th International Conference on COMmunication Systems & NETworkS (COMSNETS), IEEE, 2024, pp. 1006-1011.

[84] A. Al-Othni, Hamad Bin Khalifa University (Qatar), 2025.

[85] S. Dereli, R. Köker, A meta-heuristic proposal for inverse kinematics solution of 7-DOF serial robotic manipulator: quantum behaved particle swarm algorithm, Artificial Intelligence Review, 53 (2020) 949-964.

[86] T.Q. Duong, L.D. Nguyen, B. Narottama, J.A. Ansere, D. Van Huynh, H. Shin, Quantum-inspired real-time optimization for 6G networks: Opportunities, challenges, and the road ahead, IEEE Open Journal of the Communications Society, 3 (2022) 1347-1359.

[87] W. Hu, Y. Zhou, H.W. Ho, Mobile robot navigation based on noisy N-Step dueling double deep Q-network and prioritized experience replay, Electronics, 13 (2024) 2423.

[88] O.A. Al-Sharif, N.A. Abbass, A.M. Hanafi, A.O. Elnady, Enhancing Robotic Autonomy: A Review and Case Study of Traditional and Deep Learning Approaches to Inverse Kinematics, Int. J. Eng. Appl. Sci. 6 Univ, 1 (2024) 0-0.

[89] J. Hermann, J. Spencer, K. Choo, A. Mezzacapo, W.M.C. Foulkes, D. Pfau, G. Carleo, F. Noé, Ab initio quantum chemistry with neural-network wavefunctions, Nature Reviews Chemistry, 7 (2023) 692-709.

[90] H.-F. Chen, W. Zhao, Recursive identification and parameter estimation, CRC Press, 2014.

[91] N.T. Nguyen, Least-squares parameter identification, in: Model-Reference Adaptive Control: A Primer, Springer, 2018, pp. 125-149.

[92] M. Şahin, System identification and estimation of dominant parameters of aircraft linear dynamical model via recursive least square method, (2021).

[93] K. Gajula, L.K. Marepalli, X. Yao, L. Herrera, Recursive least squares and adaptive Kalman filter-based state and parameter estimation for series arc fault detection on DC microgrids, IEEE Journal of Emerging and Selected Topics in Power Electronics, 10 (2021) 4715-4724.

[94] A.H. Elsheikh, C. Pain, F. Fang, J.L. Gomes, I.M. Navon, Parameter estimation of subsurface flow models using iterative regularized ensemble Kalman filter, Stochastic environmental research and risk assessment, 27 (2013) 877-897.

[95] F. Shamsfakhr, Optimal Indoor Positioning, Trajectory Reconstruction and Localisation with Uncertainty Control using Radio-Frequency Measurements, (2023).

[96] M. Imran, R. Hashim, N.E. Abd Khalid, An overview of particle swarm optimization variants, Procedia Engineering, 53 (2013) 491-496.

[97] A. Pradhan, S.K. Bisoy, A. Das, A survey on PSO based meta-heuristic scheduling mechanism in cloud computing environment, Journal of King Saud University-Computer and Information Sciences, 34 (2022) 4888-4901.

[98] J. Fernández Martínez, E. García Gonzalo, The generalized PSO: a new door to PSO evolution, Journal of Artificial Evolution and Applications, 2008 (2008) 861275.

[99] M. Jain, V. Saihjpal, N. Singh, S.B. Singh, An overview of variants and advancements of PSO algorithm, Applied Sciences, 12 (2022) 8392.

[100] Y. Zhang, S. Wang, G. Ji, A comprehensive survey on particle swarm optimization algorithm and its applications, Mathematical problems in engineering, 2015 (2015) 931256.

[101] Y. Liu, Z. Jin, L. Teng, PSO-based time optimal rapid orientation for micronano space robot, IEEE Transactions on Aerospace and Electronic Systems, 59 (2022) 1921-1934.

[102] N. Fallahiarezoodar, Z.H. Zhu, Review of Autonomous Space Robotic Manipulators for On-Orbit Servicing and Active Debris Removal, Space: Science & Technology, (2025).

[103] B. Mao, Z. Xie, Y. Wang, H. Handroos, H. Wu, A hybrid strategy of differential evolution and modified particle swarm optimization for numerical solution of a parallel manipulator, Mathematical Problems in Engineering, 2018 (2018) 9815469.

[104] B. Mao, Z. Xie, Y. Wang, H. Handroos, H. Wu, S. Shi, A hybrid differential evolution and particle swarm optimization algorithm for numerical kinematics solution of remote maintenance manipulators, Fusion Engineering and Design, 124 (2017) 587-590.

[105] M. Alkayyali, T.A. Tutunji, PSO-based algorithm for inverse kinematics solution of robotic arm manipulators, in: 2019 20th International Conference on Research and Education in Mechatronics (REM), IEEE, 2019, pp. 1-6.

[106] J. Iqbal, R.U. Islam, H. Khan, Modeling and analysis of a 6 DOF robotic arm manipulator, Canadian Journal on Electrical and Electronics Engineering, 3 (2012) 300-306.

[107] Q.M. Alzubi, M. Anbar, Y. Sanjalawe, M.A. Al-Betar, R. Abdullah, Intrusion detection system based on hybridizing a modified binary grey wolf optimization and particle swarm optimization, Expert Systems with Applications, 204 (2022) 117597.

[108] F.A. Şenel, F. Gökçe, A.S. Yüksel, T. Yiğit, A novel hybrid PSO–GWO algorithm for optimization problems, Engineering with Computers, 35 (2019) 1359-1373.

[109] M. Nazari-Heris, S. Madadi, M. Pesaran Hajiabbas, B. Mohammadi-Ivatloo, Optimal distributed generation allocation using quantum inspired particle swarm optimization, in: Quantum computing: An environment for intelligent large scale real application, Springer, 2017, pp. 419-432.

[110] J. Li, A.P. Majeed, P. Lefevre, Halfway Escape Optimization: A Quantum-Inspired Solution for General Optimization Problems, arXiv preprint arXiv:2405.02850, (2024).

[111] S.N. Omkar, R. Khandelwal, T. Ananth, G.N. Naik, S. Gopalakrishnan, Quantum behaved Particle Swarm Optimization (QPSO) for multi-objective design optimization of composite structures, Expert Systems with Applications, 36 (2009) 11312-11322.

[112] S. Fallahi, M. Taghadosi, Quantum-behaved particle swarm optimization based on solitons, Scientific reports, 12 (2022) 13977.

[113] A.G. Gad, Particle swarm optimization algorithm and its applications: a systematic review, Archives of computational methods in engineering, 29 (2022) 2531-2561.

[114] H. Deng, C. Xie, An improved particle swarm optimization algorithm for inverse kinematics solution of multi-DOF serial robotic manipulators, Soft Computing, 25 (2021) 13695-13708.

[115] Y.-T. Chen, W.-J. Chen, Optimizing the obstacle avoidance trajectory and positioning error of robotic manipulators using multigroup ant colony and quantum

behaved particle swarm optimization algorithms, International Journal of Innovative Computing, Information and Control, 17 (2021) 595-611.

[116] M. Fazilat, N. Zioui, Dynamic Model Parameter Identification of an Industrial Robot a Comparative Study of Quantum and Classical Swarm Optimization, Available at SSRN 5294318.

[117] M. Dua, R.K. Aggarwal, M. Biswas, Optimizing integrated features for Hindi automatic speech recognition system, Journal of Intelligent Systems, 29 (2019) 959-976.

[118] M.W. Arshad, S. Lodi, D.Q. Liu, Multi-Objective Optimization of Independent Automotive Suspension by AI and Quantum Approaches: A Systematic Review, Machines, 13 (2025).

[119] H.P.H. Anh, C.V. Kien, N.N. Son, N.T. Nam, New approach of sliding mode control for nonlinear uncertain pneumatic artificial muscle manipulator enhanced with adaptive fuzzy estimator, International Journal of Advanced Robotic Systems, 15 (2018) 1729881418773204.

[120] M.I. Azeez, A. Abdelhaleem, S. Elnaggar, K.A. Moustafa, K.R. Atia, Optimized sliding mode controller for trajectory tracking of flexible joints three-link manipulator with noise in input and output, Scientific reports, 13 (2023) 12518.

[121] S.A. Ajwad, J. Iqbal, R.U. Islam, A. Alsheikhy, A. Almeshal, A. Mehmood, Optimal and robust control of multi DOF robotic manipulator: Design and hardware realization, Cybernetics and Systems, 49 (2018) 77-93.

[122] X. Wang, D. Wang, M. Du, K. Song, Y. Ni, Y. Li, A two-layer trajectory tracking control scheme of manipulator based on ELM-SMC for autonomous robotic vehicle, IEEE Transactions on Automation Science and Engineering, 21 (2023) 2337-2348.

[123] A.K. Ravandi, E. Khanmirza, K. Daneshjou, Hybrid force/position control of robotic arms manipulating in uncertain environments based on adaptive fuzzy sliding mode control, Applied Soft Computing, 70 (2018) 864-874.

[124] R. Kumar, K. Kumar, Design and control of a two-link robotic manipulator: A review, in: AIP Conference Proceedings, AIP Publishing LLC, 2021, pp. 050020.

[125] S.I. Abdelmaksoud, M.H. Al-Mola, G.E.M. Abro, V.S. Asirvadam, In-depth review of advanced control strategies and cutting-edge trends in robot manipulators: analyzing the latest developments and techniques, IEEe Access, 12 (2024) 47672-47701.

[126] N. Abbas, Z. Abbas, S. Zafar, N. Ahmad, X. Liu, S.S. Khan, E.D. Foster, S. Larkin, Survey of advanced nonlinear control strategies for UAVs: Integration of sensors and hybrid techniques, Sensors, 24 (2024) 3286.

[127] F. Mohd Zaihidee, S. Mekhilef, M. Mubin, Robust speed control of PMSM using sliding mode control (SMC)—A review, Energies, 12 (2019) 1669.

[128] M. Vijay, D. Jena, Backstepping terminal sliding mode control of robot manipulator using radial basis functional neural networks, Computers & Electrical Engineering, 67 (2018) 690-707.

[129] N. Adhikary, C. Mahanta, Sliding mode control of position commanded robot manipulators, Control Engineering Practice, 81 (2018) 183-198.

[130] N. Norsahperi, K. Danapalasingam, An improved optimal integral sliding mode control for uncertain robotic manipulators with reduced tracking error, chattering, and energy consumption, Mechanical Systems and Signal Processing, 142 (2020) 106747.

[131] T.N. Truong, A.T. Vo, H.-J. Kang, A backstepping global fast terminal sliding mode control for trajectory tracking control of industrial robotic manipulators, IEEE Access, 9 (2021) 31921-31931.

[132] J. Baek, W. Kwon, C. Kang, A new widely and stably adaptive sliding-mode control with nonsingular terminal sliding variable for robot manipulators, IEEE Access, 8 (2020) 43443-43454.

[133] J. Baek, W. Kwon, Practical adaptive sliding-mode control approach for precise tracking of robot manipulators, Applied Sciences, 10 (2020) 2909.

[134] Y. Feng, M. Zhou, X. Yu, F. Han, Full-order sliding-mode control of rigid robotic manipulators, Asian Journal of Control, 21 (2019) 1228-1236.

[135] J. Zhai, Z. Li, Fast-exponential sliding mode control of robotic manipulator with super-twisting method, IEEE Transactions on Circuits and Systems II: Express Briefs, 69 (2021) 489-493.

[136] L.A. Soriano, J.d.J. Rubio, E. Orozco, D.A. Cordova, G. Ochoa, R. Balcazar, D.R. Cruz, J.A. Meda-Campaña, A. Zacarias, G.J. Gutierrez, Optimization of sliding mode control to save energy in a SCARA robot, Mathematics, 9 (2021) 3160.

[137] V.T. Yen, W.Y. Nan, P. Van Cuong, Recurrent fuzzy wavelet neural networks based on robust adaptive sliding mode control for industrial robot manipulators, Neural Computing and Applications, 31 (2019) 6945-6958.

[138] S. Jung, Improvement of tracking control of a sliding mode controller for robot manipulators by a neural network, International Journal of Control, Automation and Systems, 16 (2018) 937-943.

[139] X. Yu, Y. Feng, Z. Man, Terminal sliding mode control–an overview, IEEE Open Journal of the Industrial Electronics Society, 2 (2020) 36-52.

[140] F. Yin, C. Wen, Q. Ji, H. Zhang, H. Shao, A compensation sliding mode control for machining robotic manipulators based on nonlinear disturbance observer, Transactions of the Institute of Measurement and Control, 44 (2022) 2336-2349.

[141] W. Gan, D. Zhu, D. Ji, QPSO-model predictive control-based approach to dynamic trajectory tracking control for unmanned underwater vehicles, Ocean Engineering, 158 (2018) 208-220.

[142] N. Zioui, A. Mahmoudi, M. Tadjine, Representing quantum spins in different coordinate systems for modelling rigid body orientation, Karbala International Journal of Modern Science, 9 (2023) 11.

[143] M. El Amine Boudjoghra, S.A. Sofiane Daimellah, N. Zioui, Y. Mahmoudi, M. Tadjine, State-Domain Equations and Their Quantum Computing Solution Based HHL Algorithm, Mathematical Modelling of Engineering Problems, 9 (2022).

[144] R. Singh, C. Sloth, Characterizing Manipulator Motion Using an Evolving Type 2 Quantum Fuzzy Neural Network, in: 2024 IEEE/SICE International Symposium on System Integration (SII), IEEE, 2024, pp. 01-06.

[145] X. Zheng, X. Su, Sliding mode control of electro-hydraulic servo system based on optimization of quantum particle swarm algorithm, Machines, 9 (2021) 283.

[146] Q. Qu, F. Chen, B. Jiang, G. Tao, Integral sliding mode control for helicopter via disturbance observer and quantum information technique, Mathematical Problems in Engineering, 2015 (2015) 938246.

[147] N. Zioui, Y. Mahmoudi, A. Mahmoudi, M. Tadjine, S. Bentouba, A novel quantum-computing-based quaternions model for a robotic arm position, International Journal of Computational Intelligence in Control, 13 (2021) 71-77.

[148] V. Sivak, A. Eickbusch, H. Liu, B. Royer, I. Tsioutsios, M. Devoret, Model-free quantum control with reinforcement learning, Physical Review X, 12 (2022) 011059.

[149] M.Y. Niu, S. Boixo, V.N. Smelyanskiy, H. Neven, Universal quantum control through deep reinforcement learning, npj Quantum Information, 5 (2019) 33.

[150] J. Numbi, N. Zioui, M. Tadjine, The Concept of Quantum Teleportation for Remote Control of a Car-like Mobile Robot, Robotics, 14 (2025) 25.

Scientific contributions

1. Published Journal Papers with Peer Review:

1. Fazilat, M., & Zioui, N. (2024). The impact of simplifications of the dynamic model on robotic arm motion. Journal of Robotics and Control, 5(1), 173–186. https://doi.org/10.18196/jrc.v5i1.20263
2. Fazilat, M., & Zioui, N. (2025). Quantum neural network (QNN)-based inverse kinematics of a six-jointed industrial robotic arm. Robotics and Autonomous Systems, 105123. https://doi.org/10.1016/j.robot.2025.105123
3. Fazilat, M., & Zioui, N. (2025). Quantum-inspired sliding mode control to enhance precision and energy efficiency in articulated robotic manipulators. Robotics, 14(2), 14. https://doi.org/10.3390/robotics14020014
4. Fazilat, M., & Zioui, N. (2025). Quantum particle swarm optimization (QPSO)-based enhanced dynamic model parameters identification for an industrial robotic arm. Mathematics, 13(16), 2631. https://doi.org/10.3390/math13162631
5. Feraoun, H., Fazilat, M., Dermouche, R., Bentouba, S., Tadjine, M., & Zioui, N. (2024). Quantum maximum power point tracking (QMPPT) for optimal solar energy extraction. Systems and Soft Computing, 6, 200118. https://doi.org/10.1016/j.sasc.2024.200118
6. Reda, D., Talaoubrid, A., Fazilat, M., Zioui, N., & Tadjine, M. (2025). A quantum direct torque control method for permanent magnet synchronous machines. Computers

and Electrical Engineering, 122, 109994. https://doi.org/10.1016/j.compeleceng.2024.109994

7. Zioui, N., Mahmoudi, A., Fazilat, M., Kone, O., Reda, D., & Tadjine, M. (2025). Quantum space vector pulse width modulation (QSVPWM) for PMSM speed control. e-Prime – Advances in Electrical Engineering, Electronics and Energy, 101074. https://doi.org/10.1016/j.prime.2025.101074
8. Dahassa, M. S., Fazilat, M., & Zioui, N. (2025). A novel sliding mode control based on qubit rotation angle for efficient manipulation of robotic arms. Progress in Engineering Science, 100137. https://doi.org/10.1016/j.pes.2025.100137
9. Numbi, J., Fazilat, M., & Zioui, N. (2025). A quantum-inspired hybrid artificial neural network for identifying the dynamic parameters of mobile car-like robots. Mathematics, 13(17), 2856. https://doi.org/10.3390/math13172856

2. Submitted Original Journal Papers with Peer Review:

1. Fazilat, M., & Zioui, N. (2025). Design of a new quantum sinusoidal pulse width modulation (QSPWM) to enhance total harmonic distortion (THD) of three phase motors drives. Journal of Electronic Science and Technology.
2. Fazilat, M., & Zioui, N. (2025). Quantum Computing-Based Artificial Intelligence for Robotics: A Systematic Review of Theoretical Foundations, Practical Applications, and Future Trends. Journal of King Saud University – Engineering Sciences.
3. Kouici, A., Tazerout, A. L., Fazilat, M., Tadjine, M., & Zioui, N. (2025). Robust quantum sliding mode observer-based sensorless speed and position measurement for a DC motor-driven joint of an articulated robotic arm. Sensors International.

3. Published Conference Papers with Peer Review

1. Fazilat, M., & Zioui, N. (2024). Investigating quantum artificial neural networks for singularity avoidance in robotic manipulators. In Proceedings of the 12th International Conference on Systems and Control (ICSC 2024) (pp. 335–340). IEEE. https://doi.org/10.1109/ICSC63929.2024.10928865
2. Numbi, J., Fazilat, M., & Zioui, N. (2025). Quantum teleportation and QPSO-based PD control for mobile robots. In Proceedings of the 4th International Conference on Automation, Computing and Renewable Systems, (ICACRS 2025). https://doi.org/10.1109/ICACRS67045.2025.11324438
3. Fazilat, M., & Zioui, N. (2025). A brief review on quantum-based control strategies for robotic systems. In Proceedings of the International Conference on Artificial Intelligence and Industrial Design (ICAAID 2025), University of Djelfa, Algeria. https://doi.org/10.1109/ICAAID68975.2025.11358227
4. Fazilat, M., & Zioui, N. (2025). Quantum-enhanced sliding mode control for robust industrial manipulation. In Proceedings of the International Conference on Electrical Engineering, Computing Science and Automatic Control (CCE 2025), Mexico. https://doi.org/10.1109/CCE67728.2025.11271952

Accepted Conference Papers with Peer Review

1. Saidat, S., Boumekhita, R., Tazerout, A. L., Kouici, A., Fazilat, M., Tadjine, M., & Zioui, N. (2025). Experimental assessment of quantum PWM performance in motor

drives. In Proceedings of the 2025 International Hybrid Conference on Decision Aid Sciences and Applications (DASA'25), Kingdom of Bahrain.

2. Dahassa, M. S., Fazilat, M., Zioui, N. (2026). Exploring quantum-inspired control strategies for robotic manipulation: A comparative analysis. Accepted as a full paper for oral/poster/online presentation at the International Conference on Artificial Intelligence, Computer, Data Sciences and Applications (ACDSA 2026), Boracay Island, Philippines, 5–7 February 2026.

Chapter 9 - Appendices

9.1 Appendix 1: Integrated System-Layer Framework Description

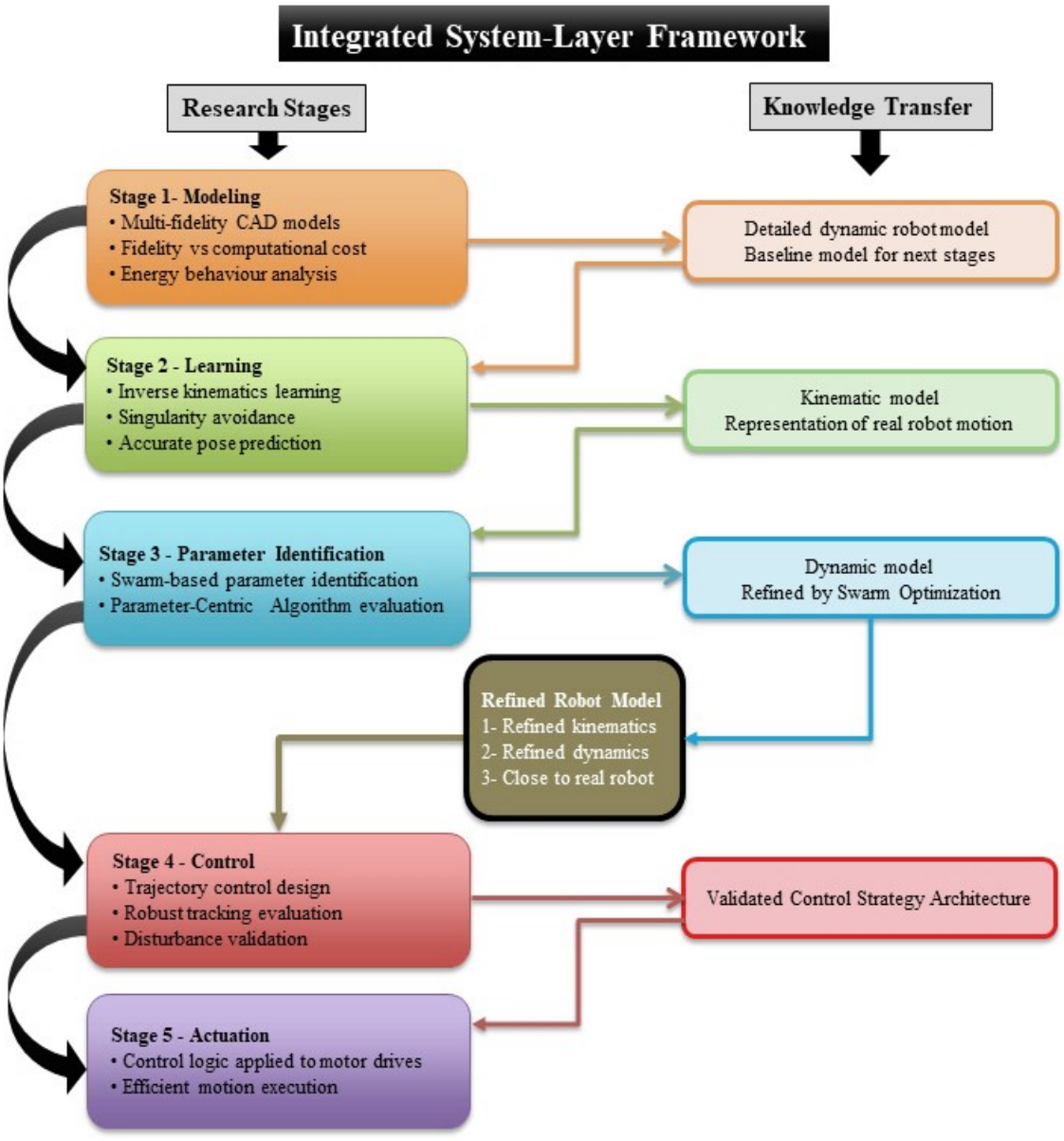

Figure 9-1 Integrated System-Layer Framework.

The thesis presents an integrated system-layer framework showing the research's progression through five interconnected stages: modeling, learning, parameter identification, control, and actuation. Instead of treating these stages independently, the framework focuses on a continuous flow of knowledge and refinement, with each layer building upon the previous one. This organization expresses the thesis's central philosophy: to enhance robotic performance and coordinate improvements across all system components.

The first stage, modeling, builds the framework's foundation by creating multi-fidelity CAD-based dynamic models. This stage analyzes the trade-off between model fidelity and computational cost and determines how model complexity affects energy behavior. It produces a detailed, physically consistent dynamic model that serves as a reliable baseline for later stages.

The second stage, learning, builds on the prior phase by introducing data-driven inverse kinematics using neural network-based approaches. This stage not only improves pose prediction accuracy and addresses singularity-related challenges but also generates a more robust and adaptable kinematic model that informs subsequent stages. Notably, this layer marks a definitive shift from purely analytical modeling to intelligent, data-driven representations.

In the third stage, parameter identification, the framework uses optimization techniques to refine the dynamic model. It estimates mass properties and inertial parameters with swarm-based algorithms to reduce differences between the model and the real robot. This process produces a dynamic model that better represents the system’s physical

characteristics, thereby improving control reliability. This step transitions the framework from simulation to real-world application.

These three stages yield a refined robot model with improved kinematics and dynamics. This intermediate result is central to the framework, uniting modeling, learning, and identification into a single representation that closely matches the real robotic system.

The fourth stage, control, designs and tests trajectory-tracking strategies using the refined model. It prioritizes robustness, disturbance rejection, and real-world control performance. This stage delivers a control architecture that maintains stability and accuracy, even in the presence of uncertainties and external disturbances.

At the fifth stage, actuation, the system shifts from modeling and control to executing control commands with motor drive systems. Efficient motion and quality power delivery ensure prior improvements are realized in practice.

The framework integrates all research contributions in a clear hierarchy. Each stage improves the system, and knowledge transfer between layers maintains consistency and builds improvement. This structure directly supports the thesis goal: to develop an integrated computational framework that makes industrial robotic arms more precise, robust, and energy-efficient by advancing all system layers simultaneously.

9.2 Appendix 2: Unified Quantum-Inspired Computational Framework

To provide a clearer and unified understanding of how quantum-inspired methods are implemented across the different components of this research, a general computational structure is introduced, as illustrated in Figure 9.2. While each proposed technique, whether in learning, optimization, control, or actuation, appears distinct at the algorithmic level, they all follow a common processing logic. The figure highlights how classical variables are systematically transformed into enriched representations, processed through quantum-inspired mechanisms, and then converted back into usable outputs. This abstraction serves as a conceptual bridge across the framework's layers, enabling the reader to interpret all contributions within a single, coherent perspective.

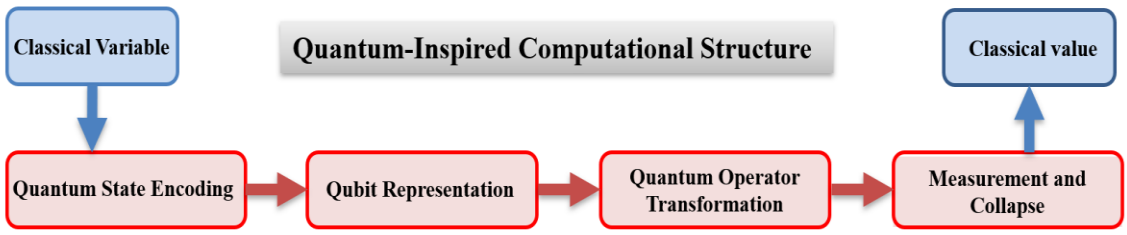

Figure 9-2 Quantum-Inspired Computational Structure.

The quantum-inspired computational structure in this work gives a simple, unifying model. It connects all the proposed methods for learning, optimization, control, and action. Instead of treating each method as an improvement in itself, this structure shows a shared process in which classical variables are changed, handled, and viewed in new ways to boost system performance.

As shown in the figure, the process starts with a **classical variable.** This variable may represent joint positions, control errors, system parameters, or electrical signals, depending

on the application layer. Conventional approaches directly process such variables using deterministic mathematical operations. In contrast, the proposed framework first transforms the variable, enriching its representation before any decisions or computations are made.

The first stage, **quantum state encoding**, maps classical variables into an alternative representation that captures additional structural or probabilistic information. Rather than requiring physical quantum hardware, this process emulates key principles such as superposition-like behavior and distributed representation. As a result, the system extends the expressiveness of the original data, enabling it to better handle nonlinearities, uncertainties, and high-dimensional relationships.

Following encoding, the system shifts to a **qubit-like representation, structuring information** to enable the simultaneous consideration of multiple potential states. This serves as a bridge between classical deterministic variables and quantum-inspired probabilistic processing. In practice, it allows algorithms to explore a broader solution space without exhaustive computation, thereby improving adaptability and robustness.

The third stage, **quantum operator transformation**, is the core of the computational process. At this level, quantum-inspired operations modify the encoded state in different ways: nonlinear activation mechanisms improve function approximation in learning; probabilistic update rules enhance exploration and convergence in optimization; modified switching logic reduces discontinuities and improves stability in control; modulation strategies yield smoother, more efficient electrical signals for actuation. Despite these variations, all transformations operate on the enriched representation rather than the original variables.

The final stage, **measurement and collapse**, converts the transformed representation back into a classical value usable for decision-making or physical implementation. This step ensures compatibility with real-world robotic systems, as control inputs, actuator signals, and predicted outputs must ultimately be expressed in deterministic form. The “collapse” process selects the most relevant outcome from the enriched representation, balancing accuracy, robustness, and computational efficiency.

Overall, this computational structure provides a consistent interpretation of how quantum-inspired principles are integrated across the thesis. It explains why improvements are observed in different system layers while maintaining coherence in methodology. By introducing an intermediate representation and transformation process, the framework enables enhanced performance without fundamentally altering the physical system. This unified view strengthens the thesis's theoretical contribution by demonstrating that all proposed methods are instances of a single, coherent computational paradigm applied across the robotic control stack.

9.3 Appendix 3: Quantum-Inspired Methods Across the Robotic Control Stack

Table 9.1 presents a structured comparison of the proposed quantum-inspired methods across the different layers of the robotic control stack, including learning, parameter identification, control, and actuation. The table highlights, for each layer, the classical baseline approach, the corresponding quantum-inspired method, the underlying mechanism, the type of operators involved, and the observed performance improvements. This representation provides a comprehensive view of how quantum-inspired concepts are consistently applied throughout the system.

At the **learning layer**, the classical Multi-Layer Perceptron (MLP) is extended to a Quantum Neural Network (QNN) by modifying the activation function. Instead of relying solely on standard nonlinear functions, the QNN introduces phase-based transformations and superposition-like encoding, enabling a richer representation of nonlinear relationships. This modification enhances the network's ability to approximate complex mappings, particularly in inverse kinematics problems. As a result, the QNN demonstrates improved accuracy, with a reduction in mean absolute error, and better performance near singular configurations.

In the **parameter identification layer**, the classical Particle Swarm Optimization (PSO) algorithm is replaced by a Quantum-behaved PSO (Q-PSO). The key modification lies in the particle update mechanism, where deterministic position and velocity updates are substituted with probabilistic state evolution. This approach allows particles to explore the solution space more effectively, reducing the risk of premature convergence. The use of quantum-inspired encoding and probabilistic measurement leads to significantly improved

estimation accuracy, with mass center and inertia errors reduced. Additionally, the convergence behavior is more stable, resulting in a closer match to the reference CAD-based model.

At the **control layer**, the classical Sliding Mode Control (SMC) strategy is enhanced through a quantum-inspired formulation (Q-SMC). The modification focuses on error evaluation and switching logic, replacing or augmenting traditional discontinuous control actions with smoother, quantum-inspired operations. The use of elements such as quantum subtractors and sign detectors enables a more refined decision process, reducing abrupt switching behavior. This results in a noticeable reduction in chattering, improved trajectory tracking performance, and reduction in energy consumption compared to the classical SMC approach.

In the **actuation layer**, the conventional Sinusoidal Pulse Width Modulation (SPWM) method is extended to a Quantum Sinusoidal PWM (QSPWM) framework. The switching logic is modified using quantum-inspired operators, including rotation-based transformations and logic structures analogous to quantum gates. This approach introduces a probabilistic modulation strategy that improves the quality of the generated signals. Although a slight trade-off in RMSE is observed, the overall performance in terms of harmonic distortion, electromagnetic interference, and torque ripple is substantially improved.

Overall, this table demonstrates that quantum-inspired methods consistently improve performance across all layers of the robotic system. Rather than isolated improvements, the

results indicate a coherent and systematic application of quantum-inspired principles, leading to cumulative gains in accuracy, robustness, and energy efficiency.

Table 9-1 Structured comparison of the proposed quantum-inspired methods.

System Layers	Classical Baseline	Proposed Method	Quantum Mechanism	Quantum Operators	Improvement
Learning	ANN (MLP)	QNN	Activation Function in MLP	Phase rotation, SU (2) transforms, superposition-like encoding	Higher accuracy near singularities
Identification	PSO	Q-PSO	Particle update Position and Velocity	Quantum angle encoding, probabilistic state measurement	Better convergence
Control	SMC	Q-SMC	Error and switching logic	Quantum subtractor, sign detector, qubit encoding	Reduced chattering; energy reduction
Actuation	SPWM	QSPWM	Modulation Switching Logic	Quantum subtractor, sign detector, Rotation gates, Hadamard/Toffoli logic	THD reduced

9.4 Appendix 4: Quantitative Summary of Contributions

Table 9.2 provides a consolidated overview of the quantitative outcomes obtained across the different stages of the proposed framework, along with their corresponding engineering interpretations. The table is structured to compare classical and quantum-inspired approaches at each system layer: modeling, learning, parameter identification, control, and actuation, highlighting both performance gains and practical implications.

At the modeling stage, three levels of dynamic model fidelity, detailed, semi-detailed, and simplified, are evaluated. The results indicate that there is no single absolute winner, as each model serves a different purpose. The detailed model provides the highest fidelity and accuracy in representing the system dynamics, while the simplified model offers significant computational advantages. Importantly, the simplified model achieves approximately 6.8% lower energy consumption compared to the semi-detailed model while preserving the overall torque trends. This demonstrates that reduced model complexity can maintain acceptable performance while improving computational efficiency, a particularly relevant feature for real-time applications.

In the learning stage, a comparison between classical Artificial Neural Networks (ANN) and Quantum Neural Networks (QNN) for inverse kinematics reveals a clear advantage for the quantum-inspired approach. The QNN achieves lower mean absolute error (MAE), with improvements of 15–17%. Specifically, the position error is reduced from approximately 2.71 mm to 1.79 mm, and the orientation error decreases significantly from about 0.021 rad to 0.00179 rad. These improvements indicate enhanced accuracy and robustness, particularly in handling nonlinear mappings and singularity-prone regions.

The parameter identification stage compares classical Particle Swarm Optimization (PSO) with Quantum-behaved PSO (Q-PSO). The results demonstrate that Q-PSO significantly improves estimation accuracy, achieving a mass center MAPE of approximately 0.43% compared to 2.94% for PSO, and an inertia MAPE of approximately 0.76% compared to 4.66%. Beyond accuracy, Q-PSO also exhibits better convergence stability and produces parameter estimates that more closely match the CAD-derived reference model. This improvement is critical for enhancing the reliability of subsequent control strategies.

At the control stage, the comparison between classical Sliding Mode Control (SMC) and Quantum-Inspired SMC (Q-SMC) shows notable performance gains. The Q-SMC approach reduces overshoot and steady-state error while producing smoother torque profiles. One of the most significant improvements is the reduction of chattering, a known limitation of classical SMC. Additionally, the energy consumption is reduced by approximately 3.79%, indicating that the quantum-inspired modifications improve both control quality and efficiency.

Finally, at the actuation stage, transitioning from classical Sinusoidal Pulse Width Modulation (SPWM) to Quantum SPWM (QSPWM) yields substantial improvements in signal quality. The Total Harmonic Distortion (THD) is reduced from 60.21% to 38.79%, corresponding to an approximate reduction of 35.6%. Although a slight increase in RMSE is observed, the overall impact is positive, with significant reductions in harmonic distortion, electromagnetic interference (EMI), and torque ripple. These improvements directly contribute to smoother, more efficient motor operation.

Overall, the table demonstrates that quantum-inspired methods consistently outperform classical approaches across multiple performance metrics. More importantly, the improvements are not isolated but accumulate across system layers, resulting in a more accurate, robust, and energy-efficient robotic system.

Table 9-2 Quantitative Summary of Thesis Contributions.

Steps	Comparison Type	Better Achievements	Engineering Interpretation
Modeling	Detailed vs Semi-detailed vs Simplified dynamic models	-	Detailed model best for fidelity; Simplified best for computational efficiency. Simplified model ~ 6.8% lower energy than semi-detailed while preserving torque trends.
Learning	ANN vs QNN for inverse kinematics	QNN	Lower MAE and position/orientation errors (~15–17%). Position error ≈1.79 mm vs 2.71 mm; Orientation error ≈0.00179 rad vs 0.021 rad.
Identification	PSO vs Q-PSO parameter identification	Q-PSO	Mass center MAPE: 0.43% vs 2.94%; Inertia MAPE: 0.76% vs 4.66%. Better convergence stability and closer match to CAD model.
Control	SMC vs Quantum-Inspired SMC	Q-SMC	Lower overshoot and steady-state error, smoother torque signals, reduced chattering. Energy reduced ~ 3.79%.
Actuation	SPWM vs QSPWM	QSPWM	THD reduced from 60.21% to 38.79% (~35.6%). Slight RMSE increase but improved EMI and torque ripple.